

2024 International Conference on Neuroprotective Agents Conference Proceedings

Issue Editors

William Slikker Jr.

Retired, United States

Slobodan M. Todorovic

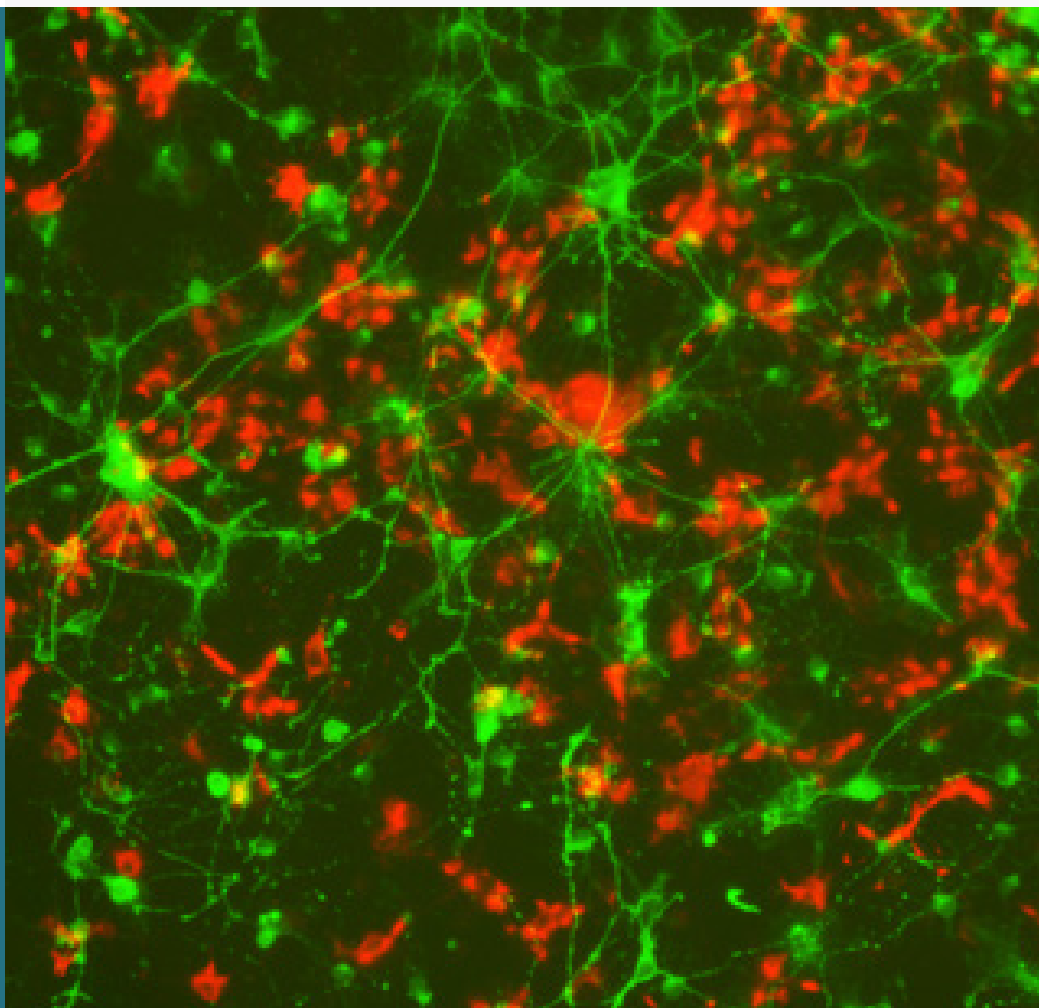
University of Colorado
Denver, United States

Russell J. Andrews

Independent researcher,
United States

Tucker A. Patterson

National Center for
Toxicological Research (FDA),
United States



2024 International Conference on Neuroprotective Agents Conference Proceedings

EBM eBook Copyright Statement

The copyright in the text of individual articles in this eBook is the property of their respective authors or their respective institutions or funders.

The copyright in graphics and images within each article may be subject to copyright of other parties. In both cases this is subject to a license granted to Frontiers.

The compilation of articles constituting this eBook is the property of Frontiers.

Each article within this eBook, and the eBook itself, are published under the most recent version of the Creative Commons CC-BY licence. The version current at the date of publication of this eBook is CC-BY 4.0. If the CC-BY licence is updated, the licence granted by Frontiers is automatically updated to the new version.

When exercising any right under the CC-BY licence, Frontiers must be attributed as the original publisher of the article or eBook, as applicable.

Authors have the responsibility of ensuring that any graphics or other materials which are the property of others may be included in the CC-BY licence, but this should be checked before relying on the CC-BY licence to reproduce those materials. Any copyright notices relating to those materials must be complied with.

Copyright and source acknowledgement notices may not be removed and must be displayed in any copy, derivative work or partial copy which includes the elements in question.

All copyright, and all rights therein, are protected by national and international copyright laws. The above represents a summary only. For further information please read Frontiers' Conditions for Website Use and Copyright Statement, and the applicable CC-BY licence.

ISSN 1535-3699

ISBN 978-2-8325-6757-9

DOI 10.3389/978-2-8325-6757-9

Generative AI statement

Any alternative text (Alt text) provided alongside figures in the articles in this ebook has been generated by Frontiers with the support of artificial intelligence and reasonable efforts have been made to ensure accuracy, including review by the authors wherever possible. If you identify any issues, please contact us.

Cover image reprinted with permission from "Assessing potential desflurane-induced neurotoxicity using nonhuman primate neural stem cell models" by Cheng Wang, Leah E. Latham, Shuliang Liu, John Talpos, Tucker A. Patterson, Joseph P. Hanig and Fang Liu, licenced under CCBY 4.0.

Table of contents

- 04 **2024 international conference on neuroprotective agents conference proceedings**
William Slikker Jr., Tucker A. Patterson, Slobodan M. Todorovic and Russell J. Andrews
- 07 **The effects of cannabidiol and its main metabolites on human neural stem cells**
Leah E. Latham, Qiang Gu, Shuliang Liu, Cheng Wang and Fang Liu
- 21 **Anesthesia-induced developmental neurotoxicity in the setting of systemic inflammation: the role of microglia**
Nemanja Useinovic, Adre Newson, Michelle Near, Stefan Maksimovic, Benjamin Volvovitz, Nidia Quillinan and Vesna Jevtovic-Todorovic
- 37 **Assessing potential desflurane-induced neurotoxicity using nonhuman primate neural stem cell models**
Cheng Wang, Leah E. Latham, Shuliang Liu, John Talpos, Tucker A. Patterson, Joseph P. Hanig and Fang Liu
- 50 **Assessing the developmental effects of fentanyl and impacts on lipidomic profiling using neural stem cell models**
Cheng Wang, Jinchun Sun, Rohini Donakonda, Richard Beger, Leah E. Latham, Leihong Wu, Shuliang Liu, Joseph P. Hanig and Fang Liu
- 62 **α -linolenic acid-induced facilitation of GABAergic synaptic transmission is mediated via acid-sensing ion channel (ASIC1a) activity in the basolateral amygdala**
Volodymyr I. Pidoplichko, Taiza H. Figueiredo, Maria F. M. Braga and Ann M. Marini
- 78 ***In vivo* silencing of the thalamic Ca_v3.1 voltage-gated calcium channels demonstrates their region-specific role in anesthetic mediated hypnosis**
Tamara Timic Stamenic, Simon Feseha, Brier Fine-Raquet, Vasilije P. Tadic and Slobodan M. Todorovic
- 89 **Comparative electrophysiological study of neuroactive steroid-induced hypnosis in mice: sex and drug-specific differences**
Abigail Martin, Ian Coulter, Reginald Cox, Douglas F. Covey, Slobodan M. Todorovic and Tamara Timic Stamenic

- 101 Cystamine reduces neurodegeneration and epileptogenesis following soman-induced status epilepticus in rats**
Abiel K. Biney, Caroline R. Schultz, Michael F. Stone, Donna A. Nguyen, Annie Wang, Marcio de Araujo Furtado and Lucille A. Lumley
- 114 Involvement of EGFR-AKT signaling in hemin-induced neurotoxicity**
Hui-Ju Huang, Yang-Jie Tseng, I-Jung Lee, Yu-Li Lo and Anya Maan-Yuh Lin
- 124 A double-edged effect of hypoxia on astrocyte-derived exosome releases**
Yang Jie Tseng, Hui-Ju Huang, Chien-Hui Lin and Anya Maan-Yuh Lin
- 135 Limitations to clinically restoring meaningful peripheral nerve function across gaps and overcoming them**
Christian A. Foy and Damien P. Kuffler
- 144 Mechanisms for reducing/eliminating chronic neuropathic pain with a focus on platelet-rich plasma**
Damien P. Kuffler and Christian A. Foy



OPEN ACCESS

*CORRESPONDENCE

William Slikker Jr.,
✉ billslikkerjr@gmail.com

†These authors have contributed equally to this work

RECEIVED 09 June 2025

ACCEPTED 30 June 2025

PUBLISHED 21 July 2025



CITATION

Slikker W Jr., Patterson TA, Todorovic SM and Andrews RJ (2025) 2024 international conference on neuroprotective agents conference proceedings. *Exp. Biol. Med.* 250:10699. doi: 10.3389/ebm.2025.10699

COPYRIGHT

© 2025 Slikker, Patterson, Todorovic and Andrews. This is an open-access article distributed under the terms of the [Creative Commons Attribution License \(CC BY\)](https://creativecommons.org/licenses/by/4.0/). The use, distribution or reproduction in other forums is permitted, provided the original author(s) and the copyright owner(s) are credited and that the original publication in this journal is cited, in accordance with accepted academic practice. No use, distribution or reproduction is permitted which does not comply with these terms.

2024 international conference on neuroprotective agents conference proceedings

William Slikker Jr. ^{1*}, Tucker A. Patterson², Slobodan M. Todorovic³ and Russell J. Andrews ^{4†}

¹Retired, Little Rock, AR, United States, ²National Center for Toxicological Research, Jefferson, AR, United States, ³University of Colorado School of Medicine, Aurora, CO, United States, ⁴World Federation of Neurosurgical Societies, Los Gatos, CA, United States

KEYWORDS

neuroprotective agents, neurochemistry, nervous system, neuroprotection, neuropharmacology

Editorial on the Research Topic

[2024 international conference on neuroprotective agents conference proceedings](#)

The purpose of the International Conference on Neuroprotective Agents (ICNA) is to assimilate basic science researchers and clinicians from many countries and disciplines in a common forum to address various approaches and advancements to achieve neuroprotection. The scientific format provides the opportunity for clinicians and basic researchers to come together in a relaxed and informal manner in order to foster the free exchange of ideas and concepts among the participants. Almost all the attendees provide an oral or a poster presentation, and informal discussions are scheduled for each session. The conferences are routinely held in small venues to encourage interaction among the participants outside of the formal sessions. Meals and coffee breaks are provided so discussions can continue throughout the day and evening. Receptions and excursions provide additional opportunities for scientific exchange. The ICNA is generally held every 2 years, and all proceedings have been published except for the very first conference held in Rockland, ME, USA, in 1991 [1]. The focus of the content in this special issue demonstrates the breadth of topics that are typical of the ICNA.

In keeping with its global aspect, the 16th ICNA was held in Bentonville, Arkansas, a small but growing city in the Northwest corner of the state. Student participation was excellent, thanks to the extensive neuroscience research being conducted throughout the state of Arkansas and elsewhere. Students at the graduate or postdoctoral level were eligible to compete in a scientific platform presentation session and competitive travel fellowships were graciously provided to Arkansas University students by the Arkansas Research Alliance.

The format was similar to previous ICNAs: a Monday evening reception, followed by a full day of presentations on Tuesday plus half-day morning presentations on

Wednesday and Thursday. A brief walking tour of the historic downtown Bentonville preceded a tour and dinner on Tuesday afternoon/evening at the beautiful and informative Crystal Bridges Museum of American Art.

Contents and summaries:

[2] *The effects of cannabidiol and its main metabolites on human neural stem cells.* Many pregnant women have been using CBD to treat pregnancy symptoms, causing fetal exposure to CBD. Using human neural stem cells in culture, the authors reported that CBD and its major metabolites 7-OH-CBD and 7-COOH-CBD reduced human NSC viability at concentrations comparable to those in human blood. In addition, CBD was observed to reduce GFAP and cannabinoid receptor 2 (CB2) expression after NSCs differentiation.

[3] *Anesthesia-induced developmental neurotoxicity in the setting of systemic inflammation: the role of microglia.* Sevoflurane neurotoxicity is enhanced in the setting of systemic inflammation induced by either LPS injection or trauma (tibia fracture) in terms of its onset, the intensity and duration that could, at least in part, be explained by a complex interplay between microglia activation and T-cell infiltration. Specifically, our mechanistic studies suggest that sevoflurane induced neuroapoptosis triggers activation of microglia, which in turn leads to the upregulation of proinflammatory cytokine MCP-1 and endothelial cell adhesion molecule, ICAM-1 mRNA levels in the hippocampus. This results in T-lymphocyte infiltration in the hippocampal subiculum, an event that further perpetuates microglial activation to control neuroapoptosis which is suggested by the fact that microglia depletion leads to a significant worsening of sevoflurane-induced developmental neuroapoptosis.

[4] *Assessing Potential Desflurane-induced Neurotoxicity Using Nonhuman Primate Neural Stem Cell Models.* Our data suggests that at the clinically relevant concentration, desflurane did not induce Neural Stem Cell (NSC) damage/death, but impaired the differentiated neuronal cells after prolonged exposure. These findings should be helpful/useful for the understanding of the diverse effects of desflurane exposure on the developing brain and could be used to optimize the usage of these agents in the pediatric setting.

[5] *Assessing the Developmental Effects of Fentanyl (Anesthetics/Analgesics) and Impacts on Lipidomic Profiling Using Neural Stem Cell Models.* These data indicated that micro molar concentrations of fentanyl exposure (24-h) did not induce detectable cell death. However, a lipidomic analysis indicated that fentanyl may affect immature neural cell functions through modifying lipid composition and lipid metabolism. These data indicated that despite the absence of clear neurodegeneration, fentanyl may still have a negative impact on the developing brain.

[6] *AlphaLinolenic acid-induced facilitation of GABAergic synaptic transmission is mediated via acid-sensing ion channel (ASIC1a) activity in the basolateral amygdala.* The selective

vulnerability of inhibitory neurons may contribute to the desynchronization of oscillations and lead to hyperexcitability disorders. By enhancing inhibitory neuronal transmission and bursting, alpha-linolenic acid may restore the synchronization of oscillations to prevent epilepsy and other hyperexcitability disorders.

[7] *In vivo silencing of the thalamic Ca_v3.1 voltage-gated calcium channels demonstrates their region-specific role in anesthetic mediated hypnosis.* The authors silenced the *Cacna1g* gene that encodes the low-threshold-activated Ca_v3.1 T-type voltage-gated calcium channel subunit by injecting short-hairpin RNA (shRNA) into midline and intralaminar - nonspecific thalamus (MIT) and sensory - specific ventrobasal (VB) thalamic nuclei in wild-type mice. They found that knocking down Ca_v3.1 channels in MIT significantly decreased inhaled isoflurane concentration that is required to induce hypnosis, but it did not affect speed of anesthetic induction and the immobilizing effect of isoflurane. In contrast, knocking down the Ca_v3.1 channel in the VB thalamus did not affect any of the measured anesthetic endpoints. Hence, they concluded that Ca_v3.1 channels in nonspecific MIT thalamus have a preferential role in anesthetic hypnosis when compared to the sensory VB thalamus.

[8] *Comparative electrophysiological study of neuroactive steroid-induced hypnosis in mice: sex and drug-specific differences.* This study investigated sex-specific effects of two common neuroactive steroids such as alphaxalone and allopregnanolone on thalamocortical (TC) oscillations in mice that are associated with their hypnotic/sedative effects. They found that females were more sensitive to both agents as evidenced by longer duration of hypnosis following intra-peritoneal injections of a dose of 100 mg/kg. Both agents had distinct electrophysiological signatures in TC circuitry that may underly their sedative/hypnotic effects with allopregnanolone inducing more profound TC suppression in females than males. The authors conclude that potential future use of neuroactive steroids for clinical anesthesia warrants consideration of their sex-specific effects.

[9] *Cystamine reduces neurodegeneration and epileptogenesis following soman-induced status epilepticus in rats.* Research efforts are continually investigating and aiming to improve therapies that may help alleviate neurodegeneration caused by injuries, toxic exposures, and/or neurological disorders. We present findings on the potential novel use of aminothiols as neuroprotectors, using a preclinical model of cholinergic-induced toxicity and associated neurodegeneration, highlighting the promising ability of aminothiols to reduce neuropathology when used as an adjunct to the current standard of care.

[10] *Involvement of EGFR-AKT signaling in hemin-induced neurotoxicity.* Using afatinib as a positive control, epithelial growth factor receptor (EGFR)-protein kinase B (aka AKT)

signaling is implicated in hemin-induced neurotoxicity and may represent a druggable target for intracerebral hemorrhage.

[11] *A double-edged effect of hypoxia on astrocyte-derived exosome releases*. Using hypoxia-preconditioned donor cells, exosome functionality appears to have both beneficial and detrimental effects on neurotoxicity, suggesting that hypoxia preconditioning plays a double-edged role.

[12] *Limitations to Clinically Restoring Meaningful Peripheral Nerve Function Across Gaps and Overcoming Them*. This review examines the efficacies, mechanisms of action, and limitations of many of the techniques used to restore meaningful function to peripheral nerves following injury that destroys a length of a nerve, creating a gap. It concludes that a novel technique using a special formulation of platelet-rich plasma (PRP) is the most effective technique and has few, if any, limitations.

[13] *Mechanisms, including PRP, for Reducing/Eliminating Chronic Neuropathic Pain*. This review examines the efficacies, mechanisms of action, and limitations of many of the techniques used to reduce neuropathic pain following peripheral nerve trauma. It concludes that a novel technique using a special formulation of platelet-rich plasma (PRP) is the most effective and can not only induce long-term chronic neuropathic pain reduction but long-term pain elimination and has few, if any, limitations.

Reference

1. Slikker W, Jr, Patterson TA, Andrews RJ. Preface: 2022 international conference on neuroprotective agents conference on neuroprotective agents. *Exp Biol Med (Maywood)* (2023) **248**(7):543–4. doi:10.1177/15353702231181136
2. Latham LE, Gu Q, Liu S, Wang C, Liu F. The effects of cannabidiol and its main metabolites on human neural stem cells. *Exp Biol Med* (2025) **250**:10608. doi:10.3389/ebm.2025.10608
3. Useinovic N, Newson A, Near M, Maksimovic S, Volvovitz B, Quillinan N, et al. Anesthesia-induced developmental neurotoxicity in the setting of systemic inflammation: the role of microglia. *Exp Biol Med* (2025) **250**:10549. doi:10.3389/ebm.2025.10549
4. Wang C, Latham LE, Liu S, Talpos J, Patterson TA, Hanig JP, et al. Assessing potential desflurane-induced neurotoxicity using nonhuman primate neural stem cell models. *Exp Biol Med* (2025) **250**:10606. doi:10.3389/ebm.2025.10606
5. Wang C, Sun J, Donakonda R, Beger R, Latham LE, Wu L, et al. Assessing the developmental effects of fentanyl and impacts on lipidomic profiling using neural stem cell models. *Exp Biol Med* (2025) **250**:10607. doi:10.3389/ebm.2025.10607
6. Pidoplichko VI, Figueiredo TH, Braga MFM, Marini AM. α -linolenic acid-induced facilitation of GABAergic synaptic transmission is mediated via acid-sensing ion channel (ASIC1a) activity in the basolateral amygdala. *Exp Biol Med* (2025) **250**:10545. doi:10.3389/ebm.2025.10545
7. Timic Stamenic T, Feseha S, Fine-Raquet B, Tadic VP, Todorovic SM. In vivo silencing of the thalamic CaV3.1 voltage-gated calcium channels demonstrates their

Author contributions

All authors listed have made a substantial, direct, and intellectual contribution to the work and approved it for publication.

Author's note

This editorial reflects the views of the authors and does not necessarily reflect those of the U.S Food and Drug Administration.

Funding

The author(s) declare that no financial support was received for the research and/or publication of this article.

Conflict of interest

The author(s) declared no potential conflicts of interest with respect to the research, authorship, and/or publication of this article.

region-specific role in anesthetic mediated hypnosis. *Exp Biol Med* (2025) **250**:10553. doi:10.3389/ebm.2025.10553

8. Martin A, Coulter I, Cox R, Covey DF, Todorovic SM, Timic Stamenic T. Comparative electrophysiological study of neuroactive steroid-induced hypnosis in mice: sex and drug-specific differences. *Exp Biol Med* (2025) **250**:10550. doi:10.3389/ebm.2025.10550

9. Biney AK, Schultz CR, Stone MF, Nguyen DA, Wang A, de Araujo Furtado M, et al. Cystamine reduces neurodegeneration and epileptogenesis following soman-induced status epilepticus in rats. *Exp Biol Med* (2025) **250**:10598. doi:10.3389/ebm.2025.10598

10. Huang H-J, Tseng Y-J, Lee I-J, Lo Y-L, Lin AM-Y. Involvement of EGFR-AKT signaling in hemin-induced neurotoxicity. *Exp Biol Med* (2025) **250**:10554. doi:10.3389/ebm.2025.10554

11. Tseng YJ, Huang H-J, Lin C-H, Lin AM-Y. A double-edged effect of hypoxia on astrocyte-derived exosome releases. *Exp Biol Med* (2025) **250**:10559. doi:10.3389/ebm.2025.10559

12. Foy CA, Kuffler DP. Limitations to clinically restoring meaningful peripheral nerve function across gaps and overcoming them. *Exp Biol Med* (2025) **250**:10566. doi:10.3389/ebm.2025.10566

13. Kuffler DP, Foy CA. Mechanisms for reducing/eliminating chronic neuropathic pain with a focus on platelet-rich plasma. *Exp Biol Med* (2025) **250**:10567. doi:10.3389/ebm.2025.10567



OPEN ACCESS

*CORRESPONDENCE

Fang Liu,
✉ fang.liu@fda.hhs.gov

RECEIVED 28 March 2025

ACCEPTED 06 May 2025

PUBLISHED 13 June 2025

CITATION

Latham LE, Gu Q, Liu S, Wang C and Liu F (2025) The effects of cannabidiol and its main metabolites on human neural stem cells.

Exp. Biol. Med. 250:10608.

doi: 10.3389/ebm.2025.10608

COPYRIGHT

© 2025 Latham, Gu, Liu, Wang and Liu. This is an open-access article distributed under the terms of the [Creative Commons Attribution License \(CC BY\)](#). The use, distribution or reproduction in other forums is permitted, provided the original author(s) and the copyright owner(s) are credited and that the original publication in this journal is cited, in accordance with accepted academic practice. No use, distribution or reproduction is permitted which does not comply with these terms.

The effects of cannabidiol and its main metabolites on human neural stem cells

Leah E. Latham, Qiang Gu, Shuliang Liu, Cheng Wang and Fang Liu*

Division of Neurotoxicology, National Center for Toxicological Research/Food and Drug Administration, Jefferson, AR, United States

Abstract

Cannabidiol (CBD) has been used for different purposes by different populations in recent years. When consumed by pregnant women, CBD can pass through the placenta and enter the fetal blood stream. There is concern over adverse effects of fetal exposure to CBD and its major metabolites (7-OH-CBD and 7-COOH-CBD). In the present study, human neural stem cells (NSCs) were treated with CBD and its metabolites at different concentrations for various durations to understand how the drug may affect fetal brain development. NSCs were also treated with delta-9 tetrahydrocannabinol (THC) for comparison purposes. CBD, 7-OH-CBD and 7-COOH-CBD dose-dependently reduced NSC viability. CBD and 7-OH-CBD reduced NSC number at the G1 phase. A 24 h exposure did not cause significant change in NSC proliferation. At concentrations comparable to those detected in human blood, longer exposures to CBD, 7-OH-CBD and 7-COOH-CBD caused more obvious cell death. After NSCs differentiation, CBD treatment reduced GFAP and cannabinoid receptor 2 (CB2) expression. THC treatment reduced the GFAP expression, but the change in CB2 expression did not reach statistical significance. The expression of cannabinoid receptor 1 (CB1) and beta-tubulin III were not significantly altered by drug exposures. The study demonstrated that clinically relevant concentrations of CBD, 7-OH-CBD and 7-COOH-CBD affect basic physiological features of human NSCs. After NSC differentiation, the reduced expression of CB2 receptors and GFAP on differentiated cells further indicated the vulnerability of developing central nervous system to CBD and THC. These data will help to contextualize *in vivo* neurodevelopmental studies that may not accurately model human metabolite profiles of CBD.

KEYWORDS

CBD, 7-OH-CBD, 7-COOH-CBD, THC, neural stem cells

Impact statement

There is a need to understand the effect of CBD on the developing brain. The current work demonstrates that exposure to CBD during early development poses a risk to the human developing brain. The work provides direct evidence on the adverse effects of 7-OH-CBD and 7-COOH-CBD on the human developing brain, helping to differentiate the effects of CBD from those of its major metabolites of 7-OH-CBD and 7-COOH-CBD. CBD and its major metabolites additively affect the developing central nervous system. The current study observes the effects of CBD and its metabolites on the brain cells, providing evidence that helps to distinguish the effects of CBD from those of its metabolites *in vivo*.

Introduction

Cannabidiol (CBD) is a non-intoxicating compound found in the plant *Cannabis Sativa*. Like with delta-9 tetrahydrocannabinol (THC), it naturally occurs in *Cannabis Sativa*. In 2018, the Farm Bill removed hemp which contains “no more than 0.3% THC on a dry weight basis” from marijuana (containing high levels of THC to have psychoactive effects, also called “cannabis”) in the Controlled Substances Act. Hemp products, especially those that contain CBD have rapidly proliferated. Preclinical and clinical studies indicate that CBD may have some therapeutic properties such as antidepressant-like, anxiolytic-like, anti-inflammatory, and antioxidative effects [1–5]. A recent clinical trial reported that CBD reduced cue-induced craving and anxiety of patients with opioid addiction [6], highlighting the potential of CBD-based therapies for treating opioid use disorder. Currently, only one CBD product (Epidiolex®) is approved by the U.S. Food and Drug Administration (FDA) for treating refractory epilepsy in children. Despite being widely available, no other CBD products are approved for the treatment of medical conditions. A survey that included a random sample of 2,543 adults from all 50 U.S. states and the DC area showed 20% of 18–29-year-old adults and 16% of 30–49-year-old adults used a CBD product in 2019 [7]. Another survey with data collected from 2,000 Americans showed 33% of American adults used CBD in 2020 [8]. Most people use CBD to medicate themselves simply due to the perception that it is natural and safer than other drugs. However, there is no data demonstrating the CBD products are safe and efficacious for the treatment of medical conditions other than seizure in very select populations, and CBD is not risk free. CBD may be hepatotoxic [9–11], actively interact with other drugs [12, 13], suppress immune function [14, 15], and adversely affect the male reproductive system [16, 17].

In humans, CBD is rapidly metabolized [18]. Among the numerous CBD metabolites, 7-COOH-CBD is the most

abundant in plasma, even more so than the parent compound. In humans, the second most abundant metabolite is 7-OH-CBD, whose concentration is comparable to CBD in plasma. While 7-OH-CBD has been reported to be bioactive [18, 19], whether 7-COOH-CBD has any bioactivity is not yet fully determined.

In the general population people use CBD for a variety of reasons. Many pregnant people report self-medicating with CBD to treat nausea, anxiety, and pain. When consumed by pregnant people, CBD can pass through the placenta [20], enter fetal blood circulation and directly interact with fetal organs. Moreover, CBD may enhance placenta permeability to other chemicals and increase the exposure of fetuses to those compounds [21]. Detection of CBD metabolites in meconium suggests that CBD is metabolized by fetuses, or that the metabolites can cross the placenta [22].

The endocannabinoid system is widely expressed in the central nervous system (CNS). It has an essential role in brain development and regulates and controls synaptic activity by releasing endogenous cannabinoids to interact with related receptors [23, 24]. CBD affects both developing and mature brains via various mechanisms, serving as a modulator of the endocannabinoid system [25]. CBD consumption during pregnancy causes fetal exposure to CBD which can accumulate in the brain due to its lipophilicity [26]. Adverse effects of CBD on the developing animal brain have been reported recently [27, 28]. With the high concentrations of 7-OH-CBD and 7-COOH-CBD in plasma, it merits further investigation to understand if the two most abundant metabolites have any effects on the human developing brain, which may contribute to the effects of CBD. Moreover, the decriminalization and legalization of cannabis for both medical and recreational use in many states in the US has caused a spike in THC consumption. THC is the most widely used illegal drug by pregnant women. It has been demonstrated that prenatal THC exposure adversely affects neurodevelopment [29], causing hyperactivity, cognition impairment, etc. in childhood [20, 30]. In the present study, we exposed human neural stem cells (NSCs) and cells that were differentiated from NSCs to CBD, 7-OH-CBD, 7-COOH-CBD and THC to assess their effects on NSC proliferation, viability and cell cycles, and the gene expression of some representative molecules on differentiated cells to get a basic idea on how they may affect brain biology at an early developmental stage.

Materials and methods

Test chemicals

CBD, 7-COOH-CBD (7-carboxy-CBD), 7-OH-CBD (7-hydroxy-CBD) and THC were purchased from Purisys (Athens, GA). CBD and the metabolites were pure; and the

purity of THC was more than 95%, as stated by the manufacturer. They were dissolved in Dimethyl sulfoxide (DMSO, MilliporeSigma, St. Louis, MO) and stored in a -20°C freezer.

Human neural stem cell (NSC) culture

Human NSCs purchased from PhoenixSongs Biologicals (Branford, CT) were used in the study. These de-identified cells were derived from the hippocampus of human fetal brain. Media for NSC proliferation (named “growth medium”) and differentiation (named “differentiation medium”) were purchased from the same vendor. These cells have been confirmed to be NSCs and capable of differentiating into neurons, astrocytes and oligodendrocytes in our previous studies [31, 32]. The cells were seeded on laminin-coated dishes of 10 cm in diameter at a density of $4.5 \times 10^4/\text{cm}^2$ and cultured with growth medium to promote NSC proliferation in a humidified incubator at 37°C with 5% CO_2 . The same cell density of $4.5 \times 10^4/\text{cm}^2$ was applied when NSCs were seeded on 96-well plates for assays. More than 95% of the seeded cells were viable 24 h after seeding. Oxygen level in the incubator was controlled at 4% as the vendor recommended to promote NSCs to differentiate into neurons. To induce NSC differentiation, NSCs were cultured in differentiation medium. After 3 days differentiation, these cells were treated with CBD, 7-OH-CBD, 7-COOH-CBD and THC in differentiation medium for 6 days before harvested. NSCs from passage 12 to 15 were used for experiments.

LDH release assay

Lactate dehydrogenase (LDH) release assay (Roche Applied Science, Indianapolis, IN) was performed as previously reported [33, 34] to determine cytotoxicity after chemical exposures for 1, 3, 5, and 7 days.

5-ethynyl-2'-deoxyuridine (EdU) incorporation assay

NSC proliferation rate was measured using an EdU staining kit [Click-iT[®] EdU Alexa Fluor[®] High-throughput Imaging (HCS) Assay, Invitrogen, Carlsbad, CA] after 24-h exposure to the chemicals, as the manufacturer instructed.

Flow cytometric analysis of cell cycle

Cell cycle status was analyzed using flow cytometry, by quantifying DNA content with DNA-binding dye propidium iodide (PI, MilliporeSigma). After 24 h exposure to drugs, human NSCs were harvested, fixed and permeabilized in cold 70%

ethanol. To ensure PI would stain DNA only, cellular RNA was digested with RNase A at 37°C for 1 h before DNA staining with PI. A LSRFortessa[™] flow cytometer with FACSDiva[™] software (BD Biosciences, San Jose, CA) was used to acquire PI signals and FCS Express (*De Novo* software, Pasadena, CA) was used to distinguish cells in each cell cycle phase. A total of 50,000 events were recorded on the flow cytometer.

Glutathione (GSH) assay

After 7 days drug exposures, the oxidative status of NSCs was assessed using GSH-Glo[™] Glutathione assay (Promega, Madison, WI) as the manufacturer described. Briefly, NSCs cultured in 96-well plates were incubated with 1X GSH-Glo[™] Reagent at room temperature, followed by incubation with Luciferin Detection Reagent and luminescence measurement.

Annexin V labeling for flow cytometry

To understand whether CBD, its metabolites or THC induced apoptosis or necrosis, human NSCs were labeled with Annexin V and PI (BD Biosciences) as manufacturer instructed after 24 h drug exposure. In brief, collected NSCs were washed with cold PBS, resuspended in Binding Buffer, and incubated with FITC Annexin V and PI, followed by flow cytometry analysis.

Terminal deoxynucleotidyl transferase dUTP nick-end labeling (TUNEL) assay

After 24 h exposure to CBD, its metabolites and THC, human NSCs were fixed with paraformaldehyde for TUNEL assay, using TUNEL Andy Fluor[™] 488 Apoptosis Detection Kit (ABP Biosciences, Rockville, MD) as previously described [35].

Western-blots of β -tubulin III, glial fibrillary acidic protein (GFAP), oligodendrocyte myelin glycoprotein (OMG), caspase 3 and cannabinoid receptors 1 and 2 (CB1 and CB2)

Western-blots of β -tubulin III, GFAP, OMG, caspase 3 (pro-caspase 3 and active caspase 3), CB1 and CB2 were conducted using Jess[™] (ProteinSimple Inc.), whose protein separation principal is based on capillary electrophoresis technology. Protein analysis was performed following the protocol provided by ProteinSimple Inc. In brief, protein samples (0.5 mg/ml) were mixed with a sample buffer containing

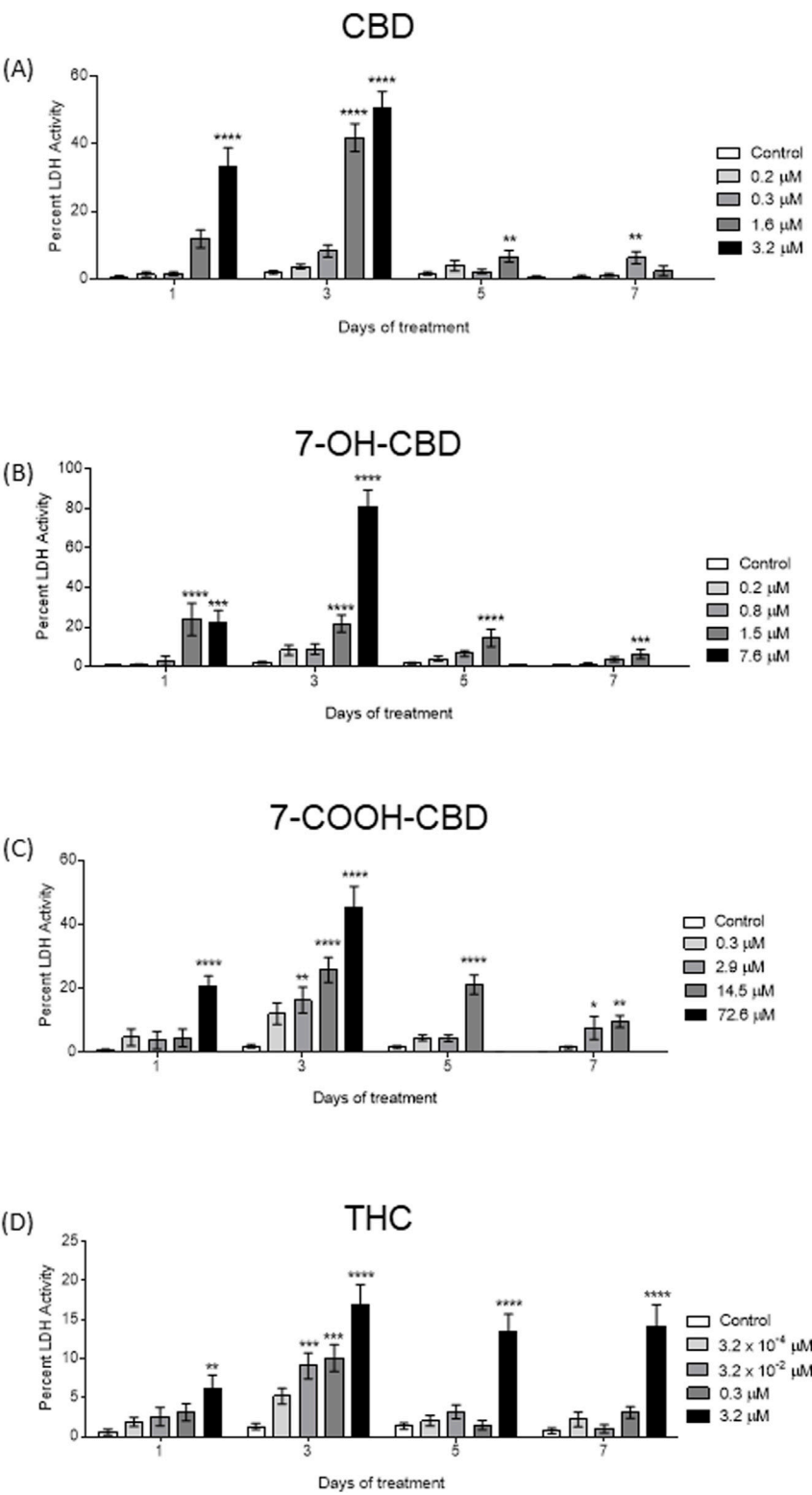


FIGURE 1 LDH release assay after CBD, 7-OH-CBD, 7-COOH-CBD and THC exposures for 1, 3, 5 and 7 days. **(A)** Exposure to 3.2 μM CBD significantly increased LDH release after 1 day and 3 days exposures; no obvious LDH release was detected after 5 days and 7 days exposures. The cytotoxic effects of 1.6 μM CBD were not significant until after 3 days exposure. Exposure to 0.3 μM CBD for 7 days caused an increase of LDH release. **(B)** 7-OH-CBD at 1.5 μM caused LDH release after 24 h exposure and continued through the entire experiment. No cells survived in 7.6 μM 7-OH- (Continued)

FIGURE 1 (Continued)

CBD group after 5 days exposure. (C) 7-COOH-CBD of 72.6 μM increased LDH release after 1 day and 3 days exposures; no obvious LDH release was detected after 5 days and 7 days exposures due to loss of cell. At 14.5 μM , 7-COOH-CBD induced higher LDH release after 3, 5 and 7 days, while 2.9 μM 7-COOH-CBD only show significant effects after 7 days exposure. (D) Exposure to 3.2 μM THC increased LDH release starting from the first day of exposure. At lower concentrations, 3.2×10^{-2} μM THC and 0.3 μM THC caused a transient LDH increase after 3 days exposure. * $P < 0.05$; ** $P < 0.01$; *** $P < 0.001$; **** $P < 0.0001$, $n = 4-6$. The experiment was repeated at least three times independently.

200 mM dithiothreitol (DTT) and fluorescent standards (4:1 vol/vol), and denatured at 95°C for 5 min. The protein samples were loaded into capillaries, separated, immobilized, incubated with respective primary antibodies (1:50, β -tubulin III, GFAP and CB1: MilliporeSigma; OMG and CB2: Abcam; caspase 3: Novus Biologicals) for 1 h, washed, and then incubated with horse radish peroxidase-conjugated anti-rabbit (GFAP, CB1 receptor, CB2 receptor and caspase 3) or anti-mouse (β -tubulin III) secondary antibodies for 1 h. After washing, the capillaries were incubated with the luminol-S/peroxide substrates, and chemiluminescence signals were captured using a charge-coupled device (CCD) camera. After the chemiluminescence signals of the target protein in each capillary were captured, the chemiluminescence signals were stripped using a RePlex kit (ProteinSimple Inc.). Then, total proteins in each capillary were determined using the Simple-Western Total Protein Detection Module (ProteinSimple Inc.), which is a chemiluminescence based total protein assay kit. The chemiluminescence signals of the target protein and the total protein in each capillary were measured using the Compass software (ProteinSimple Inc.). The signal intensity of the target protein in each capillary were normalized automatically by the Compass software based on the signals of the total proteins in that capillary. The normalized signal intensity of the target protein represents the relative abundance of the target protein. ANOVA test was used to compare the relative abundance of each target protein among the different treatment groups.

Statistical analysis

Data were analyzed with GraphPad Prism 9 (GraphPad Software Inc., San Diego, CA) using one-way ANOVA followed by Dunnett's *post hoc* test, and expressed as mean \pm SD. Each experiment was repeated at least three times independently. It was statistically different when a p value is less than 0.05.

Results

Cytotoxic effects of drugs

Human NSCs were exposed to a wide range of concentrations of CBD, 7-COOH-CBD, 7-OH-CBD and THC, which were selected according to the concentrations detected in

human blood [18]. The LDH release assay revealed that CBD, its metabolites, and THC increased LDH release in a dose- and duration-dependent manner (Figure 1), suggesting these drugs caused cell death.

After 24 h exposure to 3.2 μM CBD, LDH release was significantly increased by 32.7% compared with control; the increase reached to 48.9% after 3 days exposure. No obvious LDH release was observed on day 5 and 7 due to the loss of cells in this group. CBD at 1.6 μM caused an increase of LDH release after 24 h exposure, but it did not reach statistical significance until after 3 days of exposure, when the LDH release was significantly elevated to 41.8%, and another significant increased LDH release after 5 days exposure. It was noticed that the surviving cells in the 1.6 μM CBD-treated group were not enough to make a significant change of LDH release after 7 days exposure. In addition, exposure to 0.3 μM CBD resulted in a significant increase of LDH release by 5.7% after 7 days exposure (Figure 1A).

The toxic effect of 7.6 μM 7-OH-CBD was revealed by the elevated LDH release of 21% after 24 h exposure (Figure 1B). It induced an 79.3% increase of LDH release after 3 days exposure. There was no viable cell left in the 7.6 μM 7-OH-CBD -treated group afterwards, and no obvious LDH release was detected. 7-OH-CBD at 1.5 μM caused LDH release through the entire exposure time course: the elevated release reached 23.8%, 21.8%, 14.4%, and 6.3% when measured after 1, 3, 5, and 7 days exposure. Lower concentrations of 7-OH-CBD (0.8 μM and 0.2 μM) did not induce a significant increase of LDH release (Figure 1B).

Being the most abundant CBD metabolite, 7-COOH-CBD at 72.6 μM increased LDH release by 20.3% after 24 h exposure and increased by 43.7% after 3 days exposure. Lower concentrations of 7-COOH-CBD also stimulated LDH release after longer exposure: a continuous elevation of LDH release was observed in 14.5 μM 7-COOH-CBD-treated group after 3 days exposure, reaching 23.9%, 1.5%, and 9.7% after 3, 5, and 7 days exposure (Figure 1C). Higher levels of LDH release were detected in the 3.2 μM THC group throughout the exposure period. An elevation of 5.7%, 15.7%, 12.3% and 13.5% occurred after 1, 3, 5 and 7 days exposure, respectively (Figure 1D).

According to a pharmacokinetic study [18], CBD metabolites 7-OH-CBD and 7-COOH-CBD were detected soon after the CBD intake, and the terminal elimination half-life was 14–17 h for CBD, 14–19 h for 7-OH-CBD, and 25–30 h for 7-COOH-CBD after one dose of CBD, suggesting that the human brain could be exposed to CBD

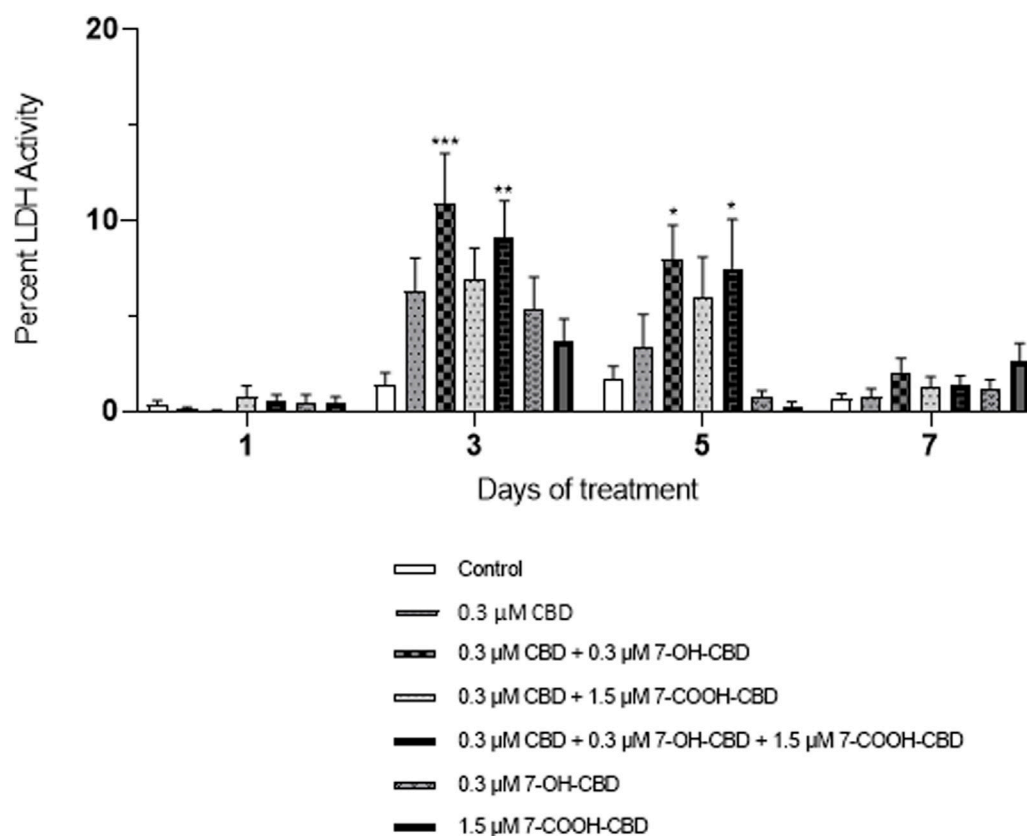


FIGURE 2

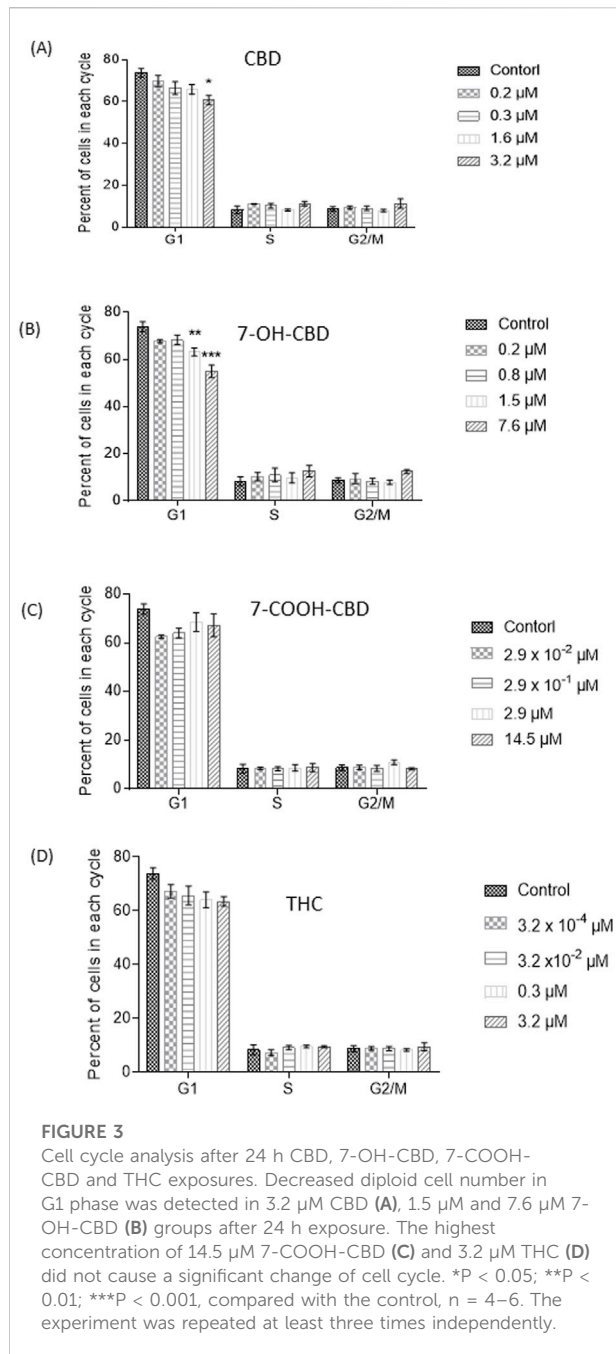
LDH assay of combination treatments. NSCs were exposed to 0.3 μM CBD and 7-OH-CBD, and 1.5 μM 7-COOH-CBD and their combinations. CBD and 7-OH-CBD additively increased LDH release starting from day 3. * $P < 0.05$; ** $P < 0.01$; *** $P < 0.001$, compared with the control, $n = 4-6$. The experiment was repeated at least three times independently.

and its metabolites simultaneously after CBD intake. Therefore, in this study, NSCs were exposed to a combination of CBD, 7-OH-CBD and 7-COOH-CBD to assess whether CBD, 7-OH-CBD and 7-COOH-CBD had any additive or synergistic toxic effects on NSCs. NSCs were exposed to 0.3 μM CBD, 0.3 μM 7-OH-CBD, and 1.5 μM 7-COOH-CBD individually or in combination. The concentrations of each compound were selected to be similar to the steady plasma concentrations of CBD, 7-OH-CBD and 7-COOH-CBD found in a clinical trial, in which subjects took 1,500 mg CBD twice a day for 6 days, with a single dose on the morning of day 7 [18]. Compared with the control group (0.1% DMSO), although the NSCs exposed to individual chemical had a higher level of LDH release after 3 days exposure, the elevation was not statistically significant. The LDH release was significantly higher in the group of NSCs exposed to a combination of CBD with 7-OH-CBD, with an increase of 9.6%. Exposure to CBD and the two metabolites stimulated LDH release from NSCs by 7.8% after 3 days exposure. There was a 6.3% increase of LDH release in the

group treated with CBD and 7-OH-CBD, and a 5.8% increase after treatment of CBD and the two metabolites for 5 days (Figure 2), while the single drug did not make a significant difference (Figure 2).

Drugs effects on NSC proliferation and cell cycle

The cell cycle analysis did not observe any changes in S phase from any treated group, suggesting no obvious effect on NSC proliferation after 24 h exposure to the chemicals. The EdU assay showed similar results (data not shown). However, the number of G1 phase cells were reduced after exposure to 3.2 μM CBD by 13.1% (Figure 3A). Both 1.5 μM and 7.6 μM 7-OH-CBD caused reductions of G1 phase cells by 10.7% and 19.0%, respectively (Figure 3B), suggesting fewer diploid cells after exposure. THC of 3.2 μM also reduced G1 phase cell number (Figure 3D), but with a p value of 0.059. 7-COOH-CBD did not show a significant effect (Figure 3C).



GSH levels in NSCs

CBD has been reported to be an antioxidant [4, 36], while THC has been shown to be an antioxidant or to increase oxidative stress, depending on different conditions [37, 38]. Whether CBD and its main metabolites affect the redox status in NSCs was determined by the measurement of GSH levels in NSCs. After 7 days exposure, CBD at 0.2 and 0.3 μM, 7-OH-CBD at 0.2 and 0.8 μM, 7-COOH-CBD at 0.3 and 2.9 μM and THC at

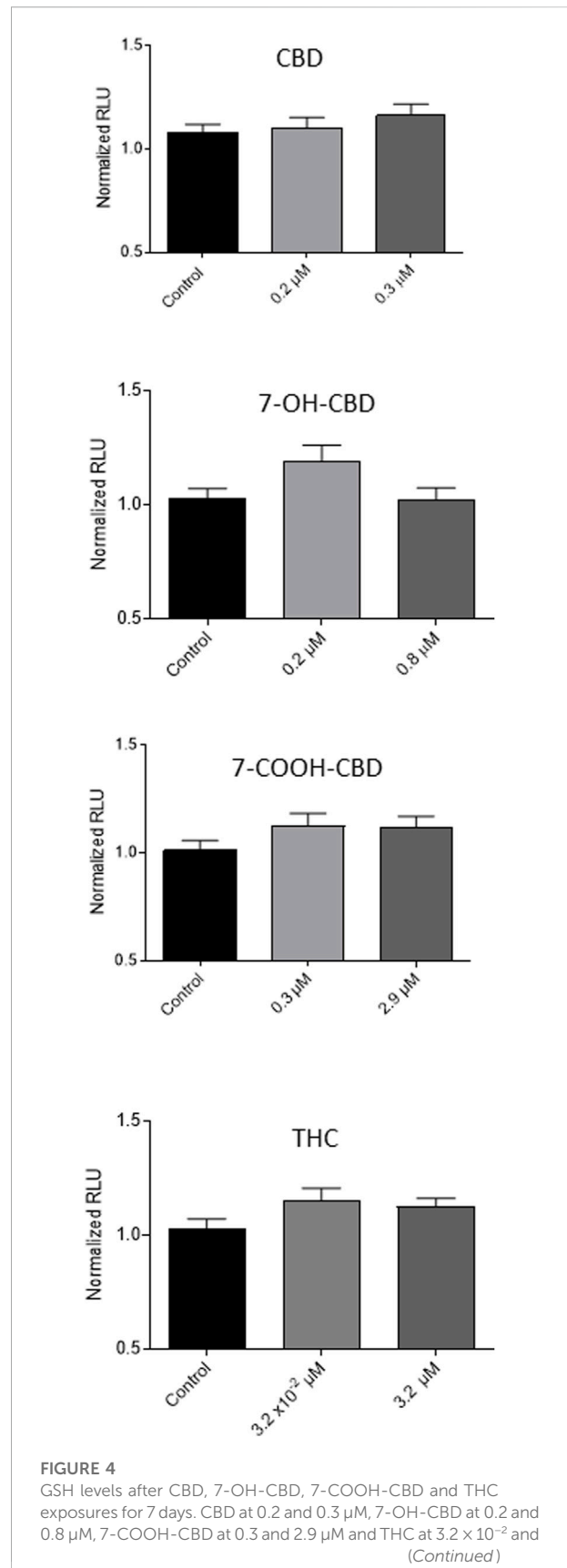


FIGURE 4 (Continued)

3.2 μ M did not make a significant change in the GSH levels in the exposed cells. N = 4–6. The experiment was repeated at least three times independently.

3.2 $\times 10^{-2}$ and 3.2 μ M did not alter GSH in NSCs significantly (Figure 4). The concentrations of each drug were selected based on the result of LDH assay, which did not show obvious cytotoxic effects on NSCs, except that 0.3 μ M of CBD caused a small but significant increase of LDH release.

NSC apoptosis detected by annexin V-PI staining and TUNEL assay

In this study, TUNEL assay and flow cytometry of Annexin V and PI staining were conducted to verify the toxic effects of cannabidiol and its main metabolites. The control group showed 14% of cells were Annexin V⁺ and PI⁺. There was a 7% increase of positive cells in 1.6 μ M CBD group, suggesting CBD-induced cell death was mainly late-stage apoptosis after 24 h exposure. However, no significant increase of Annexin V⁺ and PI⁺ positive cells was detected in 1.5 μ M 7-OH-CBD, 14.5 μ M 7-COOH-CBD or 0.3 μ M THC groups (Figure 5A). TUNEL positive cells were detected in each treated group. Although some dead cells detached during the experimental procedure, the CBD-treated group still showed obvious TUNEL positive cells. The other groups showed scattered TUNEL positive cells (Figure 5B).

Expression levels of β -tubulin III, GFAP, OMG, caspase 3, CB1 and CB2 receptors after drug exposures

From the 4th day of differentiation, the cells were treated with 0.3 μ M CBD, 0.2 μ M 7-OH-CBD and 1.5 μ M 7-COOH-CBD for 6 days, which were comparable to the steady concentrations detected in the human blood when the subjects took 1,500 mg CBD twice daily for 6 days [18]. It was reported that serum concentration of THC ranged from 13 to 63 ng/mL in cannabis smokers (from a 7% Δ 9-THC content cigarette) 0–22 h post inhalation [39]. The range of individual peak concentrations of THC is 1.6–160 μ g/L (1.6–160 ng/mL) [29]. Therefore, the differentiated cells were exposed to 0.3 μ M THC. After 10 days differentiation, markers for neurons (β -tubulin III), astrocytes (GFAP) and oligodendrocytes (OMG) were detected by Western Blots (Figures 6A–C), suggesting NSCs have differentiated into neurons and glial cells. No active caspase 3 was detected. The expression of pro-caspase 3 was similar among groups (Figure 6D). Although the signals were not as strong as

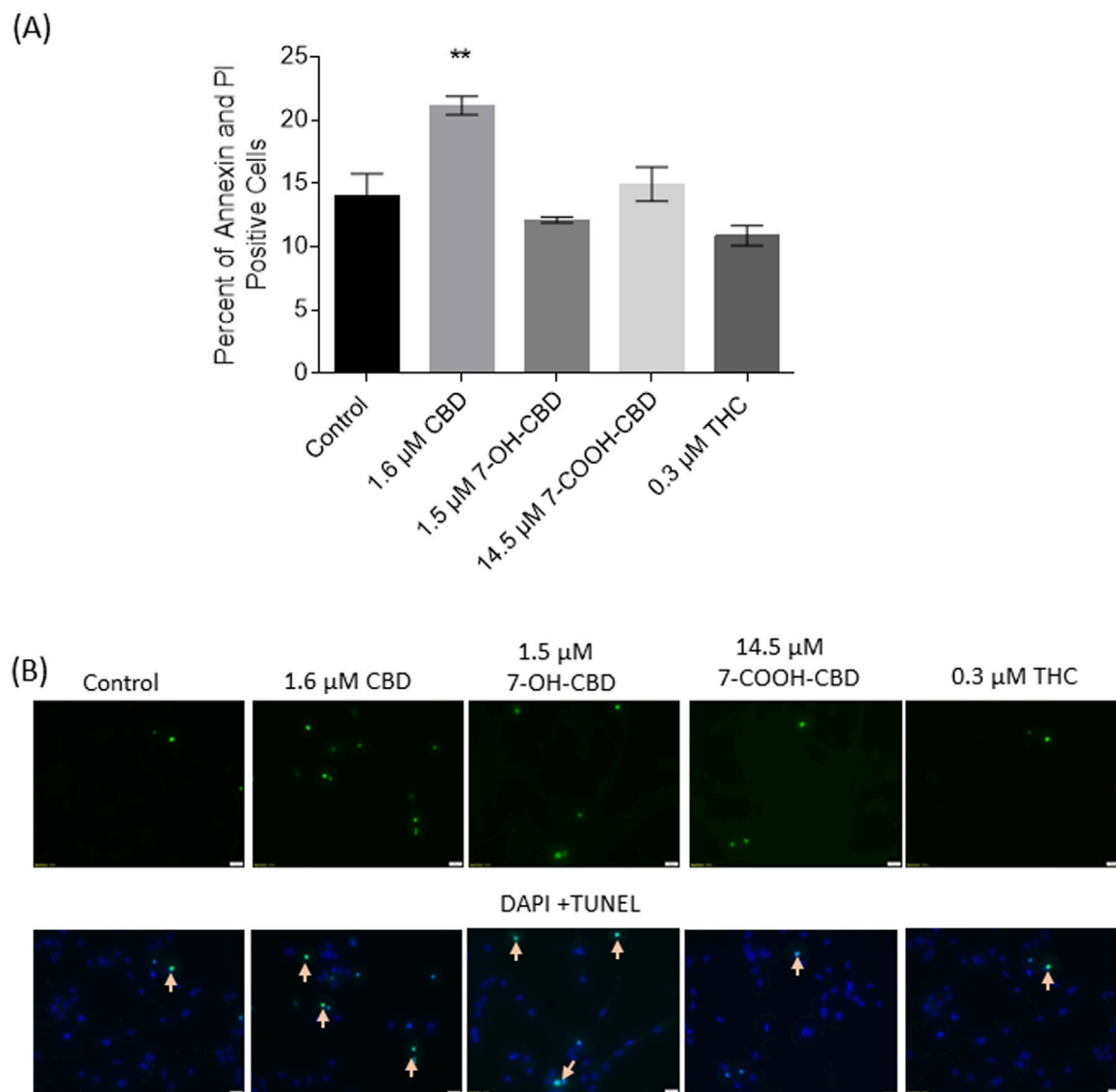
GFAP, β -tubulin III or OMG, CB1 (Figure 6E) and CB2 (Figure 6F) were detected, suggesting that differentiated cells expressed CB1 and CB2 receptors. CBD treatment resulted in decreased expression of GFAP and CB2 receptors on differentiated cells. THC treatment significantly reduced GFAP expression, while the reduction of CB2 receptors did not reach statistical significance. The CBD metabolites of 7-OH-CBD and 7-COOH-CBD did not cause significant changes in expression of β -tubulin III, GFAP, OMG, CB1 and CB2 after 6 days treatments.

Discussion

CBD products are purported to treat numerous health conditions in the popular media, but in almost every instance lack approval from a regulatory agency. While there are studies reporting the beneficial effects of CBD [1, 2, 36, 40, 41], evidence on its adverse effects has also emerged [26, 27, 42]. Its interaction with other drugs is another concern [43]. When fetuses are exposed due to pregnant women consuming CBD, the fetal central nervous system (CNS) can be more vulnerable because of their incomplete development. There is a need to determine how much and how long CBD can be consumed before it may have any adverse effects on the developing human brain. Whalley et al. [44] observed interspecies variations in endocannabinoid signaling, implying possible species-specific inaccuracies if animal models are used to predict how CBD affects the human brain. Moreover, it is not possible to explore the effects of an early-life stressor such as CBD exposure in the human fetus. To obtain data from more relevant models, we purchased human NSCs that were collected from human fetal brain at gestational week 19 to conduct dose-response and time-course studies. Cultured NSCs can proliferate and differentiated *in vitro* [31, 32]. The present study detected strong expression of β -tubulin III, GFAP and OMG (Figures 6A–C), repeatedly confirming human NSC differentiation *in vitro*. Therefore, human NSCs can recapitulate some basic biological events happening in the developing human brain, allowing for the investigation of drug exposure events in a short period of time, and in a simplified system.

Effects of CBD, its metabolites and THC on NSCs

A challenge for modeling the effects of CBD in animals is distinguishing the effects of CBD from those of its metabolites. The relative ratios of CBD metabolites in animal models (e.g., dogs, rats, etc.) are incomparable to those of humans [45–49]. Moreover, CBD concentrations in human blood vary depending on the doses, frequency and routes of administration, and the consumers' healthy state, etc. Even diet change can influence

**FIGURE 5**

Cell death detected by Annexin V-PI staining and TUNEL assay. **(A)** Twenty-four-hour exposure to 1.6 μ M CBD significantly elevated the number of both Annexin V⁺ and PI⁺ cells. **(B)** Images of TUNEL assay showed the drugs-induced apoptotic cells (indicated by arrows). ** $P < 0.01$, compared with the control, $n = 3$. The experiment was repeated three times independently.

CBD concentrations in blood [18]. There is a need to perform screening using different concentrations of CBD to estimate the consequence of brain exposure. In a clinical trial, Taylor et al. [18] measured CBD and CBD metabolites including 7-OH-CBD and 7-COOH-CBD concentrations in healthy volunteer blood after they took different doses of CBD (Epidiolex®). A dose of 1,500 mg/day CBD administration resulted in the plasma C_{max} of CBD, 7-OH-CBD and 7-COOH-CBD of 292.4 ng/mL (0.9 μ M), 238.7 ng/mL (0.7 μ M) and 3,060 ng/mL (8.9 μ M), respectively. When 4,500 mg/day of CBD was administered, the C_{max} of CBD, 7-OH-CBD and 7-COOH-CBD in plasma

reached 722.1 ng/mL, 404.8 ng/mL and 5,120 ng/mL, respectively [18]. There is no report on CBD or its metabolites concentrations in the human brain, but data from animal experiments showed CBD reached the brain with a relatively high concentration soon after it was orally administered [50]. Considering the lipophilic property of CBD, in the present study, we selected a series of concentrations for CBD and its metabolites to treat human NSCs, based on their concentrations detected in human blood and the animal brain. The utilization of NSCs helped to compare the relative toxicity of CBD, its main metabolites and THC, to

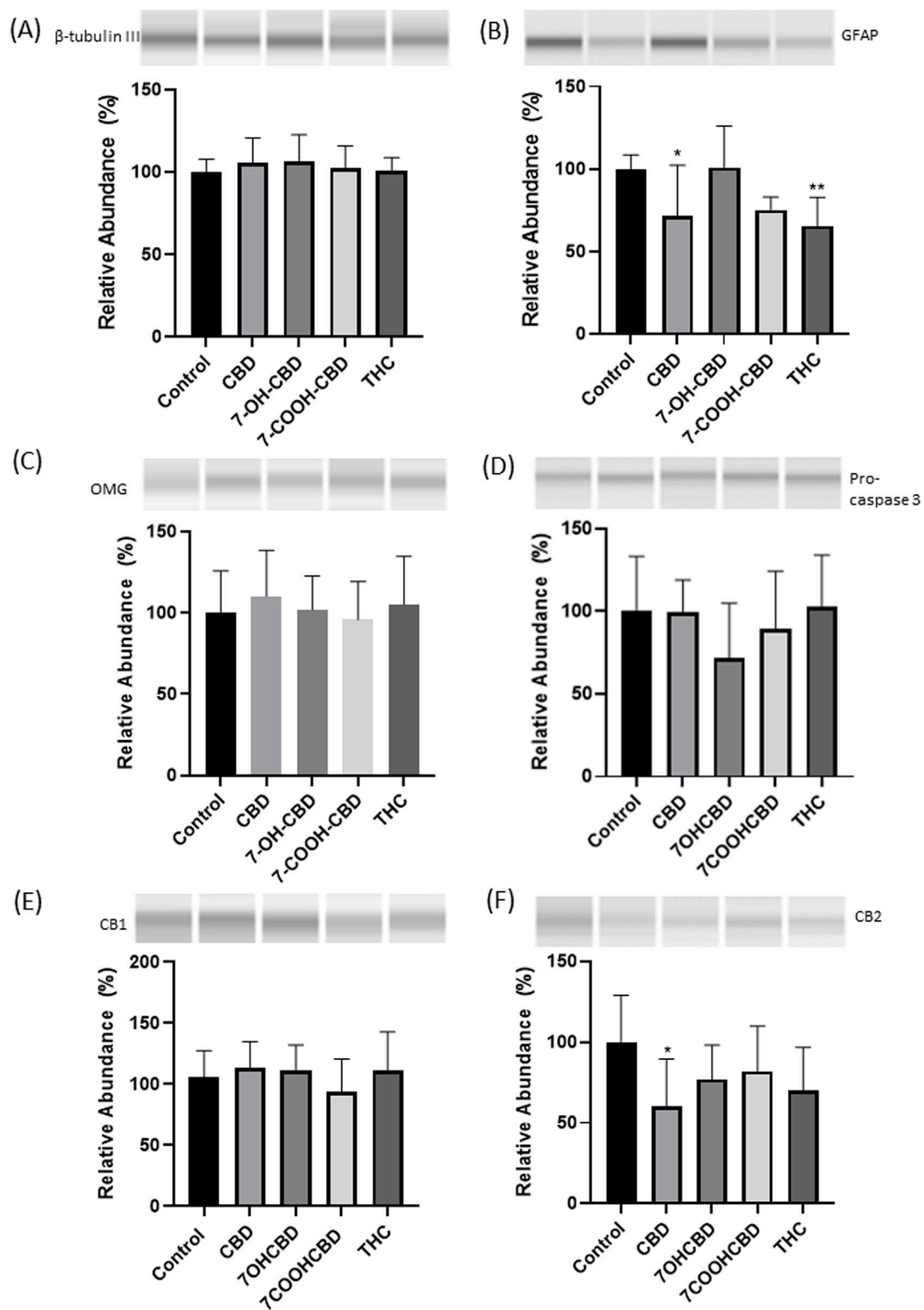


FIGURE 6

Western blots of β -tubulin III, GFAP, OMG, pro-caspase 3, CB1 and CB2 receptors in differentiated cells. No significant changes in the expression of β -tubulin III (A), OMG (C), pro-caspase 3 (D) or CB1 receptor (E). GFAP expression was lower in CBD and THC exposed groups (B). CB2 receptors expression was reduced in CBD exposed group (F). *P < 0.05; **P < 0.01; n = 3–5. The experiment was repeated at least three times independently.

predict their potential toxicity *in vivo*, which is difficult with whole animal studies. Our findings demonstrated that NSCs were vulnerable and sensitive to CBD and its metabolites as evidenced by increase cell death, after the exposure to various concentrations, at different time points. Of note, even lower concentrations of CBD and the metabolites showed slight yet significant cytotoxic effects after long term exposure (Figure 1), suggesting the potential risks of chronic exposure to CBD *in vivo*. THC concentrations in human blood vary dramatically when the amount and frequency of consumption are different [51, 52]. In this study, THC concentrations were chosen to include both low and high THC concentrations detected in humans [51, 52]. It seemed that THC had similar effects on NSC viability as those of CBD (Figure 1), although CBD does not have psychoactive effects. In addition to the effects of 7-OH-CBD in isolation, we observed additive effects of CBD and 7-OH-CBD on cell death (Figure 2), providing evidence that 7-OH-CBD has active effects on NSCs. It is well known that 7-COOH-CBD is the most abundant metabolite in plasma [18, 53]. Its direct effects on the human brain were not fully determined due to the different concentrations in human and animal models. We observed the cytotoxic effects of 7-COOH-CBD on NSCs (Figure 1), which has not been reported in other studies.

Oxidative stress is often associated with cell death [54, 55]. Cellular GSH levels are an indicator of redox status. It was reported that high levels of GSH were essential for stem cells [56]. CBD was reported to have antioxidative and neuroprotective effects mediated by various mechanisms [41, 57–59]; THC has demonstrated different effects on redox homeostasis in different situations [37, 38]. In this study, we measured cellular GSH levels to understand NSC redox status after exposure to CBD, its metabolites, and THC for 7 days. The cellular GSH levels were not dramatically changed (Figure 4). It seemed that these drugs at subtoxic concentrations (except 0.3 μ M CBD causing a subtle but detectable change in LDH release) did not significantly affect the redox status in NSCs.

Effects of CBD, its metabolites and THC on differentiated cells

In addition to NSCs, neurons and glial cells differentiated from NSCs are exposed to drugs and chemicals after they enter the fetal brain. In the present study, to determine responses of neurons, astrocytes, and oligodendrocytes after drug exposure, NSCs that had been differentiated for 3 days were treated with 0.3 μ M CBD, 0.2 μ M 7-OHCB, 1.5 μ M 7-COOHCB, and 0.3 μ M THC respectively for 6 days. No visible cell death was observed during the 6 days treatment, nor altered caspase 3 expression was detected in the differentiated cells, indicating these drugs did not cause significant death of developing neurons and glial cells. Western-blot results did not identify changes in β -tubulin

III expression (Figure 6A), suggesting neuronal differentiation was not significantly affected by CBD, its metabolites or THC at the exposed concentrations. However, GFAP expression was decreased in CBD and THC-treated groups (Figure 6B). There is research work demonstrating that THC changed GFAP expression in the animal brain during development [60–63]. A recent study by Landucci et al. presented that CBD reduced GFAP expression in CA1 region of the developing rat hippocampus [61]. Not only in early development, GFAP expression was adjusted in adolescence or adulthood after THC exposure [64]. In the present study, since no significant cell death was observed, reduced GFAP expression could suggest that the cytoskeletal structure of astrocytes was modified, which could affect astrocyte maturation and functions. Our observations and those from others indicated that the GFAP expression seems to be quite sensitive and indicative of CBD and THC exposure. In contrast to their adverse effects on NSCs, CBD metabolites of 7-OH-CBD and 7-COOH-CBD did not significantly reduce GFAP expression, although 7-COOH-CBD showed the tendency (Figure 6B).

Both CB1 and CB2 receptors have been detected on neurons and astrocytes; and CB2 receptors are found to be present on microglia too [65–69]. It has been demonstrated that CB1 and CB2 receptors are expressed in the developing brain [70]. In the present study, with the limitation of available antibodies against CB1 and CB2 receptors, it was difficult to locate CB1 and CB2 receptors on neurons or astrocytes using immunocytochemical staining, although Western blots detected CB1 and CB2 receptors expression on differentiated cells. The relative weak expression of CB2 receptor of the Western blots suggested the low abundance of CB2 receptor expression during early brain development. CBD induced down-regulation of GFAP and CB2 receptors. Therefore, it was hypothesized that CBD could have interacted with astrocytes during astrocyte differentiation, causing modulation of astrocyte functions and CB2 receptor expression on astrocytes. While the consequences of the reduced CB2 receptor expression in the developing brain have yet to be elucidated, it was reported that decreased CB2 receptor expression could increase seizure susceptibility and cause a deficiency of social memory in mice [71, 72]. It will be an intriguing topic to understand how cannabinoids would affect CB2 receptors during the brain development, and whether such effects may alter brain functions in adulthood.

Summary

In this study, we performed an evaluation of key cannabinoids on the effects of NSC biology. Our data has demonstrated the adverse effects of CBD, its metabolites, and THC on NSCs and differentiated cells, indicating their toxic effects on the human brain at an early developmental stage.

Observed effects of 7-OH-CBD and 7-COOH-CBD on NSCs highlighted their possible bioactivity *in vivo*. The cell cycle assay provided additional evidence that these drugs reduced the number of diploid cells, indicating cell death. We focused on some primary endpoints after the differentiated cells were exposed to drugs for 6 days, and detected changes in GFAP and CB2 receptors. Although more areas need to be explored, the present findings have provided evidence that CBD and its main metabolites at concentrations comparable to those detected in human blood may have adverse effects on the developing brain *in vivo*, especially after long-term exposure. Moreover, the comparative analysis of CBD and its key metabolites will also help to put findings from non-clinical studies, where metabolite profiles may not match that observed in humans, into context.

Author contributions

LL, QG, SL, and CW performed the experiments, and FL designed the study, acquired the funding and drafted the manuscript. All authors contributed to the article and approved the submitted version.

Author disclaimer

This manuscript reflects the views of its authors and does not necessarily reflect those of the U.S. Food and Drug Administration. Any mention of commercial products is for clarification only and is not intended as approval, endorsement, or recommendation.

Data availability

The original contributions presented in the study are included in the article/supplementary material, further inquiries can be directed to the corresponding author.

References

1. Schier A, Ribeiro N, Coutinho DS, Machado S, Arias-Carrion O, Crippa JA, et al. Antidepressant-like and anxiolytic-like effects of cannabidiol: a chemical compound of Cannabis sativa. *CNS & Neurological Disord - Drug Targets* (2014) **13**: 953–60. doi:10.2174/1871527313666140612114838
2. Blessing EM, Steenkamp MM, Manzanares J, Marmar CR. Cannabidiol as a potential treatment for anxiety disorders. *Neurotherapeutics* (2015) **12**:825–36. doi:10.1007/s13311-015-0387-1
3. Florensa-Zanuy E, Garro-Martinez E, Adell A, Castro E, Diaz A, Pazos A, et al. Cannabidiol antidepressant-like effect in the lipopolysaccharide model in mice: modulation of inflammatory pathways. *Biochem Pharmacol* (2021) **185**:114433. doi:10.1016/j.bcp.2021.114433
4. Atalay S, Jarocka-Karpowicz I, Skrzydlewska E. Antioxidative and anti-inflammatory properties of cannabidiol. *Antioxidants (Basel)* (2019) **9**:21. doi:10.3390/antiox9010021
5. Tripson M, Litwa K, Soderstrom K. Cannabidiol inhibits neuroinflammatory responses and circuit-associated synaptic loss following damage to a songbird vocal

Ethics statement

Ethical approval was not required for the studies on humans in accordance with the local legislation and institutional requirements because only commercially available established cell lines were used.

Funding

The author(s) declare that financial support was received for the research and/or publication of this article. This study was supported in full by the Food and Drug Administration's Perinatal Health Center of Excellence (PHCE) funding program administered by the National Center for Toxicological Research (Protocol ID: E0779301).

Acknowledgments

We would like to thank Dr. Jacqueline Yeary for her assistance in preparing the manuscript, Mr. Charles Matthew Fogle for his continuous technical support, and Drs. John Talpos, Jyotshnabala Kanungo, and Chengzhong Cai for their expert reviews on the manuscript.

Conflict of interest

The author(s) declared no potential conflicts of interest with respect to the research, authorship, and/or publication of this article.

Generative AI statement

The authors declare that no Generative AI was used in the creation of this manuscript.

pre-motor cortical-like region. *Sci Rep* (2023) **13**:7907. doi:10.1038/s41598-023-34924-z

6. Hurd YL, Spriggs S, Alishayev J, Winkel G, Gurgov K, Kudrich C, et al. Cannabidiol for the reduction of cue-induced craving and anxiety in drug-abstinent individuals with heroin use disorder: a double-blind randomized placebo-controlled trial. *Am J Psychiatry* (2019) **176**:911–22. doi:10.1176/appi.ajp.2019.18101191

7. Brennan M. 14% of Americans say they use CBD products (2019). Available online at: <https://news.gallup.com/poll/263147/americans-say-cbd-products.aspx2019>.

8. Berger K. The 2020 CBD survey. (2020).

9. Ewing LE, Skinner CM, Quick CM, Kennon-McGill S, McGill MR, Walker LA, et al. Hepatotoxicity of a cannabidiol-rich cannabis extract in the mouse model. *Molecules* (2019) **24**:1694. doi:10.3390/molecules24091694

10. Li J, Zagorski JW, Kaminski NE. Establishment of a point of departure for CBD hepatotoxicity employing human HepaRG spheroids. *Toxicology* (2023) **488**: 153469. doi:10.1016/j.tox.2023.153469
11. Watkins PB, Church RJ, Li J, Knappertz V. Cannabidiol and abnormal liver chemistries in healthy adults: results of a phase I clinical trial. *Clin Pharmacol & Ther* (2021) **109**:1224–31. doi:10.1002/cpt.2071
12. Ewing LE, McGill MR, Yee EU, Quick CM, Skinner CM, Kennon-McGill S, et al. Paradoxical patterns of sinusoidal obstruction syndrome-like liver injury in aged female CD-1 mice triggered by cannabidiol-rich cannabis extract and acetaminophen Co-administration. *Molecules* (2019) **24**:2256. doi:10.3390/molecules24122256
13. Balachandran P, Elshohly M, Hill KP. Cannabidiol interactions with medications, illicit Substances, and alcohol: a comprehensive review. *J Gen Intern Med* (2021) **36**:2074–84. doi:10.1007/s11606-020-06504-8
14. Wu HY, Chu RM, Wang CC, Lee CY, Lin SH, Jan TR. Cannabidiol-induced apoptosis in primary lymphocytes is associated with oxidative stress-dependent activation of caspase-8. *Toxicol Appl Pharmacol* (2008) **226**:260–70. doi:10.1016/j.taap.2007.09.012
15. Lee CY, Wey SP, Liao MH, Hsu WL, Wu HY, Jan TR. A comparative study on cannabidiol-induced apoptosis in murine thymocytes and EL-4 thymoma cells. *Int Immunopharmacology* (2008) **8**:732–40. doi:10.1016/j.intimp.2008.01.018
16. Carvalho RK, Santos ML, Souza MR, Rocha TL, Guimaraes FS, Anselmo-Franci JA, et al. Chronic exposure to cannabidiol induces reproductive toxicity in male Swiss mice. *J Appl Toxicol* (2018) **38**:1545. doi:10.1002/jat.3731
17. Carvalho RK, Andersen ML, Mazaro-Costa R. The effects of cannabidiol on male reproductive system: a literature review. *J Appl Toxicol* (2020) **40**:132–50. doi:10.1002/jat.3831
18. Taylor L, Gidal B, Blakey G, Tayo B, Morrison G. A phase I, randomized, double-blind, placebo-controlled, single ascending dose, multiple dose, and food effect trial of the safety, tolerability and pharmacokinetics of highly purified cannabidiol in healthy subjects. *CNS Drugs* (2018) **32**:1053–67. doi:10.1007/s40263-018-0578-5
19. Nasrin S, Coates S, Bardhi K, Watson C, Muscat JE, Lazarus P. Inhibition of nicotine metabolism by cannabidiol (CBD) and 7-hydroxycannabidiol (7-OH-CBD). *Chem Res Toxicol* (2023) **36**:177–87. doi:10.1021/acs.chemrestox.2c00259
20. Dong C, Chen J, Harrington A, Vinod KY, Hegde ML, Hegde VL. Cannabinoid exposure during pregnancy and its impact on immune function. *Cell Mol Life Sci* (2019) **76**:729–43. doi:10.1007/s00018-018-2955-0
21. Feinshtein V, Erez O, Ben-Zvi Z, Eshkoli T, Shezaf B, Sheiner E, et al. Cannabidiol enhances xenobiotic permeability through the human placental barrier by direct inhibition of breast cancer resistance protein: an *ex vivo* study. *Am J Obstet Gynecol* (2013) **209**:573.e1–573.e15. doi:10.1016/j.ajog.2013.08.005
22. Monfort A, Ferreira E, Leclair G, Lodygensky GA. Pharmacokinetics of cannabis and its derivatives in animals and humans during pregnancy and breastfeeding. *Front Pharmacol* (2022) **13**:919630. doi:10.3389/fphar.2022.919630
23. Kwan Cheung KA, Mitchell MD, Heussler HS. Cannabidiol and neurodevelopmental disorders in children. *Front Psychiatry* (2021) **12**:643442. doi:10.3389/fpsy.2021.643442
24. Lu HC, Mackie K. An introduction to the endogenous cannabinoid system. *Biological Psychiatry* (2016) **79**:516–25. doi:10.1016/j.biopsych.2015.07.028
25. Dias-de Freitas F, Pimenta S, Soares S, Gonzaga D, Vaz-Matos I, Prior C. The role of cannabinoids in neurodevelopmental disorders of children and adolescents. *Rev Neurol* (2022) **75**:189–97. doi:10.33588/rn.7507.2022123
26. Swenson KS, Gomez Wulschner LE, Hoelscher VM, Folts L, Korth KM, Oh WC, et al. Fetal cannabidiol (CBD) exposure alters thermal pain sensitivity, problem-solving, and prefrontal cortex excitability. *Mol Psychiatry* (2023) **28**: 3397–413. doi:10.1038/s41380-023-02130-y
27. Wanner NM, Colwell M, Drown C, Faulk C. Developmental cannabidiol exposure increases anxiety and modifies genome-wide brain DNA methylation in adult female mice. *Clin Epigenetics* (2021) **13**:4. doi:10.1186/s13148-020-00993-4
28. Iezzi D, Caceres-Rodriguez A, Chavis P, Manzoni OJJ. *In utero* exposure to cannabidiol disrupts select early-life behaviors in a sex-specific manner. *Transl Psychiatry* (2022) **12**:501. doi:10.1038/s41398-022-02271-8
29. Grant KS, Petroff R, Isoherranen N, Stella N, Burbacher TM. Cannabis use during pregnancy: pharmacokinetics and effects on child development. *Pharmacol & Ther* (2018) **182**:133–51. doi:10.1016/j.pharmthera.2017.08.014
30. Alpar A, Di Marzo V, Harkany T. At the tip of an iceberg: prenatal marijuana and its possible relation to neuropsychiatric outcome in the offspring. *Biological Psychiatry* (2016) **79**:e33–45. doi:10.1016/j.biopsych.2015.09.009
31. Liu F, Mahmood M, Xu Y, Watanabe F, Biris AS, Hansen DK, et al. Effects of silver nanoparticles on human and rat embryonic neural stem cells. *Front Neurosci* (2015) **9**:115. doi:10.3389/fnins.2015.00115
32. Liu F, Liu S, Patterson TA, Fogle C, Hanig JP, Wang C, et al. Protective effects of xenon on propofol-induced neurotoxicity in human neural stem cell-derived models. *Mol Neurobiol* (2020) **57**:200–7. doi:10.1007/s12035-019-01769-5
33. Wang C, Kaufmann JA, Sanchez-Ross MG, Johnson KM. Mechanisms of N-methyl-D-aspartate-induced apoptosis in phencyclidine-treated cultured forebrain neurons. *The J Pharmacol Exp Ther* (2000) **294**:287–95. doi:10.1016/s0022-3565(24)39068-8
34. Wang C, Sadovova N, Fu X, Schmued L, Scallet A, Hanig J, et al. The role of the N-methyl-D-aspartate receptor in ketamine-induced apoptosis in rat forebrain culture. *Neuroscience* (2005) **132**:967–77. doi:10.1016/j.neuroscience.2005.01.053
35. Latham LE, Dobrovolsky VN, Liu S, Talpos JC, Hanig JP, Slikker W, Jr, et al. Establishment of neural stem cells from fetal monkey brain for neurotoxicity testing. *Exp Biol Med* (Maywood) (2023) **248**:633–40. doi:10.1177/15353702231168145
36. di Giacomo V, Chiavaroli A, Recinella L, Orlando G, Cataldi A, Rapino M, et al. Antioxidant and neuroprotective effects induced by cannabidiol and cannabigerol in rat CTX-TNA2 astrocytes and isolated cortices. *Int J Mol Sci* (2020) **21**:3575. doi:10.3390/ijms21103575
37. Raja A, Ahmadi S, de Costa F, Li N, Kerman K. Attenuation of oxidative stress by cannabinoids and cannabis extracts in differentiated neuronal cells. *Pharmaceuticals* (Basel) (2020) **13**:328. doi:10.3390/ph13110328
38. Wolff V, Schlagowski AI, Rouyer O, Charles AL, Singh F, Auger C, et al. Tetrahydrocannabinol induces brain mitochondrial respiratory chain dysfunction and increases oxidative stress: a potential mechanism involved in cannabis-related stroke. *Biomed Res Int* (2015) **2015**:1–7. doi:10.1155/2015/323706
39. Natale BV, Gustin KN, Lee K, Holloway AC, Laviolette SR, Natale DRC, et al. Δ^9 -tetrahydrocannabinol exposure during rat pregnancy leads to symmetrical fetal growth restriction and labyrinth-specific vascular defects in the placenta. *Sci Rep* (2020) **10**:544. doi:10.1038/s41598-019-57318-6
40. Bonaccorso S, Ricciardi A, Zangani C, Chiappini S, Schifano F. Cannabidiol (CBD) use in psychiatric disorders: a systematic review. *Neurotoxicology* (2019) **74**: 282–98. doi:10.1016/j.neuro.2019.08.002
41. Hampson AJ, Grimaldi M, Axelrod J, Wink D. Cannabidiol and $(-)\Delta^9$ -tetrahydrocannabinol are neuroprotective antioxidants. *Proc Natl Acad Sci U S A* (1998) **95**:8268–73. doi:10.1073/pnas.95.14.8268
42. Huestis MA, Solimini R, Pichini S, Pacifici R, Carlier J, Busardo FP. Cannabidiol adverse effects and toxicity. *Curr Neuropharmacology* (2019) **17**: 974–89. doi:10.2174/1570159x17666190603171901
43. Madeo G, Kapoor A, Giorgetti R, Busardo FP, Carlier J. Update on cannabidiol clinical toxicity and adverse effects: a systematic review. *Curr Neuropharmacology* (2023) **21**:2323–42. doi:10.2174/1570159x21666230322143401
44. Whalley BJ, Lin H, Bell L, Hill T, Patel A, Gray RA, et al. Species-specific susceptibility to cannabis-induced convulsions. *Br J Pharmacol* (2019) **176**: 1506–23. doi:10.1111/bph.14165
45. Henderson RG, Welsh BT, Rogers JM, Borghoff SJ, Trexler KR, Bonn-Miller MO, et al. Reproductive and developmental toxicity evaluation of cannabidiol. *Food Chem Toxicol* (2023) **176**:113786. doi:10.1016/j.fct.2023.113786
46. Deabold KA, Schwark WS, Wolf L, Wakshlag JJ. Single-dose pharmacokinetics and preliminary safety assessment with use of CBD-rich hemp nutraceutical in healthy dogs and cats. *Animals* (Basel) (2019) **9**:832. doi:10.3390/ani9100832
47. Wakshlag JJ, Schwark WS, Deabold KA, Talsma BN, Cital S, Lyubimov A, et al. Pharmacokinetics of cannabidiol, cannabidiolic acid, δ^9 -tetrahydrocannabinol, tetrahydrocannabinolic acid and related metabolites in canine serum after dosing with three oral forms of hemp extract. *Front Vet Sci* (2020) **7**:505. doi:10.3389/fvets.2020.00505
48. Harvey DJ, Samara E, Mechoulam R. Comparative metabolism of cannabidiol in dog, rat and man. *Pharmacol Biochem Behav* (1991) **40**:523–32. doi:10.1016/0091-3057(91)90358-9
49. Schwotzer D, Kulpa J, Trexler K, Dye W, Jantzi J, Irshad H, et al. Pharmacokinetics of cannabidiol in sprague-dawley rats after oral and pulmonary administration. *Cannabis Cannabinoid Res* (2023) **8**:360–73. doi:10.1089/can.2022.0121
50. Dearborn JT, Nelvagal HR, Rensing NR, Takahashi K, Hughes SM, Wishart TM, et al. Effects of chronic cannabidiol in a mouse model of naturally occurring neuroinflammation, neurodegeneration, and spontaneous seizures. *Sci Rep* (2022) **12**:11286. doi:10.1038/s41598-022-15134-5
51. McGilveray IJ. Pharmacokinetics of cannabinoids. *Pain Res & Manag* (2005) **10** Suppl A(Suppl. A):15A–22A–22A. doi:10.1155/2005/242516
52. Oh DA, Parikh N, Khurana V, Cognata Smith C, Vetticaden S. Effect of food on the pharmacokinetics of dronabinol oral solution versus dronabinol capsules in

healthy volunteers. *Clin Pharmacol Adv Appl* (2017) **9**:9–17. doi:10.2147/cpaa.s119676

53. Perez-Acevedo AP, Busardo FP, Pacifici R, Mannocchi G, Gottardi M, Poyatos L, et al. Disposition of cannabidiol metabolites in serum and urine from healthy individuals treated with pharmaceutical preparations of medical cannabis. *Pharmaceuticals (Basel)* (2020) **13**:459. doi:10.3390/ph13120459

54. Mendez-Armenta M, Nava-Ruiz C, Juarez-Rebollar D, Rodriguez-Martinez E, Yescas Gómez P. Oxidative stress associated with neuronal apoptosis in experimental models of epilepsy. *Oxidative Med Cell Longevity* (2014) **2014**:1–12. doi:10.1155/2014/293689

55. Plascencia-Villa G, Perry G. Roles of oxidative stress in synaptic dysfunction and neuronal cell death in alzheimer's disease. *Antioxidants (Basel)* (2023) **12**:1628. doi:10.3390/antiox12081628

56. Jeong EM, Yoon JH, Lim J, Shin JW, Cho AY, Heo J, et al. Real-time monitoring of Glutathione in living cells reveals that high Glutathione levels are required to maintain stem cell function. *Stem Cell Rep* (2018) **10**:600–14. doi:10.1016/j.stemcr.2017.12.007

57. El-Remessy AB, Khalil IE, Matragoon S, Abou-Mohamed G, Tsai NJ, Roon P, et al. Neuroprotective effect of (-)-Delta9-tetrahydrocannabinol and cannabidiol in N-methyl-D-aspartate-induced retinal neurotoxicity: involvement of peroxynitrite. *The Am J Pathol* (2003) **163**:1997–2008. doi:10.1016/s0002-9440(10)63558-4

58. Esposito G, Scuderi C, Valenza M, Togna GI, Latina V, De Filippis D, et al. Cannabidiol reduces $\alpha\beta$ -induced neuroinflammation and promotes hippocampal neurogenesis through PPAR γ involvement. *PLoS One* (2011) **6**:e28668. doi:10.1371/journal.pone.0028668

59. Pagano C, Savarese B, Coppola L, Navarra G, Avilia G, Laezza C, et al. Cannabinoids in the modulation of oxidative signaling. *Int J Mol Sci* (2023) **24**:2513. doi:10.3390/ijms24032513

60. Suarez I, Bodega G, Ramos JA, Fernandez-Ruiz JJ, Fernandez B. Neuronal and astroglial response to pre- and perinatal exposure to delta-9-tetrahydrocannabinol in the rat substantia nigra. *Dev Neurosci* (2000) **22**:253–63. doi:10.1159/000017449

61. Landucci E, Mazzantini C, Lana D, Giovannini MG, Pellegrini-Giampietro DE. Neuronal and astrocytic morphological alterations driven by prolonged exposure with δ 9-tetrahydrocannabinol but not cannabidiol. *Toxics* (2022) **10**:48. doi:10.3390/toxics10020048

62. Krassnitzer M, Boisvert B, Beiersdorf J, Harkany T, Keimpema E. Resident astrocytes can limit injury to developing hippocampal neurons upon THC exposure. *Neurochem Res* (2023) **48**:1242–53. doi:10.1007/s11064-022-03836-1

63. Suarez I, Bodega G, Fernandez-Ruiz JJ, Ramos JA, Rubio M, Fernandez B. Reduced glial fibrillary acidic protein and glutamine synthetase expression in astrocytes and bergmann glial cells in the rat cerebellum caused by δ 9-tetrahydrocannabinol administration during development. *Dev Neurosci* (2002) **24**:300–12. doi:10.1159/000066744

64. Ramos-Jimenez C, Petkau S, Mizrahi R. A systematic review of delta-9-tetrahydrocannabinol (Δ 9-THC) in astrocytic markers. *Cells* (2024) **13**:1628. doi:10.3390/cells13191628

65. Sheng WS, Hu S, Min X, Cabral GA, Lokensgard JR, Peterson PK. Synthetic cannabinoid WIN55,212-2 inhibits generation of inflammatory mediators by IL-1 β -stimulated human astrocytes. *Glia* (2005) **49**:211–9. doi:10.1002/glia.20108

66. Stella N. Cannabinoid and cannabinoid-like receptors in microglia, astrocytes, and astrocytomas. *Glia* (2010) **58**:1017–30. doi:10.1002/glia.20983

67. De Simone U, Pignatti P, Villani L, Russo LA, Sargenti A, Bonetti S, et al. Human astrocyte spheroids as suitable *in vitro* screening model to evaluate synthetic cannabinoid mam2201-induced effects on CNS. *Int J Mol Sci* (2023) **24**:1421. doi:10.3390/ijms24021421

68. Garcia MC, Cinquina V, Palomo-Garo C, Rabano A, Fernandez-Ruiz J. Identification of CB(2) receptors in human nigral neurons that degenerate in Parkinson's disease. *Neurosci Lett* (2015) **587**:1–4. doi:10.1016/j.neulet.2014.12.003

69. Stempel A, Stumpf A, Zhang HY, Özdoğan T, Pannasch U, Theis AK, et al. Cannabinoid type 2 receptors mediate a cell type-specific plasticity in the Hippocampus. *Neuron* (2016) **90**:795–809. doi:10.1016/j.neuron.2016.03.034

70. Zurolo E, Iyer AM, Spliet WG, Van Rijen PC, Troost D, Gorter JA, et al. CB1 and CB2 cannabinoid receptor expression during development and in epileptogenic developmental pathologies. *Neuroscience* (2010) **170**:28–41. doi:10.1016/j.neuroscience.2010.07.004

71. Shapiro L, Wong JC, Escayg A. Reduced cannabinoid 2 receptor activity increases susceptibility to induced seizures in mice. *Epilepsia* (2019) **60**:2359–69. doi:10.1111/epi.16388

72. Komorowska-Muller JA, Ravichandran KA, Zimmer A, Schurmann B. Cannabinoid receptor 2 deletion influences social memory and synaptic architecture in the hippocampus. *Sci Rep* (2021) **11**:16828. doi:10.1038/s41598-021-96285-9



OPEN ACCESS

*CORRESPONDENCE

Nemanja Useinovic,
✉ 94nemanjau@gmail.com

RECEIVED 25 February 2025

ACCEPTED 22 April 2025

PUBLISHED 16 May 2025

CITATION

Useinovic N, Newson A, Near M, Maksimovic S, Volvovitz B, Quillinan N and Jevtovic-Todorovic V (2025) Anesthesia-induced developmental neurotoxicity in the setting of systemic inflammation: the role of microglia. *Exp. Biol. Med.* 250:10549. doi: 10.3389/ebm.2025.10549

COPYRIGHT

© 2025 Useinovic, Newson, Near, Maksimovic, Volvovitz, Quillinan and Jevtovic-Todorovic. This is an open-access article distributed under the terms of the [Creative Commons Attribution License \(CC BY\)](#). The use, distribution or reproduction in other forums is permitted, provided the original author(s) and the copyright owner(s) are credited and that the original publication in this journal is cited, in accordance with accepted academic practice. No use, distribution or reproduction is permitted which does not comply with these terms.

Anesthesia-induced developmental neurotoxicity in the setting of systemic inflammation: the role of microglia

Nemanja Useinovic^{1*}, Adre Newson¹, Michelle Near¹, Stefan Maksimovic¹, Benjamin Volvovitz¹, Nidia Quillinan^{1,2} and Vesna Jevtovic-Todorovic¹

¹Department of Anesthesiology, University of Colorado Anschutz Medical Campus, Aurora, CO, United States, ²Neuronal Injury and Plasticity Program, University of Colorado Anschutz Medical Campus, Aurora, CO, United States

Abstract

Although it is well documented in animal research that an early exposure to general anesthetics during critical stages of synaptogenesis disturbs normal brain development ultimately leading to cognitive and affective impairments, it is less clear whether and how surgical interventions and/or underlying systemic inflammation impact the detrimental effects of general anesthetics. Some emerging evidence suggests that aseptic systemic inflammation preceding exposure to the commonly used general anesthetics worsens anesthesia-induced neuroapoptosis and activates inflammasome pathways while resulting in impaired cognitive-affective behaviors. To improve our understanding of the underlying mechanisms, here we focused on multicellular interactions between damaged neurons and microglia since microglia is the resident macrophages within the brain that respond to stress. Using infant rats (post-natal day 7) and most commonly used inhaled anesthetic, sevoflurane, we examine microglia role in sevoflurane-induced inflammation-propagated developmental neurotoxicity. We show that sevoflurane exposure leads to a significant neuroapoptosis in young rat pup hippocampal subiculum, a neuroapoptosis that is worsened in the setting of systemic inflammation caused by either lipopolysaccharide (LPS) injection or trauma (tibial fracture). The worsening is not only shown in terms of the intensity of neuroapoptosis but in its duration and onset. We further report that sevoflurane-induced neuroapoptosis triggers activation of microglia, which in turn releases proinflammatory cytokine MCP-1 and upregulates endothelial cell adhesion molecule, ICAM-1. This leads to T-lymphocyte infiltration in the hippocampal subiculum, an event that further perpetuates microglia activation in an attempt to control neuroapoptosis which is suggested by the fact that microglia depletion leads to a significant worsening of sevoflurane-induced developmental neuroapoptosis. Our work gets us a step closer to making our animal work more relevant to the clinical setting

and hence more translational. This is vitally important considering that exposure to anesthesia is exceedingly rare in the absence of any kind of a pathological process.

KEYWORDS

tibial fracture, neonatal rats, sevoflurane, lipopolysaccharide, microglia, neuroinflammation, developmental neurotoxicity

Impact statement

Over four million children are exposed to general anesthesia annually in the US alone. The work over the past couple of decades suggests that anesthesia exposure of a developing young brain may result in neuroapoptosis and long-lasting impairments of socio-cognitive development. Since exposure seldom occurs in the absence of an underlying disease and/or inflammation, the question remains whether and how this may affect anesthesia-induced developmental neurotoxicity. Our work and the work of others would suggest that disease-associated inflammation worsens neurotoxicity. Understanding the underlying mechanisms is crucially important in the field of clinical anesthesiology and fundamental science alike. We believe that our investigation of the role of microglia and their interplay with T-lymphocyte in the setting of sevoflurane-induced inflammation-propagated neuronal damage gets us a step closer to better understanding this phenomenon, hence allowing us to develop promising strategies for the use of general anesthesia in a true disease setting.

Introduction

Based on numerous preclinical and emerging clinical findings over the past couple of decades, it is becoming apparent that an early exposure to general anesthetics (GAs) during critical stages of synaptogenesis disturbs normal brain development ultimately leading to cognitive and affective impairments [1–9]. Preclinical studies thus far have aimed to understand this worrisome phenomenon by performing studies with GAs largely in isolation from underlying disease processes that necessitate GA exposure in the first place. While this strategy had been extremely valuable in mechanistic analyses of GA-induced neurotoxicity, it has been repeatedly criticized. This is understandable since there is a significant gap in our understanding as to whether and how surgical interventions and/or underlying systemic inflammation impact the detrimental effects of GAs, especially considering that general anesthesia without an underlying illness or trauma is rare. In fact, systemic inflammation is prevalent in many disease processes and, importantly, surgical interventions themselves can initiate aseptic inflammatory responses [10, 11].

The work presented herein builds on our recently published observations that aseptic systemic inflammation preceding

exposure to the commonly used inhaled GA sevoflurane, worsens sevoflurane-induced neuroapoptosis and activates inflammasome pathways while resulting in impaired cognitive-affective behaviors [12]. Here we focus on multicellular interactions between damaged neurons and microglia since microglia is the resident macrophages within the brain that respond to stress, typically triggering a pro-inflammatory state [13–16]. Hence, we set out to examine their role in several aspects of sevoflurane-induced inflammation-propagated developmental neurotoxicity. Our interest in the interactions between neurons and microglia is based on the fact that brain is considered an immune privileged organ lacking circulating immune cells [17, 18].

In the context of neuronal injury, damage associated molecular patterns (DAMPs) released by dying neurons trigger pro-inflammatory microglial activation and release of cytokines, in particular monocyte chemoattractant protein-1 (MCP-1) among others [19–22]. Since we have previously reported an increase in sevoflurane-induced neuroapoptosis in the setting of systemic inflammation [12], the question we asked here was whether infiltrating immune cells contribute to ongoing inflammatory processes and hence, whether they play a detrimental role in herein presented ongoing and enhanced neuronal destruction long after the offending agents (sevoflurane and biochemical products of inflammation) are no longer present. Furthermore, we also examine the expression of intercellular adhesion molecule-1 (ICAM-1) that enables peripheral immune cells to enter the brain [23] and assess the role of immune cell brain infiltration.

We introduce two disease-type systemic inflammatory states in neonatal rodents at peak of their brain development (post-natal day 7): lipopolysaccharide (LPS) injection and a novel neonatal tibial fracture model of trauma, each initiated prior to sevoflurane exposure thus enabling us to focus on the role of preemptive systemic inflammation.

In this study we first confirm that systemic inflammation enhances sevoflurane-induced neuroapoptosis and report that this is accompanied by heightened activation of microglia, upregulation of cytokine, MCP-1 which is known to upregulate cell adhesion molecules that allow peripheral immune cells to enter the brain [21, 24] and increased expression of ICAM-1, a cell adhesion molecule and transmembrane glycoprotein that could be induced by upregulated MCP-1. We also report a role of microglia in subsequent T-lymphocyte infiltration in subiculum

of sevoflurane-exposed animals in the setting of systemic inflammation.

Materials and methods

Ethical statement

All experimental procedures were approved by the Institutional Animal Care and Use Committee of the University of Colorado Anschutz Medical Campus and adhered to the NIH Guide for the Care and Use of Laboratory animals. All efforts were made to minimize the number of animals used and procedures were performed in full compliance with Public Health Service's Policy on Humane Care and Use of Laboratory Animals.

Animals

Sprague-Dawley dams were purchased with PND 4-5 pups of equal gender (Envigo, Indianapolis, IN, United States), and housed under a 14/10 light-dark cycle with *ad libitum* access to food and water until pups were appropriate age for experiments. Upon arrival, animals were allowed a minimum of 36 h acclimation period prior to use.

Tibial fracture

PND6 rat pups were anesthetized with 3% sevoflurane. Animals were transferred to surgical station pre-heated to 37°C, and anesthesia was maintained with 2-3% sevoflurane administered via a nose cone. Animals were positioned supine, and the entire body was covered with sterile drapes except the right lower extremity. Skin was disinfected with iodine and alcohol swabs hip to ankle.

Under sterile conditions, the knee of the lower right extremity was flexed to expose the tibial plateau and patellar ligament. Stainless steel 0.38 mm inner rod of 22-gauge Quincke style spinal needle (McKesson, Irving, TX, United States) was advanced through the tibial medullary canal from the superomedial aspect of the tibial plateau to 1 cm above the ankle joint. The trajectory of the needle was parallel to the tibial shaft, 1-2 mm medial to the patellar ligament projection.

Upon secure placement, the proximal end of the needle was clipped off at the entry point using wire cutters. A small skin incision was made on the medial surface of the tibia midway along the shaft to expose the underlying bone. Transverse fracture was produced using sterilized straight Bonn scissors (Fine Science Tools, Foster City, CA, United States). Fracture point was confirmed, and stability

verified with gentle manual manipulation of proximal and distal fragments. External pressure was applied to achieve hemostasis, and skin was reapproximated and sealed with veterinarian glue. Neosporin ointment was applied to spinal needle entry point as well as the skin incision site. Animal was disconnected from the anesthesia and placed on a heated blanket until they regained consciousness and were able to remain sternal. Animal was subsequently returned to the home cage and reunion with the dam closely observed over 30 min for signs of distress such as hypomobility, nursing difficulties, symptoms of agitation and unusual vocalization.

Sham surgery counterparts, randomly selected within the same litters, were similarly induced with 3% sevoflurane and transferred to the surgical station. Animals were kept under anesthesia for a duration of time equivalent to the average procedure time of the surgery animals within the litter. During this time, small incision was made mid-tibia medially, and soft tissues were gently manipulated with sterile tools to emulate injury of surrounding soft tissue. Neither intramedullary fixation nor sharp tibial fracture were performed. Skin incision was closed with veterinary glue, and animals were returned to the home cage and observed as described for fracture procedure.

LPS treatment

Lipopolysaccharide (LPS) model of systemic inflammation was induced as previously described [12]. Briefly, LPS (*E. coli*, O55:B5) was purchased from Sigma Aldrich (St. Louis, MO, United States) and dissolved in 1x phosphate buffered saline (PBS). On PND6, animals were randomly assigned to receive 1 mg/kg LPS intraperitoneally (i.p.) or PBS vehicle.

Microglial manipulations

Minocycline hydrochloride was purchased from Sigma Aldrich (St. Louis, MO, United States). PLX-5622 was purchased from Cayman Chemical (Ann Arbor, MI, United States). Immediately prior to injection, minocycline was dissolved in warm PBS, whereas PLX-5622 was dissolved in 10% dimethyl sulfoxide (DMSO) and 25% β -cyclodextrin (Santa Cruz Biotechnology, Santa Cruz, CA, United States).

To inhibit microglial activation, animals were randomly administered two i.p. doses of minocycline 40 mg/kg, based on the published literature [25, 26], or PBS vehicle. The first loading dose was administered 1 h prior to LPS, and second given 12 h later, 1 h before anesthesia exposure. To deplete microglia from the developing brain, 65 mg/kg PLX-5622 or DMSO-cyclodextrin vehicle were administered i.p. in 3 doses 24 h apart on PND4, 5 and 6, as determined by our pilot study.

Anesthesia exposure

Twelve hours after the tibial fracture or LPS injection, animals now at PND7 were exposed to 3% sevoflurane administered in 30% oxygen carrier gas or 30% oxygen carrier gas only for 3 hours, as described in our previous study [12]. In addition to being relevant in dose and duration [27, 28], this anesthesia regimen proved to be reliable and reproducible method in our previous study of inducing neuroapoptosis in PND7 rat pups [12]. Ambient temperature of 35.5°C and gas concentrations (oxygen, CO₂ and sevoflurane) were continuously monitored in real time for the duration of the exposure (Datex Ohmeda Capnomac Ultima, Helsinki, Finland). Heart rate, blood glucose and oxygen measurements were obtained at the end of the 3 h exposure period in a subset of animals. Left ventricular blood sample was transcardially obtained for arterial blood gas analyses (i-STAT 1 Analyzer, Abbott Laboratories, Abbott Park, IL, United States) in a dedicated cohort, and given the terminal nature of the procedure, these animals were not used for further data analysis.

Tissue collection

Euthanasia and tissue collection were performed at predetermined timepoints (1 h, 2 h, and 8 h) following sevoflurane exposure. For histological evaluation, animals were deeply anesthetized with isoflurane and transcardially perfused with ice-cold PBS followed by 4% paraformaldehyde (PFA). Brains were extracted and placed in 4% PFA overnight for post-fixation, then transferred to PBS + 0.025% sodium-azide and stored at 4°C.

For gene expression assays, animals were deeply anesthetized with isoflurane and brains rapidly extracted on ice. Left and right hippocampi were combined and flash-frozen in liquid nitrogen, then stored at -80°C prior to further processing.

Neuroapoptosis quantification

Activated caspase-3 staining was performed as previously described [12]. Briefly, vibratome-cut sections were mounted on a slide, washed, quenched by submersion in Bloxall (Vector Labs, Newark, CA, United States) for 10 min and then blocked with 5% normal goat serum for 1 h at room temperature prior to staining. Stained serial 50 µm thick coronal brain slices (n = 4 subicula per animal) corresponding to -5.80 and -6.04 mm from bregma [29] were examined under Nikon Eclipse E800 microscope (Nikon Instruments, Melville, NY, United States). Images were obtained using a Nikon DS-Fi3 camera under a ×10 objective. Stained profiles were manually counted using a 500 µm² grid placed over the regions of

interest by an investigator blinded to treatment condition and multiplied by 2 to obtain the number of positive immunoprofiles per mm², using NIS-Elements BR-5.11.02 software (Tokyo, Japan).

Immunofluorescence staining and analysis

For microglial visualization, free floating sections (n = 4 subicula per animal) were washed three times in PBS+0.1% Triton X-100. Slices were blocked in 5% normal donkey serum (NDS) (Sigma Aldrich, St. Louis, MO, United States) for 1 h at room temperature, then incubated overnight at 4°C with goat anti-rat Iba1 primary antibody (1:500; Abcam, Cambridge, UK, ab5076). The following day, slices were washed three times with PBS+0.1% Triton X-100, then incubated with Alexa Fluor 488 donkey anti-goat secondary antibody (1:500, Jackson ImmunoResearch, West Grove, PA, United States, 705-545-003) for 2 h at room temperature protected from light. Slices were then washed three times, mounted, coverslipped and kept at 4°C until imaging.

High resolution confocal images were obtained under ×10 objective on Olympus FV-1200 confocal laser scanning microscope (Olympus Corporation, Tokyo, Japan). An investigator blinded to treatment conditions performed qualitative analysis of microglial morphology. Microglia were deemed inactive if they exhibited small somas and long branching processes, whereas activated state was identified by substantial soma enlargement and retraction of processes. Percent activation was calculated as a proportion of activated to the total number of microglia in the rat subicula per visual field, multiplied by 100 and averaged across all slices per individual animal.

RNA extraction and quantitative polymerase chain reaction

Whole left and right hippocampus of each animal were combined, and total RNA isolated using RNeasy mini kit (Qiagen, Germany) according to the manufacturer's instructions. 1,000 ng of RNA was used for cDNA synthesis (iScript Advance cDNA kit, Bio-rad, CA, United States). Quantitative real-time PCR was performed on a CFX Connect Real time system (Bio-rad, CA, United States) using SsoAdvanced Universal Probe Supermix (Bio-rad, CA, United States) and TaqMan gene expression assay probes for MCP-1 and ICAM-1 (Thermo Fisher Scientific, Waltham, MA, United States). Each sample was done in triplicate and normalized to the levels of GAPDH as a housekeeping gene. Results were expressed as fold changes compared to controls, which were assigned value of 1.

TABLE 1 Blood glucose concentration, hemoglobin saturation and heart rate in each animal group.

	Control (n = 6) PBS injection 30% oxygen for 3 h	LPS (n = 6) 1 mg/kg LPS 30% oxygen for 3 h	Sevo (n = 6) PBS injection 3% sevo for 3 h	LPS + Sevo (n = 5) 1 mg/kg LPS 3% sevo for 3 h
Glucose (mg/dL)	98.17 ± 32.88	64.83 ± 14.22	115.3 ± 7.257	77.00 ± 36.38
SpO ₂ (%)	98.83 ± 0.4082	97.50 ± 1.975	95.00 ± 2.828	93.60 ± 2.608
Heart rate (per min)	343.5 ± 44.93	312.2 ± 15.35	217.5 ± 57.36 (***)	221.0 ± 34.27 (***)

Statistically significant differences in means are indicated in bold letters. PBS, phosphate buffered saline; LPS, lipopolysaccharide; SpO₂, saturation of peripheral blood oxygen. ***p < 0.001.

TABLE 2 Arterial blood chemistry in each animal group.

	Control (n = 8) PBS injection 30% oxygen for 3 h	LPS (n = 9) 1 mg/kg LPS 30% oxygen for 3 h	Sevo (n = 8) PBS injection 3% sevo for 3 h	LPS + Sevo (n = 10) 1 mg/kg LPS 3% sevo for 3 h
pH	7.33 ± 0.05	7.32 ± 0.05	7.30 ± 0.06	7.30 ± 0.11
SpO ₂ (%)	95.50 ± 2.13	97.00 ± 0.76	93.22 ± 2.33	93.90 ± 3.57
paO ₂ (mmHg)	88.13 ± 9.77	98.50 ± 10.23	77.89 ± 5.64	81.90 ± 8.99
pCO ₂ (mmHg)	57.56 ± 6.72	47.68 ± 6.82	64.50 ± 8.88	49.50 ± 12.96

PBS, phosphate buffered saline; pH, potential of hydrogen; paO₂, partial pressure of arterial oxygen; paCO₂, partial pressure of arterial carbon dioxide; SpO₂, saturation of peripheral oxygen.

Flow cytometry

Two hours after exposure, freshly harvested hippocampi were finely minced and incubated in calcium- and magnesium-free Hanks Buffered Salt Solution (HBSS) with addition of collagenase/dispase digestive enzymes (Sigma Aldrich, St. Louis, MO, United States) for 30 min at 37°C. Digested sample was diluted with excess HBSS, passed through 100 µm cell strainer, and pelleted in refrigerated centrifuge at 500 × g for 7 min. Pellet was resuspended in 70/30 Cytiva Percoll gradient centrifugation media (Thermo Fischer Scientific, Waltham, MA, United States) and centrifuged at 800 × g for 30 min with deceleration brakes disengaged. Interphase layer was collected, resuspended in HBSS and centrifuged at 500 × g for 7 min to wash away the Percoll. Single cell suspension was obtained by resuspending the pellet in 250 µL flow cytometry buffer.

All antibodies and dyes were purchased from BioLegend (San Diego, CA, United States). Staining steps were performed at 4°C. Cells and appropriate single-stain and fluorescence-minus-one (FMO) controls were blocked with anti-CD16/32 antibody (1:100) for 5 min, then incubated for 30 min with mastermix staining solution containing following antibody-fluorochrome products: ZombieYellow viability dye (1:1800), CD45-Pacific Blue (1:400), CD3-APC (1:100), B220-PE (1:200). Cells were then washed, resuspended in flow cytometry buffer and analyzed immediately on Gallios 561 flow cytometer (Beckmann Coulter, Brea, CA, United States). Briefly, single cells were identified using

scatter features, live cells identified with viability dye, and CD45⁺ cells were gated then further separated into T-lymphocyte and B-lymphocyte populations.

Statistical analysis

Statistical analysis was performed in GraphPad Prism 9.3. Differences between groups were assessed by the ANOVA followed by Tukey's or Sidak's *post hoc* test for one-way or two-way analyses, respectively. α was set at 0.05, thus *p*-values < 0.05 were considered statistically significant. Data were graphed as mean ± SEM, and level of significance indicated by elbow connectors with asterisks. For each dataset, males and females were separated and compared within each treatment group to establish the effect of sex differences. Analysis was performed using Two-way ANOVA and Sidak's *post hoc*. Since we found no sex differences, the final set of data combined both sexes in each treatment group.

Results

Based on our previous published work, it has been suggested that systemic inflammation results in worsening of sevoflurane-induced neuroapoptosis and upregulation of cytokines responsible for inflammasome activation [12]. Here we set out to further explore the severity of anesthesia-induced

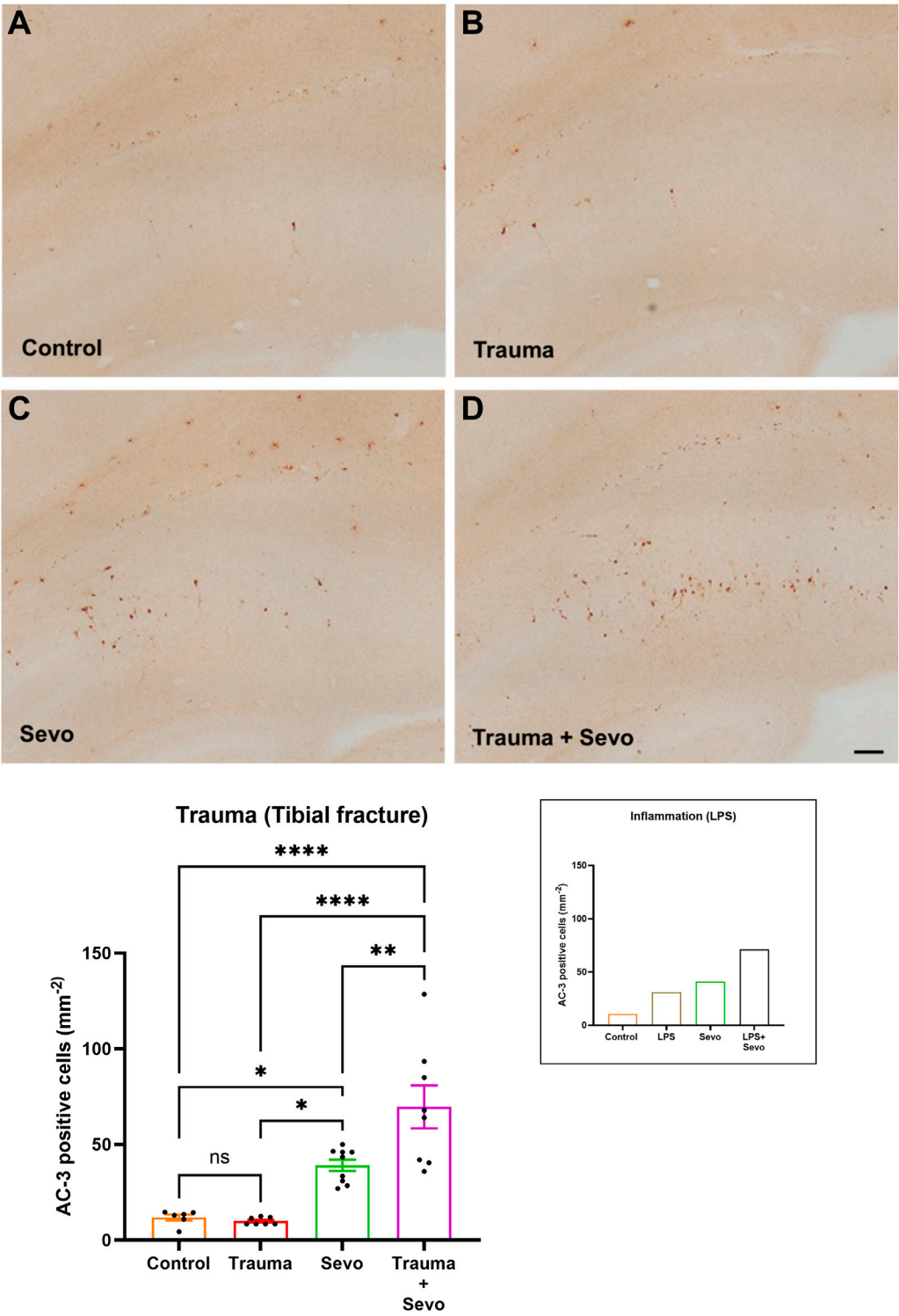


FIGURE 1
Preceding tibial fracture worsens sevoflurane-induced neuroapoptosis in the hippocampal subiculum of PND7 rat pups. Histomorphological analyses of neuronal apoptosis in the hippocampal subiculum are shown in the representative images of activated caspase-3 (AC-3⁺) staining in the hippocampal subiculum in control (A), trauma (B), sevoflurane (C) and trauma + sevoflurane (D) groups. The number of AC-3⁺ cells was increased in trauma + sevoflurane group compared with controls. x10 magnification, scale bar is 100 μ m. Bar graphs show the quantification analysis of AC-3⁺ cells. (Continued)

FIGURE 1 (Continued)

3⁺ positive cells per square millimeter in the hippocampal subiculum. Although trauma alone was indistinguishable from the control group, 3 hours of sevoflurane exposure significantly increased AC-3⁺ cells compared with the control or trauma group. However, sevoflurane exposure in the setting of trauma (trauma + sevo group) the number of AC-3⁺ cells were greater compared with either treatment alone. Because there were no gender differences in AC-3⁺ cells densities, the results from both sexes were combined. For the ease of side-by-side comparisons, we include shadow bar graph in the upper right corner that shows previously published effects of lipopolysaccharide (LPS) on sevo-(sevoflurane) induced developmental neuroapoptosis. [12]. One-way ANOVA with Tukey's *post hoc*. ns - non-significant, **p* < 0.05, ***p* < 0.01, *****p* < 0.0001.

developmental neurotoxicity in the disease setting where we focus on a couple of timepoints of neuroapoptosis post-sevoflurane exposure as well as the role of microglia and cell adhesion molecules which allow for infiltration of circulating immune cells into the brain [21, 23, 24].

To continue to examine GA-induced inflammation-propagated developmental neurotoxicity we used two disease models: 1) systemic LPS injection and 2) trauma (tibia fracture as described in the Methods). The neurotoxicity was examined using activated caspase-3 (AC3⁺) staining as a reliable marker of neuroapoptosis. Our focus was on hippocampal subiculum for two main reasons: hippocampal subiculum is exquisitely sensitive to anesthesia-induced neurotoxicity [6, 30] and, as an extension of CA1 hippocampus, it plays an important role in socio-emotional development found to be impaired after an early exposure to anesthesia [2, 3, 31–34].

To assess the stability of relevant biological variables we carefully monitored and continuously recorded sevoflurane concentration, ambient temperature, oxygen delivery and CO₂ concentration in anesthesia chamber to confirm the setting as stipulated in the Methods section. In addition, vital signs such as heart rate and oxygen saturation (using non-invasive pulse oximetry - SpO₂) and blood glucose level were assessed in each animal group (control, LPS alone, sevoflurane alone and LPS + sevo). As shown in Table 1 we found no major changes in blood glucose concentration and SpO₂ between groups when recorded at the end of sevoflurane exposure with an expected decrease in heart rate [35] in sevo and LPS + sevo groups. In addition, we studied arterial blood chemistry in a subset of animals within each cohort (sample sizes are included in Table 2). When collected and analyzed at the end of a 3-h sevoflurane exposure we confirmed that arterial blood chemistry, which reliably captures disturbances in tissue perfusion and oxygenation, was comparable to controls in each of the three experimental groups (Table 2).

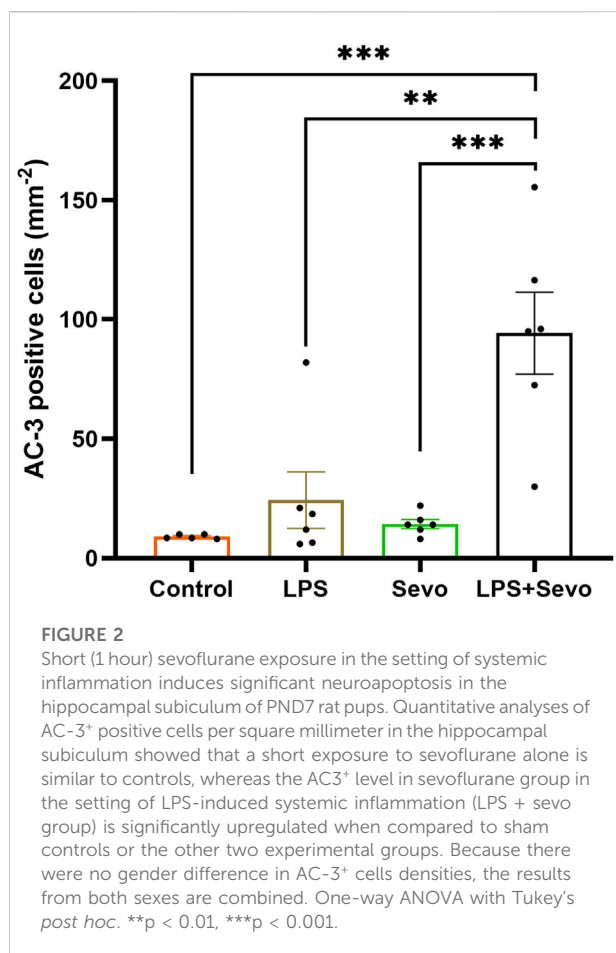
We then proceeded to perform histomorphological analysis of developmental neuroapoptosis in each animal group (Figure 1A–D). As shown in Figure 1 we found that both LPS-induced systemic inflammation (previously reported [12] and shown here as a shadow graph in right upper corner) and trauma cause significant increase in activated caspase-3 positive cells (AC3⁺) in the developing subiculum of the animals exposed to sevoflurane for 3 hours compared to either sevoflurane alone or LPS/trauma alone. Interestingly, unlike LPS, trauma alone did

not result in upregulated AC3⁺ cells when compared to sham controls. However, preemptive systemic inflammation caused by either LPS or trauma (*p* < 0.01) worsens developmental neuroapoptosis in young hippocampal subiculum of the animals exposed to sevoflurane at the peak of their synaptogenesis (PND7) compared to sevoflurane alone group.

To assess the severity of GA-induced inflammation-propagated developmental neurotoxicity we set out to further examine the importance of inflammatory priming. Hence, we shortened the exposure to sevoflurane from 3 h (as shown in Figure 1) to only 1 h (Figure 2). We noted that although such short exposure has no bearing on AC3⁺ levels in sevoflurane alone groups when compared to controls, the AC3⁺ levels in sevoflurane group in the setting of LPS-induced systemic inflammation are significantly upregulated when compared to sham controls or the other two experimental groups (sevoflurane, *p* < 0.001 or LPS alone, *p* < 0.01) (Figure 2). Importantly, a short, 1-h sevoflurane exposure in the setting of inflammation is found to be as harmful as a 3-h exposure in the setting of systemic inflammation (Figure 2).

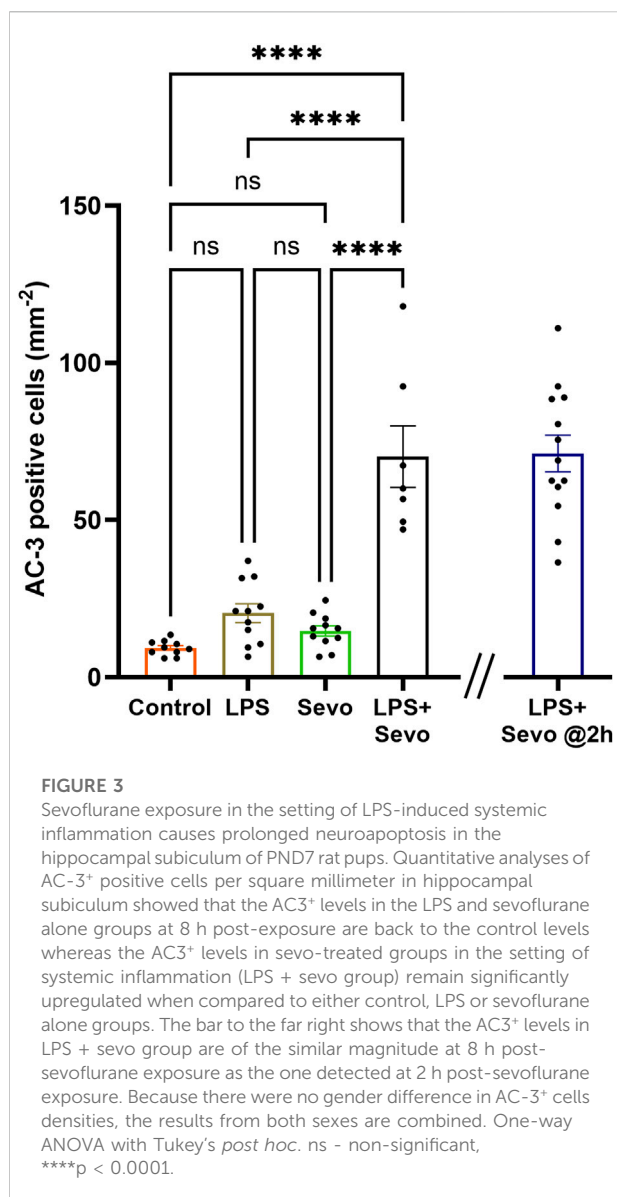
Furthermore, when we examined the delayed signs of neuroapoptosis, we found that the AC3⁺ levels in the LPS and sevoflurane alone groups at 8 h post-exposure are back to the control levels whereas the AC3⁺ levels in sevo-treated groups in the setting of systemic inflammation (LPS + sevo group) remain significantly upregulated when compared to either control, LPS or sevoflurane alone groups (*p* < 0.0001) (Figure 3). Interestingly, an ongoing neuroapoptosis in LPS + sevo group appears to be of the same intensity at 8 h timepoint post-sevoflurane exposure for 3 hours, as the one detected at the earlier timepoint, 2 h post-sevoflurane exposure (also shown in Figure 1). In aggregate, these findings suggest that the interactions between the inflammatory processes and general anesthesia result in amplified and prolonged neuronal demise hours after the offending agent (sevoflurane) is discontinued.

In view of the observed intensity and duration of sevoflurane-induced neuroapoptosis in the setting of systemic inflammation, we set out to examine the role of microglia since they serve as the resident macrophages within the brain and respond to stress, typically triggering and propagating a pro-inflammatory state. Microglia are ramified with processes that probe the extracellular environment and become amoeboid with retracted processes in an activated state (Figure 4A). We assessed microglia activation using morphological features of Iba1⁺ labelled microglia in the



hippocampal subiculum. Our data collected 2 h after sevoflurane exposure demonstrate that LPS, trauma (tibial fracture), or sevoflurane alone can independently cause a ~2-fold increase in microglia activation in the subiculum compared to their respective controls. When sevoflurane was administered following LPS (Figure 4B) or trauma (Figure 4C), a further increase in microglial activation was observed (~3- and ~4.5-fold above controls, respectively; *p* < 0.0001).

Considering that the pattern of microglia activation (Figure 4) mimics the pattern of neuroapoptosis (Figure 1) we set out to further probe whether activated microglia may be, at least in part, responsible for amplified sevoflurane neurotoxicity in the setting of systemic inflammation. We exposed PND7 rat pups to minocycline to block microglial activation [36, 37] at the time of LPS administration and again 12 h later at the time of sevoflurane exposure. AC3⁺ cells were evaluated 2 h post-sevoflurane exposure. We observed significant increase in neuroapoptosis in minocycline-treated pups exposed to LPS + sevo compared to those without minocycline (*p* < 0.0001) (Figure 5). Considering that minocycline is not selective for microglia but can also downregulate other cell types (e.g., T-lymphocytes), we



repeated this experiment with a more selective microglia-depleting agent, PLX5622. PLX5622 was administered once daily for 3 consecutive days to deplete the microglia prior to LPS administration and again 12 h later at the time of sevoflurane exposure. This treatment resulted in almost complete removal of microglia as shown in the representative microphotographs (Figure 6). AC3⁺ cells were quantified 2 h post sevoflurane exposure. Similarly to minocycline (Figure 5), we observed a significant increase in neuroapoptosis in PLX5622-treated pups exposed to LPS + sevo compared to those not pretreated with PLX5622 (*p* < 0.01) (Figure 6). These findings would suggest that microglia in the inflammatory setting is very important for cleaning damaged neurons demonstrating that their loss could result in the accumulation of neuronal debris and further

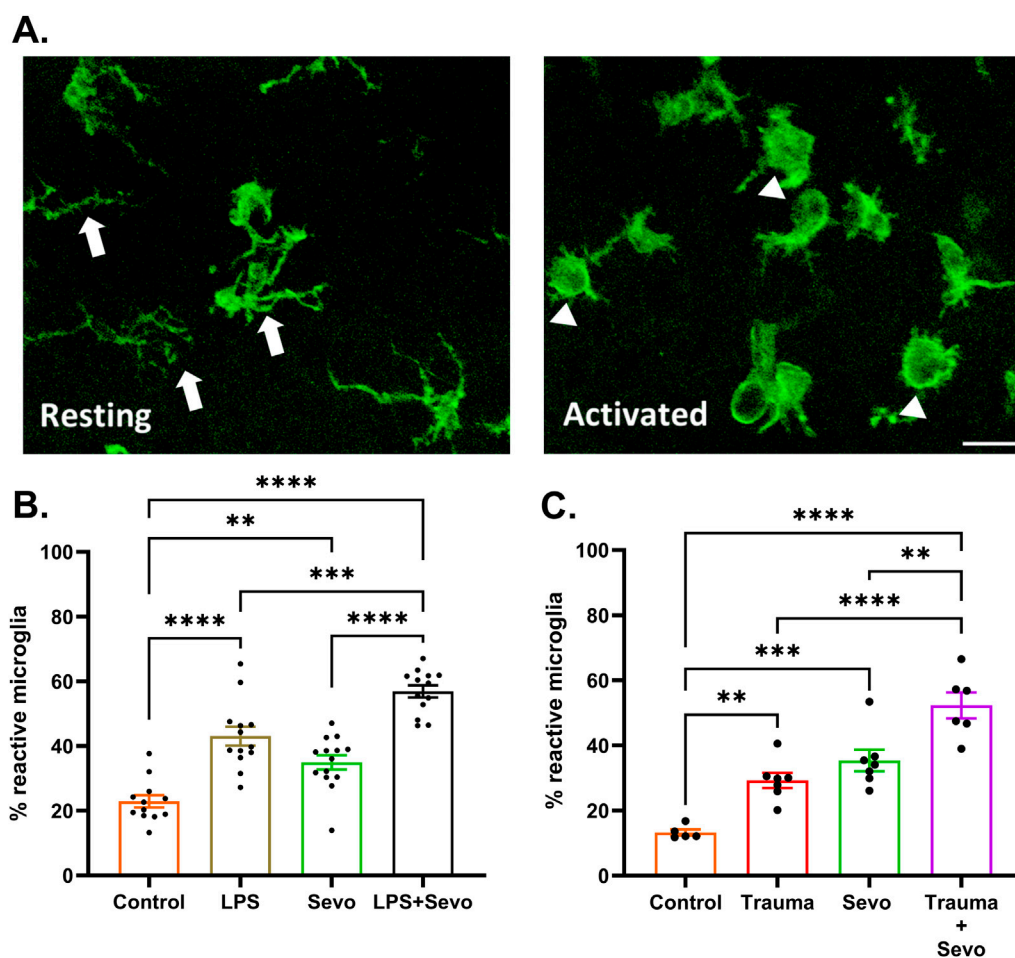


FIGURE 4

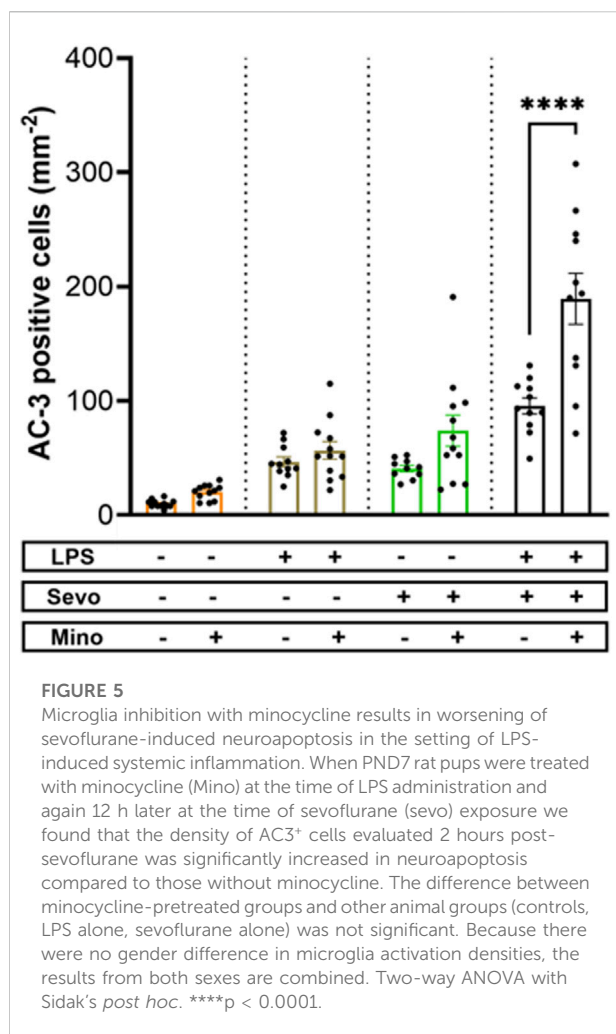
Sevoflurane exposure causes microglia activation in the hippocampal subiculum of PND7 rat pups that is worsened in the setting of trauma- and LPS-induced systemic inflammation. **(A)** Resting microglia (left panel) are ramified with processes (arrows) that probe the extracellular environment and become amoeboid (right panel) in activated state (arrowheads). x60 magnification, scale bar 20 μ m. **(B)** At 2 h post-sevoflurane exposure we detect significant (~2-fold) increase in microglia activation in LPS or sevoflurane alone groups in the subiculum compared to their respective controls. When sevoflurane was administered following LPS, we report a further increase in microglial activation (~3-fold above controls). **(C)** At 2 h post-sevoflurane exposure we detect significant (~2-fold) increase in microglia activation in trauma (tibia fracture) or sevoflurane alone groups in the subiculum compared to their respective controls. When sevoflurane was administered following trauma, we report a further increase in microglial activation (~4.5-fold above controls). Because there were no gender difference in microglia activation densities, the results from both sexes are combined. One-way ANOVA with Tukey's *post hoc*. **p < 0.01, ***p < 0.001, ****p < 0.0001.

promulgation of the inflammatory responses and enhanced neuronal damage.

We have previously published that pro-inflammatory cytokines, IL-1 β and possibly IL-18 are upregulated in the brains of the animals exposed to systemic inflammation [12]. To further probe the role of proinflammatory cytokines, we examined the levels of MCP-1, known to upregulate cell adhesion molecules that allow peripheral immune cells to enter the brain [21, 24]. In the same vein we examined the expression of ICAM-1, a cell adhesion molecule and transmembrane glycoprotein that could be induced by upregulated MCP-1. We observed a significant 4.7-fold increase in MCP-1 (Figure 7A) and 2.5-fold increase in

ICAM-1 mRNA expressions (Figure 7B) ($p < 0.05$) in LPS + sevo treated rats compared to controls.

Since upregulated MCP-1 promotes T-lymphocyte infiltration, we decided to determine the presence of peripheral immune cells in sevoflurane exposed rat pups in the setting of LPS-induced systemic inflammation using flow cytometry. To minimize the risk of contamination from within the traversing blood vessels, animals were thoroughly perfused with ice-cold PBS immediately prior to hippocampal dissection. As shown in Figure 7C, we found a significant increase ($p < 0.01$) in the proportion of T-lymphocytes in the hippocampus of LPS + sevo rat pups compared to controls (representative flow scatter plots are shown in Figures 7D,E). No differences in proportions of B-cells or neutrophils were observed in



our CD45⁺ population (data not shown). Based on this finding we suggest that sevoflurane anesthesia in the setting of systemic inflammation results in significant T-lymphocyte infiltration in hippocampal subiculum.

Discussion

Here we show that an early exposure to sevoflurane during critical stages of synaptogenesis leads to significant neuroapoptosis in young rat pup subiculum, which is worsened in the setting of systemic inflammation caused by either LPS injection or trauma (tibial fracture). The worsening is not only shown in terms of the intensity of neuroapoptosis but in its duration and onset. Our mechanistic studies presented herein suggest that sevoflurane-induced neuroapoptosis triggers activation of microglia, which in turn leads to the upregulation of proinflammatory cytokine MCP-1 and endothelial cell adhesion molecule, ICAM-1 mRNA levels in the hippocampus. This results in T-lymphocyte infiltration in the

hippocampal subiculum, an event that further perpetuates microglial activation in an attempt to control neuroapoptosis which is suggested by the fact that microglia depletion leads to a significant worsening of sevoflurane-induced developmental neuroapoptosis. The series of proposed events is depicted in Figure 8.

Due to its complexity, the studies assessing the role of inflammation in anesthesia-induced developmental neurotoxicity have been limited and sometimes at odds with each other [38] with some reporting the worsening of neurotoxicity and long-lasting impairment of cognitive function [12, 39] and other showing amelioration of anesthesia neurotoxicity [40, 41]. Most recent report indicates that sevoflurane, in the setting of LPS-induced systemic inflammation, causes significant upregulation of activated caspase-1 and NLRP1 (NLR family pyrin domain containing 1) along with related proinflammatory cytokines, IL-1 β , and IL-18 [12]. This was suggested to result in the formation of caspase-1/NLRP1 inflammasome complex which in turn activates caspases-9 and -3 thus further propagating sevoflurane-driven neuronal demise [12]. Importantly, it also resulted in worsening of learning and memory deficits in male rodents and heightened anxiety-related behavior in female rodents, a sex-specific change noted when tested in young adulthood [12]. As complex as the phenomenon may be, it is becoming more apparent that systemic inflammation could be detrimental to anesthesia-induced developmental neurotoxicity thus suggesting that studying clinically relevant conditions of a disease is paramount. Our work presented herein would suggest that similarly to systemic inflammation caused by LPS, a seemingly regional inflammation caused by bone injury, namely, tibial fracture, followed by surgical repair, using open reduction and internal fixation approach, could result in very similar neurotoxic effects in very young brain.

Based on currently available knowledge which suggests that cytokines and inflammasomes play an important role in the setting of systemic inflammation, we reasoned that microglia could play an important role as well. As specialized macrophages, microglia is considered the innate immune cells in the brain responsible for neuronal protection against different pathogens [13–16, 42, 43]. Through their phagocytic activity microglia control neuronal pruning and the refinement of neuronal circuitries and as such, they play an important role in brain development since they control every important aspect of synaptogenesis [44–49]. The complex role of activated microglia includes not only promotion of inflammation and neurotoxicity (neurotoxic phenotype) [50, 51] but depending on the activation stimulus, they may promote anti-inflammatory and neuroprotective effects (neuroprotective phenotype) [52]. It has been reported that, as the first line of defense, neurotoxic microglia release pro-inflammatory factors with potentially neurotoxic effects. Along those lines, we have previously reported the upregulation of pro-inflammatory cytokines, IL-1 β and IL-18 immediately post-sevoflurane exposure in the setting of LPS-

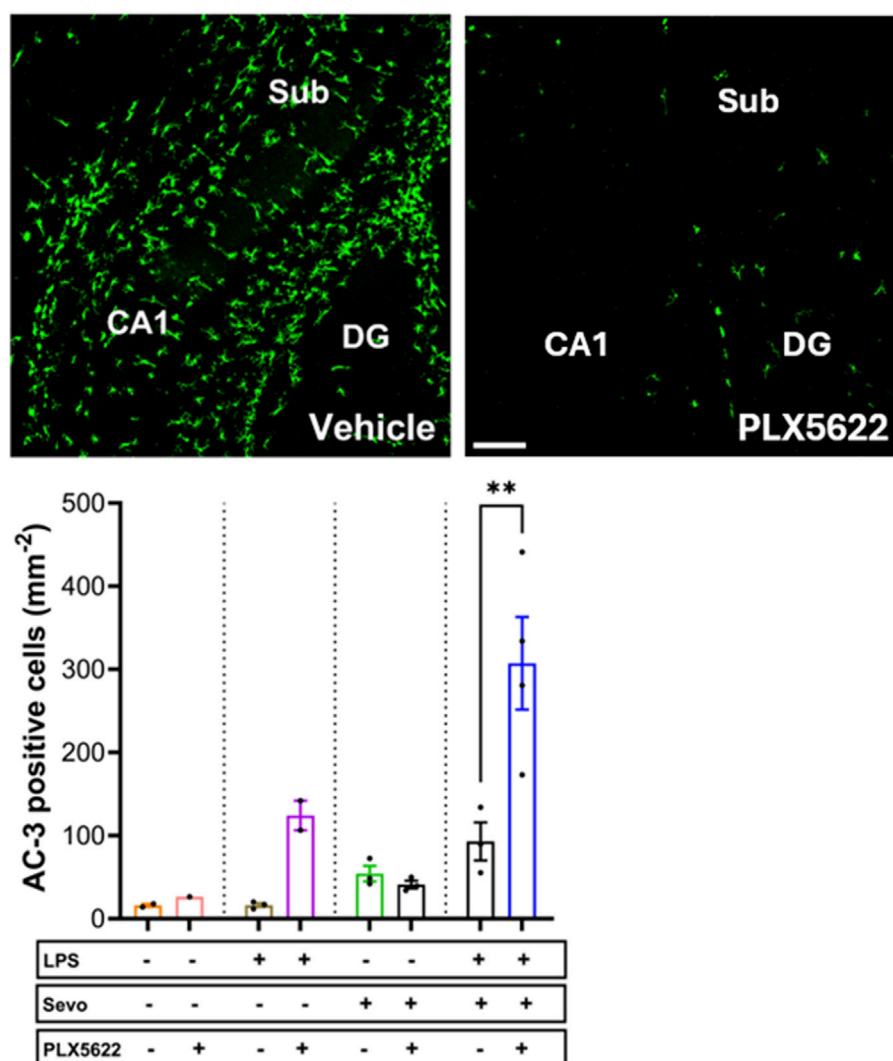
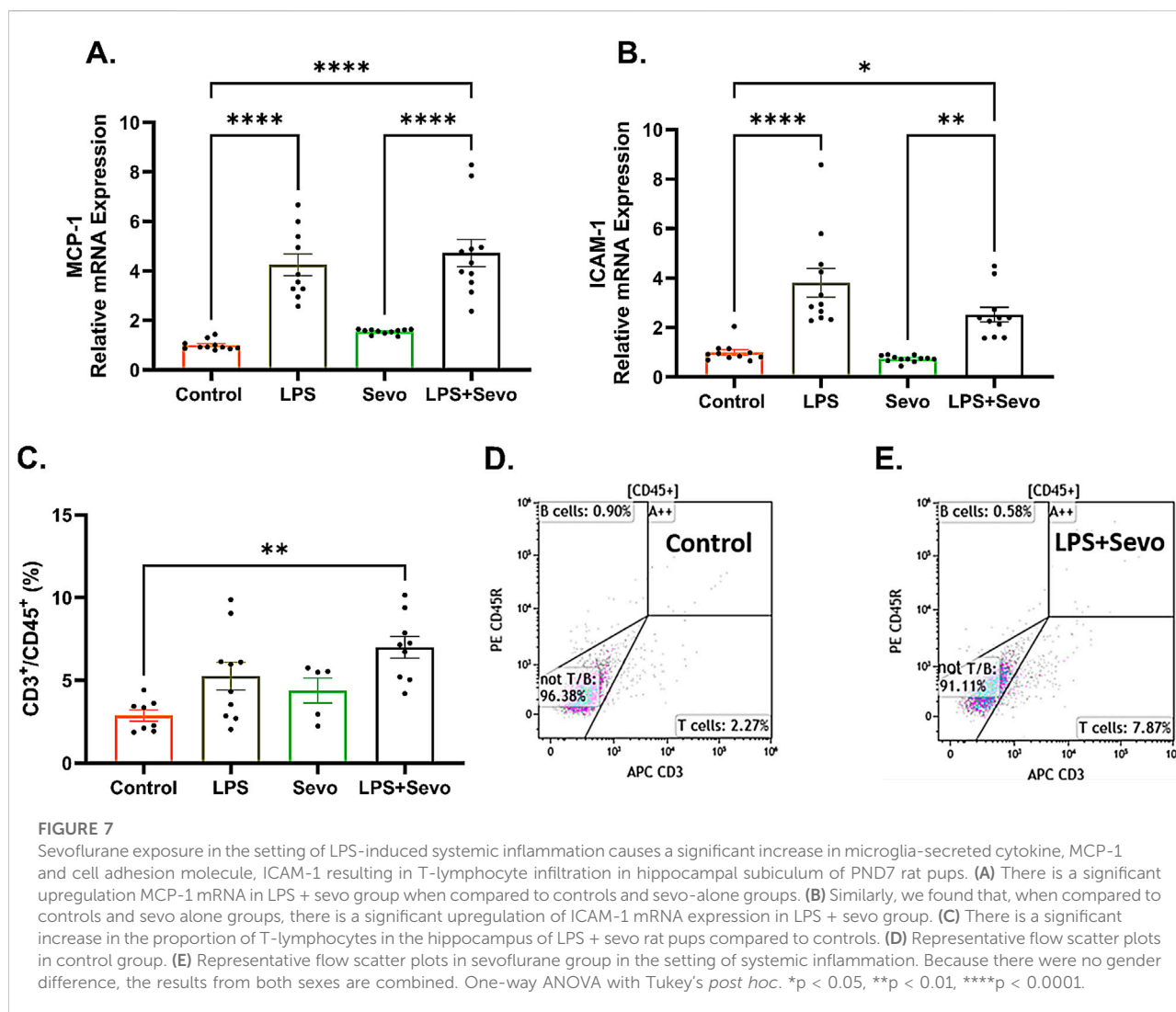


FIGURE 6

Microglia depletion with PLX5622 results in worsening of sevoflurane-induced neuroapoptosis in the setting of LPS-induced systemic inflammation. When PND7 rat pups were treated with a more selective microglia inhibitor, PLX5622 at the time of LPS administration and again 12 h later at the time of sevoflurane exposure, we found that the density of AC3⁺ cells evaluated 2 hours post-sevoflurane was significantly increased compared to vehicle-treated counterparts. The difference between PLX5622-pretreated animals and corresponding vehicle-treated animals within groups (controls, LPS alone, sevoflurane alone) was not significant. Because there were no gender difference in microglia activation densities, the results from both sexes are combined. x10 magnification, scale bar 150 μ m. Two-way ANOVA with Sidak's *post hoc*, ***p* < 0.01.

induced systemic inflammation [12]. However, if only neurotoxic phenotype gets activated in this setting, one would expect that global microglia inhibition post-minocycline or depletion post-PLX5622 pretreatment would result in ameliorated caspase-3 activation and not enhanced one as we report herein. This prompted us to hypothesize that neuroprotective subset of microglia which suppress inflammation and promote repair of damaged neuropil [53–55] are important in controlling sevoflurane-induced neuroapoptosis in the setting of systemic inflammation. The suggested mechanism supported by our findings would indicate that the observed rise in activated microglia we report herein could

be, at least in part, due to an increase in a subset of neuroprotective microglia in the setting of sevoflurane-induced inflammation-propagated developmental neurotoxicity. It has been reported that a conversion of microglia to neuroprotective phenotype gives rise to so-called ‘acute central inflammation’ deemed to be neuroprotective due to its clearing and repairing properties [13, 56]. The puzzling question though remains whether microglia inhibition with minocycline or depletion with PLX5622 targets neuroprotective microglial phenotype more so than the neurotoxic one thus disturbing the fine balance between microglia-dependent neurotoxic and



neuroprotective pathways leading to a more substantial neuronal damage post-sevoflurane treatment in the inflammation setting. Further detailed analysis of neurotoxic and neuroprotective microglial phenotype and their interplay in this experimental setting would shed more light on this interesting proposition.

Microglia are instrumental in cleaning up damaged neurons and are considered to be irreplaceable in maintaining neuronal health and timely synaptic development [44–49]. Because of the substantial crosstalk and synergistic activity between microglia and adaptive immune system components during inflammatory conditions [57], an important consideration in this setting is the interaction between T-lymphocytes and neuroprotective microglia. It has been reported that neuroprotective microglia promote local infiltration of T-lymphocytes by expressing MHC-I (major histocompatibility complex-I) [58, 59] and by releasing neuroprotective cytokines such as IL-4, -10 and -13, TGF- β and IGF-1 in the local milieu [55, 60]. Importantly, this in turn can induce the differentiation of

naïve T-cells to neuroprotective Th2 and Treg T-cell phenotypes which can release their own anti-inflammatory cytokines, IL-4, -10 and -13 and promote further T-cell infiltration while decreasing the conversion to neurotoxic microglia and reducing the activation of pro-inflammatory type T-cells [57, 61]. Although not designed to examine such complex interaction between infiltrated T-lymphocytes and their various phenotypes on the one side with neuroprotective microglia on the other, our results would suggest that local infiltration of T-cell (but not B-cells), is important in controlling neuroprotective microglia activation and neuronal demise in the setting of sevoflurane-induced neuroapoptosis. This notion is supported by our findings that microglia depletion results in worsening of neuronal damage, most likely due to a disturbed feedback loop between microglia activation and T-lymphocyte infiltration known to play an important role in microglia phagocytosis which improves the clearing of the debris and repairing of damaged neuropil [57, 61]. More detailed assessment of T-cell and microglia phenotypes

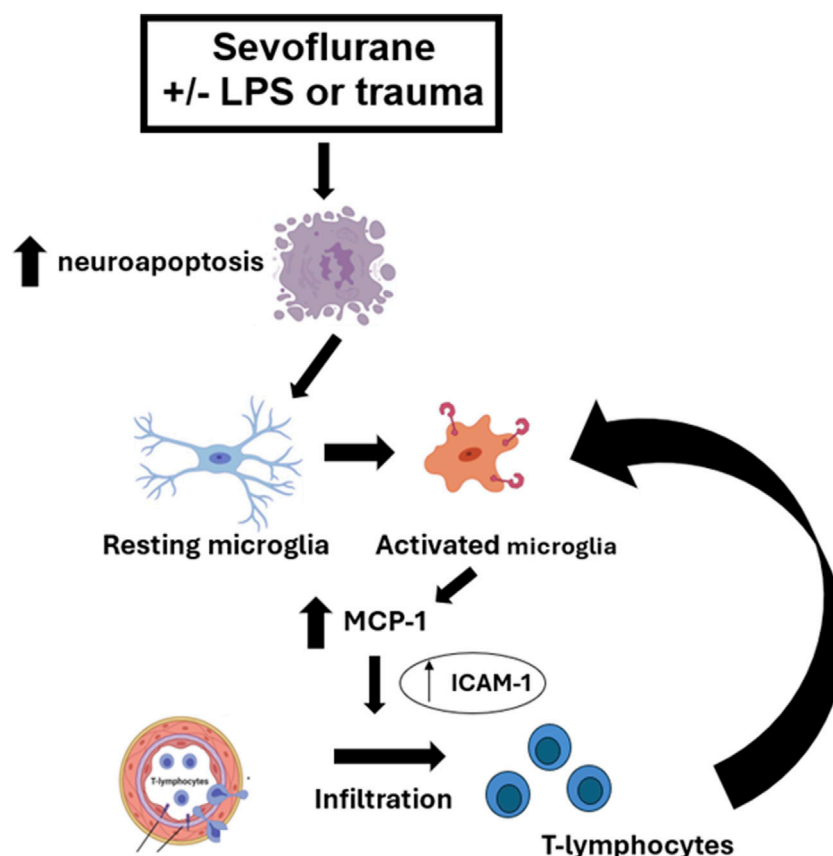


FIGURE 8

Schematic diagram of the proposed pathway in the setting of sevoflurane-induced systemic inflammation-propagated developmental neuroapoptosis in the hippocampal subiculum of PND7 rat pups. Sevoflurane-induced neuroapoptosis triggers activation of neuroprotective microglia, which in turn releases proinflammatory cytokine, MCP-1 and activates endothelial cell adhesion molecule, ICAM-1. This leads to T-lymphocyte infiltration in the subiculum, an event that further propagates neuroprotective microglia activation in an attempt to control neuroapoptosis, clear the debris and restore the neuropil.

and secreting properties would be necessary to examine this view. It is worth noting that our work presented herein was focused on the acute timeline, i.e., at 17 h after the initiation of inflammation and only 2 h after the end of sevoflurane exposure. Although this is the optimal time for the assessment of the severity of neuroapoptosis, it is relatively early for detection of T-cell infiltration and its phenotype conversion [16]. Based on previously published work, it appears that later timepoints would be useful in assessing the full scope of T-cells and microglia interactions in the setting of sevoflurane-induced inflammation-propagated neuronal demise.

In the attempt to make our animal work more relevant to the clinical setting and hence more translational, we introduce for the first time a model of trauma in very young animals that is caused by bone fracture. Since the vulnerability to GA-induced developmental neurotoxicity has been reported in pediatric groups up to 4 years of age [62–67], we believe that using orthopedic trauma model is relevant since orthopedic injuries occur in that age group [68, 69] in otherwise healthy and active

children. A trauma model of tibial fracture simulates aseptic inflammation since it entails a small skin nick, blunt manipulation of soft tissue and tibial fracture followed by internal fixation, the components relevant to trauma-like disease state [10, 11]. In view of our findings that trauma-induced propagation of sevoflurane-induced neurotoxicity mimics one described with well-known model of systemic inflammation caused by LPS [12, 16, 20], we believe that tibia fracture is a promising model that could get us a step closer to improving our understanding of a very complex phenomenon of anesthesia-induced developmental neurotoxicity in the setting of a disease. This is vitally important considering that exposure to anesthesia is exceedingly rare in the absence of any kind of pathological process.

While GA-induced developmental neurotoxicity was greatly amplified after orthopedic trauma compared to sham procedure, in our studies the insult of trauma alone was not sufficient to induce quantifiable degree of neuroapoptosis, and the reasons

behind this observation are not entirely clear. We propose that the systemic inflammation in the case of tibia fracture is not as robust as what has been reported after the LPS injection. Furthermore, LPS easily crosses blood-brain barrier and is well-known as a powerful inducer of not only systemic and but neuroinflammation as well. Hence, LPS alone is capable of initiating neuroapoptotic cascade of events through massive release of inflammatory cytokines and accumulation of reactive oxygen species in the brain which in turn activates caspases-8, -9, and -3. Trauma, on the other hand, relies on circulatory systemic inflammatory markers to initiate a neuroinflammation. Hence, it appears that while effective at priming the intracellular inflammatory machinery, a second signal provided by the GA is needed to trigger the full scope of GA-induced, inflammation-amplified developmental neuroapoptosis [12, 70, 71].

In conclusion, our work presented herein suggests that sevoflurane neurotoxicity is enhanced in the setting of systemic inflammation in terms of its onset, the intensity and duration that could, at least in part, be explained by a complex interplay between microglia activation and T-cell infiltration.

Author contributions

All authors participated in the design, interpretation of the studies and analysis of the data and review of the article; NU conducted the experiments, performed data quantification and interpretation and statistical analysis, and was responsible for writing the final version of the article; AN conducted the experiments, performed confocal imaging and finalized the figures and tables; MN helped with the experiments and performed confocal imaging; SM performed the qPCR analyses of gene expression; BV participated in article writing and data interpretation; NQ and VJ-T are senior authors responsible for study design, data analysis and interpretation, article preparation, and overall project supervision. All authors contributed to the article and approved the submitted version.

References

- Jevtovic-Todorovic V, Hartman RE, Izumi Y, Benshoff ND, Dikranian K, Zorumski CF, et al. Early exposure to common anesthetic agents causes widespread neurodegeneration in the developing rat brain and persistent learning deficits. *J Neurosci* (2003) 23:876–82. doi:10.1523/jneurosci.23-03-00876.2003
- Raper J, Alvarado MC, Murphy KL, Baxter MG. Multiple anesthetic exposure in infant monkeys alters emotional reactivity to an acute stressor. *Anesthesiology* (2015) 123:1084–92. doi:10.1097/ALN.0000000000000851
- Raper J, De Biasio JC, Murphy KL, Alvarado MC, Baxter MG. Persistent alteration in behavioural reactivity to a mild social stressor in rhesus monkeys repeatedly exposed to sevoflurane in infancy. *Br J Anaesth* (2018) 120:761–7. doi:10.1016/j.bja.2018.01.014
- Paule MG, Li M, Allen RR, Liu F, Zou X, Hotchkiss C, et al. Ketamine anesthesia during the first week of life can cause long-lasting cognitive deficits in rhesus monkeys. *Neurotoxicology and Teratology* (2011) 33:220–30. doi:10.1016/j.ntt.2011.01.001
- Slikker W, Jr, Zou X, Hotchkiss CE, Divine RL, Sadovova N, Twaddle NC, et al. Ketamine-induced neuronal cell death in the perinatal rhesus monkey. *Toxicol Sci* (2007) 98:145–58. doi:10.1093/toxsci/kfm084
- Rizzi S, Carter LB, Ori C, Jevtovic-Todorovic V. RESEARCH ARTICLE: clinical anesthesia causes permanent damage to the fetal Guinea pig brain. *Brain Pathol* (2008) 18:198–210. doi:10.1111/j.1750-3639.2007.00116.x
- Yon JH, Daniel-Johnson J, Carter LB, Jevtovic-Todorovic V. Anesthesia induces neuronal cell death in the developing rat brain via the intrinsic and extrinsic apoptotic pathways. *Neuroscience* (2005) 135:815–27. doi:10.1016/j.neuroscience.2005.03.064
- Boscolo A, Milanovic D, Starr JA, Sanchez V, Oklopčić A, Moy L, et al. Early exposure to general anesthesia disturbs mitochondrial fission and fusion in the developing rat brain. *Anesthesiology* (2013) 118:1086–97. doi:10.1097/ALN.0b013e318289bc9b

Data availability

The raw data supporting the conclusions of this article will be made available by the authors, without undue reservation.

Ethics statement

The animal study was approved by Institutional Animal Care and Use Committee, University of Colorado Anschutz Medical Campus. The study was conducted in accordance with the local legislation and institutional requirements.

Funding

The author(s) declare that financial support was received for the research and/or publication of this article. This work was supported by the Department of Anesthesiology at the University of Colorado Anschutz Medical Campus, Aurora, CO; Eunice Kennedy Shriver National Institute of Child Health and Human Development, Bethesda, MD (R01HD097990, R01HD044517, R01HD044517S); National Institute of General Medical Sciences, Bethesda, MD (R01GM118197, R01GM118197-11S1); CU Medicine Endowments, Aurora, CO.

Conflict of interest

The author(s) declared no potential conflicts of interest with respect to the research, authorship, and/or publication of this article.

Generative AI statement

The authors declare that no Generative AI was used in the creation of this manuscript.

9. Lunardi N, Ori C, Erisir A, Jevtovic-Todorovic V. General anesthesia causes long-lasting disturbances in the ultrastructural properties of developing synapses in young rats. *Neurotox Res* (2010) 17:179–88. doi:10.1007/s12640-009-9088-z
10. Caballero-Herrero MJ, Jumilla E, Buitrago-Ruiz M, Valero-Navarro G, Cuevas S. Role of damage-associated molecular patterns (DAMPs) in the postoperative period after colorectal surgery. *Int J Mol Sci* (2023) 24:3862. doi:10.3390/ijms24043862
11. Leijte GP, Custers H, Gerretsen J, Heijne A, Roth J, Vogl T, et al. Increased plasma levels of danger-associated molecular patterns are associated with immune suppression and postoperative infections in patients undergoing cytoreductive surgery and hyperthermic intraperitoneal chemotherapy. *Front Immunol* (2018) 9:663. doi:10.3389/fimmu.2018.00663
12. Useinovic N, Maksimovic S, Liechty C, Cabrera OH, Quillinan N, Jevtovic-Todorovic V. Systemic inflammation exacerbates developmental neurotoxicity induced by sevoflurane in neonatal rats. *Br J Anaesth* (2022) 129:555–66. doi:10.1016/j.bja.2022.05.008
13. Zrzavy T, Höftberger R, Berger T, Rauschka H, Butovsky O, Weiner H, et al. Pro-inflammatory activation of microglia in the brain of patients with sepsis. *Neuropathol Appl Neurobiol* (2019) 45:278–90. doi:10.1111/nan.12502
14. Riazzi K, Galic MA, Kuzmiski JB, Ho W, Sharkey KA, Pittman QJ. Microglial activation and TNF α production mediate altered CNS excitability following peripheral inflammation. *Proc Natl Acad Sci U S A* (2008) 105:17151–6. doi:10.1073/pnas.0806682105
15. Perry VH, Teeling J. Microglia and macrophages of the central nervous system: the contribution of microglia priming and systemic inflammation to chronic neurodegeneration. *Semin Immunopathol* (2013) 35:601–12. doi:10.1007/s00281-013-0382-8
16. Hoogland IC, Houbolt C, van Westerloo DJ, van Gool WA, van de Beek D. Systemic inflammation and microglial activation: systematic review of animal experiments. *J Neuroinflammation* (2015) 12:114. doi:10.1186/s12974-015-0332-6
17. Forrester JV, McMenamin PG, Dando SJ. CNS infection and immune privilege. *Nat Rev Neurosci* (2018) 19:655–71. doi:10.1038/s41583-018-0070-8
18. Abbott NJ, Patabendige AA, Dolman DE, Yusof SR, Begley DJ. Structure and function of the blood-brain barrier. *Neurobiol Dis* (2010) 37:13–25. doi:10.1016/j.nbd.2009.07.030
19. Zhang K, Wang H, Xu M, Frank JA, Luo J. Role of MCP-1 and CCR2 in ethanol-induced neuroinflammation and neurodegeneration in the developing brain. *J Neuroinflammation* (2018) 15:197. doi:10.1186/s12974-018-1241-2
20. Qin L, Wu X, Block ML, Liu Y, Breese GR, Hong JS, et al. Systemic LPS causes chronic neuroinflammation and progressive neurodegeneration. *Glia* (2007) 55:453–62. doi:10.1002/glia.20467
21. Deshmeh SL, Kremlev S, Amini S, Sawaya BE. Monocyte chemoattractant protein-1 (MCP-1): an overview. *J Interferon & Cytokine Res* (2009) 29:313–26. doi:10.1089/jir.2008.0027
22. Faustino JV, Wang X, Johnson CE, Klibanov A, Derugin N, Wendland MF, et al. Microglial cells contribute to endogenous brain defenses after acute neonatal focal stroke. *J Neurosci* (2011) 31:12992–3001. doi:10.1523/jneurosci.2102-11.2011
23. Adamson P, Etienne S, Couraud PO, Calder V, Greenwood J. Lymphocyte migration through brain endothelial cell monolayers involves signaling through endothelial ICAM-1 via a rho-dependent pathway. *The J Immunol* (1999) 162:2964–73. doi:10.4049/jimmunol.162.5.2964
24. Jiang Y, Beller DI, Frenzl G, Graves DT. Monocyte chemoattractant protein-1 regulates adhesion molecule expression and cytokine production in human monocytes. *The J Immunol* (1992) 148:2423–8. doi:10.4049/jimmunol.148.8.2423
25. Giri PK, Lu Y, Lei S, Li W, Zheng J, Lu H, et al. Pretreatment with minocycline improves neurogenesis and behavior performance after midazolam exposure in neonatal rats. *Neuroreport* (2018) 29:153–9. doi:10.1097/wnr.0000000000000937
26. Lu Y, Giri PK, Lei S, Zheng J, Li W, Wang N, et al. Pretreatment with minocycline restores neurogenesis in the subventricular zone and subgranular zone of the hippocampus after ketamine exposure in neonatal rats. *Neuroscience* (2017) 352:144–54. doi:10.1016/j.neuroscience.2017.03.057
27. Orliaguet G, Vivien B, Langeron O, Bouhemad B, Coriat P, Riou B. Minimum alveolar concentration of volatile anesthetics in rats during postnatal maturation. *Anesthesiology* (2001) 95:734–9. doi:10.1097/0000542-200109000-00028
28. Xiao A, Feng Y, Yu S, Xu C, Chen J, Wang T, et al. General anesthesia in children and long-term neurodevelopmental deficits: a systematic review. *Front Mol Neurosci* (2022) 15:972025. doi:10.3389/fnmol.2022.972025
29. Paxinos G, Watson C. *The rat brain in stereotaxic coordinates*. 5th ed. Amsterdam ; Boston: Elsevier Academic Press (2005).
30. Sanchez V, Feinstein SD, Lunardi N, Jokovic PM, Boscolo A, Todorovic SM, et al. General anesthesia causes long-term impairment of mitochondrial morphogenesis and synaptic transmission in developing rat brain. *Anesthesiology* (2011) 115:992–1002. doi:10.1097/aln.0b013e3182303a63
31. Matsumoto N, Kitanishi T, Mizuseki K. The subiculum: unique hippocampal hub and more. *Neurosci Res* (2019) 143:1–12. doi:10.1016/j.neures.2018.08.002
32. Witter MP, Ostendorf RH, Groenewegen HJ. Heterogeneity in the dorsal subiculum of the rat. Distinct neuronal zones project to different cortical and subcortical targets. *Eur J Neurosci* (1990) 2:718–25. doi:10.1111/j.1460-9568.1990.tb00462.x
33. Coleman K, Robertson ND, Dissen GA, Neuringer MD, Martin LD, Cuzon Carlson VC, et al. Isoflurane anesthesia has long-term consequences on motor and behavioral development in infant rhesus macaques. *Anesthesiology* (2017) 126:74–84. doi:10.1097/aln.0000000000001383
34. Ing C, Landau R, DeStephano D, Miles CH, von Ungern-Sternberg BS, Li G, et al. Prenatal exposure to general anesthetic and childhood behavioral deficit. *Anesth & Analgesia* (2021) 133:595–605. doi:10.1213/ane.0000000000005389
35. Tesic V, Joksimovic SM, Quillinan N, Krishnan K, Covey DF, Todorovic SM, et al. Neuroactive steroids alphaxalone and CDNC24 are effective hypnotics and potentiators of GABA(A) currents, but are not neurotoxic to the developing rat brain. *Br J Anaesth* (2020) 124:603–13. doi:10.1016/j.bja.2020.01.013
36. Ren Z, Wang X, Xu M, Frank JA, Luo J. Minocycline attenuates ethanol-induced cell death and microglial activation in the developing spinal cord. *Alcohol* (2019) 79:25–35. doi:10.1016/j.alcohol.2018.12.002
37. Tikka T, Fiebich BL, Goldsteins G, Keinänen R, Koistinaho J. Minocycline, a tetracycline derivative, is neuroprotective against excitotoxicity by inhibiting activation and proliferation of microglia. *J Neurosci* (2001) 21:2580–8. doi:10.1523/jneurosci.21-08-02580.2001
38. Useinovic N, Jevtovic-Todorovic V. Controversies in anesthesia-induced developmental neurotoxicity. *Best Pract & Res Clin Anaesthesiology* (2023) 37:28–39. doi:10.1016/j.bpa.2023.03.004
39. Shu Y, Zhou Z, Wan Y, Sanders RD, Li M, Pac-Soo CK, et al. Nociceptive stimuli enhance anesthetic-induced neuroapoptosis in the rat developing brain. *Neurobiol Dis* (2012) 45:743–50. doi:10.1016/j.nbd.2011.10.021
40. Liu JR, Liu Q, Li J, Baek C, Han XH, Athiraman U, et al. Noxious stimulation attenuates ketamine-induced neuroapoptosis in the developing rat brain. *Anesthesiology* (2012) 117:64–71. doi:10.1097/aln.0b013e31825ae693
41. Anand KJ, Garg S, Rovnaghi CR, Narsinghani U, Bhutta AT, Hall RW. Ketamine reduces the cell death following inflammatory pain in newborn rat brain. *Pediatr Res* (2007) 62:283–90. doi:10.1203/pdr.0b013e3180986d2f
42. Rodríguez AM, Rodríguez J, Giambartolomei GH. Microglia at the crossroads of pathogen-induced neuroinflammation. *ASN Neuro* (2022) 14:17590914221104566. doi:10.1177/17590914221104566
43. Kofler J, Wiley CA. Microglia: key innate immune cells of the brain. *Toxicol Pathol* (2011) 39:103–14. doi:10.1177/0192623310387619
44. Han Q, Lin Q, Huang P, Chen M, Hu X, Fu H, et al. Microglia-derived IL-1 β contributes to axon development disorders and synaptic deficit through p38-MAPK signal pathway in septic neonatal rats. *J Neuroinflammation* (2017) 14:52. doi:10.1186/s12974-017-0805-x
45. Sierra A, Abiega O, Shahrz A, Neumann H. Janus-faced microglia: beneficial and detrimental consequences of microglial phagocytosis. *Front Cell Neurosci* (2013) 7(6):6. doi:10.3389/fncel.2013.00006
46. Xiong Y, Chen J, Li Y. Microglia and astrocytes underlie neuroinflammation and synaptic susceptibility in autism spectrum disorder. *Front Neurosci* (2023) 17:1125428. doi:10.3389/fnins.2023.1125428
47. Xu ZX, Kim GH, Tan JW, Riso AE, Sun Y, Xu EY, et al. Elevated protein synthesis in microglia causes autism-like synaptic and behavioral aberrations. *Nat Commun* (2020) 11:1797. doi:10.1038/s41467-020-15530-3
48. Ball JB, Green-Fulham SM, Watkins LR. Mechanisms of microglia-mediated synapse turnover and synaptogenesis. *Prog Neurobiol* (2022) 218:102336. doi:10.1016/j.pneurobio.2022.102336
49. Miyamoto A, Wake H, Ishikawa AW, Eto K, Shibata K, Murakoshi H, et al. Microglia contact induces synapse formation in developing somatosensory cortex. *Nat Commun* (2016) 7:12540. doi:10.1038/ncomms12540
50. Colonna M, Butovsky O. Microglia function in the central nervous system during health and neurodegeneration. *Annu Rev Immunol* (2017) 35:441–68. doi:10.1146/annurev-immunol-051116-052358
51. Saitgareeva AR, Bulygin KV, Gareev IF, Beylerli OA, Akhmadeeva LR. The role of microglia in the development of neurodegeneration. *Neurol Sci* (2020) 41:3609–15. doi:10.1007/s10072-020-04468-5

52. Qin J, Ma Z, Chen X, Shu S. Microglia activation in central nervous system disorders: a review of recent mechanistic investigations and development efforts. *Front Neurol* (2023) **14**:1103416. doi:10.3389/fneur.2023.1103416
53. Yao K, Zu HB. Microglial polarization: novel therapeutic mechanism against Alzheimer's disease. *Inflammopharmacology* (2020) **28**:95–110. doi:10.1007/s10787-019-00613-5
54. Li Y, Xia Y, Yin S, Wan F, Hu J, Kou L, et al. Targeting microglial α -synuclein/TLRs/NF- κ B/NLRP3 inflammasome Axis in Parkinson's disease. *Front Immunol* (2021) **12**:719807. doi:10.3389/fimmu.2021.719807
55. Guo S, Wang H, Yin Y. Microglia polarization from M1 to M2 in neurodegenerative diseases. *Front Aging Neurosci* (2022) **14**:815347. doi:10.3389/fnagi.2022.815347
56. Jin X, Yamashita T. Microglia in central nervous system repair after injury. *J Biochem* (2016) **159**:491–6. doi:10.1093/jb/mvv009
57. Schettters STT, Gomez-Nicola D, Garcia-Vallejo JJ, Van Kooyk Y. Neuroinflammation: microglia and T cells get ready to tango. *Front Immunol* (2017) **8**:1905. doi:10.3389/fimmu.2017.01905
58. Goddery EN, Fain CE, Lipovsky CG, Ayasoufi K, Yokanovich LT, Malo CS, et al. Microglia and perivascular macrophages act as antigen presenting cells to promote CD8 T cell infiltration of the brain. *Front Immunol* (2021) **12**:726421. doi:10.3389/fimmu.2021.726421
59. Kellogg CM, Pham K, Machalinski AH, Porter HL, Blankenship HE, Tooley K, et al. Microglial MHC-I induction with aging and Alzheimer's is conserved in mouse models and humans. *GeroScience* (2023) **45**:3019–43. doi:10.1007/s11357-023-00859-6
60. Cherry JD, Olschowka JA, O'Banion MK. Neuroinflammation and M2 microglia: the good, the bad, and the inflamed. *J Neuroinflammation* (2014) **11**:98. doi:10.1186/1742-2094-11-98
61. Ebner F, Brandt C, Thiele P, Richter D, Schliesser U, Siffrin V, et al. Microglial activation milieu controls regulatory T cell responses. *The J Immunol* (2013) **191**:5594–602. doi:10.4049/jimmunol.1203331
62. Flick RP, Katusic SK, Colligan RC, Wilder RT, Voigt RG, Olson MD, et al. Cognitive and behavioral outcomes after early exposure to anesthesia and surgery. *Pediatrics* (2011) **128**:e1053–61. doi:10.1542/peds.2011-0351
63. Sprung J, Flick RP, Katusic SK, Colligan RC, Barbaresi WJ, Bojanić K, et al. Attention-deficit/hyperactivity disorder after early exposure to procedures requiring general anesthesia. *Mayo Clinic Proc* (2012) **87**:120–9. doi:10.1016/j.mayocp.2011.11.008
64. Wilder RT, Flick RP, Sprung J, Katusic SK, Barbaresi WJ, Mickelson C, et al. Early exposure to anesthesia and learning disabilities in a population-based birth cohort. *Anesthesiology* (2009) **110**:796–804. doi:10.1097/01.anes.0000344728.34332.5d
65. DiMaggio C, Sun LS, Li G. Early childhood exposure to anesthesia and risk of developmental and behavioral disorders in a sibling birth cohort. *Anesth & Analgesia* (2011) **113**:1143–51. doi:10.1213/ane.0b013e3182147f42
66. Ing C, DiMaggio C, Whitehouse A, Hegarty MK, Brady J, von Ungern-Sternberg BS, et al. Long-term differences in language and cognitive function after childhood exposure to anesthesia. *Pediatrics* (2012) **130**:e476–85. doi:10.1542/peds.2011-3822
67. Reighard C, Junaid S, Jackson WM, Arif A, Waddington H, Whitehouse AJO, et al. Anesthetic exposure during childhood and neurodevelopmental outcomes: a systematic review and meta-analysis. *JAMA Netw Open* (2022) **5**:e2217427. doi:10.1001/jamanetworkopen.2022.17427
68. Chaudhary S, Javed M, Figueroa J, Bayakly R, Mays E, Shaikh S, et al. Pediatric falls ages 0-4: understanding demographics, mechanisms, and injury severities. *Pediatrics* (2018) **142**:718. doi:10.1542/peds.142.1ma8.718
69. Monget F, Sapienza M, McCracken KL, Nectoux E, Fron D, Andreacchio A, et al. Clinical characteristics and distribution of pediatric fractures at a tertiary hospital in northern France: a 20-year-distance comparative analysis (1999-2019). *Medicina (Kaunas)* (2022) **58**:610. doi:10.3390/medicina58050610
70. Liao Y, Kong Y, Chen H, Xia J, Zhao J, Zhou Y. Unraveling the priming phase of NLRP3 inflammasome activation: molecular insights and clinical relevance. *Int Immunopharmacology* (2025) **146**:113821. doi:10.1016/j.intimp.2024.113821
71. Swanson KV, Deng M, Ting JP. The NLRP3 inflammasome: molecular activation and regulation to therapeutics. *Nat Rev Immunol* (2019) **19**:477–89. doi:10.1038/s41577-019-0165-0



OPEN ACCESS

*CORRESPONDENCE

Cheng Wang,
✉ cheng.wang@fda.hhs.gov

RECEIVED 28 March 2025

ACCEPTED 20 May 2025

PUBLISHED 13 June 2025

CITATION

Wang C, Latham LE, Liu S, Talpos J, Patterson TA, Hanig JP and Liu F (2025) Assessing potential desflurane-induced neurotoxicity using nonhuman primate neural stem cell models. *Exp. Biol. Med.* 250:10606. doi: 10.3389/ebm.2025.10606

COPYRIGHT

© 2025 Wang, Latham, Liu, Talpos, Patterson, Hanig and Liu. This is an open-access article distributed under the terms of the [Creative Commons Attribution License \(CC BY\)](https://creativecommons.org/licenses/by/4.0/). The use, distribution or reproduction in other forums is permitted, provided the original author(s) and the copyright owner(s) are credited and that the original publication in this journal is cited, in accordance with accepted academic practice. No use, distribution or reproduction is permitted which does not comply with these terms.

Assessing potential desflurane-induced neurotoxicity using nonhuman primate neural stem cell models

Cheng Wang^{1*}, Leah E. Latham¹, Shuliang Liu¹, John Talpos¹, Tucker A. Patterson², Joseph P. Hanig³ and Fang Liu¹

¹Division of Neurotoxicology, National Center for Toxicological Research/FDA, Jefferson, AR, United States, ²Office of Center Director, National Center for Toxicological Research/Food and Drug Administration (FDA), Jefferson, AR, United States, ³Office of Pharmaceutical Quality, Center for Drug Evaluation and Research/FDA, Silver Spring, MD, United States

Abstract

Safety concerns about general anesthetics (GA), such as desflurane (a commonly used gaseous anesthetic agent), arose from studies documenting neural cell death and behavioral changes after early-life exposure to anesthetics and compounds with related modes of action. Neural stem cells (NSCs) can recapitulate most critical events during central nervous system (CNS) development *in vivo* and, therefore, represent a valuable *in vitro* model for evaluating potential desflurane-induced developmental neurotoxicity. In this study, NSCs harvested from the hippocampus of a gestational day 80 monkey brain were applied to explore the temporal relationships between desflurane exposures and neural stem cell health, proliferation, differentiation, and viability. At clinically relevant doses (5.7%), desflurane exposure did not result in significant changes in NSC viability [lactate dehydrogenase (LDH) release] and NSC proliferation profile/rate by Cell Cycle Assay, in both short term (3 h) and prolonged (24 h) exposure groups. However, when monkey NSCs were guided to differentiate into neural cells (including neurons, astrocytes, and oligodendrocytes), and then exposed to desflurane (5.7%), no significant changes were detected in LDH release after a 3-h exposure, but a significant elevation in LDH release into the culture medium was observed after a 24-h exposure. Desflurane (24 h)-induced neural damage was further supported by increased expression levels of multiple cytokines, e.g., G-CSF, IL-12, IL-9, IL-10, and TNF- α compared with the controls. Additionally, our immunocytochemistry and flow cytometry data demonstrated a remarkable attenuation of differentiated neurons as evidenced by significantly decreased numbers of polysialic acid neural cell adhesion molecule (PSA-NCAM)-positive cells in the desflurane-exposed (prolonged) cultures. Our data suggests that at the clinically relevant concentration, desflurane did not induce NSC damage/death, but impaired the differentiated neuronal cells after prolonged exposure. Collectively, PSA-NCAM could be essential for neuronal viability. Desflurane-induced neurotoxicity was primarily associated with the loss of differentiated neurons. Changes in the neuronal specific marker, PSA-NCAM, may help understand the underlying mechanisms associated with anesthetic-induced

neuronal damage. These findings should be helpful/useful for the understanding of the diverse effects of desflurane exposure on the developing brain and could be used to optimize the usage of these agents in the pediatric setting.

KEYWORDS

anesthetics, desflurane,, developing neurons, neural differentiation, neurotoxicity

Introduction

While controversial, it is suspected that extended or multiple early-life exposures to general anesthetics may lead to later adverse cognitive development [1–8]. However, it remains uncertain if the neurodevelopmental deficits are caused by general anesthesia, the surgery/procedure used to treat the condition, or the condition itself [9, 10]. All approved general anesthetics including desflurane, have NMDA-type glutamate receptor-blocking or GABA_A receptor-enhancing properties. Desflurane belongs to the group of medicines known as general anesthetics. Inhaled desflurane is used to cause general anesthesia (loss of consciousness) before and during surgery in adults. It is also used as a maintenance anesthesia in adults and children after receiving other anesthetics before and during surgery. Available findings indicate that decreased excitation of NMDA receptors or increased activation of GABA_A receptors can induce wide-spread neurodegeneration in the developing rodent or monkey brain [11–14] and cause cognitive impairments [15–17]. Additionally, a population-based study showed that early exposure to anesthesia could be a significant risk factor for later learning disabilities [1]. Appropriate studies performed have not demonstrated pediatric-specific problems that would limit the usefulness of inhaled desflurane [18] in children after receiving other anesthetics. However, children 6 years of age and younger are more likely to have unwanted side effects, such as coughing, chest tightness, or trouble breathing, which may require caution in patients receiving this agent. Previous studies have demonstrated that exposure of the developing brain to gaseous anesthetics such as nitrous oxide plus isoflurane during the period of synaptogenesis produced exposure duration-dependent increases in neurotoxicity [4, 7, 8, 12, 19] and lasting behavioral changes [6, 16]. A growing body of data indicates that prolonged bouts of anesthesia in the developing brain may lead to neurodegeneration. It is proposed that anesthetic-induced neurotoxicity depends upon the concentration of drug used, the duration of exposure, and the age of neurodevelopment at the time of exposure [12].

Most nonclinical models of neurotoxicity rely on animals, however, some *in vitro* models [11, 13, 20, 21] have emerged that can provide similar data. Particularly, NSC models [14] with their capacity to reproduce the most critical developmental processes including proliferation and differentiation, may serve as an effective alternative when evaluating anesthesia-related neurotoxicity. Since nonhuman primates have a central nervous system comparable to

humans relative to anatomy, physiology and development, monkey NSCs [21, 22] can reach a high degree of concordance. Thus, the utilization of highly relevant *in vitro* monkey NSC models, might serve as a “bridging” system to evaluate the cellular and molecular changes after anesthetic exposure. Translational observations could also be made by exploring issues related to pediatric desflurane exposure from nonhuman primate neural stem cells, thereby providing valuable information on the ability to better interrogate specific mechanisms and the ability to do large scale of science research that cannot easily occur *in vivo*.

The neural cell adhesion molecule (NCAM) serves as a temporally and spatially regulated modulator of a variety of cell-cell interactions. It is known that cells expressing polysialylated isoforms of NCAM (PSA-NCAM) have a markedly increased capacity for structural plasticity [23–25], and the polysialic acid modification of the neural cell adhesion molecule is involved in spatial learning and hippocampal long-term potentiation [26]. Meanwhile, as a neuronal specific marker, PSA-NCAM has been used to identify/define developing neurons [21, 25, 27].

For this study, it was hypothesized that: 1) NSCs from nonhuman primates (NHP) could recapitulate key findings from *in vivo* work that support “clinical-like” studies in the NHP; 2) desflurane-induced neural damage, if any, most likely depends on the duration of exposure; 3) desflurane-induced neural damage/neuronal-loss could be evaluated using biological assays and monitoring PSA-NCAM expression levels; and 4) measuring PSA-NCAM levels could serve as a key step (as a target molecule) to dissect the underlying mechanisms associated with anesthetic-induced neurotoxicity.

Materials and methods

Test agents

Desflurane was purchased from NexAir, LLC (Memphis, TN). Desflurane (5.7%) was driven by the delivery gas (mixed gas) of 21% oxygen, 5% CO₂, and balanced by nitrogen.

Cultures

Media for NSC proliferation (named “growth medium”) and for NSC differentiation (named “differentiation medium”) were

purchased from VESTA Biotherapeutics (Branford, CT). Monkey NSCs were harvested from the gestational day 80 fetal monkey [28]. The cells were seeded on poly-D-lysine/laminin-coated dishes. Monkey NSCs were cultured in NSC growth medium [Vesta Biotherapeutics; Branford, CT (changed every 48 h)] until the cells reached confluence. The cells were then transferred to 35 mm Petri dishes (Corning Incorporated; Corning, NY) with round cover slips at a seeding density of 6×10^3 cells/cm², and 24 h after seeding the cells were used for NSC characterization, and/or were directed to differentiate using neural differentiation medium (Vesta Biotherapeutics; Branford, CT) for another 5 days, with culture medium changed every other day. The cells were cultured in a standard culture incubator with humidified air and 5% carbon dioxide at 37°C. The concentrations of oxygen and carbon dioxide in the chamber were continuously monitored.

To expose to desflurane, the cells/cultures were loaded into a VitroCell System (VITROCELL Systems GmbH; Waldkirch, Germany) where the concentrations of desflurane, oxygen, and carbon dioxide (CO₂) were accurately maintained during the experiment. Control cultures were also loaded to the same system without exposure to desflurane.

5-ethynyl-2'-deoxyuridine (EdU) incorporation assay

The NSC proliferation rate was measured using an EdU staining kit [Click-iT® EdU Alexa Fluor® High-throughput Imaging (HCS) Assay, Invitrogen; Carlsbad, CA] as previously described [13, 14].

Cell cycle

NSCs were detached and washed twice in cold PBS and centrifuged at 200 *g* for 5 min at 4°C. Cells were fixed in 70% ethanol for 1 h on ice. Cells were washed and treated with 0.25 mg/mL RNase (Qiagen) for 1 h at 37°C. Cells were then immediately stained with 10 µg/mL propidium iodide (PI; Millipore; Burlington, MA) for 30 min on ice. Samples were run on a BD LSR Fortessa flow cytometer and at least 100,000 events were captured. Cells were analyzed for PI positivity using FCS Express version 6 (*De Novo* Software).

Assessment of neurotoxicity

Lactate dehydrogenase (LDH) release

The release of LDH into the culture medium occurs with loss of plasma membrane integrity, a process most often associated with acute cell death. The LDH (Roche Applied Science; Indianapolis, IN)

release assay was performed as previously reported [20, 29] to determine cytotoxicity after desflurane exposure.

Cytokine immunoassay

Cell lysate was collected from NSCs after exposure to desflurane or delivery of mixed air (control) using the Bio-Plex Cell Lysis kit (Bio-Rad; Kansas City MO) and protein concentration was measured by the DC Protein Assay kit (Bio-Rad; Kansas City MO). Cell lysates were then probed with cytokines and growth factors using the Bio-Plex Pro Human Cytokine 27-plex assay (M500KCAF0Y; Bio-Rad; Kansas City MO) according to the manufacturer's instructions. During the assay, antibody specifically directed against the cytokine of interest was coupled to a color-coded bead and allowed to incubate with the sample. Then a biotinylated detection antibody was added creating a sandwich of antibodies around the cytokine. This mixture was then detected by streptavidin-PE. When each reaction was run through the bio-plex system the fluorescent intensity was measured and calculated by the Bio-Plex 200 (Bio-Rad; Kansas City MO) software using a standard curve, and data were analyzed in Bio-Plex Data Pro software.

Immunocytochemistry and nuclear staining

Immunocytochemical staining was performed as previously described [21]. Specifically, a mouse monoclonal antibody to nestin (1:100 dilution in PBS/0.5% BSA/0.03% Triton X-100 solution, Millipore; Burlington, MA) was used to label neural stem cells; a mouse monoclonal antibody to polysialic acid neural cell adhesion molecule (PSA-NCAM; 1:500; Miltenyi Biotec Inc; Auburn, CA); and polyclonal antibody to GFAP (1:200, Millipore; Burlington, MA) were used to identify glial cells. Briefly, the cells were rinsed with phosphate-buffered saline (PBS), fixed with ice-cold 4% paraformaldehyde in PBS and permeabilized with 0.5% bovine serum albumin (BSA)/Triton X-100 in PBS for 1 h. The cells were incubated with primary antibody at 4°C overnight. Bound antibodies were revealed with FITC-conjugated sheep anti-mouse IgG second antibody, or rhodamine-conjugated sheep anti-rabbit IgG secondary antibody. DAPI, a nuclear stain dye, in the mounting medium was applied to determine total cell counts in the cultures. Cells were viewed using an Olympus IX71 microscope (Olympus; Center Valley, PA).

Flow cytometry analysis of PSA-NCAM staining

Cultured neural cells were dissociated from culture dishes using Accutase™ Cell Detachment Solution (BD

Neural Stem Cells Derived from Monkey

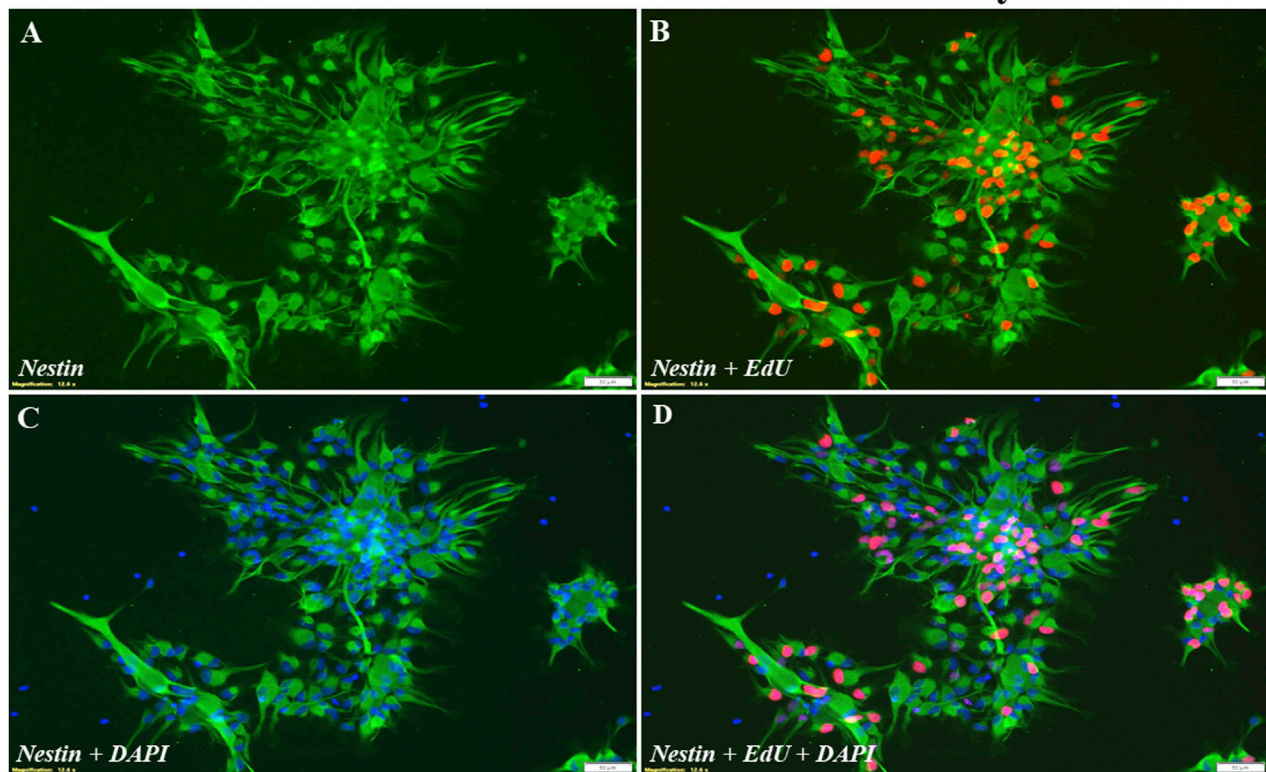


FIGURE 1

Representative photographs of immunostaining of nestin and EdU incorporation. In this control culture, numerous nestin positive NSCs [(A); green] were EdU-positive [(B); red]. These cells were undifferentiated NSCs when the cultures were maintained in the NSC growth medium. The total number of cells in the culture was revealed by DAPI-labeled nuclei (C), and a merged image (D). Approximately, on the day *in vitro* 8, the cells are confluent/ready for experiments. Scale bar = 50 μ m.

Biosciences; San Jose, CA), washed with PBS, filtered through a 70- μ m Falcon[®] cell strainer (Life Sciences; Tewksbury, MA), fixed in BD Cytofix Fixation buffer (BD Biosciences; San Jose, CA) and permeabilized with BD Phosflow Perm Buffer III (BD Biosciences; San Jose, CA). Non-specific antibody binding was blocked using Human Fc Block (1:300) (catalog #564220, BD Biosciences; San Jose, CA) for 30 min at 4°C in cell staining buffer. Cells were washed and resuspended in PE conjugated PSA-NCAM (1:50) (Miltenyi Biotec Inc; Auburn, CA) for 1 h at room temperature. Samples were washed twice and immediately ran on a BD Bioscience LSR Fortessa flow cytometer. Data were analyzed using FCS Express version 6 (De Novo Software).

Statistical analysis

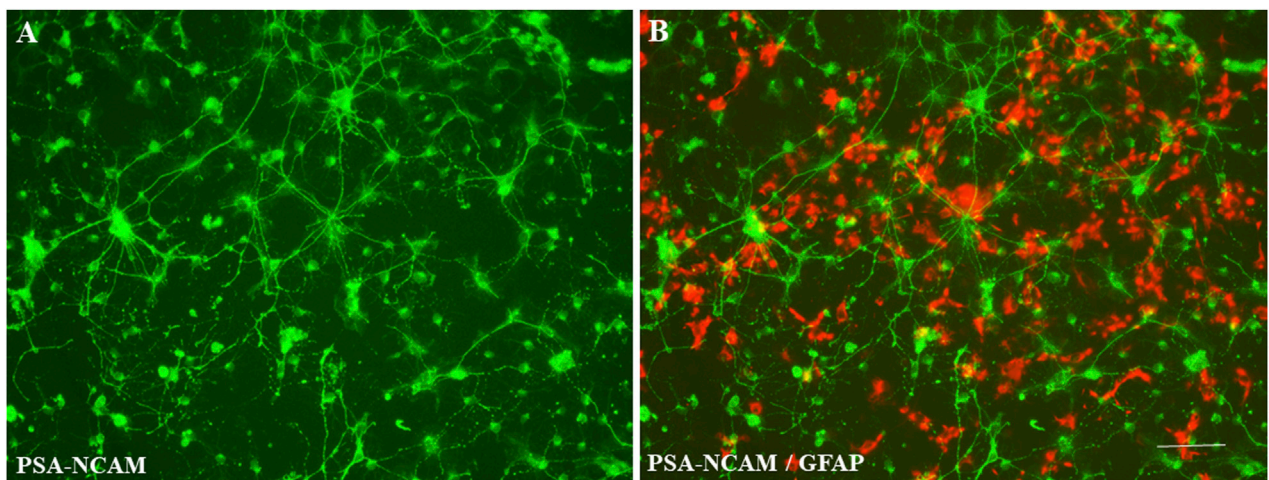
Statistical analyses were performed, and graphs were produced using GraphPad Prism 9 (GraphPad Software

Inc.; San Diego, CA). Data were analyzed with GraphPad Prism 9 using the unpaired t-test, and expressed as mean \pm SD. A p-value less than 0.05 was considered statically significant. Each treatment condition was assessed at least in triplicate, and experiments were repeated three times independently.

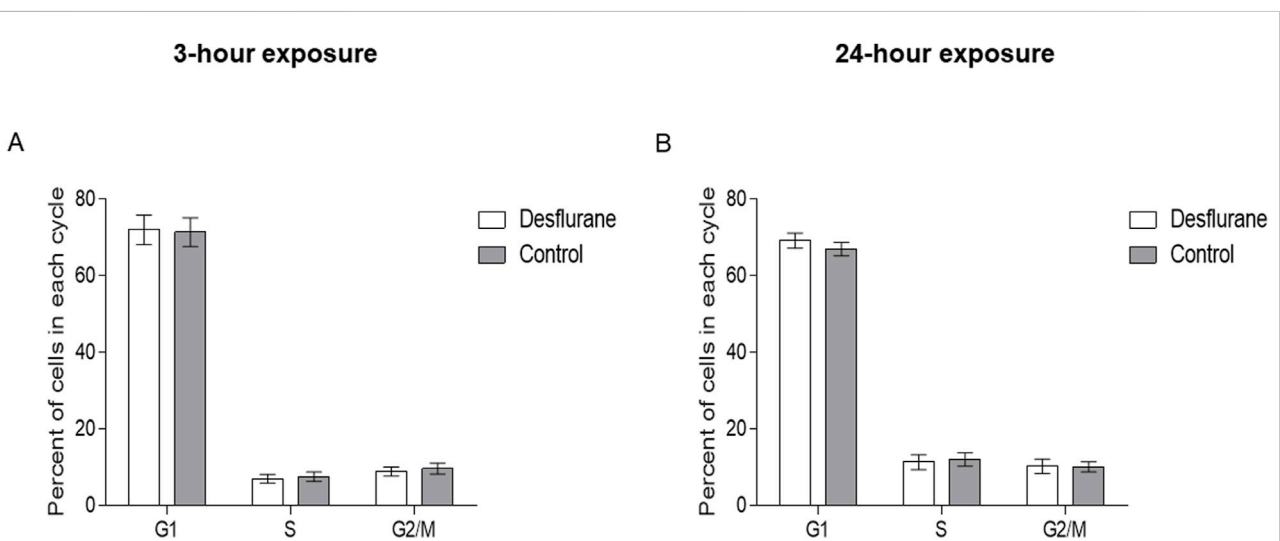
Results

Characterization of NSCs

The cultured monkey NSCs demonstrated the features of being able to self-renew (Figures 1A–C) and differentiate to generate lineages of neurons as well as glia including astrocytes and oligodendrocytes (Figure 2). As shown in Figure 1, numerous morphologically bipolar monkey NSCs were generated on day *in vitro* (DIV) 8, and most of these cells were positively stained by a NSC marker, nestin. In this control culture, the NSC proliferation was further

**FIGURE 2**

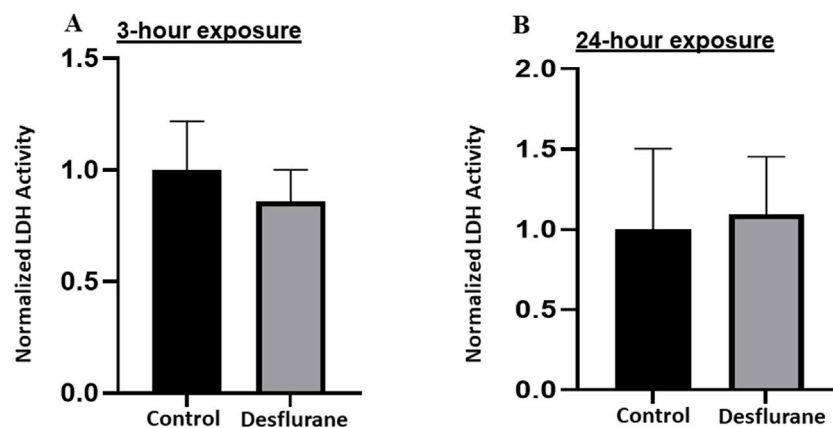
Representative photographs of NSC differentiation. Different neural cells (derived from monkey NSCs) with multiple processes and a clear neural network could be observed when the control cultures were maintained in neural differentiation medium. Morphologically defined neurons were positively stained by a monoclonal antibody to PSA-NCAM [(A); green]. Typical astrocytes were labeled with the anti-GFAP antibody [(B); red]. Scale bar = 50 μ m.

**FIGURE 3**

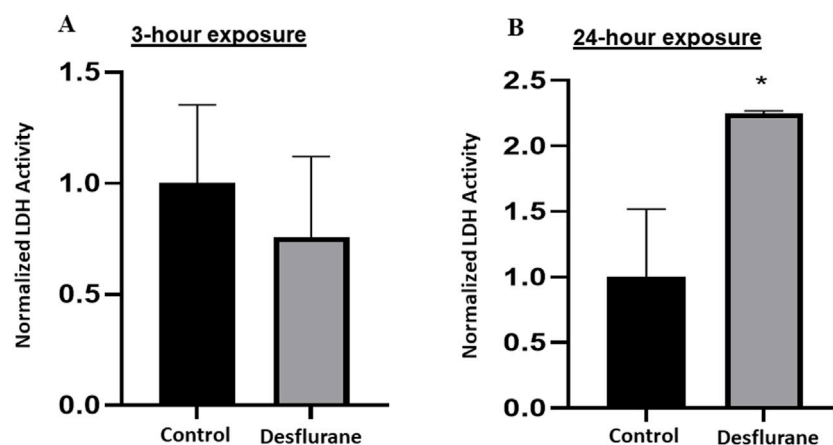
Proportion of cells in each phase of the cell cycle. Monkey NSCs were treated with 5.7% desflurane or delivery mixed air for 3 (A) or 24 (B) hours. Immediately following exposure, cells were collected and treated as described in the methods. Desflurane exposure does not significantly affect the proportion of NSCs in each phase of the cell cycle. Results are pooled from 3 independent experiments; a student's T-test revealed no statistical significance.

confirmed using a commercially available EdU incorporation assay. The merged picture (Figure 1D; nestin/EdU/DAPI) shows that many of nestin-positive NSCs (green) were EdU-positive (red), demonstrating the capability of NSCs to proliferate.

Differentiated cells with multiple processes and a clear neural network were observed (Figure 2), when the cultures were maintained in neural differentiation medium for 5 days. Morphologically defined developing neurons were positively stained with specific neuronal marker, PSA-NCAM [A

**FIGURE 4**

To study the vulnerability of NSCs to desflurane-induced neurotoxicity, LDH levels in the culture medium were monitored. No significant changes in the LDH release were detected when the monkey NSCs were exposed to desflurane (5.7%) in both short term (3 h) cultures (A) and prolonged (24 h) cultures (B). The experiments were repeated three times independently.

**FIGURE 5**

To study the vulnerability of differentiated neuronal cells to desflurane-induced neurotoxicity, LDH levels in the culture medium were monitored. Differentiated neuronal cell viability was not significantly affected after short term (3 h) desflurane exposure (A). However, a significant elevation in LDH release into the culture medium was observed when these neuronal cells (derived/differentiated from monkey NSCs) were exposed to desflurane (5.7%) for 24 h (B). The experiments were repeated three times independently. * $p \leq 0.05$.

(green)], and typical astrocytes were labeled with the anti-GFAP antibody [B (red)].

Cell cycle

Desflurane did not significantly affect the proportion of NSCs in each phase of the cell cycle, after 3-h (Figure 3A) or 24-h (Figure 3B) exposures, compared with the controls. There was no difference in the number of cells in S phase, indicating desflurane did not alter NSC differentiation. Results are pooled from three independent experiments.

LDH release from NSCs and the differentiated cells

At clinically relevant doses (5.7%), desflurane did not induce significant changes in LDH release, in both short (3 h) term (Figure 4A), and prolonged (24 h) exposure groups (Figure 4B).

On the other hand, differentiated cells had a significant elevation in LDH release into the culture medium after 24-h exposure (Figure 5B), however, the 3-h exposure did not show a difference (Figure 5A). (Figure 5 about here)

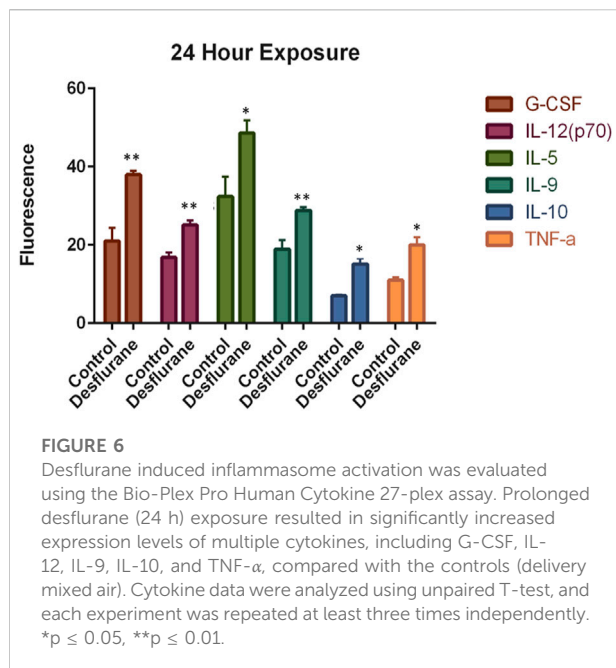
TABLE 1 Summary of Cytokines change in differentiated neural cells.

	P value	Mean1	Mean2	Difference	SE of difference	t ratio	df
Eotaxin	0.180113	14.3889	19.5833	−5.19444	3.20241	1.62204	4
FGF Basic	0.29853	18.9167	24.9722	−6.05556	5.0727	1.19376	4
G-CSF	0.00780072	21	38	−17	3.43929	4.94288	4
GM-CSF	0.67853	26.4444	30.1944	−3.75	8.40396	0.446218	4
IFN-g	0.141982	27.3611	39.3889	−12.0278	6.58908	1.82541	4
IL-10	0.538916	13.0278	14.6667	−1.63889	2.44208	0.671105	4
IL-12(p70)	0.00797281	16.7778	25.0556	−8.27777	1.68508	4.91238	4
IL-13	0.513043	11.9167	15.2222	−3.30555	4.61061	0.716945	4
IL-15	0.731475	26.9444	28.25	−1.30555	3.54708	0.368064	4
IL-17	0.510721	11.7222	15.5556	−3.83333	5.31565	0.721141	4
IL-1b	0.532207	9.22222	12.4444	−3.22222	4.71887	0.682837	4
IL-1ra	0.553413	8.86111	10.7778	−1.91667	2.96651	0.646102	4
IL-2	0.0763289	14.75	29.7222	−14.9722	6.3017	2.3759	4
IL-4	0.563121	8.63889	10.6944	−2.05556	3.26481	0.62961	4
IL-5	0.0532313	32.3889	48.6111	−16.2222	5.97384	2.71555	4
IL-6	0.510306	14.6389	17.3333	−2.69444	3.73247	0.721893	4
IL-7	0.943022	15	15.5833	−0.583332	7.66908	0.0760628	4
IL-8	0.922356	15.6389	15.8056	−0.166667	1.60631	0.103757	4
IL-9	0.015421	18.9444	28.8056	−9.86111	2.43226	4.0543	4
IL-10	0.004156	6.97222	15.1389	−8.16667	1.38666	5.88944	4
MCP-1(MCAF)	0.463354	18.8056	24.8333	−6.02777	7.44133	0.810039	4
MIP-1a	0.534612	8.44444	10.1667	−1.72222	2.53783	0.67862	4
MIP-1b	0.323724	20.1389	27.3611	−7.22222	6.42274	1.12448	4
PDGF-bb	0.745631	166.417	179.806	−13.3889	38.5134	0.347642	4
RANTES	0.063974	29.8056	39.3056	−9.5	3.74001	2.5401	4
TNF-α	0.0123884	10.9722	20	−9.02777	2.08685	4.32603	4
VEGF	0.213373	48	60.5556	−12.5556	8.49256	1.47842	4

Cytokine changes in the differentiated cells

Desflurane exposure resulted in significant increases in levels of the key proinflammatory cytokines: interleukin 12 (IL-12) with an average 1.3-fold increase, G-CSF with an average 1.85-fold increase, TNF-α with an average 1.66-fold increase and anti-inflammatory cytokine such as interleukin 9 (IL-9) with an average 1.25-fold increase and interleukin 10 (IL-10) with an average 2.0-fold increase. These results (summarized in Table 1 and Figure 6) indicate that an enduring increase in systemic inflammatory cytokines may occur after 24-h desflurane exposure.

Potential toxic effects after prolonged desflurane exposure (24 h) on differentiated neural cells were examined using immunocytochemical markers including neuronal and glial specific antibodies such as PSA-NCAM (neuronal specific marker), GFAP (astrocyte specific marker) and Galc [oligodendrocyte specific markers (data not shown)]. Numerous typical neurons were labeled by PSA-NCAM on their membrane surface of both cell bodies and processes in the control cultures (Figure 7A), and many differentiated astrocytes were labeled with the anti-GFAP antibody [Figure 7B (red)]. The number of PSA-NCAM positive neurons was obviously reduced after desflurane exposure.



PSA-NCAM expression in the desflurane group exhibited typically condensed residue pieces, fragmentation and shrinking profiles (Figure 7C) compared with control (Figure 7A). In contrast, GFAP labeled astrocytes were not remarkably affected by desflurane (Figure 7D).

Analysis of PSA-NCAM expression by flow cytometry

Desflurane exposure diminished PSA-NCAM expression. Figure 8A shows a representative histogram. The black filled histogram is the unstained control. The light blue striped histograms are the desflurane exposed cells, and the solid dark blue histograms are the control air exposed cells. Figure 8B shows the percentage of single cells expressing PSA-NCAM after exposure to desflurane or control air. The data is pooled from three experiments. The experiments were repeated three times independently. Consistent with the immunocytochemistry data, the flow cytometry analysis (Figure 8) illustrates that 24-h desflurane exposure reduced the number of positively labeled PSA-NCAM cells, suggesting the reduction/damage of the developing neurons.

Discussion

NSC culture is a key tool that can be used to assess potential anesthetic-induced neurotoxicity [13, 14]. Here, we used NSCs derived from fetal monkey multipotent stem cells to create a vitro model of the developing nervous system to study the

pathophysiology of neurodegeneration associated with anesthetic (such as desflurane)-induced neurotoxicity [28]. Our data demonstrated that cultured monkey NSCs can proliferate on a dish and differentiate into neural cells (including neurons and glial cells). Our data highlights the effectiveness of the nonhuman primate NSC model to study anesthetic (e.g., desflurane)-induced neurotoxicity in the developing CNS.

Links between anesthesia exposure in developing brains and subsequent cognitive deficiencies have been identified in many pre-clinical studies [30–32]. Pre-clinically, both cell-culture and animal studies [11–14, 21] suggest that anesthetics may cause neural apoptosis, caspase activation, neurodegeneration, neuroinflammation, and ultimately, deficits in cognition. Desflurane is not often used for induction of anesthesia in children due to its potent airway irritant properties, which can lead to coughing, laryngospasm, and other complications. However, it can be used for maintaining anesthesia in children. Previously, an animal study in neonatal and adult mice demonstrated that desflurane exposure induced more neural apoptosis in neonatal mice compared to sevoflurane and isoflurane [33]. Further, adult mice exposed to desflurane demonstrated greater impairments in working memory compared to adult mice exposed to sevoflurane and isoflurane. It is important that any potentially deleterious side effects of anesthetics be elucidated and properly addressed. In the present study, the short-term or prolonged exposure of NSCs to a clinically relevant concentration of desflurane did not affect NSC proliferation and viability, suggesting NSCs are not sensitive to anesthetic-induced neurotoxicity. In contrast, the developing neurons were vulnerable to desflurane. The possible reason for the vulnerability may be due to the expression of GABA_A receptors on neurons. Our previous data demonstrated that no GABA_A receptor immuno-reactive staining was detected on nestin-positive NSCs (lacking physiological activation). However, strong immunoreactive staining for the GABA_A receptor was observed on neurons that were differentiated from NSCs [13]. Therefore, after differentiation, prolonged exposure to desflurane caused significant elevation of neuronal cell death and changes in cytokine levels, providing evidence that neuronal cells are a more vulnerable cell population than uncommitted NSCs to anesthetic-induced adverse effects in the developing nervous system.

Numerous preclinical animal studies suggest some evidence of neurotoxicity of volatile anesthetics [30, 34–36]. Moreover, numerous *in vivo* studies using a variety of models have demonstrated the potential of cognitive/developmental issues in children exposed to early-life anesthesia [35–37]. These concerns are balanced by a risk–benefit analysis. Currently, it is unknown if the *in vitro* models used here will have similar baseline and cell signaling (molecules) responses to desflurane exposure (short or prolonged) and alter developing neuronal transmission systems in corresponding *in vivo* models. Previously, neuroleptic anesthesia with a surgical insult (splenectomy) in rats resulted in signs of CNS

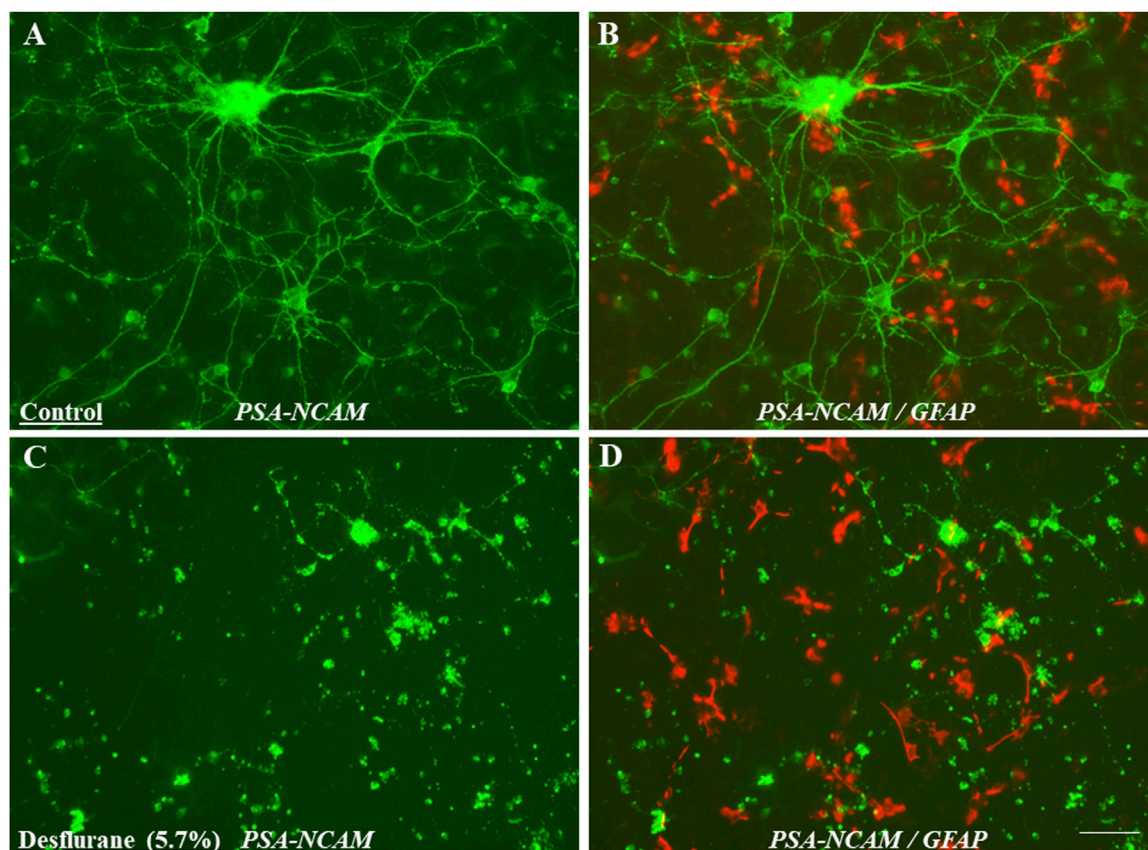


FIGURE 7

Differentiated neural cells with multiple processes and a clear neural network (cellular interactions facilitated through contact between cellular protrusions) could be observed after 5 days differentiation. Morphologically defined neurons were positively stained with monoclonal PSA-NCAM (neuron specific marker) antibody (A). However, the number of PSA-NCAM positive neurons was obviously reduced in desflurane-exposed (prolonged) cultures. PSA-NCAM expression in desflurane group was exhibiting typically condensed residue pieces, fragmentation and shrinking profiles [(C); green] compared with control [(A); green]. In contrast, GFAP labeled astrocytes were not remarkably affected in the desflurane group [(D); red], compared with control group [(B); red].

inflammation and cognitive impairment on the first and third postoperative days, whereas control and anesthesia-only groups showed neither inflammatory changes nor behavioral effects [37]. Also, our previous *in vivo* studies [22] demonstrated that at a clinically relevant dosage, inhaled anesthetics (e.g., sevoflurane) induced and maintained a stable surgical anesthesia status in postnatal day 5 monkeys, and prolonged sevoflurane exposure resulted in significant alterations in gene expression profiles, cytokine secretion, lipid composition, and neuronal cell death. These data/findings are consistent with the view that prolonged exposure to inhaled agents could stimulate an inflammatory reaction in the CNS, which may contribute to cell death or other lasting negative consequences of early-life exposure to anesthesia.

Cytokines, key modulators of inflammation, are signaling molecules and are produced in response to invading pathogens [38–41]. It is well known that cytokines mediate neuronal and glial cell function to facilitate neuronal regeneration or

neurodegeneration, and cytokine dysregulation is linked to microglial activation, neuroinflammation, neuronal damage, and cognitive deficits. In the present study, prolonged desflurane exposure of differentiated neural cells increased levels of multiple cytokines, including G-CSF, IL-12, IL-9, IL-10, and TNF- α , compared with controls. Neuroinflammation could play critical roles in the pathogenesis after longer durations of inhaled anesthetic exposure [22, 42]. Thus, altered cytokines could primarily be responsible for the development of increased neuroinflammation, and subsequent neuronal damage. Our data indicated that an enduring increase in systemic inflammatory cytokines (pro and anti-inflammatory cytokine accumulation) may occur after desflurane exposure. Elevated neurodegeneration after prolonged anesthetic exposure may involve an imbalance of pro- and anti-inflammatory cytokines [37, 42]. Since disturbed proinflammatory cytokines, especially TNF- α , have a fundamental role in modulating inflammation and could be responsible for a diverse range of signaling events within

Intensity of Polysialic Acid Neural Cell Adhesion Molecule (PSA-NCAM) *Flow cytometry*

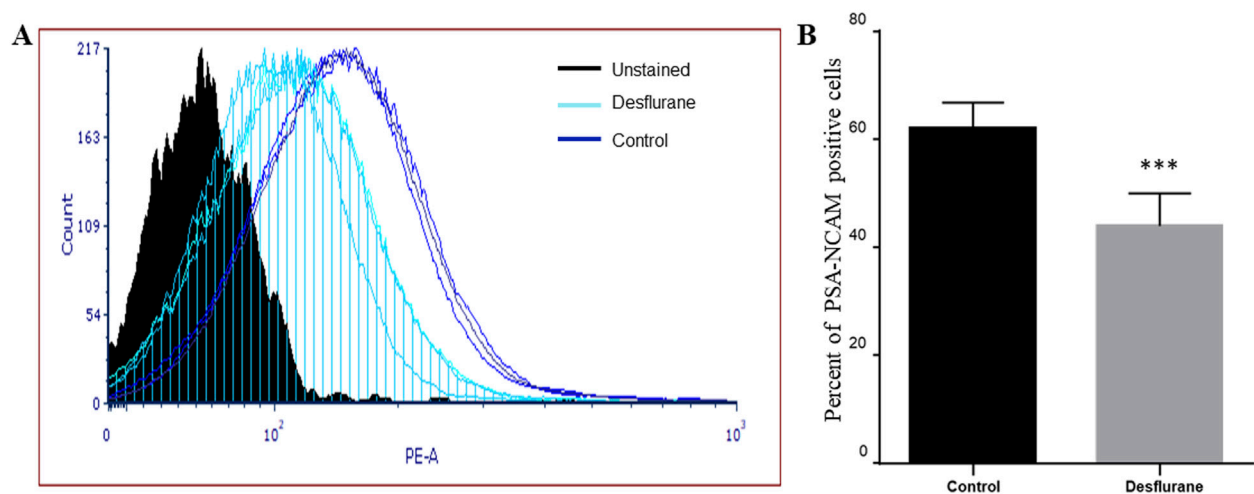


FIGURE 8

Representative flow cytometry histogram, normalized to mode, of PSA-NCAM staining. The black filled histogram is the unstained control. The light blue striped histograms are the desflurane exposed cells, and the solid dark blue histograms are the control air (delivery mixed air) exposed cells (A). The percentage of single cells expressing PSA-NCAM after exposure to desflurane or control air is shown (B). Our data indicated that prolonged (24 h) desflurane exposure at clinically relevant concentration specifically resulted in PSA-NCAM diminished expression. The data were pooled from three independent experiments. *** $p < 0.0001$.

cells, leading to cell damage/death, it is tempting to speculate the potential of anti-proinflammatory drugs (and/or antibodies) to ameliorate/preclude anesthetic-induced neurotoxicity.

It has been reported that exposure to inhaled anesthetics produced transient changes in dendritic spine density in the developing brain [43], which may result in lasting changes to synaptic ultrastructure [44]. Longer durations of inhaled anesthetic exposure could inhibit LTP [45], and prolonged sevoflurane exposure decreased survival of neurons [46]. PSA-NCAM is a specific marker for developing neurons [21, 22]. Ultrastructural studies showed that during early development the polysialylated form of NCAM is expressed by growth cones, neuronal processes, and neuronal bodies [27, 47]. In the current study, substantial downregulation of PSA-NCAM expression was observed on the neuronal surface and their processes in prolonged desflurane-exposed neurons. In contrast, no significant differences including the number, size, form, and distribution of GFAP labeled astrocytes were observed between desflurane-exposed and control (mixed delivery air) cultures. Our flow cytometry analysis provided quantitative information on a reduced number of developing neurons and downregulation of PSA-NCAM expression levels with desflurane (24 h) exposure versus their control. These results highlight that differentiated neurons, not glia, are the most vulnerable cell population to prolonged desflurane-induced toxicity. In fact, PSA-NCAM is of protective interest/effect for its key role in promoting neuritogenesis and synaptic plasticity. Altered PSA-NCAM

expression levels could result in significant changes in synaptic activity, synaptic formation, and synaptic remodeling [27, 48, 49], and consequently neuronal damage. Also, synaptic pruning and subsequent neuronal loss, whether by programmed cell death or necrosis, are critical to plasticity and stabilization of circuits in the developing nervous system and these are active processes that are tightly controlled by neurotrophins signaling mechanisms to ensure normal development and facilitate synaptic plasticity [50]. Previously, it was reported that PSA-NCAM interacts with NMDA-type glutamate receptors [51, 52]. PSA-NCAM could prevent glutamate-induced cell death [52] by restraining the signaling through GluN2B-containing NMDA receptors and regulating GluN2B-mediated Ca^{2+} influx in CA1 pyramidal cells in hippocampal slices [53]. It should be noted that PSA-NCAM may increase the sensitivity of neurons to brain derived neurotrophic factor (BDNF) and ciliary neurotrophic factor (CNTF) [54]. Also, PSA-NCAM could induce the activation of fibroblast growth factor receptor 1 (FGFR1) [55], and FGFR1/FGFs could critically impact retinal ganglion cells (RGCs; bridging neurons that connect the retinal input to the visual processing centers) survival [56]. Therefore, the dysregulated PSA-NCAM expression, after prolonged desflurane exposure, could suggest: 1) early neurodegeneration, 2) interruption of synaptic communication, 3) functional and/or behavioral deficits, 4) altered neuronal viability and plasticity, and 5) a target molecule in dissecting underlying mechanisms associated with prolonged anesthetic-induced neurotoxicity on uncommitted NSCs and differentiated neuronal cells. Collectively, the present

study demonstrated that prolonged desflurane-induced downregulation/shedding of PSA-NCAM was closely related to the observed loss/damage of developing neurons.

It should also be mentioned that the VitroCell system used for toxicological testing of desflurane has some limitations. For example, 1) although temperature and humidity of the test have been conditioned and well controlled to meet specific requirements of the cell cultures, owing to the complexity of the physical processes governing desflurane transport and deposition, the submersed state of a cell culture is not exactly/absolutely representative of the situation in the respiratory tract. And 2) although each treatment condition was assayed at least in triplicate and the experiments were repeated three times independently, toxicological testing of desflurane requires more experimental replicates than three replicates which matters to ensure/facilitate the correct amount of drug was applied to each well and in a reasonably uniform/consistent manner and should be addressed in our future desflurane studies.

Summary

Our findings suggest that at clinically relevant doses (5.7%) desflurane did not result in significant changes in NSC viability and NSC proliferation. In contrast, after differentiation, significantly elevated neuronal damage was detected after prolonged desflurane exposure. Our results indicated that an enduring increase in systemic inflammatory cytokines occurred after desflurane exposure, and the cytokine dysregulation could be a critical contributing factor to prolonged desflurane-induced neurotoxicity. In addition, the changes in PSA-NCAM expression confirmed the vulnerability of neurons in desflurane-induced neurotoxicity. Our experimental analyses provided quantitatively accurate and reproducible information regarding reduced neuronal viability and remarkable attenuation of PSA-NCAM levels after prolonged desflurane exposure.

Future work

Continued pre-clinical investigation may have significant impact on desflurane's clinical practice. Associated perturbations of the nervous system could be involved in blocking excitatory ion channels and increasing the activity of inhibitory ion channels. Since neural receptors/ion channels and PSA-NCAM expression levels, as well as calcium signaling, play crucial roles in receiving external signals and regulating intracellular signaling in numerous neurological processes, a study to monitor the baseline responsivity to neurotransmitters and changes in intracellular calcium concentrations would be informative for measuring states of cellular activity, neuronal viability and neuronal plasticity associated with anesthetic (desflurane)-induced neurotoxicity.

Author contributions

All authors listed have made a substantial, direct, and intellectual contribution to the work and approved it for publication.

Author disclaimer

This document reflects the views of its authors and does not necessarily reflect those of the United States Food and Drug Administration. Any mention of commercial products is for clarification only and is not intended as approval, endorsement, or recommendation.

Data availability

The raw data supporting the conclusions of this article will be made available by the authors, without undue reservation.

Ethics statement

The animal study was approved by NCTR/FDA Institutional Animal Care and Use Committee. The study was conducted in accordance with the local legislation and institutional requirements.

Funding

The author(s) declare that financial support was received for the research and/or publication of this article. This research was funded by the Food and Drug Administration.

Acknowledgments

We would like to thank Dr. Jacqueline Yeary for her assistance in performing cytokine assay/analysis, and Mr. Charles Matthew Fogle for his technical support.

Conflict of interest

The author(s) declared no potential conflicts of interest with respect to the research, authorship, and/or publication of this article.

Generative AI statement

The authors declare that no Generative AI was used in the creation of this manuscript.

References

1. Wilder RT, Flick RP, Sprung J, Katusic SK, Barbaresi WJ, Mickelson C, et al. Early exposure to anesthesia and learning disabilities in a population-based birth cohort. *Anesthesiology* (2009) **110**:796–804. doi:10.1097/01.anes.0000344728.34332.5d
2. Wei H, Kang B, Wei W, Liang G, Meng QC, Li Y, et al. Isoflurane and sevoflurane affect cell survival and BCL-2/BAX ratio differently. *Brain Res* (2005) **1037**:139–47. doi:10.1016/j.brainres.2005.01.009
3. Ikonomidou C, Bosch F, Miksa M, Bittigau P, Vöckler J, Dikranian K, et al. Blockade of NMDA receptors and apoptotic neurodegeneration in the developing brain. *Science* (1999) **283**:70–4. doi:10.1126/science.283.5398.70
4. Loepke AW, Istaphanous GK, McAuliffe JJ, 3rd, Miles L, Hughes EA, McCann JC, et al. The effects of neonatal isoflurane exposure in mice on brain cell viability, adult behavior, learning, and memory. *Anesth and Analgesia* (2009) **108**:90–104. doi:10.1213/ane.0b013e31818c8db29
5. Satomoto M, Satoh Y, Terui K, Miyao H, Takishima K, Ito M, et al. Neonatal exposure to sevoflurane induces abnormal social behaviors and deficits in fear conditioning in mice. *Anesthesiology* (2009) **110**:628–37. doi:10.1097/aln.0b013e3181974fa2
6. Stratmann G, May LD, Sall JW, Alvi RS, Bell JS, Ormerod BK, et al. Effect of hypercarbia and isoflurane on brain cell death and neurocognitive dysfunction in 7-day-old rats. *Anesthesiology* (2009) **110**:849–61. doi:10.1097/aln.0b013e31819c7140
7. Fredriksson A, Ponten E, Gordh T, Eriksson P. Neonatal exposure to a combination of N-methyl-D-aspartate and gamma-aminobutyric acid type A receptor anesthetic agents potentiates apoptotic neurodegeneration and persistent behavioral deficits. *Anesthesiology* (2007) **107**:427–36. doi:10.1097/01.anes.0000278892.62305.9c
8. Viberg H, Ponten E, Eriksson P, Gordh T, Fredriksson A. Neonatal ketamine exposure results in changes in biochemical substrates of neuronal growth and synaptogenesis, and alters adult behavior irreversibly. *Toxicology* (2008) **249**:153–9. doi:10.1016/j.tox.2008.04.019
9. O'Leary JD, Janus M, Duku E, Wijeyesundera DN, To T, Li P, et al. Influence of surgical procedures and general anesthesia on child development before primary school entry among matched sibling pairs. *JAMA Pediatr* (2019) **173**:29–36. doi:10.1001/jamapediatrics.2018.3662
10. Walkden GJ, Pickering AE, Gill H. Assessing long-term neurodevelopmental outcome following general anesthesia in early childhood: challenges and opportunities. *Anesth and Analgesia* (2019) **128**:681–94. doi:10.1213/ane.0000000000004052
11. Wang C, Fridley J, Johnson KM. The role of NMDA receptor upregulation in phencyclidine-induced cortical apoptosis in organotypic culture. *Biochem Pharmacol* (2005) **69**:1373–83. doi:10.1016/j.bcp.2005.02.013
12. Slikker W, Jr, Zou X, Hotchkiss CE, Divine RL, Sadovova N, Twaddle NC, et al. Ketamine-induced neuronal cell death in the perinatal rhesus monkey. *Toxicol Sci* (2007) **98**:145–58. doi:10.1093/toxsci/kfm084
13. Liu F, Patterson TA, Sadovova N, Zhang X, Liu S, Zou X, et al. Ketamine-induced neuronal damage and altered N-methyl-D-aspartate receptor function in rat primary forebrain culture. *Toxicol Sci* (2013) **131**:548–57. doi:10.1093/toxsci/kfs296
14. Liu F, Rainosek SW, Sadovova N, Fogle CM, Patterson TA, Hanig JP, et al. Protective effect of acetyl-L-carnitine on propofol-induced toxicity in embryonic neural stem cells. *Neurotoxicology* (2014) **42**:49–57. doi:10.1016/j.neuro.2014.03.011
15. Paule MG, Li M, Allen RR, Liu F, Zou X, Hotchkiss C, et al. Ketamine anesthesia during the first week of life can cause long-lasting cognitive deficits in rhesus monkeys. *Neurotoxicology and Teratology* (2011) **33**:220–30. doi:10.1016/j.ntt.2011.01.001
16. Talpos JC, Chelonis JJ, Li M, Hanig JP, Paule MG. Early life exposure to extended general anesthesia with isoflurane and nitrous oxide reduces responsiveness on a cognitive test battery in the nonhuman primate. *Neurotoxicology* (2019) **70**:80–90. doi:10.1016/j.neuro.2018.11.005
17. Raper J, De Biasio JC, Murphy KL, Alvarado MC, Baxter MG. Persistent alteration in behavioural reactivity to a mild social stressor in rhesus monkeys repeatedly exposed to sevoflurane in infancy. *Br J Anaesth* (2018) **120**:761–7. doi:10.1016/j.bja.2018.01.014
18. Nishikawa K, Harrison NL. The actions of sevoflurane and desflurane on the gamma-aminobutyric acid receptor type A: effects of TM2 mutations in the alpha and beta subunits. *Anesthesiology* (2003) **99**:678–84. doi:10.1097/00000542-200309000-00024
19. Zou X, Patterson TA, Divine RL, Sadovova N, Zhang X, Hanig JP, et al. Prolonged exposure to ketamine increases neurodegeneration in the developing monkey brain. *Int J Developmental Neurosci* (2009) **27**:727–31. doi:10.1016/j.jdevneu.2009.06.010
20. Wang C, Sadovova N, Fu X, Schmued L, Scallet A, Hanig J, et al. The role of the N-methyl-D-aspartate receptor in ketamine-induced apoptosis in rat forebrain culture. *Neuroscience* (2005) **132**:967–77. doi:10.1016/j.neuroscience.2005.01.053
21. Wang C, Sadovova N, Hotchkiss C, Fu X, Scallet AC, Patterson TA, et al. Blockade of N-methyl-D-aspartate receptors by ketamine produces loss of postnatal day 3 monkey frontal cortical neurons in culture. *Toxicol Sci* (2006) **91**:192–201. doi:10.1093/toxsci/kfj144
22. Liu F, Rainosek SW, Frisch-Daiello JL, Patterson TA, Paule MG, Slikker W, Jr, et al. Potential adverse effects of prolonged sevoflurane exposure on developing monkey brain: from abnormal lipid metabolism to neuronal damage. *Toxicol Sci* (2015) **147**:562–72. doi:10.1093/toxsci/kfv150
23. Kiss JZ, Rougon G. Cell biology of polysialic acid. *Curr Opin Neurobiol* (1997) **7**:640–6. doi:10.1016/s0959-4388(97)80083-9
24. Rougon G. Structure, metabolism and cell biology of polysialic acids. *Eur J Cell Biol* (1993) **61**:197–207.
25. Liu F, Liu S, Patterson TA, Fogle C, Hanig JP, Wang C, et al. Protective effects of xenon on propofol-induced neurotoxicity in human neural stem cell-derived models. *Mol Neurobiol* (2020) **57**:200–7. doi:10.1007/s12035-019-01769-5
26. Becker CG, Artola A, Gerardy-Schahn R, Becker T, Welzl H, Schachner M. The polysialic acid modification of the neural cell adhesion molecule is involved in spatial learning and hippocampal long-term potentiation. *J Neurosci Res* (1996) **45**:143–52. doi:10.1002/(sici)1097-4547(19960715)45:2<143::aid-jnr6>3.3.co;2-y
27. Wang C, Inselman A, Liu S, Liu F. Potential mechanisms for phencyclidine/ketamine-induced brain structural alterations and behavioral consequences. *Neurotoxicology* (2020) **76**:213–9. doi:10.1016/j.neuro.2019.12.005
28. Latham LE, Dobrovolsky VN, Liu S, Talpos JC, Hanig JP, Slikker W, Jr, et al. Establishment of neural stem cells from fetal monkey brain for neurotoxicity testing. *Exp Biol Med (Maywood)* (2023) **248**:633–40. doi:10.1177/15353702231168145
29. McInnis J, Wang C, Anastasio N, Hultman M, Ye Y, Salvemini D, et al. The role of superoxide and nuclear factor- κ B signaling in N-Methyl-D-aspartate-Induced necrosis and apoptosis. *The J Pharmacol Exp Ther* (2002) **301**:478–87. doi:10.1124/jpet.301.2.478
30. Jevtovic-Todorovic V, Benshoff N, Olney JW. Ketamine potentiates cerebrotectal damage induced by the common anaesthetic agent nitrous oxide in adult rats. *Br J Pharmacol* (2000) **130**:1692–8. doi:10.1038/sj.bjp.0703479
31. Olney JW, Wozniak DF, Jevtovic-Todorovic V, Farber NB, Bittigau P, Ikonomidou C. Drug-induced apoptotic neurodegeneration in the developing brain. *Brain Pathol* (2002) **12**:488–98. doi:10.1111/j.1750-3639.2002.tb00467.x
32. Olney JW, Young C, Wozniak DF, Jevtovic-Todorovic V, Ikonomidou C. Do pediatric drugs cause developing neurons to commit suicide? *Trends Pharmacol Sci* (2004) **25**:135–9. doi:10.1016/j.tips.2004.01.002
33. Kodama M, Satoh Y, Otsubo Y, Araki Y, Yonamine R, Masui K, et al. Neonatal desflurane exposure induces more robust neuroapoptosis than do isoflurane and sevoflurane and impairs working memory. *Anesthesiology* (2011) **115**:979–91. doi:10.1097/aln.0b013e318234228b
34. Culley DJ, Baxter MG, Crosby CA, Yukhananov R, Crosby G. Impaired acquisition of spatial memory 2 weeks after isoflurane and isoflurane-nitrous oxide anesthesia in aged rats. *Anesth analgesia* (2004) **99**:1393–7. doi:10.1213/01.ane.0000135408.14319.cc
35. Steinmetz J, Christensen KB, Lund T, Lohse N, Rasmussen LS, Group I. Long-term consequences of postoperative cognitive dysfunction. *Anesthesiology* (2009) **110**:548–55. doi:10.1097/aln.0b013e318195b569
36. Koblin DD. Characteristics and implications of desflurane metabolism and toxicity. *Anesth Analg* (1992) **75**:S10–6.
37. Wan Y, Xu J, Ma D, Zeng Y, Cibelli M, Maze M. Postoperative impairment of cognitive function in rats: a possible role for cytokine-mediated inflammation in the hippocampus. *Anesthesiology* (2007) **106**:436–43. doi:10.1097/00000542-200703000-00007
38. Dickson DW, Lee SC, Mattiace LA, Yen SH, Brosnan C. Microglia and cytokines in neurological disease, with special reference to AIDS and Alzheimer's disease. *Glia* (1993) **7**:75–83. doi:10.1002/glia.440070113
39. Wilson CJ, Finch CE, Cohen HJ. Cytokines and cognition--the case for a head-to-toe inflammatory paradigm. *J Am Geriatr Soc* (2002) **50**:2041–56. doi:10.1046/j.1532-5415.2002.50619.x

40. McGeer PL, McGeer EG. The inflammatory response system of brain: implications for therapy of Alzheimer and other neurodegenerative diseases. *Brain Res Rev* (1995) **21**:195–218. doi:10.1016/0165-0173(95)00011-9
41. Wu X, Lu Y, Dong Y, Zhang G, Zhang Y, Xu Z, et al. The inhalation anesthetic isoflurane increases levels of proinflammatory TNF- α , IL-6, and IL-1 β . *Neurobiol Aging* (2012) **33**:1364–78. doi:10.1016/j.neurobiolaging.2010.11.002
42. Wei H, Liang G, Yang H, Wang Q, Hawkins B, Madesh M, et al. The common inhalational anesthetic isoflurane induces apoptosis via activation of inositol 1,4,5-trisphosphate receptors. *Anesthesiology* (2008) **108**:251–60. doi:10.1097/01.anes.0000299435.59242.0e
43. Qiu L, Zhu C, Bodogan T, Gomez-Galan M, Zhang Y, Zhou K, et al. Acute and long-term effects of brief sevoflurane anesthesia during the early postnatal period in rats. *Toxicol Sci* (2016) **149**:121–33. doi:10.1093/toxsci/kfv219
44. Fehr T, Janssen WGM, Park J, Baxter MG. Neonatal exposures to sevoflurane in rhesus monkeys alter synaptic ultrastructure in later life. *iScience* (2022) **25**:105685. doi:10.1016/j.isci.2022.105685
45. Xiao H, Liu B, Chen Y, Zhang J. Learning, memory and synaptic plasticity in hippocampus in rats exposed to sevoflurane. *Int J Developmental Neurosci* (2016) **48**:38–49. doi:10.1016/j.ijdevneu.2015.11.001
46. Fang F, Xue Z, Cang J. Sevoflurane exposure in 7-day-old rats affects neurogenesis, neurodegeneration and neurocognitive function. *Neurosci Bull* (2012) **28**:499–508. doi:10.1007/s12264-012-1260-4
47. Butler AK, Uryu K, Morehouse V, Rougon G, Chesselet MF. Regulation of the polysialylated form of the neural cell adhesion molecule in the developing striatum: effects of cortical lesions. *J Comp Neurol* (1997) **389**:289–308. doi:10.1002/(sici)1096-9861(19971215)389:2<289::aid-cne8>3.0.co;2-y
48. Regan CM, Fox GB. Polysialylation as a regulator of neural plasticity in rodent learning and aging. *Neurochem Res* (1995) **20**:593–8. doi:10.1007/bf01694541
49. Ronn LC, Hartz BP, Bock E. The neural cell adhesion molecule (NCAM) in development and plasticity of the nervous system. *Exp Gerontol* (1998) **33**:853–64. doi:10.1016/s0531-5565(98)00040-0
50. Perouansky M, Hemmings HC, Jr, Riou B. Neurotoxicity of general anesthetics: cause for concern? *Anesthesiology* (2009) **111**:1365–71. doi:10.1097/aln.0b013e3181bf1d61
51. Bai N, Aida T, Yanagisawa M, Katou S, Sakimura K, Mishina M, et al. NMDA receptor subunits have different roles in NMDA-induced neurotoxicity in the retina. *Mol Brain* (2013) **6**:34. doi:10.1186/1756-6606-6-34
52. Hammond MS, Sims C, Parameshwaran K, Suppiramaniam V, Schachner M, Dityatev A. Neural cell adhesion molecule-associated polysialic acid inhibits NR2B-containing N-methyl-D-aspartate receptors and prevents glutamate-induced cell death. *J Biol Chem* (2006) **281**:34859–69. doi:10.1074/jbc.m602568200
53. Kochlamazashvili G, Senkov O, Grebenyuk S, Robinson C, Xiao MF, Stummeyer K, et al. Neural cell adhesion molecule-associated polysialic acid regulates synaptic plasticity and learning by restraining the signaling through GluN2B-containing NMDA receptors. *J Neurosci* (2010) **30**:4171–83. doi:10.1523/jneurosci.5806-09.2010
54. Hildebrandt H, Muhlenhoff M, Weinhold B, Gerardy-Schahn R. Dissecting polysialic acid and NCAM functions in brain development. *J Neurochem* (2007) **103**(Suppl. 1):56–64. doi:10.1111/j.1471-4159.2007.04716.x
55. Kiselyov VV, Skladchikova G, Hinsby AM, Jensen PH, Kulahin N, Soroka V, et al. Structural basis for a direct interaction between FGFR1 and NCAM and evidence for a regulatory role of ATP. *Structure* (2003) **11**:691–701. doi:10.1016/s0969-2126(03)00096-0
56. Blanco RE, Lopez-Roca A, Soto J, Blagburn JM. Basic fibroblast growth factor applied to the optic nerve after injury increases long-term cell survival in the frog retina. *J Comp Neurol* (2000) **423**:646–58. doi:10.1002/1096-9861(20000807)423:4<646::aid-cne9>3.0.co;2-u



OPEN ACCESS

*CORRESPONDENCE

Cheng Wang,
✉ cheng.wang@fda.hhs.gov

[†]These authors share first authorship

RECEIVED 28 March 2025

ACCEPTED 28 May 2025

PUBLISHED 25 June 2025

CITATION

Wang C, Sun J, Donakonda R, Beger R, Latham LE, Wu L, Liu S, Hanig JP and Liu F (2025) Assessing the developmental effects of fentanyl and impacts on lipidomic profiling using neural stem cell models.
Exp. Biol. Med. 250:10607.
doi: 10.3389/ebm.2025.10607

COPYRIGHT

© 2025 Wang, Sun, Donakonda, Beger, Latham, Wu, Liu, Hanig and Liu. This is an open-access article distributed under the terms of the [Creative Commons Attribution License \(CC BY\)](https://creativecommons.org/licenses/by/4.0/). The use, distribution or reproduction in other forums is permitted, provided the original author(s) and the copyright owner(s) are credited and that the original publication in this journal is cited, in accordance with accepted academic practice. No use, distribution or reproduction is permitted which does not comply with these terms.

Assessing the developmental effects of fentanyl and impacts on lipidomic profiling using neural stem cell models

Cheng Wang^{1*†}, Jinchun Sun^{2†}, Rohini Donakonda², Richard Beger², Leah E. Latham¹, Leihong Wu³, Shuliang Liu¹, Joseph P. Hanig⁴ and Fang Liu¹

¹Division of Neurotoxicology, National Center for Toxicological Research/FDA, Jefferson, AR, United States, ²Division of Systems Biology, National Center for Toxicological Research/U.S. Food and Drug Administration (FDA), Jefferson, AR, United States, ³Division of Bioinformatics and Biostatistics, National Center for Toxicological Research/FDA, Jefferson, AR, United States, ⁴Office of Pharmaceutical Quality, Center for Drug Evaluation and Research/U.S. Food and Drug Administration (FDA), Silver Spring, MD, United States

Abstract

Fentanyl is a potent and short-acting opioid that is often given to pediatric patients during surgery to relieve pain and as an adjunct to anesthesia. Its effects on the developing brain are yet to be determined. In the present study, commercially available human neural stem cells (NSCs) were used to model the effects of fentanyl on the developing human brain. We determined the dose dependent effects and temporal relationships between fentanyl exposures and NSC health, viability, and differentiation. Markers of mitochondrial health [3-(4,5-dimethylthiazol-2-yl)-2,5-diphenyltetrazolium bromide (MTT)] and cell death/damage [lactate dehydrogenase (LDH)] were monitored to determine the dose response effects of fentanyl on NSC viability. In addition, lipidomics analysis was conducted to investigate lipid profile changes in differentiated neural cells treated with fentanyl. Fentanyl did not cause a significant increase in LDH release, nor MTT reduction after 24-h exposure at concentrations of 0.5, 1.0, 3.0, 10, or 100 μ M, for both NSCs and differentiated neural cells. Lipidomics data showed the top 15 most variable important in projection (VIP) lipid species (the higher the VIP scores, the bigger changes in treated groups vs. controls), including lysophosphatidylcholines (LPCs), lysophosphatidylethanolamines (LPEs), ceramides (CER), cholesterol esters (ChEs) and sphingosine (SPH). The lipidomic data indicate that LPC (16:0), LPC (16:1), LPC (18:1), CER (d18:0_22:0), CER (d18:2_18:0), CER(d18:2_24:1) were significantly increased, and only ChE (24:5) and SPH (d18:1) were significantly decreased in the highest dose group versus control. These data indicated that fentanyl exposure (24-h) did not induce detectable cell death. However, a lipidomic analysis indicated that fentanyl may affect immature neural cell functions through modifying lipid

composition and lipid metabolism. These data indicated that despite the absence of clear neurodegeneration, fentanyl may still have a negative impact on the developing brain.

KEYWORDS

development, fentanyl, lipidomic analysis, anesthetics, neurotoxicity

Impact statement

Opioids, such as fentanyl, are used as pediatric analgesics in pain management. Our data indicate/provide important information to understand how to continue to use these medications safely. In the present study, advanced lipidomic analysis using ultra-high-performance liquid chromatography coupled with high-resolution mass spectrometry was utilized to investigate underlying mechanisms and the impacts of different doses of fentanyl on NSCs and neural cells differentiated from NSCs. Although markers of neurotoxic assays showed that no detectable cell death occurred after fentanyl exposure at micromolar concentrations for 24 h, lipidomic analysis indicated that fentanyl may affect immature neural cell functions through modifying lipid composition and lipid metabolism. These data indicated that despite the absence of clear neurodegeneration, fentanyl may still have a negative impact on the developing brain, and changes in lipid composition may help explain the progression of neurodegeneration and could ultimately provide therapeutic/neuroprotective potential.

Introduction

Opioids, including natural compounds, semi-synthetic and synthetic derivatives, are used as analgesics in pain management [1]. Children may be prescribed opioids to control severe pain resulting from their operations or injuries [2]. Opioids decrease severe pain by blocking pain signals in the brain and spinal cord [3]. Public concerns of prescription opioids include misuse, abuse, addiction, overdose, and death from respiratory depression [4, 5]. Also, fatal poisonings from opioid overdoses are increasing among children and teens [6]. It is important to understand how to continue to use these medications safely.

The most prescribed opioid analgesic (non-oral) in pediatric hospitalizations is fentanyl [7, 8]. Fentanyl is a lipid-soluble synthetic opioid and a strong mu receptor agonist with less respiratory suppression compared to morphine [9, 10]. It is a potent, short-acting opioid medication that is often given to pediatric patients during surgery to relieve pain and as an adjunct to anesthesia [6]. Despite the frequency of its use in young children, little is known about the effects of fentanyl on the developing brain.

Due to the complexity and temporal dynamics of the developing nervous system, it is difficult to determine the adverse effects of fentanyl on human infant and children brain development [11–16]. However, application of highly relevant preclinical models, such as NSCs derived from humans, might serve as a bridging model to evaluate the sensitivity/vulnerability of the developing nervous system, and to address FDA's regulatory needs.

Human NSCs can mimic or model particular developmental stages of the human brain, thus, providing a valuable model for conducting systematic dose-dependent response and time-course studies. Application of this approach may reduce the number of animals, and the amount of time/money required for developmental neurotoxicity assessments. In this study, commercialized hippocampus (HIP) NSCs from a fetal human brain were used to evaluate the vulnerability of the developing nervous system. The transformation of NSCs to neurons and glial cells occurs in two basic steps: 1) undifferentiated and proliferative NSCs replicate to form small clusters of cells; and 2) differentiation into neurons, astrocytes, and oligodendrocytes. Our previous data demonstrated that NSC viability and their ability to self-renew could be affected when NSCs were exposed to general anesthetics at relatively high concentrations [12], suggesting NSCs may be a good platform for evaluating developmental neurotoxicity. Markers of mitochondrial health (MTT Assay) and cell death/damage (LDH Release) were monitored to determine the dose-related effects of fentanyl on NSCs and differentiated cells.

General anesthetics (including a range of structurally diverse inhaled and injectable compounds) are highly lipid soluble and can dissolve in every membrane, penetrate organelles, and interact with numerous cellular constituents. Their actions have long been considered rapid and fully reversible, within the pharmacodynamic time course of anesthesia [17]. Although in most patients physiologic homeostasis is restored soon after general anesthesia, anesthetics have potentially profound and long-lasting effects that, in animal models, seem particularly consequential in specific developmental periods and pathophysiologic contexts [17]. Lipids are essential for cellular functioning considering their role in membrane composition, signaling, and energy metabolism. Neural cells contain a wide variety of lipid classes and lipid species in the brain. Abnormal lipid constitution and changes in their metabolic rates could be related to earlier stages of neural

degenerative disorders and neural damage [11, 18–20]. In the central nervous system (CNS) lipid dysregulation has been linked to etiology, progression, and severity of neurodegenerative diseases/disorders including prolonged anesthetic-induced neurotoxicity [11–13]. Thus, changes in lipid composition may help explain the progression of neurodegeneration and could ultimately provide therapeutic/neuroprotective potential [11, 18, 21]. In the present study, lipidomic analysis using ultra-high-performance liquid chromatography (UHPLC) coupled with high-resolution mass spectrometry (HRMS) was utilized to investigate underlying mechanisms and the impacts of different doses of fentanyl on NSCs and neural cells differentiated from NSCs.

Materials and methods

Test chemicals

Fentanyl was purchased from Sigma Aldrich (St. Louis, MO), and freshly dissolved in culture media (VESTA Biotherapeutics) upon the experiments.

Cultures

Commercially available, de-identified human NSCs derived from human fetal brains were utilized (VESTA Biotherapeutics). Media for NSC proliferation (named Neural StemCell Growth Medium) and for NSC differentiation (named Neural Differentiation Medium) were purchased from the same vendor (VESTA Biotherapeutics). The cells were seeded on laminin-coated dishes. Briefly, cultured cells on slides or in flasks were placed in a low oxygen (5% oxygen) culture incubator with humidified air and 5% carbon dioxide at 37°C. The culture media was changed every 3 days. The concentrations of oxygen and carbon dioxide in the chamber were continuously monitored. Control experiments were performed in the same manner. Cultured NSCs and/differentiated neural cells were exposed to fentanyl at 0.5, 1, 3, 10, and 100 µM [22] respectively, for 24 h.

Assessment of neurotoxicity

MTT assay

The MTT dye is metabolized by viable mitochondria forming a colored product that can be dissolved in dimethyl sulfoxide (DMSO) and detected photometrically. Thus, the extent of MTT metabolism is an indicator of mitochondrial function. Briefly, after the removal of media for use in the lactate dehydrogenase (LDH) assay, 100 µL MTT (5 mg/10 mL of medium) was added to each well, and the plate was incubated for 2 h at 37°C. The MTT solution

was removed and followed by the addition of 100 µL of DMSO to each well. The color intensity was assessed with a plate reader at 590 nm, as previously described [14, 23].

LDH release

LDH is a cytoplasmic enzyme retained by viable cells with intact plasma membranes. The release of LDH into the cell culture medium occurs with loss of plasma membrane integrity, a process most often associated with acute cell death [12]. After exposure (24 h) to different concentrations of fentanyl, the media were collected and assayed for LDH activity using a cytotoxicity detection kit from Roche Applied Science (Indianapolis, IN). Briefly, LDH catalyzes the conversion of lactate to pyruvate upon reduction of NAD⁺ to NADH/H⁺; the added tetrazolium salt (yellow) is then reduced to formazan (red). The amount of formazan formed correlates to LDH activity. The formazan product was measured with a plate reader at 490 nm, as previously described [14, 23].

Lipidomic methods

Sample preparation (lipid extraction)

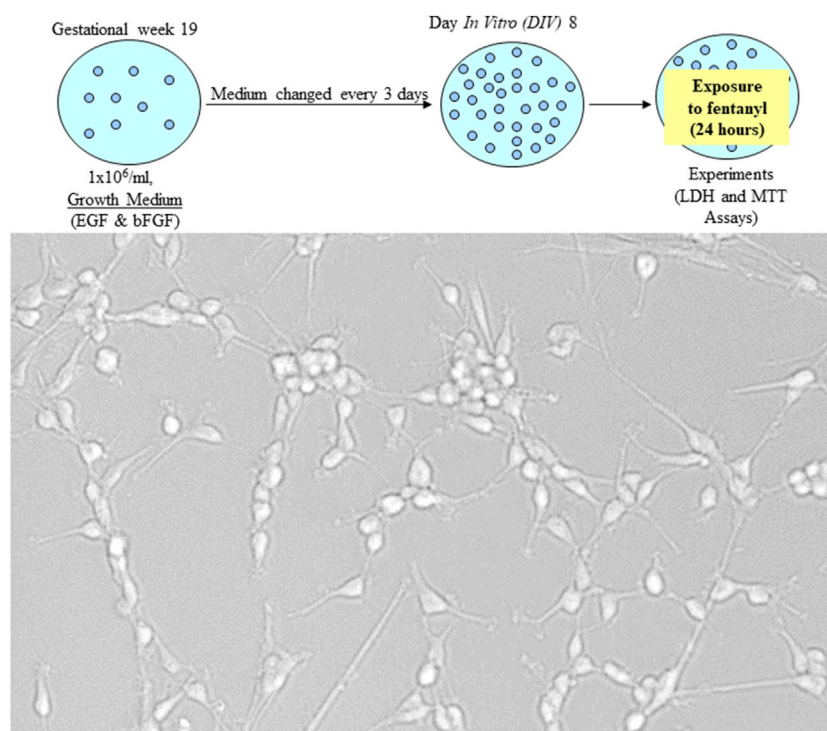
Protein content was used to normalize the determined lipid levels for the individual samples. LC/MS grade water (1 mL) was added to the Eppendorf tube containing differentiated cells (~1 M counts), followed by vortexing for 40 s. The cell suspension was then transferred to glass tubes for lipid extraction. Lipid extraction was achieved using a modified version of the Bligh and Dyer extraction protocol [24], whereby 2 mL methanol and 0.9 mL dichloromethane (DCM) were added to the 1 mL cell suspension and mixed gently, but thoroughly for 5 s. Aliquots of stable internal standard mixtures-SPLASH® Lipidomix® Mass Spec Standard, which contained 14 individual isotope-labeled standards that cover 14 lipid classes, were spiked into all samples. Following two rounds of extraction, the bottom layers were combined and dried under nitrogen flow and reconstituted in 1 mL ethanol and centrifuged just prior to analysis.

Quality control in open-profiling lipidomics

Pooled lipid extracts were run every 10 sample injections by UHPLC/Exploris 240 MS to monitor the analytical equipment variability, also were used for data filtering as described in the raw data analysis.

UHPLC/HRMS analysis

Lipid extract (4 µL) was separated using a Thermo Accucore C30 column on a Thermo Vanquish Ultimate 3000 UPLC (Thermo Scientific, Waltham, MA). Chromatography was operated at a flow rate of 0.4 mL/min, and the column was maintained at 40°C during a 30 min gradient. The mobile phase consisted of solvent A (5 mM ammonium formate in 60%

**FIGURE 1**

NSCs are multipotent cells in the nervous system. They have the features of being able to self-renew and give rise to differentiated progenitor cells to generate lineages of neurons as well as glia, such as astrocytes and oligodendrocytes. Human NSCs were seeded at a cell density of 1×10^6 /mL. When the cultures were maintained in the growth medium, the bipolar NSCs continuously proliferated.

acetonitrile with 0.1% formic acid) and solvent B (5 mM ammonium formate in 10% acetonitrile and 90% isopropanol with 0.1% formic acid). Lipids were eluted using linear gradients of 40–55% solution B from 0 to 7 min, 55–65% solution B from 7 to 8 min, maintained at 65% B until 12 min, 65–95% solution B from 12 to 20 min, 95–100% solution B from 20 to 22 min and maintained at 100% B until 27 min, and finally returned to 40% B at 27.1 min.

Mass spectrometric (MS) data were collected with a Thermo Orbitrap Exploris 240 mass spectrometer (Thermo Scientific, Waltham, MA) operated in positive and negative ionization electrospray modes. Data were acquired in full-scan mode (m/z 70–1,000) at a resolution of 120,000 for all samples. The capillary voltage was set to 3.5 kV for positive ionization mode and 2.5 kV for negative ionization mode. Other parameters used for the data collection were an ion transfer tube temperature of 325°C, a vaporizer temperature of 350°C, sheath gas (arb) 50, auxiliary gas (arb) 10, and sweep gas (arb) 1. Internal mass calibration EASY-IC was used for mass accuracy. MS/MS data was collected in a sequence of separate runs operated by the intelligence-driven software AcquireX (Thermo Scientific) to acquire more MS/MS spectra from the detected ion features than data-dependent acquisition. The raw data were processed using LipidSearch

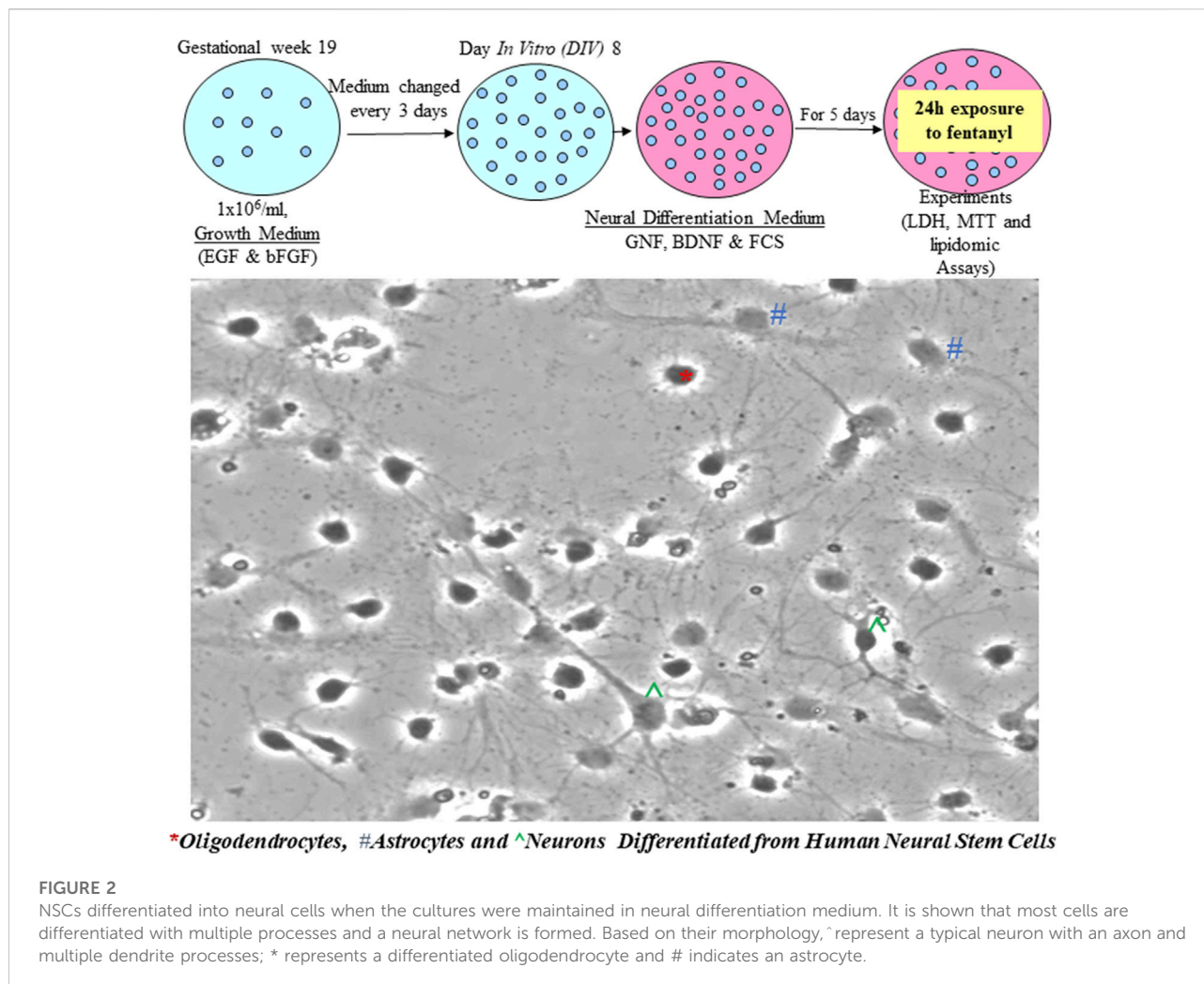
(vers. 5.0; Thermo Scientific). Data were filtered using pooled QC samples based on the following criteria: *i*) ions with %RSD less than 30% in the pooled QC samples were included, *ii*) ions present in $\geq 70\%$ of QC samples were included.

Statistical analysis

Each condition/experiment, including lipidomics, was assessed in triplicate, and experiments were repeated three times independently. For the LDH and MTT assays, statistical analyses were performed, and graphs generated using SigmaPlot. Data were analyzed using one-way ANOVA followed by Dunnett's *post hoc* test and expressed as mean \pm SD. Significance was considered at a p value < 0.05 .

For lipidomics, the resulting dataset from LipidSearch processing was further analyzed by supervised partial least squares discriminant analysis (PLS-DA) using MetaboAnalyst v. 6.0¹ [25]. The values in the treated group were compared to their

¹ www.metaboanalyst.ca



respective control group, as mean \pm SD. A value of $p < 0.05$ from the unpaired t -Test was considered statistically significant. Lipid intensity data was log-transformed prior to PLS-DA. Repeated measures ANOVA were performed using MetaboAnalyst v. 6.0¹.

Results

Characterization of the *in vitro* models

The cultured NSCs were typically bipolar in shape. More and more cells were generated and gathered when the cultures were maintained in NSC growth media, demonstrating their capability of proliferation (Figure 1).

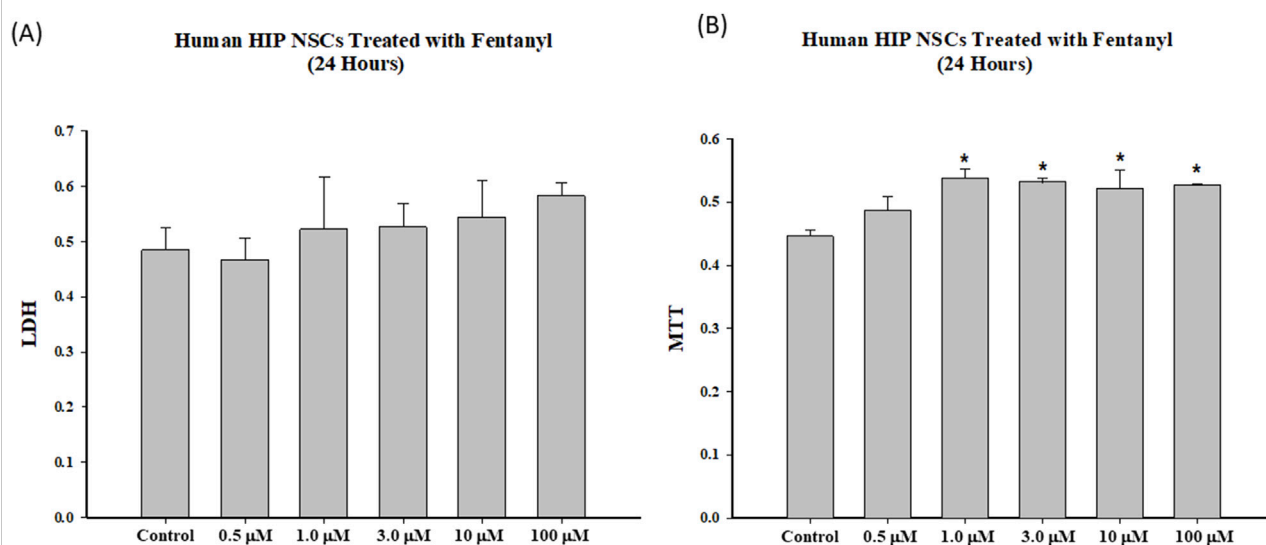
Given the importance of NSC differentiation in the assessment of fentanyl-induced adverse effects/cell viability, starting from day *in vitro* 8 (DIV 8), NSCs were cultured in neural differentiation medium. After 5-day of differentiation, the differentiated neural/neuronal cells showed multiple processes, and a typical neural

network was formed (Figure 2). Meanwhile, differentiated neurons, astrocytes, and oligodendrocytes (derived from human NSCs) could be morphologically identified (Figure 2).

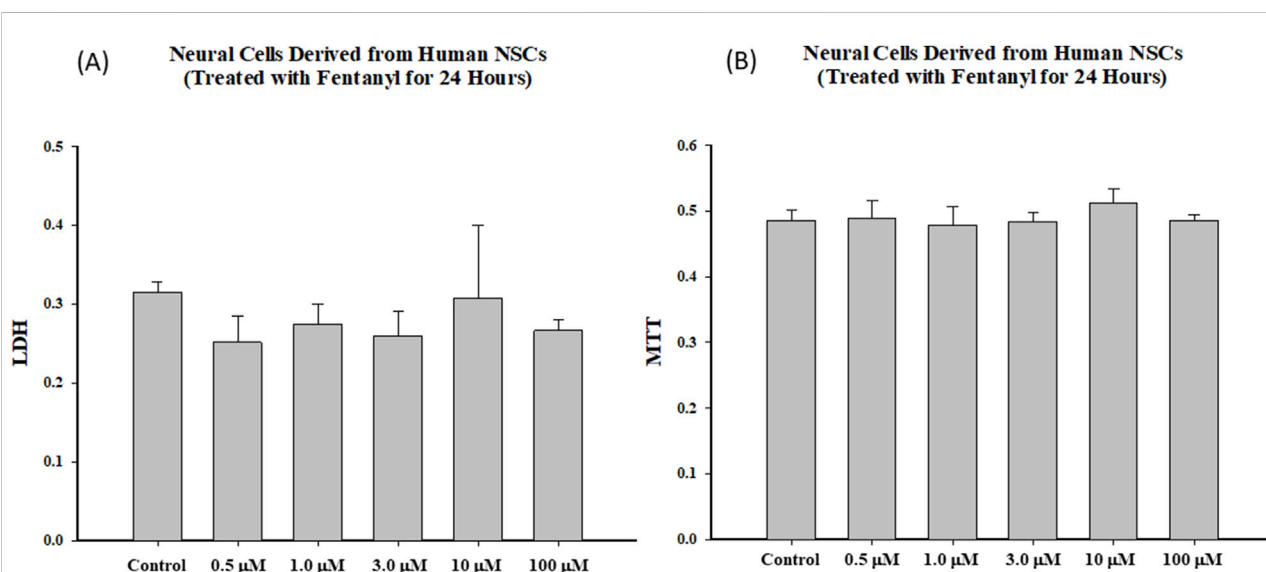
Cytotoxicity of fentanyl on NSCs and/or differentiated neural cells

The LDH assays demonstrated that 24-h fentanyl exposure of NSCs at concentrations of 0.5, 1.0, 3.0, 10 or 100 μ M resulted in a subtle, but a non-significant increase in the release of LDH into the cell culture medium. No significant MTT reduction was observed when the cultured NSCs were exposed to any of these five concentrations of fentanyl compared with controls (Figure 3). In contrast, 24-h fentanyl exposure at concentrations of 1.0, 3.0, 10 or 100 μ M caused an elevation of MTT uptake (Figure 3).

Markers of cell death/damage were also used to assess the dose response effects of fentanyl exposure on the viability of

**FIGURE 3**

To determine the dose response effects and temporal relationships of fentanyl on cell viability, NSCs were exposed to fentanyl for 24 h at concentration of 0.5, 1.0, 3.0, 10 or 100 μM. Fentanyl exposure resulted in a slight dose-related increase (not significant) in the release of LDH (A) into the cell culture medium, compared with controls. No reduction in MTT (B) was observed in the fentanyl exposed group, compared with controls.

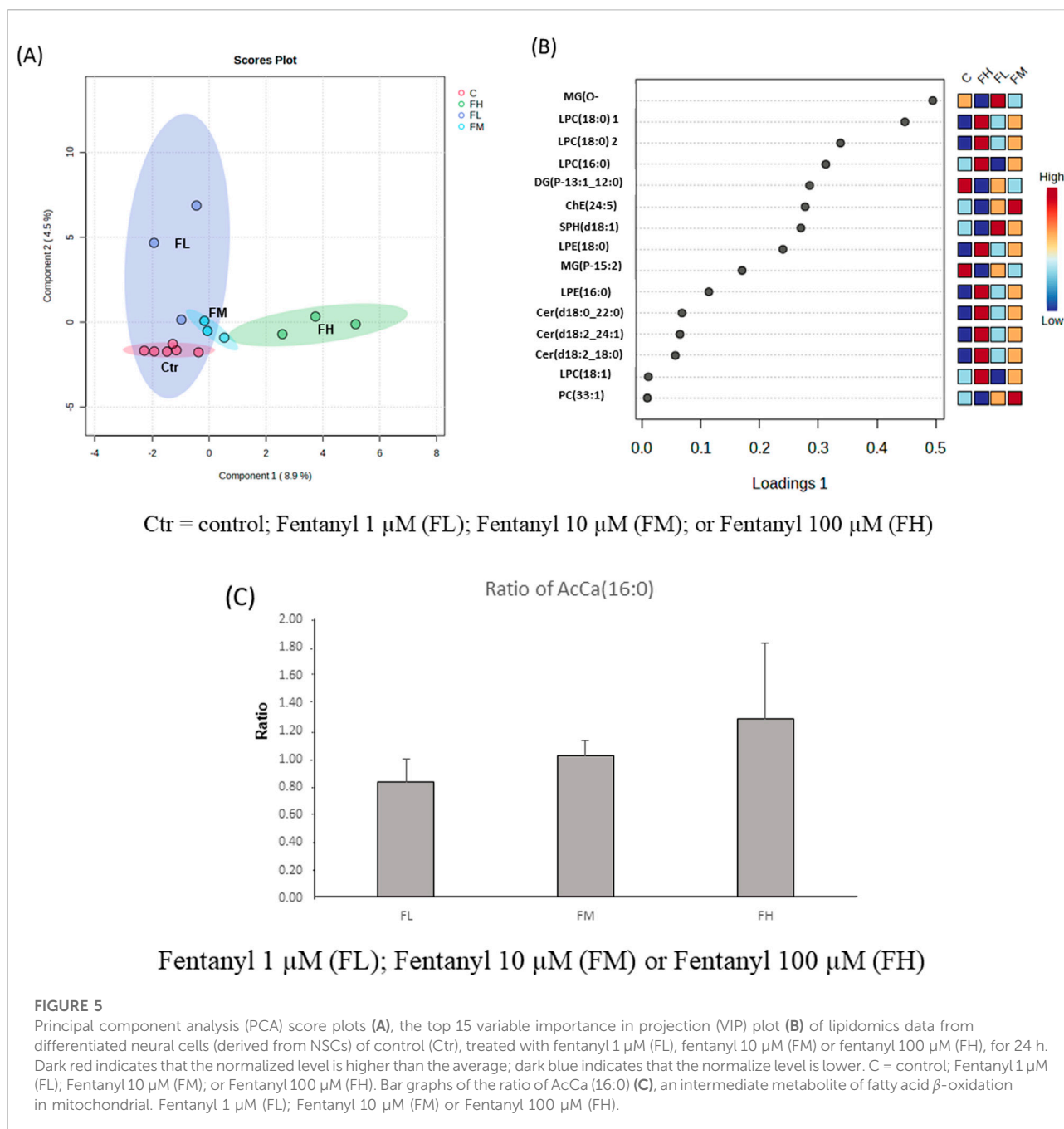
**FIGURE 4**

Exposure of differentiated cells to fentanyl for 24 h did not lead to changes in LDH release (A) or MTT reduction (B). Each treatment condition was assessed at least in triplicate, and experiments were repeated three times independently.

differentiated neural cells. Like NSCs, fentanyl did not produce a remarkable increase in the release of LDH or a significant decrease of MTT uptake in the differentiated neural cells after 24-h exposure, compared with control (Figure 4). Each treatment condition was assayed at least in triplicate and the experiments were repeated three times independently.

Lipidomic data

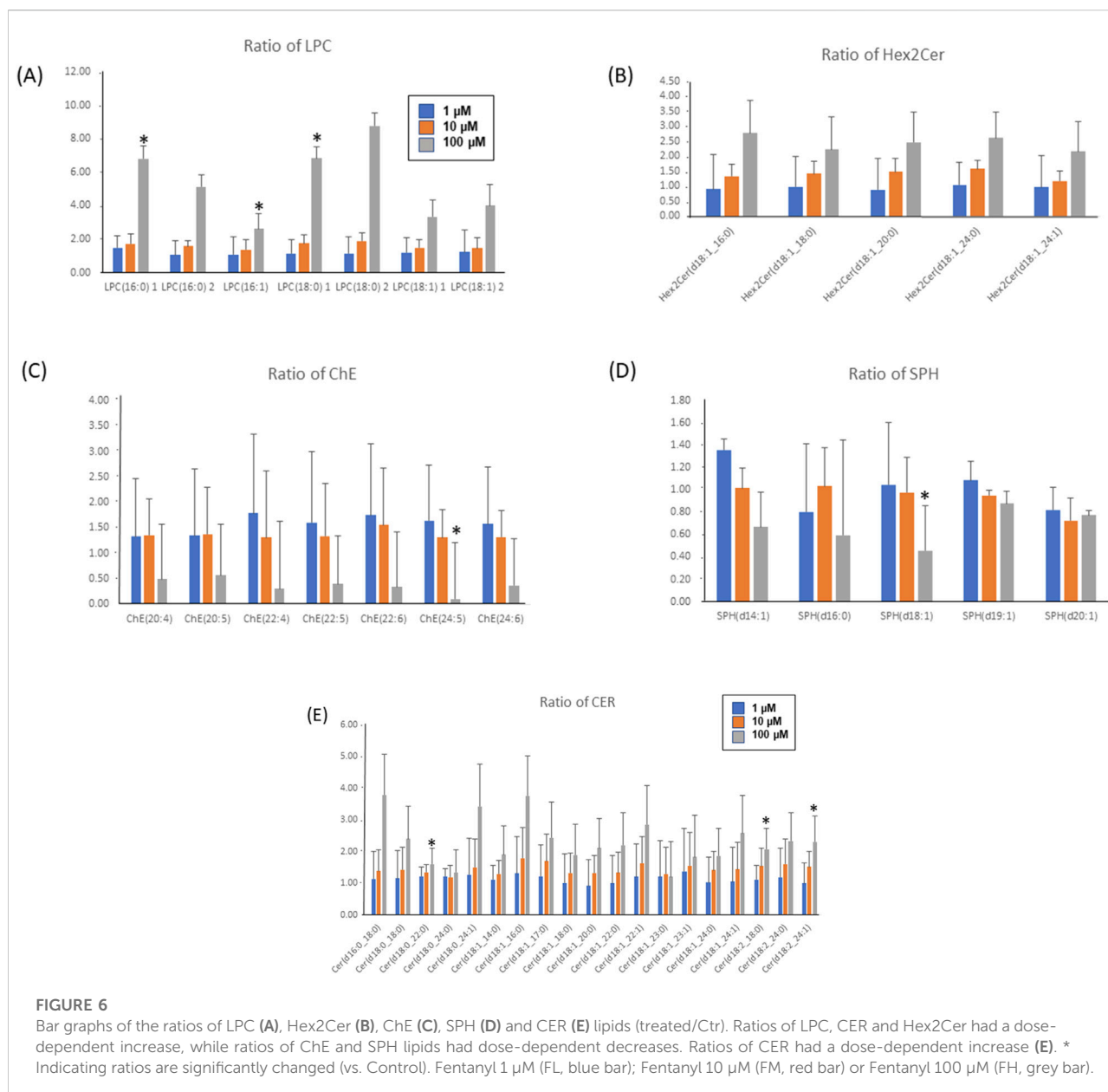
In total, 919 lipid species from 20 lipid classes were detected from differentiated cells treated with vehicle (Control, $n = 6$), or 1 μM (FL, $n = 3$), 10 μM (FM, $n = 3$) or 100 μM (FH, $n = 3$) fentanyl for 24 h (the experiments were repeated three times independently).



The Partial Least Squares Discriminant Analysis (PLSDA) effectively distinguishes between control and fentanyl-treated groups, and the high-dose group (FH) is located furthest from the control group (Figure 5A). The top 15 most variable important in projection (VIP) lipid species (based on VIP scores), which are responsible for the group separations, included LPC (16:0), LPC (16:1), LPC (18:1), CER (d18:0_22:0), CER (d18:2_18:0), CER(d18:2_24:1) which were significantly increased, while ChE (24:5) and SPH (d18:1) significantly decreased (Figure 5B). Despite these

alterations, palmitoyl carnitine levels, indicative of mitochondrial function, remained unaffected by fentanyl exposure (Figure 5C), aligning with the findings from the MTT assays that showed no detectable mitochondrial damage after fentanyl exposure.

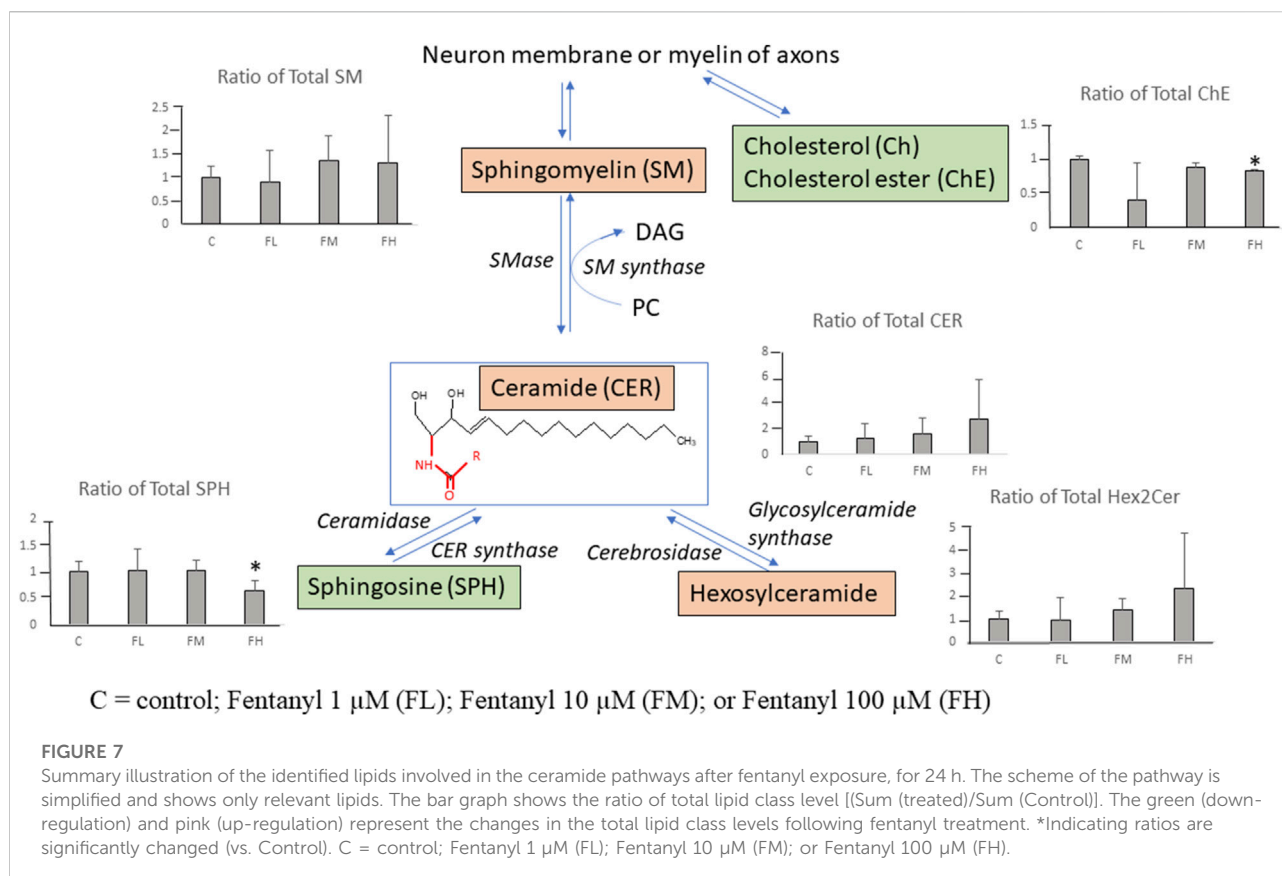
In Figure 6, the bar graphs delineate the dose-responsive modulation of lipid species upon fentanyl exposure, showcasing significant increments in LPCs (Figure 6A), CERs (Figure 6E), and di-hexosylceramides (Hex2Cer, Figure 6B), with the high-dose group (FH) demonstrating



more than a twofold increase compared to the controls. Conversely, cholesterol esters (ChEs, Figure 6C) and sphingosines (SPHs, Figure 6D) manifest dose-dependent down-regulations, with reductions exceeding twofold in the high-dose scenario (Supplementary Table S1). This vividly illustrates the impacts of fentanyl on lipid metabolism, underscoring the substance's capacity to induce profound alterations in cellular lipid profiles in a dose-dependent manner. It must be noted that only LPC (16:0), LPC (16:1), LPC (18:0), CER(d18:0_22:0), CER(d18:2_18:0), CER(d18:2_24:1) significantly increased, and only ChE(24:5) and SPH(d18:1) significantly decreased in the FH group vs. control.

The affected lipids species involved in the CER pathways are summarized in Figure 7. Ratios of total lipid class of CER and Hex2Cer show dose-dependent increases.

Ratios of total lipid class of sphingomyelin (SM) had minor increases (~1.3 fold) in the FH group vs. control. Ratios of total lipid class of ChE and SPH had significant decreases with <2-fold decreases in the FH group vs. control. Among the 20 detected lipid classes the total abundance of cholesterol ester and sphingosine classes significantly decreased while ceramide and hexosylceramide classes significantly increased (>2-fold increase) in the high-dose group (FH) vs. control. These lipidomic data indicate that the ceramide pathway might be disturbed by fentanyl treatment.



Discussion

Accumulating data have suggested that an *in vitro* neuronal culture system could recapitulate some major events of CNS development *in vivo*. Culture models, such as NSC cultures, facilitate mechanistic dissections including potential fentanyl-induced neurotoxicity [14–16, 26–29, 30], which is difficult using *in vivo* systems. Originally, we hypothesized that: 1) application of *in vitro* NSC models and/or differentiated cells should be able to provide data that can inform clinical interventions and preclinical toxicology studies; 2) fentanyl-induced neural damage, if any, could depend on the dose given and the duration of exposure. In this study, commercially available and de-identified human NSCs were employed. The cultured cells exhibited typical features including self-renew and differentiation to generate neurons, astrocytes, and oligodendrocytes. Our data (Figures 1, 2) show that the model was successful, despite the minimal impact of fentanyl.

Fentanyl, a synthetic opioid, is widely used to supplement general anesthesia. The clinical response to given doses of an opioid varies considerably, and this is at least in part a result of variability in disposition [31]. Consequently, the influence of several factors, such as the patient's age, sex, body weight, cardiac output, or type and duration of surgery and anesthesia, on the pharmacokinetics of opioids have been investigated [32–36]. In the present study, to determine dose-dependent

effect curves and the temporal relationships between fentanyl exposures and NSC health, differentiation, and viability, a range of fentanyl at micromolar concentrations was tested. The selection of micromolar concentration was based on the fact that the reference concentrations in human blood (plasma) vary greatly depending on the doses, frequency, routes of administration, and as a primary anesthetic agent, for example, fentanyl is administered in very high doses during cardiac surgery [37–39]. Our data demonstrated that 24-h exposure of NSCs to fentanyl at micromolar concentrations did not significantly affect mitochondrial functions in NSCs, nor reduced cell viability. In fact, 24-h fentanyl exposure at concentrations of 1.0, 3.0, 10 or 100 μM even caused a certain level of elevation of MTT uptake into NSCs. Additionally, with up to 100 μM fentanyl no significant adverse effects were observed on cell viability (LDH) or mitochondrial health status (MTT). Therefore, these results suggest that at micromolar levels (concentrations) [32, 35], NSCs and immature neuronal cells were not sensitive to fentanyl-induced cell death, indicating the apoptotic cascades and acute neuronal damage (necrotic cascades/pathways) did not seem to contribute to the fentanyl-induced adverse effects.

Approximately 60% of the human brain is comprised of lipids. Despite this, the impact of chemicals on lipid composition is rarely considered. Lipidomics analysis was conducted to investigate whether the lipidome of neural cells derived from human NSCs

was changed by fentanyl exposure. Currently, few studies have evaluated whether and/or how analgesics/anesthetics might affect the biodynamics of lipids [11, 36]. Identifying alterations of lipid composition may help to evaluate the adverse effects associated with fentanyl exposure at a variety of micromolar concentrations. Since neural/neuronal cells contain a wide variety of lipid classes and lipid species, lipidomic analysis using UHPLC/HRMS was conducted to investigate the impacts of different concentrations of fentanyl on neural/neuronal cells. Notably, the dose-dependent increases in LPCs and CERs, along with decreases in ChEs and SPH, hints at a disruption in the ceramide pathway, a potential mechanism for fentanyl-induced functional deficits and/or early states of neurotoxicity. Sphingolipids, the second most abundant membrane lipids after phospholipids [34], are classified into three lipid classes: ceramides, sphingomyelins (SM), and glycosphingolipids (Hex2Cer) [33] as displayed in Figure 7, where CER is a central point for both sphingolipid biosynthesis and catabolism. Sphingolipids play important roles in the development and maintenance of the functional integrity of the nervous system [40]. Dysregulated sphingolipid metabolism has been reported to be associated with a variety of neurodegenerative diseases [40–42], specifically accumulation of ceramides contributes to the neuroinflammatory process in a wide range of neurodegenerative diseases [40, 43, 44]. The sphingolipid pathway was disturbed as shown by dose-dependent increases in CER and Hex2Cer and decreases in SPH. These data indicate that the neural cells might experience inflammation associated changes caused by fentanyl exposure at 100 μ M, in the absence of negative effects on LDH and MTT. The increases in CER and Hex2Cer and decreases in ChE by fentanyl might affect the structure, function, and stability of myelin, as well as for axonal growth of neurons. The lipidomic shifts underscore the intricate role of lipid metabolism in the neurotoxic effects associated with opioid exposure, particularly in pediatric settings. By highlighting the importance of the ceramide pathway and lipid metabolism, our findings advocate for a deeper exploration into how fentanyl alters cellular biochemistry, contributing to a more comprehensive understanding of their neurotoxic potential.

Given the paucity of research on how analgesics and anesthetics influence lipid biodynamics (crucial for brain structure and function), our lipidomics analysis using UHPLC/HRMS represents a significant step forward. Investigating the effect of various fentanyl dosages on neural cells derived from human NSCs has provided valuable insight into fentanyl's effects at the cellular level, suggesting that lipidomic profiling provides complementary information to biological tests (for instances, LDH release and MTT assay) for evaluating the nuanced mechanisms of fentanyl-induced neurotoxicity and for developing strategies to protect vulnerable pediatric populations during opioid therapy. It should also be mentioned that the current study has some limitations. For example, 1) although each treatment condition was assayed at least in triplicate and the experiments were repeated

three times independently, untargeted-lipidomics requires more experimental replicates than three replicates which matters in terms of statistical data analysis [45]. And 2) although, at our preliminary experiments, it is indicated that shorter periods of fentanyl exposure (including 1-, 3- and 6-h) did not induce dose-related adverse effects (data not shown) on NSC and differentiated neural cell viability, the effects of shorter exposure time on lipidomic profiles should be more impactful and should be addressed in our future fentanyl projects.

Summary

MTT and LDH data showed that no detectable cell death occurred after fentanyl exposure at micromolar concentrations for 24 h. However, lipidomics analysis showed that the sphingolipid pathway was disturbed by fentanyl exposure at 100 μ M for 24 h. Further, CER(d18:0_22:0), CER(d18:2_18:0) and CER (d18:2_24:1) may be potential biomarkers for neural cell inflammation status. Monitoring alteration of lipid composition and aberrant lipid metabolism may provide a more in depth understanding of the neurotoxic mechanisms, neuroinflammation, and neuronal viability/plasticity associated with fentanyl exposures.

Author contributions

All authors listed have made a substantial, direct, and intellectual contribution to the work and approved it for publication.

Author disclaimer

This article reflects the views of its authors and does not necessarily reflect those of the U.S. Food and Drug Administration. Any mention of commercial products is for clarification only and is not intended as approval, endorsement, or recommendation.

Data availability

The original contributions presented in the study are included in the article/Supplementary Material, further inquiries can be directed to the corresponding author.

Ethics statement

Ethical approval was not required for the studies on humans in accordance with the local legislation and institutional requirements because only commercially available established cell lines were used.

Funding

The author(s) declare that financial support was received for the research and/or publication of this article. This work was funded by the National Center for Toxicological Research (NCTR E0769301).

Conflict of interest

The author(s) declared no potential conflicts of interest with respect to the research, authorship, and/or publication of this article.

References

1. Kwanten LE, O'Brien B, Anwar S. Opioid-based anesthesia and analgesia for adult cardiac surgery: history and narrative review of the literature. *J Cardiothorac Vasc Anesth* (2019) 33(3):808–16. doi:10.1053/j.jvca.2018.05.053
2. Thigpen JC, Odle BL, Harirforoosh S. Opioids: a review of pharmacokinetics and pharmacodynamics in neonates, infants, and children. *Eur J Drug Metab Pharmacokinet* (2019) 44(5):591–609. doi:10.1007/s13318-019-00552-0
3. Twycross AM, Chorney JM, McGrath PJ, Finley GA, Boliver DM, Mifflin KA. A Delphi study to identify indicators of poorly managed pain for pediatric postoperative and procedural pain. *Pain Res Management* (2013) 18(5):e68–74. doi:10.1155/2013/570478
4. Berde CB, Sethna NF. Analgesics for the treatment of pain in children. *N Engl J Med* (2002) 347(14):1094–103. doi:10.1056/nejmra012626
5. Vargas-Schaffer G. Is the WHO analgesic ladder still valid? Twenty-four years of experience. *Can Fam Physician* (2010) 56(6):514–7.
6. Odell S, Logan DE. Pediatric pain management: the multidisciplinary approach. *J Pain Res* (2013) 6:785–90. doi:10.2147/jpr.s37434
7. Lasky T, Ernst FR, Greenspan J. Use of analgesic, anesthetic, and sedative medications during pediatric hospitalizations in the United States 2008. *Anesth and Analgesia* (2012) 115(5):1155–61. doi:10.1213/ane.0b013e31825b6fb2
8. Stevens BJ, Harrison D, Rashotte J, Yamada J, Abbott LK, Coburn G, et al. Pain assessment and intensity in hospitalized children in Canada. *The J Pain* (2012) 13(9):857–65. doi:10.1016/j.jpain.2012.05.010
9. Jang Y, Yoburn BC. Evaluation of receptor mechanism mediating fentanyl analgesia and toxicity. *Eur J Pharmacol* (1991) 197(2-3):135–41. doi:10.1016/0014-2999(91)90512-o
10. Stanley TH. The fentanyl story. *The J Pain* (2014) 15(12):1215–26. doi:10.1016/j.jpain.2014.08.010
11. Liu F, Rainosek SW, Frisch-Daiello JL, Patterson TA, Paule MG, Slikker W, Jr, et al. Potential adverse effects of prolonged sevoflurane exposure on developing monkey brain: from abnormal lipid metabolism to neuronal damage. *Toxicol Sci* (2015) 147(2):562–72. doi:10.1093/toxsci/kfv150
12. Liu F, Rainosek SW, Sadovova N, Fogle CM, Patterson TA, Hanig JP, et al. Protective effect of acetyl-L-carnitine on propofol-induced toxicity in embryonic neural stem cells. *Neurotoxicology* (2014) 42:49–57. doi:10.1016/j.neuro.2014.03.011
13. Wang C, Han X, Liu F, Patterson TA, Hanig JP, Paule MG, et al. Lipid profiling as an effective approach for identifying biomarkers/adverse events associated with pediatric anesthesia. *Toxicol Appl Pharmacol* (2018) 354:191–5. doi:10.1016/j.taap.2018.03.017
14. Wang C, Sadovova N, Fu X, Schmued L, Scallet A, Hanig J, et al. The role of the N-methyl-D-aspartate receptor in ketamine-induced apoptosis in rat forebrain culture. *Neuroscience* (2005) 132(4):967–77. doi:10.1016/j.neuroscience.2005.01.053
15. Wang C, Sadovova N, Hotchkiss C, Fu X, Scallet AC, Patterson TA, et al. Blockade of N-methyl-D-aspartate receptors by ketamine produces loss of postnatal day 3 monkey frontal cortical neurons in culture. *Toxicol Sci* (2006) 91(1):192–201. doi:10.1093/toxsci/kfj144
16. Liu F, Patterson TA, Sadovova N, Zhang X, Liu S, Zou X, et al. Ketamine-induced neuronal damage and altered N-methyl-D-aspartate receptor function in rat primary forebrain culture. *Toxicol Sci* (2013) 131(2):548–57. doi:10.1093/toxsci/kfs296

Generative AI statement

The author(s) declare that no Generative AI was used in the creation of this manuscript.

Supplementary material

The Supplementary Material for this article can be found online at: <https://www.ebm-journal.org/articles/10.3389/ebm.2025.10607/full#supplementary-material>

17. Perouansky M, Hemmings HC, Jr, Riou B. Neurotoxicity of general anesthetics: cause for concern? *Anesthesiology* (2009) 111(6):1365–71. doi:10.1097/aln.0b013e3181bf1d61
18. Castellanos DB, Martín-Jiménez CA, Rojas-Rodríguez F, Barreto GE, González J. Brain lipidomics as a rising field in neurodegenerative contexts: perspectives with Machine Learning approaches. *Front Neuroendocrinology* (2021) 61:100899. doi:10.1016/j.yfrne.2021.100899
19. Kosicek M, Zetterberg H, Andreasen N, Peter-Katalinic J, Hecimovic S. Elevated cerebrospinal fluid sphingomyelin levels in prodromal Alzheimer's disease. *Neurosci Lett* (2012) 516(2):302–5. doi:10.1016/j.neulet.2012.04.019
20. Sato H, Tomimoto H, Ohtani R, Kitano T, Kondo T, Watanabe M, et al. Astroglial expression of ceramide in Alzheimer's disease brains: a role during neuronal apoptosis. *Neuroscience* (2005) 130(3):657–66. doi:10.1016/j.neuroscience.2004.08.056
21. Motyl J, Strosznajder JB. Sphingosine kinase 1/sphingosine-1-phosphate receptors dependent signalling in neurodegenerative diseases. The promising target for neuroprotection in Parkinson's disease. *Pharmacol Rep* (2018) 70(5):1010–4. doi:10.1016/j.pharep.2018.05.002
22. Fritz HG, Holzmayr M, Walter B, Moeritz KU, Lupp A, Bauer R. The effect of mild hypothermia on plasma fentanyl concentration and biotransformation in juvenile pigs. *Anesth and Analgesia* (2005) 100(4):996–1002. doi:10.1213/01.ane.0000146517.17910.54
23. Wang C, Kaufmann JA, Sanchez-Ross MG, Johnson KM. Mechanisms of N-methyl-D-aspartate-induced apoptosis in phencyclidine-treated cultured forebrain neurons. *The J Pharmacol Exp Ther* (2000) 294(1):287–95. doi:10.1016/s0022-3565(24)39068-8
24. Cao Z, Schmitt TC, Varma V, Sloper D, Beger RD, Sun J. Evaluation of the performance of lipidizer platform and its application in the lipidomics analysis in mouse heart and liver. *J Proteome Res* (2020) 19(7):2742–9. doi:10.1021/acs.jproteome.9b00289
25. Pang Z, Zhou G, Ewald J, Chang L, Hacariz O, Basu N, et al. Using MetaboAnalyst 5.0 for LC-HRMS spectra processing, multi-omics integration and covariate adjustment of global metabolomics data. *Nat Protoc* (2022) 17(8):1735–61. doi:10.1038/s41596-022-00710-w
26. Liu F, Wang C. Application of omics technologies to neural stem cell studies. *J Pharmacogenomics and Pharmacoproteomics* (2015) 6(3). doi:10.4172/2153-0645.1000e146
27. Bai X, Yan Y, Canfield S, Muravyeva MY, Kikuchi C, Zaja I, et al. Ketamine enhances human neural stem cell proliferation and induces neuronal apoptosis via reactive oxygen species-mediated mitochondrial pathway. *Anesth and Analgesia* (2013) 116(4):869–80. doi:10.1213/ane.0b013e3182860fc9
28. Wang C, Liu F, Patterson TA, Paule MG, Slikker W, Jr. Anesthetic drug-induced neurotoxicity and compromised neural stem cell proliferation. *J Drug Alcohol Res* (2015) 4:1–8. doi:10.4303/jdar/235905
29. Slikker W, Jr, Liu F, Rainosek SW, Patterson TA, Sadovova N, Hanig JP, et al. Ketamine-induced toxicity in neurons differentiated from neural stem cells. *Mol Neurobiol* (2015) 52(2):959–69. doi:10.1007/s12035-015-9248-5
30. Liu F, Mahmood M, Xu Y, Watanabe F, Biris AS, Hansen DK, et al. Effects of silver nanoparticles on human and rat embryonic neural stem cells. *Front Neurosci* (2015) 9(115). doi:10.3389/fnins.2015.00115
31. Bjorkman S, Wada R, Stanski DR. Application of physiologic models to predict the influence of changes in body composition and blood flows on the pharmacokinetics of fentanyl and alfentanil in patients. *Anesthesiology* (1998) 88(3):657–67. doi:10.1097/0000542-199803000-00016

32. Kahraman S, Zup SL, McCarthy MM, Fiskum G. GABAergic mechanism of propofol toxicity in immature neurons. *J Neurosurg Anesthesiology* (2008) **20**(4): 233–40. doi:10.1097/ana.0b013e31817ec34d
33. Lahiri S, Futerman AH. The metabolism and function of sphingolipids and glycosphingolipids. *Cell Mol Life Sci* (2007) **64**(17):2270–84. doi:10.1007/s00018-007-7076-0
34. Merrill AH, Jr, Schmelz EM, Dillehay D, Spiegel S, Shayman J, Schroeder J, et al. Sphingolipids--the enigmatic lipid class: biochemistry, physiology, and pathophysiology. *Toxicol Appl Pharmacol* (1997) **142**(1):208–25. doi:10.1006/taap.1996.8029
35. Spahr-Schopfer I, Vutskits L, Toni N, Buchs PA, Parisi L, Muller D. Differential neurotoxic effects of propofol on dissociated cortical cells and organotypic hippocampal cultures. *Anesthesiology* (2000) **92**(5):1408–17. doi:10.1097/00005542-200005000-00032
36. Wang C, Liu F, Frisch-Daiello JL, Martin S, Patterson TA, Gu Q, et al. Lipidomics reveals a systemic energy deficient state that precedes neurotoxicity in neonatal monkeys after sevoflurane exposure. *Analytica Chim Acta* (2018) **1037**: 87–96. doi:10.1016/j.aca.2017.11.052
37. Gillespie TJ, Gandolfi AJ, Maiorino R, Vaughan R. Gas chromatographic determination of fentanyl and its analogues in human plasma. *J Anal Toxicol* (1981) **5**(3):133–7. doi:10.1093/jat/5.3.133
38. Huynh NH, Tyrefors N, Ekman L, Johansson M. Determination of fentanyl in human plasma and fentanyl and norfentanyl in human urine using LC-MS/MS. *J Pharm Biomed Anal* (2005) **37**(5):1095–100. doi:10.1016/j.jpba.2004.09.024
39. Scholz J, Steinfath M, Schulz M. Clinical pharmacokinetics of alfentanil, fentanyl and sufentanil. An update. *Clin Pharmacokinet* (1996) **31**(4):275–92. doi:10.2165/00003088-199631040-00004
40. van Echten-Deckert G, Herget T. Sphingolipid metabolism in neural cells. *Biochim Biophys Acta* (2006) **1758**(12):1978–94. doi:10.1016/j.bbamem.2006.06.009
41. Martinez Martinez P, Mielke MM. Sphingolipids in alzheimer's disease and related disorders. *J Alzheimer's Dis* (2017) **60**(3):753–6. doi:10.3233/jad-170735
42. Xing Y, Tang Y, Zhao L, Wang Q, Qin W, Ji X, et al. Associations between plasma ceramides and cognitive and neuropsychiatric manifestations in Parkinson's disease dementia. *J Neurol Sci* (2016) **370**:82–7. doi:10.1016/j.jns.2016.09.028
43. Hardy J, Selkoe DJ. The amyloid hypothesis of Alzheimer's disease: progress and problems on the road to therapeutics. *Science* (2002) **297**(5580):353–6. doi:10.1126/science.1072994
44. Maceyka M, Spiegel S. Sphingolipid metabolites in inflammatory disease. *Nature* (2014) **510**(7503):58–67. doi:10.1038/nature13475
45. Wee HN, Lee L, Han S, Zhou J, Yen P, Ching J. Lipidomics workflow for analyzing lipid profiles using multiple reaction monitoring (MRM) in liver homogenate of mice with non-alcoholic steatohepatitis (NASH). *Bio Protoc* (2023) **13**(13):e4773. doi:10.21769/bioprotoc.4773
46. Liu F, Mahmood M, Xu Y, Watanabe F, Biris AS, Hansen DK, et al. Effects of silver nanoparticles on human and rat embryonic neural stem cells. *Front Neurosci* (2015) **9**:115. doi:10.3389/fnins.2015.00115



OPEN ACCESS

*CORRESPONDENCE

Ann M. Marini,
✉ ann.marini@usuhs.edu

RECEIVED 24 February 2025

ACCEPTED 22 April 2025

PUBLISHED 15 May 2025

CITATION

Pidoplichko VI, Figueiredo TH, Braga MFM and Marini AM (2025) α -linolenic acid-induced facilitation of GABAergic synaptic transmission is mediated via acid-sensing ion channel (ASIC1a) activity in the basolateral amygdala. *Exp. Biol. Med.* 250:10545. doi: 10.3389/ebm.2025.10545

COPYRIGHT

© 2025 Pidoplichko, Figueiredo, Braga and Marini. This is an open-access article distributed under the terms of the [Creative Commons Attribution License \(CC BY\)](https://creativecommons.org/licenses/by/4.0/). The use, distribution or reproduction in other forums is permitted, provided the original author(s) and the copyright owner(s) are credited and that the original publication in this journal is cited, in accordance with accepted academic practice. No use, distribution or reproduction is permitted which does not comply with these terms.

α -linolenic acid-induced facilitation of GABAergic synaptic transmission is mediated via acid-sensing ion channel (ASIC1a) activity in the basolateral amygdala

Volodymyr I. Pidoplichko¹, Taiza H. Figueiredo¹,
Maria F. M. Braga¹ and Ann M. Marini^{2*}

¹Department of Anatomy, Physiology and Genetics, Uniformed Services University of the Health Sciences, Bethesda, MD, United States, ²Department of Neurology, Neuroscience, Molecular and Cellular Biology, Graduate School of Nursing, Uniformed Services University of the Health Sciences, Bethesda, MD, United States

Abstract

Epilepsy affects more than 70 million people worldwide. A seizure focus that develops in different cortical brain regions can present as either focal or generalized seizures. Temporal lobe epilepsy is a highly pharmacoresistant form of epilepsy that involves the amygdala, hippocampus with or without hippocampal sclerosis as well as other limbic structures. Loss and/or dysfunction of GABAergic inhibitory neurons play a critical role in tipping the balance toward excitation. Synchronous burst firing is a feature of inhibitory neurons that is thought to regulate and rectify large excitatory neuronal networks in the BLA and is thought to underlie higher cognitive function. Acid sensing ion channels (ASIC) activated by decreases in pH, the presence of ammonium ion or a slight lowering of temperature are present on excitatory and inhibitory neurons and can alter excitability. The net effect of the activation of ASIC1a channels in the BLA is inhibition. ASIC1a channels are active in the basal state, enhancing primarily GABAergic inhibition by direct depolarization of interneurons but also by indirect excitation of interneurons via ASIC1a-mediated depolarization of pyramidal neurons. In this study, we examine the contribution of ASIC1a channel activation on alpha-linolenic acid (ALA)-induced GABAergic inhibitory synchronous burst firing in the BLA. Our results show that ALA initiates inhibitory bursts that are dependent, in part, on the activation of ASIC1a channels that may in turn be mediated by mature brain-derived neurotrophic factor.

KEYWORDS

alpha-linolenic acid, rat, GABA, inhibitory bursts, ASIC1a channels

Impact statement

Hyperexcitability is associated with informational processing deficits that may lead to disconnection and clinical cognitive impairment. Brain injuries caused by acute and chronic neurological disorders can impair neuronal function and/or lead to neuronal loss. GABAergic inhibitory neurons carry out diverse functions in brain. One major function of GABAergic inhibitory interneurons is to arrange and generate oscillations. Oscillations in the brain can either synchronize or desynchronize neural ensembles. Loss or dysfunction of GABAergic inhibitory neurons may contribute to epilepsy and lead to the disruption of oscillations in the BLA. The novel finding that alpha-linolenic acid facilitates inhibitory bursts suggests that this nutraceutical may compensate for the loss and/or dysfunction of inhibitory neurons to reduce seizures and restore oscillatory function.

Introduction

Epilepsy is one of the most common neurological disorders and affects more than 70 million people around the world. Epilepsy, defined as spontaneous recurrent seizures or as two unprovoked seizures separated by more than twenty-four hours, is commonly treated with anticonvulsant therapy. There are approximately 150,000 individuals that have experienced one unprovoked seizure in the United States [1] and those that have had a brain insult, an electroencephalogram (EEG) with epileptic discharges or an abnormality on brain imaging and a nocturnal seizure are at greatest risk of having a second unprovoked seizure over the next 2 years [2]. Whether to treat a single seizure requires clinical judgement in weighing the risks of having a second seizure versus anticonvulsant side effects [2]. There are social implications for anyone that has had their first seizure including loss of driving privileges and potential employment issues.

Epilepsy has intriguing features beginning with epileptogenesis, the process of converting a normal functioning brain with a variable latent period without seizures into one that generates spontaneous recurrent seizures. A seizure is a transient synchronous discharge of neuronal activity in the brain but the process of conversion to an epileptic state is complicated. In fact, the details of how normal neuronal circuits develop into transient abnormal synchronous discharges are unknown. The pathophysiology has been attributed, at least in part, to the imbalance of excitatory and inhibitory neurons and/or function in the brain. However, this is not the entire story. Absence seizures, for example, result from an aberrant increase in inhibition due to impaired uptake of γ -aminobutyric acid [GABA] [3] although recent evidence suggests that a reduction in cortical inhibition may be a significant contributing factor in these generalized seizures [4].

The amygdala is an almond-shaped structure that is located in the mesial temporal lobe of the brain [5]. At least thirteen

different nuclei define the amygdala where they carry out diverse functions including emotional memory, and normal behavioral functions [6]. The basolateral division of the amygdala (BLA) is a relatively new division of the amygdala that is associated with the cortex [6]. The BLA has reciprocal connections with the ventral hippocampus and prefrontal cortex, areas critically involved in fear memory, among others [7–9].

The amygdala plays a fundamental role in temporal lobe epilepsy [10, 11]. Temporal lobe epilepsy (TLE) is the most common type of focal epilepsy and, in the presence of hippocampal sclerosis, at least one-third of patients suffer from pharmacoresistance [12, 13]. The amygdala is one of the brain regions that shows extensive damage in patients with TLE [11, 14–16]. Studies show that the seizure focus resides in the amygdala and/or hippocampus although the seizure focus is most commonly found in both brain regions [11, 17, 18].

The amygdala, however, may be the most common brain region of the seizure focus. It is well-known that kindling, the use of repeated electrical stimulation in laboratory animals, results in spontaneous recurrent seizures much faster when performed in the amygdala compared with the hippocampus [19, 20]. Moreover, the earliest indication of interictal spike activity or epileptiform discharges occurs in the amygdala and piriform cortex even if kindling was performed in the hippocampus [21, 22]. Seizure spread from the amygdala to other areas may be due to its extensive reciprocal connections to temporal and other cortical brain regions [23] that facilitates the spread of seizures to the hippocampus and to other brain regions. The mechanisms of the vulnerability of the amygdala to the generation of seizures are largely unknown [11, 24].

The BLA plays an important role in the normal and abnormal functions of the amygdala. Sensory information from thalamocortical areas project to the BLA [25, 26]. Importantly, BLA activation is particularly responsible for the generation of status epilepticus in animal models of seizures even when the seizures are generated in extra-amygdalar brain regions [27, 28]. In addition, prolonged electrical stimulation of the amygdala sets off status epilepticus more readily when it is done in the BLA compared with other areas of the amygdala [29]. However, the reasons behind the susceptibility of the BLA in the generation of status epilepticus are unclear.

The BLA contains two types of neurons, glutamatergic pyramidal (principal) neurons and γ -amino-butyric acidergic (GABAergic) inhibitory neurons [30, 31]. The vast majority of neurons in the BLA are glutamatergic or principal neurons (80–85%) whereas GABAergic inhibitory neurons represent 15–20% of neurons [5, 32, 33]. GABAergic inhibitory interneurons co-express neuropeptides such as the calcium binding proteins calbindin or calretinin, cholecystokinin (CCK), vasoactive intestinal peptide (VIP), somatostatin or parvalbumin [34–38]. Interestingly, GABAergic inhibitory neurons co-expressing the neuropeptide parvalbumin comprise about 40% of the total number of GABAergic

inhibitory neurons and are the principle foundation of perisomatic innervation of principal neurons that may be involved in feedback inhibition in the BLA. In contrast, GABAergic inhibitory interneurons that co-express calretinin make up about 25–30% and mostly synapse on other inhibitory interneurons [37, 39–41].

GABAergic inhibitory interneurons tightly regulate the excitability of the BLA [42], despite representing only about 20% of the total number of neurons. The GABA_A receptor mediates fast inhibitory synaptic neurotransmission but there are modulators that also regulate neuronal excitability in the BLA. The glutamate receptor subtype, kainic acid, is involved in synaptic transmission and modulates the presynaptic release of glutamate [43] and GABA [44–47]. Moreover, kainic acid is involved in epilepsy [24, 48, 49]. The kainic acid receptor consist of five different subtypes: GluK1-3 (previously called GluR5-7), and GluK4-5 (previously called KA1-2) [50]. Kainic acid receptors are tetramers forming homomeric or heteromeric receptors; GluK4-5 subunits form functional receptors only in combination with GluK1-3 subunits [51, 52]. The N-terminal amino terminal domain (ATD) plays a major role in the assembly of heterodimers and homodimers because the formation of dimers begins at the ATD domains [53]. Alternative splicing and mRNA editing alter substrate binding and ion fluxes [51, 54, 55]. Thus, the combination of subunits results in a diverse complement of distinct receptors with different pharmacological and biophysical properties. High levels of mRNA coding for GluK1-3 are expressed in the amygdala [56–58]. The mRNA levels of GluK1 are especially elevated in the BLA, higher than in the hippocampus [56, 57]. It has been shown that GluK1-containing kainate receptors contribute to excitatory postsynaptic currents (EPSCs) when recorded from BLA glutamatergic neurons [59, 60] and increases the amplitude and frequency of action-potential spontaneous GABAergic inhibitory postsynaptic currents (IPSCs) recorded from BLA excitatory neurons [57].

Several studies implicate the GluK1-containing kainate receptors in temporal lobe epilepsy or complex partial seizures. ATPA, a GluK1 agonist, induces spontaneous epileptiform bursting in rat amygdala slices [56], and limbic status epilepticus when administered intravenously or when the compound is directly injected into the rat amygdala [24, 49]; the seizure-generating effects of ATPA are blocked by the GluK1 antagonist, LY293558 [61]. Also, antagonists of GluK1-containing receptors block limbic seizures beginning in the hippocampus induced by pilocarpine, a muscarinic agonist, or electrical stimulation *in vitro* or *in vivo* [24, 48]. Topiramate, a GluK1 antagonist [60], prevents ATPA-induced seizures but has no anti-seizure effect on other ionotropic glutamate receptor subtypes [49] i.e., NMDA or α -amino-3-hydroxyl-5-methyl-4-isoxazole-propionate (AMPA). These results suggest that blocking GluK1-containing kainic acid receptors is a major mechanism of stopping seizures by topiramate. Expression

levels of GluK1 are markedly increased in epileptic temporal lobe brain regions in human as well as in rats [62, 63]. Although GluK1-containing receptors can increase EPSCs, and therefore, excitability, in glutamatergic neurons and increase the release of GABA from presynaptic terminals of GABAergic inhibitory neurons to reduce excitability of glutamatergic neurons at low glutamate concentrations, elevated concentrations of glutamate as occurs during a seizure suppresses the release of GABA from presynaptic terminals [57] thereby exacerbating seizure activity. Additional studies have shown that the overall effect of elevated activation of GluK1-containing kainate receptors is a striking increase in neuronal excitability in the BLA and generation of spontaneous epileptiform discharges [61].

Physiological synchronous burst firing, a property of inhibitory neurons [64–66], resets and controls excitatory activity [64, 67]. As a result, GABAergic inhibitory interneurons play a central role in arranging and generating oscillations [68–71]. Synchronous oscillations in the BLA appear to be important for safety perception [72] and fear response [73]. Recently, spontaneous rhythmic oscillatory GABA_A receptor-mediated inhibitory bursts were recorded with an average burst frequency of 0.5 Hz from the rat BLA that were dependent upon NMDA receptor activation, specifically the NR2A subunit, located on GABAergic inhibitory neurons [74]. However, the role of other receptors and/or channels in the generation of inhibitory burst activity is unknown.

A small reduction in the pH or temperature, or the presence of ammonium ion activates H⁺-gated sodium channels called acid-sensing ion channels (ASICs) [75, 76]. The channel was cloned from rat brain and three types of ASIC channels have been identified, ASIC1, ASIC2 and ASIC [3, 77]. ASICs are members of the epithelial/degnerin sodium channel family with different biophysical properties. ASIC1 has two splice variants, ASIC1a and ASIC1b; ASIC1a is broadly distributed in brain with the highest expression found in the amygdala, among other brain regions [76, 78]. Pidoplichko et al., (2014) [79] demonstrated that activation of ASIC1a channels by a reduction in pH or in the presence of ammonium evokes inward currents depolarizing excitatory neurons and interneurons and enhanced IPSCs more than EPSCs from excitatory neurons and increase inhibitory activity in the BLA by the activation of inhibitory neurons and indirect activity by the synaptic activation of glutamatergic neurons. Pharmacological manipulation in rat BLA slices to induce epileptiform activity using elevated potassium or low magnesium, a strategy that relieves the magnesium block of NMDA receptors to increase activity, was completely blocked by ammonium [79]. These results confirm that activation of ASIC1a channels enhance inhibition over excitation in the BLA.

We have shown previously that alpha-linolenic acid (ALA), an omega-3 polyunsaturated fatty acid (PUFA), increases the facilitation of GABA_A receptor-mediated neurotransmission in the BLA [80]. An increase in GABA_A receptor-mediated

neurotransmission induced by mature brain-derived neurotrophic factor (mBDNF) elicited a similar increase in inhibitory activity. These results suggest that ALA may protect neurons via a bidirectional effect by reducing excitation through activation of a background potassium channel [81] and enhancing inhibition [80]. We now show that ALA enhances inhibitory burst activity in the BLA by activating ASIC1a channels possibly via a mBDNF-mediated mechanism.

Ethics statement

The experiments followed the Guide for the Care and Use of Laboratory Animals (Institute of Laboratory Animal Resources, National Research Council) and were in accordance with the guidelines and approved by the Uniformed Services University of the Health Sciences Institutional Animal Care and Use Committees (IACUC). The animal care and use programs of both institutions are accredited by the Association for Assessment and Accreditation of Laboratory Animal Care International.

Animals

Experiments were performed using 8–16 weeks old male, Sprague–Dawley rats (Charles River, Wilmington, MA, United States). Rats were pair-housed on arrival and acclimated for 3 days. A total of ten rats were used for the study. Animals were housed on an environmentally controlled room (20–23°C, ~44% humidity, 12-h light/12-h dark cycle [350–400 lux], lights on at 6:00 am), with food (Harlan Teklad Global Diet 2018, 18% protein rodent diet; Harlan Laboratories; Indianapolis, IN) and water available *ad libitum*. All rats used were not injected with substances prior to electrophysiological experiments.

Electrophysiological experiments

The procedures for obtaining the whole-cell recordings from the BLA region have been previously described [80, 82]. The rats were anesthetized with isoflurane before decapitation. Coronal brain slices (400 μ m thick) containing the amygdala were cut in ice-cold solution (in mM: 115 sucrose; 70 N-methyl-D-glucamine-gluconate (NMDG); 1 KCl; 2 CaCl₂; 4 MgCl₂; 1.25 NaH₂PO₄; 30 NaHCO₃) with the use of a vibratome (Leica VT 1200 S; Leica Microsystems, Buffalo Grove, IL, United States). The slices were transferred to a holding chamber at room temperature of about 23°C, in a bath solution containing (in mM): 125 NaCl; 2.5 KCl; 1.25 NaH₂PO₄; 21 NaHCO₃; 2 CaCl₂; 1 MgCl₂; and 25 D-glucose. The recording solution (artificial cerebrospinal

fluid; ACSF) was the same as the holding bath solution. All of the solutions were saturated with 95% O₂/5% CO₂ to achieve a pH near 7.4. The recording chamber (0.7 mL capacity) had continuously flowing ACSF (~8 mL/min) at 30–31°C. The osmolality of the ACSF was adjusted to 325 mOsm with D-glucose.

To visualize the neurons, we used a $\times 40$ water immersion objective equipped with a CCD-100 camera (Dage-MTI, Michigan City, IN, United States), under infrared light, using Nomarski optics of an upright microscope (Zeiss Axioskop 2, Thornwood, NY, United States).

The recording electrodes had resistances of 3.5–4.5 m Ω when filled with the internal solution (in mM): 60 CsCH₃SO₃; 60 KCH₃SO₃; 5 KCl; 10 EGTA; 10 HEPES; 5 Mg-ATP; 0.3 Na₃GTP (pH 7.2; osmolality was adjusted to 295 mOsm with potassium gluconate). Tight-seal (over 1 Giga Ohm) whole-cell recordings were obtained from the cell body of the principal neurons, distinguished from the interneurons by their larger size, pyramidal shape, and electrophysiological characteristics. Access resistance not exceeding 20 Mega Ohms was monitored during the recordings, and the cells were rejected if the resistance changed by more than 15% during the experiment. The currents were amplified and filtered (2 kHz) using the Axopatch 200B amplifier (Axon Instruments, Foster City, CA, United States) with a four-pole, low-pass Bessel filter, digitally sampled (up to 2 kHz) using the Clampex 10.7 software (Molecular Devices, Sunnyvale, CA, United States), and subsequently analyzed using Origin2019b software (OriginLab Corporation, Northampton, MA, United States).

GABA_A receptors (GABA_ARs)-mediated sIPSCs were recorded in a voltage-clamp mode at holding potential (V_h) of +30 mV in the presence of D-AP5 (50 μ M); SCH50911 (10 μ M); LY341495 (3 μ M). After a BLA cell was patch-clamped, the holding potential was switched from conventional –58 to +30 mV. The cell was left to equilibrate with the new V_h for about 4 min in drug-free bath solution (ACSF) and then another 4 min in antagonists-containing bath solution. Spontaneous IPSCs were recorded after that. Pressure-application of substances was performed with the help of the technique described previously [83]. Substances used in this study were as follows: D-AP5, a competitive NMDA receptor antagonist, NMDA, Ammonium chloride and all chemicals used for buffers were purchased from Sigma-Aldrich Chemical Co (St. Louis, MO). Mature BDNF and Ibuprofen were purchased from Tocris Bioscience, (Ellisville, MO). Alpha-linolenic acid (ALA) was purchased from Nu-Chek Prep Inc (Elysian, MN) and was freshly prepared on the day of experimentation. ALA was dissolved in ethanol at a molar concentration and then diluted in ACSF solution to reach a final concentration of 50, 100 or 200 μ M. It was reported that ALA undergo auto-oxidation [84], therefore all manipulations of ALA were made under nitrogen.

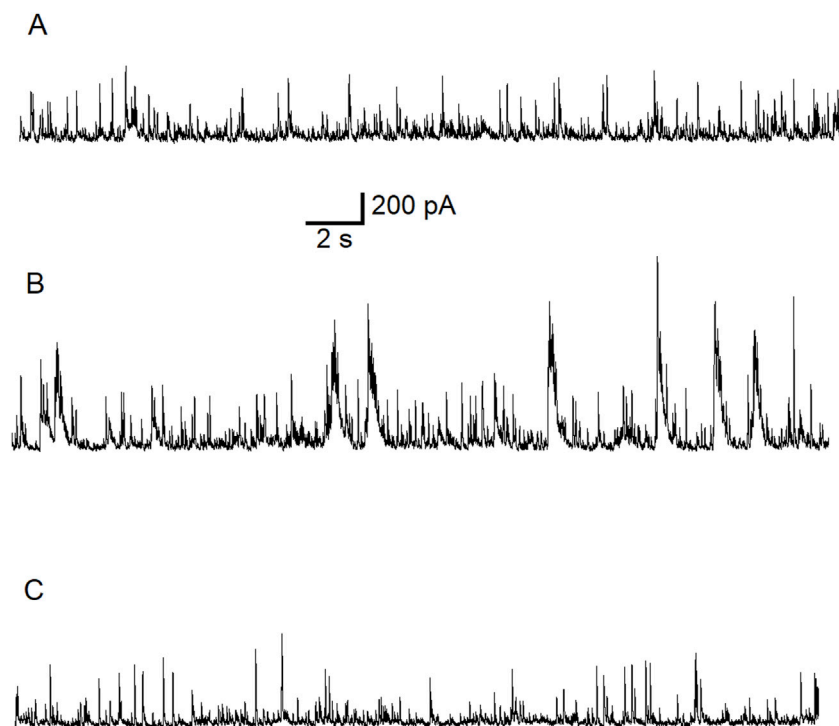


FIGURE 1

Typical potentiating effect of bath-applied ALA on inhibitory activity mediated via GABA_ARs. The experiment was conducted at $V_h = +30$ mV in the presence of NMDARs antagonist D-AP5 (50 μ M). Control current traces are demonstrated (A). Bath-applied ALA (50 μ M) facilitated inhibitory activity (bursts) (B). Note the initiation of inhibitory bursts in the presence of the NMDA receptor antagonist D-AP5. Inhibitory activity subsided during wash-out of ALA (C).

The experiments were performed in the presence of the NMDA receptor antagonist D-AP5, unless specified in the description of results and figure legend.

Statistical analysis

Statistical values are presented as means \pm standard error (SE) of the mean, and comparisons were made using paired-t test. Results were considered statistically significant when the p value was <0.05 . Sample sizes (n) refers to the number of currents.

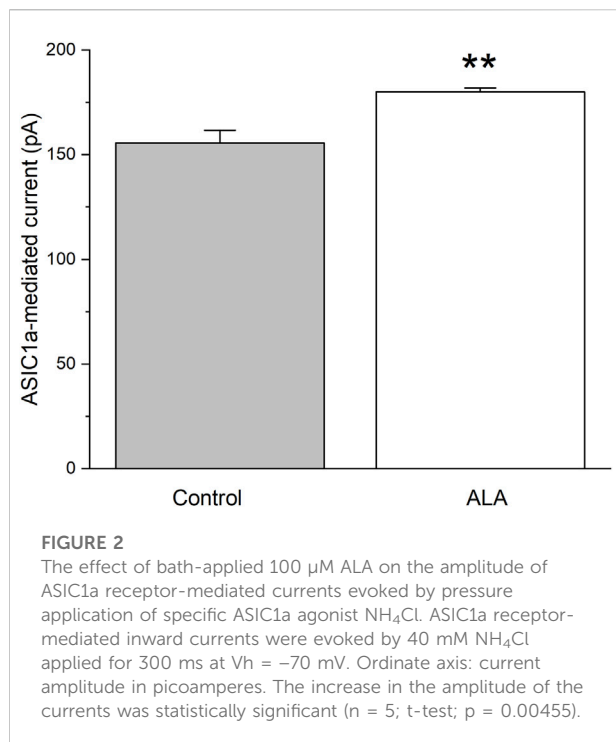
Results

In the first experiment we replicate the effects of ALA on GABAergic neurotransmission in the BLA (Figure 1). Control current trace is shown in Figure 1A. We demonstrate that bath application of 50 μ M ALA, a lower concentration than used previously [80] (Figure 5), enhances the facilitation of GABAergic activity in the BLA in slices (Figure 1B) and this effect was reversed after wash out with control bath solution (Figure 1C). To show that the effect was not due to activation of

NMDA receptors, this experiment was performed in the presence of the NMDA receptor antagonist D-AP5.

Since we have demonstrated that the ALA enhancing GABAergic inhibitory currents in the basolateral amygdala is not dependent on activation of NMDA receptors, we tested the hypothesis that this enhancing effect is dependent on the activation of ASIC1a channels. To investigate the direct effect of ALA on ASIC1a receptor (ASIC1aRs)-mediated currents at $V_h = -70$ mV, we conducted a second experiment consisting of pressure application of ammonium chloride for 300 ms, under control and bath-applied ALA (100 μ M) conditions. Comparisons of ASIC1a-mediated currents, measured in picoAmperes (pA), tested under control (156 ± 6 , $n = 5$) and 100 μ M ALA (180 ± 2 , $n = 5$) showed a significant increase ($p = 0.004$) when ALA was present in the bath solution (Figure 2).

To confirm that inhibitory effect of ALA is dependent on ASIC1aRs activation, we conducted a third experiment recording ASIC1a-dependent inhibitory neuronal bursts in the BLA. Figure 3 shows 40 min of continuous recording performed on pyramidal BLA neurons in v-clamp mode at $V_h = +30$ mV. In panel Figure 3A bath-application of ALA initiates ASIC1aRs-dependent inhibitory bursts. Bursts were initiated also via specific facilitation of ASIC1aRs by reducing the bath temperature, as



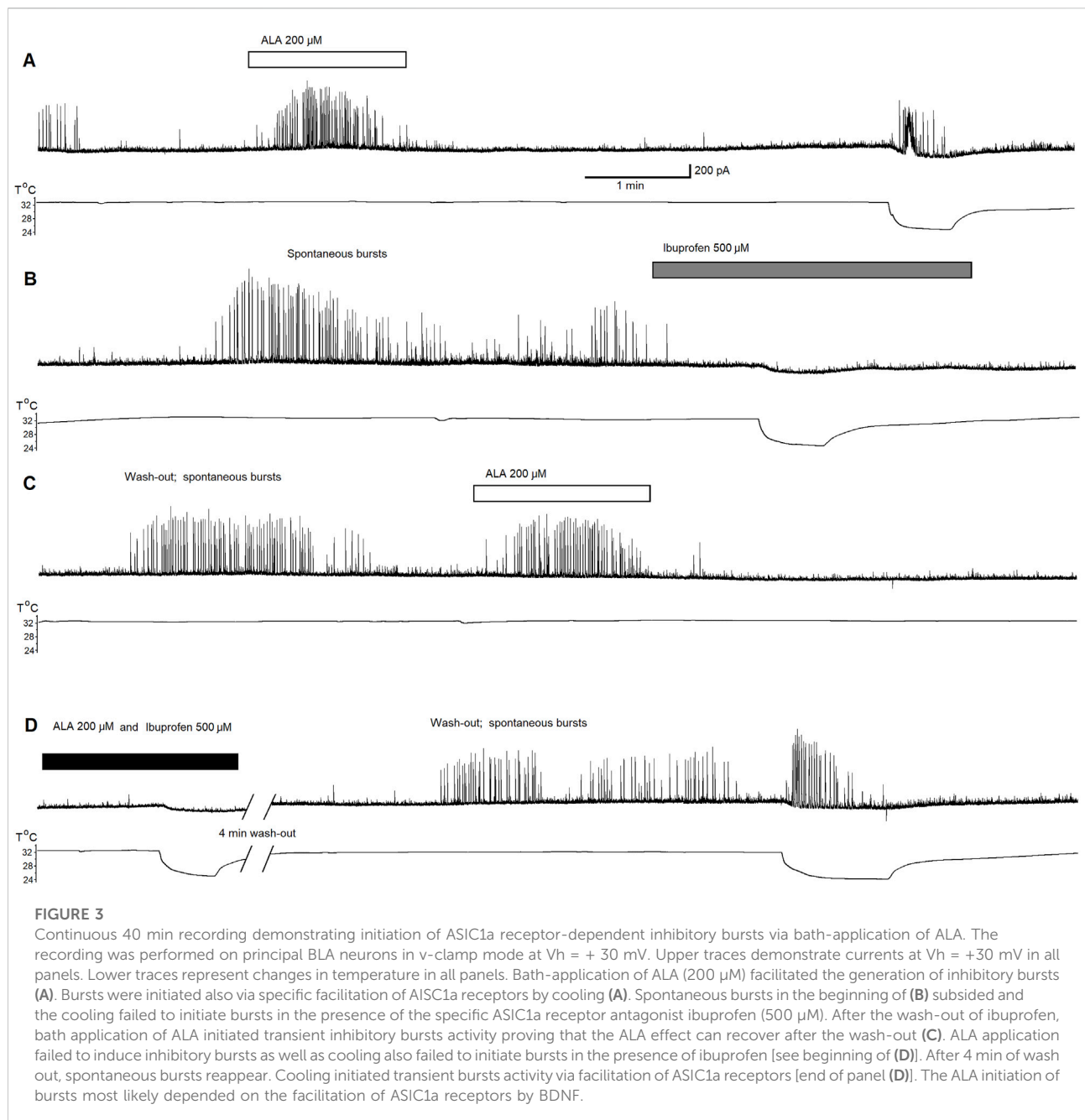
shown in [Figure 3A](#) where the lower line is indicating drop of temperature. In [Figure 3B](#), the bath-application of the specific ASIC1a receptor antagonist, ibuprofen (500 μM), extinguished spontaneous inhibitory bursts and when cooling was applied it failed to initiate bursts. In [Figure 3C](#), after wash-out of ibuprofen, bath application of ALA (200 μM) initiated transient inhibitory bursts activity showing that ALA can recover bursts activity after the washout. [Figure 3D](#) shows that in the presence of ibuprofen, ALA application failed to induce inhibitory bursts as well as cooling also failed to initiate bursts. After 4 min of washout, spontaneous bursts reappear and cooling initiated transient bursts activity via facilitation of ASIC1a receptors. The pharmacological induced changes on inhibitory neuronal bursts in the BLA clearly demonstrate that the effects of ALA are dependent on ASIC1aRs activation.

Since we have previously demonstrated that the ALA enhances the inhibitory GABAergic currents of pyramidal neurons through a BDNF-tyrosine receptor kinase (Trk)-mediated pathway [80] ([Figure 7](#)), we hypothesized that ALA initiation of bursts may occur due to activation of ASIC1a receptors by BDNF. Therefore, we investigated the effects of BDNF on ASIC1a currents. The specific ASIC1a receptor agonist, ammonium chloride, was pressure applied to BLA principal neurons (demonstrated by arrowheads in [Figures 4A–C](#)). Bath-applied mBDNF increased ASIC1a receptor-mediated inward currents in control ([Figure 4A](#); v-clamp mode, $V_h = -70$ mV) by about 40% ([Figure 4B](#)) and the effect was reversed after wash-out ([Figure 4C](#)).

To test the hypothesis that mBDNF may enhance NMDA receptor-mediated evoked currents in the BLA, we conducted an experiment with pressure application of NMDA in BLA principal neurons. During this experiment, the NMDA antagonist D-AP5 was not present at the control bath solution. [Figure 5](#) shows recordings of the current evoked by pressure-applied NMDA (100 μM for 100 ms; arrowheads) under control bath-solution [Figure 5A](#), BDNF (20 ng/mL) bath applied [Figure 5B](#), wash-out [Figure 5C](#), NMDA receptor antagonist D-AP5 (50 μM) bath-applied [Figure 5D](#) and wash-out [Figure 5E](#). Results showed that NMDA receptor-mediated currents are completely inhibited by D-AP5 and there was an incomplete recovery of the current amplitude after washout. No changes in NMDA receptor-mediated currents were observed in the presence of mBDNF, demonstrating that mBDNF does not facilitate NMDA receptor-evoked currents in principal BLA neurons.

Since the effects of mBDNF on inhibitory GABAergic currents in the BLA did not depend on facilitation of NMDA receptor-evoked currents, we further investigated the effects of BDNF on ASIC1a-dependent inhibitory bursts. [Figure 6](#) shows recording of inhibitory currents in the absence of the NMDA antagonist D-AP5: [Figure 6A](#) regular excitatory bursts were recorded at holding potential (V_h) = +30 mV and bursts frequency is about 0.5 Hz under control conditions; [Figure 6B](#) the initial effect of bath applied of the NMDA receptor antagonist D-AP5 (50 μM) shows disruption of NMDA receptor-dependent wide excitatory bursts generation; [Figure 6C](#) After 6 min in D-AP5, mBDNF (20 ng/mL) was bath-applied and results show the restoration of bursts generation; [Figure 6D](#) Bursts persisted after the washout of BDNF suggesting an ASIC1a receptor-mediated mechanism although the bursts become more narrow; [Figure 6E](#) Bursts are again recorded after the washout of D-AP5; [Figure 6F](#) the ASIC1a receptor antagonist, ibuprofen (1 mM) completely blocked inhibitory bursts generation; [Figure 6G](#) addition of BDNF shows no effect; [Figure 6H](#) After a 10 min washout, generation of bursts show recovery. The pharmacological induced changes on inhibitory neuronal bursts in the BLA principal neurons demonstrated that mBDNF restores inhibitory bursts generation that are prevented by NMDA receptor inhibition.

To confirm that mBDNF is enhancing GABAergic currents in the BLA via ASIC1aRs activation, we recorded depolarizing bursts on BLA interneurons. In [Figure 7](#), we demonstrate that regular depolarizing bursts recorded at $V_h = -70$ mV under control bath-solution show bursts frequencies at about 0.8 Hz [Figure 7A](#). When 1 mM of Ibuprofen, the ASIC1a receptor antagonist, was bath applied there was a reduction in bursts activity to about 0.5 Hz. After 8 min of ibuprofen application, bursts frequency decreased further to about 0.3 Hz [Figure 7B](#). Bath application of mBDNF (20 ng/mL) on the background of ibuprofen produced no effect [Figure 7C](#). After 10 min washout [Figure 7D](#), regular bursts pattern was restored (bursts frequency 0.8 Hz). Addition of mBDNF to the bath [Figure 7E](#) increased bursts frequency to about 1.3 Hz. The pharmacological induced changes on inhibitory neuronal bursts in

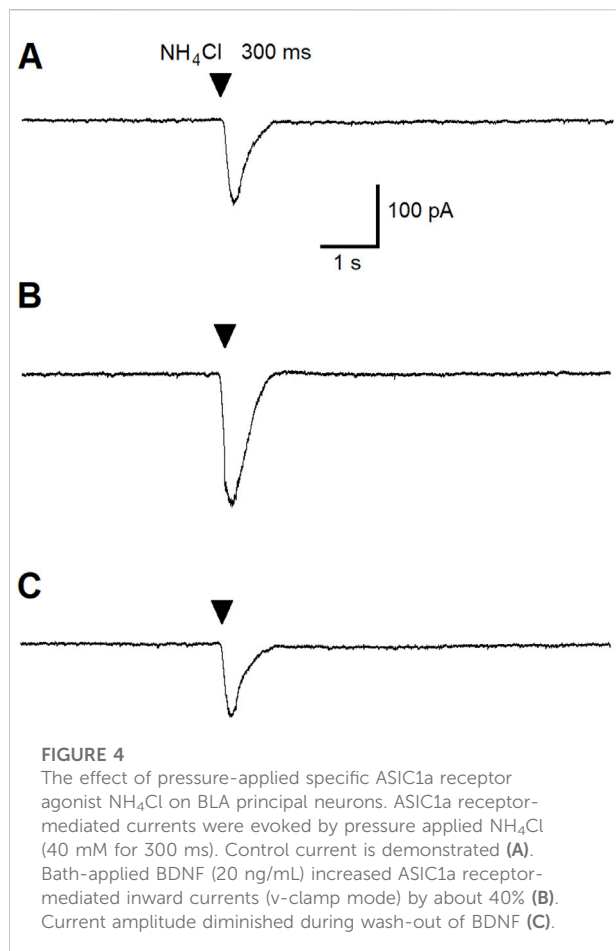


the BLA principal interneurons demonstrated that mBDNF enhances depolarizing burst activity in interneurons in the BLA, therefore increasing GABAergic inhibitory activation.

Discussion

An epileptic focus of an idiopathic nature can develop in any area of the cortex that results in the appearance of enduring spontaneous recurrent seizures and neurocognitive and

psychosocial consequences [85]. A prior brain injury, structural lesion and seizures during sleep are predisposition factors associated with seizure recurrence [2]. Seizures are transient events characterized by abnormal synchronous neuronal discharges that spread to cortical and subcortical areas in the brain [86]. Generalized epilepsy is associated with a higher rate of freedom from seizures (64–82%) compared with focal epilepsies (25–70%) during the first 2 years after diagnosis [87]. The mortality rate in epileptic individuals is 1.6–9.3 times higher than in the general population. Dire consequences of

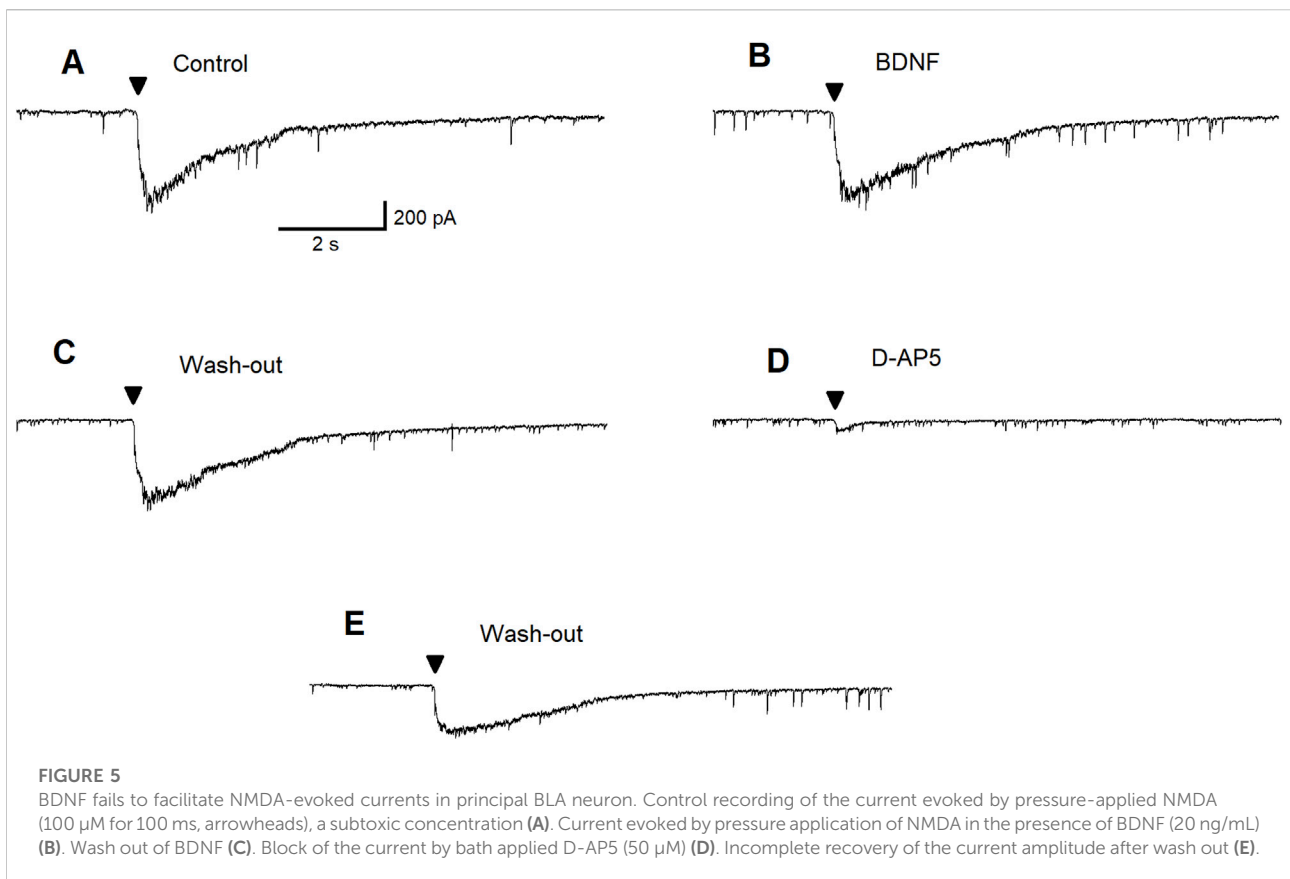


epilepsy commonly include sudden unexpected death in epilepsy, drowning, status epilepticus, and suicide [88]. Unfortunately, the seizure-free rate, defined as the absence of seizures over a 5-year period in focal and generalized epilepsy, has remained unchanged over the last twenty years despite the addition of seventeen anti-convulsants to the armamentarium of anti-seizure medications [88].

The detailed cellular and molecular mechanisms of epileptogenesis and epilepsy are unknown. Surgical removal of human epileptic tissue from patients with intractable seizures has provided insight into the electrophysiological properties of ictal and interictal events, synapse formation and characteristics of pyramidal and inhibitory interneurons. Data acquired from human epileptic tissue has shown that afferent fiber stimulation, resulting in excitatory bursts with variable latencies, were formed in the temporal or frontal cortex that depended in part on the glutamate receptor subtype, NMDA receptors [89]. Prolonged responses with after-discharges are observed in the dentate gyrus by low frequency perforant path stimulation in the hippocampus from epileptic human tissue that is only found in healthy tissue when GABA_A receptors are partially blocked [90]. There may be decreased inhibition in

dentate neurons from epileptic human tissue with hippocampal sclerosis. Single high frequency stimulation of the perforant path resulted in dentate neuronal depolarization that was amplified with the addition of a low concentration of bicuculline, a GABA_A receptor antagonist, suggesting that reduced inhibition may be a critical component of hyperexcitability in sclerotic hippocampal epileptic tissue [91]. Hippocampal epileptic tissue with sclerosis shows reduced GABAergic neurotransmission by fast and slow inhibitory post-synaptic potentials (IPSCs) in the dentate gyrus providing additional evidence of impaired inhibition [92].

In the absence of extracellular magnesium, a manipulation that relieves the magnesium block on the NMDA receptor-associated channel, both interictal bursts and long ictal synchronous epileptiform discharges were observed from the cortex of human epileptic brain tissue; ictal events were blocked by the NMDA receptor antagonist, 2-amino-5-phosphonopentanoic acid [APV], while non-NMDA receptor antagonists had no effect on the ictal discharges in the absence of magnesium [93]. In the hippocampus, repetitive low frequency stimulation resulted in spontaneous epileptiform discharges and were reduced in the presence of the NMDA receptor antagonist, 3-(2-Carboxypiperazin-4-yl)propyl-1-phosphonic acid (CPP). The investigators also showed spontaneous rhythmic positive polarity potentials that became more hyperpolarizing when the neuronal membrane became less negative relative to the resting membrane potential and these potentials were markedly attenuated or abolished with the addition of bicuculline. The spontaneous epileptiform discharges resulting from repetitive focal stimulation of the human epileptic tissue was associated with a reduction in the GABA_A receptor-mediated spontaneous rhythmic currents. These results suggest that the initiation of epileptiform discharges may be due in part to a reduced GABA_A receptor inhibitory-mediated mechanism even though GABA-mediated inhibition is functional in human epileptic brain tissue and confirmed in human and animal models of chronic epilepsy [94, 95]. In these cases, the human brain tissue was obtained from patients with intractable epilepsy where the tissue was described as having neuronal loss and gliosis [93]. Curiously, interictal-like discharges have been observed in the subiculum, the outflow region of the hippocampus in patients with hippocampal sclerosis. This type of activity was not detected in the CA1, CA3, dentate gyrus or entorhinal cortex. Interictal field potentials in the subiculum are significantly reduced by ionotropic glutamate and GABA_A receptor antagonists [96]. Inhibitory interneurons fire just before and during interictal-like discharges. Curiously, some of the subicular pyramidal neurons have an impaired chloride homeostasis and analysis of human epileptic tissue *in vitro* confirmed the subiculum's role in epileptogenesis [97]. It is interesting that subicular pyramidal and inhibitory interneurons abundantly express Ca_v 3.1 T-channels that contribute burst firing in the subiculum. That is, when T-channels are antagonized in the subiculum, burst firing changed to spike firing with low depolarizing stimuli; the



absence of T-channels by genetic manipulation resulted in suppression of burst and spike firing [98].

The number of GABAergic inhibitory interneurons in the brain is relatively small (about 20%) compared with the number of excitatory neurons. Loss of GABAergic inhibitory neurons in a non-primate model of focal epilepsy was first reported by Ribak et al., (1982) [99]. More reports of GABAergic inhibitory loss or abnormalities in GABAergic function in human and animal models of status epilepticus/epilepsy followed [100–106].

When GABA_A receptors are activated, the chloride-associated channel opens that in turn influxes chloride. This is due to a higher extracellular concentration of chloride compared with the intracellular concentration. However, the regulation of chloride is more complex and involves the sodium-potassium-chloride (NKCC1) and potassium-chloride (KCC2) cotransporters. NKCC1 increases the intracellular concentration of chloride using the sodium ion electrochemical gradient whereas KCC2 effluxes chloride from the cell by the chemical gradient of potassium ions [107]. In normal tissue, KCC2 is highly expressed whereas the expression levels of NKCC1 may be low or inhibited [108], thereby keeping the intracellular concentration of chloride low in part so that when GABA_A receptors are activated, the chloride-associated channel opens and chloride goes down the electrochemical gradient and influxes into the neuron. The dynamics of

chloride regulation are not just a matter of an intellectual exercise. Emerging evidence suggests that inflammation is implicated in the process of epileptogenesis and drives seizure severity, frequency and excitotoxicity [109, 110]. In a recent study, a single injection of lipopolysaccharide (LPS) into the peritoneum of male and female mice, a method known to induce a cytokine cascade in the brain within 60 min after injection, leads to a significant reduction in the efflux of chloride and an uptake of chloride into neurons in the dentate gyrus and hyperexcitability and increases the probability of spike activity 24 h after injection [111]. Thus, a reversal of the normal role of the KCC2 and NKCC1 cotransporters occurs that results in hyperexcitability in the brain after an episode of acute peripheral inflammation. This novel finding *in vivo* provides new mechanistic insights into epileptogenesis that may involve systemic inflammatory insults that result in an inflammatory response in brain in addition to genetics and other traditional etiologies.

An episode of status epilepticus (SE) can trigger epileptogenesis. In the kainic acid model of status epilepticus, prior work showed profound loss in GABAergic inhibitory neurons compared with the loss of excitatory neurons in the rat BLA seven to 10 days after status epilepticus. These changes were associated with an increase in the $\alpha 1$ GABA_A receptor subunit, glutamate decarboxylase (GAD), the enzyme that

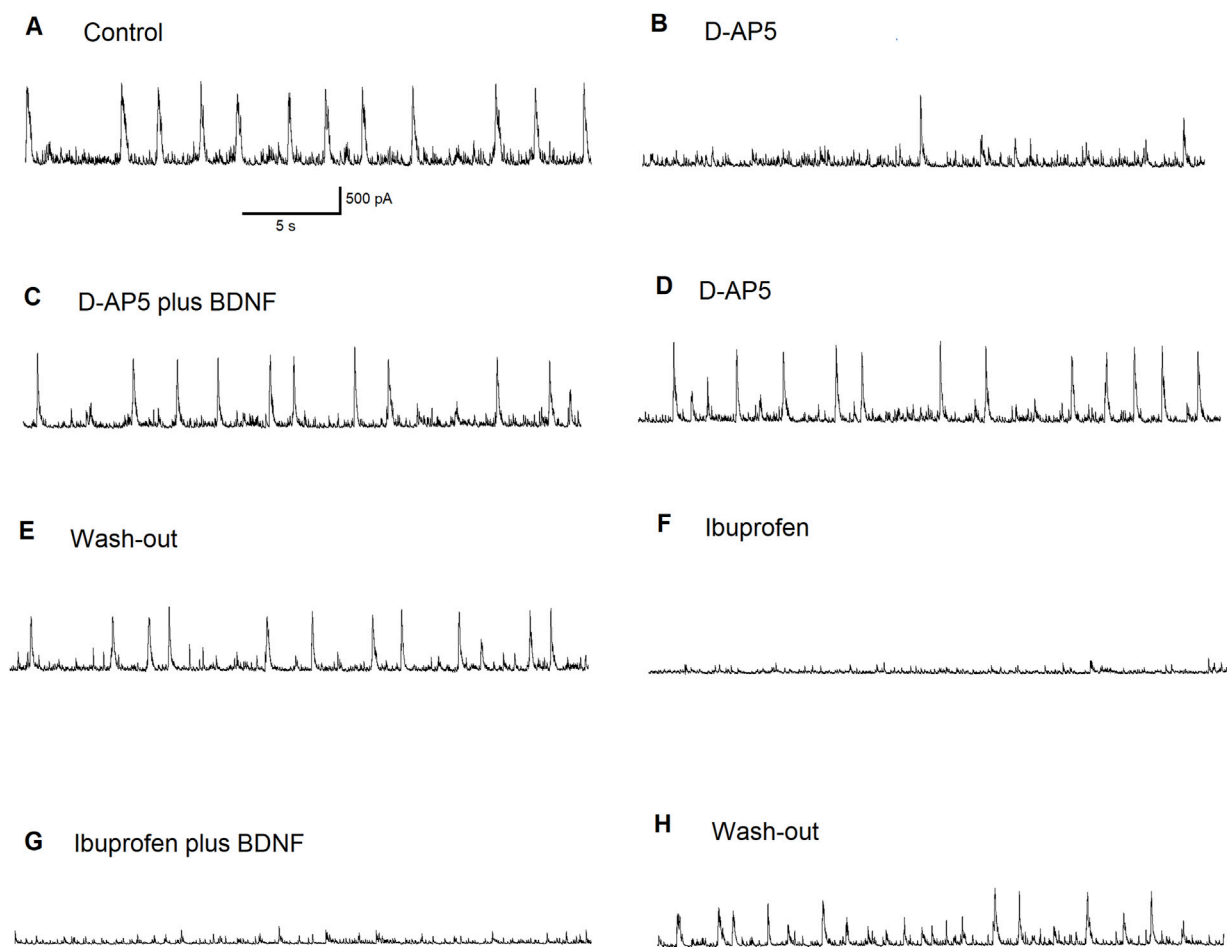


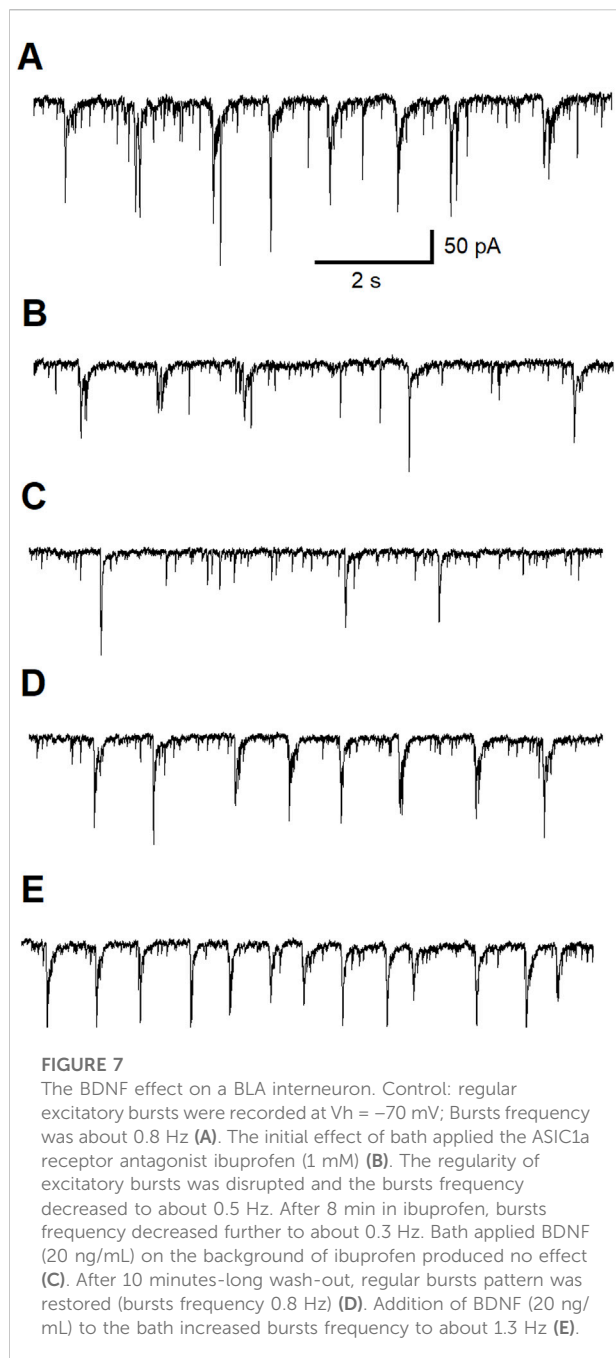
FIGURE 6

The effect of BDNF on principal BLA neuron supports the importance of ASIC1a receptors in inhibitory bursts generation. Regular inhibitory bursts have been recorded at $V_h = +30$ mV. Bursts frequency was about 0.5 Hz in control (A). The initial effect of the bath applied NMDA receptor antagonist D-AP5 (50 μ M). NMDARs-dependent wide excitatory bursts generation was disrupted (B). After 6 min in D-AP5, the addition of BDNF restored the burst generation (C). Bursts persisted after wash-out of BDNF (ASIC1a receptors were involved: please note that the profile of the bursts became narrow) (D). Bursts were recorded after the wash-out of D-AP5 (E). The ASIC1a receptor antagonist ibuprofen (1 mM) blocked inhibitory bursts generation completely (F). Addition of BDNF produced no effect (G). After 10 min-long wash-out, the generation of bursts has recovered (H).

converts glutamate to GABA, and a decrease in the glutamate ionotropic receptor kainate type subunit 1 (GluK1). Whole-cell recordings showed a significant reduction in the amplitude and frequency of spontaneous action potential-dependent IPSCs, a reduction in the frequency but not amplitude of miniature IPSCs and an impairment in the modulation of IPSCs via GluK1-containing receptors [112]. These results underscore the striking vulnerability of GABAergic inhibitory interneurons after SE that is not compensated by surviving GABAergic inhibitory neurons that expressed increased levels of the $\alpha 1$ subunit of the GABA_A receptor and the increase in GAD. These alterations may set the stage of the development of an epileptic focus due to the loss of GABAergic inhibitory neurons in the rat BLA.

Because loss or impairment of GABAergic function has been implicated in human and animal models of temporal lobe epilepsy, compounds that positively affect the GABAergic system would be beneficial in controlling and/or preventing epilepsy. Anticonvulsants that enhance GABAergic function have been approved by the FDA such as valproic acid, and lamotrigine and are already in use today. Unfortunately, many of the anticonvulsants have side effects, with some that are serious and/or debilitating [88].

Alpha-linolenic acid is an omega-3 essential polyunsaturated fatty acid (PUFA) found in plants including flaxseed, nuts, and vegetable oils [113]. In contrast to anticonvulsant drugs, ALA has a wide safety margin. There is ample literature to suggest that omega-3 polyunsaturated fatty acids, including alpha-linolenic



acid, have therapeutic potential for neurologic and psychiatric disorders. Therapeutic efficacy of ALA has been observed in animal models of stroke [114–119] that improves outcome [120], spinal cord injury [121], kainic acid-induced status epilepticus [81], a temporal lobe epilepsy model, after soman-induced status epilepticus [122] that reduces behavioral and cognitive impairment [123, 124] in part via an mammalian target of rapamycin-mediated mechanism [125] and in a mild traumatic brain injury model [126]. ALA is metabolized to oxylipins by exposure to air [84], lipoxygenase, and

cyclooxygenase pathways [127]. Polyunsaturated fatty acids also undergo metabolism by the CYP450 pathway [128]. A new report showed that ALA is metabolized to linotrans and these oxylipins exert anti-inflammatory properties in cultured microglia exposed to lipopolysaccharide [113].

Administration of three doses of ALA at 30 min, 3 days and 7 days after injury was originally found to enhance brain plasticity including a two-fold increase in mBDNF in the hippocampus and cortex, two brain regions involved in neuronal plasticity, a significant increase in neurogenesis in the subgranular zone of the dentate gyrus, an increase in expression in key proteins involved in synaptogenesis and glutamate neurotransmission; This same dosing schedule also exerts an anti-depressant effect [129]. The administration of three doses or subchronic treatment of ALA was used to show neuroprotective efficacy in animal models of stroke, mTBI and soman-induced status epilepticus. It's been known for about 20 years that ALA activates a neuronal TREK (TWIK-related potassium channel)-1 channel. TREK-1 channels are 2-pore domain background potassium channels that are open at membrane potentials and likely contribute to the resting membrane potential [130]. Activation of TREK-1 channels by ALA hyperpolarizes the membrane to advantage the magnesium block and reduce NMDA receptor activation on post-synaptic membranes as well as reduce the excessive release of glutamate from presynaptic sites. Activated TREK-1 channels by ALA are also involved in cerebral vasodilation to increase blood flow and protect against stroke [117].

There are some reports showing that ALA reduces seizures. An early study showed that a mixture of ALA and linoleic acid, an omega-6 PUFA, in a ratio of 1:4 administered over 3 weeks prior to exposure to four different models of seizures reduced the seizure latency 22-fold in up to 84% in the number of rats with seizures and up to a 97% reduction in the duration of seizures [131]. Recently, intra-gastric administration of ALA for 40 days after injection of pentylenetetrazol (PTZ), a convulsant compound, reduced the frequency of epileptic seizures, improved the cognitive and behavior impairment and reduced neuronal apoptosis via downregulating the JAK/STAT-3 pathway [132]. The exact mechanisms of how ALA reduces the various elements of seizures i.e., duration, frequency, latency, are unknown.

We have shown previously that a single dose of ALA (1500 nmol/kg) injected subcutaneously into male Sprague-Dawley rats increased the charge transfer of inhibitory postsynaptic potential currents mediated by GABA_A receptors in pyramidal neurons by 52% in the BLA and by 92% in the CA1. Bath application of ALA also increases the facilitation of GABA_A receptor-mediated neurotransmission in the BLA and CA1 subfield of the hippocampus in naïve male rats. Interestingly, K252a, the high affinity and selective TrkB inhibitor, completely blocked the ALA-induced increase in GABAergic neurotransmission in the BLA and CA1, suggesting an mBDNF-mediated mechanism. Bath application of mBDNF (20 ng/mL) also enhanced

GABAergic inhibitory activity in the BLA and CA1 pyramidal neurons similar to what was observed with ALA [80]. We proposed that low-level activation of NMDA receptors results in the immediate release of mBDNF from either presynaptic neurons [133] or astroglial cells [134] to mediate this effect.

Here, we show that bath application of ALA elicits ASIC1a-dependent GABA_A receptor-mediated inhibitory bursts located on glutamatergic and GABAergic inhibitory neurons in rat BLA slices. Because we suggested that the enhanced facilitation of GABAergic neurotransmission was elicited via a TrkB-mediated mechanism, we tested whether mBDNF might be involved in the ASIC1a-dependent GABAergic inhibitory bursts. To this end, mBDNF (20 ng/mL) was bath applied in the presence of the NMDA receptor antagonist, D-AP5. Because the effects of mBDNF on inhibitory GABAergic currents in the BLA did not depend on activation of NMDA receptor-evoked currents, we investigated the effects of mBDNF on ASIC1a-dependent inhibitory bursts. Activation of NMDA receptor-evoked currents elicit inhibitory bursts. However, in the presence of the NMDA receptor antagonist, D-AP5, NMDA receptor-mediated excitatory bursts showed disruption. Mature BDNF (20 ng/mL) was bath applied 6 minutes after the addition of D-AP5 and results showed restoration of bursts generation (Figure 6). The bursts persisted after the washout of mBDNF suggesting an ASIC1a receptor-mediated mechanism and this mechanism was confirmed when the ASIC1a receptor antagonist, ibuprofen (1 mM) was added and inhibitory bursts generation was completely blocked. Washout resulted in the return of bursts. These results show that mBDNF restores inhibitory burst generation in the presence of AP-5, an NMDA receptor antagonist.

To provide confirmatory data that mBDNF enhances GABAergic currents in the BLA via ASIC1aR activation, depolarizing bursts were recorded on BLA interneurons. Burst frequencies in the bath solution recorded at a holding voltage of -70 mV show bursts frequencies about 0.8 Hz; addition of Ibuprofen reduced bursts activity to about 0.5 Hz. Eight minutes later, bursts frequency decreased further to about 0.3 Hz. Addition of mBDNF to the bath on the background of ibuprofen showed no effect. Washout for 10 min showed regular bursts pattern restoration (bursts frequency 0.8 Hz) and bath application of mBDNF increased bursts frequency to about 1.3 Hz. These results show that mBDNF enhances depolarizing burst activity in interneurons in the BLA, thereby enhancing GABAergic inhibitory activation.

The amygdala is critically involved in TLE and shows extensive damage in TLE patients. The amygdala's reciprocal connections with the hippocampus and other temporal structures likely mediate the spread of the seizure focus. In addition, the amygdala may be the location of the seizure focus as kindling produces seizures in the amygdala faster than the hippocampus and the earliest interictal spikes or epileptiform discharges occur in the amygdala even if kindling was performed in the hippocampus. Moreover, BLA activation is especially implicated in the generation of status epilepticus in animal models of seizures even when the seizures are generated in extra-amygdalar brain regions. Our results show

that ALA enhances the facilitation of GABAergic inhibitory activity and initiate GABAergic inhibitory bursts via the facilitation of ASIC1a channels. Because ALA increases GABAergic inhibitory bursts directly on inhibitory neurons and indirectly via activation of ASIC1a channels located on glutamatergic neurons in the BLA and activation of ASIC1a channels produce an overall reduction in neuronal excitability, we suggest that chronic administration of ALA, an omega-3 PUFA with a wide safety margin may reduce seizure activity in the BLA via enhancing GABAergic inhibitory activity and by facilitating the activation of ASIC1a channels. We showed previously that ALA enhances GABAergic inhibitory activity in the CA1 subfield in the hippocampus. Our results may also explain recent results showing that ALA exhibits anti-convulsant properties in generalized seizures [132].

Author contributions

VIP conducted the experiments; TF, AM, and MB contributed to the writing and editing of this manuscript; TF and VP prepared the figures. All authors contributed to the article and approved the submitted version.

Author disclaimer

The opinions and assertions expressed herein are those of the author(s) and do not reflect the official policy or position of the Uniformed Services University of the Health Sciences or the Department of Defense.

Data availability

The raw data supporting the conclusions of this article will be made available by the authors, without undue reservation.

Ethics statement

The animal study was approved by Institutional Animal Care and Use Committee. The study was conducted in accordance with the local legislation and institutional requirements.

Funding

The author(s) declare that financial support was received for the research and/or publication of this article. Supported by the CounterACT Program, National Institutes of Health, Office of the Director and the National Institute of Neurologic Disorders and Stroke (Grant Numbers U01 NS123252-01A1 and R21NS136126-01).

Conflict of interest

The author(s) declared no potential conflicts of interest with respect to the research, authorship, and/or publication of this article.

Generative AI statement

The authors declare that no Generative AI was used in the creation of this manuscript.

References

- Hauser WA, Beghi E. First seizure definitions and worldwide incidence and mortality. *Epilepsia* (2008) 49(Suppl. 1):8–12. doi:10.1111/j.1528-1167.2008.01443.x
- Krumholz A, Wiebe S, Gronseth GS, Gloss DS, Sanchez AM, Kabir AA, et al. Evidence-based guideline: management of an unprovoked first seizure in adults: report of the guideline development subcommittee of the American academy of neurology and the American epilepsy society. *Epilepsy Curr* (2015) 15(3):144–52. doi:10.5698/1535-7597-15.3.144
- Cope DW, Di Giovanni G, Fyson SJ, Orbán G, Errington AC, Lőrincz ML, et al. Enhanced tonic GABA_A inhibition in typical absence epilepsy. *Nat Med* (2009) 15(12):1392–8. doi:10.1038/nm.2058
- Mangan KP, Nelson AB, Petrou S, Cirelli C, Jones MV. Cortical tonic inhibition gates the expression of spike-and-wave discharges associated with absence epilepsy. *J Integr Neurosci* (2024) 23(1):24. doi:10.31083/j.jin2301024
- Hajos N. Interneuron types and their circuits in the basolateral amygdala. *Front Neural Circuits* (2021) 15:687257. doi:10.3389/fncir.2021.687257
- LeDoux J. The amygdala. *Curr Biol* (2007) 17(20):R868–74. doi:10.1016/j.cub.2007.08.005
- LeDoux J, Cicchetti P, Xagoraris A, Romanski L. The lateral amygdaloid nucleus: sensory interface of the amygdala in fear conditioning. *J Neurosci* (1990) 10:1062–9. doi:10.1523/jneurosci.10-04-01062.1990
- Campeau S, Davis M. Involvement of subcortical and cortical afferents to the lateral nucleus of the amygdala in fear conditioning measured with fear-potentiated startle in rats trained concurrently with auditory and visual conditioned stimuli. *J Neurosci* (1995) 15(3 Pt 2):2312–27. doi:10.1523/JNEUROSCI.15-03-02312.1995
- Fanselow MS, Kim JJ. Acquisition of contextual Pavlovian fear conditioning is blocked by application of an NMDA receptor antagonist D,L-2-amino-5-phosphonopentanoic acid to the basolateral amygdala. *Behav Neurosci* (1994) 108(1):210–2. doi:10.1037/0735-7044.108.1.210
- Gloor P. Role of the amygdala in temporal lobe epilepsy. In: Aggleton JP, editor. *The amygdala: neurobiological aspects of emotion, memory, and mental dysfunction*. New York: Wiley-Liss (1992). p. 505–38.
- Pitkänen A, Tuunanen J, Kälviäinen R, Partanen K, Salmenperä T. Amygdala damage in experimental and human temporal lobe epilepsy. *Epilepsy Res* (1998) 32(1–2):233–53. doi:10.1016/s0920-1211(98)00055-2
- Bruxel EM, do Canto AM, Bruno DCF, Geraldine JC, Lopes-Cendes I. Multi-omic strategies applied to the study of pharmacoresistance in mesial temporal lobe epilepsy. *Epilepsia Open* (2022) 7(Suppl. 1):S94–S120. doi:10.1002/epi4.12536
- van Vliet EA, Aronica E, Gorter JA. Role of blood-brain barrier in temporal lobe epilepsy and pharmacoresistance. *Neuroscience* (2014) 277:455–73. doi:10.1016/j.neuroscience.2014.07.030
- Cendes F, Andermann F, Dubeau F, Gloor P, Evans A, Jones-Gotman M, et al. Early childhood prolonged febrile convulsions, atrophy and sclerosis of mesial structures, and temporal lobe epilepsy: an MRI volumetric study. *Neurology* (1993) 43(6):1083–7. doi:10.1212/wnl.43.6.1083
- Cendes F, Andermann F, Gloor P, Evans A, Jones-Gotman M, Watson C, et al. MRI volumetric measurement of amygdala and hippocampus in temporal lobe epilepsy. *Neurology* (1993) 43(4):719–25. doi:10.1212/wnl.43.4.719
- Saukkonen A, Kälviäinen R, Partanen K, Vainio P, Riekkinen P, Pitkänen A. Do seizures cause neuronal damage? An MRI study in newly diagnosed and chronic epilepsy. *Neuroreport* (1994) 6(1):219–23. doi:10.1097/00001756-199412300-00055
- Dewar S, Passaro E, Fried I, Engel J, Jr. Intracranial electrode monitoring for seizure localization: indications, methods and the prevention of complications. *J Neurosci Nurs* (1996) 28(5):280–92. doi:10.1097/01376517-199610000-00002
- Morimoto K, Fahnestock M, Racine RJ. Kindling and status epilepticus models of epilepsy: rewiring the brain. *Prog Neurobiol* (2004) 73(1):1–60. doi:10.1016/j.pneurobio.2004.03.009
- Goddard GV. Development of epileptic seizures through brain stimulation at low intensity. *Nature* (1967) 214(5092):1020–1. doi:10.1038/2141020a0
- McIntyre DC, Racine RJ. Kindling mechanisms: current progress on an experimental epilepsy model. *Prog Neurobiol* (1986) 27(1):1–12. doi:10.1016/0301-0082(86)90010-9
- Kairiss EW, Racine RJ, Smith GK. The development of the interictal spike during kindling in the rat. *Brain Res* (1984) 322(1):101–10. doi:10.1016/0006-8993(84)91185-5
- Racine RJ, Paxinos G, Mosher JM, Kairiss EW. The effects of various lesions and knife-cuts on septal and amygdala kindling in the rat. *Brain Res* (1988) 454(1–2):264–74. doi:10.1016/0006-8993(88)90826-8
- Stefanacci L, Farb CR, Pitkänen A, Go G, LeDoux JE, Amaral DG. Projections from the lateral nucleus to the basal nucleus of the amygdala: a light and electron microscopic PHA-L study in the rat. *J Comp Neurol* (1992) 323(4):586–601. doi:10.1002/cne.903230411
- Rogawski MA, Gryder D, Castaneda D, Yonekawa W, Banks MK, Li He. GluR5 kainate receptors, seizures, and the amygdala. *Ann New York Acad Sci* (2003) 985(Apr):150–62. doi:10.1111/j.1749-6632.2003.tb07079.x
- McDonald AJ. Cortical pathways to the mammalian amygdala. *Prog Neurobiol* (1998) 55(3):257–332. doi:10.1016/s0301-0082(98)00003-3
- Pitkänen A, Pikkarainen M, Nurminen N, Ylinen A. Reciprocal connections between the amygdala and the hippocampal formation, perirhinal cortex, and postrhinal cortex in rat. A review. *Ann New York Acad Sci* (2000) 911(Jun):369–91. doi:10.1111/j.1749-6632.2000.tb06738.x
- White LE, Price JL. The functional anatomy of limbic status epilepticus in the rat. I. Patterns of 14C-2-deoxyglucose uptake and Fos immunocytochemistry. *J Neurosci* (1993) 13(11):4787–809. doi:10.1523/JNEUROSCI.13-11-04787.1993
- White LE, Price JL. The functional anatomy of limbic status epilepticus in the rat. II. The effects of focal deactivation. *J Neurosci* (1993) 13(11):4810–30. doi:10.1523/JNEUROSCI.13-11-04810.1993
- Mohapel P, Dufresne C, Kelly ME, McIntyre DC. Differential sensitivity of various temporal lobe structures in the rat to kindling and status epilepticus induction. *Epilepsy Res* (1996) 23(3):179–87. doi:10.1016/0920-1211(95)00084-4
- McDonald A. Cell types and intrinsic connections of the amygdala. In: Aggleton J, editor. *The amygdala: neurobiological aspects of emotion, memory, and mental dysfunction*. New York, NY: Wiley-Liss, Inc (1992).
- Paré D, Smith Y. Intrinsic circuitry of the amygdaloid complex: common principles of organization in rats and cats. *Trends Neurosciences* (1998) 21(6):240–1. doi:10.1016/s0166-2236(98)01240-5
- Sah P, Faber ES, Lopez De Armentia M, Power J. The amygdaloid complex: anatomy and physiology. *Physiol Rev* (2003) 83(3):803–34. doi:10.1152/physrev.00002.2003
- Spampanato J, Polepalli J, Sah P. Interneurons in the basolateral amygdala. *Neuropharmacology* (2011) 60(5):765–73. doi:10.1016/j.neuropharm.2010.11.006
- Dávila JC, Olmos L, Legaz I, Medina L, Guirado S, Real MA. Dynamic patterns of colocalization of calbindin, parvalbumin and GABA in subpopulations of mouse basolateral amygdalar cells during development. *J Chem Neuroanat* (2008) 35(1):67–76. doi:10.1016/j.jchemneu.2007.06.003
- Kempainen S, Pitkänen A. Distribution of parvalbumin, calretinin, and calbindin-D(28k) immunoreactivity in the rat amygdaloid complex and colocalization with gamma-aminobutyric acid. *J Comp Neurol* (2000) 426(3):441–67. doi:10.1002/1096-9861(20001023)426:3<441::aid-cne8>3.0.co;2-7
- Mascagni F, McDonald AJ. Immunohistochemical characterization of cholecystokinin containing neurons in the rat basolateral amygdala. *Brain Res* (2003) 976(2):171–84. doi:10.1016/s0006-8993(03)02625-8
- McDonald AJ, Mascagni F. Colocalization of calcium-binding proteins and GABA in neurons of the rat basolateral amygdala. *Neuroscience* (2001) 105(3):681–93. doi:10.1016/s0306-4522(01)00214-7
- McDonald AJ, Mascagni F. Immunohistochemical characterization of somatostatin containing interneurons in the rat basolateral amygdala. *Brain Res* (2002) 943(2):237–44. doi:10.1016/s0006-8993(02)02650-1

39. Capogna M. GABAergic cell type diversity in the basolateral amygdala. *Curr Opin Neurobiol* (2014) **26**:110–6. doi:10.1016/j.conb.2014.01.006
40. Muller JF, Mascagni F, McDonald AJ. Synaptic connections of distinct interneuronal subpopulations in the rat basolateral amygdala nucleus. *J Comp Neurol* (2003) **456**(3):217–36. doi:10.1002/cne.10435
41. Muller JF, Mascagni F, McDonald AJ. Pyramidal cells of the rat basolateral amygdala: synaptology and innervation by parvalbumin-immunoreactive interneurons. *J Comp Neurol* (2006) **494**(4):635–50. doi:10.1002/cne.20832
42. Prager EM, Bergstrom HC, Wynn GH, Braga MF. The basolateral amygdala γ -aminobutyric acidergic system in health and disease. *J Neurosci Res* (2016) **94**(6):548–67. doi:10.1002/jnr.23690
43. Chittajallu R, Vignes M, Dev KK, Barnes JM, Collingridge GL, Henley JM. Regulation of glutamate release by presynaptic kainate receptors in the hippocampus. *Nature* (1996) **379**(6560):78–81. doi:10.1038/379078a0
44. Cunha RA, Constantino MD, Ribeiro JA. Inhibition of [3H] gamma-aminobutyric acid release by kainate receptor activation in rat hippocampal synaptosomes. *Eur J Pharmacol* (1997) **323**(2–3):167–72. doi:10.1016/s0014-2999(97)00043-5
45. Jiang L, Xu J, Nedergaard M, Kang J. A kainate receptor increases the efficacy of GABAergic synapses. *Neuron* (2001) **30**(2):503–13. doi:10.1016/s0896-6273(01)00298-7
46. Huettner JE. Kainate receptors and synaptic transmission. *Prog Neurobiol* (2003) **70**(5):387–407. doi:10.1016/s0301-0082(03)00122-9
47. Lerma J. Roles and rules of kainate receptors in synaptic transmission. *Nat Rev Neurosci* (2003) **4**(6):481–95. doi:10.1038/nrn1118
48. Smolders I, Bortolotto ZA, Clarke VR, Warre R, Khan GM, O'Neill MJ, et al. Antagonists of GLU(K5)-containing kainate receptors prevent pilocarpine-induced limbic seizures. *Nat Neurosci* (2002) **5**(8):796–804. doi:10.1038/nn880
49. Kaminski RM, Banerjee M, Rogawski MA. Topiramate selectively protects against seizures induced by ATPA, a GluR5 kainate receptor agonist. *Neuropharmacology* (2004) **46**(8):1097–104. doi:10.1016/j.neuropharm.2004.02.010
50. Gaidin SG, Kosenkov AM. mRNA editing of kainate receptor subunits: what do we know so far? *Rev Neurosciences* (2022) **33**(6):641–55. doi:10.1515/revneuro-2021-0144
51. Herb A, Burnashev N, Werner P, Sakmann B, Wisden W, Seeburg PH. The KA-2 subunit of excitatory amino acid receptors shows widespread expression in brain and forms ion channels with distantly related subunits. *Neuron* (1992) **8**(4):775–85. doi:10.1016/0896-6273(92)90098-x
52. Schiffer HH, Swanson GT, Heinemann SF. Rat GluR7 and a carboxy-terminal splice variant, GluR7b, are functional kainate receptor subunits with a low sensitivity to glutamate. *Neuron* (1997) **19**(5):1141–6. doi:10.1016/s0896-6273(00)80404-3
53. Kumar J, Schuck P, Mayer ML. Structure and assembly mechanism for heteromeric kainate receptors. *Neuron* (2011) **71**(2):319–31. doi:10.1016/j.neuron.2011.05.038
54. Bettler B, Boulter J, Hermans-Borgmeyer I, O'Shea-Greenfield A, Deneris ES, Moll C, et al. Cloning of a novel glutamate receptor subunit, GluR5: expression in the nervous system during development. *Neuron* (1990) **5**(5):583–95. doi:10.1016/0896-6273(90)90213-y
55. Sommer B, Köhler M, Sprengel R, Seeburg PH. RNA editing in brain controls a determinant of ion flow in glutamate-gated channels. *Cell* (1991) **67**(1):11–9. doi:10.1016/0092-8674(91)90568-j
56. Li H, Chen A, Xing G, Wei ML, Rogawski MA. Kainate receptor-mediated heterosynaptic facilitation in the amygdala. *Nat Neurosci* (2001) **4**(6):612–20. doi:10.1038/88432
57. Braga MF, Aroniadou-Anderjaska V, Xie J, Li H. Bidirectional modulation of GABA release by presynaptic glutamate receptor 5 kainate receptors in the basolateral amygdala. *J Neurosci* (2003) **23**(2):442–52. doi:10.1523/JNEUROSCI.23-02-00442.2003
58. Braga MF, Aroniadou-Anderjaska V, Li H. The physiological role of kainate receptors in the amygdala. *Mol Neurobiol* (2004) **30**(2):127–42. doi:10.1385/MN:30:2:127
59. Li H, Rogawski MA. GluR5 kainate receptor mediated synaptic transmission in rat basolateral amygdala *in vitro*. *Neuropharmacology* (1998) **37**(10–11):1279–86. doi:10.1016/s0028-3908(98)00109-9
60. Gryder DS, Rogawski MA. Selective antagonism of GluR5 kainate receptor-mediated synaptic currents by topiramate in rat basolateral amygdala neurons. *J Neurosci* (2003) **23**(18):7069–74. doi:10.1523/JNEUROSCI.23-18-07069.2003
61. Aroniadou-Anderjaska V, Qashu F, Braga MF. Mechanisms regulating GABAergic inhibitory transmission in the basolateral amygdala: implications for epilepsy and anxiety disorders. *Amino Acids* (2007) **32**(3):305–15. doi:10.1007/s00726-006-0415-x
62. Palma E, Esposito V, Mileo AM, Di Gennaro G, Quarato P, Giangaspero F, et al. Expression of human epileptic temporal lobe neurotransmitter receptors in *Xenopus* oocytes: an innovative approach to study epilepsy. *Proc Natl Acad Sci U S A*. (2002) **99**(23):15078–83. doi:10.1073/pnas.232574499
63. Ullal G, Fahnestock M, Racine R. Time-dependent effect of kainate-induced seizures on glutamate receptor GluR5, GluR6, and GluR7 mRNA and Protein Expression in rat hippocampus. *Epilepsia* (2005) **46**(5):616–23. doi:10.1111/j.1528-1167.2005.49604.x
64. Thomson AM. Neurotransmission: chemical and electrical interneuron coupling. *Curr Biol* (2000) **10**(3):R110–2. doi:10.1016/s0960-9822(00)00305-5
65. Muller JF, Mascagni F, McDonald AJ. Coupled networks of parvalbumin-immunoreactive interneurons in the rat basolateral amygdala. *J Neurosci* (2005) **25**(32):7366–76. doi:10.1523/JNEUROSCI.0899-05.2005
66. Woodruff AR, Sah P. Networks of parvalbumin-positive interneurons in the basolateral amygdala. *J Neurosci* (2007) **27**(3):553–63. doi:10.1523/JNEUROSCI.3686-06.2007
67. Woodruff AR, Sah P. Inhibition and synchronization of basal amygdala principal neuron spiking by parvalbumin-positive interneurons. *J Neurophysiol* (2007) **98**(5):2956–61. doi:10.1152/jn.00739.2007
68. Bartos M, Vida I, Jonas P. Synaptic mechanisms of synchronized gamma oscillations in inhibitory interneuron networks. *Nat Rev Neurosci* (2007) **8**(1):45–56. doi:10.1038/nrn2044
69. Sohal VS, Zhang F, Yizhar O, Deisseroth K. Parvalbumin neurons and gamma rhythms enhance cortical circuit performance. *Nature* (2009) **459**(7247):698–702. doi:10.1038/nature07991
70. Stark E, Eichler R, Roux L, Fujisawa S, Rotstein HG, Buzsáki G. Inhibition-induced theta resonance in cortical circuits. *Neuron* (2013) **80**(5):1263–76. doi:10.1016/j.neuron.2013.09.033
71. Allen K, Monyer H. Interneuron control of hippocampal oscillations. *Curr Opin Neurobiol* (2015) **31**(Apr):81–7. doi:10.1016/j.conb.2014.08.016
72. Stujenske JM, Likhtik E, Topiwala MA, Gordon JA. Fear and safety engage competing patterns of theta-gamma coupling in the basolateral amygdala. *Neuron* (2014) **83**(4):919–33. doi:10.1016/j.neuron.2014.07.026
73. Karalis N, Dejean C, Chaudun F, Khoder S, Rozeske RR, Wurtz H, et al. 4-Hz oscillations synchronize prefrontal-amygdala circuits during fear behavior. *Nat Neurosci* (2016) **19**(4):605–12. doi:10.1038/nn.4251
74. Aroniadou-Anderjaska V, Pidoplichko VI, Figueiredo TH, Braga MFM. Oscillatory synchronous inhibition in the basolateral amygdala and its primary dependence on nr2a-containing NMDA receptors. *Neuroscience* (2018) **373**:145–58. doi:10.1016/j.neuroscience.2018.01.021
75. Krishtal OA, Pidoplichko VI. A receptor for protons in the nerve cell membrane. *Neuroscience* (1980) **5**(12):2325–7. doi:10.1016/0306-4522(80)90149-9
76. Waldmann R, Champigny G, Bassilana F, Heurteaux C, Lazdunski M. A proton-gated cation channel involved in acid-sensing. *Nature* (1997) **386**(6621):173–7. doi:10.1038/386173a0
77. Waldmann R, Lazdunski M. H(+)-gated cation channels: neuronal acid sensors in the NaC/DEG family of ion channels. *Curr Opin Neurobiol* (1998) **8**(3):418–24. doi:10.1016/s0959-4388(98)80070-6
78. Biagini G, Babinski K, Avoli M, Marcinkiewicz M, Séguéla P. Regional and subunit-specific downregulation of acid-sensing ion channels in the pilocarpine model of epilepsy. *Neurobiol Dis* (2001) **8**(1):45–58. doi:10.1006/nbdi.2000.0331
79. Pidoplichko VI, Aroniadou-Anderjaska V, Prager EM, Figueiredo TH, Almeida-Suhett CP, Miller SL, et al. ASIC1a activation enhances inhibition in the basolateral amygdala and reduces anxiety. *J Neurosci* (2014) **34**(9):3130–41. doi:10.1523/JNEUROSCI.4009-13.2014
80. Pidoplichko VI, Figueiredo TH, Braga MF, Pan H, Marini AM. Alpha-linolenic acid enhances the facilitation of GABAergic neurotransmission in the BLA and CA1. *Exp Biol Med (Maywood)* (2023) **248**(7):596–604. doi:10.1177/15353702231165010
81. Lauritzen I, Blondeau N, Heurteaux C, Widmann C, Romey G, Lazdunski M. Polyunsaturated fatty acids are potent neuroprotectors. *EMBO J* (2000) **19**(8):1784–93. doi:10.1093/emboj/19.8.1784
82. Figueiredo T, Harbert CL, Pidoplichko V, Almeida-Suhett CP, Rossetti K, Braga MFM, et al. The recovery of GABAergic function in the Hippocampus CA1 region after mTBI. *Mol Neurobiol* (2020) **57**(1):23–31. doi:10.1007/s12035-019-01753-z
83. Pidoplichko VI, Dani JA. Acid-sensitive ionic channels in midbrain dopamine neurons are sensitive to ammonium, which may contribute to hyperammonemia

damage. *Proc Natl Acad Sci U S A.* (2006) **103**(30):11376–80. doi:10.1073/pnas.0600768103

84. Yan S, Liang Y, Zhang J, Chen Z, Liu CM. Autoxidized linolenic acid inhibits aflatoxin biosynthesis in *Aspergillus flavus* via oxylipin species. *Fungal Genet Biol* (2015) **81**(Aug):229–37. doi:10.1016/j.fgb.2014.11.005

85. Fisher RS, Acevedo C, Arzimanoglou A, Bogacz A, Cross JH, Elger CE, et al. ILAE official report: a practical clinical definition of epilepsy. *Epilepsia* (2014) **55**(4): 475–82. doi:10.1111/epi.12550

86. Fisher RS, Boas Wv E, Blume W, Elger C, Genton P, Lee P, et al. Epileptic seizures and epilepsy: definitions proposed by the international league against epilepsy (ILAE) and the international bureau for epilepsy (IBE). *Epilepsia* (2005) **46**(4):470–2. doi:10.1111/j.0013-9580.2005.66104.x

87. Seneviratne U, Cook M, D'Souza W. The prognosis of idiopathic generalized epilepsy. *Epilepsia* (2012) **53**(12):2079–90. doi:10.1111/j.1528-1167.2012.03723.x

88. Kanner AM, Bicchi MM. Antiseizure medications for adults with epilepsy: a review. *JAMA* (2022) **327**(13):1269–81. doi:10.1001/jama.2022.3880

89. Avoli M, Olivier A. Electrophysiological properties and synaptic responses in the deep layers of the human epileptogenic neocortex *in vitro*. *J Neurophysiol* (1989) **61**(3):589–606. doi:10.1152/jn.1989.61.3.589

90. Masukawa LM, Higashima M, Kim JH, Spencer DD. Epileptiform discharges evoked in hippocampal brain slices from epileptic patients. *Brain Res* (1989) **493**(1):168–74. doi:10.1016/0006-8993(89)90102-3

91. Isokawa M, Fried I. Extracellular slow negative transient in the dentate gyrus of human epileptic hippocampus *in vitro*. *Neuroscience* (1996) **72**(1):31–7. doi:10.1016/0306-4522(95)00544-7

92. Williamson A, Patrylo PR, Spencer DD. Decrease in inhibition in dentate granule cells from patients with medial temporal lobe epilepsy. *Ann Neurol* (1999) **45**(1):92–9. doi:10.1002/1531-8249(199901)45:1<92::aid-art15>3.0.co;2-n

93. Avoli M, Louvel J, Drapeau C, Pumain R, Kurcewicz I. GABA-mediated inhibition and *in vitro* epileptogenesis in the human neocortex. *J Neurophysiol* (1995) **73**(2):468–84. doi:10.1152/jn.1995.73.2.468

94. Williams S, Vachon P, Lacaille JC. Monosynaptic GABA-mediated inhibitory postsynaptic potentials in CA1 pyramidal cells of hyperexcitable hippocampal slices from kainic acid-treated rats. *Neuroscience* (1993) **52**(3):541–54. doi:10.1016/0306-4522(93)90404-4

95. Nagao T, Avoli M, Gloor P. Interictal discharges in the hippocampus of rats with long-term pilocarpine seizures. *Neurosci Lett* (1994) **174**(2):160–4. doi:10.1016/0304-3940(94)90011-6

96. Huberfeld G, Blauwblomme T, Miles R. Hippocampus and epilepsy: findings from human tissues. *Revue Neurologique* (2015) **171**(3):236–51. doi:10.1016/j.neurol.2015.01.563

97. Fabo D, Magloczky Z, Wittner L, Pek A, Eross L, Czirjak S, et al. Properties of *in vivo* interictal spike generation in the human subiculum. *Brain* (2008) **131**(Pt 2): 485–99. doi:10.1093/brain/awn297

98. Joksimovic SM, Eggan P, Izumi Y, Joksimovic SL, Tesic V, Dietz RM, et al. The role of T-type calcium channels in the subiculum: to burst or not to burst? *The J Physiol* (2017) **595**(19):6327–48. doi:10.1113/JP274565

99. Ribak CE, Bradburne R, Harris AB. A preferential loss of GABAergic, symmetric synapses in epileptic foci: a quantitative ultrastructural analysis of monkey neocortex. *J Neurosci* (1982) **2**:1725–35. doi:10.1523/JNEUROSCI.02-12-01725.1982

100. de Lanerolle NC, Kim JH, Robbins RJ, Spencer DD. Hippocampal interneuron loss and plasticity in human temporal lobe epilepsy. *Brain Res* (1989) **495**:387–95. doi:10.1016/0006-8993(89)90234-5

101. Toth K, Eross L, Vajda J, Halasz P, Freund TF, Magloczky Z. Loss and reorganization of calretinin-containing interneurons in the epileptic human hippocampus. *Brain* (2010) **133**(9):2763–77. doi:10.1093/brain/awq149

102. Kobayashi M, Buckmaster PS. Reduced inhibition of dentate granule cells in a model of temporal lobe epilepsy. *J Neurosci* (2003) **23**:2440–52. doi:10.1523/JNEUROSCI.23-06-02440.2003

103. Ratté S, Lacaille JC. Selective degeneration and synaptic reorganization of hippocampal interneurons in a chronic model of temporal lobe epilepsy. *Adv Neurol* (2006) **97**:69–76.

104. Liu YQ, Yu F, Liu WH, He XH, Peng BW. Dysfunction of hippocampal interneurons in epilepsy. *Neurosci Bull* (2014) **30**(6):985–98. doi:10.1007/s12264-014-1478-4

105. Papp P, Kovács Z, Szocsics P, Juhász G, Maglóczy Z. Alterations in hippocampal and cortical densities of functionally different interneurons in rat models of absence epilepsy. *Epilepsy Res* (2018) **145**(Sep):40–50. doi:10.1016/j.epilepsyres.2018.05.013

106. Giacomoni J, Bruzelius A, Stamouli CA, Rylander Ottosson D. Direct conversion of human stem cell-derived glial progenitor cells into GABAergic interneurons. *Cells* (2020) **9**(11):2451. doi:10.3390/cells9112451

107. Payne JA, Rivera C, Voipio J, Kaila K. Cation-chloride co-transporters in neuronal communication, development and trauma. *Trends Neurosciences* (2003) **26**(4):199–206. doi:10.1016/S0166-2236(03)00068-7

108. Dzhalal VI, Talos DM, Sdrulla DA, Brumback AC, Mathews GC, Benke TA, et al. NKCC1 transporter facilitates seizures in the developing brain. *Nat Med* (2005) **11**(11):1205–13. doi:10.1038/nm1301

109. Vezzani A, French J, Bartfai T, Baram TZ. The role of inflammation in epilepsy. *Nat Rev Neurol* (2011) **7**(1):31–40. doi:10.1038/nrneurol.2010.178

110. Rana A, Musto AE. The role of inflammation in the development of epilepsy. *J Neuroinflammation* (2018) **15**(1):144. doi:10.1186/s12974-018-1192-7

111. Kurki SN, Srinivasan R, Laine J, Virtanen MA, Ala-Kurikka T, Voipio J, et al. Acute neuroinflammation leads to disruption of neuronal chloride regulation and consequent hyperexcitability in the dentate gyrus. *Cell Rep* (2023) **42**(11):113379. doi:10.1016/j.celrep.2023.113379

112. Fritsch B, Qashu F, Figueiredo TH, Aroniadou-Anderjaska V, Rogawski MA, Braga MF. Pathological alterations in GABAergic interneurons and reduced tonic inhibition in the basolateral amygdala during epileptogenesis. *Neuroscience* (2009) **163**(1):415–29. doi:10.1016/j.neuroscience.2009.06.034

113. Balas L, Dey SK, Béraud-Dufour S, Riechers DE, Landau OA, Bertrand-Michel J, et al. Linotrans: omega-3 oxylipins featuring an E,Z,E conjugated triene motif are present in the plant kingdom and alleviate inflammation in LPS-challenged microglial cells. *Eur J Med Chem* (2022) **231**:114157. doi:10.1016/j.ejmech.2022.114157

114. Blondeau N, Widmann C, Lazdunski M, Heurteaux C. Activation of the nuclear factor- κ B is a key event in brain tolerance. *J Neurosci* (2001) **21**(13): 4668–77. doi:10.1523/JNEUROSCI.21-13-04668.2001

115. Blondeau N, Widmann C, Lazdunski M, Heurteaux C. Polyunsaturated fatty acids induce ischemic and epileptic tolerance. *Neuroscience* (2002) **109**(2):231–41. doi:10.1016/s0306-4522(01)00473-0

116. Heurteaux C, Laigle C, Blondeau N, Jarretou G, Lazdunski M. Alpha-linolenic acid and riluzole treatment confer cerebral protection and improve survival after focal brain ischemia. *Neuroscience* (2006) **137**(1):241–51. doi:10.1016/j.neuroscience.2005.08.083

117. Blondeau N, Pétrault O, Manta S, Giordanengo V, Gounon P, Bordet R, et al. Polyunsaturated fatty acids are cerebral vasodilators via the TREK-1 potassium channel. *Circ Res* (2007) **101**(2):176–84. doi:10.1161/CIRCRESAHA.107.154443

118. Nguemni C, Delplanque B, Rovère C, Simon-Rousseau N, Gandin C, Agnani G, et al. Dietary supplementation of alpha-linolenic acid in an enriched rapeseed oil diet protects from stroke. *Pharmacol Res* (2010) **61**(3):226–33. doi:10.1016/j.phrs.2009.12.007

119. Blondeau N. The nutraceutical potential of omega-3 alpha-linolenic acid in reducing the consequences of stroke. *Biochimie* (2016) **120**:49–55. doi:10.1016/j.biochi.2015.06.005

120. Bourourou M, Heurteaux C, Blondeau N. Alpha-linolenic acid given as enteral or parenteral nutritional intervention against sensorimotor and cognitive deficits in a mouse model of ischemic stroke. *Neuropharmacology* (2016) **108**:60–72. doi:10.1016/j.neuropharm.2016.04.040

121. Lang-Lazdunski L, Blondeau N, Jarretou G, Lazdunski M, Heurteaux C. Linolenic acid prevents neuronal cell death and paraplegia after transient spinal cord ischemia in rats. *J Vasc Surg* (2003) **38**(3):564–75. doi:10.1016/s0741-5214(03)00473-7

122. Pan H, Hu XZ, Jacobowitz DM, Chen C, McDonough J, Van Shura K, et al. Alpha-linolenic acid is a potent neuroprotective agent against soman-induced neuropathology. *Neurotoxicology* (2012) **33**(5):1219–29. doi:10.1016/j.neuro.2012.07.001

123. Pan H, Piermartiri TC, Chen J, McDonough J, Oppel C, Driewech W, et al. Repeated systemic administration of the nutraceutical alpha-linolenic acid exerts neuroprotective efficacy, an antidepressant effect and improves cognitive performance when given after soman exposure. *Neurotoxicology* (2015) **51**: 38–50. doi:10.1016/j.neuro.2015.09.006

124. Piermartiri T, Pan H, Figueiredo TH, Marini AM. α -Linolenic acid, A nutraceutical with pleiotropic properties that targets endogenous neuroprotective pathways to protect against organophosphate nerve agent-induced neuropathology. *Molecules* (2015) **20**(11):20355–80. doi:10.3390/molecules201119698

125. Piermartiri TC, Pan H, Chen J, McDonough J, Grunberg N, Aplan JP, et al. Alpha-linolenic acid-induced increase in neurogenesis is a key factor in

the improvement in the passive avoidance task after soman exposure. *NeuroMolecular Med* (2015) **17**(3):251–69. doi:10.1007/s12017-015-8353-y

126. Figueiredo TH, Harbert CL, Pidoplichko V, Almeida-Suhett CP, Pan H, Rossetti K, et al. Alpha-linolenic acid treatment reduces the contusion and prevents the development of anxiety-like behavior induced by a mild traumatic brain injury in rats. *Mol Neurobiol* (2018) **55**(1):187–200. doi:10.1007/s12035-017-0732-y

127. Liu M, Chen P, Véricel E, Lelli M, Béguin L, Lagarde M, et al. Characterization and biological effects of di-hydroxylated compounds deriving from the lipoxygenation of ALA. *J Lipid Res* (2013) **54**(8):2083–94. doi:10.1194/jlr.M035139

128. Capdevila JH, Falck JR, Harris RC. Cytochrome P450 and arachidonic acid bioactivation. Molecular and functional properties of the arachidonate monooxygenase. *J Lipid Res* (2000) **41**(2):163–81. doi:10.1016/s0022-2275(20)32049-6

129. Blondeau N, Nguemeni C, Debruyne DN, Piens M, Wu X, Pan H, et al. Subchronic alpha-linolenic acid treatment enhances brain plasticity and exerts an antidepressant effect: a versatile potential therapy for stroke. *Neuropsychopharmacology* (2009) **34**(12):2548–59. doi:10.1038/npp.2009.84

130. Heurteaux C, Guy N, Laigle C, Blondeau N, Duprat F, Mazzuca M, et al. TREK-1, a K⁺ channel involved in neuroprotection and general anesthesia. *EMBO J* (2004) **23**(13):2684–95. doi:10.1038/sj.emboj.7600234

131. Yehuda S, Carasso RL, Mostofsky DI. Essential fatty acid preparation (SR-3) raises the seizure threshold in rats. *Eur J Pharmacol* (1994) **254**(1-2):193–8. doi:10.1016/0014-2999(94)90387-5

132. Zeng X, Luo F, Cheng YH, Gao J, Hong D. α -Linolenic acid ameliorates pentylenetetrazol-induced neuron apoptosis and neurological impairment in mice with seizures via down-regulating JAK2/STAT3 pathway. *Br J Nutr* (2024) **132**(1):1–12. doi:10.1017/S0007114524000989

133. Xu B, Gottschalk W, Chow A, Wilson RI, Schnell E, Zang K, et al. The role of brain-derived neurotrophic factor receptors in the mature hippocampus: modulation of long-term potentiation through a presynaptic mechanism involving TrkB. *J Neurosci* (2000) **20**(18):6888–97. doi:10.1523/JNEUROSCI.20-18-06888.2000

134. Lalo U, Bogdanov A, Moss GW, Pankratov Y. Astroglia-derived BDNF and MSK-1 mediate experience- and diet-dependent synaptic plasticity. *Brain Sci* (2020) **10**(7):462. doi:10.3390/brainsci10070462



OPEN ACCESS

*CORRESPONDENCE

Slobodan M. Todorovic,
✉ slobodan.todorovic@ucdenver.edu

RECEIVED 26 February 2025

ACCEPTED 29 April 2025

PUBLISHED 16 May 2025

CITATION

Timic Stamenic T, Feseha S, Fine-Raquet B, Tadic VP and Todorovic SM (2025) *In vivo* silencing of the thalamic $\text{Ca}_v3.1$ voltage-gated calcium channels demonstrates their region-specific role in anesthetic mediated hypnosis. *Exp. Biol. Med.* 250:10553. doi: 10.3389/ebm.2025.10553

COPYRIGHT

© 2025 Timic Stamenic, Feseha, Fine-Raquet, Tadic and Todorovic. This is an open-access article distributed under the terms of the [Creative Commons Attribution License \(CC BY\)](https://creativecommons.org/licenses/by/4.0/). The use, distribution or reproduction in other forums is permitted, provided the original author(s) and the copyright owner(s) are credited and that the original publication in this journal is cited, in accordance with accepted academic practice. No use, distribution or reproduction is permitted which does not comply with these terms.

In vivo silencing of the thalamic $\text{Ca}_v3.1$ voltage-gated calcium channels demonstrates their region-specific role in anesthetic mediated hypnosis

Tamara Timic Stamenic¹, Simon Feseha¹, Brier Fine-Raquet¹, Vasilije P. Tadic¹ and Slobodan M. Todorovic^{1,2,3*}

¹Department of Anesthesiology, University of Colorado, Aurora, CO, United States, ²Department of Neuroscience, University of Colorado, Aurora, CO, United States, ³Department of Pharmacology Graduate Programs, University of Colorado, Aurora, CO, United States

Abstract

Although substantial progress has been made in the last three decades towards our understanding of how general anesthetics (GAs) act at the molecular level, much less is known about how GAs cause loss of consciousness at the level of neuronal networks. The role of thalamus as an important brain region in anesthetic-induced hypnosis is relatively well established, but the specific roles of voltage-gated ion channels in different functional regions of the thalamus in anesthetic mechanisms are not well studied. To address this gap in knowledge, we selectively silenced the *Cacna1g* gene that encodes the low-threshold-activated $\text{Ca}_v3.1$ T-type voltage-gated calcium channel subunit by injecting short-hairpin RNA (shRNA) into midline and intralaminar - nonspecific thalamus (MIT) and sensory - specific ventrobasal (VB) thalamic nuclei in wild-type (WT) mice. Control animals were injected with scrambled shRNA. To validate our silencing approach, we performed patch-clamp experiments in acute thalamic slices *ex vivo*. In injected animals we determined anesthetic endpoints such as hypnosis measured with loss of righting reflex (LORR) and immobilization measured with loss of withdrawal reflex (LOWR) *in vivo* after administration of a traditional volatile GA isoflurane. Effective $\text{Ca}_v3.1$ channel knock-down was documented by greatly diminished amplitudes of T-currents and absence of rebound burst firing in our patch-clamp recordings from thalamic slices. We found that knocking down $\text{Ca}_v3.1$ channels in MIT significantly decreased inhaled isoflurane concentration that is required to induce LORR, but it did not affect speed of anesthetic induction and the immobilizing effect of isoflurane. In contrast, knocking down the $\text{Ca}_v3.1$ channel in the VB thalamus did not affect any of the measured

anesthetic endpoints. Hence, we concluded that $\text{Ca}_v3.1$ channels in nonspecific MIT thalamus have a preferential role in anesthetic hypnosis when compared to the sensory VB thalamus.

KEYWORDS

calcium ion channels, thalamus, anesthesia, isoflurane, hypnosis

Impact Statement

General anesthetics (GAs) have been clinically used for nearly two centuries, but the mechanisms whereby different classes of these agents achieve different clinical effects are still not well understood. We found that knocking down $\text{Ca}_v3.1$ channels in MIT significantly decreased inhaled isoflurane concentration that is required to induce LORR, but it did not affect speed of anesthetic induction and immobilizing effect of isoflurane. In contrast, knocking down $\text{Ca}_v3.1$ channel in the VB thalamus did not affect any of the measured anesthetic endpoints.

Introduction

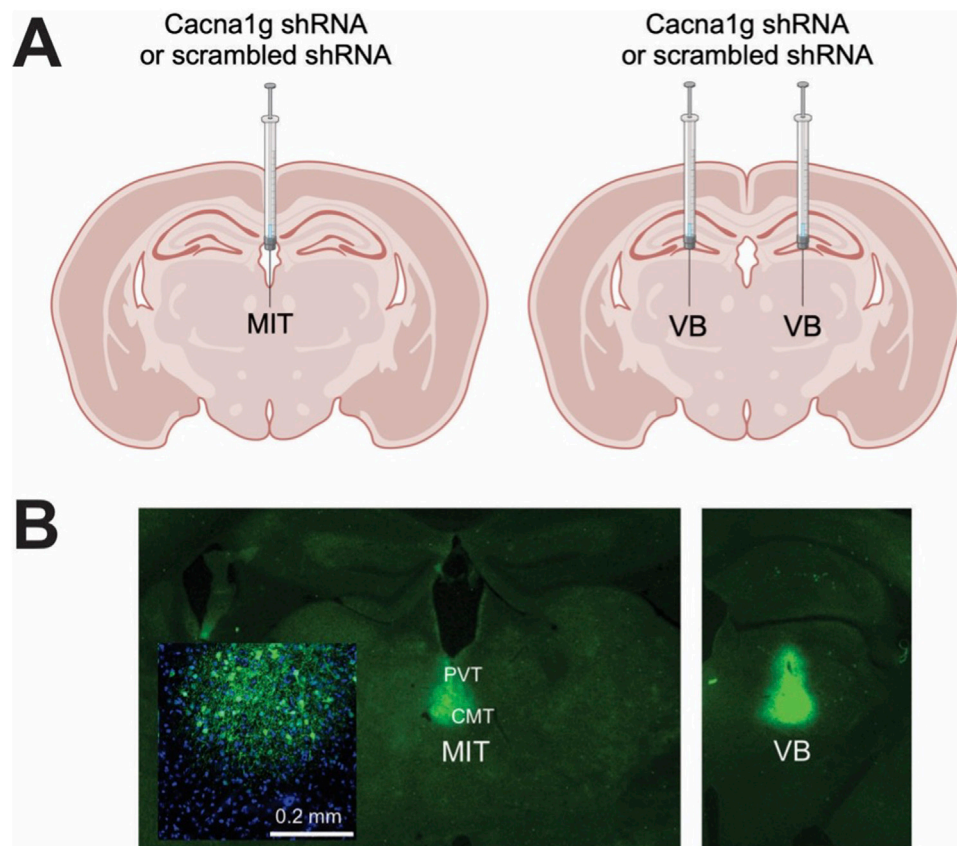
General anesthetics (GAs) have been clinically used for nearly two centuries, but the mechanisms whereby different classes of these agents achieve different clinical effects are still not well understood. A complete anesthetic state involves loss of consciousness (hypnosis) and movement (immobilization), as well as loss of both pain sensation (analgesia) and recollection of the event (amnesia). Research advances in the last three decades strongly suggest that GAs act through specific sites on the neuronal membrane and that different ion channels that control neuronal excitability may mediate their clinical effects [1, 2]. It is well known that most GAs currently in use have either N-methyl-D-aspartate (NMDA) receptor-blocking or/and γ -aminobutyric acid A (GABA_A) receptor-mimetic properties that can account for anesthetic hypnosis [1]. However, a family of neuronal voltage-gated calcium channels (VGCCs) was also implicated in the mechanisms of anesthesia because VGCC inhibition may be important in anesthetic action by decreasing neuronal excitability and presynaptic excitatory transmission [3].

Thalamus is one of the brain regions implicated in regulation of arousal, natural sleep-wake cycle and a very relevant site of anesthetic actions. The thalamus has traditionally been divided into three anatomical and functional groups: the principal (relay, sensory or motor) nuclei, the association nuclei, and the midline and intralaminar nuclei (MIT) [4, 5]. Since the sensory nuclei receive sensory information through ascending pathways and transmit it to distinct regions of the cortex, they are known as a specific part of thalamus [4, 5]. On the other hand, MIT are historically known as a nonspecific thalamus because of diffuse

projections to different cortical and subcortical areas [4, 5]. Various thalamic nuclei are important in awareness, cognitive functions, and as targets for many GAs [1, 6, 7]. Importantly, most thalamic nuclei express different isoforms of T-type VGCCs that activate with small membrane depolarizations. The T-channels are crucial for the rhythmic oscillations between mutually interconnected cortical, inhibitory GABAergic neurons in the nucleus reticularis thalami (nRT) and glutamatergic relay neurons in the sensory thalamic nuclei (VB) and MIT. Our previous studies established that nRT neurons are enriched in $\text{Ca}_v3.2$ and $\text{Ca}_v3.3$ isoforms of T-channels that underlie their low-threshold-calcium spikes (LTSS) and burst firing [8]. In contrast to nRT, neurons of the VB and MIT express almost exclusively the $\text{Ca}_v3.1$ isoform of T-channels [9–11]. In addition, we reported that $\text{Ca}_v2.3$ R-type of VGCCs is also expressed in central medial nucleus of the thalamus (CMT, part of intralaminar thalamus) and in concert with the $\text{Ca}_v3.1$ T-type channels regulate neuronal excitability [11, 12].

Recent findings have suggested that the intralaminar parts of thalamus (CMT) may act as a key hub through which GA-induced hypnosis and natural sleep are initiated [6]. Additionally, the CMT has been identified as the neuroanatomical site mediating the arousal response by manipulating activity of voltage-gated potassium channels [13–15]. Moreover, studies demonstrated that the paraventricular thalamus (PVT, part of the midline thalamus), is a key wakefulness-controlling nucleus in the thalamus [16, 17]. However, despite the proposed roles of the CMT and PVT in regulation of the state of arousal, the ability of GAs to regulate activity of VGCCs and specifically $\text{Ca}_v3.1$ channels in MIT in the context of anesthetic endpoints is not well established.

We previously reported that T-currents in the CMT, nRT and VB are inhibited by clinically relevant concentrations of volatile GAs [11, 18, 19]. This strongly suggests that thalamic T-currents participate in anesthetic action, however, new genetic tools are needed for proof-of-concept studies for the role of T-channels in the clinical effects of GAs. Further, potential region-specific differences of T-channel inhibition within the thalamus are not known. To address this gap in knowledge, here we selectively silenced the *Cacna1g* gene that encodes the $\text{Ca}_v3.1$ T-channel subunit by injecting short-hairpin RNA (shRNA) [20] into MIT and VB thalamic nuclei in wild-type (WT) mice. We then determined anesthetic endpoints such as

**FIGURE 1**

Generation of selective thalamic $\text{Ca}_v3.1$ T-channels knock-down mice. **(A)** Diagram of stereotaxic injections; control (scrambled shRNA) or *Cacna1g* shRNA injection in the non-specific thalamus (midline and intralaminar thalamus - MIT) or specific – sensory thalamus (ventrobasal thalamus - VB). **(B)** Stereotaxic injections confirmation by immunohistochemistry.

hypnosis and immobilization after administration of a traditional volatile GA isoflurane.

Materials and methods

To investigate the potential role of thalamic T-channels in anesthesia, we used a methodology which silences the *Cacna1g* gene that encodes the $\text{Ca}_v3.1$ channel pore-forming subunit by injecting short-hairpin RNA (shRNA); this is the same procedure employed by others [21] and in our recent study [20]. In short, high-titer AAV2 vectors expressing $\text{Ca}_v3.1\text{shRNA}$ (*AAV2-GFP-U6-mCACNA1G-shRNA*) or control (scrambled shRNA) were obtained from Vector BioLabs, prepared and delivered either into the MIT targeting the intralaminar (CMT) and midline parts of thalamus (PVT) (in mm from bregma, AP: -1.35 , ML: 0 , DV: 3.95) or targeting both the right and left VB thalamus (AP: -1.75 , ML: ± 1.60 , DV: 4.00) of WT male mice by stereotaxic injections using a $5\text{-}\mu\text{L}$ Hamilton syringe at a rate of $0.1\text{ }\mu\text{L/min}$. Figure 1 shows a schematic of

these areas. The induction of anesthesia in mice was performed in an anesthesia chamber with 3% isoflurane, after which they were placed on a stereotaxic frame and kept anesthetized via nose cone that continuously delivered 2–3% isoflurane throughout the whole procedure. Mice were monitored for the changes in the respiratory rate and the concentration of isoflurane was adjusted accordingly. The frame was equipped with automated drilling, followed by ultraprecise injection (Robot Stereotaxic, Neurostar). After surgery mice were treated with the analgesic Banamine 2 days and allowed to recover if no major neurological deficits were noticed. The effects of *Cacna1g* shRNA or control (scrambled shRNA) were studied at least 2 weeks following injections to allow adequate time for virus spread in the targeted areas.

Immunohistochemistry (IHC)

Following completion of behavioral experiments, brains of all mice injected with *Cacna1g* shRNA or scrambled shRNA were

processed for localization verification. Mice were deeply anesthetized with 5% isoflurane and transcardially perfused with phosphate buffered saline (PBS pH 7.4, Life Technologies), followed by 4% paraformaldehyde in 0.1 M phosphate buffer, pH 7.4 (PFA). Whole brains were extracted and post-fixed in PFA for 24 h. Brains were rinsed in PBS, embedded in 3% agarose and brain sections (50 μ m) were prepared on a microtome (Leica VT1200). Slices were rinsed three times in PBS, mounted on slides and an antigen retrieval process was performed by exposing slides to a boiling citric buffer solution (0.1 M, pH 6.0). Sections were permeabilized in 1% glycine in PBST for 15 min and rinsed in PBS for 5 min. Sections were then blocked with 5% normal donkey serum in PBST (0.1% Triton X-100 in PBS) for 30 min, and incubated with primary antibody (rabbit anti-GFP; 1:1000; A11122; Invitrogen) diluted in 1% normal donkey serum in PBST overnight at 4°C. Slices were rinsed 3 \times 5 min in PBST followed by a 5-min rinse in PBS and then incubated for 2 h with secondary anti-rabbit antibody (anti-rabbit Alexa 488: 1:500, Invitrogen) at room temperature and washed 3 \times 5 min in PBS. Sections were coverslipped using a fluorescent mounting medium containing DAPI (Vector laboratories) and images were taken using a confocal laser scanning microscope (Olympus FluoView FV1200) at \times 20 magnification using image stitching to obtain the entire region of interest. Although, in our stereotaxic injections we targeted the CMT, we found using confocal microscopy that GFP immunofluorescence has spread into adjacent nuclei [PVT and/or interomediodorsal nucleus of thalamus (IMD), Figure 1] in most of our experiments. Hence, due to this technical limitation we refer to nonspecific thalamic injections as targeting MIT, not just CMT. Only the mice that had viral GFP expression localized to the MIT or VB were included in analysis.

Brain slice preparation for patch-clamp electrophysiology experiments

Patch-clamp experiments using brain slices from the virus-injected mice began at least 2 weeks after injection. Animals were anesthetized briefly with isoflurane, decapitated, and their brains rapidly removed. Fresh horizontal brain slices, 250 μ m-thick, were sectioned at 4°C in a pre-chilled solution containing (in mM): sucrose 260, D-glucose 10, NaHCO₃ 26, NaH₂PO₄ 1.25, KCl 3, CaCl₂ 2, MgCl₂ 2, using a vibrating micro slicer (Leica VT 1200S). Brain slices were immediately incubated for 45 min in a solution containing (in mM): NaCl 124, D-glucose 10, NaHCO₃ 26, NaH₂PO₄ 1.25, KCl 4, CaCl₂ 2, MgCl₂ 2 at 37°C prior to use in electrophysiology experiments, which were conducted at room temperature. During incubation, slices were constantly perfused with a gas mixture of 95% O₂ and 5% CO₂ (v/v).

Patch-clamp electrophysiology recordings

The external solution for whole-cell voltage-clamp recordings consisted of (in mM): NaCl 125, D-glucose 25, NaHCO₃ 25, NaH₂PO₄ 1.25, KCl 2.5, MgCl₂ 1, and CaCl₂ 2. This solution was equilibrated with a mixture of 95% O₂ and 5% CO₂ (v/v) for at least 30 min with a resulting pH of approximately 7.4. The internal solution for recording well isolated T-currents consisted of (in mM): tetramethyl ammonium (TMA)-OH 135, EGTA 10, MgCl₂ 2, and HEPES 40, titrated to pH 7.2 with hydrofluoric acid (HF) [22].

The current-voltage (I-V) curves were generated by stepping from the holding potential (V_h) of -90 mV to depolarized test potentials (V_t) from -80 to -40 mV in 2.5 mV increments. The voltage dependencies of steady-state activation were described with single Boltzmann distributions of the following forms: Activation: $G(V) = G_{\max} / (1 + \exp[-(V - V_{50})/k])$; G_{\max} is the maximal conductance (calculated by dividing current amplitude by estimated reversal potential), V_{50} is the voltage at which half of the current is activated, and k represents the voltage dependence (slope) of the distribution. The T-currents from the inactivation protocol were recorded by using a standard double-pulse protocol with 3.6-s-long prepulses to variable voltages (from -120 to -60 mV in 5 mV increments) and test potentials to -50 mV.

For the whole-cell current-clamp recordings, the internal solution consisted of (in mM): potassium-D-gluconate 130, EGTA 5, NaCl 4, CaCl₂ 0.5, HEPES 10, Mg ATP 2, Tris GTP 0.5, pH 7.2. Glass micropipettes (Sutter Instruments O.D. 1.5 mm) were pulled using a Sutter Instruments Model P-1000 and fabricated to maintain an initial resistance of 3–5 M Ω . GFP-expressing thalamic neurons were identified using the microscope with epifluorescence and IR-DIC optics. Intrinsic excitability of thalamic neurons was characterized by using a multi-step protocol which consisted of injecting a family of depolarizing (50–300 pA) current pulses of 400 ms duration in 25 pA increments followed by a series of hyperpolarizing currents of the same duration stepping from -50 to -250 pA in 25 pA increments. Subsequent action potential (AP) tonic and rebound firing frequencies (per pulse and per burst) and input resistances were determined. The membrane potential was measured at the beginning of each recording and was not corrected for the liquid junction potential, which was around 10 mV in our experiments. The membrane input resistance was calculated by dividing the end of steady-state hyperpolarizing voltage deflection by the injected current. Neuronal membrane responses were recorded using a Multiclamp 700B amplifier (Molecular Devices, CA, United States). Voltage current commands and digitization of the resulting voltages and currents were performed with Clampex 8.3 software

(Molecular Devices), and voltage and current traces were analyzed using Clampfit 10.5 (Molecular Devices).

Animals

Experimental procedures with animals were performed according to the guidelines approved by the Institutional Animal Care and Use Committee (IACUC) of the University of Colorado Anschutz Medical Campus. Treatments of animals adhered to guidelines set forth in the NIH Guide for the Care and Use of Laboratory Animals. Our study was approved by the ethics committee of the University of Colorado Anschutz Medical Campus. The adult male C57BL/6J wild type (WT) mice (between 2 and 4 months of age) were used for behavioral experiments. C57BL/6J mice were obtained from the Jackson laboratory (USA). We opted for male mice, as very little is known about sex differences in activity of volatile anesthetics in the thalamus. All animals were maintained on a 14/10 h light-dark cycle with food and water *ad libitum*. Anesthetic endpoints were measured as we previously reported [23] as follows.

Loss of righting reflex (LORR) and loss or withdrawal reflex (LOWR)

LORR is assessed by placing the mouse on its back until animal loses righting reflex. The criterion for the LORR is failure of mouse to right within a 30-s period. For LOWR, an alligator clip covered with airway tubing was used on proximal 1/3 tail and LOWR was considered when there was no withdrawal for a minimum of 30-s. All mice were placed on a heating pad in a chamber equilibrated with 0.5% isoflurane. Isoflurane was then increased by 0.1% every 10 min until LORR and LOWR was obtained. Illustration of the experiments with LORR and LOWR determination is depicted on top panels of Figures 4A, 5A.

Anesthetic induction

Induction time was assessed by measuring the time to LORR (TTLORR) at a constant inhaled concentration of 1.2% isoflurane. Mice were placed on the heating pad in anesthetic chamber that was set at 1.2% isoflurane after a 30-min wait. Successful induction was determined when a mouse failed to right within a 30-s period.

Drugs

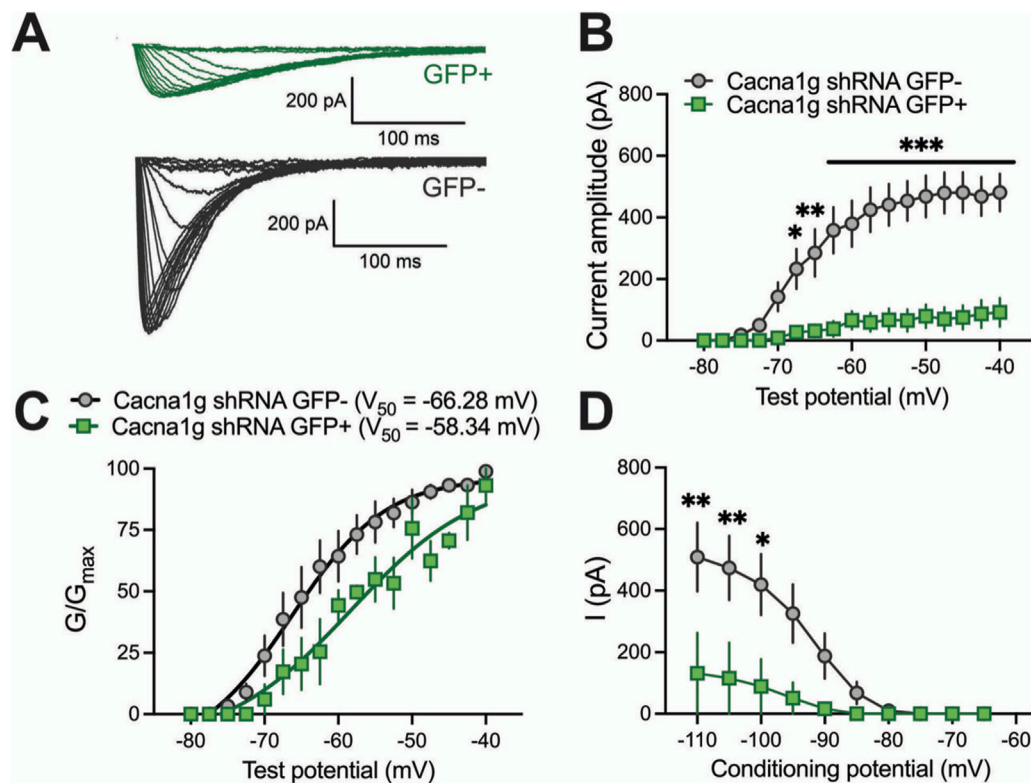
Isoflurane was purchased from McKesson (San Francisco, CA) and Banamine (Merck) was obtained from the University of Colorado Hospital pharmacy.

Data analysis

In every experiment, we attempted to minimize the number of animals used. All animals with complete data set and physiological parameters were included in the study. Statistical analysis was performed using two-way repeated measure (RM) ANOVA as well as student unpaired and two-tailed *t*-test, where appropriate. We used *Sidak's multiple comparisons test* where interaction between factors after two-way RM ANOVA was significant. Significance was accepted with *p* values < 0.05. Statistical and graphical analysis was performed using GraphPad Prism 8.00 software (GraphPad Software, La Jolla, CA, United States) and Origin 2018 (OriginLab, Northampton, MA, United States).

Results

To validate functional knock-down of T-currents we first performed patch-clamp recordings using acute brain slices from WT mice injected with *Cacna1g* shRNA (Figure 2). Transfected neurons were readily identified in our recordings from live brain slices with bright GFP immunofluorescence. Specifically, we compared T-current biophysical properties from the acute thalamic slices in GFP positive (GFP+) and GFP negative (GFP-) neurons. T-currents were evoked using our standard current-voltage (I-V) protocols with depolarizing steps to test potentials (*V_t*) from −80 to −40 mV from holding (*V_h*) potentials of −90 mV. Original traces of inward calcium currents from representative recordings in the CMT in GFP+ neurons (green traces) and GFP- neurons (black traces) are depicted in Figure 2A. On average, we found that peak T-currents in GFP+ neurons (*n* = 7, green symbols) were almost completely abolished as evidenced by about 90% decreased amplitudes when compared to GFP- neurons (*n* = 7, gray symbols) across most of the test potentials in our I-V recordings (Figure 2B). We next compared steady-state activation curves in two groups and found that GFP+ neurons exhibited a small but insignificant depolarizing shift in *V₅₀* of channel activation when compared to GFP- neurons (Figure 2C). Finally, we used an independent protocol of recordings T-current amplitudes (*V_t* −50 mV) after conditioning pre-pulses from −110 to −60 mV. Average graphs from these experiments showing largely decreased T-current amplitudes in GFP+ neurons (green symbols) when compared to GFP- neurons (gray symbols) is summarized on Figure 2D. Our results showing greatly decreased T-current amplitudes strongly suggest that excitability of GFP+ neurons may be decreased as result of injections of *Cacna1g* shRNA. Hence, in ensuing current-clamp experiments we compared tonic and burst firing properties of GFP+ and GFP- neurons in CMT as summarized on Figure 3. Original traces of a rebound action potential (AP) and a T-channel-dependent low-threshold-calcium spike (LTS) from a GFP- neuron (gray trace) are

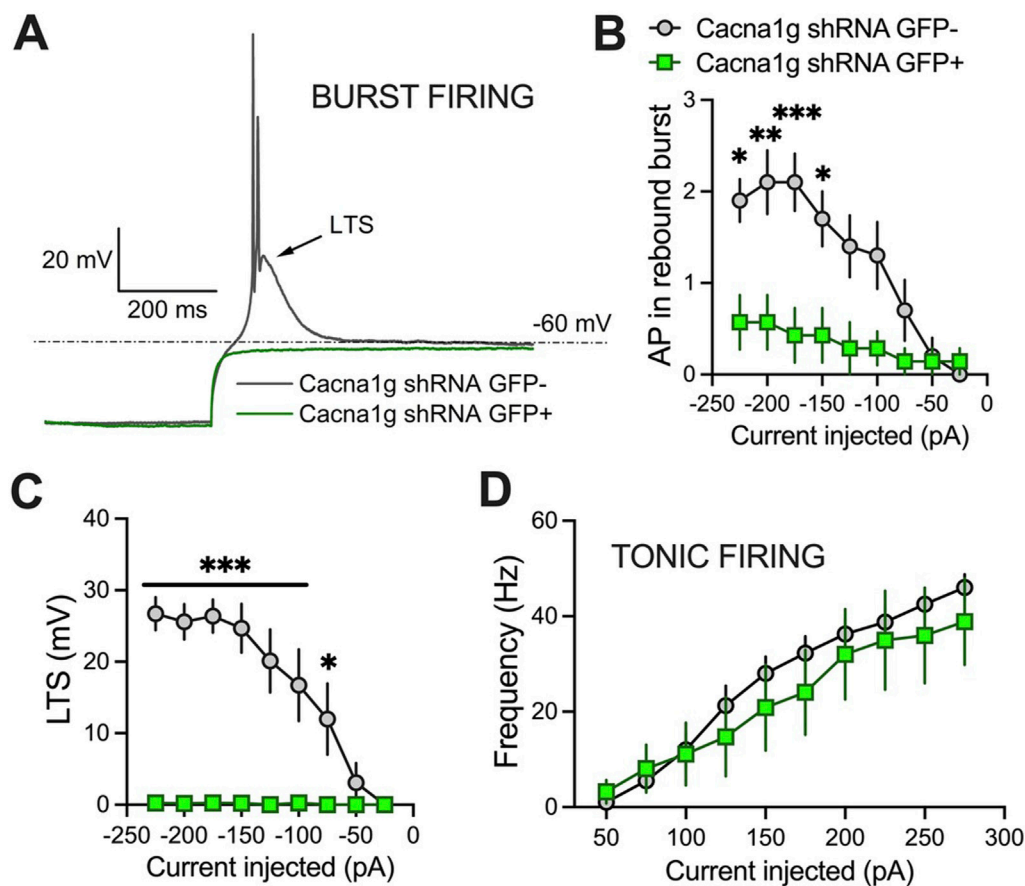
**FIGURE 2**

Biophysical properties of thalamic T-currents in Cacna1g shRNA GFP+ and GFP- neurons. **(A)** T-current $I-V$ traces from representative GFP+ (green) and GFP- (black) neurons in the voltage range for V_t of -80 to -40 mV from an initial holding potential (V_h) of -90 mV in 2.5 mV increments. Note that the T-currents recorded from the GFP+ cells are smaller and don't show typical criss-crossing pattern. **(B)** Average T-current amplitude, as calculated from the steady-state activation protocol was reduced in Cacna1g shRNA GFP+ neurons in comparison to GFP- cells (two-way RM ANOVA: interaction $F_{(16,129)} = 12.54$, $p < 0.001$; test potential $F_{(16,192)} = 25.01$, $p < 0.001$, GFP $F_{(1,12)} = 27.34$, $p < 0.001$; Sidak's *post hoc* presented on Figure). $N = 7$ cells per group, note that 3 GFP+ cells did not have T-currents. **(C)** The average voltage dependence of a steady-state activation (G/G_{max}) curve with V_{50} value noted on the graph for GFP+ and GFP- thalamic neurons. The difference between V_{50} for T-current activation was not statistically significant between GFP+ and GFP- cells. $N = 3$ GFP+, $N = 7$ GFP-neurons. **(D)** Average T-current amplitude, as calculated from the steady-state inactivation protocol (double-pulse protocol with 3.6 -s-long prepulses to variable voltages (from -120 to -50 mV in 5 mV increments) and a test potential (V_t) of -50 mV) was greatly reduced in Cacna1g shRNA GFP+ neurons in comparison to GFP- cells (two-way RM ANOVA: interaction $F_{(9,72)} = 4.61$, $p < 0.001$; potential $F_{(9,72)} = 12.24$, $p < 0.001$, GFP $F_{(1,8)} = 4.99$, $p = 0.056$; Sidak's *post hoc* presented on Figure). $N = 4$ GFP+, $N = 6$ GFP- cells per group, note that just one of four GFP+ cells had measurable T-currents. * $p < 0.05$, ** $p < 0.01$, *** $p < 0.001$.

depicted on Figure 3A. The same figure shows a lack of rebound APs and completely abolished LTS in a GFP+ neuron (green trace). In the summary graph on Figure 3B we depict the average number of rebound APs in GFP- neurons ($n = 10$ neurons, gray symbols) resulting from progressively stronger hyperpolarizing steps from -50 to -250 pA. In contrast, the same figure shows only minimal active membrane response upon injections of the same currents ($n = 7$ neurons, gray symbols). Likewise, Figure 3C shows that in the same two groups when we compared LTSs are completely absent in GFP+ neurons (green symbols) while in GFP- neurons (gray symbols) they show typical voltage-dependence with larger amplitudes associated with stronger current injections. As expected, we found very little difference in the two groups when we compared properties of tonic firing of APs in response to escalating depolarizing current injections from $+50$ to $+300$ pA (Figure 3D). Overall, our patch-clamp

recordings from thalamic neurons *ex vivo* in animals injected with Ca v 3.1shRNA show that GFP+ neurons exhibited largely decreased T-current amplitudes and greatly diminished rebound burst firing.

In the ensuing *in vivo* experiments, we tested control groups (mice injected with scrambled shRNA) and experimental groups (mice injected with Cacna1g shRNA) for anesthetic endpoints, as determined by concentrations of inhaled isoflurane required to induce LORR. The examiner was blinded to the experimental and control groups. Figure 4 summarizes our data from the experiments where the Cacna1g shRNA or scrambled shRNA (control group) were injected into MIT. We found no significant difference in speed of induction as measured by TTLORR in Cacna1g shRNA group ($n = 6$, green symbols) when compared to our controls ($n = 8$, scrambled shRNA, gray symbols) as depicted on Figure 4B. In

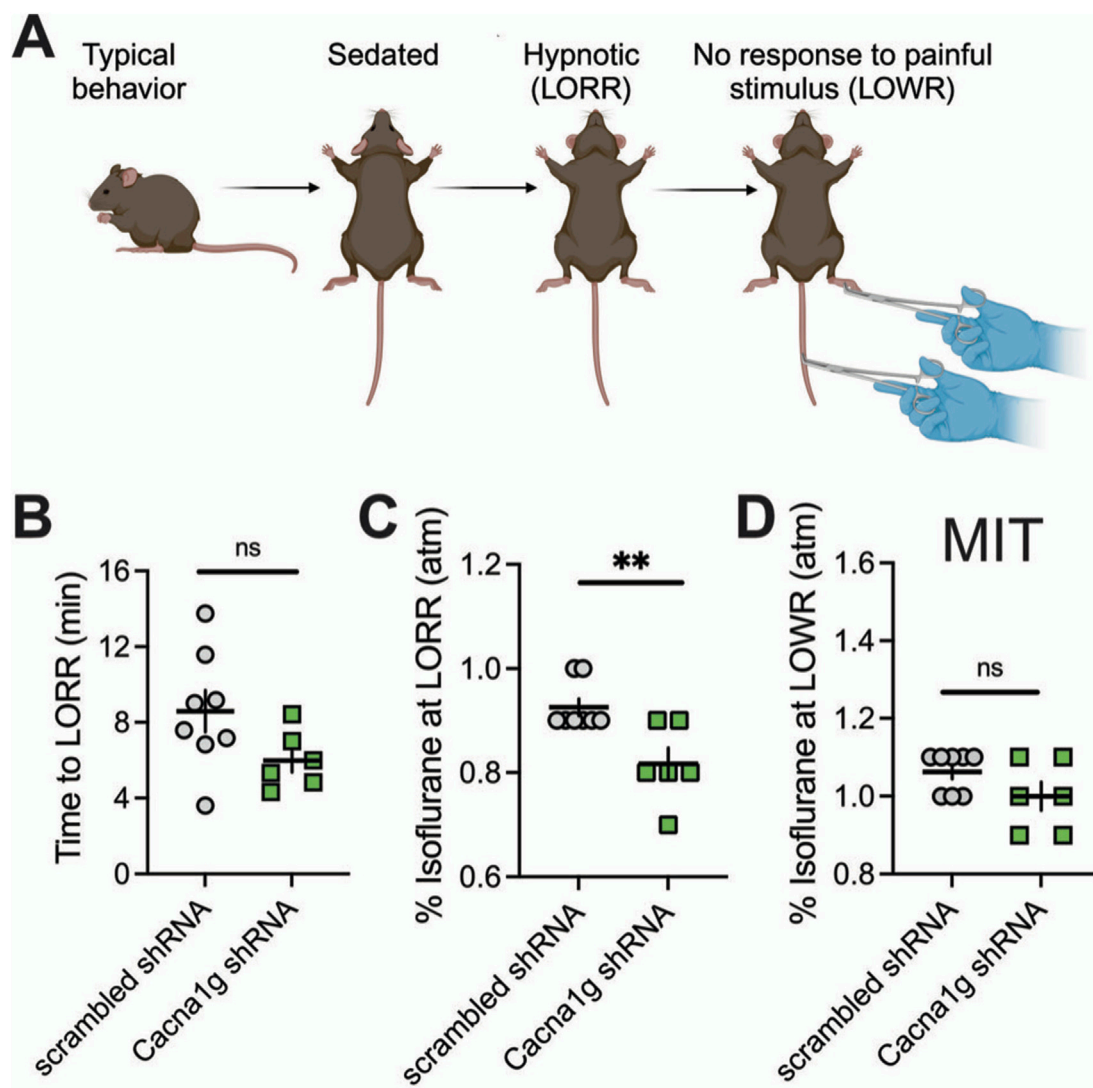
**FIGURE 3**

Excitability differences between GFP+ and GFP- thalamic neurons from Cacna1g shRNA injected animals. **(A)** Original traces from representative thalamic neurons recorded from GFP+ (green) and GFP- (gray) neurons show active membrane responses to a hyperpolarizing (-225 pA) current injection. Note that GFP+ neuron does not show APs nor low threshold spike (LTS) after membrane hyperpolarization. **(B)** Number of action potentials (AP) in rebound burst was statistically significant smaller in GFP+ neurons (two-way RM ANOVA: interaction $F_{(8,120)} = 5.34$, $p < 0.001$; current injected $F_{(8,120)} = 11.95$, $p < 0.001$, GFP $F_{(1,15)} = 9.07$, $p = 0.009$; Sidak's *post hoc* presented on Figure). **(C)** LTS was not observed in GFP+ neurons (two-way RM ANOVA: interaction $F_{(8,120)} = 12.06$, $p < 0.001$; current injected $F_{(8,120)} = 12.51$, $p < 0.001$, GFP $F_{(1,15)} = 31.07$, $p < 0.001$; Sidak's *post hoc* presented on Figure). **(D)** Graph of averages of tonic AP firing frequency and current injections of 50–275 pA from multiple experiments shows no difference between GFP+ and GFP- Cacna1g shRNA injected thalamic neurons. $N = 7$ GFP+, $N = 10$ GFP- cells. * $p < 0.05$, ** $p < 0.01$, *** $p < 0.001$.

contrast, we found about 10% decrease in inhaled % atm isoflurane needed to induce LORR in group where Cacna1g shRNA was injected in the MIT region (Figure 4C). Finally, we found that the immobilizing effect measured by LOWR after injections of Cacna1g shRNA and scrambled shRNA into MIT region was not different in the two groups (Figure 4D). In contrast, mice injected with Cacna1g shRNA in the VB region ($n = 9$) did not show any difference in the speed of anesthetic induction (Figure 5B), or concentration of isoflurane required to induce LORR when compared to controls ($n = 9$) (Figure 5C). Similarly to injections to MIT, we found that LOWR response was not different between Cacna1g shRNA ($n = 9$) and scrambled shRNA ($n = 9$) group in our VB injections (Figure 5D). We conclude that *in vivo* silencing of $Ca_v3.1$ channels in two functionally different regions of the

thalamus, such as the MIT and the VB, differentially affected the required hypnotic concentration of isoflurane without an apparent difference in the speed of anesthetic induction and immobilizing properties of isoflurane.

In the ensuing *in vivo* experiments, we also tested the ability of mice injected either with scrambled shRNA or with Cacna1g shRNA into the MIT or the lateral thalamus targeting bilateral VB to perform behavioral tasks in an open-field test. We found that performance of mice during 10 min of testing in the groups injected either with scrambled or Cacna1g shRNA when compared to the naive, uninjected mice, was not different in the open-field testing ($n = 5$ – 10 mice per group, data not shown). Hence, it appears that intrathalamic injection of viral vectors did not cause any major neurological deficit *per se* because it did not affect the general motor ability of mice.

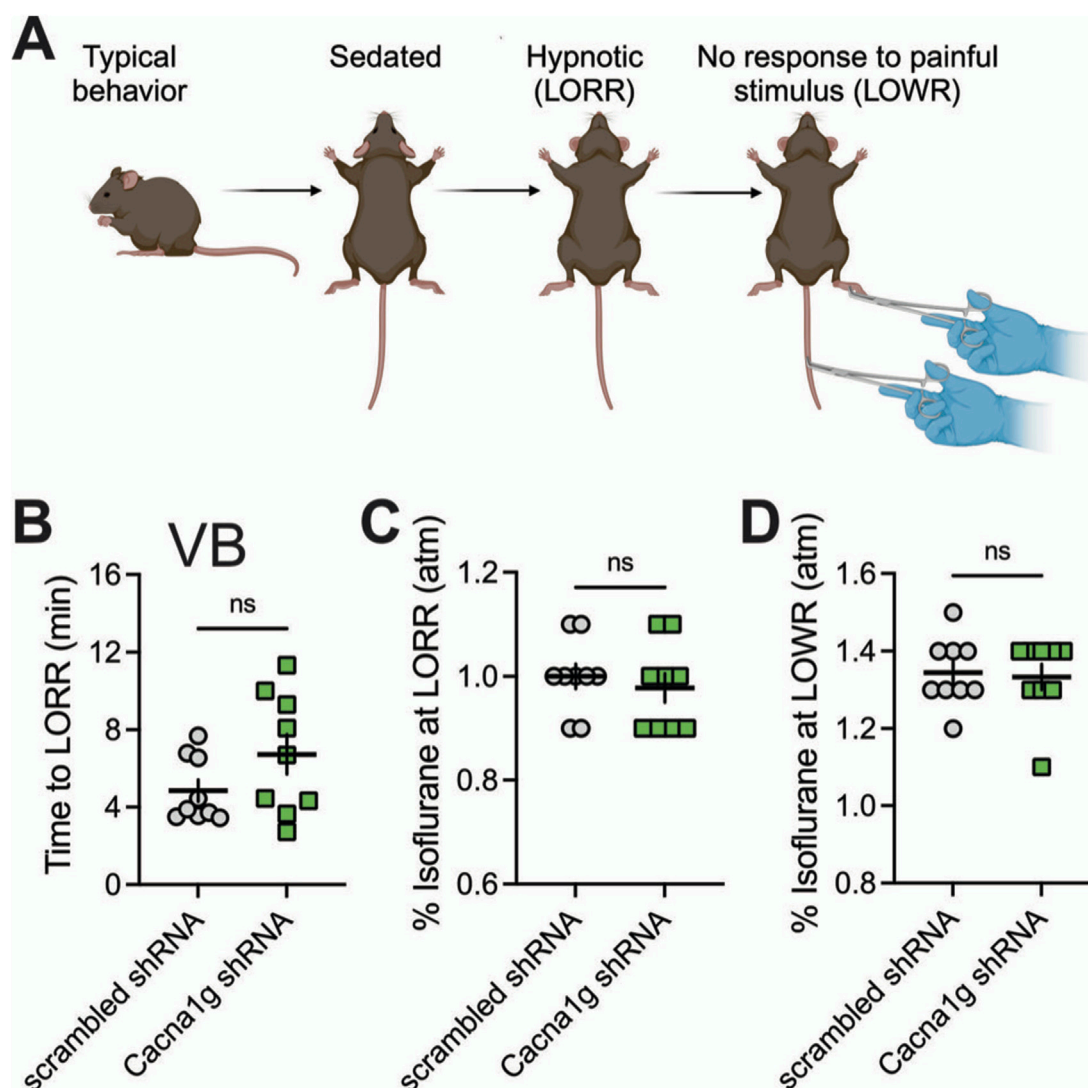
**FIGURE 4**

Effect of knocking-down of $Ca_v3.1$ T-channels from MIT on LORR. (A) Schematic representation of LORR and LOWR experiments. (B) Time to LORR was not statistically significant between control (scrambled shRNA) and Cacna1g shRNA MIT injected mice. (C) Cacna1g shRNA MIT injected animals required less isoflurane for achieving LORR (hypnotic effect) in comparison to control male mice (unpaired two-tailed t-test: $t_{(12)} = 3.34$, $p = 0.006$). (D) There was no difference in isoflurane requirement for LOWR between control scrambled shRNA and Cacna1g shRNA MIT injected animals. $N = 8$ control scrambled shRNA and $N = 6$ Cacna1g shRNA animals. ** $p < 0.01$.

Discussion

One of the compelling reasons to study VGCCs in the mechanisms of anesthetic actions is that these channels are essential in regulation of synaptic transmission and excitability in the neuronal sleep pathway such as thalamus. The thalamus is the major gateway for the flow of sensory information from the periphery to the cortex and the disruption of thalamocortical connectivity may be an essential common feature of the hypnotic effects of many GAs. Indeed, both human and animal studies *in vivo* have indicated that the thalamus is deactivated during anesthesia [24]. Two thalamic

regions are particularly relevant for our considerations as neuronal network targets for GAs. One such region, the thalamic VB nucleus, receives direct sensory projections from the periphery and projects mostly to the barrel cortex, it is a principal thalamic nucleus often referred to as a specific or sensory thalamus [5, 25]. The other region of interest, known as a nonspecific thalamus, consists of the CMT and PVT, parts of the MIT, which project diffusely to the different cortical and subcortical areas [5]. The parts of MIT are interposed between the brain stem “arousal” system and are ideally suited to control the overall level of thalamic and cortical activity [5, 26, 27]. Importantly, our previous *ex vivo* studies using acute brain slices

**FIGURE 5**

Effect of knocking-down of $\text{Ca}_v3.1$ T-channels from VB on LORR. **(A)** Schematic representation of LORR and LOWR experiments. **(B)** Time to LORR was not statistically significant between control (scrambled shRNA) and *Cacna1g* shRNA in VB injected mice. **(C)** There was no difference in isoflurane requirement for LORR (hypnotic effect) between control and *Cacna1g* shRNA in VB injected mice. **(D)** There was no difference in isoflurane requirement for LOWR between control and *Cacna1g* shRNA in VB injected animals. $N = 9$ control scrambled shRNA and $N = 9$ *Cacna1g* shRNA animals.

have demonstrated that $\text{Ca}_v3.1$ channel-mediated excitability in both the VB [19] and in the CMT [11] is diminished with clinically relevant concentrations of isoflurane. Hence, we hypothesized that knocking-down $\text{Ca}_v3.1$ channels in the CMT and VB neurons may have different effects on loss of consciousness induced by GAs. To test this hypothesis, we produced region-specific knock-down of $\text{Ca}_v3.1$ channels in MIT and VB nuclei to determine if diminished excitability of these neurons *ex vivo* correlate with the ability of a traditional volatile GA such as isoflurane to induce hypnosis in mice. These experiments addressed a long-standing unresolved issue of whether inhibition of $\text{Ca}_v3.1$ T-channels in different functional

regions of the thalamus is important for GA-induced hypnosis. Most thalamic neurons fire APs in a regular (tonic) mode when depolarized from the resting membrane potential, and high frequency burst firing mode that crowns low-threshold calcium spikes (LTS) if they are hyperpolarized sufficiently to de-inactivate T-type calcium channels [11, 28]. Indeed, we showed that knocking down $\text{Ca}_v3.1$ channels in thalamus completely abolished LTS and greatly diminished rebound burst firing pattern while it had only a minimal effect on the tonic firing pattern (Figure 3). Our voltage- and current-clamp experiment validated our silencing technique using an shRNA approach that we also used to study the functional

role of $\text{Ca}_v3.1$ channel in the subiculum [20]. A previous study used a global knockout mouse to investigate the role of $\text{Ca}_v3.1$ channels in anesthetic sensitivities. Petrenko and colleagues reported that global $\text{Ca}_v3.1$ KO mice showed no change in anesthetic requirements (isoflurane, halothane, sevoflurane, pentobarbital) for LORR and LOWR but have delay in the onset of anesthetic induction measured by TTLORR [29]. They further concluded that the timely induction of anesthesia/hypnosis by volatile anesthetic agents and some intravenous anesthetic agents may require the normal functioning of the $\text{Ca}_v3.1$ channel isoform. However, since $\text{Ca}_v3.1$ channels are expressed in many different parts of the thalamus, hippocampus and cortex, we opted for the knock-down approach to be able to target specific thalamic regions and minimize compensatory changes in neuronal circuitry that are more likely with global knockouts. In contrast to this study with global KO mice, we found that knocking down this T-channel isoform in MIT leads to a decreased requirement for hypnosis induced by isoflurane. Our finding is consistent with another study that examined the specific role of the VB and CMT in anesthetic hypnosis [6]. Specifically, Baker and colleagues recorded local field potentials (LFPs) from four brain regions (barrel neocortex, VB, anterior cingulate cortex, and CMT) simultaneously in freely moving rodents during transitions into natural sleep and anesthetic-induced (propofol and dexmedetomidine) LORR. They found that for propofol-induced LORR and natural sleep, the LFP changes with neuronal oscillations occur first in the nonspecific thalamus before changes could be detected in the neocortex. With dexmedetomidine, they found that initial LFP changes occurred simultaneously in the nonspecific thalamus and neocortex. Overall, they concluded that CMT acts as key hub through which both anesthetic hypnosis and natural sleep are initiated. Our results are consistent with the idea that the nonspecific MIT region of the thalamus is more important for isoflurane-induced hypnosis than the specific sensory VB thalamus. In addition, we validated important role of $\text{Ca}_v3.1$ isoform of T-type channels in this mechanism of anesthetic hypnosis. Towards this end, we recently reported that other classes of GAs like neuroactive steroids induce hypnosis in rodents at least in part by inhibiting $\text{Ca}_v3.1$ channels in the thalamus [30, 31]. Hence, our future experiments will address the issue if $\text{Ca}_v3.1$ T-type channels in MIT region of the thalamus show a similar preferential role in neurosteroid-induced hypnosis.

Author contributions

Conceptualization, TTS and SMT; analysis, TTS; experiment, TTS, SF, BF-R, VT; writing—original draft preparation, SMT; writing—review and editing, TTS, SF, BF-R, VT; supervision, SMT; funding acquisition, TTS and SMT.

Data availability

The raw data supporting the conclusions of this article will be made available by the authors, without undue reservation.

Ethics statement

Experimental procedures with animals were performed according to the guidelines approved by the Institutional Animal Care and Use Committee (IACUC) of the University of Colorado Anschutz Medical Campus. Treatments of animals adhered to guidelines set forth in the NIH Guide for the Care and Use of Laboratory Animals. Our study was approved by the ethics committee of the University of Colorado Anschutz Medical Campus.

Funding

The author(s) declare that financial support was received for the research and/or publication of this article. This study was funded in part by grants from the National Institutes of Health (GRANT# GM141802 and VA Merit I01BX004763 to SMT and DA055258 to TTS) and funds from the Department of Anesthesiology and School of Medicine at Anschutz Medical Campus.

Acknowledgments

We thank MacKenzie Walz and Sarah Kawell for maintaining the mouse colonies.

Conflict of interest

The author(s) declared no potential conflicts of interest with respect to the research, authorship, and/or publication of this article.

Generative AI statement

The authors declare that no Generative AI was used in the creation of this manuscript.

References

1. Franks NP. General anaesthesia: from molecular targets to neuronal pathways of sleep and arousal. *Nat Rev Neurosci* (2008) **9**:370–86. doi:10.1038/nrn2372
2. Herold KF, Sanford RL, Lee W, Andersen OS, Hemmings HC. Clinical concentrations of chemically diverse general anesthetics minimally affect lipid bilayer properties. *Proc Natl Acad Sci* (2017) **114**:3109–14. doi:10.1073/pnas.1611717114
3. Orestes P, Todorovic SM. Are neuronal voltage-gated calcium channels valid cellular targets for general anesthetics? *Channels (Austin)* (2010) **4**:518–22. doi:10.4161/chan.4.6.12873
4. Vertes RP, Linley SB, Hoover WB. Limbic circuitry of the midline thalamus. *Neurosci and Biobehavioral Rev* (2015) **54**:89–107. doi:10.1016/j.neubiorev.2015.01.014
5. Vertes RP, Linley SB, Rojas AKP. Structural and functional organization of the midline and intralaminar nuclei of the thalamus. *Front Behav Neurosci* (2022) **16**:964644. doi:10.3389/fnbeh.2022.964644
6. Baker R, Gent TC, Yang Q, Parker S, Vyssotski AL, Wisden W, et al. Altered activity in the central medial thalamus precedes changes in the neocortex during transitions into both sleep and propofol anesthesia. *The J Neurosci* (2014) **34**:13326–35. doi:10.1523/jneurosci.1519-14.2014
7. Alkire MT, Haier RJ, Fallon JH. Toward a unified theory of narcosis: brain imaging evidence for a thalamocortical switch as the neurophysiologic basis of anesthetic-induced unconsciousness. *Conscious Cogn* (2000) **9**:370–86. doi:10.1006/cog.1999.0423
8. Joksovic PM, Nelson MT, Jevtovic-Todorovic V, Patel MK, Perez-Reyes E, Campbell KP, et al. Cav3.2 is the major molecular substrate for redox regulation of T-type Ca²⁺ channels in the rat and mouse thalamus. *The J Physiol* (2006) **574**:415–30. doi:10.1113/jphysiol.2006.110395
9. Talley EM, Cribbs LL, Lee JH, Daud A, Perez-Reyes E, Bayliss DA. Differential distribution of three members of a gene family encoding low voltage-activated (T-type) calcium channels. *J Neurosci* (1999) **19**:1895–911. doi:10.1523/jneurosci.19-06-01895.1999
10. Kim D, Song I, Keum S, Lee T, Jeong MJ, Kim SS, et al. Lack of the burst firing of thalamocortical relay neurons and resistance to absence seizures in mice lacking $\alpha 1G$ T-type Ca²⁺ channels. *Neuron* (2001) **31**:35–45. doi:10.1016/s0896-6273(01)00343-9
11. Timic ST, Feseha S, Valdez R, Zhao W, Klawitter J, Todorovic SM. Alterations in oscillatory behavior of central medial thalamic neurons demonstrate a key role of Cav3.1 isoform of T-channels during isoflurane-induced anesthesia. *Cereb Cortex* (2019) **29**:1–18. doi:10.1093/cercor/bhz002
12. Timic Stamenic T, Manzella FM, Maksimovic S, Krishnan K, Covey DF, Jevtovic-Todorovic V, et al. Further evidence that inhibition of neuronal voltage-gated calcium channels contributes to the hypnotic effect of neurosteroid analogue, 3 β -OH. *Front Pharmacol* (2022) **13**:850658. doi:10.3389/fphar.2022.850658
13. Alkire MT, Asher CD, Franciscus AM, Hahn EL. Thalamic microinfusion of antibody to a voltage-gated potassium channel restores consciousness during anesthesia. *Anesthesiology* (2009) **110**:766–73. doi:10.1097/aln.0b013e31819c461c
14. Lioudyno MI, Birch AM, Tanaka BS, Sokolov Y, Goldin AL, Chandy KG, et al. Shaker-related potassium channels in the central medial nucleus of the thalamus are important molecular targets for arousal suppression by volatile general anesthetics. *The J Neurosci* (2013) **33**:16310–22. doi:10.1523/jneurosci.0344-13.2013
15. Alkire MT, McReynolds JR, Hahn EL, Trivedi AN. Thalamic microinjection of nicotine reverses sevoflurane-induced loss of righting reflex in the rat. *Anesthesiology* (2007) **107**:264–72. doi:10.1097/01.anes.0000270741.33766.24
16. Ren S, Wang Y, Yue F, Cheng X, Dang R, Qiao Q, et al. The paraventricular thalamus is a critical thalamic area for wakefulness. *Science* (2018) **362**:429–34. doi:10.1126/science.aat2512
17. Colavito V, Tesoriero C, Wirtu AT, Grassi-Zucconi G, Bentivoglio M. Limbic thalamus and state-dependent behavior: the paraventricular nucleus of the thalamic midline as a node in circadian timing and sleep/wake-regulatory networks. *Neurosci and Biobehavioral Rev* (2015) **54**:3–17. doi:10.1016/j.neubiorev.2014.11.021
18. Joksovic PM, Todorovic SM. Isoflurane modulates neuronal excitability of the nucleus reticularis thalami *in vitro*. *Ann New York Acad Sci* (2010) **1199**:36–42. doi:10.1111/j.1749-6632.2009.05172.x
19. Eckle VS, DiGrucio MR, Uebele VN, Renger JJ, Todorovic SM. Inhibition of T-type calcium current in rat thalamocortical neurons by isoflurane. *Neuropharmacology* (2012) **63**:266–73. doi:10.1016/j.neuropharm.2012.03.018
20. Joksimovic SM, Ghodsi SM, Heinsbroek JA, Orfila JE, Busquet N, Tesic V, et al. Cav3.1 T-type calcium channels are important for spatial memory processing in the dorsal subiculum. *Neuropharmacology* (2023) **226**:109400. doi:10.1016/j.neuropharm.2022.109400
21. Gangadharan G, Shin J, Kim S-W, Kim A, Paydar A, Kim D-S, et al. Medial septal GABAergic projection neurons promote object exploration behavior and type 2 theta rhythm. *Proc Natl Acad Sci* (2016) **113**:6550–5. doi:10.1073/pnas.1605019113
22. Todorovic SM, Lingle CJ. Pharmacological properties of T-type Ca²⁺ current in adult rat sensory neurons: effects of anticonvulsant and anesthetic agents. *J Neurophysiol* (1998) **79**:240–52. doi:10.1152/jn.1998.79.1.240
23. Feseha S, Timic Stamenic T, Wallace D, Tamag C, Yang L, Pan JQ, et al. Global genetic deletion of Cav3.3 channels facilitates anaesthetic induction and enhances isoflurane-sparing effects of T-type calcium channel blockers. *Sci Rep* (2020) **10**:21510–0. doi:10.1038/s41598-020-78488-8
24. Schiff ND. Central thalamic contributions to arousal regulation and neurological disorders of consciousness. *Ann New York Acad Sci* (2008) **1129**:105–18. doi:10.1196/annals.1417.029
25. Crunelli V, David F, Leresche N, Lambert RC. Role for T-type Ca²⁺ channels in sleep waves. *Pflügers Archiv - Eur J Physiol* (2014) **466**:735–45. doi:10.1007/s00424-014-1477-3
26. Vertes RP, Hoover WB, Rodriguez JJ. Projections of the central medial nucleus of the thalamus in the rat: node in cortical, striatal and limbic forebrain circuitry. *Neuroscience* (2012) **219**:120–36. doi:10.1016/j.neuroscience.2012.04.067
27. Vertes RP, Hoover WB. Projections of the paraventricular and paratenial nuclei of the dorsal midline thalamus in the rat. *J Comp Neurol* (2008) **508**:212–37. doi:10.1002/cne.21679
28. Stamenic TT, Todorovic SM. Cytosolic ATP relieves voltage-dependent inactivation of T-type calcium channels and facilitates excitability of neurons in the rat central medial thalamus. *eNeuro* (2018) **5**:ENEURO.0016–8.2018. doi:10.1523/eneuro.0016-18.2018
29. Petrenko AB, Tsujita M, Kohno T, Sakimura K, Baba H. Mutation of $\alpha 1GT$ -type calcium channels in mice does not change anesthetic requirements for loss of the righting reflex and minimum alveolar concentration but delays the onset of anesthetic induction. *Anesthesiology* (2007) **106**:1177–85. doi:10.1097/01.anes.0000267601.09764.e6
30. Timic Stamenic T, Feseha S, Manzella FM, Wallace D, Wilkey D, Corrigan T, et al. The T-type calcium channel isoform Cav3.1 is a target for the hypnotic effect of the anaesthetic neurosteroid (3 β ,5 β ,17 β)-3-hydroxyandrostane-17-carbonitrile. *Br J Anaesth* (2021) **126**:245–55. doi:10.1016/j.bja.2020.07.022
31. Manzella FM, Cabrera OH, Wilkey D, Fine-Raquet B, Klawitter J, Krishnan K, et al. Sex-specific hypnotic effects of the neuroactive steroid (3 β ,5 β ,17 β)-3-hydroxyandrostane-17-carbonitrile are mediated by peripheral metabolism into an active hypnotic steroid. *Br J Anaesth* (2023) **130**:154–64. doi:10.1016/j.bja.2022.09.025



OPEN ACCESS

*CORRESPONDENCE

Tamara Timic Stamenic,
✉ tamara.timicstamenic@
cuanschutz.edu

RECEIVED 25 February 2025

ACCEPTED 30 May 2025

PUBLISHED 10 June 2025

CITATION

Martin A, Coulter I, Cox R, Covey DF, Todorovic SM and Timic Stamenic T (2025) Comparative electrophysiological study of neuroactive steroid-induced hypnosis in mice: sex and drug-specific differences. *Exp. Biol. Med.* 250:10550. doi: 10.3389/ebm.2025.10550

COPYRIGHT

© 2025 Martin, Coulter, Cox, Covey, Todorovic and Timic Stamenic. This is an open-access article distributed under the terms of the [Creative Commons Attribution License \(CC BY\)](#). The use, distribution or reproduction in other forums is permitted, provided the original author(s) and the copyright owner(s) are credited and that the original publication in this journal is cited, in accordance with accepted academic practice. No use, distribution or reproduction is permitted which does not comply with these terms.

Comparative electrophysiological study of neuroactive steroid-induced hypnosis in mice: sex and drug-specific differences

Abigail Martin¹, Ian Coulter¹, Reginald Cox¹, Douglas F. Covey^{2,3}, Slobodan M. Todorovic^{1,4} and Tamara Timic Stamenic^{1*}

¹Department of Anesthesiology, University of Colorado Anschutz Medical Campus, Aurora, CO, United States, ²Department of Developmental Biology, Washington University School of Medicine, Saint Louis, MO, United States, ³Taylor Family Institute for Innovative Psychiatric Research, Washington University School of Medicine, Saint Louis, MO, United States, ⁴Neuroscience and Pharmacology Graduate Program, University of Colorado Anschutz Medical Campus, Aurora, CO, United States

Abstract

Since the discovery of their anesthetic effects, some neuroactive steroids have been used as general anesthetics. However, their effects on thalamocortical oscillations and potential sex differences that are associated with their hypnotic/sedative effects are not well studied. Here, we investigated spectral characteristics and sex differences in hypnotic effect of two common neuroactive steroids: Allopregnanolone (AlloP) and its synthetic analog Alphaxalone (Alpx) in wild type mice using behavioral testing (loss of righting reflex – LORR) and *in vivo* electrophysiology. Our data revealed sex-differences in LORR duration with 100 mg/kg intraperitoneally injected AlloP and Alpx confirming that females are more sensitive to neuroactive steroid-induced hypnosis. Spectral analysis, thalamocortical and corticocortical phase synchronization showed notable differences between two neuroactive steroids. AlloP induced a profound reduction in local field potential (LFP) and electroencephalogram (EEG) after LORR with higher LFP/EEG suppression in females during first 60 min after injection. Also, we observed a decrease in thalamocortical synchronization in lower (delta, theta, alpha) and increase in higher low gamma frequency in AlloP group; similar effects were observed in Alpx treated animals with no change in delta thalamocortical phase locking values. Synchronization between right and left cortex was reduced in all frequencies except low gamma in AlloP-treated group. Similarly, Alpx induced reduction in corticocortical synchronization for theta, alpha and

beta frequencies. We conclude that AlloP and Alpx have distinct electrophysiological signatures in thalamocortical circuitry that may underly their sedative/hypnotic effects.

KEYWORDS

neuroactive steroids, hypnosis, electroencephalogram, phase locking value, sex-differences

Impact statement

While clinically used general anesthetics are considered relatively safe, there is an ongoing interest in the development of new, potentially safer general anesthetics, especially for specific populations such as children. Neuroactive steroids are utilized as anesthetic agents due to their ability to modulate the activity of γ -aminobutyric acid type A (GABA_A) receptors in the brain, leading to a sedative and anesthetic effect. Currently, neuroactive steroids are primarily used for the induction and maintenance of general anesthesia in veterinary medicine (Alphaxalone), but there is ongoing interest in exploring their potential for human use as well. Here, we are comparing the spectral characteristics and sex differences in the hypnotic effect of two neuroactive steroids, Allopregnanolone and its synthetic analogue, Alphaxalone. Our data demonstrate that it is important to consider the use of neuroactive steroids for clinical anesthesia, particularly for their potential to be safer than traditional anesthetics.

Introduction

Neuroactive steroids are endogenous or exogenous steroids with direct effects on neuronal excitability. It has been shown that the spatial arrangement of the hydroxyl group at the C3 position of the steroid skeleton dramatically affects the biological properties of the neuroactive steroids [1, 2]. Previous reports demonstrated that 3 α -hydroxy neuroactive steroids, like endogenous Allopregnanolone (AlloP, 3 α -hydroxy-5 α -pregnan-20-one) or its synthetic analog Alphaxalone (Alpx, 3 α -hydroxy-5 α -pregnane-11,20-dione), act like positive allosteric modulators of γ -aminobutyric acid type A (GABA_A) receptors in nanomolar concentrations [3–6]. This effect on γ -aminobutyric acid (GABA) currents is consistent with known behavioral effects of neuroactive steroids including anxiolysis, analgesia, anticonvulsant activity, sedation, hypnosis and anesthesia [7].

Furthermore, neuroactive steroids have been used in human and veterinary clinics as potentially safer anesthetic agents [8]. In comparison to traditional general anesthetics, many neuroactive steroids have favorable clinical properties: minimal cardiorespiratory depression, rapid onset and recovery, less neurotoxicity in young populations [2, 8–10]. It has been shown that AlloP is a potent hypnotic drug not just in wild-

type (WT) animals but also in animals that lack progesterone receptors, suggesting that progesterone receptors are not involved in the hypnotic response to AlloP [11, 12]. Similarly, a synthetic drug, Alpx, has potent hypnotic/anesthetic and sedative properties [2, 8]. Although it was abandoned for clinical use due to unwanted side effects caused by its vehicle, there has been recent interest in the therapeutic value of Alpx: a new aqueous formulation (Phaxan[®]) has been developed for use as an intravenous sedative and anesthetic in humans [9, 13]. While the sex-differences in various behavioral effects of neuroactive steroids are well documented in the literature, their neurophysiological signature is poorly understood [14].

Central medial nucleus of thalamus (CMT), as a part of intralaminar thalamic complex is implicated in arousal and is a key hub through which general anesthesia and sleep are initiated [15]. Here, we investigated sex-differences and spectral characteristics in the hypnotic effect of AlloP and Alpx in WT mice using behavioral testing (loss of righting reflex - LORR) and *in vivo* electrophysiology by recording local field potential (LFP) from CMT and electroencephalogram (EEG) from barrel cortex. Since there is an ongoing interest in developing new hypnotics and general anesthetics, we hope that our study may rekindle interest in clinical use of these agents as safer alternative to other common sedatives and anesthetics.

Materials and methods

All experimental procedures with mice were performed according to a protocol approved by the Institutional Animal Care and Use Committee of the University of Colorado Anschutz Medical Campus, Aurora, CO, USA. Treatments of animals adhered to guidelines set forth in the NIH Guide for the Care and Use of Laboratory Animals. All efforts were made to minimize animal suffering and to use only the necessary number of animals to produce reliable scientific data. The authors confirm that the study complies with the ARRIVE guidelines.

Male and female adult C57BL/6J WT 3–4 months old mice (Jackson Laboratory, Bar Harbor, ME, USA) were used for behavioral and *in vivo* electrophysiology studies. All mice were maintained on a 14/10h light-dark cycle with food and water *ad libitum*. All tests were done in a blinded fashion. The estrus cycle of the female animals was not monitored during the experiments and can be a limitation of the study.

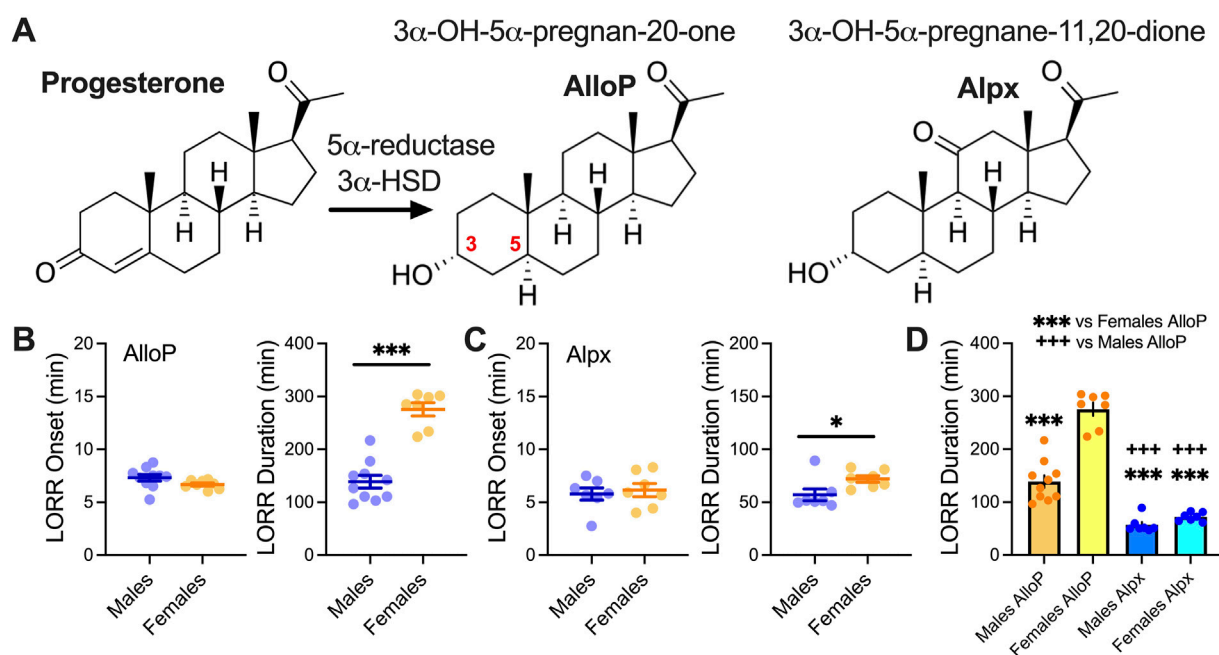


FIGURE 1

LORR with 100 mg/kg AlloP and Alpx. (A) Schematic presentation of AlloP synthesis from progesterone (3α-hydroxysteroid dehydrogenase - 3α-HSD) and AlloP synthetic analog Alpx. (B) Left LORR onset with 100 mg/kg AlloP (10 male and 7 female animals); (B) Right LORR duration with 100 mg/kg AlloP; unpaired two-tailed t-test $t_{(15)} = 7.74$, $p < 0.001$. (C) Left LORR onset with 100 mg/kg Alpx (7 mice per group); (C) Right LORR duration with 100 mg/kg Alpx; unpaired two-tailed t-test $t_{(12)} = 2.36$, $p = 0.036$. (D) Differences between AlloP and Alpx in LORR duration, one-way ANOVA $F(3,27) = 89.64$, $p < 0.001$, Tukey's post hoc presented on Figure. Blue-males, orange-females * $p < 0.05$, *** $p < 0.001$.

Neuroactive steroid preparation

AlloP and Alpx (Figure 1A) were synthesized and obtained from Dr. Covey (Saint Louis, MO, USA) and were dissolved in 25% (2-Hydroxypropyl)-β-cyclodextrin (Santa Cruz Biotechnology Inc, Dallas, TX, USA) in H₂O to yield the desired concentration for intraperitoneal (i.p.) injection. The solutions were prepared on the same day as they were injected into the mice. Mice were weighed and injected with the appropriate volume of neuroactive steroids to achieve desired dose (100 mg/kg). Our preliminary experiments showed that with this dose all injected animals exhibited loss of righting reflex (LORR).

Assessment of hypnotic behavior in mice

One desirable endpoint of general anesthesia is the state of unconsciousness, also known as hypnosis [16]. A widely used behavioral surrogate for hypnosis in rodents is the loss of righting reflex (LORR), or the point at which the animal no longer responds to their innate instinct to avoid the vulnerability of dorsal recumbency [16]. We measured hypnosis by assessing the LORR. After 30 min of habituation to the testing chamber male and female mice

received i.p. injections of 100 mg/kg AlloP or Alpx and placed on a heating pad in a clear plastic cage. This cage was intermittently gently tilted to roll a given mouse onto its back. Loss of righting reflex was measured as inability to right self within 30 s. To assess duration of the LORR we measured the gain of righting reflex time. Animals were placed on a heating pad to prevent hypothermia and oxygen levels were checked intermittently during LORR experiments using pulse oximetry.

EEG data acquisition and spectral analysis

Synchronized, time locked video and EEG/LFP signals were recorded using the Pinnacle system (Pinnacle Technology Inc., Lawrence, KS, USA). The EEG and LFP signals were amplified (100×) and digitized at a sampling frequency rate of 2000 Hz (high pass filter 0.5 Hz and low pass filter 500 Hz) and stored on a hard disk for offline analysis. The electrodes (two screw-type cortical [AP: −1 mm, MD: ± 3 mm, DV: 0]) and one depth coated tungsten in CMT [anteroposterior-AP: −1.35 mm, mediolateral-MD: 0 and dorsoventral-DV: −3.6 mm], were implanted under continuous 2.5 vol% isoflurane anesthesia. Banamine® – Merck (i.p. 2.5 mg/kg) was applied right after surgery and every 24 h for 48 h. Seven to 10 days after

surgery animals were put in the recording chamber ($(H \times W \times L)$ $15.2 \times 16.5 \times 31.1$ cm) and EEG/LFP were recorded 30 min before (baseline recordings) and 60 min after i.p. injection of neuroactive steroid. To compare spectra, 5 min of signal in baseline (wake state) and during 100 mg/kg i.p. of neuroactive steroid were analyzed. After completion of experiments, mice were briefly anesthetized with ketamine (100 mg/kg i.p.) and electrolytic lesions were made by passing 5 μ A current for 1 s (5 times) to verify placement of the deep electrode. Mice were anesthetized additionally with isoflurane and perfused with ice-cold 0.1M phosphate buffer containing 1% of potassium-ferrocyanide. The brains were extracted, kept in 4% formalin (PFA) for 2 days and sliced (100–150 μ m) using a vibrating micro slicer (Laica VT 1200 S). Photos of coronal slices with electrode location conformation were obtained using bright-field Zeiss stereoscope and Zen Blue software.

We excluded thalamic recordings from 4 animals in the analysis; one female animal that did not have good deep (CMT) electrode placement, two female and one male animal did not have good quality of thalamic recording.

Data analysis

Statistical analysis was performed using one- or two-way repeated measure (RM) ANOVA as well as Student unpaired two-tailed t-test where appropriate. Generally one-way RM ANOVA was used for LORR analysis between neuroactive steroids, two-way RM ANOVA for spectral analysis, and unpaired t-test for sex-differences in LORR. Where interaction between factors after two-way RM ANOVA was significant, Sidak's multiple comparisons test was used. If one-way ANOVA was significant, Tukey's comparison test was used. Significance was accepted with p values <0.05 . Statistical and graphical analysis was performed using GraphPad Prism 8.00 software (GraphPad Software, La Jolla, CA, USA). The EEG frequency spectrum was divided into the following frequency bands: delta (0.5–4 Hz), theta (4–8 Hz), alpha (8–13 Hz), beta (13–30 Hz) and low gamma (30–50 Hz). Power density, total power and relative power spectral analysis were calculated using LabChart 8 software (ADInstruments Inc., Colorado Springs, CO). For additional EEG/LFP analysis we used Brainstorm software package implemented in MATLAB [17, 18]. We calculated thalamocortical and corticocortical phase locking values for functional connectivity using the Hilbert transform based phase synchronization analysis [19]. The phase locking values were used as non-directed functional connectivity metrics to capture interdependence between two signals—thalamocortical (CMT and cortex) and corticocortical (right and left cortex) [20]. All data are presented as mean \pm SEM.

Data availability

Data will be made available from the corresponding author on request.

Results

Sex-differences in LORR after 100 mg/kg AlloP and Alpx injections

Figure 1A shows chemical structure of neuroactive steroids and a biosynthesis of the AlloP from progesterone; AlloP is derived from progesterone by reduction at the 5- and 3-positions of the steroid A-ring via 5 α -reductase and 3 α -hydroxysteroid dehydrogenase [7]. We examined the effect of 100 mg/kg AlloP and Alpx on LORR in male and female mice (Figures 1B,C). All tested animals lost righting reflex after drug injection. While the onset of LORR was not changed, both neuroactive steroids showed a sex-dependent effect in LORR duration. Specifically, female mice had longer times for LORR duration than males (Figures 1B,C). Interestingly, both male and female animals injected with the 100 mg/kg AlloP had longer LORR durations in comparison to mice injected with Alpx. Furthermore, sex differences were more notable in AlloP group where LORR in females was about 2-fold longer than in males (Figure 1D). Onset of LORR was not different between different sexes for both neuroactive steroids.

Changes in total thalamic and cortical oscillatory power under AlloP and Alpx over time

To analyze further sex-differences during AlloP- and Alpx-induced hypnosis we recorded LFP from CMT and EEG from right and left barrel cortex. CMT has been previously implicated in the mechanisms of both general anesthesia and sleep initiation [15]. In animals that received 100 mg/kg AlloP, we observed a very strong LFP/EEG suppression of total power (dB) in all analyzed frequencies after LORR during the first 60 min after injection (Figures 2A,C,E,G,I). By contrast, animals that were injected with 100 mg/kg Alpx showed very little change in LFP/EEG signals after LORR in comparison to the wakeful state (Figures 2B,D,F,H,J). Consistent with its longer hypnotic effect, suppression under AlloP was more profound in females in thalamic delta (Figure 2A left), thalamic and cortical theta, alpha and beta power (Figures 2C,E,G, respectively). On the contrary, we did not observe sex differences in LFP and EEG recordings after Alpx injection.

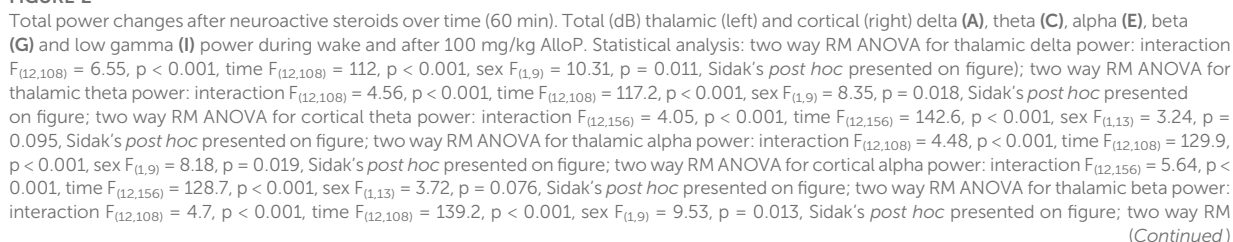


FIGURE 2 (Continued)

ANOVA for cortical beta power: interaction $F_{(12,156)} = 4.66$, $p < 0.001$, time $F_{(12,156)} = 121.4$, $p < 0.001$, sex $F_{(1,13)} = 3.47$, $p = 0.085$, Sidak's *post hoc* presented on figure. Total thalamic (left) and cortical (right) delta (B), theta (D), alpha (F), beta (H) and low gamma (J) power during wake and after 100 mg/kg Alpx. Note that we did not observe statistical difference between male and female animals after Alpx during first 60 min in all analyzed frequencies. Blue-males, orange-females, number of mice per group are presented on figure, red line presents statistically significant *post hoc* test.

Spectral signatures and spectrograms 30 min after AlloP and Alpx injection

We chose 25–30 min after injection to further investigate neuroactive steroid-induced spectral changes (Figure 3). During wakeful periods before AlloP and Alpx injection we did not observe sex-differences in either thalamic or cortical power densities (Figures 3A,C). However, AlloP induced a profound suppression of power densities in comparison to wake state in both thalamus and cortex. Power densities in both the thalamus (2–8 Hz frequency range) and cortex (2–6 Hz frequency range, Figure 3B) were about 2-fold higher in male mice after AlloP injection. Moreover, there was a shift in maximal (peak) power density towards slower oscillations, from dominant wake theta frequency (8Hz, Figure 3A) to dominant delta oscillations during AlloP exposure (4Hz, Figure 3B). The same shift in maximal power density peak was observed with Alpx (Figures 3E,F), except instead of suppression in power density, increase in slower frequencies (2–6 Hz) was observed in thalamus in comparison to wake state (Figure 3E).

Difference in relative power and functional connectivity between two neuroactive steroids

We did not detect significant sex-differences in relative power and corticocortical and thalamocortical phase locking values before or under neuroactive steroids, hence we combined the data from male and female mice to perform statistical analysis (Figure 4). We found no significant differences in thalamic and cortical relative powers during baseline (wake state) between the two neuroactive steroids (Figure A,B left). Both AlloP and Alpx increased delta and decreased alpha relative power in thalamus (Figure 4A right). Alpx increased thalamic theta and decreased beta and low gamma relative power (Figure 4A right). In cortex, delta relative power was increased only in the Alpx group but not in the AlloP-treated mice (Figure 4B right). However, AlloP decreased beta, alpha and increased beta and low gamma cortical relative powers (Figure 4B right). Additionally, Alpx-treated group had higher relative powers of slower frequencies (delta and theta) and had lower relative powers of higher frequencies (beta and low gamma) in comparison to AlloP in thalamus (Figure 4A middle) and cortex (Figure 4B middle).

To investigate functional thalamocortical and corticocortical connectivity we analyzed phase locking values before (wake) and after AlloP and Alpx injections. We detected about 3-fold higher corticocortical phase locking values in comparison to thalamocortical phase locking values during wake stage (Figures 3C,D left). Under AlloP there was a decrease in slower frequencies (delta, theta and alpha) and an increase in low gamma thalamocortical phase locking values (Figure 4C right). Similar results were observed with Alpx except for no change in delta thalamocortical phase locking values (Figure 4C, right). Additionally, there was a decrease in delta, theta, alpha and beta corticocortical phase locking values under AlloP (Figure 4D right). Similarly to thalamic data, Alpx did not change delta corticocortical phase locking values but decreased corticocortical synchronization for beta, alpha and beta frequency range (Figure 4D right). Alpx-treated mice also had higher delta and lower beta thalamocortical phase locking values (Figure 4C middle), and higher delta, theta and alpha corticocortical phase locking values in comparison to AlloP injected animals (Figure 4D middle).

Discussion

Although the introduction of Alpx and related 3 α -OH analogues with hypnotic/anesthetic properties occurred in the 1970s, there is an increased interest recently in the development of new neuroactive steroids as therapeutic agents. For example, AlloP was formulated and FDA-approved as a medicine for postpartum depression (Brexanolone[®]), and a 3 β -methylated analogue of AlloP (Ganaxalone[®]) was FDA-approved for treatment of seizure associated with the rare disease cyclin-dependent kinase-like 5 deficiencies [10]. Furthermore, a new aqueous formulation of Alpx (Phaxan[®]) has been developed for use as an intravenous sedative and anesthetic in humans [9, 13].

As expected, we found that both AlloP and Alpx can reliably produce LORR in male and female mice. We further found that there are notable sex-differences in the effects of both neuroactive steroids in tested behavior. Specifically, the female animals are more sensitive to the hypnotic effect. Previous studies reported sex specific effect with both endogenous neuroactive steroids and synthetic analogues [21, 22]. The longer duration of LORR in females was previously described with Alpx in both mice and rats [22–24]. It was postulated that the interactions of neuroactive steroids with synaptic membranes may be more sex-specific [22, 23] and can potentially explain why the female mice in our study

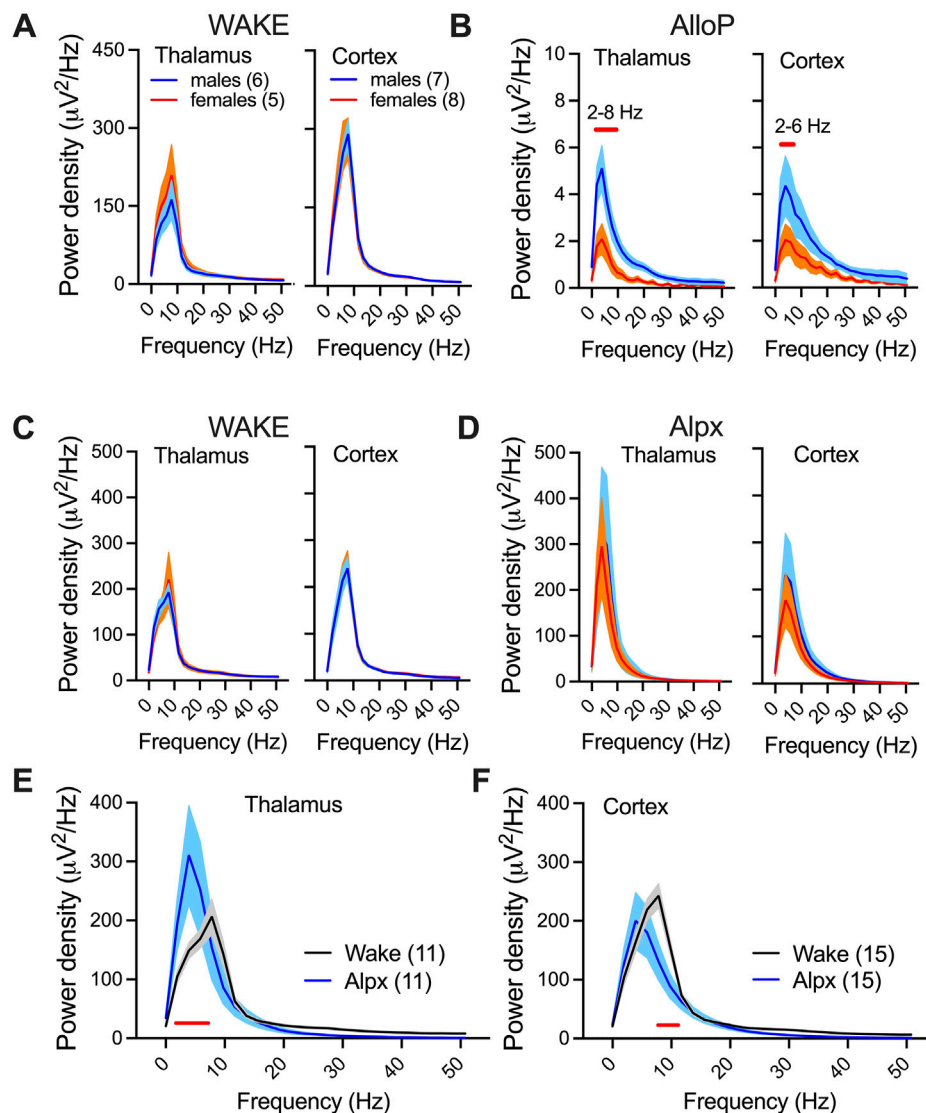


FIGURE 3

Spectral changes and sex-differences under AlloP and Alpx. Thalamic (left) and cortical (right) power densities during wake state (A) and 25–30 min after 100 mg/kg AlloP injection (B). Female mice had reduction in 2–10 Hz thalamic and 2–6 Hz cortical power densities in comparison to male mice under AlloP; two way RM ANOVA for thalamic power density: interaction $F_{(26,234)} = 4.75$, $p < 0.001$, frequency $F_{(26,234)} = 27.22$, $p < 0.001$, sex $F_{(1,9)} = 8.7$, $p = 0.016$, Sidak's *post hoc* presented on figure; two way RM ANOVA for cortical power density: interaction $F_{(26,338)} = 1.74$, $p = 0.016$, frequency $F_{(26,338)} = 13.72$, $p < 0.001$, sex $F_{(1,13)} = 4.53$, $p = 0.053$, Sidak's *post hoc* presented on figure. E, Thalamic (left) and cortical (right) power densities during wake state (C) and 25–30 min after 100 mg/kg Alpx injection (D). We did not observe sex differences in power densities after Alpx and analyzed females and males together (E,F). Alpx-induced changes in power density in thalamus (E) and cortex (F); two way RM ANOVA: interaction $F_{(26,234)} = 3.37$, $p < 0.001$, frequency $F_{(26,234)} = 23.95$, $p < 0.001$, Alpx $F_{(1,9)} = 0.05$, $p = 0.83$, Sidak's *post hoc* significant 2–6 Hz; and cortex (F); two way RM ANOVA: interaction $F_{(26,338)} = 2.72$, $p < 0.001$, frequency $F_{(26,234)} = 75.70$, $p < 0.001$, Alpx $F_{(1,13)} = 1.03$, $p = 0.329$, Sidak's *post hoc* significant 8–10 Hz. Blue-males, orange-females, number of mice per group are presented on figure; red line presents statistically significant *post hoc* test.

had a longer duration of hypnosis with the same dose of AlloP and Alpx. The authors found that the sex differences with Alpx is age-dependent, can be abolished by administering estrogen to the males, does not depend on sexual differentiation of the brain, and cannot be attributed to a sex difference in the metabolic clearance rate of neuroactive steroids [22].

Similarly, it was reported that neuroactive steroids such as AlloP exhibit sex differences in their anticonvulsant activity indicating reduced potency in the males relative to females [25]. This effect can be likely due to a greater abundance of extra-synaptic δ subunit of GABA_A receptors that mediates neuroactive steroid-sensitive, tonic GABA currents and seizure

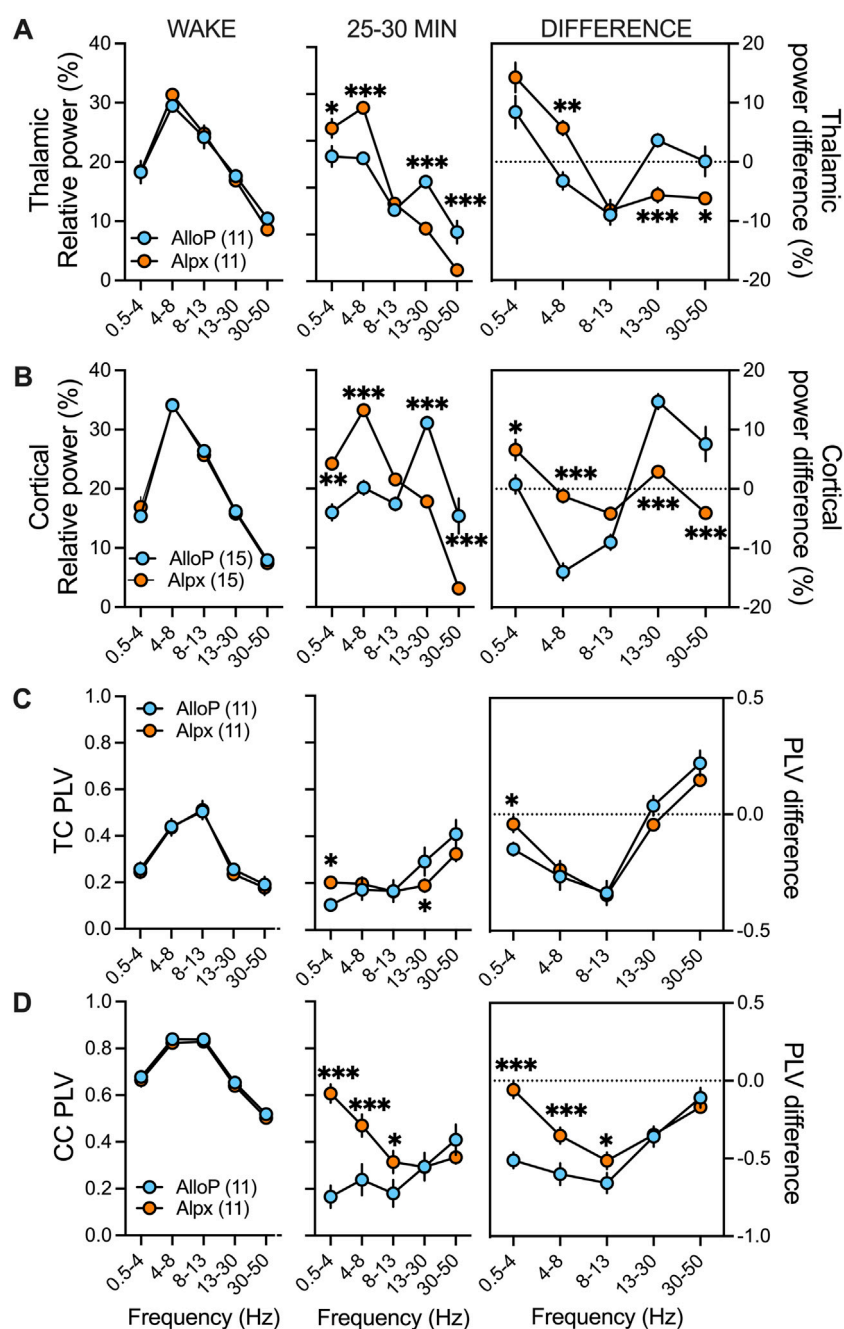


FIGURE 4

Differences in spectral characteristics between AlloP and Alpx. Since there was no statistical significance in thalamocortical (TC) and corticocortical (CC) phase locking values (PLVs) and relative power (%) between sexes during wake periods and 25–30 min after neuroactive steroid injection both female and male data are combined together for this figure. (A) Thalamic relative power during wake state (left), after AlloP and Alpx injection (middle) and change in relative power from wake state (right). We did not observed differences during wake periods. Animals injected with Alpx had higher delta and theta but lower beta and low gamma relative powers in comparison to Alpx group; two-way RM ANOVA: interaction $F_{(4,40)} = 22.17$, $p < 0.001$, frequency $F_{(4,40)} = 56.24$, $p < 0.001$, neuroactive steroid $F_{(1,10)} = 0.56$, $p = 0.471$, Sidak's *post hoc* presented on figure. Change in relative power from wake state showed increase in Alpx theta and decrease in beta and low gamma thalamic relative power that was not seen in AlloP treated animals; two-way RM ANOVA: interaction $F_{(4,40)} = 11.79$, $p < 0.001$, frequency $F_{(4,40)} = 19.02$, $p < 0.001$, neuroactive steroid $F_{(1,10)} = 0.52$, $p = 0.486$, Sidak's *post hoc* presented on figure. (B) Cortical relative power during wake state (left), after AlloP and Alpx injection (middle) and change in relative power from wake state (right). We did not observed differences during wake periods. Animals injected with Alpx had higher delta and theta but lower beta and low gamma relative powers in comparison to Alpx group; two-way RM ANOVA: interaction $F_{(4,56)} = 33.92$, $p < 0.001$, frequency $F_{(4,56)} = 44.49$, $p < 0.001$, neuroactive steroid $F_{(1,14)} = 4.1$, $p = 0.062$, Sidak's *post hoc* presented on figure. Interestingly, AlloP treated animals showed increase in beta and low gamma relative powers from wake state and decrease in beta relative power while animals in Alpx group had increase in delta

(Continued)

FIGURE 4 (Continued)

cortical relative power that was not seen with AlloP; two-way RM ANOVA: interaction $F_{(4,108)} = 21.37$, $p < 0.001$, frequency $F_{(4,108)} = 33.63$, $p < 0.001$, neuroactive steroid $F_{(1,27)} = 1.54$, $p = 0.226$, Sidak's *post hoc* presented on figure. **(C)** TC PLVs during wake (left), after AlloP or Alpx (middle) and change in PLV from wake state (right). We did not observe PLVs differences during wake state. There was increase in delta and decrease in beta TC PLVs in Alpx group in comparison to AlloP; two-way RM ANOVA: interaction $F_{(4,40)} = 6.298$, $p = 0.001$, frequency $F_{(4,40)} = 21.19$, $p < 0.001$, neuroactive steroid $F_{(1,10)} = 0.13$, $p = 0.725$, Sidak's *post hoc* presented on figure. Analysis of PLV difference showed decrease in delta TC PLVs in AlloP but not in Alpx group; two-way RM ANOVA: interaction $F_{(4,40)} = 4.78$, $p = 0.003$, frequency $F_{(4,40)} = 59.60$, $p < 0.001$, neuroactive steroid $F_{(1,10)} = 0.03$, $p = 0.876$, Sidak's *post hoc* presented on figure. **(D)** CC PLVs during wake (left), after AlloP or Alpx (middle) and change in PLV from wake state (right). We did not observe PLVs differences during wake state. There was increase in delta, theta and alpha CC PLVs in Alpx group in comparison to AlloP; two-way RM ANOVA: interaction $F_{(4,40)} = 5.71$, $p < 0.001$, frequency $F_{(4,40)} = 5.71$, $p = 0.001$, neuroactive steroid $F_{(1,10)} = 7.90$, $p = 0.019$, Sidak's *post hoc* presented on figure. Similarly, analysis of PLV difference showed more profound decrease in delta, theta and alpha CC PLVs after AlloP than after Alpx injection; two-way RM ANOVA: interaction $F_{(4,40)} = 15.98$, $p < 0.001$, frequency $F_{(4,40)} = 36.64$, $p < 0.001$, neuroactive steroid $F_{(1,10)} = 10.76$, $p = 0.008$, Sidak's *post hoc* presented on figure. Blue-males, orange-females, number of mice per group is presented on figure, * $p < 0.05$, ** $p < 0.01$, *** $p < 0.001$.

protection [26] and can at least partially explain sex specific effect in our experiments.

Interestingly, recent studies demonstrated that the female brain in mice and humans is less responsive to the hypnotic effects of volatile anesthetics largely due to acute effects of sex hormones [27]. Despite clear behavioral sex differences in anesthetic sensitivity, sex-differences were not visible in clinically used EEG but were detected in subcortical recordings [27]. This hidden resistance to volatile anesthetics may explain the higher incidence of awareness under anesthesia in females and requires investigation of sex-differences using both EEG (cortical) and LFP recordings [27].

Neuronal inhibition in the brain is predominantly provided by activation of GABA_A receptors - heteropentameric receptors formed from an array of subunits ($\alpha 1-6$, $\beta 1-3$, $\gamma 1-3$, δ , ϵ , π , θ and $\rho 1-3$) [28, 29]. Synaptic receptors typically comprise $\alpha 1-3$, β and γ subunits, while extra-synaptic receptors contain $\alpha 4/6$, β and δ subunits [30]. It has been shown that AlloP has higher selectivity for tonic δ -containing GABA_A receptors, and that by being more selective to extra-synaptic GABA_A receptors, AlloP plays an essential neurophysiological role in the fine-tuning of neuronal inhibition mediated by GABA_A receptors [31, 32]. However, when injected in high doses, as in our case (100 mg/kg, i.p.), AlloP produced drastic suppression of total power in both male and female mice after LORR probably by acting on both synaptic and extra-synaptic GABA_A receptors. The clinically relevant dose range for AlloP in rodents varies depending on the desired effect and route of administration, and for anesthetic effect is higher (15–20 mg/kg i.v) than for anxiolytic/sedative effect in animals [28]. Additionally, the typical dose range for Alpx with hypnotic effect is between 50 and 60 mg/kg i.p. in females but higher doses are needed for male rodents [23]. To compare hypnotic effect of AlloP and Alpx, based on our preliminary dose-response experiments, we used the lowest dose of neuroactive steroids that induces LORR in all tested female and male mice.

Since the introduction of EEG, neural oscillations have been systematically categorized across behavioral states into canonical frequency bands: delta, theta, alpha, beta, gamma [33]. Both natural sleep and general anesthesia are associated with

synchronized, high-amplitude slow oscillations, whereas conscious wakefulness is dominated by faster, desynchronized activity patterns [34]. Low doses of sedative-hypnotic agents, such as positive allosteric modulators of GABA_A receptors (e.g., propofol, barbiturates, etomidate), can paradoxically induce cortical excitation, typically reflected as enhanced β -band activity [35]. As anesthetic depth increases, EEG signatures progress through characteristic stages: Phase 1 (light sedation) is marked by reduced beta and elevated alpha power; Phase 2 (intermediate depth) displays prominent alpha and delta oscillations, closely resembling non-rapid eye movement slow-wave sleep; Phase 3 exhibits burst-suppression patterns; and Phase 4 is characterized by a near-isoelectric EEG, indicative of profound cortical silencing [35]. Although full anesthesia can be assessed by investigating withdrawal reflex to a painful stimulus, like tail or toe clamping and pinching, here we investigated just the hypnotic effect and were unable to assess if AlloP or Alpx induce surgical levels of anesthesia in high dose. However, strong EEG/LFP suppression that we observed with AlloP resembles burst suppression seen with potent volatile general anesthetics [36]. Similarly to sex-differences observed in behavioral test, the EEG/LFP suppression seen with AlloP was more profound in female animals in comparison to males. On the contrary, with the same dose of Alpx we did not observe LFP/EEG suppression, confirming previous results that Alpx alone can induce hypnosis or light anesthesia but even in higher doses probably cannot induce deeper surgical levels of general anesthesia [23, 24]. The observed changes between AlloP and Alpx-induced hypnosis could be at least partially explained by the differences in modulation of synaptic $\alpha 1\beta 2\gamma 2$ GABA_A receptors; AlloP is a more potent positive allosteric modulator of these receptors than Alpx (ED₅₀ for $\alpha 1$ containing GABA_A receptors for AlloP $0.18 \pm 0.002 \mu\text{M}$ (mean \pm SEM) and for Alpx $2.2 \pm 0.04 \mu\text{M}$) [37]. The same rationale can explain longer LORR durations induced by AlloP in comparison to Alpx in both female and male mice. Somewhat surprisingly, sex-differences in total EEG/LFP power in our experiments were not seen with the Alpx.

In the cortex and thalamus, power density analysis showed a shift in the power density peak from theta during wakefulness to delta frequencies after both neuroactive steroids, accompanied

with a drastic suppression of EEG/LFP power density only in the AlloP group. On the contrary, thalamic spectral analysis showed increase in power density in slower frequencies under Alpx in comparison to the wake state. Similarly to other general anesthetics that act as GABA_A positive allosteric modulators, analysis of relative power showed increase in thalamic relative delta power in AlloP and Alpx animals while increase in EEG delta relative power was observed just with Alpx [38, 39]. Although both alpha and slow-delta oscillations are dominant EEG signature for propofol-induced hypnosis and hypnosis with other GABA_A positive allosteric modulators, with neuroactive steroids we observed a decrease and not an increase in thalamic and cortical alpha relative power [38, 39]. The difference in effect between neuroactive steroids and other GABA_A positive allosteric modulators was previously reported and might be related to effects on different GABA_A receptor isoforms [2, 10, 40, 41]. Additionally, neuroactive steroids have higher affinity for extra-synaptic GABA_A receptors responsible for persistent non-desensitizing inhibitory conductance [42]. Interestingly, we observed a substantial rise in relative cortical beta/low gamma powers after AlloP-induced LORR. A similar rise in low gamma range was seen in rodents after injections of ketamine, an N-methyl-D-aspartate (NMDA) antagonist [43, 44]. By contrast, we found that Alpx decreased thalamic beta and slightly increased cortical beta relative power and reduced low gamma relative power in both the thalamus and cortex. Overall, our data showed that in AlloP-treated mice, relative powers of slower (delta and theta) frequencies are lower but relative powers of higher (beta and low gamma) frequencies are higher than in the Alpx group.

Additionally, we used the Hilbert transform based phase synchronization analysis [19], to investigate the phase coupling during neuroactive steroid-induced hypnosis. Systematic phase synchronization changes were detected after injection of both neuroactive steroids. Generally, we observed reduction in corticocortical phase synchronization in AlloP animals that was more profound in slower than in higher frequency ranges. Similarly, Alpx induced drop in corticocortical synchronization in all except delta frequencies. We observed existence of higher corticocortical phase locking values under Alpx in comparison to AlloP in delta, theta and alpha frequencies. Previous models predicted that anesthesia would induce a decrease in slow wave EEG phase coherence as the cortex transitions away from the wakeful state [45]. In line with these findings, some experiments have confirmed that phase coherence during induction with propofol produces a significant drop in slow-wave bands synchronization between frontal, occipital, and frontal-occipital electrode pairs in humans [45, 46]. With AlloP we observed a similar decrease in cortical delta phase locking values. Previous findings reported that traditional general anesthetics can induce a large and localized increase in synchronization in alpha band as well as

smaller and widespread synchrony increases in gamma frequency bands [47]. Studies using propofol in humans have reported that alpha band synchronization between cortical sites increases during induction and decreases during recovery [46]. By contrast, with neuroactive steroids we observed a profound decrease in alpha frequency synchronization in both corticocortical and thalamocortical leads in all treatment groups. Interestingly, we found increased synchronization in thalamocortical low gamma oscillation in both AlloP and Alpx treatment groups. This finding further denotes that neuroactive steroids induce very distinctive spectral changes that were not described with other similar GABA-mimetic general anesthetics.

Furthermore, in contrast to commonly used general anesthetics, both AlloP and Alpx activate progesterone receptors, and have neuroprotective effects that is independent of their GABA_A actions [48]. Recently, it has been shown that Alpx treated subjects scored better than propofol and sevoflurane anesthetized patients in the cognition tests, and that the higher cognition scores were accompanied by higher serum m-Brain-Derived Neurotrophic Factor levels in the Alpx-anesthetized patients [13]. Having this in mind, we posit that use of neuroactive steroids as general anesthetics may have beneficial effects in comparison to commonly clinically used drugs.

In conclusion, our data from behavioral assessments and LFP/EEG changes support the idea that female mice are more sensitive to neuroactive steroid-induced hypnosis. Our data also showed that neuroactive steroid-induced hypnosis has similar spectral characteristics as common general anesthetics with some unique LFP/EEG properties. While most used general anesthetics act as positive allosteric modulators of GABA_A receptors, they have different binding sites in comparison to neuroactive steroids and have markedly different side effects suggesting major differences in off-target binding and clinical effect [10]. Thus, we posit that future clinical use of neuroactive steroids for clinical anesthesia warrants consideration.

Author contributions

Performed experiments TTS (*in vivo* electrophysiology), IC and RC (LORR); analysed the data AM and TTS; designed the studies TTS and SMT, performed final manuscript preparation: AM, IC, DC, SMT, and TTS. All authors contributed to the article and approved the submitted version.

Data availability

The original contributions presented in the study are included in the article/supplementary material, further inquiries can be directed to the corresponding author.

Ethics statement

The animal study was approved by Institutional Animal Care and Use Committee of the University of Colorado Anschutz Medical Campus, Aurora, CO, USA. The study was conducted in accordance with the local legislation and institutional requirements.

Funding

The author(s) declare that financial support was received for the research and/or publication of this article. This study was funded by grants from the National Institutes of Health (GRANT# R35GM141802 to SMT and K01DA055258 to TTS).

References

1. Miller PS, Scott S, Masiulis S, De Colibus L, Pardon E, Steyaert J, et al. Structural basis for GABAA receptor potentiation by neurosteroids. *Nat Struct Mol Biol* (2017) **24**:986–92. doi:10.1038/nsmb.3484
2. Jevtovic-Todorovic V, Todorovic SM. The role of neuroactive steroids in analgesia and anesthesia: an interesting comeback? *Biomolecules* (2023) **13**:1654. doi:10.3390/biom13111654
3. Lambert JJ, Belelli D, Peden DR, Vardy AW, Peters JA. Neurosteroid modulation of GABA A receptors. *Prog Neurobiol* (2003) **71**:67–80. doi:10.1016/j.pneurobio.2003.09.001
4. Maguire JL, Mennerick S. Neurosteroids: mechanistic considerations and clinical prospects. *Neuropsychopharmacology* (2024) **49**:73–82. doi:10.1038/s41386-023-01626-z
5. Cottrell GA, Lambert JJ, Peters JA. Modulation of GABAA receptor activity by alphaxalone. *Br J Pharmacol* (1987) **90**:491–500. doi:10.1111/j.1476-5381.1987.tb11198.x
6. Sugawara Y, Cheng WWL, Bracamontes JR, Chen ZW, Wang L, Germann AL, et al. Site-specific effects of neurosteroids on gabaa receptor activation and desensitization. *Elife* (2020) **9**:e55331–32. doi:10.7554/elife.55331
7. Reddy DS. Neurosteroids: endogenous role in the human brain and therapeutic potentials. *Prog Brain Res* (2010) **186**:113–37. doi:10.1016/B978-0-444-53630-3.00008-7
8. Manzella FM, Covey DF, Jevtovic-Todorovic V, Todorovic SM. Synthetic neuroactive steroids as new sedatives and anesthetics: back to the future. *J Neuroendocrinol* (2022) **34**:e13086. doi:10.1111/JNE.13086
9. Monagle J, Siu L, Worrell J, Goodchild CS, Serrao JM. A phase 1c trial comparing the efficacy and safety of a new aqueous formulation of alphaxalone with propofol. *Anesth & Analgesia* (2015) **121**:914–24. doi:10.1213/ane.0000000000000856
10. Tateiwa H, Evers AS. Neurosteroids and their potential as a safer class of general anesthetics. *J Anesth* (2024) **38**:261–74. doi:10.1007/s00540-023-03291-4
11. Reddy DS, Zeng YC. Differential anesthetic activity of ketamine and the GABAergic neurosteroid allopregnanolone in mice lacking progesterone receptor A and B subtypes. *Methods Find Exp Clin Pharmacol* (2007) **29**:659–64. doi:10.1358/mf.2007.29.10.1147766
12. Korniyev A, Costa E. Allopregnanolone (THP) mediates anesthetic effects of progesterone in rat brain. *Horm Behav* (1996) **30**:37–43. doi:10.1006/hbeh.1996.0006
13. Serrao JM, Goodchild CS. Alphaxalone anaesthesia increases brain derived neurotrophic factor levels and preserves postoperative cognition by activating pregnane-X receptors: an *in vitro* study and a double blind randomised controlled trial. *BMC Anesthesiol* (2022) **22**:401–13. doi:10.1186/S12871-022-01940-X
14. Sze Y, Brunton PJ. Sex, stress and steroids. *Eur J Neurosci* (2020) **52**:2487–515. doi:10.1111/ejn.14615

Acknowledgments

We thank the University of Colorado Anschutz Medical Campus Rodent *In Vivo* Neurophysiology Core for providing facilities to acquire and review video-EEG data.

Conflict of interest

The author(s) declared no potential conflicts of interest with respect to the research, authorship, and/or publication of this article.

Generative AI statement

The author(s) declare that no Generative AI was used in the creation of this manuscript.

15. Baker R, Gent TC, Yang Q, Parker S, Vyssotski AL, Wisden W, et al. Altered activity in the central medial thalamus precedes changes in the neocortex during transitions into both sleep and propofol anesthesia. *The J Neurosci* (2014) **34**:13326–35. doi:10.1523/jneurosci.1519-14.2014
16. McCarren HS, Moore JT, Kelz MB. Assessing changes in volatile general anesthetic sensitivity of mice after local or systemic pharmacological intervention. *J visualized experiments: JoVE* (2013):e51079. doi:10.3791/51079
17. Tadel F, Baillet S, Mosher JC, Pantazis D, Leahy RM. Brainstorm: a user-friendly application for MEG/EEG analysis. *Comput Intelligence Neurosci* (2011) **2011**:1–13. doi:10.1155/2011/879716
18. Tadel F, Bock E, Niso G, Mosher JC, Cousineau M, Pantazis D, et al. MEG/EEG group analysis with brainstorm. *Front Neurosci* (2019) **13**:76. doi:10.3389/fnins.2019.00076
19. Liang Z, Ren Y, Yan J, Li D, Voss LJ, Sleight JW, et al. A comparison of different synchronization measures in electroencephalogram during propofol anesthesia. *J Clin Monit Comput* (2016) **30**:451–66. doi:10.1007/s10877-015-9738-z
20. Bastos AM, Schoffelen JM. A tutorial review of functional connectivity analysis methods and their interpretational pitfalls. *Front Syst Neurosci* (2015) **9**:175. doi:10.3389/fnsys.2015.00175
21. Selye H. Anesthetic effect of steroid hormones. *Exp Biol Med* (1941) **46**:116–21. doi:10.3181/00379727-46-11907
22. Fink G, Sarkar DK, Dow RC, Dick H, Borthwick N, Malnick S, et al. Sex difference in response to alphaxalone anaesthesia may be oestrogen dependent. *Nature* (1982) **298**:270–2. doi:10.1038/298270a0
23. Siriachavatana P, Ayers JD, Kendall LV. Anesthetic activity of alphaxalone compared with ketamine in mice. *J Am Assoc Lab Anim Sci* (2016) **55**: 426–30. Available online at: <https://pmc.ncbi.nlm.nih.gov/articles/PMC4943613/>.
24. Arenillas M, Gomez de Segura IA. Anaesthetic effects of alphaxalone administered intraperitoneally alone or combined with dexmedetomidine and fentanyl in the rat. *Lab Anim* (2018) **52**:588–98. doi:10.1177/0023677218764214
25. Samba Reddy D. Sex differences in the anticonvulsant activity of neurosteroids. *J Neurosci Res* (2017) **95**:661–70. doi:10.1002/jnr.23853
26. Reddy DS, Carver CM, Clossen B, Wu X. Extrasynaptic γ -aminobutyric acid type A receptor-mediated sex differences in the antiseizure activity of neurosteroids in status epilepticus and complex partial seizures. *Epilepsia* (2019) **60**:730–43. doi:10.1111/epi.14693
27. Wasilczuk AZ, Rinehart C, Aggarwal A, Stone ME, Mashour GA, Avidan MS, et al. Hormonal basis of sex differences in anesthetic sensitivity. *Proc Natl Acad Sci U S A* (2024) **121**:e2312913120. doi:10.1073/pnas.2312913120
28. Belelli D, Lambert JJ. Neurosteroids: endogenous regulators of the GABAA receptor. *Nat Rev Neurosci* (2005) **6**:565–75. doi:10.1038/nrn1703

29. Lambert JJ, Belelli D, Hill-Venning C, Peters JA. Neurosteroids and GABAA receptor function. *Trends Pharmacol Sci* (1995) **16**:295–303. doi:10.1016/s0165-6147(00)89058-6
30. Sigel E, Steinmann ME. Structure, function, and modulation of GABAA receptors. *J Biol Chem* (2012) **287**:40224–31. doi:10.1074/jbc.r112.386664
31. Pinna G, Uzunova V, Matsumoto K, Puia G, Mienville JM, Costa E, et al. Brain allopregnanolone regulates the potency of the GABAA receptor agonist muscimol. *Neuropharmacology* (2000) **39**:440–8. doi:10.1016/s0028-3908(99)00149-5
32. Paul SM, Pinna G, Guidotti A. Allopregnanolone: from molecular pathophysiology to therapeutics. A historical perspective. *Neurobiol Stress* (2020) **12**:100215. doi:10.1016/j.ynstr.2020.100215
33. Crunelli V, Lörincz ML, Connelly WM, David F, Hughes SW, Lambert RC, et al. Dual function of thalamic low-vigilance state oscillations: rhythm-regulation and plasticity. *Nat Rev Neurosci* (2018) **19**:107–18. doi:10.1038/nrn.2017.151
34. Scharf MT, Kelz MB. Sleep and anesthesia interactions: a pharmacological appraisal. *Curr Anesthesiol Rep* (2013) **3**:1–9. doi:10.1007/s40140-012-0007-0
35. Brown EN, Lydic R, Schiff ND. General anesthesia, sleep, and coma. *New Engl J Med* (2010) **363**:2638–50. doi:10.1056/nejmra0808281
36. Kenny JD, Westover MB, Ching SN, Brown EN, Solt K. Propofol and sevoflurane induce distinct burst suppression patterns in rats. *Front Syst Neurosci* (2014) **8**:237. doi:10.3389/FNSYS.2014.00237
37. Weir CJ, Ling ATY, Belelli D, Wildsmith JAW, Peters JA, Lambert JJ. The interaction of anaesthetic steroids with recombinant glycine and GABAA receptors. *Br J Anaesth* (2004) **92**:704–11. doi:10.1093/bja/aei125
38. Timic Stamenic T, Todorovic SM. Thalamic T-type calcium channels as targets for hypnotics and general anesthetics. *Int J Mol Sci* (2022) **23**:2349. doi:10.3390/ijms23042349
39. Akeju O, Brown EN. Neural oscillations demonstrate that general anesthesia and sedative states are neurophysiologically distinct from sleep. *Curr Opin Neurobiol* (2017) **44**:178–85. doi:10.1016/j.conb.2017.04.011
40. Sieghart W, Sperk G. Subunit composition, distribution and function of GABA-A receptor subtypes. *Curr Top Med Chem* (2002) **2**:795–816. doi:10.2174/1568026023393507
41. Olsen RW, Sieghart W. GABA A receptors: subtypes provide diversity of function and pharmacology. *Neuropharmacology* (2009) **56**:141–8. doi:10.1016/j.neuropharm.2008.07.045
42. Carver CM, Reddy DS. Neurosteroid interactions with synaptic and extrasynaptic GABAA receptors: regulation of subunit plasticity, phasic and tonic inhibition, and neuronal network excitability. *Psychopharmacology (Berl)* (2013) **230**:151–88. doi:10.1007/s00213-013-3276-5
43. Kulikova SP, Tolmacheva EA, Anderson P, Gaudias J, Adams BE, Zheng T, et al. Opposite effects of ketamine and deep brain stimulation on rat thalamocortical information processing. *Eur J Neurosci* (2012) **36**:3407–19. doi:10.1111/j.1460-9568.2012.08263.x
44. Hunt MJ, Raynaud B, Garcia R. Ketamine dose-dependently induces high-frequency oscillations in the nucleus accumbens in freely moving rats. *Biol Psychiatry* (2006) **60**:1206–14. doi:10.1016/j.biopsych.2006.01.020
45. Wang K, Steyn-Ross ML, Steyn-Ross DA, Wilson MT, Sleight JW. EEG slow-wave coherence changes in propofol-induced general anesthesia: experiment and theory. *Front Syst Neurosci* (2014) **8**:215. doi:10.3389/fnsys.2014.00215
46. Koskinen M, Seppänen T, Tuukkanen J, Yli-Hankala A, Jäntti V. Propofol anesthesia induces phase synchronization changes in EEG. *Clin Neurophysiol* (2001) **112**:386–92. doi:10.1016/s1388-2457(00)00538-1
47. Nicolaou N, Georgiou J. Spatial analytic phase difference of EEG activity during anesthetic-induced unconsciousness. *Clin Neurophysiol* (2014) **125**:2122–31. doi:10.1016/j.clinph.2014.02.011
48. Langmade SJ, Gale SE, Frolov A, Mohri I, Suzuki K, Mellon SH, et al. Pregnane X receptor (PXR) activation: a mechanism for neuroprotection in a mouse model of Niemann-Pick C disease. *Proc Natl Acad Sci U S A* (2006) **103**:13807–12. doi:10.1073/pnas.0606218103



OPEN ACCESS

*CORRESPONDENCE

Lucille A. Lumley,
✉ lucille.a.lumley@health.mil

RECEIVED 24 March 2025

ACCEPTED 20 May 2025

PUBLISHED 09 June 2025

CITATION

Biney AK, Schultz CR, Stone MF, Nguyen DA, Wang A, de Araujo Furtado M and Lumley LA (2025) Cystamine reduces neurodegeneration and epileptogenesis following soman-induced status epilepticus in rats.

Exp. Biol. Med. 250:10598.

doi: 10.3389/ebm.2025.10598

COPYRIGHT

© 2025 Biney, Schultz, Stone, Nguyen, Wang, de Araujo Furtado and Lumley. This is an open-access article distributed under the terms of the [Creative Commons Attribution License \(CC BY\)](https://creativecommons.org/licenses/by/4.0/). The use, distribution or reproduction in other forums is permitted, provided the original author(s) and the copyright owner(s) are credited and that the original publication in this journal is cited, in accordance with accepted academic practice. No use, distribution or reproduction is permitted which does not comply with these terms.

Cystamine reduces neurodegeneration and epileptogenesis following soman-induced status epilepticus in rats

Abiel K. Biney¹, Caroline R. Schultz¹, Michael F. Stone¹, Donna A. Nguyen¹, Annie Wang¹, Marcio de Araujo Furtado² and Lucille A. Lumley^{1*}

¹Neuroscience Department, U.S. Army Medical Research Institute of Chemical Defense (USAMRICD), Aberdeen, MD, United States, ²BioSEaD, LLC, Rockville, MD, United States

Abstract

Acute exposure to a seizure-inducing dose of an organophosphorus nerve agent inhibits acetylcholinesterase, leading to pharmacoresistance if benzodiazepine treatment is delayed. Following soman-induced status epilepticus (SE) in rats, prolonged seizure is associated with severe and widespread neurodegeneration. We evaluated the aminothiols cystamine, the oxidized form of cysteamine, for neuroprotective potential against soman-induced SE and associated neurodegeneration. Cystamine has a myriad of effects including antioxidant properties, neuroprotective effects, and immunomodulation, among others, which is of interest in evaluating neuroprotective efficacy against cholinergic-induced neurodegeneration. Adult male rats implanted with telemetry transmitters for continuous EEG recording were exposed to soman and treated with the muscarinic antagonist atropine sulfate and the oxime asoxime dimethanesulfonate 1 min after exposure to increase survival. Midazolam was administered 30 min after seizure onset. Cystamine (10 or 50 mg/kg) or vehicle was administered 30 min after seizure onset and again 4 h after soman exposure. The initial seizure duration, the EEG power integral at 6 h after exposure, and the percentage of rats that developed spontaneous recurrent seizure were reduced in rats treated with cystamine, compared to those that received only midazolam. In addition, cystamine reduced neurodegeneration in seizure-sensitive brain regions following soman exposure, compared to midazolam. Our findings highlight the potential for aminothiols to serve as adjunctive therapy to midazolam in treating cholinergic-induced toxicity and suggest broader applications of aminothiols in neuroprotection and neurological disorders.

KEYWORDS

organophosphorus nerve agents, seizures, status epilepticus, cystamine, neuroprotection

Impact statement

Current research faces challenges in addressing long-term neurodegeneration. Using a preclinical model of cholinergic-induced status epilepticus and associated neurodegeneration, our study investigated the neuroprotective potential of the aminothiol cystamine, demonstrating its ability to reduce chronic neuropathology when used as an adjunct to the current standard of care. The findings presented here not only emphasize the efficacy of cystamine in mitigating cholinergic-induced neurodegeneration, but also suggest its potential role in reducing initial time in seizure, neuroinflammation and epileptogenesis. Our findings contribute valuable insight into the broader applications of aminothiols in neuroprotection.

Introduction

Recent studies suggests that aminothiols, such as cystamine and cysteamine, may serve as promising novel neuroprotectants (reviewed in Paul and Snyder, 2019) [1]. The aminothiol cystamine is the oxidized form of cysteamine, which is a decarboxylated derivative of cysteine. Cysteamine is FDA-approved for use in treatment of nephropathic and ocular cystinosis; cystinosis is a genetic disorder in which cystine crystals build up in tissues. More recently, cysteamine and cystamine, are under evaluation for potential treatment of neurodegenerative disorders. Cystamine and cysteamine are recognized for their antioxidant properties, capable of scavenging harmful free radicals and mitigating oxidative stress as observed in emerging studies investigating neurodegenerative diseases like Huntington's, Alzheimer's, and Parkinson's disease (reviewed in Paul and Snyder, 2019) [1]. Cystamine's inhibition of transglutaminase, an enzyme linked to neuronal death, along with its ability to reduce oxidative stress has shown to preserve neuronal integrity in Huntington's disease models, highlighting its protective role against neurodegeneration [2, 3]. Similarly, its analog cysteamine reduced the toxic effects of mutant huntingtin proteins by modulating mitochondrial dysfunction and preventing apoptosis [4]. Both aminothiols increase brain-derived neurotrophic factor (BDNF) levels in mouse brain, enhancing neuronal survival and repair [2, 5, 6]. Calkins et al. (2010) [7] reported that cystamine attenuated oxidative damage in a neurotoxicity model involving exposure to 3-nitropropionic (3-NP) acid, a neurotoxin that induces mitochondrial dysfunction, similar to that observed in Parkinson's disease. Cystamine and cysteamine have demonstrated efficacy in rescuing dopaminergic neurons and promoting restorative mechanisms in rodent models of Parkinson's disease and 1-methyl-4-phenyl-1,2,3,6-tetrahydropyridine (MPTP)-induced toxicity [6, 8, 9], with cysteamine further identified as a potential disease-modifying agent that improved cognitive and motor function, and delayed disease progression in mice (reviewed in Cicchetti et al., 2019 [10]). While much of the current research on

cystamine treatments centers on neurological conditions that are progressive and long-term in nature, this study investigates the acute effects of cystamine. The findings presented here may suggest its potential application in mitigating neurological injury and disease, but further research to include long-term studies are needed. We evaluated cystamine for its neuroprotective efficacy in a rat model of cholinergic-induced status epilepticus and associated neurodegeneration caused by organophosphorus nerve agent exposure.

Organophosphorus nerve agents are potent, fast acting irreversible inhibitors of acetylcholinesterase, which, if left untreated, rapidly lead to a cholinergic crisis and fatality due to respiratory failure [11, 12]. In preclinical studies, exposure to a seizure-inducing dose of nerve agent, such as soman, resulted in long-term, progressive pathophysiology characterized by neurodegeneration, epileptogenesis, neuroinflammation, and neurological dysfunction [13–17]. This pathological progression is also demonstrated by the onset of status epilepticus, a condition marked by recurrent seizures that impede neurological recovery and exacerbate long-term damage [15, 16, 18]. Chen et al. (2012) [17] and Jett et al. (2020) [19] discussed findings in human and animal studies, where disruptions to the cholinergic system caused by nerve agent exposure is linked to increased levels of oxidative stress and persistent cognitive deficits such as impaired learning, memory loss, mood disturbances, and attention deficits. The current therapeutic standard of treatment for nerve agent exposure includes the muscarinic antagonist atropine, an oxime such as 2-pralidoxime, and a first-line benzodiazepine such as midazolam or diazepam [20, 21]. Although this therapeutic strategy increases survival, delayed treatment, which is anticipated in a mass casualty event, may result in benzodiazepine refractory status epilepticus and failure to fully protect against the neuroinflammation and neurodegeneration induced by status epilepticus [22–24]. These events underscore the need for improved medical and public health preparedness, particularly in mass casualty scenarios.

Considering current drug limitations and lack of approved neuroprotectants to mitigate the secondary neurodegeneration that follows nerve agent exposure, we evaluated the potential neuroprotective efficacy of the aminothiol cystamine as a novel adjunct to midazolam against soman-induced status epilepticus in rats. The organophosphorus nerve agent soman was used to assess the neuroprotective efficacy of cystamine, since in preclinical models, exposure to a lethal dose of soman consistently induces seizure [24, 25] and seizure-associated brain damage [26, 27]. Soman's rapid induction of seizure activity makes it more reliable for neuroprotection studies compared to nerve agent VX, which although highly toxic, has less consistent SE compared to soman [24, 28]. In addition, the most effective anticonvulsant drugs in soman-induced seizures are either equally or more effective in treating seizures induced by other nerve agents (tabun, sarin, cyclosarin, VX) [24], suggesting therapies effective against soman may be broadly applicable to other nerve agents. Soman is

difficult to treat since it undergoes a rapid “aging” process, within minutes [29], whereby nerve agent inhibited acetylcholinesterase (AChE) is converted to an inactive form, limiting the window for oxime reactivation. In addition, in rats exposed to soman, the U.S. fielded oxime pralidoxime chloride (2-PAM) afforded no protection [30].

Early control of nerve agent-induced seizure is critical for both survival and neuroprotection [24] as there is a time-dependent reduction in efficacy of benzodiazepines in terminating nerve-agent induced seizure [31, 32]. Our laboratory developed a preclinical rat model of soman-induced seizure to evaluate therapies to treat SE, epileptogenesis and associated neurodegeneration [18, 33–36]. Soman’s reliability in producing severe, benzodiazepine-resistant SE in rats makes it particularly valuable for studying neuroprotection in refractory SE scenarios. In sum, the well characterized preclinical rat model of soman-induced SE results in benzodiazepine refractory SE and severe neuropathology, making it a reliable and rigorous model for testing therapeutics against cholinergic-induced seizure and associated neurodegeneration. Animal studies conducted in our laboratory using this preclinical model, along with evidence in literature suggests that aminothiols may serve as promising novel adjunctive therapies for counteracting nerve-induced neurodegeneration, neuroinflammation, and epileptogenesis.

Materials and methods

Animals

Adult male Sprague Dawley rats (276–300 g; Charles River Laboratories; Kingston, NY, United States) were pair-housed upon arrival and then housed in individual cages at the time of surgery. Animals were kept in temperature and humidity-controlled quarters with food and water available *ad libitum*. Rooms were set on a standard 12:12 h light-dark cycle (lights on at 0600) and rats were weighed daily (M-F) with exception of weekends and federal holidays. The experimental protocol was approved by the Animal Care and Use Committee at the United States Army Medical Research Institute of Chemical Defense, an AAALAC accredited facility, and all procedures were conducted in accordance with the principles stated in the Guide for the Care and Use of Laboratory Animals and the Animal Welfare Act of 1966 (P.L. 89–544), as amended.

Telemetry transmitter implantation for electroencephalographic recording

Rats were implanted subcutaneously (SC) with electroencephalographic (EEG) telemetry transmitters. For

pain management, rats were pretreated with meloxicam (1 mg/kg, SC; Patterson Veterinary; St. Paul, MN, United States) prior to being anesthetized with isoflurane (Patterson Veterinary; 5% chamber induction, 1–5% maintenance with 0.5–10 L/oxygen). Once rats were secured in a Kopf stereotaxic apparatus (David Kopf Instruments, Tujunga, CA, United States), four stainless steel screw electrodes were implanted cortically through the skull 2 mm from each side of the midline at 2 mm anterior and 4 mm posterior to bregma. HD-S02 or F40-EET transmitters (Data Sciences International [DSI], Inc., St. Paul, MN, United States) were implanted SC, with the ends of the four stainless-steel wires wrapped around each screw electrode. Electrodes and wrapped wires were secured in place with self-curing dental acrylic (Ortho-Jet™, Lang Dental Manufacturing Company, Inc., Wheeling, IL, United States). Buprenorphine sustained release (SR) or extended release (ER) (1.2 mg/kg, SC; ZooPharm, Laramie, WY, United States) was administered as a post-operative analgesic immediately after removal from anesthesia. Rats were given food pellets dissolved in water with a few grains of sugar to aid with post-operative recovery and at least 1 week of surgical recovery prior to experimentation. EEG activity was continuously recorded using the Ponemah V6 or Dataquest Art Acquisition (digitized at 500 Hz, DSI, Inc.).

Agent exposure and treatments

Rats were exposed to saline (Hospira; Lake Forest, IL, United States) or a seizure-inducing dose of soman (GD; 0.5 mL/kg, 236.2 µg/mL, SC; obtained from the United States Army Combat Capabilities Development Command Chemical Biological Center; Aberdeen Proving Ground, Gunpowder, MD, United States) then treated with an admix of atropine sulfate (ATS; 2 mg/kg, IM; Sigma-Aldrich; St. Louis, MO, United States) and asoxime dimethanesulfonate (HI-6 in DMS; 118.5 mg/kg, IM, Kalexyn Medicinal Chemistry, Kalamazoo, MI, United States) 1 min after exposure, followed by midazolam (3 mg/kg, SC; Hospira) 30 min after seizure onset. In our study, we administered a dose of 1.2 LD₅₀ soman which is approximately the LD₉₀ for subcutaneous exposure in untreated adult male rats (data generated in our laboratory) [37]. The ATS and HI-6 admix treatments were administered to simulate the standard medical response following exposure and to increase survival. Controls (No GD) did not receive the admix. EEG recordings were monitored in real time to identify the onset of seizure defined as rhythmic, high amplitude spikes (>2 × baseline values) lasting ≥10 s.

Cystamine (10 or 50 mg/kg, IP) or vehicle was administered 30 min after seizure onset and again 4 h later. The experimental setup consisted of four groups: control (No GD, n = 14), midazolam (GD/MDZ/VEH, n = 14), midazolam-cystamine 10 mg/kg (GD/MDZ/CYS10, n = 7), and midazolam-

cystamine 50 mg/kg (GD/MDZ/CYS50, $n = 10$). Cystamine given at doses of 10 and 50 mg/kg were previously shown to be neuroprotective in rodents (10, 50, and 100 mg/kg [38]; 30 and 60 mg/kg [39]). Both studies administered cystamine repeatedly over multiple weeks. For the present study, we gave a single additional dose of cystamine. Seven out of the fourteen rats in the control group and eight out of the fourteen rats in the midazolam group are historical controls. Three rats from the control (No GD) group had nonfunctional transmitters (no remaining battery life) and were excluded from temperature, activity, and power band analysis. Histological analysis for NeuN was performed for a subset of $n = 11$ rats in the control (No GD) group. Histological analysis for Iba1 was performed for a subset of $n = 11$ rats in the control (No GD) group. Data missing values because of death, include one rat in the cystamine (10 mg/kg) group that died after nerve agent exposure before receiving the second treatment and was excluded from all data analysis. One rat in the cystamine (10 mg/kg) group was euthanized early for humane endpoint 4 days after exposure and excluded from body weight, spontaneous recurrent seizures (SRS), activity, and neuropathological analysis. One rat in the cystamine (50 mg/kg) group did not survive to 24 h and was excluded from all analysis except toxic signs and power integral.

Analysis of EEG seizure and behavioral seizure

Continuous recording of EEG, temperature, and activity data were recorded using the Ponemah software (DSI, Inc.) and Dataquest Art Acquisition (DSI, Inc.) for subjects with HD-S02 and F40-EET transmitters. Home cages were placed on RPC-1 PhysioTel receivers (DSI, Inc.), where baseline EEG was recorded at least 1 day prior to exposure and continuously for 14 days after exposure. The EEG power spectrum was divided into delta (0.1–4.0 Hz), theta (4.1–8.0 Hz), alpha (8.1–12 Hz), beta (12.1–25 Hz), and gamma (25.1–50 Hz) bands. The mean power was calculated for each band (see de Araujo Furtado et al., 2009 for methods) [40] and integrated in 10-min bins. Calculation of the EEG power integral to measure seizure severity was determined by taking the average of power spectra of each hour period using a customized MATLAB algorithm and applying a formula $\{\text{decibels} = 10 \times [\text{Log}(V^2_{\text{sample}}/V^2_{\text{baseline}})]\} \times 60 \text{ min}$, resulting in decibels/h (see Niquet et al., 2016 and Lumley et al., 2019 for methods) [41, 42]. The frequency range was 0.1–100 Hz, with the data representing the full spectrum and the ratio of EEG power in specific time periods after onset of SE or treatment. Noldus Observer XT (Noldus Information Technology Inc., Leesburg, VA, United States) was used for real-time monitoring and to input behavioral seizure continuously for 2 h after exposure and then every 30 min until close of business. A modified Racine scale [43] was used to score behavioral seizures, comprised of the

following five stages: 1, masticatory movements; 2, head myoclonus; 3, limb clonus and/or tonus; 4, forelimb clonus with rearing; 5, rearing and falling and/or tonic-clonic convulsions. EEG was also monitored throughout this observation period. Additional sterile saline (5 mL, SC) treatments and food pellets dissolved in water with grains of sugar were provided 1–2 times daily to aid with weight recovery and dehydration for the first 3–4 days after exposure.

Neuropathology assessments

Two weeks after soman exposure, rats were deeply anesthetized with sodium pentobarbital (75 mg/kg, 1.0 mL, IP; Euthasol, Virbac or Fatal-Plus, Patterson Veterinary) and then transcardially exsanguinated with 0.9% heparinized saline in 0.1 M phosphate buffer (PB; FD Neurotechnologies, Columbia, MD, United States), followed by 4% paraformaldehyde in 0.1 M PB (FD Neurotechnologies) for tissue fixation. Following perfusions, brains were removed and post-fixed in 4% paraformaldehyde for 6 h at 4–8°C then cryoprotected in 20% sucrose (FD Neurotechnologies) in PB for up to 1 week. Brains were later flash frozen at –70°C in preparation for sectioning and staining. Brain tissue was sectioned coronally at 30 μm and stained with mature neuronal marker NeuN (mouse anti-NeuN IgG 1:1000; Millipore, Billerica, MA, United States) or microglial marker ionized calcium-binding adaptor molecule 1 (Iba1; rabbit anti-Iba1 IgG 1:10,000; Wako Chemicals, Richmond, VA, United States). Processing for the stains was conducted by FD Neurotechnologies. Viable neurons were quantified through analysis of NeuN-positive (NeuN+) cells and neuroinflammation was quantified through analysis of Iba1-positive (Iba1+) cell density and cell body-to-size ratio in the following brain regions, which our laboratory and others [21, 33, 36] previously observed soman-induced neurodegeneration: layer 3 of the piriform cortex, CA1 of the hippocampus, amygdala, medial thalamus, and lateral thalamus.

An Olympus brightfield microscope and VSI slide scanning software were utilized to obtain images of slides. NeuN-stained coronal sections (30 μm , scanned at $\times 10$ magnification, slides between Bregma –2.40 to –3.24 mm) were analyzed using ImagePro v7.0 (Media Cybernetics, Inc., Rockville, MD, United States) to evaluate NeuN-positive (NeuN+) cell density and density values (areas measured in μm) were obtained using automated counts. Inverted contrast was applied to aid in the visualization and counting of NeuN+ cells. StereoInvestigator (MBF Biosciences, Williston, VT, United States) was utilized to manually count NeuN+ cell densities in the highly dense region of the CA1 of the hippocampus. Iba1-stained coronal sections (30 μm , scanned at $\times 20$ magnification, slides between Bregma –2.40 to –3.24 mm) were analyzed in ImageJ (National Institutes of Health, NIH, Bethesda, MD, United States) for Iba1-positive (Iba1+) cell density and Iba1+ cell body-to-size ratio to evaluate microglial activation. Control

(No GD) subjects served as comparisons for neuropathology evaluation; subjects that did not survive until study endpoint of 14 days after exposure were excluded from neuropathological analysis.

Data analysis

Statistical analyses were performed using SPSS (IBM Inc. Armonk, NY, United States) and graphs generated using Prism GraphPad 10 (Dotmatics; Boston, MA, United States). For group comparisons of body weight, temperature, activity, EEG power band, and EEG power integral, repeated measures analysis was used followed by an analysis of variance with a Tukey's test. For comparisons of initial seizure duration, NeuN+ density, and Iba+ density and ratio, a one-way ANOVA was done followed by Tukey's test. Treatment effect on median latency to SRS onset was determined with a Kaplan-Meier analysis. The effect of treatment on the endpoint percent of subjects that developed SRS was determined using a binary logistic regression analysis followed by a Chi-Square Fisher's exact test. The effect of group on the number of SRS occurrences was determined based on a negative binomial model. Behavioral seizure score was analyzed using a Kruskal-Wallis test.

Results

Body weight, body temperature, and home cage activity after soman exposure

Five out of the seven rats treated with the 10 mg/kg dose and nine out of the ten rats treated with the 50 mg/kg of cystamine survived exposure to soman. All rats that received midazolam monotherapy survived exposure to soman and only surviving historical rats were included. All soman-exposed groups experienced a reduction in body weight within 24 h of exposure ($p < 0.05$; [Supplementary Figure S1](#)). Body weight in soman-exposed rats that received cystamine (50 mg/kg) as adjunct to midazolam did not differ from control rats in body weight by post-exposure day 3, whereas those that received midazolam monotherapy weighed less than control rats until 1 week after exposure. Following soman exposure, rats experienced a decline in body temperature in the first few hours after exposure, with temperatures stabilizing close to baseline levels after approximately 36–42 h after exposure ([Figure 1](#)). While all three soman-exposed groups experienced a drop in body temperature following exposure, the temperatures of the group that received 50 mg/kg of cystamine returned to baseline within 18 h of exposure while those that received 10 mg/kg of cystamine returned within 26 h, and those that received midazolam monotherapy returned within 37 h of exposure ($p < 0.05$). In addition, rats treated with cystamine

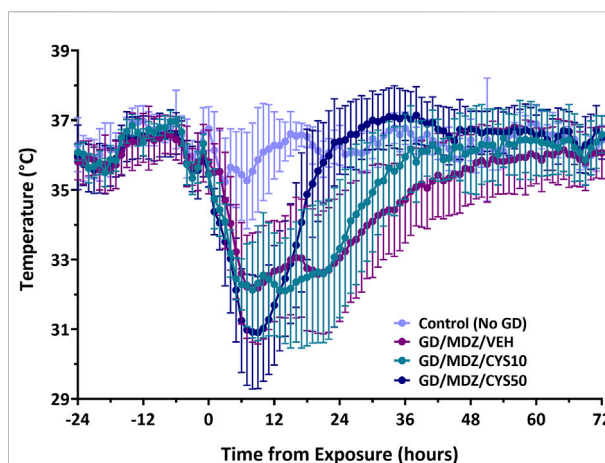


FIGURE 1

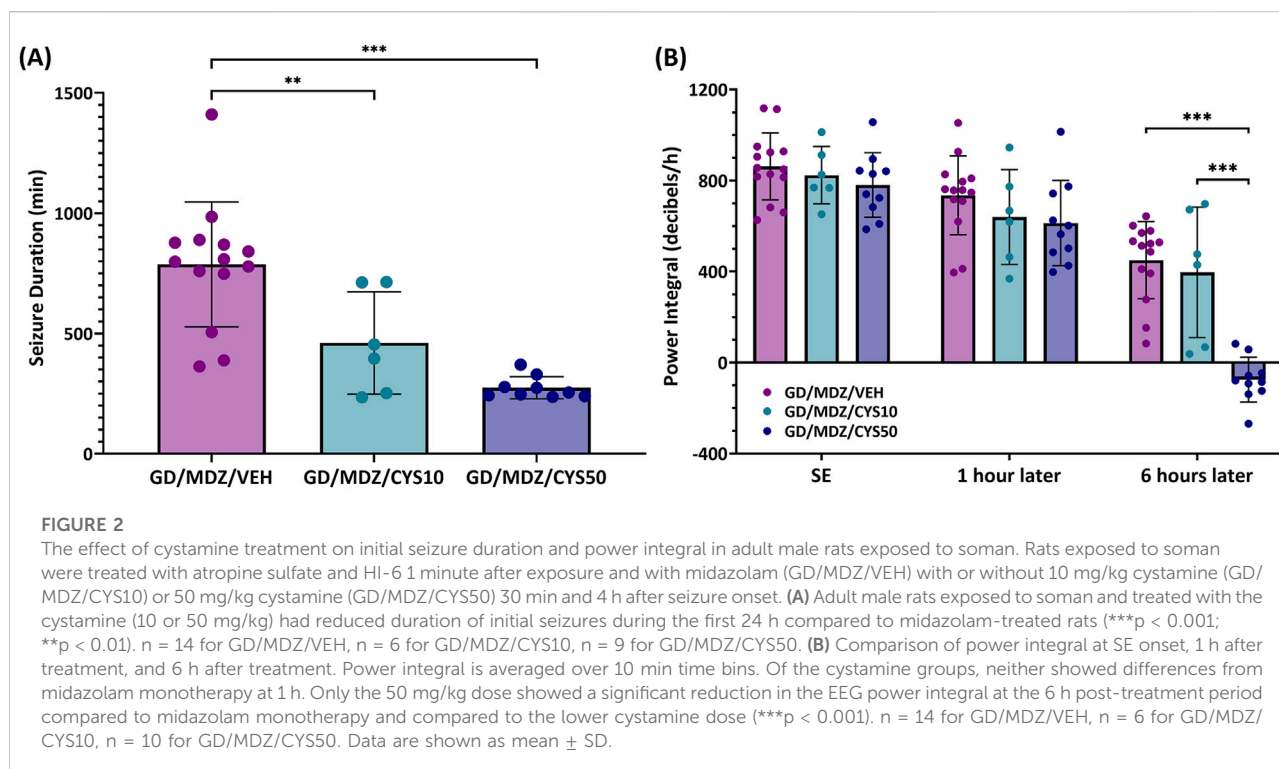
The effect of cystamine treatment on body temperature in adult male rats exposed to soman. Rats exposed to soman were treated with atropine sulfate and HI-6 1 minute after exposure and with midazolam (GD/MDZ/VEH) with or without 10 mg/kg cystamine (GD/MDZ/CYS10) or 50 mg/kg cystamine (GD/MDZ/CYS50) 30 min and 4 h after seizure onset. In all soman-exposed groups, body temperature was reduced within a few hours compared to baseline and to Control (No GD). The GD/MDZ/CYS50 group had lower body temperature at 1 h and 2 h compared to the GD/MDZ/VEH group ($p < 0.05$), yet recovered body temperature more rapidly; from 18 to 44 h, 46–48 h, and 56 h after exposure. The GD/MDZ/CYS50 rats had significantly higher body temperature compared to GD/MDZ/VEH ($p < 0.05$). In addition, the GD/MDZ/CYS50 group returned to baseline temperature by 18 h, the GD/MDZ/CYS10 within 26 h and the GD/MDZ/VEH within 37 h after exposure. $n = 11$ for Control (No GD), $n = 14$ for GD/MDZ/VEH, $n = 6$ for GD/MDZ/CYS10, $n = 9$ for GD/MDZ/CYS50. Data are shown as mean \pm SD.

(50 mg/kg) and midazolam had higher temperature compared to midazolam monotherapy, from 18–44, 46–48 and at 56 h after soman exposure. The group that received 10 mg/kg of cystamine returned to baseline within 29 h.

Home cage activity increased in the dark cycle of soman-exposed rats treated with either midazolam or with the lower dose of cystamine (10 mg/kg), compared to control (No GD) rats ($p < 0.05$; [Supplementary Figure S2](#)). Significance was found in rats treated with cystamine (10 mg/kg) during the dark cycle on days 8 and 9 and in rats treated with midazolam-only on days 10 and 11 following exposure compared to controls. Rats that received midazolam and cystamine (10 mg/kg) also had increased activity on days 2–3 after exposure. In contrast, activity in rats treated with the higher dose of cystamine (50 mg/kg) as adjunct to midazolam did not differ from control.

Behavioral seizure, EEG seizure activity, power integral, and epileptogenesis

All soman-exposed adult rats experienced moderate-to-severe behavioral seizure within minutes of exposure. Animals

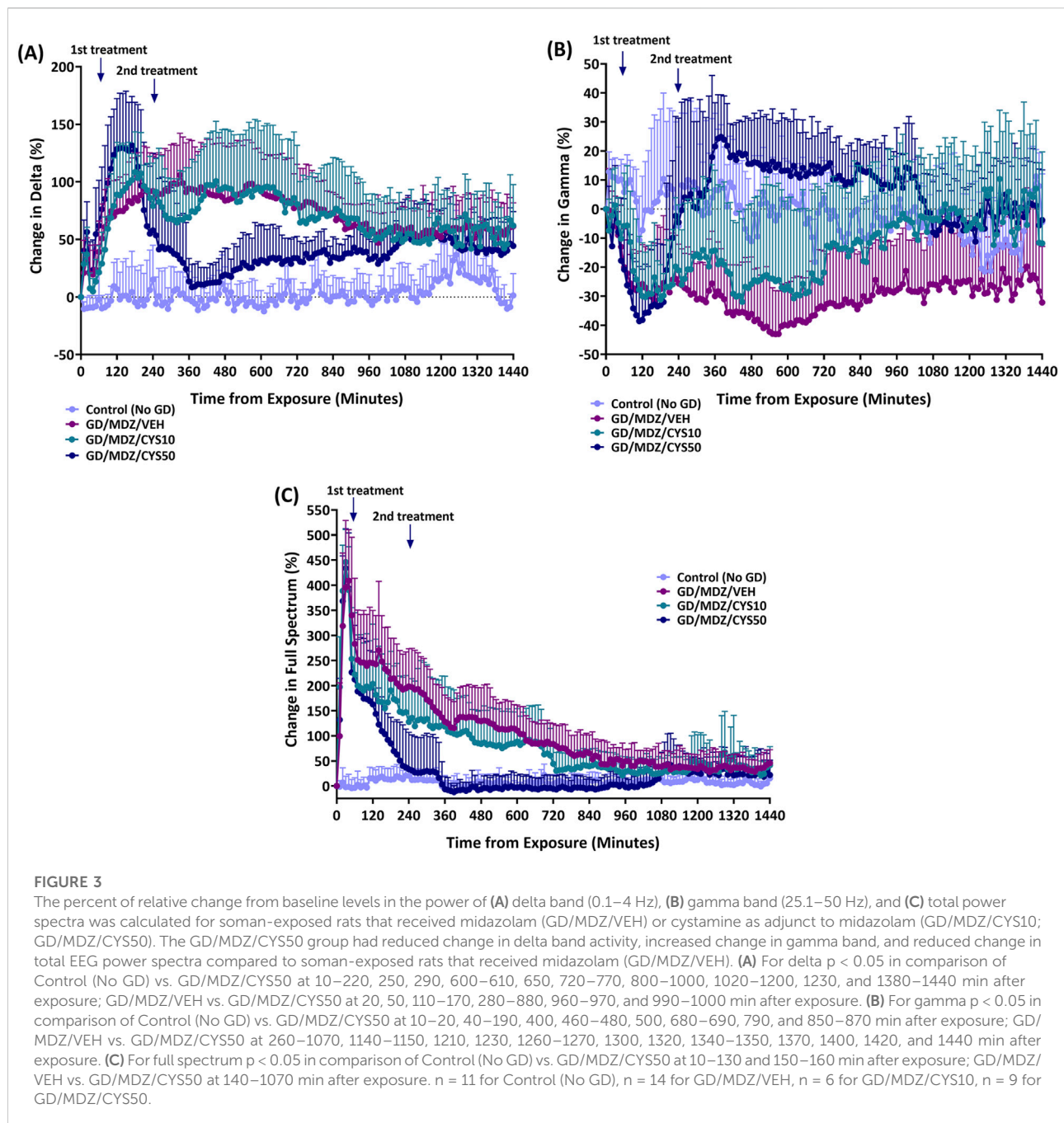


exhibited behavioral seizure corresponding to stages 4–5 within the first hour following exposure and signs persisted at stages 2–3 over the 6-h period after exposure. Neither dose of cystamine dose as adjunct with midazolam reduced severity of behavioral seizures shortly after treatment compared to midazolam monotherapy; however, the 50 mg/kg dose of cystamine had significantly reduced behavioral seizure scores at the 210-min time point ($p < 0.05$). Acute (24 h) seizure duration and EEG power integral were monitored in adult rats that had received telemetry implants 7–10 days prior to soman exposure. Among rats treated with the cystamine, the duration of initial seizures during the first 24 h was significantly reduced compared to midazolam-only treated rats, with the 50 mg/kg dose showing the greatest reduction ($p < 0.001$; Figure 2A). In addition, the 50 mg/kg dose of cystamine reduced EEG power integral 6 h post-treatment when compared to midazolam alone ($p < 0.001$; Figure 2B).

The percent of relative change from baseline levels in the power of (A) delta power band (0.1–4 Hz), (B) gamma power band (25.1–50 Hz), and (C) full spectrum power band are shown in Figure 3. All soman-exposed rats had an increase in percent change from baseline levels in delta power band ($p < 0.05$). Midazolam monotherapy delta levels returned to Control (No GD) levels briefly at 1240–1250, and 1270 min after exposure but otherwise had increased change from Control (No GD) levels for the full 24 h following exposure ($p < 0.05$). Rats treated with the

50 mg/kg dose of cystamine, when compared to midazolam monotherapy, had a greater initial increase in delta power band levels at 20, 50, and 110–170 min after exposure ($p < 0.05$) but had reduced change compared to midazolam monotherapy at 280–880 min after exposure ($p < 0.05$). All soman-exposed rats had an initial reduction in percent change in gamma power band compared to Control (No GD) levels ($p < 0.05$). Change in gamma power band levels for rats treated with the 50 mg/kg dose of cystamine was increased compared to midazolam monotherapy at 260–1070, 1140–1150, 1210, 1230, 1260–1270, 1300, 1320, 1340–1350, 1370, 1400, 1420, and 1440 min after exposure ($p < 0.05$). All soman-exposed rats had an initial increase in full spectrum power band compared to Control (No GD) levels ($p < 0.05$). Rats treated with the 50 mg/kg dose of cystamine returned to Control (No GD) levels earlier (at 170 min after exposure) than other treatment groups ($p < 0.05$); cystamine (10 mg/kg) treatment returned to Control (No GD) levels at 720 min after exposure ($p < 0.05$) and midazolam monotherapy treatment group returned to Control (No GD) levels at 1100 min after exposure ($p < 0.05$). Change in full spectrum power band levels was significantly reduced for rats treated with cystamine 50 mg/kg compared with midazolam monotherapy, 140–1070 min after soman exposure ($p < 0.05$).

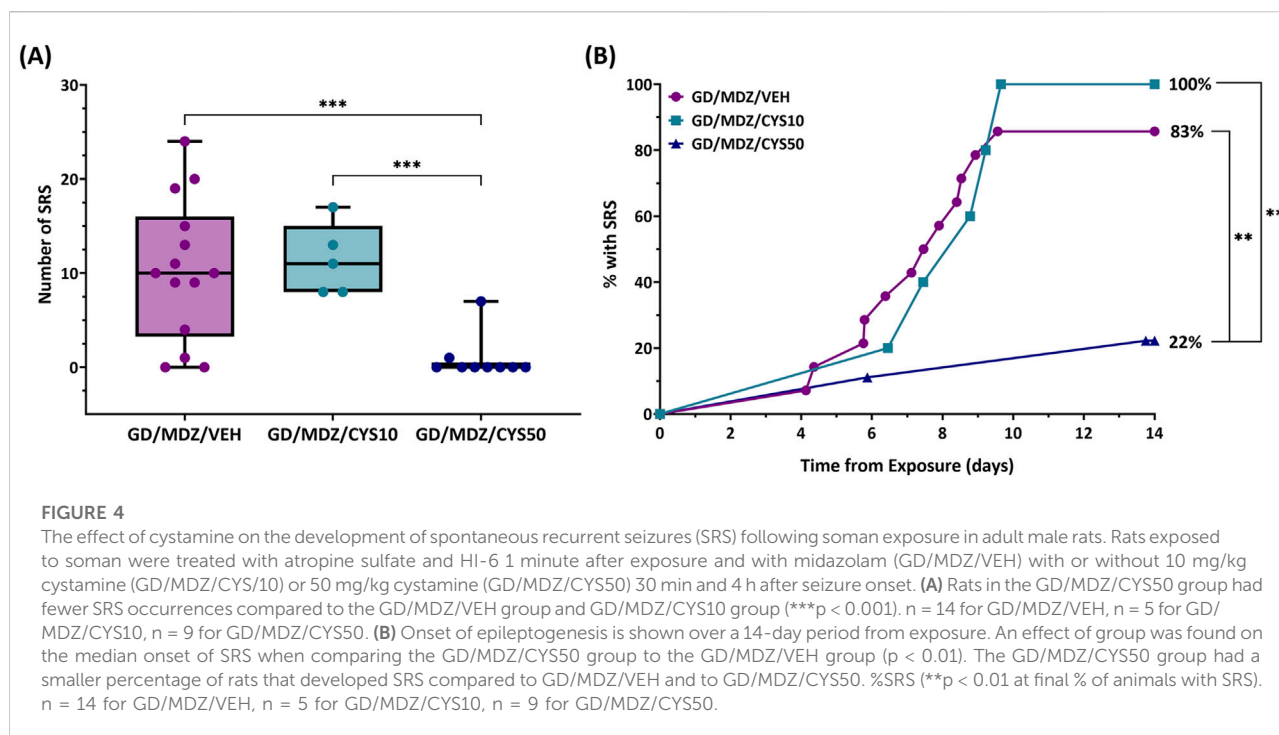
Continuous monitoring of EEG data for the 14-day duration following soman exposure allowed for detection of spontaneous recurrent seizures (SRS). Rats that received the 50 mg/kg



cystamine dose adjunct with midazolam had a lower number of SRS events compared to rats treated with the monotherapy and 10 mg/kg dual therapy 14 days after exposure ($p < 0.001$; Figure 4A). All treatment groups contained at least one subject that developed SRS approximately 4–6 days after exposure. While 100% of rats in the 10 mg/kg dual-therapy group developed SRS, the 50 mg/kg dual-therapy group had a substantial reduction in incidence, with only about 22% of rats affected ($p < 0.01$; Figure 4B).

Neuronal loss and microglial activation after soman exposure

Neuronal loss was demonstrated by a lower density of NeuN+ cells. Exposure to soman led to varying degrees of neuronal loss in the regions of interest across all groups (Figure 5A). Adjunct treatment with the 50 mg/kg cystamine dose significantly reduced neuronal loss in the CA1, amygdala, medial thalamus, and the lateral thalamus, compared to



midazolam monotherapy ($p < 0.01$, $p < 0.001$). The 10 mg/kg dose did not afford significant neuroprotection overall. Representative photomicrographs of NeuN-stained coronal sections visualize treatment group differences in the piriform cortex, CA1 region of the hippocampus, amygdala, medial thalamus, and lateral thalamus (Figure 5B). Sparsely stained areas reflect the absence of neurons and greater damage, in contrast to denser or darker-stained regions where neuronal populations were better preserved; this difference was most pronounced when comparing the brain regions of the 50 mg/kg cystamine and monotherapy groups.

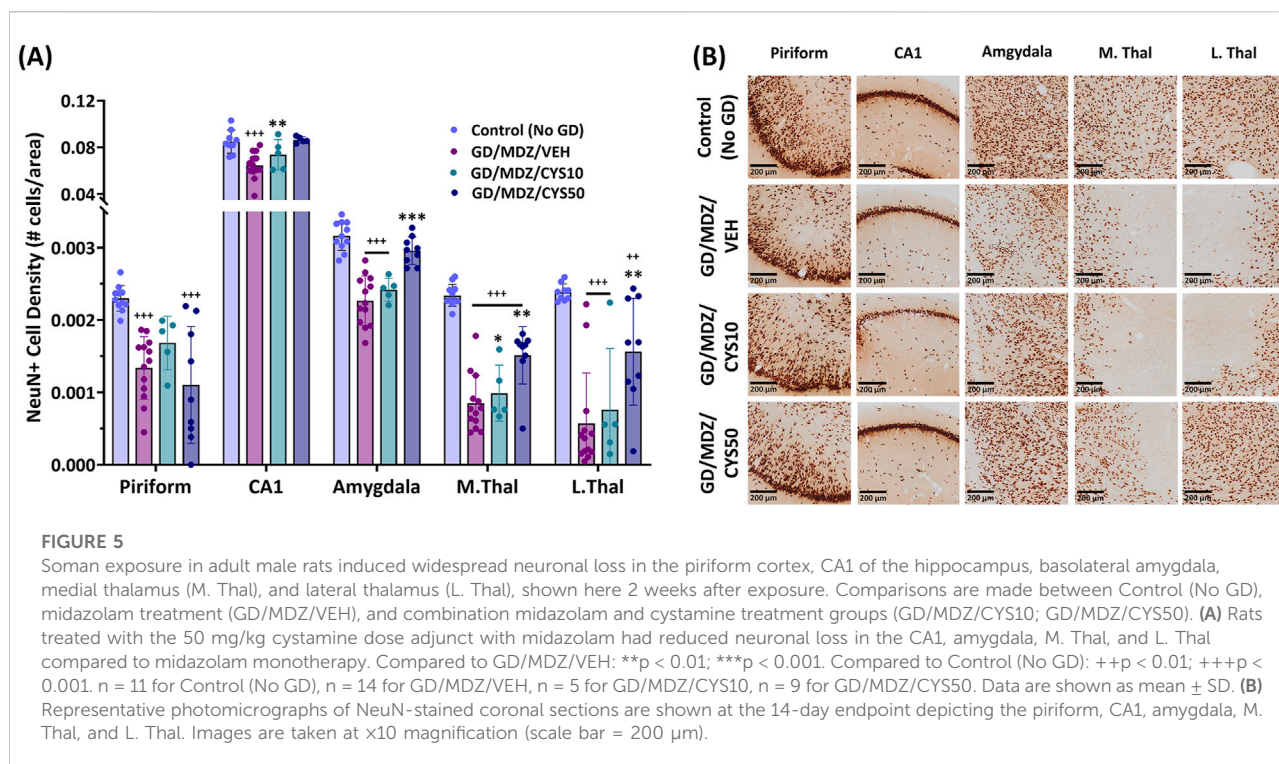
An increase in Iba1+ cell density represents an increase in cell proliferation and an increase in cell body-to-size ratio represents the morphological changes that resident microglia undergo in response to seizure activity and central nervous system (CNS) damage. Varying degrees of microglial activation and proliferation were observed in animals treated with either the midazolam monotherapy or the midazolam-cystamine dual therapies based on qualitative observations of Iba1+ cell density and Iba1+ cell body-to-size ratio (Figures 6A,B). Adjunct treatment with the 50 mg/kg cystamine dose reduced soman-induced increase in Iba1+ cell density in the lateral thalamus compared to midazolam monotherapy ($p < 0.01$). This dose also decreased cell body-to-size ratio in the CA1 of the hippocampus compared to midazolam-treated rats after soman exposure ($p < 0.01$). The 10 mg/kg dose did not afford significant mitigation of microglial activation and proliferation. Representative photomicrographs of Iba1-stained coronal sections with a cresyl violet co-stain visualize treatment

group differences in the piriform cortex, CA1 region of the hippocampus, amygdala, medial thalamus, and lateral thalamus (Figure 6C). An increased number of microglial cells and their aggregation, along with visibly enlarged cell bodies, indicate heightened activation in response to damage, whereas fewer cells with less density and reduced enlargement suggest attenuation of that response. This difference is most apparent when comparing the brain regions of the 50 mg/kg cystamine and monotherapy groups.

Discussion

This study utilized a rodent model of soman-induced status epilepticus to investigate the therapeutic potential of an aminothiols in mitigating neurodegeneration. Compared to midazolam monotherapy, the midazolam and cystamine dual therapy demonstrated anti-seizure effects following soman exposure as observed in its reduction of initial time spent in seizure, fewer occurrences of SRS, reduced EEG power integral, and modulation of power band spectra, which may indicate reduced seizure severity. Furthermore, cystamine as adjunct to midazolam treatment ameliorated neuronal damage and suppressed microglial activation, which occurs following exposure to a seizure-inducing dose of soman in rodents [22, 36, 44, 45].

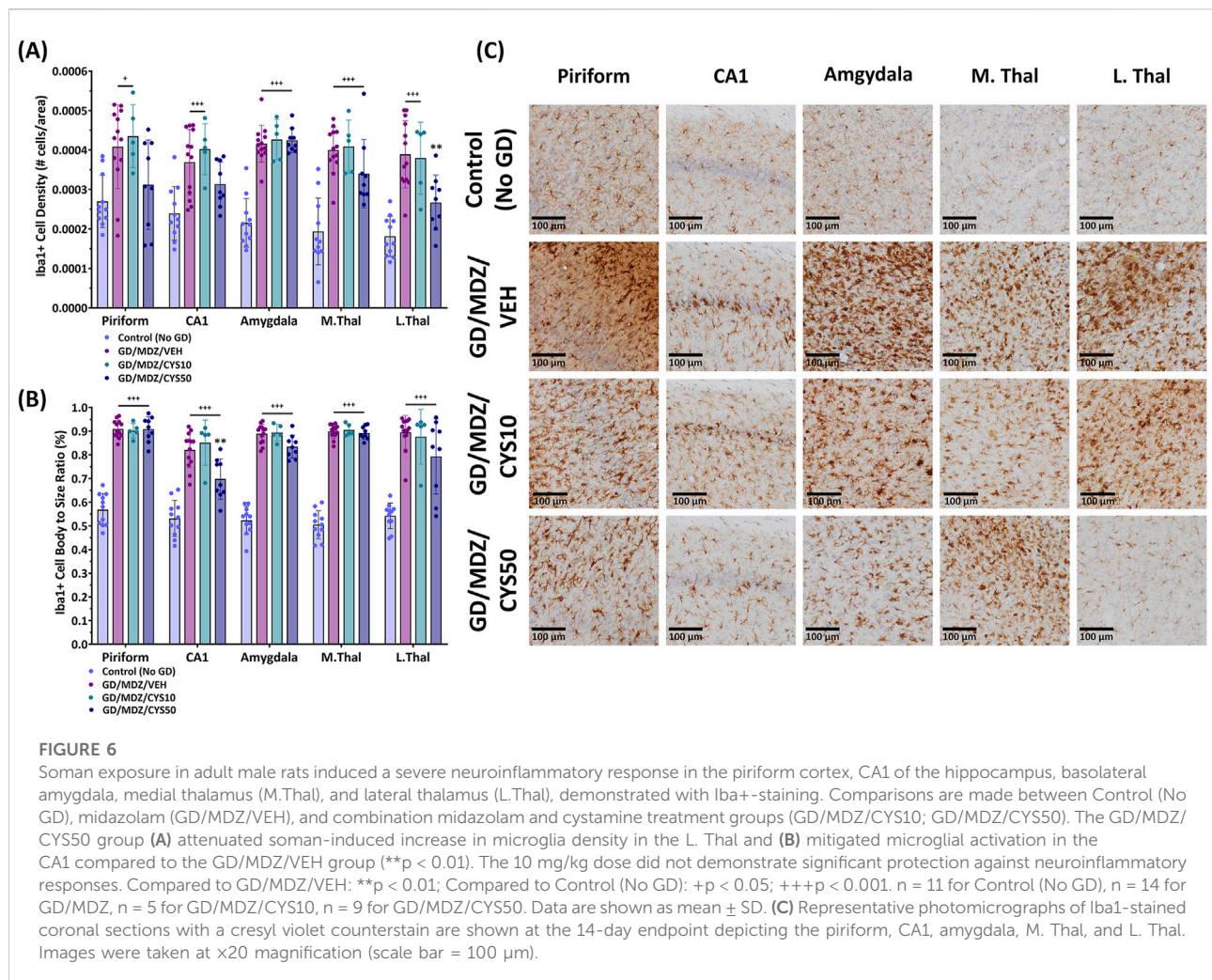
The higher dose of cystamine (50 mg/kg) in combination with midazolam was more effective than the lower dose (10 mg/kg) in reducing soman-induced status epilepticus,



specifically by reducing the total time spent in initial seizures as well as a lower occurrence and percentage of rats that developed SRS, compared to midazolam monotherapy. The duration of initial seizure was associated with the extent of neurodegeneration, with less time in seizure resulting in less brain damage [16]. The development of SRS after soman exposure in rats treated with a benzodiazepine is associated with greater hippocampal damage compared to rats that do not develop SRS [46]. Greater suppression of soman-induced seizure duration and reduction in SRS development by cystamine (50 mg/kg) as an adjunct to midazolam likely contributed to reduced neuronal loss compared to rats treated with midazolam only. The longer time in seizure and high occurrences of SRS may have contributed to the greater neuropathology observed in animals that received the lower dose (10 mg/kg) of cystamine. In addition, attenuation of soman-induced increases in delta band activity, as observed in our findings with rats treated with the cystamine 50 mg/kg dose, corresponded to less neurodegeneration [47, 48]. It is important to note however, extensive neurodegeneration can still occur in the absence of recurrent seizures, possibly driven by mechanisms such as excitotoxicity from initial seizure events or inflammation that persists beyond the initial trauma after exposure [17].

Cystamine as adjunct therapy to midazolam reduced neurodegeneration in the CA1, amygdala, and regions of the thalamus. Immunohistochemical analysis of our findings showing reduced neuronal loss and reduced microglia

proliferation activity in the CA1 of rats that received the 50 mg/kg dual treatment presents an intriguing insight about cystamine's mechanism of action. The hippocampus, which encompasses the CA1 subregion, is one of the seizure-sensitive brain regions most vulnerable to severe neuronal damage after nerve agent exposure [24, 49, 50]. An excessive reactive microglial response, as observed in other models of nerve agent-induced toxicity [44], can exacerbate neurodegeneration, where these immune cells can contribute to neuronal injury through the release of pro-inflammatory cytokines and reactive oxygen species (ROS) [51, 52]. This aligns with broader observations in neurodegenerative disease such as Alzheimer's and Parkinson's disease, where chronic neuroinflammation and dysregulated glial activity are hallmarks of disease progression [53–55]. By reducing the degree of microglial activation in soman-exposed rats, it is possible that cystamine as an adjunct to midazolam is also reducing the exacerbation of neuronal degeneration. Although the current study shows promising results, its short-term duration (2 weeks) offers only a preliminary understanding. Further studies are needed to investigate the long-term neuroprotective effects of treatment with aminothiols cystamine and cysteamine in models of status epilepticus, as well as to assess the efficacy of sub-chronic and chronic treatment with aminothiols in these models. In addition, future studies would benefit from a larger sample size, especially in cases of reduced survivors to soman exposure.



The precise mechanism of action of cystamine is not fully understood, but evidence suggests its protective effects are largely indirect. Cystamine is rapidly metabolized into cysteamine, resulting in the accumulation of the cellular antioxidant cysteine [1, 56, 57]. The accumulation of cysteine (also proposed to be neuroprotective) supports the synthesis of glutathione, another powerful antioxidant that helps counteract oxidative stress via the neutralization of ROS [56, 58, 59]. Beyond its influence on antioxidant levels, cystamine metabolites are thought to interact with several neuroprotective pathways. Notably, cystamine has been shown to inhibit transglutaminase, an enzyme implicated in the neurodegenerative process and cell death, where it catalyzes the crosslinking of toxic protein aggregates during times of stress [60]. Additionally, cysteamine, the active form of cystamine, has been linked to an increase in BDNF levels, which has been shown to play a crucial role in neuronal survival and plasticity [2, 5, 6]. Interestingly, our laboratory previously observed that low dose exposure to the nerve agent

O-ethyl-S-(2-diisopropylaminoethyl)-methylphosphonothiolate (VX) in mice increased BDNF in CA3 of the hippocampus and suggested that elevated BDNF may have been an adaptive response in this model [61]. Overall, it appears that cystamine potentially triggered a cascade of biochemical changes that collectively bolstered neuronal resilience against damage.

Our findings reinforce existing evidence of cystamine's neuroprotective potential. Cystamine has demonstrated efficacy in other models of neurotoxicity, including 3-nitropropionic (3-NP), 6-hydroxydopamine (6-OHDA), and 1-methyl-4-phenyl-1,2,3,6-tetrahydropyridine (MPTP), which resulted in damage to the substantia nigra and striatum [6, 7, 9]. Like the brain regions examined in this study, substantia nigra and striatum are highly susceptible to severe neuronal damage following exposure [62–64]. For instance, in a 3-NP model, cystamine reduced striatal lesion size [7], while in 6-OHDA and MPTP preclinical models of Parkinson's disease it mitigated neuronal loss in the substantia nigra and preserved dopaminergic projections to the striatum [9]. Moreover, cysteamine, an analog

of cystamine, exhibited a dose-dependent protection of striatal dopaminergic neurons and substantia nigra neurons in a mouse model of neurodegeneration [6]. Comparable effects of cystamine treatment on neuroprotection were observed in our findings where viable neurons were preserved, and reactive microglia response was attenuated in seizure sensitive brain regions following soman exposure. Although the toxicity-induced models cited here differ in their mechanisms of toxicity from soman, there may be overlap in the secondary mechanisms of cell death such as oxidative stress, which may be protected by treatment with cystamine. Additionally, while the brain regions of interest we report here differ from those investigated in the aforementioned studies, they share susceptibility to neurotoxic damage, further supporting cystamine's therapeutic potential across diverse neural systems and regions.

Neuronal injury often results in the integrity of the blood brain barrier (BBB) being compromised, as reported in epilepsy models from a multitude of etiologies [65] and in nerve agent animal models [66]. This phenomenon allows for the recruitment of peripheral immune cells in the brain with less resistance [67]. Despite this impairment of BBB integrity, the BBB itself is still a significant challenge to the clinical application of many neuroactive compounds. Cystamine, through its reduced form, cysteamine, has been reported to effectively cross the blood brain barrier, where it has been shown to enhance neuronal survival through its mitigation of mitochondrial dysfunction [1], which is central to the pathophysiology of many neurodegenerative conditions. Bousquet et al., (2010) [3] reports cystamine facilitates cysteamine brain transport as evidenced by their findings in determining the brain transport coefficient which indicates the degree of brain uptake. It is possible that infiltration of peripheral immune cells in the brain to assist with the neuroinflammatory response, coupled with cystamine's neuroprotective mechanisms is why less neurodegeneration is observed in animals treated with the cystamine dual therapies. Further studies are needed to better understand cystamine's long-term effects on the BBB in the context of nerve agent-induced status epilepticus as well as other neurodegenerative disease models.

Much of the existing research regarding organophosphorus nerve agents primarily focused on management of seizures and therefore limits attention to the underlying neurodegeneration, neuroinflammation, and excitotoxicity that can persist after exposure. Although our focus was on neuroprotective potential of cystamine, as an adjunct treatment with midazolam our present finding of reduced time in seizure and reduced incidence of SRS may have contributed to our observed neuroprotective findings in rats treated with cystamine and midazolam, over midazolam monotherapy. Whether the multi-faceted neuroprotective mechanisms of action of cystamine [1] provided added benefit over that of reduction in initial seizure requires further study. The neuroprotective efficacy of cystamine as adjunct to midazolam

tested in this study against soman-induced toxicity offers a promising approach to this challenge and extends the current understanding of the neuroprotective potential of aminothiols. Managing oxidative stress caused by soman-induced toxicity with cystamine may reduce the overactivation of microglia, thereby limiting their potentially damaging effects and allowing for a more reparative neuroimmune response. Furthermore, since cystamine influences metabolic pathways, further research should explore whether treatments to endogenously enhance these natural processes might provide a sustained and multifaceted defense against cell death.

Author contributions

All authors participated in conducting the experiments, data acquisition, and data compilation, as well as in the review of the manuscript. MS, AW, MA, CS, DN, and LL performed formal analysis. CS and LL conducted statistical analysis. MA contributed to software. DN and MS generated the representative photomicrograph images. AB and CS generated the figure images. AB and LL wrote and edited the manuscript. MS, MA, CS, and LL contributed to methodology. LL contributed to conceptualization, design of the study, and funding acquisition. All authors contributed to the article and approved the submitted version.

Author disclaimer

The views expressed here are those of the author(s) and do not reflect the official policy and views of DOD, DOE, or ORAU/ORISE.

Data availability

The raw data supporting the conclusions of this article will be made available by the authors, without undue reservation.

Ethics statement

The animal study was approved by Institute Animal Care and Use Committee. The study was conducted in accordance with the local legislation and institutional requirements.

Funding

The author(s) declare that financial support was received for the research and/or publication of this article. The research was supported by an interagency agreement (AOD24006-001-00000)

between the NIH Office of the Director (OD); and the U.S. Army Medical Research Institute of Chemical Defense under the oversight of the Chemical Countermeasures Research Program (CCRP) within the Office of Biodefense Research (OBRS) at the National Institute of Allergy and Infectious Diseases (NIAID/NIH).

Acknowledgments

The authors appreciate technical support of Sou Chen and Sabrina Orta in compilation of figures and assisting with experiments, respectively. In addition, we appreciate Hailey Steier for editorial review. This research was supported in part by an appointment to the Department of Defense (DOD) Research Participation Program administered by the Oak Ridge Institute for Science and Education (ORISE) through an interagency agreement between the U.S. Department of Energy (DOE) and the DOD. ORISE is managed by ORAU under DOE contract number DE-SC0014664.

References

- Paul BD, Snyder SH. Therapeutic applications of cysteamine and cystamine in neurodegenerative and neuropsychiatric diseases. *Front Neurol* (2019) **10**:1315. doi:10.3389/fneur.2019.01315
- Borrell-Pages M, Canals JM, Cordelieres FP, Parker JA, Pineda JR, Grange G, et al. Cystamine and cysteamine increase brain levels of BDNF in Huntington disease via HSP1b and transglutaminase. *J Clin Invest* (2006) **116**:1410–24. doi:10.1172/JCI27607
- Bousquet M, Gibrat C, Ouellet M, Rouillard C, Calon F, Cicchetti F. Cystamine metabolism and brain transport properties: clinical implications for neurodegenerative diseases. *J Neurochem* (2010) **114**:1651–8. doi:10.1111/j.1471-4159.2010.06874.x
- Arbez N, Roby E, Akimov S, Eddings C, Ren M, Wang X, et al. Cysteamine protects neurons from mutant huntingtin toxicity. *J Huntington's Dis* (2019) **8**: 129–43. doi:10.3233/jhd-180312
- Gibrat C, Bousquet M, Saint-Pierre M, Levesque D, Calon F, Rouillard C, et al. Cystamine prevents MPTP-induced toxicity in young adult mice via the up-regulation of the brain-derived neurotrophic factor. *Prog Neuro-Psychopharmacology Biol Psychiatry* (2010) **34**:193–203. doi:10.1016/j.pnpbp.2009.11.005
- Sun L, Xu S, Zhou M, Wang C, Wu Y, Chan P. Effects of cysteamine on MPTP-induced dopaminergic neurodegeneration in mice. *Brain Res* (2010) **1335**:74–82. doi:10.1016/j.brainres.2010.03.079
- Calkins MJ, Townsend JA, Johnson DA, Johnson JA. Cystamine protects from 3-nitropropionic acid lesioning via induction of nf-e2 related factor 2 mediated transcription. *Exp Neurol* (2010) **224**:307–17. doi:10.1016/j.expneurol.2010.04.008
- Cisbani G, Drouin-Ouellet J, Gibrat C, Saint-Pierre M, Lagace M, Badrinarayanan S, et al. Cystamine/cysteamine rescues the dopaminergic system and shows neurorestorative properties in an animal model of Parkinson's disease. *Neurobiol Dis* (2015) **82**:430–44. doi:10.1016/j.nbd.2015.07.012
- Stack EC, Ferro JL, Kim J, Del Signore SJ, Goodrich S, Matson S, et al. Therapeutic attenuation of mitochondrial dysfunction and oxidative stress in neurotoxin models of Parkinson's disease. *Biochim Biophys Acta (Bba) - Mol Basis Dis* (2008) **1782**:151–62. doi:10.1016/j.bbadis.2007.12.006
- Cicchetti F, David LS, Siddu A, Denis HL. Cysteamine as a novel disease-modifying compound for Parkinson's disease: over a decade of research supporting a clinical trial. *Neurobiol Dis* (2019) **130**:104530. doi:10.1016/j.nbd.2019.104530
- Hulse EJ, Haslam JD, Emmett SR, Woolley T. Organophosphorus nerve agent poisoning: managing the poisoned patient. *Br J Anaesth* (2019) **123**:457–63. doi:10.1016/j.bja.2019.04.061
- Savolainen K. CHAPTER 50 - understanding the toxic actions of organophosphates. (2001).

Conflict of interest

Author MA was employed by BioSeAD, LLC.

The remaining author declared no potential conflicts of interest with respect to the research, authorship, and/or publication of this article.

Generative AI statement

The authors declare that no Generative AI was used in the creation of this manuscript.

Supplementary material

The Supplementary Material for this article can be found online at: <https://www.ebm-journal.org/articles/10.3389/ebm.2025.10598/full#supplementary-material>

- Reddy DS. Chapter 20 - advances in targeted therapy of organophosphate neurotoxicity and chemical warfare nerve agents. (2023).
- Kadar T, Cohen G, Sahar R, Alkalai D, Shapira S. Long-term study of brain lesions following soman, in comparison to DFP and metrazol poisoning. *Hum Exp Toxicol* (1992) **11**:517–23. doi:10.1177/096032719201100613
- Petrus JM. Neurology and neuropathology of Soman-induced brain injury: an overview. *J Exp Anal Behav* (1994) **61**:319–29. doi:10.1901/jeab.1994.61-319
- McDonough JH, Jr, Shih TM. Neuropharmacological mechanisms of nerve agent-induced seizure and neuropathology 1 The animals used in studies performed in, or sponsored by, this Institute were handled in accordance with the principles stated in the Guide for the Care and use of laboratory animals, proposed by the committee on Care and use of laboratory animals of the Institute of laboratory animal resources, national research council, DHHA, national Institute of health publication #85–23, 1985, and the animal Welfare Act of 1966, as amended. The opinions, or assertions contained herein are the private views of the authors, and are not to be construed as reflecting the views of the department of the Army or the department of defense. *Neurosci & Biobehavioral Rev* (1997) **21**:559–79. doi:10.1016/s0149-7634(96)00050-4
- Chen Y. Organophosphate-induced brain damage: mechanisms, neuropsychiatric and neurological consequences, and potential therapeutic strategies. *Neurotoxicology* (2012) **33**:391–400. doi:10.1016/j.neuro.2012.03.011
- de Araujo Furtado M, Lumley LA, Robison C, Tong LC, Lichtenstein S, Yourick DL. Spontaneous recurrent seizures after status epilepticus induced by soman in Sprague-Dawley rats. *Epilepsia* (2010) **51**:1503–10. doi:10.1111/j.1528-1167.2009.02478.x
- Jett DA, Sibrizzi CA, Blain RB, Hartman PA, Lein PJ, Taylor KW, et al. A national toxicology program systematic review of the evidence for long-term effects after acute exposure to sarin nerve agent. *Crit Rev Toxicol* (2020) **50**:474–90. doi:10.1080/10408444.2020.1787330
- Cannard K. The acute treatment of nerve agent exposure. *J Neurol Sci* (2006) **249**:86–94. doi:10.1016/j.jns.2006.06.008
- Newmark J. Therapy for acute nerve agent poisoning: an update. *Neurol Clin Pract* (2019) **9**:337–42. doi:10.1212/cpj.0000000000000641
- Marrero-Rosado B, de Araujo Furtado M, Schultz CR, Stone M, Kundrick E, Walker K, et al. Soman-induced status epilepticus, epileptogenesis, and neuropathology in carboxylesterase knockout mice treated with midazolam. *Epilepsia* (2018) **59**:2206–18. doi:10.1111/epi.14582
- Reddy SD, Reddy DS. Midazolam as an anticonvulsant antidote for organophosphate intoxication--A pharmacotherapeutic appraisal. *Epilepsia* (2015) **56**:813–21. doi:10.1111/epi.12989

24. Shih TM, Duniho SM, McDonough JH. Control of nerve agent-induced seizures is critical for neuroprotection and survival. *Toxicol Appl Pharmacol* (2003) **188**:69–80. doi:10.1016/s0041-008x(03)00019-x
25. Shih TM, McDonough JH. Efficacy of biperiden and atropine as anticonvulsant treatment for organophosphorus nerve agent intoxication. *Arch Toxicol* (2000) **74**:165–72. doi:10.1007/s002040050670
26. Petras JM. Soman neurotoxicity. *Toxicol Sci* (1981) **1**:242. doi:10.1093/toxsci/1.2.242
27. Shih TM, McDonough JH, Jr. Neurochemical mechanisms in soman-induced seizures. *J Appl Toxicol* (1997) **17**:255–64. doi:10.1002/(sici)1099-1263(199707)17:4<255::aid-jat441>3.3.co;2-4
28. Shih TM, McDonough JH, Jr. Organophosphorus nerve agents-induced seizures and efficacy of atropine sulfate as anticonvulsant treatment. *Pharmacol Biochem Behav* (1999) **64**:147–53. doi:10.1016/s0091-3057(99)00114-8
29. Talbot BG, Anderson DR, Harris LW, Yarbrough LW, Lermox WJ. A comparison of *in vivo* and *in vitro* rates of aging of soman-inhibited erythrocyte acetylcholinesterase in different animal species. *Drug Chem Toxicol* (1988) **11**:289–305. doi:10.3109/01480548809017884
30. Tsung-Ming S, Whalley CE, Valdes JJ. A comparison of cholinergic effects of HI-6 and pralidoxime-2-chloride (2-PAM) in soman poisoning. *Toxicol Lett* (1991) **55**:131–47. doi:10.1016/0378-4274(91)90128-s
31. McDonough JH, McMonagle JD, Shih TM. Time-dependent reduction in the anticonvulsant effectiveness of diazepam against soman-induced seizures in Guinea pigs. *Drug Chem Toxicol* (2010) **33**:279–83. doi:10.3109/01480540903483417
32. Shih T, McDonough JH, Jr, Koplovitz I. Anticonvulsants for soman-induced seizure activity. *J Biomed Sci* (1999) **6**:86–96. doi:10.1007/bf02256439
33. Moffett MC, Schultz MK, Schwartz JE, Stone MF, Lumley LA. Impaired auditory and contextual fear conditioning in soman-exposed rats. *Pharmacol Biochem Behav* (2011) **98**:120–9. doi:10.1016/j.pbb.2010.11.022
34. Rossetti F, de Araujo Furtado M, Pak T, Bailey K, Shields M, Chanda S, et al. Combined diazepam and HDAC inhibitor treatment protects against seizures and neuronal damage caused by soman exposure. *Neurotoxicology* (2012) **33**:500–11. doi:10.1016/j.neuro.2012.02.010
35. Lumley LA, Marrero-Rosado B, Rossetti F, Schultz CR, Stone MF, Niquet J, et al. Combination of antiseizure medications phenobarbital, ketamine, and midazolam reduces soman-induced epileptogenesis and brain pathology in rats. *Epilepsia Open* (2021) **6**:757–69. doi:10.1002/epi4.12552
36. Nguyen DA, Stone MF, Schultz CR, de Araujo Furtado M, Niquet J, Wasterlain CG, et al. Evaluation of midazolam-ketamine-allopregnanolone combination therapy against cholinergic-induced status epilepticus in rats. *The J Pharmacol Exp Ther* (2024) **388**:376–85. doi:10.1124/jpet.123.001784
37. Wright LK, Lee RB, Vincelli NM, Whalley CE, Lumley LA. Comparison of the lethal effects of chemical warfare nerve agents across multiple ages. *Toxicol Lett* (2016) **241**:167–74. doi:10.1016/j.toxlet.2015.11.023
38. Tremblay ME, Saint-Pierre M, Bourhis E, Lévesque D, Rouillard C, Cicchetti F. Neuroprotective effects of cystamine in aged parkinsonian mice. *Neurobiol Aging* (2006) **27**:862–70. doi:10.1016/j.neurobiolaging.2005.04.004
39. Wang S, Li X, Li M, Jiang L, Yuan H, Han W, et al. Cystamine attenuated behavioral deficiency via increasing the expression of BDNF and activating PI3K/Akt signaling in 2,5-hexanedione intoxicated rats. *Toxicol Res (Camb)* (2017) **6**:199–204. doi:10.1039/c6tx00409a
40. de Araujo Furtado M, Zheng A, Sedigh-Sarvestani M, Lumley L, Lichtenstein S, Yourick D. Analyzing large data sets acquired through telemetry from rats exposed to organophosphorus compounds: an EEG study. *J Neurosci Methods* (2009) **184**:176–83. doi:10.1016/j.jneumeth.2009.07.020
41. Lumley LA, Rossetti F, de Araujo Furtado M, Marrero-Rosado B, Schultz CR, Schultz MK, et al. Dataset of EEG power integral, spontaneous recurrent seizure and behavioral responses following combination drug therapy in soman-exposed rats. *Data in Brief* (2019) **27**:104629. doi:10.1016/j.dib.2019.104629
42. Niquet J, Baldwin R, Norman K, Suchomelova L, Lumley L, Wasterlain CG. Midazolam-ketamine dual therapy stops cholinergic status epilepticus and reduces Morris water maze deficits. *Epilepsia* (2016) **57**:1406–15. doi:10.1111/epi.13480
43. Racine RJ, Burnham WM, Gartner JG. First trial motor seizures triggered by amygdaloid stimulation in the rat. *Electroencephalogr Clin Neurophysiol* (1973) **35**:487–94. doi:10.1016/0013-4694(73)90024-2
44. Lumley LA, Nguyen DA, de Araujo Furtado M, Niquet J, Linz EO, Schultz CR, et al. Efficacy of lacosamide and rufinamide as adjuncts to midazolam-ketamine treatment against cholinergic-induced status epilepticus in rats. *The J Pharmacol Exp Ther* (2024) **388**:347–57. doi:10.1124/jpet.123.001789
45. Reddy DS. Mechanism-based novel antidotes for organophosphate neurotoxicity. *Curr Opin Toxicol* (2019) **14**:35–45. doi:10.1016/j.cotox.2019.08.001
46. de Araujo Furtado M, Rossetti F, Chanda S, Yourick D. Exposure to nerve agents: from status epilepticus to neuroinflammation, brain damage, neurogenesis and epilepsy. *Neurotoxicology* (2012) **33**:1476–90. doi:10.1016/j.neuro.2012.09.001
47. Carpentier P, Foquin A, Kamenka JM, Rondouin G, Lerner-Natoli M, de Groot DM, et al. Effects of thienylphenylcyclidine (TCP) on seizure activity and brain damage produced by soman in Guinea-pigs: ECoG correlates of neurotoxicity. *Neurotoxicology* (2001) **22**:13–28. doi:10.1016/s0161-813x(00)00016-4
48. McDonough JH, Jr, Clark TR, Slone TW, Jr, Zoeffel D, Brown K, Kim S, et al. Neural lesions in the rat and their relationship to EEG delta activity following seizures induced by the nerve agent soman. *Neurotoxicology* (1998) **19**:381–91.
49. Aplan JP, Figueiredo TH, Qashu F, Aroniadou-Anderjaska V, Souza AP, Braga MF. Higher susceptibility of the ventral versus the dorsal hippocampus and the posterodorsal versus anterodorsal amygdala to soman-induced neuropathology. *Neurotoxicology* (2010) **31**:485–92. doi:10.1016/j.neuro.2010.05.014
50. McDonough JH, Jr, Jaax NK, Crowley RA, Mays MZ, Modrow HE. Atropine and/or diazepam therapy protects against soman-induced neural and cardiac pathology. *Toxicol Sci* (1989) **13**:256–76. doi:10.1093/toxsci/13.2.256
51. Simpson DSA, Oliver PL. ROS generation in microglia: understanding oxidative stress and inflammation in neurodegenerative disease. *Antioxidants (Basel)* (2020) **9**:743. doi:10.3390/antiox9080743
52. Streit WJ, Mrak RE, Griffin WS. Microglia and neuroinflammation: a pathological perspective. *J Neuroinflammation* (2004) **1**:14. doi:10.1186/1742-2094-1-14
53. Gao C, Jiang J, Tan Y, Chen S. Microglia in neurodegenerative diseases: mechanism and potential therapeutic targets. *Signal Transduction Targeted Ther* (2023) **8**:359. doi:10.1038/s41392-023-01588-0
54. Isik S, Yeman Kiyak B, Akbayir R, Seyhali R, Arpacı T. Microglia mediated neuroinflammation in Parkinson's disease. *Cells* (2023) **12**:1012. doi:10.3390/cells12071012
55. Cai Y, Liu J, Wang B, Sun M, Yang H. Microglia in the neuroinflammatory pathogenesis of alzheimer's disease and related therapeutic targets. *Front Immunol* (2022) **13**:856376. doi:10.3389/fimmu.2022.856376
56. Fox JH, Barber DS, Singh B, Zucker B, Swindell MK, Norflus F, et al. Cystamine increases L-cysteine levels in Huntington's disease transgenic mouse brain and in a PC12 model of polyglutamine aggregation. *J Neurochem* (2004) **91**:413–22. doi:10.1111/j.1471-4159.2004.02726.x
57. Pinto JT, Van Raamsdonk JM, Leavitt BR, Hayden MR, Jeitner TM, Thaler HT, et al. Treatment of YAC128 mice and their wild-type littermates with cystamine does not lead to its accumulation in plasma or brain: implications for the treatment of Huntington disease. *J Neurochem* (2005) **94**:1087–101. doi:10.1111/j.1471-4159.2005.03255.x
58. Jokay I, Kelemenics K, Gyuris A, Minarovits J. S-methylthio-cysteine and cystamine are potent stimulators of thiol production and glutathione synthesis. *Life Sci* (1997) **62**:PL27–33. doi:10.1016/s0024-3205(97)01066-7
59. Lesort M, Lee M, Tucholski J, Johnson GV. Cystamine inhibits caspase activity. *J Biol Chem* (2003) **278**:3825–30. doi:10.1074/jbc.m205812200
60. Jeitner TM, Pinto JT, Cooper AJL. Cystamine and cysteamine as inhibitors of transglutaminase activity *in vivo*. *Biosci Rep* (2018) **38**. doi:10.1042/bsr20180691
61. Pizarro JM, Chang WE, Bah MJ, Wright LK, Saviolakis GA, Alagappan A, et al. Repeated exposure to sublethal doses of the organophosphorus compound VX activates BDNF expression in mouse brain. *Toxicol Sci* (2012) **126**:497–505. doi:10.1093/toxsci/kfr353
62. Beal MF, Brouillet E, Jenkins BG, Ferrante RJ, Kowall NW, Miller JM, et al. Neurochemical and histologic characterization of striatal excitotoxic lesions produced by the mitochondrial toxin 3-nitropropionic acid. *J Neurosci* (1993) **13**:4181–92. doi:10.1523/jneurosci.13-10-04181.1993
63. Bossi SR, Simpson JR, Isacson O. Age dependence of striatal neuronal death caused by mitochondrial dysfunction. *Neuroreport* (1993) **4**:73–6. doi:10.1097/00001756-199301000-00019
64. Pandey M, Borah A, Varghese M, Barman PK, Mohanakumar KP, Usha R. Striatal dopamine level contributes to hydroxyl radical generation and subsequent neurodegeneration in the striatum in 3-nitropropionic acid-induced Huntington's disease in rats. *Neurochem Int* (2009) **55**:431–7. doi:10.1016/j.neuint.2009.04.013
65. DePaula-Silva AB. The contribution of microglia and brain-infiltrating macrophages to the pathogenesis of neuroinflammatory and neurodegenerative diseases during TMEM infection of the central nervous system. *Viruses* (2024) **16**:119. doi:10.3390/v16010119
66. Nguyen DA, Niquet J, Marrero-Rosado B, Schultz CR, Stone MF, de Araujo Furtado M, et al. Age differences in organophosphorus nerve agent-induced seizure, blood brain barrier integrity, and neurodegeneration in midazolam-treated rats. *Exp Neurol* (2025) **385**:115122. doi:10.1016/j.expneurol.2024.115122
67. Chen T, Dai Y, Hu C, Lin Z, Wang S, Yang J, et al. Cellular and molecular mechanisms of the blood-brain barrier dysfunction in neurodegenerative diseases. *Fluids Barriers CNS* (2024) **21**:60. doi:10.1186/s12987-024-00557-1



OPEN ACCESS

*CORRESPONDENCE

Yu-Li Lo,
✉ yulilo@nycu.edu.tw
Anya Maan-Yuh Lin,
✉ myalin@vghtpe.gov.tw,
✉ myalin@nycu.edu.tw

RECEIVED 27 February 2025

ACCEPTED 24 April 2025

PUBLISHED 15 May 2025

CITATION

Huang H-J, Tseng Y-J, Lee I-J, Lo Y-L
and Lin AM-Y (2025) Involvement of
EGFR-AKT signaling in hemin-
induced neurotoxicity.
Exp. Biol. Med. 250:10554.
doi: 10.3389/ebm.2025.10554

COPYRIGHT

© 2025 Huang, Tseng, Lee, Lo and Lin.
This is an open-access article
distributed under the terms of the
[Creative Commons Attribution License](#)
(CC BY). The use, distribution or
reproduction in other forums is
permitted, provided the original
author(s) and the copyright owner(s) are
credited and that the original
publication in this journal is cited, in
accordance with accepted academic
practice. No use, distribution or
reproduction is permitted which does
not comply with these terms.

Involvement of EGFR-AKT signaling in hemin-induced neurotoxicity

Hui-Ju Huang¹, Yang-Jie Tseng², I-Jung Lee³, Yu-Li Lo^{4*} and
Anya Maan-Yuh Lin^{1,2,5*}

¹Department of Medical Research, Taipei Veterans General Hospital, Taipei, Taiwan, ²Ph.D. Program in
Regulatory Science and Policy, National Yang-Ming Chiao-Tung University, Taipei, Taiwan,

³Pharmaceutical Botany Research Laboratory, Yokohama University of Pharmacy, Yokohama, Japan,
⁴Institute of Pharmacology, National Yang-Ming Chiao-Tung University, Taipei, Taiwan, ⁵Department
of Pharmacy, National Yang-Ming Chiao-Tung University, Taipei, Taiwan

Abstract

Intracerebral hemorrhage (ICH), as bleeding from ruptured vessels within the brain, is the second leading neuropathological problem following ischemic stroke. In the present study, the involvement of epithelial growth factor receptor (EGFR)-tyrosine kinase (TK) signaling underlying ICH-related neurodegeneration was investigated using afatinib, a clinically available EGFR-tyrosine kinase inhibitor (EGFR-TKI). We employed hemin (a breakdown product of hemoglobin) to mimic the pathophysiology of ICH in primary cultured cortical neurons. Using a lactate dehydrogenase (LDH) assay, incubation of hemin concentration- and time-dependently induced neuronal death. Simultaneous incubation of afatinib (10 nM) significantly inhibited hemin (30 μ M)-induced neuronal death. Immunofluorescent data demonstrated that co-treatment of afatinib for 1 h attenuated hemin (30 μ M)-induced elevation in phosphorylated-EGFR (p-EGFR) immunoreactivity and neurite impairment. Western blot assay demonstrated that co-incubation of afatinib for 16 h diminished hemin-induced elevation in p-EGFR and p-AKT, tumor necrosis factor- α and cyclooxygenase 2 (two proinflammatory biomarkers) as well as heme oxygenase-1 (HO-1, an enzyme catalyzing heme/hemin), glutathione hydroperoxidase 4 and receptor-interacting protein 3 (two biomarkers of ferroptosis and necroptosis). In addition, co-treatment of afatinib for 24 h inhibited hemin-induced NO production in the culture medium. In conclusion, our study shows that afatinib via blocking EGFR-AKT signaling inhibits hemin-induced EGFR-AKT activation, neuroinflammation, HO-1 expression and programmed cell death, suggesting that EGFR-AKT signaling is involved in hemin-induced neurotoxicity and may be a druggable target for ICH.

KEYWORDS

hemin, EGFR-AKT signaling, afatinib, primary cultured cortical neurons, ferroptosis

Impact statement

To find potential therapies for the secondary injury in ICH, the involvement of EGFR-TK signaling in ICH was investigated *in vitro*. We found that hemin induced neuronal death as well as EGFR-AKT activation, neuroinflammation, HO-1 expression, ferroptosis and necroptosis in primary cultured cortical neurons. Furthermore, afatinib, a clinically available EGFR-TK inhibitor, is capable of blocking hemin-induced EGFR-AKT activation and neurotoxicity. Our data suggest that EGFR-AKT signaling may be a druggable target for ICH.

Introduction

Intracerebral hemorrhage (ICH) is due to the rupture of blood vessels in the parenchyma. ICH reportedly induces primary and secondary brain injuries [1, 2]. The primary injury is initiated acutely by local pressure and mechanical damage due to hematoma in the brain. The secondary injury results from released blood which is degraded to blood derived products, including heme/hemin and iron. These blood-derived products reportedly induce oxidative injury, neuroinflammation and protein aggregation that lead to cell death [1, 3–5]. Current therapies for the primary injury include surgical removal of blood clots and drug treatment to reduce the elevated intracranial pressure [5]. Neuroprotective strategies toward the secondary injury are urged.

Cellular growth factors and its kinase pathways, such as epidermal growth factor receptor (EGFR) [6], have been used as cancer therapies for decades [7, 8] and are now proposed for central nervous system (CNS) neurodegenerative diseases [9, 10]. Physiologically, EGFR is involved in the developing nervous system by regulating growth, differentiation and repair [9]. In a healthy adult brain, EGFR is expressed in specific regions, such as the subventricular zone [11]. However, a clinical report showed intensive EGFR expression in the neurites in affected brain tissues of patients with Alzheimer disease (AD), suggesting an EGFR reactivation in response to insults [12]. In support of this notion, an Alzheimer's pre-clinical study demonstrated that EGFR inhibitors ameliorated A β 42-induced neurotoxicity [13]. Furthermore, both AG1478 (an EGFR antagonist) and C225 (anti-EGFR monoclonal antibody) reportedly reduced the expression of phosphorylated EGFR (p-EGFR), enhanced axonal outgrowth and promoted functional recovery in rats subjected to spinal cord injury (SCI) [14]. Moreover, AZD 3759, a blood brain barrier permeable EGFR-tyrosine kinase inhibitor (EGFR-TKI), was found to reduce the phosphorylated α -synuclein levels, a pathological biomarker of Parkinson's Disease [10]. Our previous study showed that afatinib, a clinically available EGFR-TKI for lung cancer therapy, attenuated oxygen-glucose deprivation (OGD)-induced neuroinflammation in primary cultured astrocytes [15].

Accordingly, a pathological role of EGFR signaling is suggested in CNS neurodegenerative diseases.

Many studies have focused on the involvement of EGFR in ischemic stroke [16–18]. However, only one pre-clinical study demonstrated that AG1478 inhibited neuronal apoptosis in mice subjected to subarachnoid hemorrhage [19]. In the present study, the involvement of EGFR in the pathophysiology of ICH was investigated using hemin to mimic ICH-related neurotoxicity [20, 21]. Moreover, afatinib, via binding to the EGFR-ATP binding activation site [22], was repurposed to block hemin-induced EGFR activation and hemin-induced neurotoxicity in neurons to delineate the EGFR-AKT signaling in the pathophysiology of ICH.

Materials and methods

Chemicals

The chemicals used were hemin (Sigma, St. Louis, MO, United States) and afatinib (AdooQ Bioscience, Irvine, CA, United States). Hemin was dissolved in ammonia water and pH value was corrected to pH 7.4. Afatinib was dissolved in dimethyl sulfoxide (DMSO, Sigma) and diluted with DMEM or Neurobasal (NB, Thermo Fisher Scientific, Waltham, MA, United States) medium.

Animals

Twenty-three pregnant female Sprague-Dawley (SD) rats were supplied by BioLASCO Taiwan Co., Ltd. (Yilan, Taiwan). All animals (one rat/individually ventilated cage) were housed in an air-conditioned room ($22 \pm 2^\circ\text{C}$) on a 12 hr-light/dark cycle (07:00–19:00h light) and had free access to food and water. Pregnant female Sprague-Dawley (SD) rats of 17-day gestation were sacrificed by an overdose of Zoletil® (Virbac, Taiwan) to minimize pain or discomfort. Embryonic day 17 fetal rat brains obtained from pregnant female SD rats were used to prepare primary cultured cortical neurons. The use of animals and all experiments conducted were under approved protocols from the Institutional Animal Care and Use Committee (IACUC) of Taipei Veterans General Hospital, Taipei, Taiwan. The approval number is IACUC2022-235. All experiments were performed in accordance with relevant guidelines and regulations.

Primary culture of cortical neurons

Cerebral cortices of fetal rats were isolated and dissociated mechanically. The dissociated cells were suspended in the Basal Medium Eagle (BME, Thermo Fisher Scientific) medium

containing 20% fetal bovine serum, and were seeded onto 35-mm culture dishes (IWAKI, Tokyo, Japan) with a density of 5×10^6 cells per dish. Afterwards, cells were maintained with serum-free Neurobasal medium supplemented with B27 (Thermo Fisher Scientific) in the incubator with 5% CO₂ at 37°C. Four experimental treatments included vehicle (as control), hemin (30 µM), hemin (30 µM) plus afatinib (10 nM) and afatinib (10 nM).

Cytotoxicity assay

In brief, primary cultured cortical neurons were seeded on a 24-well plate. Concentration-dependent effects (10–60 µM) of hemin were performed for 16 and 24 h. The effect of afatinib was investigated 16 h after simultaneous addition of afatinib (10 nM) and hemin (30 µM). Cytotoxicity was determined by a Lactate Dehydrogenase (LDH) assay. The LDH released in the culture medium was assessed by adding β-nicotinamide adenine dinucleotide and sodium pyruvate (Sigma). LDH activity was determined by measuring the absorbance at 340 nm for 6 min using an enzyme-linked immunosorbent assay (ELISA) reader (TECAN Sunrise, Männedorf, Switzerland). The LDH activity of cells treated with 0.1% Triton X-100 was used as control set to 100%.

Western blots analysis

At the end of 16-h treatments, the cells were collected, washed with phosphate buffered saline (PBS), and lysed in a radioimmunoprecipitation assay (RIPA, Cell Signaling Tech., Beverly, MA, United States) lysis buffer containing 20 mM Tris HCl, 150 mM NaCl, 1% (v/v) NP-40, 1% (w/v) sodium deoxycholate, 1 mM ethylenediaminetetraacetates (EDTA), 0.1% (w/v) sodium dodecyl sulfate polyacrylamide (SDS) and 0.01% (w/v) sodium azide (pH 7.5) for 20 min on ice. Lysates were then centrifuged at 13,800g for 10 min, and the protein concentrations of supernatants were determined by Pierce BCA Protein Assay Kit (Thermo Fisher Scientific). Protein samples (30 µg) were run on 12%–13.5% SDS-polyacrylamide gel electrophoresis and then transferred onto a polyvinylidene difluoride (PVDF, Bio-Rad, Hercules, CA, United States) at 100 V for 120 min. Blots were probed with primary antibodies including antibodies against p-EGFR/total-EGFR, p-AKT/total-AKT (Cell Signaling Tech.), Tumor necrosis factor (TNF)-α, Cyclooxygenase 2 (COX2), Heme oxygenase-1 (HO-1) (StressGen, Victoria, CA, United States), Glutathione hydroperoxidase 4 (GPX4) and Receptor-interacting serine/threonine-protein kinase 3 (RIP3) (Cell Signaling Tech.) overnight at 4°C. After incubation of primary antibodies, the membrane was washed and incubated with a secondary antibody for 1 h at room

temperature. The secondary antibodies were horseradish peroxidase-conjugated secondary IgG (Chemicon, Temecula, CA, United States). The immunoreaction was visualized using Amersham Enhanced Chemiluminescence (Amersham Pharmacia Biotech, Piscataway, NJ, United States). After this measurement, the bound primary and secondary antibodies were stripped by incubating the membrane in stripping buffer (100 mM 2-mercaptoethanol, 2% SDS) at 50°C for 5 min. The membrane was reprobed with a primary antibody against β-actin (Millipore, Billerica, MA, United States).

Immunofluorescent staining

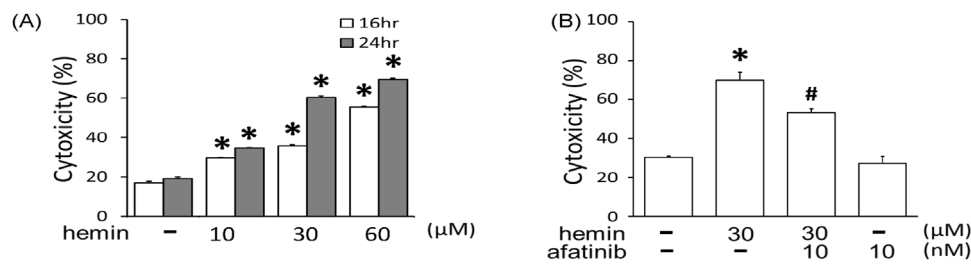
At the end of 1-hr treatments, the cells were fixed with 4% paraformaldehyde (Merck, Boston, MA, United States). Cells were then washed with 0.1 M PBS, incubated with 0.3% Triton X-100 (Sigma) and 1% goat serum (GS; Jackson ImmunoResearch, West Grove, PA, United States), and blocked with 3% GS for 60 min. Next, cells were processed for immunostaining using mouse monoclonal antibody specific for rat p-EGFR and microtubule-associated protein 2 (MAP-2, Millipore) in 1% GS-PBS at 4°C for 24 h. The cells were then incubated in fluorescein conjugated-IgG (FITC) (Jackson ImmunoResearch) and Texas Red dye-conjugated IgG fraction monoclonal mouse anti-biotin (Jackson ImmunoResearch) for 1 h at room temperature, mounted in glycerol (Merck). Controls consisted of omission of primary antibodies. The sections were visualized by a fluorescence confocal microscope (Olympus FluoView, Norfolk, VA, United States).

Nitric oxide (NO) production

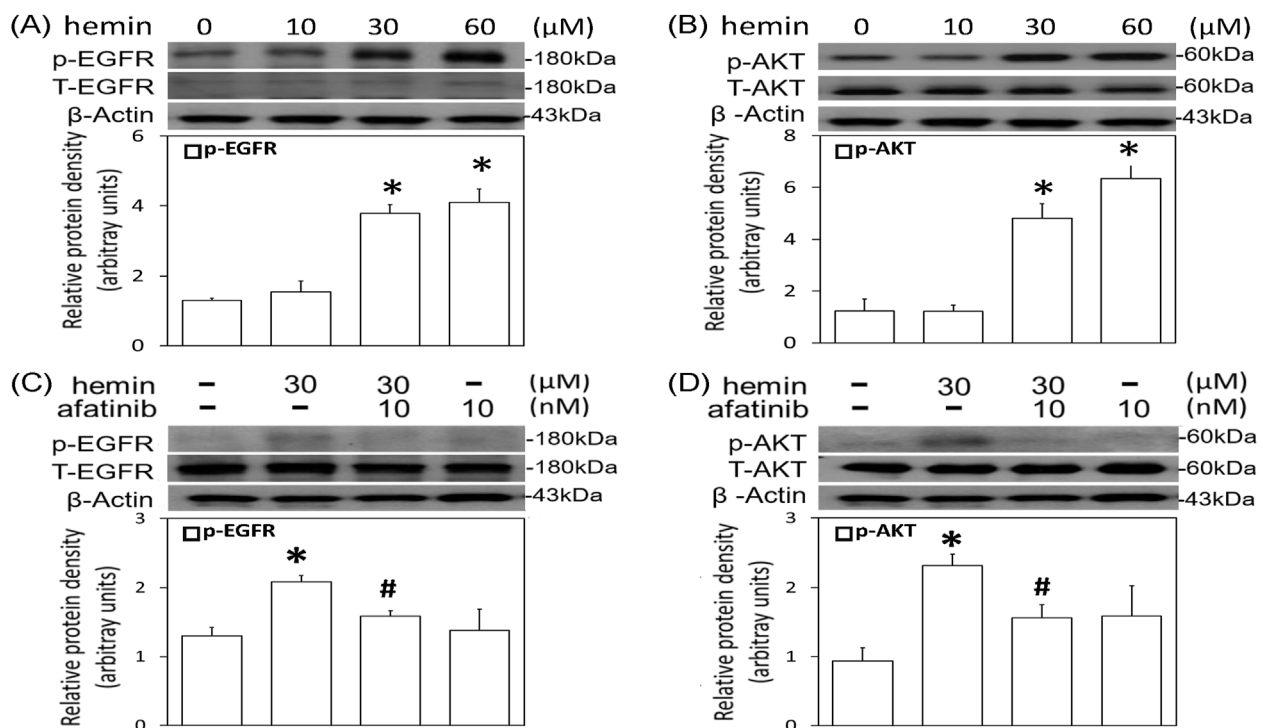
At the end of 24-h treatments, the culture medium was collected to measure NO production. The culture medium was mixed with an equal volume of the Griess reagent (1% sulfanilamide, 0.1% N-(1-Naphthyl)ethylenediamine in 2.5% H₃PO₄) and incubated for 15 min at room temperature in the dark. Nitrite concentration was determined by measuring the absorbance at 550 nm using an ELISA plate reader (TECAN Sunrise, Männedorf, Schweiz).

Statistics

All data are expressed as the mean ± standard error of the mean (S.E.M.). The results were analyzed by one-way analysis of variance (one-way ANOVA) followed by the least significance difference (LSD) test as post-hoc method. The significance level was set at $p < 0.05$.

**FIGURE 1**

Effects of afatinib on hemin-induced cytotoxicity. **(A)** Primary cultured cortical neurons were treated with hemin (10–60 μM) for 16 h and 24 h. **(B)** Primary cultured cortical neurons were treated with hemin (30 μM) plus afatinib (10 nM) simultaneously for 16 h. Cell death was measured by LDH assay. Values are the mean ± S.E.M. (n = 3/each group). *p < 0.05 statistically significant in the hemin groups compared with the control groups; #P < 0.05 in hemin plus afatinib compared with hemin alone by one-way ANOVA followed by the LSD test as post-hoc method.

**FIGURE 2**

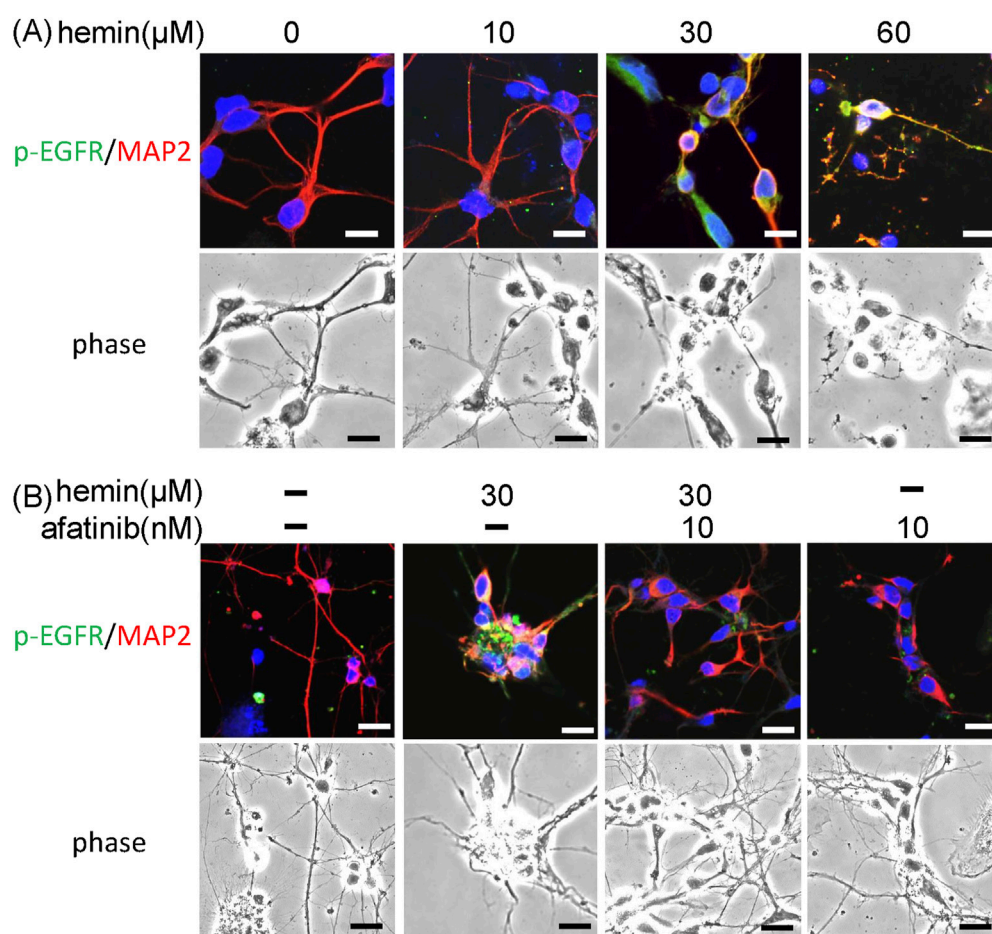
Effects of afatinib on hemin-induced EGFR-AKT activation. **(A,B)** Primary cultured cortical neurons were treated with hemin (10–60 μM) for 1 h **(C,D)** Primary cultured cortical neurons were treated with hemin (30 μM) plus afatinib (10 nM) for 1h. Western blot assay was employed to measure phosphorylated EGFR (p-EGFR) **(A,C)**, and phosphorylated AKT (p-AKT) **(B,D)**. Each lane contained 30 μg protein for all experiments. Graphs show statistical results from relative optical density of bands on the blots. Values are the mean ± S.E.M. (n = 3/each group). *p < 0.05 statistically significant in the hemin groups compared with the control groups; #P < 0.05 in hemin plus afatinib compared with hemin alone by one-way ANOVA followed by the LSD test as post-hoc method.

Results

Afatinib attenuated hemin-induced neuronal death

To mimic the neurodegeneration in ICH, a hemin-induced neurotoxicity model was established in primary cultured

cortical neurons. The LDH assay showed that incubation of hemin (10–60 μM) for 16 and 24 h increased neuronal death in time- and concentration-dependent manners (Figure 1A). The IC₅₀ of hemin in primary cortical neurons was about 30 μM after 24-hr incubation. Co-incubation with afatinib (10 nM) for 16 h significantly attenuated hemin-induced cell death in primary cultured cortical neurons (Figure 1B), indicating

**FIGURE 3**

Effects of afatinib on hemin-induced impairment of neurite outgrowth. **(A)** Primary cultured cortical neurons were treated with hemin (10–60 μM) for 1 h. Representative immunofluorescent data show concentration-dependent damages of hemin on neurite outgrowth. **(B)** Primary cultured cortical neurons were treated with hemin (30 μM) plus afatinib (10 nM) for 1 h. The neurites were immunostained with phosphorylated EGFR (p-EGFR) and MAP-2. Calibration: 10 μm . The results were duplicated.

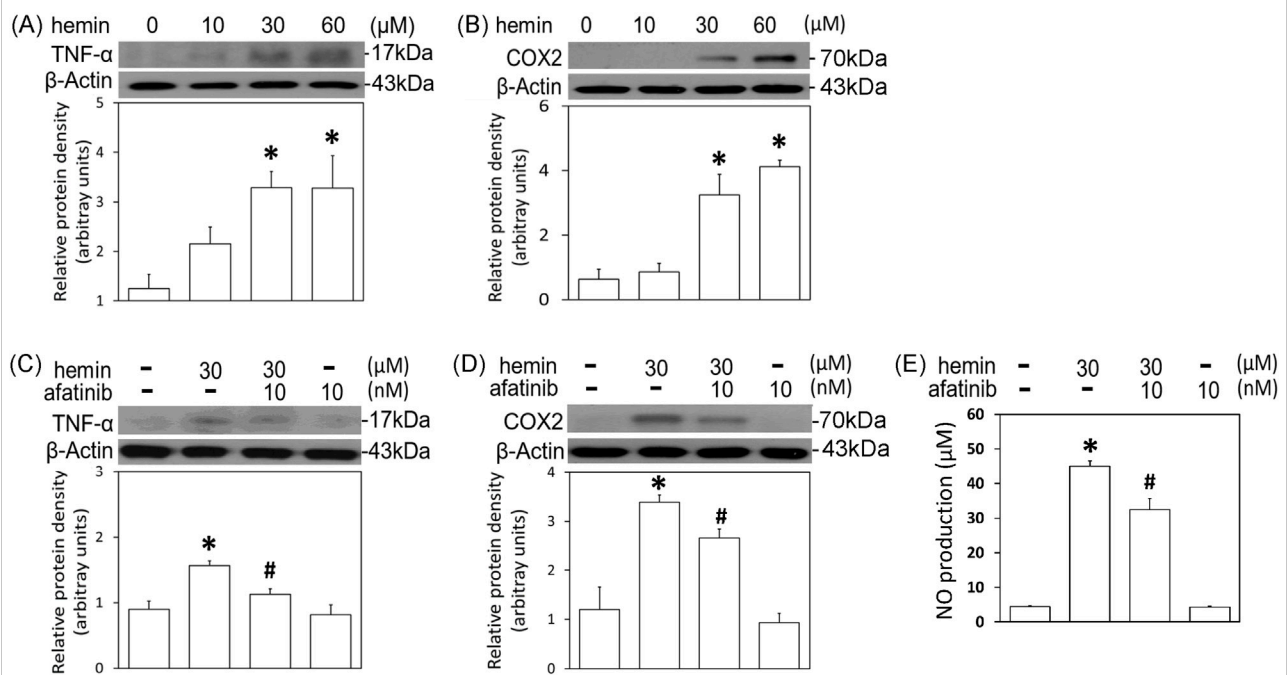
that afatinib is capable of inhibiting hemin-induced neuronal death.

Afatinib attenuated hemin-induced EGFR-AKT activation and morphological changes

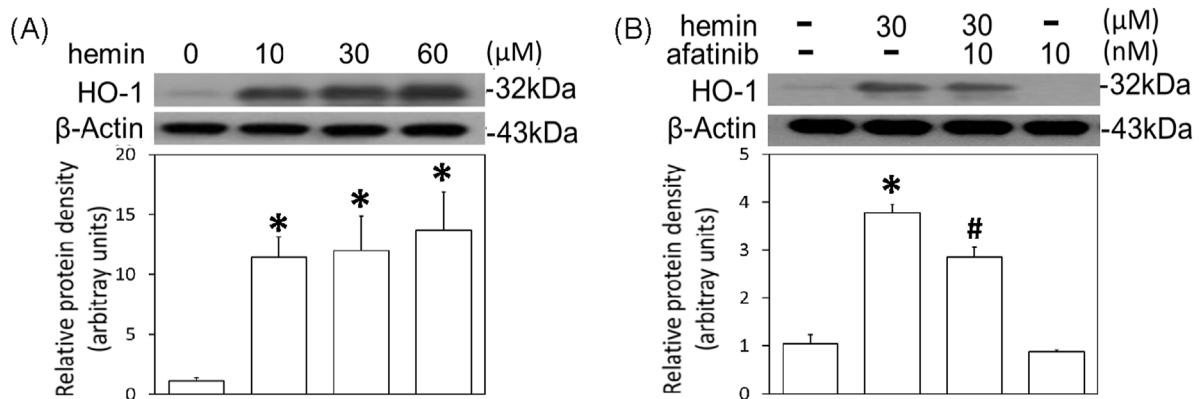
The involvement of EGFR signaling in the hemin-induced neurotoxicity was investigated by measuring p-EGFR levels in primary cultured cortical neurons. We found that 1-h incubation of hemin (10–60 μM) concentration-dependently increased EGFR phosphorylation (Figure 2A). EGFR phosphorylation was evident when cells were treated with 30 μM hemin and maintained elevated with 60 μM hemin (Figure 2A). Similarly, incubation of hemin for 1 h significantly elevated p-AKT levels in a concentration-dependent manner (Figure 2B). Co-incubation

of afatinib (10 nM) significantly attenuated hemin-induced EGFR phosphorylation (Figure 2C) and AKT phosphorylation (Figure 2D), indicating hemin indeed activated EGFR-AKT signaling in primary cultured cortical neurons.

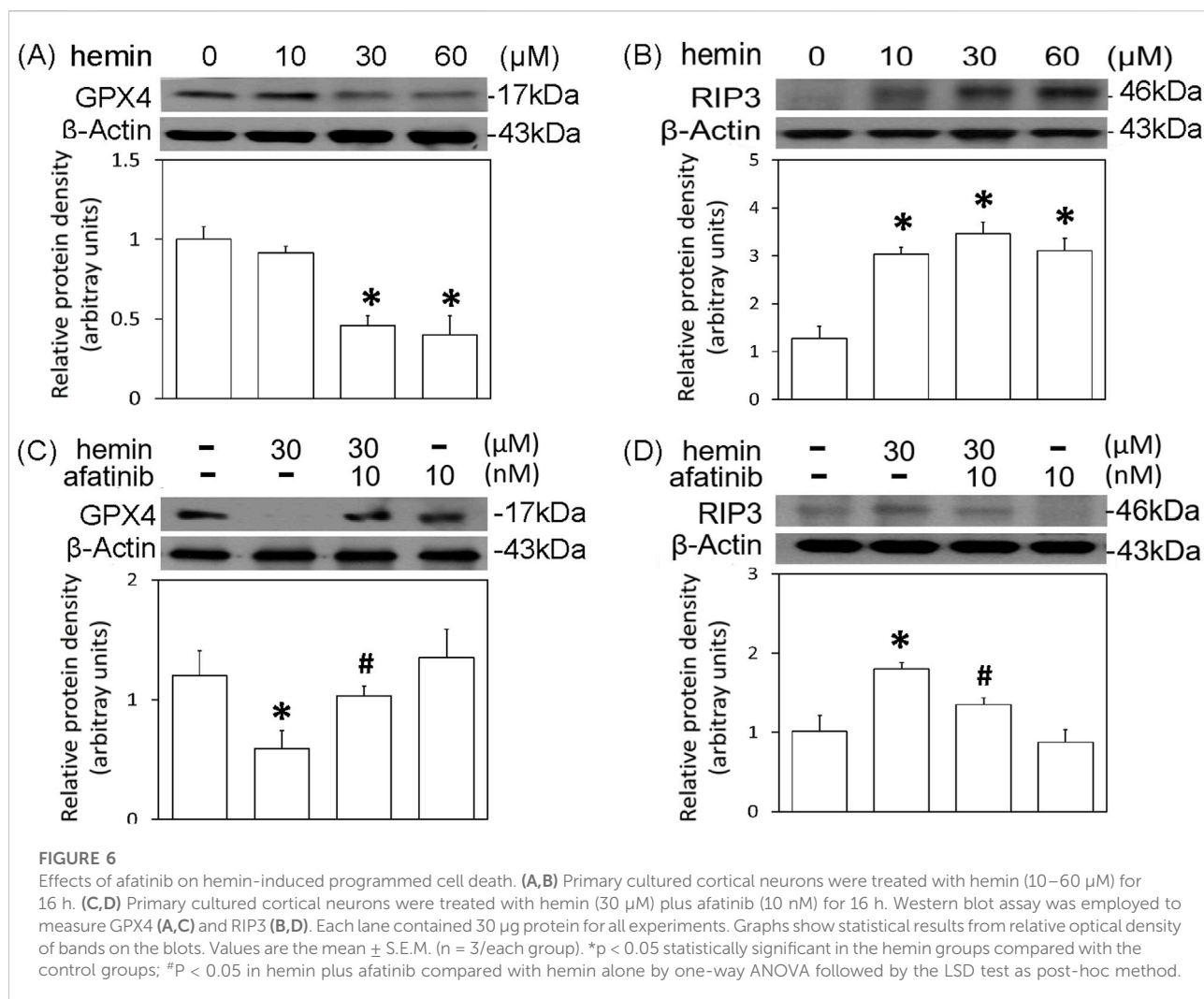
Furthermore, we investigated the effect of afatinib on hemin-induced morphological changes in primary cultured cortical neurons. Compared with the vehicle-treated cells, immunofluorescent staining data showed that hemin concentration-dependently (10–60 μM) increased p-EGFR immunoreactivity and damaged neurite outgrowth (Figure 3A). Incubation of hemin (10 μM) for 8 h did not cause significant changes in the neurite outgrowth. However, higher concentrations of hemin (30–60 μM) induced strong p-EGFR immunoreactivity. At the same time, hemin caused focal bead-like swellings, neuritic beading and discontinuities of neurites in primary cultured cortical neurons (Figure 3A). Co-incubation with afatinib (10 nM) attenuated hemin-induced

**FIGURE 4**

Effects of afatinib on hemin-induced neuroinflammation. **(A, B)** Primary cultured cortical neurons were treated with hemin (10–60 μM) for 16 h. **(C, D)** Primary cultured cortical neurons were treated with hemin (30 μM) plus afatinib (10 nM) for 16 h. Western blot assay was employed to measure TNF- α **(A, C)** and COX2 **(B, D)**. Each lane contained 30 μg protein for all experiments. Graphs show statistical results from relative optical density of bands on the blots. **(E)** Primary cultured cortical neurons were treated with hemin (30 μM) plus afatinib (10 nM) for 24 h. The levels of NO in culture medium were measured using Griess reaction. Values are the mean \pm S.E.M. ($n = 3$ /each group). * $p < 0.05$ statistically significant in the hemin groups compared with the control groups; # $P < 0.05$ in hemin plus afatinib compared with hemin alone by one-way ANOVA followed by the LSD test as post-hoc method.

**FIGURE 5**

Effects of afatinib on hemin-induced HO-1 expression. **(A)** Primary cultured cortical neurons were treated with hemin (10–60 μM) for 16 h. **(B)** Primary cultured cortical neurons were treated with hemin (30 μM) plus afatinib (10 nM) for 16 h. Western blot assay was employed to measure HO-1. Each lane contained 30 μg protein for all experiments. Graphs show statistical results from relative optical density of bands on the blots. Values are the mean \pm S.E.M. ($n = 3$ /each group). * $p < 0.05$ statistically significant in the hemin groups compared with the control groups; # $P < 0.05$ in hemin plus afatinib compared with hemin alone by one-way ANOVA followed by the LSD test as post-hoc method.



elevation in p-EGFR immunoreactivity and impairment in neurite outgrowth (Figure 3B), suggesting that the EGFR signaling pathway is responsible for the hemin-induced damage to neurite outgrowth in primary cultured cortical neurons.

Afatinib attenuated hemin-induced neuroinflammation, HO-1 expression and programmed cell death

To further confirm the involvement of EGFR-AKT signaling in ICH, afatinib was employed to block hemin-induced activation of EGFR-TK signaling and related neurotoxicity. First, we established hemin-induced neuroinflammation in primary cultured cortical neurons. Western blot assay showed that a 16-hr incubation of hemin concentration-dependently (10–60 μ M) increased TNF- α (Figure 4A) and COX2 protein levels (Figure 4B) in primary cultured cortical neurons. Co-incubation with afatinib (10 nM)

prevented hemin (30 μ M)-induced elevations in TNF- α (Figure 4C) and COX2 (Figure 4D) as well as NO production in the culture medium of treated neurons (Figure 4E), suggesting that afatinib is capable of reducing hemin-induced neuroinflammation. At the same time, we investigated the effect of afatinib on HO-1 expression (an enzyme catalyzing hemin). Western blot assay showed that a 16-h incubation of hemin (10–60 μ M) increased HO-1 levels (Figure 5A). Co-incubation with afatinib (10 nM) prevented hemin (30 μ M)-induced elevation in HO-1 (Figure 5B), suggesting that afatinib is capable of reducing hemin-induced HO-1 expression.

The cell death mechanisms underlying hemin-induced neurotoxicity were investigated by measuring GPX4 (a biomarker of ferroptosis) and receptor-interacting protein 3 (RIP3, a biomarker of necroptosis). Western blot assay demonstrated that hemin concentration-dependently (10–60 μ M) reduced GPX4 (Figure 6A) and increased RIP3 (Figure 6B). Co-incubation with afatinib (10 nM) inhibited the hemin (30 μ M)-induced reduction in GPX4 (Figure 6C) and

elevation in RIP3 (Figure 6D). These data indicate that afatinib is capable of reducing hemin-induced ferroptosis and necroptosis.

Discussion

In the present study, the EGFR-TK signaling was involved in the pathophysiology of ICH in several areas. First, hemin-induced neurotoxicity was demonstrated by neuronal death, neurite outgrowth impairment, neuroinflammation, HO-1 expression, ferroptosis and necroptosis. Furthermore, hemin consistently activated EGFR-AKT signaling in primary cultured cortical neurons. Finally, afatinib significantly attenuated hemin-induced EGFR-AKT activation and neurotoxicity. Taken together, these data suggest that the EGFR-AKT signaling may be a druggable target when developing therapies for ICH.

A pathological role of EGFR signaling has been demonstrated in CNS neurodegenerative diseases, including SCI, AD, brain ischemia and subarachnoid hemorrhage [10, 13–15, 19] but not ICH. In the present study, we are the first to show the involvement of EGFR in the pathophysiology of ICH. To mimic ICH-related neurotoxicity, several *in vitro* studies used PC12 cells and primary cortical neurons subjected to hemin ranging from 30 μ M to 50 mM [21, 23–25]. Furthermore, an animal study reported high micromolar (\approx 390 μ M) hemin in the hematomas [26]. In the present study, hemin (10–60 μ M) was found to induce concentration-dependent increases in EGFR-AKT phosphorylation and neurotoxicity in primary cultured cortical neurons. Consistent with Zhou's study [25], we chose 30 μ M hemin to further delineate the involvement of EGFR-AKT signaling in ICH by studying the effect of afatinib, a second-generation EGFR-TKI for lung cancers [7], in primary cultured cortical neurons. Due to its covalent bonding to the EGFR-AKT activation site [27], nanomolar range (1 and 10 nM) of afatinib was found to effectively attenuate EGFR activation in cancer cells [7, 27]. Similar to Chen's studies [15], we used 10 nM afatinib in the present study to successfully block hemin-induced EGFR-AKT signaling and neurotoxicity in primary cultured cortical neurons.

A “vicious cycle” containing oxidative stress, protein aggregation and cell death has been proposed for the pathophysiology of CNS neurodegenerative diseases; neuroinflammation is at the center of this “vicious cycle” [28]. Both clinical [29] and non-clinical studies [1, 2, 30] showed significant neuroinflammation in the ICH-affected brain tissues, including increases in inflammatory enzymes and proinflammatory cytokines. Our study supports this notion by demonstrating hemin-induced elevations in TNF- α and COX2 expression, as well as NO production. Similar to the afatinib-induced anti-inflammation in the OGD model [15], the present study using an ICH model demonstrated that afatinib attenuated hemin-induced neuroinflammation, suggesting that afatinib is anti-inflammatory in ICH.

Hemin is reportedly an HO-1 inducer [31, 32] to catalyze the degradation of heme/hemin [3, 33] and thus release iron [34] which is known as a Fenton's reagent [35]. In the present study, hemin consistently elevated HO-1 expression which elevated iron levels that overproduced free radicals and oxidative injury [1]. Accordingly, in addition to anti-oxidant therapies [24, 36, 37], HO-1 inhibitors appear to be beneficial to ICH. Our study supports this notion that afatinib may exert its neuroprotective effect via attenuating HO-1 expression in ICH.

A significant body of literature has demonstrated several cell death mechanisms in ICH, including ferroptosis [21, 38] which is a programmed cell death related to iron metabolism [39–41]. Consistently, we identified hemin-induced ferroptosis in primary cultured cortical neurons. Moreover, we demonstrated that afatinib is capable of blocking hemin-induced ferroptosis. This may be due to afatinib-induced inhibition of hemin-elevated HO-1 expression which reduced iron accumulation, prevented Fenton's reaction and then attenuated hemin-induced ferroptosis. In addition, we detected hemin-induced necroptosis, which was inhibited by afatinib, too. The afatinib-induced inhibition of necroptosis may be due to afatinib's inhibition of hemin-elevated TNF- α levels because TNF- α reportedly initiates necroptosis and leads to RIP3 activation [42]. These data suggest that afatinib is capable of ameliorating ferroptosis and necroptosis in ICH.

In conclusion, the present study demonstrates that afatinib inhibited hemin-induced EGFR-AKT activation and neurotoxicity in primary cultured cortical neurons, suggesting that EGFR-AKT signaling is involved in the pathophysiology of ICH. Along with our previous study showing that afatinib inhibited OGD-induced neuroinflammation in astrocytes [15], it appears that EGFR-TKIs may be a novel repurposing drug for CNS neurodegenerative diseases, including ICH.

Author contributions

All authors listed have made a substantial, direct, and intellectual contribution to the work and approved it for publication.

Data availability

The original contributions presented in the study are included in the article/supplementary material, further inquiries can be directed to the corresponding authors.

Ethics statement

The animal study was approved by The Institutional Animal Care and Use Committee (IACUC) of Taipei Veterans General

Hospital (TVGH), Taipei, Taiwan. The approval number is IACUC2022-235. The study was conducted in accordance with the local legislation and institutional requirements.

Funding

The author(s) declare that financial support was received for the research and/or publication of this article. The MOST grant 110-2320-B-A49A-509-MY3 and VGHTPE grant V112C-147.

References

- Shao Z, Tu S, Shao A. Pathophysiological mechanisms and potential therapeutic targets in intracerebral hemorrhage. *Front Pharmacol* (2019) **10**:1079. doi:10.3389/fphar.2019.01079
- Tschoe C, Bushnell CD, Duncan PW, Alexander-Miller MA, Wolfe SQ. Neuroinflammation after intracerebral hemorrhage and potential therapeutic targets. *J Stroke* (2020) **22**:29–46. doi:10.5853/jos.2019.02236
- Robinson SR, Dang TN, Dringen R, Bishop GM. Hemin toxicity: a preventable source of brain damage following hemorrhagic stroke. *Redox Rep* (2009) **14**:228–35. doi:10.1179/135100009x12525712409931
- Bai Q, Liu J, Wang G. Ferroptosis, a regulated neuronal cell death type after intracerebral hemorrhage. *Front Cell Neurosci* (2020) **14**:591874. doi:10.3389/fncel.2020.591874
- Magid-Bernstein J, Girard R, Polster S, Srinath A, Romanos S, Awad IA, et al. Cerebral hemorrhage: pathophysiology, treatment, and future directions. *Circ Res* (2022) **130**:1204–29. doi:10.1161/circresaha.121.319949
- Wee P, Wang Z. Epidermal growth factor receptor cell proliferation signaling pathways. *Cancers (Basel)* (2017) **9**:52. doi:10.3390/cancers9050052
- Liao BC, Lin CC, Yang JC. Second and third-generation epidermal growth factor receptor tyrosine kinase inhibitors in advanced nonsmall cell lung cancer. *Curr Opin Oncol* (2015) **27**:94–101. doi:10.1097/cco.0000000000000164
- Varela L, Garcia-Rendueles MER. Oncogenic pathways in neurodegenerative diseases. *Int J Mol Sci* (2022) **23**:3223–6. doi:10.3390/ijms23063223
- Romano R, Bucci C. Role of EGFR in the nervous system. *Cells* (2020) **9**:1887. doi:10.3390/cells9081887
- Tavassoly O, Del Cid Pellitero E, Larroquette F, Cai E, Thomas RA, Soubannier V, et al. Pharmacological inhibition of brain EGFR activation by a BBB-penetrating inhibitor, AZD3759, attenuates α -synuclein pathology in a mouse model of α -synuclein propagation. *Neurotherapeutics* (2021) **18**:979–97. doi:10.1007/s13311-021-01017-6
- Suh Y, Obernier K, Hölzl-Wenig G, Mandl C, Herrmann A, Wörner K, et al. Interaction between DLX2 and EGFR regulates proliferation and neurogenesis of SVZ precursors. *Mol Cell Neurosci* (2009) **42**:308–14. doi:10.1016/j.mcn.2009.08.003
- Birecree E, Whetsell WO, Jr, Stoscheck C, King LE, Jr, Nanney LB. Immunoreactive epidermal growth factor receptors in neuritic plaques from patients with Alzheimer's disease. *J Neuropathol Exp Neurol* (1988) **47**:549–60. doi:10.1097/00005072-198809000-00006
- Mansour HM, Fawzy HM, El-Khatib AS, Khattab MM. Potential repositioning of anti-cancer EGFR inhibitors in alzheimer's disease: current perspectives and challenging prospects. *Neuroscience* (2021) **469**:191–6. doi:10.1016/j.neuroscience.2021.06.013
- Qu WS, Tian DS, Guo ZB, Fang J, Zhang Q, Yu Z, et al. Inhibition of EGFR/MAPK signaling reduces microglial inflammatory response and the associated secondary damage in rats after spinal cord injury. *J Neuroinflammation* (2012) **9**:642. doi:10.1186/1742-2094-9-178
- Chen YJ, Hsu CC, Shiao YJ, Wang HT, Lo YL, Lin AMY. Anti-inflammatory effect of afatinib (an EGFR-TKI) on OGD-induced neuroinflammation. *Sci Rep* (2019) **9**:2516. doi:10.1038/s41598-019-38676-7
- Planas AM, Justicia C, Soriano MA, Ferrer I. Epidermal growth factor receptor in proliferating reactive glia following transient focal ischemia in the rat brain. *Glia* (1998) **23**:120–9. doi:10.1002/(sici)1098-1136(199806)23:2<120::aid-glia3>3.0.co;2-a
- Peng DH, Liu YY, Chen W, Hu HN, Luo Y. Epidermal growth factor alleviates cerebral ischemia-induced brain injury by regulating expression of neutrophil gelatinase-associated lipocalin. *Biochem Biophysical Res Commun* (2020) **524**:963–9. doi:10.1016/j.bbrc.2020.02.025
- Yu Y, Zhang X, Han Z, Zhao W, Zhang L. Expression and regulation of miR-449a and AREG in cerebral ischemic injury. *Metab Brain Dis* (2019) **34**:821–32. doi:10.1007/s11011-019-0393-9
- Nakano F, Kanamaru H, Kawakita F, Liu L, Nakatsuka Y, Nishikawa H, et al. Epidermal growth factor receptor mediates neuronal apoptosis after subarachnoid hemorrhage in mice. *Stroke* (2023) **54**:1616–26. doi:10.1161/strokeaha.122.041977
- Min H, Choi B, Jang YH, Cho IH, Lee SJ. Heme molecule functions as an endogenous agonist of astrocyte TLR2 to contribute to secondary brain damage after intracerebral hemorrhage. *Mol Brain* (2017) **10**:27. doi:10.1186/s13041-017-0305-z
- Zille M, Karuppagounder SS, Chen Y, Gough PJ, Bertin J, Finger J, et al. Neuronal death after hemorrhagic stroke *in vitro* and *in vivo* shares features of ferroptosis and necroptosis. *Stroke* (2017) **48**:1033–43. doi:10.1161/strokeaha.116.015609
- Zhou J, Du T, Li B, Rong Y, Verkhatsky A, Peng L. Crosstalk between MAPK/ERK and PI3K/AKT signal pathways during brain ischemia/reperfusion. *ASN Neuro* (2015) **7**:1759091415602463. doi:10.1177/1759091415602463
- Karuppagounder SS, Alim I, Khim SJ, Bourassa MW, Sleiman SF, John R, et al. Therapeutic targeting of oxygen-sensing prolyl hydroxylases abrogates ATF4-dependent neuronal death and improves outcomes after brain hemorrhage in several rodent models. *Sci Transl Med* (2016) **8**:328ra29. doi:10.1126/scitranslmed.aac6008
- Duan L, Zhang Y, Yang Y, Su S, Zhou L, Lo PC, et al. Baicalin inhibits ferroptosis in intracerebral hemorrhage. *Front Pharmacol* (2021) **12**:629379. doi:10.3389/fphar.2021.629379
- Zhou YF, Zhang C, Yang G, Qian ZM, Zhang MW, Ma J, et al. Hepcidin protects neuron from hemin-mediated injury by reducing iron. *Front Physiol* (2017) **8**:332. doi:10.3389/fphys.2017.00332
- Letarte PB, Lieberman K, Nagatani K, Haworth RA, Odell GB, Duff TA. Hemin: levels in experimental subarachnoid hematoma and effects on dissociated vascular smooth-muscle cells. *J Neurosurg* (1993) **79**:252–5. doi:10.3171/jns.1993.79.2.0252
- Solca F, Dahl G, Zoephel A, Bader G, Sanderson M, Klein C, et al. Target binding properties and cellular activity of afatinib (BIBW 2992), an irreversible ErbB family blocker. *The J Pharmacol Exp Ther* (2012) **343**:342–50. doi:10.1124/jpet.112.197756
- Zhang W, Xiao D, Mao Q, Xia H. Role of neuroinflammation in neurodegeneration development. *Signal Transduction Targeted Ther* (2023) **8**:267. doi:10.1038/s41392-023-01486-5
- Almarghalani DA, Sha X, Mrak RE, Shah ZA. Spatiotemporal cofilin signaling, microglial activation, neuroinflammation, and cognitive impairment following hemorrhagic brain injury. *Cells* (2023) **12**:1153. doi:10.3390/cells12081153
- Mayne M, Ni W, Yan HJ, Xue M, Johnston JB, Del Bigio MR, et al. Antisense oligodeoxynucleotide inhibition of tumor necrosis factor- α expression is neuroprotective after intracerebral hemorrhage. *Stroke* (2001) **32**:240–8. doi:10.1161/01.str.32.1.240
- Ouyang Y, Li D, Wang H, Wan Z, Luo Q, Zhong Y, et al. MiR-21-5p/dual-specificity phosphatase 8 signalling mediates the anti-inflammatory effect of haem

Conflict of interest

The author(s) declared no potential conflicts of interest with respect to the research, authorship, and/or publication of this article.

Generative AI statement

The author(s) declare that no Generative AI was used in the creation of this manuscript.

oxygenase-1 in aged intracerebral haemorrhage rats. *Aging Cell* (2019) **18**:e13022. doi:10.1111/accel.13022

32. Le LL, Li XY, Meng D, Liang Q, Wang X, Li N, et al. Heme oxygenase-1 mediated memorial and revivable protective effect of ischemic preconditioning on brain injury. *CNS Neurosci Ther* (2013) **19**:963–8. doi:10.1111/cns.12152

33. Chen-Roetling J, Lu X, Regan RF. Targeting heme oxygenase after intracerebral hemorrhage. *Ther Targets Neurol Dis* (2015) **2**:474. doi:10.14800/ttnd.474

34. Hu S, Hua Y, Keep RF, Feng H, Xi G. Deferoxamine therapy reduces brain hemin accumulation after intracerebral hemorrhage in piglets. *Exp Neurol* (2019) **318**:244–50. doi:10.1016/j.expneurol.2019.05.003

35. Winterbourn CC. Toxicity of iron and hydrogen peroxide: the Fenton reaction. *Toxicol Lett* (1995) **82-83**:969–74. doi:10.1016/0378-4274(95)03532-x

36. Duan X, Wen Z, Shen H, Shen M, Chen G. Intracerebral hemorrhage, oxidative stress, and antioxidant therapy. *Oxidative Med Cell Longevity* (2016) **2016**:1203285. doi:10.1155/2016/1203285

37. Zheng Y, Li R, Fan X. Targeting oxidative stress in intracerebral hemorrhage: prospects of the natural products approach. *Antioxidants (Basel)* (2022) **11**:1811–24. doi:10.3390/antiox11091811

38. Zhang Y, Khan S, Liu Y, Zhang R, Li H, Wu G, et al. Modes of brain cell death following intracerebral hemorrhage. *Front Cell Neurosci* (2022) **16**:799753. doi:10.3389/fncel.2022.799753

39. Lu C, Tan C, Ouyang H, Chen Z, Yan Z, Zhang M. Ferroptosis in intracerebral hemorrhage: a panoramic perspective of the metabolism, mechanism and theranostics. *Aging Dis* (2022) **13**:1348–64. doi:10.14336/ad.2022.01302

40. Tang D, Chen X, Kang R, Kroemer G. Ferroptosis: molecular mechanisms and health implications. *Cell Res* (2021) **31**:107–25. doi:10.1038/s41422-020-00441-1

41. Li Q, Han X, Lan X, Gao Y, Wan J, Durham F, et al. Inhibition of neuronal ferroptosis protects hemorrhagic brain. *JCI Insight* (2017) **2**:e90777. doi:10.1172/jci.insight.90777

42. Sun X, Lee J, Navas T, Baldwin DT, Stewart TA, Dixit VM. RIP3, a novel apoptosis-inducing kinase. *J Biol Chem* (1999) **274**:16871–5. doi:10.1074/jbc.274.24.16871



OPEN ACCESS

*CORRESPONDENCE

Anya Maan-Yuh Lin,
✉ myalin@nycu.edu.tw

RECEIVED 02 March 2025

ACCEPTED 02 May 2025

PUBLISHED 21 May 2025

CITATION

Tseng YJ, Huang H-J, Lin C-H and
Lin AM-Y (2025) A double-edged effect
of hypoxia on astrocyte-derived
exosome releases.

Exp. Biol. Med. 250:10559.

doi: 10.3389/ebm.2025.10559

COPYRIGHT

© 2025 Tseng, Huang, Lin and Lin. This
is an open-access article distributed
under the terms of the [Creative
Commons Attribution License \(CC BY\)](#).
The use, distribution or reproduction in
other forums is permitted, provided the
original author(s) and the copyright
owner(s) are credited and that the
original publication in this journal is
cited, in accordance with accepted
academic practice. No use, distribution
or reproduction is permitted which does
not comply with these terms.

A double-edged effect of hypoxia on astrocyte-derived exosome releases

Yang Jie Tseng¹, Hui-Ju Huang², Chien-Hui Lin³ and
Anya Maan-Yuh Lin^{1,2,4*}

¹Ph.D. Program in Regulatory Science and Policy, National Yang-Ming Chiao-Tung University, Hsin-Chu, Taiwan, ²Department of Medical Research, Taipei Veterans General Hospital, Taipei, Taiwan, ³Institute of Physiology, National Yang-Ming Chiao-Tung University, Hsin-Chu, Taiwan, ⁴Department of Pharmacy, National Yang-Ming Chiao-Tung University, Hsin-Chu, Taiwan

Abstract

Exosomes are the smallest extracellular vesicles secreted from cells, carrying different cargos, including nucleic acids, proteins and others which transfer from cells to cells. The properties of exosomes depend on the donor cells. Hypoxia, referring to a sublethal and insufficient oxygen supply, reportedly influences exosome secretion of hypoxic cells. In the present study, we focused on the effects of hypoxia on exosomes obtained from CTX-TNA2 astrocyte cells exposed to different durations of hypoxia followed by normoxia as a model of hypoxic preconditioning. To evaluate the functions of exosomes, primary cultured cortical neurons were treated with hemin, a potent neurotoxin. Our sulforhodamine B assay showed that incubation of hemin (30 μ M) consistently induced neuronal death. Co-incubation of exosomes from CTX-TNA2 cells subjected to 2 hr-hypoxia plus 6 hr-renormoxia (2H/6R exosomes), but not 12 hr-hypoxia plus 24 hr-renormoxia (12H/24R exosomes), attenuated hemin-induced cell death and reduction in growth associated protein 43 level (a biomarker of neurite outgrowth). Western blot assay demonstrated that 2H/6R exosomes attenuated hemin-induced elevations in inducible nitric oxide synthase (iNOS) and cyclooxygenase-2 (COX-2) levels (two proinflammatory biomarkers) as well as heme oxygenase-1 (HO-1). In contrast, 12H/24R exosomes did not alter hemin-induced elevation in HO-1 but further augmented hemin-induced increases in iNOS and COX-2. Moreover, 2H/6R exosomes attenuated hemin-induced reduction in glutathione hydroperoxidase 4 (a biomarker of ferroptosis) and elevation in active caspase 3 (a biomarker of apoptosis) while 12H/24R exosomes did not effectively alter hemin-induced programmed cell death. In conclusion, our study showed that 2H/6R exosomes possessed neuroprotective activities while 12H/24R exosomes had mild pro-inflammatory activities, suggesting that different hypoxic preconditionings influenced CTX-TNA2 cells which then secreted exosomes with differential biological activities. These findings highlight a double-edged role of hypoxia on exosome functions.

KEYWORDS

hypoxic preconditioning, double-edged role, exosomes, hemin, CTX-TNA2

Impact statement

To delineate the role of hypoxic preconditioning on the exosome's secretion and functions, the CTX-TNA2 cells were exposed to different durations of hypoxia plus renormoxia and were found to secrete exosomes with opposite functions. One was to attenuate hemin-induced neurotoxicity and the other was to augment hemin-induced neuroinflammation. Our data suggests that in addition to exosomes secretion, hypoxic treatment plays a crucial role in modulating exosomes functions.

Introduction

Cells are known to secrete small membrane-bound vesicles, namely, extracellular vesicles (EVs). Extracellular vesicles differ in size, density, morphology, contents, and biomarkers [1–3]. Exosomes are the smallest subgroup of EVs, ranging from 30 to 160 nm. Exosomes carry various biomolecules, including proteins, lipids, and nucleic acids (RNA, DNA) which are reportedly transferred from donor cells to target cells [4]. Accordingly, the function of exosomes depends on the status of donor cells [2]. Protective exosomes from good cells are suggested to carry “good” cargos while detrimental exosomes from bad cells carry “bad” cargos [4, 5]. Many non-clinical and clinical studies have demonstrated cytoprotective roles of exosomes against various diseases [1, 5–10]. For example, non-clinical studies showed that exosomes from cardiac fibroblasts inhibited heart failure and myocardial ischemic damage [7]. Furthermore, exosomes derived from umbilical cord mesenchymal stem cells (MSC) reportedly prevented acute liver damage in mice [8]. Exosomes from hypoxic MSC exert its protective action via attenuating neurological deficits, and program cell death in stroke and Alzheimer's models [9] as well as promoting bone fracture healing [10]. At the same time, many clinical trials focused on the protective effects of exosomes on renal diseases, type 1 diabetes, osteoarthritis, stroke, Alzheimer's disease, and cancers [1, 6].

Hypoxia refers to a condition in which oxygen supply is insufficient in cells, tissues, organs, and systems [11, 12]. A variety of protective functions via hypoxia-induced adaptation has been demonstrated. For example, a non-lethal hypoxia in the tumor microenvironment is reportedly cytoprotective to cancer cells [13, 14]. Furthermore, our previous studies have demonstrated that hypoxic preconditioning is neuroprotective against kainic acid-induced neurotoxicity [15] and ischemic stroke [16]. The proposed mechanisms underlying hypoxia-induced adaptation included induction of hypoxia-inducible factor- α , a transcription factor which is reportedly up-regulated to activate genes and is responsible for adaptation-related cellular responses [12]. Furthermore, hypoxia-induced adaptation may be mediated via regulation of anti-oxidative defense systems, induction of autophagy [17], exosome secretion [4, 10] and others.

Due to the intersection of hypoxia and exosomes, the present study focused on the effects of hypoxia on CTX-TNA2 cells-derived exosomes using hemin-induced neurotoxicity, an intracerebral hemorrhage (ICH) *in vitro* model [18]. Astrocytes are reportedly involved in homeostasis and defense of the central nervous system (CNS) [19]. During the insults, astrocytes are activated and may damage the nearby cells. However, recent studies proposed a neuroprotective role of astrocytes in the astrocyte polarization [20] following brain injury. These findings indicate that astrocytes may play beneficial or detrimental roles in CNS neurodegenerative diseases [19–21]. Given that astrocytes are the most numerous cell type in the brain, astrocytes-derived exosomes may have a substantial influence on the progression of CNS neurodegenerative disorders, including ICH. In the present study, CTX-TNA2 astrocyte cells were exposed to different durations of hypoxia and subsequent renormoxia, including 2-h hypoxia followed by 6-h normoxia (2H/6R) and 12-h hypoxia followed by 24-h normoxia (12H/24R). Both 2H/6R exosomes and 12H/24R exosomes were collected and their functions were characterized. Our data showed that 2H/6R exosomes attenuated hemin-induced neurotoxicity while 12H/24R exosomes possessed proinflammatory activities, indicating that the role of hypoxia is double-edged in exosomes' functions.

Materials and methods

Chemicals

The chemicals used were hemin (Sigma, St. Louis, MO, United States). Hemin was dissolved in ammonia water and pH value was corrected to pH 7.4. Hemin was diluted with DMEM or Neurobasal medium (NB, Thermo Fisher Scientific, Waltham, MA, United States).

Hypoxic preconditioning of CTX-TNA2 cells

CTX-TNA2, an astrocyte cell line isolated from the cortex of 1-day old rats, was purchased from Bioresource Collection and Research Center (Taiwan) and maintained in Dulbecco's Modified Eagle Medium (Sigma) supplemented with 10% (v/v) fetal bovine serum (Cytiva, Marlborough, MA, United States) and 1% penicillin-streptomycin-amphotericin B (Cytiva) in an incubator under 5% CO₂ at 37°C. Prior to the hypoxic preconditioning, CTX-TNA2 cells were seeded at a density of 1×10^6 cells in a 10-cm culture dish and were incubated in 5 mL NB without exosomes. Hypoxic treatment was conducted by incubating cells in an incubator with 1% oxygen. Two hypoxic preconditionings were designed as follows. One hypoxic treatment was to expose CTX-TNA2 cells to 2-h hypoxia

followed by 6-h normoxia. The other was to expose CTX-TNA2 cells to 12-h hypoxia followed by 24-h normoxia.

Exosomes preparation

At the end of hypoxia-renormoxia treatments, exosomes obtained from the culture medium were isolated using ExoQuick (System Biosciences, Palo Alto, CA, United States). In brief, the culture medium from 10-cm culture dishes was collected and centrifuged at $2600 \times g$ for 30 min at 4°C. The supernatant was transferred to a new centrifuge tube. Five milliliters of culture medium mixed with 1 mL of ExoQuick and the tube was placed in a refrigerator at 4°C overnight. The supernatant was collected and centrifuged at $1,500 \times g$ for 30 min at 4°C. Again, the supernatant was collected and centrifuged at $1,500 \times g$ for 5 min. After removing the remaining supernatant, the exosome pellet was re-dissolved in PBS at 4°C and stored at 4°C. Approximately, 5×10^8 exosome particles obtained from 1×10^6 cells in a 10-cm culture dish were used for further experiments as 1-fold (1x) of exosomes.

Nanoparticle tracking analysis and detection of zeta potentials

Nanoparticle Tracking Analysis (NTA) was employed to characterize exosomes, including size distribution and exosome particle concentration by NanoSight NS300 (Malvern Panalytical, Malvern, UK). This technique was capable of detecting vesicles with sizes between 0.05 and 1 μm . At the same time, zeta potential of exosomes was analyzed using the Nano ZS (Malvern Panalytical).

Transmission electron microscopy

An aliquot of exosomes was applied onto an electron microscopy grid and incubated for 5 min and fixed with 2% paraformaldehyde for 5 min. The samples were counterstained with 1% uranyl acetate for 1 min, air-dried overnight, and observed using a Transmission Electron Microscope JEM-1400Plus (JEOL Ltd., Tokyo, Japan).

RNA sequencing analysis

MicroRNA(miRNA) libraries were prepared using the QIAseq miRNA UDI Library Kit (Qiagen, Venlo, Netherlands) and evaluated for size distribution using the Agilent 4150 TapeStation with HS D1000 ScreenTape (Agilent, Santa Clara, CA, United States). Sequencing was conducted with single end reads (100 bp) at a depth

exceeding 10 million reads per sample. miRNA expression levels were quantified using the Qiagen GeneGlobe platform (Qiagen) with UMI-based correction.

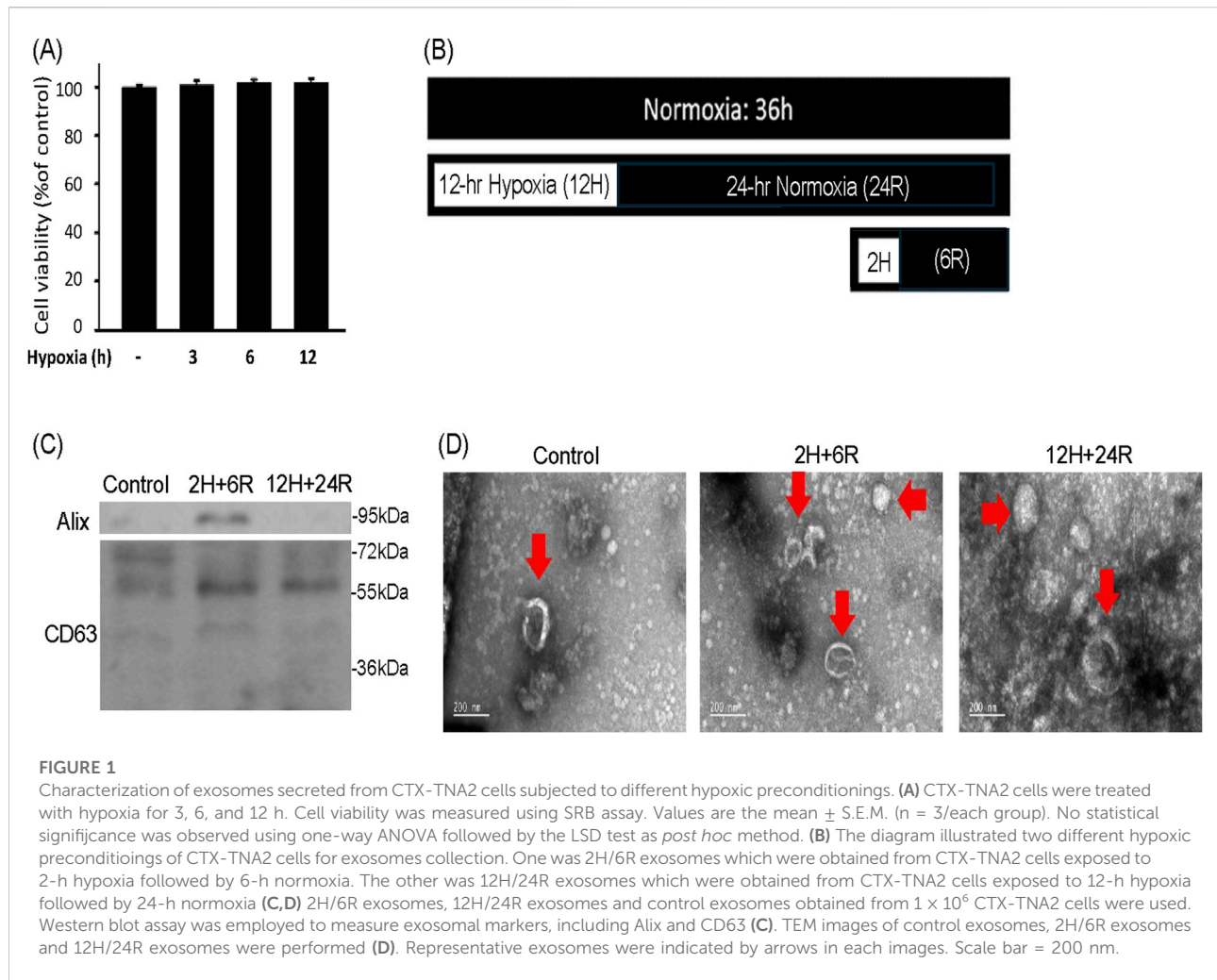
Primary cultured cortical neurons

Pregnant female Sprague-Dawley (SD) rats were supplied by BioLASCO Taiwan Co., Ltd. (Yilan, Taiwan). All animals (one rat/individually ventilated cage) were housed in an air-conditioned room ($22 \pm 2^\circ\text{C}$) on a 12 hr-light/dark cycle (07:00–19:00 h light) and had free access to food and water. To prepare primary cultured cortical neurons, embryonic day 17 fetal rat brains were obtained from pregnant female SD rats of 17-day gestation which were sacrificed by an overdose of Zoletil® (Virbac, Taipei, Taiwan) to minimize pain or discomfort used. The use of animals and all experiments conducted were under approved protocols from the Institutional Animal Care and Use Committee (IACUC) of Taipei Veterans General Hospital, Taipei, Taiwan. The approval number is IACUC2022-235. In addition, the authors complied with the ARRIVE guidelines. All experiments were performed in accordance with relevant guidelines and regulations.

Cerebral cortices of fetal rats were isolated and dissociated mechanically. The dissociated cells were suspended in the Basal Medium Eagle medium (BME, Thermo Fisher Scientific) containing 20% fetal bovine serum, and were seeded onto a 35-mm culture dish (IWAKI, Tokyo, Japan) with a density of 5×10^6 cells per dish. Afterwards, cells were maintained with serum-free NB medium supplemented with B27 (Thermo Fisher Scientific) in the incubator with 5% CO₂ at 37°C. Hemin-induced neurotoxicity was established by exposing primary cultured cortical neurons with hemin (30 μM).

Cytotoxicity assay

A modified sulforhodamine B (SRB) assay was employed to measure cell viability. At the end of experiment, cells in 96-well plates were washed with phosphate-buffered saline (PBS) and 10% trichloroacetic acid (TCA, Merck, Boston, MA, United States) and were then incubated at 4°C for 1h. Afterwards, TCA solution was removed, and the cells were washed with double distilled H₂O. Cells were then incubated with SRB solution (0.4% in 1% acetic acid, Merck) for 10 min. Afterwards, SRB solution was removed, and the cells were washed with 1% acetic acid. After removing acetic acid, the sample was air-dried and 20 mM unbuffered Tris base was used to dissolve the resulting formazan product. The absorption was measured by an ELISA reader (TECAN Sunrise, Männedorf, United States) at 540 nm with a reference wavelength of 690 nm.



Western blots analysis

At the end of 16-h treatments, the cells were collected, washed with phosphate buffered saline (PBS), and lysed in radioimmunoprecipitation assay (RIPA, Cell Signaling Tech. Beverly, MA, United States) lysis buffer containing 20 mM Tris HCl, 150 mM NaCl, 1% (v/v) NP-40, 1% (w/v) sodium deoxycholate, 1 mM ethylenediaminetetraacetates (EDTA), 0.1% (w/v) sodium dodecyl sulfate polyacrylamide (SDS) and 0.01% (w/v) sodium azide (pH 7.5) for 20 min on ice. Lysates were then centrifuged at $13800 \times g$ for 10 min, and the protein concentrations of supernatants were determined by Pierce BCA Protein Assay Kit (Thermo Fisher Scientific). Protein samples (30 μ g) were run on 12–13.5% SDS-polyacrylamide gel electrophoresis and then transferred onto a polyvinylidene difluoride (PVDF, Bio-Rad, Hercules, CA, United States) at 100 V for 120 min. Blots were probed with primary antibodies including antibodies against GAP43 (Cell Signaling Technology), iNOS, COX-2, HO-1 (StressGen, Victoria, CA, United States), GPX4 and active-

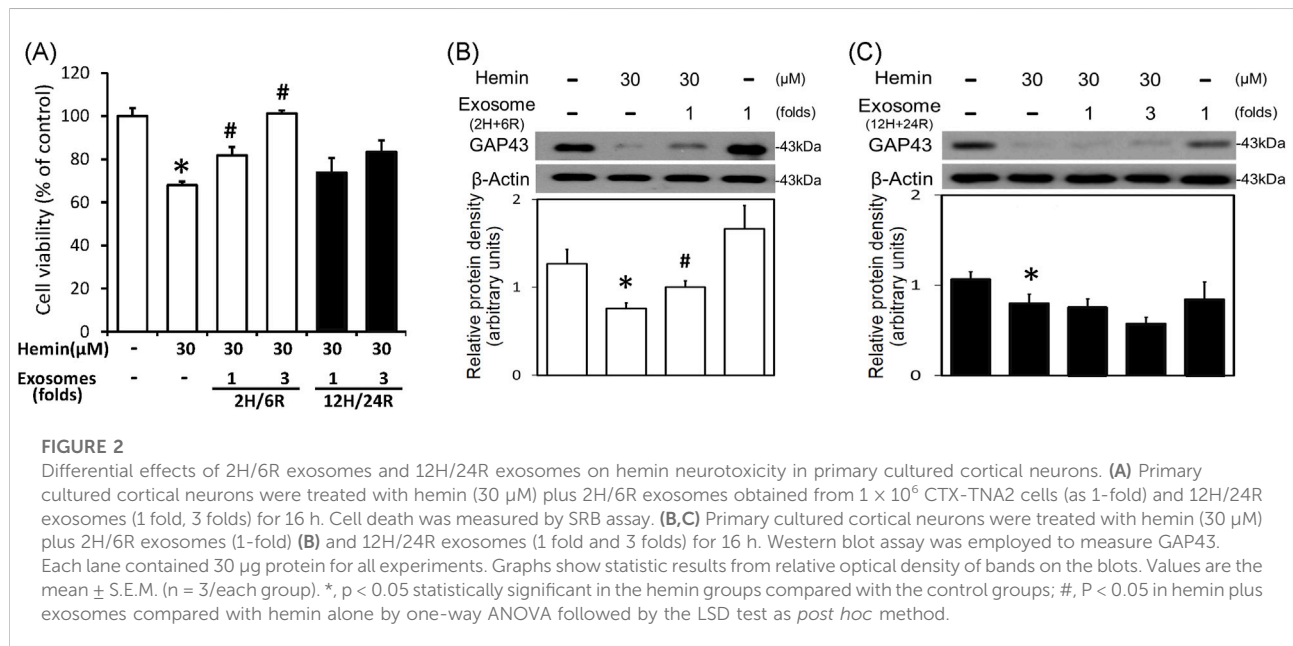
caspase 3 (Cell Signaling Technology) overnight at 4°C. After incubation of primary antibodies, the membrane was washed and incubated with a secondary antibody for 1 h at room temperature. The secondary antibodies were horseradish peroxidase-conjugated secondary IgG (Chemicon, Temecula, CA, United States). The immunoreaction was visualized using Amersham Enhanced Chemiluminescence (Amersham Pharmacia Biotech, Piscataway, NJ, United States). After this measurement, the bound primary and secondary antibodies were stripped by incubating the membrane in stripping buffer (100 mM 2-mercaptoethanol, 2% SDS) at 50°C for 5 min. The membrane was reprobed with a primary antibody against β -actin (Millipore, Billerica, MA, United States).

Immunofluorescent staining

At the end of treatments, the primary cultured cortical neurons were fixed with 4% paraformaldehyde (Merck). Cells

TABLE 1 NTA assay of 2H/6R exosomes and 12H/24R exosomes. 2H/6R exosomes were obtained from CTX-TNA2 cells exposed to 2-h hypoxia followed by 6-h normoxia. The other was 12H/24R exosomes obtained from cells exposed to 12-h hypoxia followed by 24-h normoxia. NTA assay and zeta potential assay were performed. Values are the mean \pm S.E.M. ($n = 3$ /each group). No statistical significance was observed using one-way ANOVA followed by the Tukey multiple comparison as *post hoc* method.

Exosomes' conditions	Size (nm)	Concentration (particles/mL)	Zeta potential (mV)
Control exosomes	89.8 \pm 9.9	1.25 \pm 0.35 $\times 10^{10}$	-8.57 \pm 0.27
2H/6R exosomes	99.4 \pm 9.0	1.04 \pm 0.29 $\times 10^{10}$	-8.72 \pm 0.87
12H/24R exosomes	105.1 \pm 22.3	1.40 \pm 0.64 $\times 10^{10}$	-7.48 \pm 0.80



were then washed with 0.1 M PBS, incubated with 0.3% Triton X-100 (Sigma) and 1% goat serum (GS; Jackson ImmunoResearch, West Grove, PA, United States), and blocked with 3% GS for 60 min. Next, cells were processed for immunostaining using monoclonal antibody specific for rat Neu N (Cell Signaling Technology) in 1% GS-PBS at 4°C for 24 h. The cells were then incubated in fluorescein conjugated-IgG (FITC) (Jackson ImmunoResearch) for 1 h at room temperature, mounted in glycerol (Merck) and exosome stained with PKH26 (Sigma). Controls consisted of omissions of primary antibodies. The sections were visualized by a fluorescence confocal microscope (Olympus FluoView, Norfolk, VA, United States).

Statistics

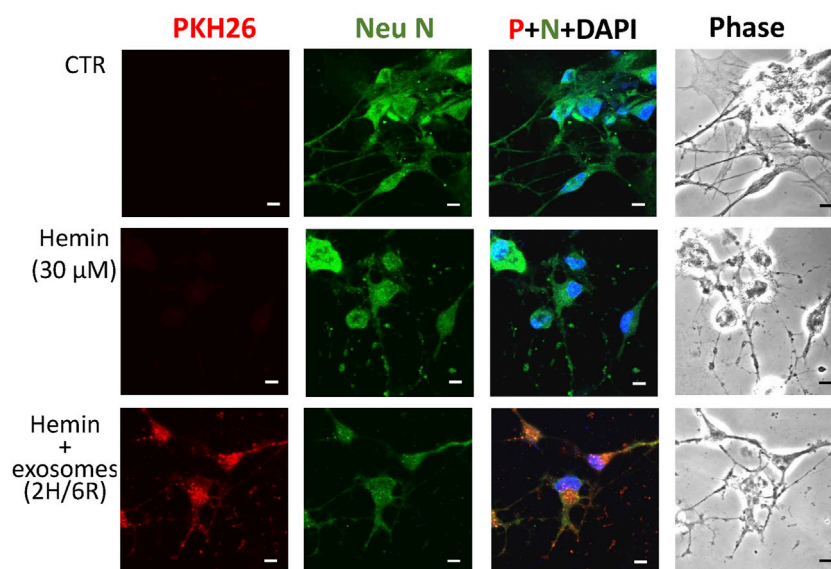
All data are expressed as the mean \pm S.E.M. The results were analyzed by one-way analysis of variance (one-way ANOVA) followed by the LSD test (cell viability and Western blot assay) or

Tukey multiple comparison (NTA) as *post hoc* methods. The significance level was set at $p < 0.05$.

Results

Characterization of exosomes of hypoxic preconditioned CTX-TNA2 cells

To delineate the effect of hypoxic preconditionings on exosome secretion, CTX-TNA2 astrocyte cells were treated with 3, 6, and 12 h hypoxia. SRB assay showed that hypoxia (1% oxygen) for 3, 6, 12 h did not cause significant cell loss of CTX-TNA2 cells (Figure 1A). Therefore, 2-h hypoxia followed by 6-h normoxia (2H/6R) and 12-h hypoxia followed by 24-h normoxia (12H/24R) were designed to treat CTX-TNA2 cells to harvest exosomes (Figure 1B). Western blot assay showed that compared with the control, AIX and CD 63 levels were elevated in the 2H/6R exosomes and 12H/24R exosomes (Figure 1C). TEM analysis showed that control exosomes, 2H/6R exosomes and

**FIGURE 3**

Differential effects of 2H/6R exosomes and 12H/24R exosomes on hemin-induced impairment of neurite outgrowth in primary cultured cortical neurons. Primary cultured cortical neurons were treated with hemin (30 μ M) plus 2H/6R exosomes obtained from 1×10^6 CTX-TNA2 cells for 1 h. The cells were immunostained with Neu N, PKH26 and DAPI. Calibration: 10 μ m. The results were duplicated.

12H/24R exosomes all exhibited a spherical morphology with an intact lipid bilayer membrane (Figure 1D). Furthermore, the NTA assay showed that the sizes of 2H/6R exosomes and 12H/24R exosomes were slightly larger but not statistically different from the control exosomes, ranging from 89.8 ± 9.9 nm in the control exosomes to 99.4 ± 12.7 nm in 2H/6R exosomes and 105.1 ± 22.3 nm in the 12H/24R exosomes ($n = 3/\text{group}$) (Table 1). At the same time, the concentrations of exosomes particles were not statistically different among 3 exosomes (Table 1). Furthermore, no statistical differences were observed in zeta potentials of 3 exosomes (Table 1).

Differential effects of exosomes of hypoxic preconditioned CTX-TNA2 cells on hemin-induced cell death and morphological changes

To delineate the effects of 2H/6R exosomes and 12H/24R exosomes, a hemin-induced neurotoxicity model was established in primary cultured cortical neurons. The SRB assay showed that 16-h incubation of hemin (30 μ M) increased neuronal death (Figure 2A). Co-incubation with 2H/6R exosomes concentration-dependently attenuated hemin-induced neuronal death. In contrast, 12H/24R exosomes did not significantly alter hemin-induced neuronal death (Figure 2A). At the same time, Western blot assay showed that hemin reduced GAP43 levels (a biomarker of neurite outgrowth). Co-incubation

of 2H/6R exosomes, but not 12H/24R exosomes, attenuated hemin-induced reduction in GAP 43 levels, indicating that 2H/6R exosomes may attenuate hemin-induced reduction of neurite outgrowth (Figures 2B,C). Moreover, the immunofluorescent staining data showed focal bead-like swellings, neuritic beading and discontinuities of neurites in hemin-treated primary cultured cortical neurons after 1-h incubation of hemin, indicating hemin-induced impairments in neurite outgrowth (Figure 3). Co-incubation of 2H/6R exosomes significantly attenuated hemin-induced neurite impairment (Figure 3). At the same time, intensive PKH26 fluorescence (a fluorescent dye specific for exosomes) was detected in the cytosol of primary cultured cortical neurons treated with hemin plus 2H/6R exosomes, suggesting that exosomes were successfully endocytosed by primary cultured cortical neurons.

Differential effects of exosomes of hypoxic preconditioned CTX-TNA2 cells on hemin-induced neuroinflammation, HO-1 expression and programmed cell death

To further investigate the differential effects of 2H/6R exosomes and 12H/24R exosomes, iNOS and COX-2 (two proinflammatory biomarkers) were measured in the primary cultured cortical neurons. Western blot assay demonstrated

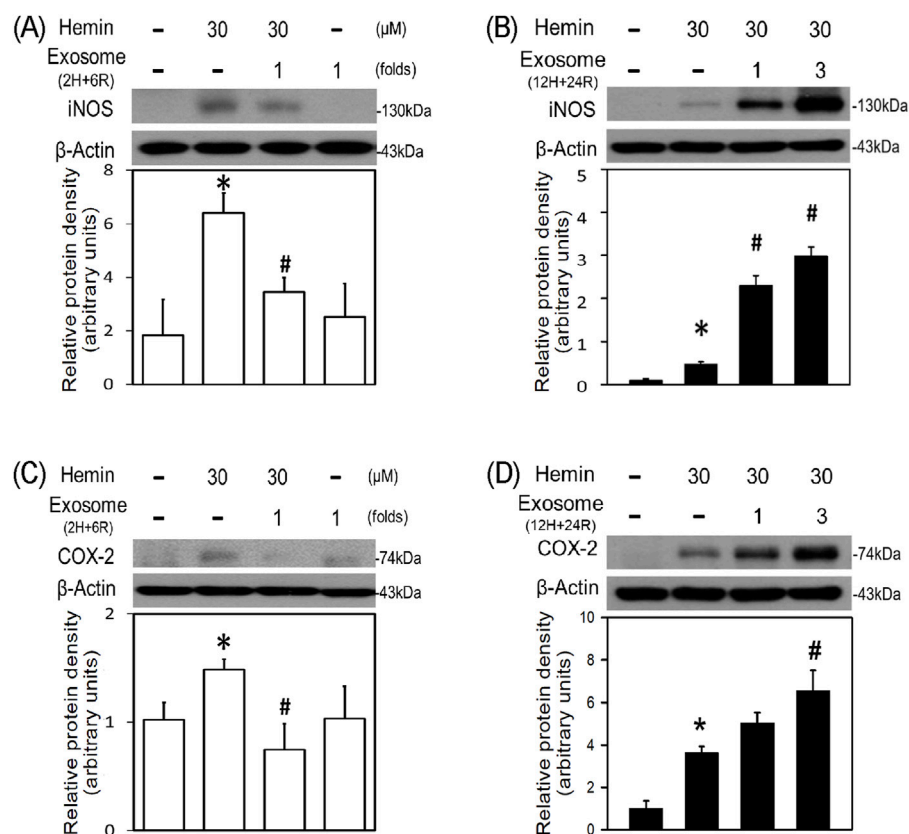


FIGURE 4

Differential effects of 2H/6R exosomes and 12H/24R exosomes on hemin-induced neuroinflammation in primary cultured cortical neurons. (A,C) Primary cultured cortical neurons were treated with hemin (30 μ M) plus 2H/6R exosomes obtained from 1×10^6 CTX-TNA2 cells (as 1 fold) for 16 h (B,D) Primary cultured cortical neurons were treated with hemin (30 μ M) plus 12H/24R exosomes (1 fold and 3 folds) for 16 h. Western blot assay was employed to measure iNOS (A,B) and COX-2 (C,D). Each lane contained 30 μ g protein for all experiments. Graphs show statistic results from relative optical density of bands on the blots. Values are the mean \pm S.E.M. ($n = 3$ /each group). *, $p < 0.05$ statistically significant in the hemin groups compared with the control groups; #, $P < 0.05$ in hemin plus exosomes compared with hemin alone by one-way ANOVA followed by the LSD test as *post hoc* method.

hemin (30 μ M)-induced neuroinflammation by increasing iNOS (Figures 4A,B) and COX-2 (Figures 4C,D) in hemin-treated primary cultured cortical neurons. Co-incubation with 2H/6R exosomes significantly prevented hemin-induced elevations in iNOS (Figure 4A) and COX-2 (Figure 4C). In contrast, 12H/24R exosomes further increased hemin-elevated iNOS (Figure 4B) and COX-2 (Figure 4D). These data indicated opposite effects of 2H/6R exosomes and 12H/24R exosomes on hemin-induced neuroinflammation. At the same time, we investigated the effects of exosomes on HO-1 expression (an enzyme catalyzing hemin). Western blot assay showed that co-incubation of H/6R exosomes but not 12H/24R significantly attenuated hemin-induced elevation in HO-1 expression (Figure 5), suggesting that 2H/6R exosomes can reduce hemin-induced HO-1 expression.

The neurotoxic mechanisms underlying hemin-induced neuronal death were investigated by measuring glutathione hydroperoxidase 4 (GPX4, a biomarker of ferroptosis) and

active caspase 3 (a biomarker of apoptosis). Western blot assay demonstrated that hemin (30 μ M) reduced GPX4 (Figures 6A,B) and increased active caspase 3 (Figures 6C,D). Co-incubation with 2H/6R exosomes attenuated hemin-induced reduction in GPX4 (Figure 6A) and elevation in active caspase 3 (Figure 6C). In contrast, 12H/24R exosomes did not alter hemin-induced reduction in GPX4 (Figure 6B) and elevation in active caspase 3 (Figure 6D), indicating indicate that 2H/6R exosomes appear to reduce hemin-induced ferroptosis and apoptosis.

Diverse cargos in 2H/6R exosomes and 12H/24R exosomes

So far, we have demonstrated differential effects of 2H/6R exosomes and 12H/24R exosomes on hemin-induced neurotoxicity; 2H/6R exosomes, but not 12H/24R exosomes, possessed a neuroprotective activity. The cargos, especially

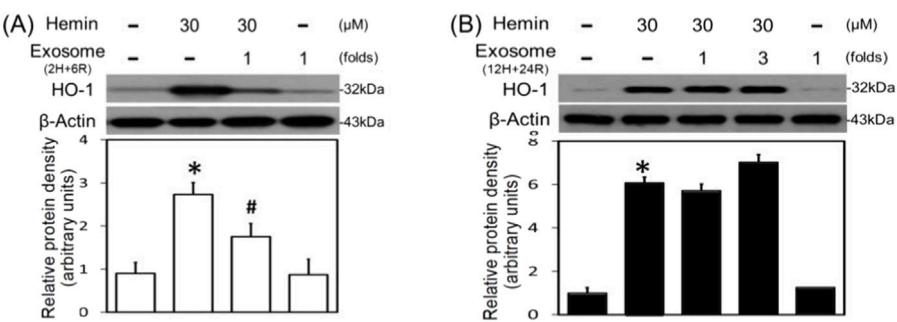


FIGURE 5 Differential effects of 2H/6R exosomes and 12H/24R exosomes on hemin-induced HO-1 expression in primary cultured cortical neurons. **(A)** Primary cultured cortical neurons were treated with hemin (30 μ M) plus 2H/6R exosomes obtained from 1×10^6 CTX-TNA2 cells (as 1-fold) for 16 h. **(B)** Primary cultured cortical neurons were treated with hemin (30 μ M) plus 12H/24R exosomes (1 fold and 3 folds) for 16 h. Western blot assay was employed to measure HO-1. Each lane contained 30 μ g protein for all experiments. Graphs show statistic results from relative optical density of bands on the blots. Values are the mean \pm S.E.M. (n = 3/each group). *, p < 0.05 statistically significant in the hemin groups compared with the control groups; #, P < 0.05 in hemin plus exosomes compared with hemin alone by one-way ANOVA followed by the LSD test as *post hoc* method.

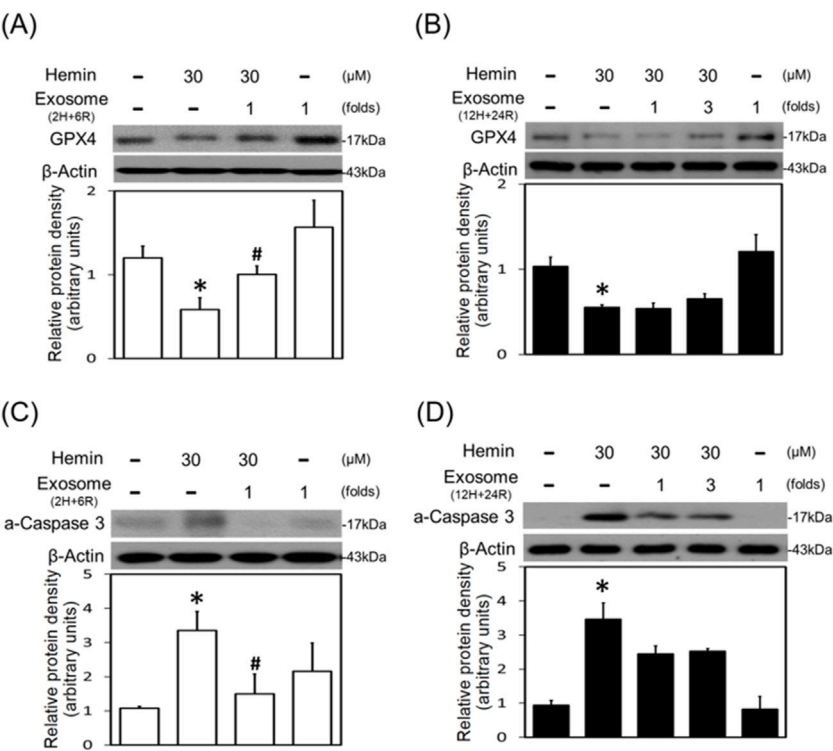


FIGURE 6 Differential effects of 2H/6R exosomes and 12H/24R exosomes on hemin-induced programmed cell death in primary cultured cortical neurons. **(A,C)** Primary cultured cortical neurons were treated with hemin (30 μ M) plus 2H/6R exosomes obtained from 1×10^6 CTX-TNA2 cells (as 1 fold) for 16 h **(B,D)** Primary cultured cortical neurons were treated with hemin (30 μ M) plus 12H/24R exosomes (1 fold and 3 folds) for 16 h. Western blot assay was employed to measure GPX4 **(A,B)** and active-caspase 3 **(C,D)**. Each lane contained 30 μ g protein for all experiments. Graphs show statistic results from relative optical density of bands on the blots. Values are the mean \pm S.E.M. (n = 3/each group). *, p < 0.05 statistically significant in the hemin groups compared with the control groups; #, P < 0.05 in hemin plus exosomes compared with hemin alone by one-way ANOVA followed by the LSD test as *post hoc* method.

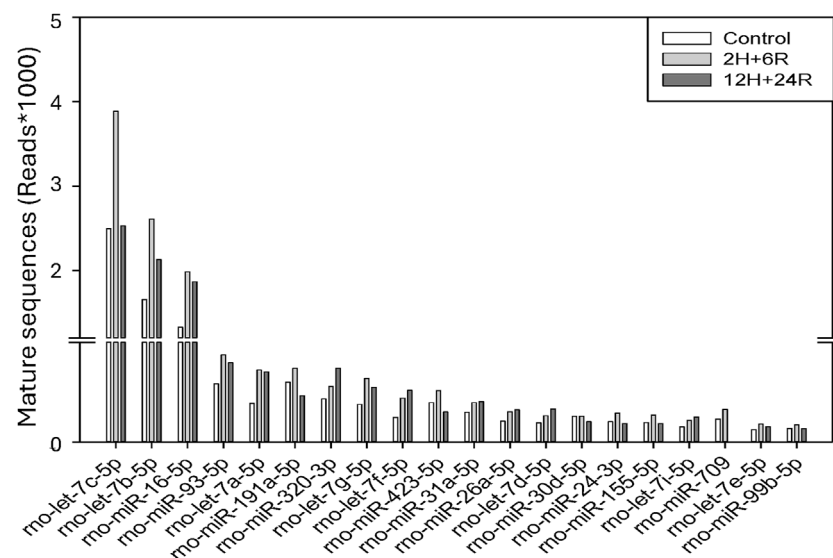


FIGURE 7

Cargos in control exosomes, 2H/6R and 12H/24R exosomes by miRNA sequencing analysis. Sequencing was performed with single-end reads (100 bp) at a depth exceeding 10 million reads per sample. miRNA expression levels were analyzed on the Qiagen GeneGlobe platform with UMI-based correction.

miRNA in both exosomes were analyzed using RNA Sequencing Analysis. We found significant changes in the miRNA expression profiles, including the expression levels of let-7c-5p, miR-191a-5p, and miR-709 in 2H/6R exosomes (Figure 7).

Discussion

In the present study, the effects of hypoxia on exosomes obtained from CTX-TNA2 cells exposed to different hypoxic preconditionings were delineated using hemin-induced neurotoxicity as follows. First, compared to the control exosomes, 2H/6R exosomes and 12H/24R exosomes did not show significant difference in exosomes secretion. Secondly, 2H/6R exosomes showed neuroprotective properties by attenuating hemin-induced neurotoxicity. However, 12H/24R exosomes appear to be proinflammatory by augmenting hemin-induced neuroinflammation. Our study showed that exosomes from CTX-TNA2 cells subjected to different hypoxic preconditionings possess opposite properties, suggesting that hypoxia plays a double-edged role in exosome's functions.

Hypoxia, a condition of insufficient oxygen, is reportedly an external factor that stimulates exosome secretion [22, 23]. Several *in vitro* studies on cancer biology have demonstrated that incubation of cancer cells under hypoxia (1% oxygen for 24–72 h) which mimicked hypoxia in the tumor microenvironment, increased exosome releases [14, 23]. At the

same time, exosomes from hypoxic cancer cells contain proangiogenic miRNA and growth factors for angiogenesis and cancer cell proliferation, respectively [14, 24], indicating that in addition to exosome secretion, hypoxia is capable of altering exosome's properties [23, 24]. To support this notion, two different hypoxic preconditionings were designed to treat CTX-TNA2 cells and collect exosomes from the cultured medium individually. Our data showed that hypoxia preconditionings significantly increased exosome biomarkers and slight increases in exosome size. Due to the lack of differences in particle concentration, one possible explanation is that more exosome biomarkers are expressed in each exosome. Our data suggested that hypoxic preconditioning did not significantly affect exosome secretion.

In contrast, hypoxic preconditioning significantly changed the properties of exosomes. To delineate the exosome's properties, we employed hemin [18] which is commonly used to mimic ICH-related secondary injury [25], including cytotoxicity, neurite impairment, HO-1 expression, neuroinflammation and program cell death. Hemin, a byproduct of hemoglobin degradation [26], is known as an HO-1 inducer to catalyze the degradation of heme/hemin and release iron [27], a Fenton's reagent which induce oxidative injury and subsequent cell death [28]. We found that 2H/6R exosomes attenuated hemin-induced neuronal death, neurite impairment and neuroinflammation. More importantly, 2H/6R exosomes significantly inhibited hemin-elevated HO-1 levels which resulted in less iron accumulation and

ameliorated subsequent apoptosis and ferroptosis, a programmed cell death related to iron metabolism. In contrast to the 2H/6R exosomes-induced neuroprotection, 12H/24R exosomes significantly augmented hemin-induced elevation in iNOS and COX-2, indicating that 12H/24R exosomes is proinflammatory. Due to the opposite effects of 2H/6R exosomes and 12H/24R exosomes on hemin-induced neurotoxicity, our data further support that hypoxia plays a double-edged role in regulating exosome functions.

A significant body of studies has focused on the pathological effects of hypoxia on CNS, including ICH. The pathophysiology of hypoxia depends on the duration of hypoxia, including acute, subacute and chronic hypoxia [29]. In addition to 2H/6R and 12H/24R, more hypoxia-renormoxia treatments were tested, including 3H/24R, 6H/24R, and 12H/24R (unpublished data). To avoid obtaining exosomes from unhealthy cells, we chose hypoxic duration from 2 to 12 h because hypoxia duration less than 12 h did not cause significant cytotoxicity. All cells are capable of releasing exosomes [1–3], including brain cells. In addition to CTX-TNA2 cells, we have tested different hypoxia-renormoxia conditions on primary cultured cortical neurons. The exosomes from primary cultured cortical neurons showed different biological activities from those from CTX-TNA2 (unpublished data). Accordingly, types and conditions of donor cells are the critical factors for exosome production [30].

To obtain “good” exosomes from hypoxic cells, it is important to design an ideal hypoxic condition, including optimal duration (2–72 h) [14] and intensity (0.1%–5% oxygen) [13, 31]. For example, exosomes obtained from MSCs subjected to 48-h hypoxia (1% O₂) were reportedly more efficacious to bone fracture healing [10]. In addition, exosomes from hypoxic donor cells (3% for 24 h) were found to be neuroprotective to attenuate program cell death induced by OGD/reperfusion [32]. “As an important intercellular mediator, “cargos” in the exosomes, including miRNAs, are the key element for its functions [30]. For example, miR-92b-3p in the exosomes released from OGD-treated astrocytes has been suggested to mediate the neuroprotection against OGD-induced neurotoxicity [33]. Furthermore, exosome-delivered miR216a-5p from hypoxic preconditioned-MSCs is suggested to repair spinal cord injury [34]. In the present study, we identified several miRNAs elevated in the 2H/6R exosomes, including let-7c-5p which has been suggested to be neuroprotective against cerebral ischemia [35]. Accordingly, 2H/6R treatment may produce “good” exosomes for neuroprotection.

In conclusion, hypoxia has been used as a strategy to enhance exosome secretion. However, beyond the quantity of released exosomes, it is equally important to characterize how hypoxia simultaneously affects exosomes’ properties. Given that function

of exosomes is closely tied to the conditions of donor cells, our data demonstrated that CTX-TNA2 cells exposed to varying hypoxia-renormoxia treatments produce exosomes with opposite functional profiles. The present study demonstrates the complex effects of hypoxia as well as a double-edged role of hypoxia on exosome functionality.

Author contributions

All authors listed have made a substantial, direct, and intellectual contribution to the work and approved it for publication.

Data availability

The original contributions presented in the study are included in the article/supplementary material, further inquiries can be directed to the corresponding author.

Ethics statement

The animal study was approved by the Institutional Animal Care and Use Committee (IACUC) of Taipei Veterans General Hospital (TVGH), Taipei, Taiwan. The study was conducted in accordance with the local legislation and institutional requirements.

Funding

The author(s) declare that financial support was received for the research and/or publication of this article. The NSTC grant NSTC 113-2320-B-A49-033 and VGHTPE grant V113C-022.

Conflict of interest

The author(s) declared no potential conflicts of interest with respect to the research, authorship, and/or publication of this article.

Generative AI statement

The authors declare that no Generative AI was used in the creation of this manuscript.

References

- Zhang Y, Liu Y, Liu H, Tang WH. Exosomes: biogenesis, biologic function and clinical potential. *Cell Biosci* (2019) 9:19. doi:10.1186/s13578-019-0282-2
- Stahl AL, Johansson K, Mossberg M, Kahn R, Karpman D. Exosomes and microvesicles in normal physiology, pathophysiology, and renal diseases. *Pediatr Nephrol* (2019) 34:11–30. doi:10.1007/s00467-017-3816-z
- Krylova SV, Feng D. The machinery of exosomes: biogenesis, release, and uptake. *Int J Mol Sci* (2023) 24:1337. doi:10.3390/ijms24021337
- Jiang H, Zhao H, Zhang M, He Y, Li X, Xu Y, et al. Hypoxia induced changes of exosome cargo and subsequent biological effects. *Front Immunol* (2022) 13:824188. doi:10.3389/fimmu.2022.824188
- Rahmati S, Shojai F, Shojaei A, Rezakhani L, Dehkordi MB. An overview of current knowledge in biological functions and potential therapeutic applications of exosomes. *Chem Phys Lipids* (2020) 226:104836. doi:10.1016/j.chemphyslip.2019.104836
- Lotfy A, AboQuella NM, Wang H. Mesenchymal stromal/stem cell (MSC)-derived exosomes in clinical trials. *Stem Cell Res Ther* (2023) 14:66. doi:10.1186/s13287-023-03287-7
- Rosand Ø, Høydal MA. Cardiac exosomes in ischemic heart disease- A narrative review. *Diagnostics* (Basel) (2021) 11:269. doi:10.3390/diagnostics11020269
- Shokravi S, Borisov V, Zaman BA, Niazvand F, Hazrati R, Khah MM, et al. Mesenchymal stromal cells (MSCs) and their exosome in acute liver failure (ALF): a comprehensive review. *Stem Cell Res Ther* (2022) 13:192. doi:10.1186/s13287-022-02825-z
- Yamashita T, Takahashi Y, Takakura Y. Possibility of exosome-based therapeutics and challenges in production of exosomes eligible for therapeutic application. *Biol Pharm Bull* (2018) 41:835–42. doi:10.1248/bpb.b18-00133
- Liu W, Li L, Rong Y, Qian D, Chen J, Zhou Z, et al. Hypoxic mesenchymal stem cell-derived exosomes promote bone fracture healing by the transfer of miR-126. *Acta Biomater* (2020) 103:196–212. doi:10.1016/j.actbio.2019.12.020
- Michiels C. Physiological and pathological responses to hypoxia. *Am J Pathol* (2004) 164:1875–82. doi:10.1016/s0002-9440(10)63747-9
- Lee P, Chandel NS, Simon MC. Cellular adaptation to hypoxia through hypoxia inducible factors and beyond. *Nat Rev Mol Cell Biol* (2020) 21:268–83. doi:10.1038/s41580-020-0227-y
- King HW, Michael MZ, Gleadle JM. Hypoxic enhancement of exosome release by breast cancer cells. *BMC Cancer* (2012) 12:421. doi:10.1186/1471-2407-12-421
- Zeng Z, Zhao Y, Chen Q, Zhu S, Niu Y, Ye Z, et al. Hypoxic exosomal HIF-1 α -stabilizing circZNF91 promotes chemoresistance of normoxic pancreatic cancer cells via enhancing glycolysis. *Oncogene* (2021) 40:5505–17. doi:10.1038/s41388-021-01960-w
- Wang CH, Chang A, Tsai MJ, Cheng H, Liao L, Lin AM. Kainic acid-induced oxidative injury is attenuated by hypoxic preconditioning. *Ann N Y Acad Sci* (2005) 1042:314–24. doi:10.1196/annals.1338.054
- Lin AM, Dung SW, Chen CF, Chen W, Ho L. Hypoxic preconditioning prevents cortical infarction by transient focal ischemia-reperfusion. *Ann N Y Acad Sci* (2003) 993:168–78. doi:10.1111/j.1749-6632.2003.tb07527.x
- Tzeng YW, Lee LY, Chao PL, Lee H, Wu R, Lin A. Role of autophagy in protection afforded by hypoxic preconditioning against MPP $^{+}$ -induced neurotoxicity in SH-SY5Y cells. *Free Radic Biol Med* (2010) 49:839–46. doi:10.1016/j.freeradbiomed.2010.06.004
- Syed B, Nirwane A, Yao Y. *In vitro* models of intracerebral hemorrhage. *Brain Hemorrhages* (2022) 3:105–7. doi:10.1016/j.hest.2022.06.002
- Sofroniew MV, Vinters HV. Astrocytes: biology and pathology. *Acta Neuropathol* (2010) 119:7–35. doi:10.1007/s00401-009-0619-8
- Fan YY, Huo J. A1/A2 astrocytes in central nervous system injuries and diseases: angels or devils? *Neurochem Int* (2021) 148:105080. doi:10.1016/j.neuint.2021.105080
- Verkhatsky A, Butt A, Li B, Illes P, Zorec R, Semyanov A, et al. Astrocytes in human central nervous system diseases: a frontier for new therapies. *Signal Transduction Targeted Ther* (2023) 8:396. doi:10.1038/s41392-023-01628-9
- Debbi L, Guo S, Safina D, Levenberg S. Boosting extracellular vesicle secretion. *Biotechnol Adv* (2022) 59:107983. doi:10.1016/j.biotechadv.2022.107983
- Tse SW, Tan CF, Park JE, Gnanasekaran J, Gupta N, Low JK, et al. Microenvironmental hypoxia induces dynamic changes in lung cancer synthesis and secretion of extracellular vesicles. *Cancers (Basel)* (2020) 12:2917. doi:10.3390/cancers12102917
- Shao C, Yang F, Miao S, Liu W, Wang C, Shu Y, et al. Role of hypoxia-induced exosomes in tumor biology. *Mol Cancer* (2018) 17:120. doi:10.1186/s12943-018-0869-y
- Shao Z, Tu S, Shao A. Pathophysiological mechanisms and potential therapeutic targets in intracerebral hemorrhage. *Front Pharmacol* (2019) 10:1079. doi:10.3389/fphar.2019.01079
- Ponka P. Cell biology of heme. *Am J Med Sci* (1999) 318:241–56. doi:10.1097/0000441-199910000-00004
- Le LL, Li XY, Meng D, Liang Q, Wang X, Li N, et al. Heme oxygenase-1 mediated memorial and revivable protective effect of ischemic preconditioning on brain injury. *CNS Neurosci Ther* (2013) 19:963–8. doi:10.1111/cns.12152
- Winterbourn CC. Toxicity of iron and hydrogen peroxide: the Fenton reaction. *Toxicol Lett* (1995) 82:83:969–74. doi:10.1016/0378-4274(95)03532-x
- Mukandala G, Tynan R, Lanigan S, O'Connor J. The effects of hypoxia and inflammation on synaptic signaling in the CNS. *Brain Sci* (2016) 6:6. doi:10.3390/brainsci6101006
- Yang R, Li Z, Xu J, Luo J, Qu Z, Chen X, et al. Role of hypoxic exosomes and the mechanisms of exosome release in the CNS under hypoxic conditions. *Front Neurol* (2023) 14:1198546. doi:10.3389/fneur.2023.1198546
- Han Y, Ren J, Bai Y, Pei X, Han Y. Exosomes from hypoxia-treated human adipose-derived mesenchymal stem cells enhance angiogenesis through VEGF/VEGF-R. *Int J Biochem and Cel Biol* (2019) 109:59–68. doi:10.1016/j.biocel.2019.01.017
- Deng C, Dong K, Liu Y, Chen K, Min C, Cao Z, et al. Hypoxic mesenchymal stem cell-derived exosomes promote the survival of skin flaps after ischaemia-reperfusion injury via mTOR/ULK1/FUNDC1 pathways. *J Nanobiotechnology* (2023) 21:340. doi:10.1186/s12951-023-02098-5
- Xu L, Cao H, Xie Y, Zhang Y, Du M, Xu X, et al. Exosome-shuttled miR-92b-3p from ischemic preconditioned astrocytes protects neurons against oxygen and glucose deprivation. *Brain Res* (2019) 1717:66–73. doi:10.1016/j.brainres.2019.04.009
- Liu W, Rong Y, Wang J, Zhou Z, Ge X, Ji C, et al. Exosome-shuttled miR-216a-5p from hypoxic preconditioned mesenchymal stem cells repair traumatic spinal cord injury by shifting microglial M1/M2 polarization. *J Neuroinflammation* (2020) 17:47. doi:10.1186/s12974-020-1726-7
- Ni J, Wang X, Chen S, Liu H, Wang Y, Xu X, et al. MicroRNA let-7c-5p protects against cerebral ischemia injury via mechanisms involving the inhibition of microglia activation. *Brain Behav Immun* (2015) 49:75–85. doi:10.1016/j.bbi.2015.04.014



OPEN ACCESS

*CORRESPONDENCE

Damien P. Kuffler,
✉ dkuffler@hotmail.com

RECEIVED 05 March 2025

ACCEPTED 29 April 2025

PUBLISHED 27 May 2025

CITATION

Foy CA and Kuffler DP (2025) Limitations to clinically restoring meaningful peripheral nerve function across gaps and overcoming them.
Exp. Biol. Med. 250:10566.
doi: 10.3389/ebm.2025.10566

COPYRIGHT

© 2025 Foy and Kuffler. This is an open-access article distributed under the terms of the [Creative Commons Attribution License \(CC BY\)](https://creativecommons.org/licenses/by/4.0/). The use, distribution or reproduction in other forums is permitted, provided the original author(s) and the copyright owner(s) are credited and that the original publication in this journal is cited, in accordance with accepted academic practice. No use, distribution or reproduction is permitted which does not comply with these terms.

Limitations to clinically restoring meaningful peripheral nerve function across gaps and overcoming them

Christian A. Foy¹ and Damien P. Kuffler^{2*}

¹Section of Orthopedic Surgery, University of Puerto Rico, San Juan, PR, United States, ²Institute of Neurobiology, Medical School, University of Puerto Rico, San Juan, PR, United States

Abstract

Clinically, reliably restoring meaningful peripheral sensory and motor nerve function across peripheral nerve gaps is limited. Thus, although autografts are the clinical “gold standard” repair technique for bridging nerve gaps, even under relatively good conditions, <50% of patients recover meaningful function. Due to this low recovery rate, many patients are not even provided repair surgery and, consequently, suffer permanent loss of function. This paper examines intrinsic and extrinsic changes associated with injured neurons and Schwann cells that reduce the extent of axon regeneration and recovery. It also examines how these changes can be reversed, leading to enhanced regeneration and recovery. It next examines the efficacy of platelet-rich plasma (PRP) in promoting axon regeneration and two novel techniques involving bridging nerve gaps with an autograft within a platelet-rich (PRP) collagen tube or only a PRP-filled collagen tube, which induce meaningful recovery under conditions where autografts alone are not effective. Finally, it looks at potential mechanisms by which platelet-released factors may enhance axon regeneration and recovery. This review shows that although there are many limitations to restoring meaningful function following peripheral nerve trauma, there are a number of ways these can be overcome. Presently, the most promising techniques involve using PRP.

KEYWORDS

allograft, axon regeneration, collagen tube, nerve gap, nerve trauma, peripheral nerve repair, platelet-rich fibrin, PRP

Impact statement

Restoring clinical function following peripheral nerve trauma is restricted by neuron and Schwann cell intrinsic and extrinsic limitations. Further, autografts, the current clinical “gold stand” technique for bridging nerve gaps to restore function, suffer many significant limitations in restoring meaningful functional recovery. This review discusses intrinsic and extrinsic limitations to regeneration and how they can be overcome. It also discusses how the application of platelet-rich plasma (PRP) promotes axon regeneration

and how its influences can be increased or decreased. It then discusses how, clinically, bridging nerve gaps with autograft within a PRP-filled collagen tube induces axon regeneration and recovery under currently impossible conditions. It concludes with a discussion of the potential mechanisms by which platelet-released factors may exert their influences. Understanding what limits axon regeneration and recovery and how these limitations can be overcome will lead to developing new clinical techniques that induce more extensive axon regeneration and recovery.

Introduction

Sensory nerve autografts, the clinical “gold standard” technique for restoring function across peripheral nerve gaps [1], have substantial limitations. Therefore, there is a good prognosis for reliable, meaningful sensory and motor function only when (1) the repairs are performed ≤ 5 months post-trauma [2–4], with recovery decreasing with longer delays [3–6] (2) the gaps are < 5 (cm) [7, 8], with recovery decreasing for longer gaps [2, 3, 8, 9], few axons regenerate across grafts ≥ 8 cm in length [2, 10, 11], and none across autografts > 10 cm [3, 5], and (3) patients are ≤ 20 –25 years old, with recovery decreasing with increasing ages [3, 4, 6]. Finally, there is little to no recovery when the values of two or all three variables increase simultaneously [9, 12]. Therefore, $< 50\%$ of subjects recover meaningful sensory or motor functions [13]. These findings raise the question of what underlies these limitations and how can they be reduced, leading to improved recovery.

Injury-induced intrinsic neuronal changes reduce their capacity to extend axons

Partly underlying the decreased capacity of aged and long-term axotomized neurons to extend axons are changes in their intrinsic properties [14]. These neurons lose their capacity to extend axons, and those extended regenerate only short distances [15, 16] while regenerating more slowly than normal [17]. Thus, by > 4 months post-nerve injury, only about 33% of neurons can extend an axon [15, 18], and for those that retain the capacity, it is reduced to $\sim 10\%$ of normal [16].

Reduced protein synthesis

The c-Jun transcription factor is critical for neurons' capacity to extend axons, and nerve injury induces neuronal up-regulation of c-Jun expression. However, with increasing time of axotomy, c-Jun expression decreases, paralleling the loss of neurons' capacity to extend axons [19]. This change is also associated with the down-regulation of genes for regeneration-

promoting neurotrophic factors, such as GAP-43 and $\alpha 1$ -tubulin [20], NGF [21], BDNF, and CNTF [16, 22]. Thus, the age-associated decrease in axon regeneration is due to reduced protein synthesis, which is required to induce the neurons' soma to respond to injury by triggering the regeneration process and growth cone extension [23–25]. This process also involves decreased levels of axonal translation proteins and the inability of neurons to increase the translation of regeneration-promoting axonal mRNAs released from stress granules [26]. The decrease is also associated with an increasing age-associated decrease in neurofilament mRNA levels and neurofilament proteins [27], and the loss of Nrg1, which reduces axon-Schwann cell interactions and remyelination after nerve crush, further reducing neurons' capacity to extend axons [28].

Decreased metabolism and axoplasmic transport

Neurite outgrowth from neonatal neurons *in vitro* is 40% faster than adult neurons [29]. This is attributed to an age-related decrease in cytoskeletal protein expression [30] and axoplasmic transport, which are required for axon elongation [30, 31]. This is because axon regeneration requires energy metabolism, which involves oxidative glycolysis and the formation of high-energy phosphate compounds, most importantly creatine phosphate and ATP [32]. Increasing age is also associated with a decrease in the levels of endoneurial ATP and creatine phosphate [30], which would, therefore, restrict the extent of axon regeneration.

Reversing injury-induced intrinsic neuronal changes allows neurons to extend axons by promoting neuron protein synthesis

Axon regeneration following a sciatic nerve crush is promoted by enhanced protein synthesis due to enhanced local translation and production of the protein synthesis machinery [26]. This involves dissolving stress granules, resulting in their releasing sequestered mRNAs and translation factors [33]. Further, following rat sciatic nerve injury, Nrg1 treatment increases axon diameter, myelin thickness, distance axons regenerate, and both the extent [34] and rate of recovery [35]. These effects are partly induced by neuron-released Nrg1 promoting Schwann cell differentiation, proliferation, migration, and myelination [28, 36–41].

Electrical stimulation

As mentioned, long-term axotomy results in 33% of neurons losing their capacity to extend axons. However, electrical stimulation results in a 34%–50% increase in the number of

neurons extending axons [42] and a 2.3-fold increase in the extent of axon sprouting from transected axons [43] while also increasing the speed of axon regeneration [17, 42]. This influence is exerted through various mechanisms, including direct actions on axotomized neurons [17, 44–47]. The influence of electrical stimulation is similar when applied to acute and long-term injured neurons [46, 48].

Injury-induced extrinsic neuronal changes reduce their capacity to extend axons

Reduced Schwann cell capacity to support neuron

Schwann cells release the cytokines MCP-1 and LIF [49], which recruit macrophages and convert them from the M1 to the M2 phenotype. These macrophages secrete high levels of cytokines, which promote axonal outgrowth [50]. However, nerve injury deprives Schwann cells of axon contact, causing them to become senescent and stop producing and releasing neurotrophic factors. Schwann cell development of senescence parallels the decrease in the extent of axon regeneration [8]. Thus, long autografts do not induce axon regeneration and recovery because by the time the axons reach the distal end of the autograft, the Schwann cells have become senescent and do not support axon regeneration [8].

Schwann cell senescence is also associated with a reduction in their c-Jun expression [51], loss of their injury-induced repair phenotype [8, 22, 38, 52], and their down-regulation of the genes for factors required for Schwann cells to support axon regeneration and proteins required to myelinate axons [30]. These include S100, p75, GFAP, BDNF, NGF, NT-3, NT-4, CNTF, GDNF, and small molecule trkB agonists.

Schwann cell senescence also leads to their inability to synthesize and release VEGF [53]. VEGF is essential for inducing vascularization and recruiting macrophages [54, 55] to the injury site, where the macrophage normally also releases VEGF [55, 56]. In addition, senescent Schwann cells lose their capacity to phagocytize axon and myelin debris [57], and without its removal, it inhibits axon regeneration [30]. Therefore, maximizing functional recovery requires nerve repairs be performed <3–6 months post-trauma [3, 9, 58].

Reversing injury-induced extrinsic neuronal changes by reactivating Schwann cells: applying neurotrophic factors and restoring c-Jun

Nerve injury induces Schwann cell up-regulation of Shh, which induces c-Jun expression [59–61], which leads to c-Jun

enhancing axon regeneration through autografts and *in vitro* [62]. However, with prolonged denervation and aging, c-Jun expression decreases in Schwann cells, which is associated with decreased axon regeneration [51]. Nevertheless, axon regeneration can be promoted by reactivating senescent Schwann cells by applying neurotrophic factors, which restores normal levels of Shh and c-Jun expression [63].

Reactivating Schwann cells: applying electrical stimulation

Electrical stimulation reactivates Senescent Schwann cells. This induces their expression of P0, Par-3, BDNF, NGF, and GDNF, which initiate and enhance axon regeneration and myelination [64–66].

PRP promotes axon regeneration

Platelet-released factors

Platelets contain and release an evolutionarily complex cocktail of factors, including high levels of neurotrophic and other growth factors, such as IL-10, insulin-like growth factors 1 and 2, VEGF [67], BDNF [68], transforming growth factor- β 1, HGF, and FGF. This allows platelets to play different essential roles in tissue healing and promoting axon regeneration [69–72].

In animal model studies, PRP significantly enhances the extent of axon regeneration when injected into a nerve following a nerve crush [73], is applied to sites of a nerve crush [74–78], neurorrhaphy [69, 79–82], site of rat prostatectomy [83], following nerve crush, *mycobacterium leprae* (leprosy bacteria) -induced lesion [84], sucrose-induced injury [85], autografts [86, 87], acellular allografts [88], when applied onto or injected into neurorrhaphy sites [89–92], is injected onto injured nerves [89, 93, 94], or short nerve gaps within the preserved epineurium [95], PRP exosomes are injected under the perineurium [96], and site of carpal tunnel syndrome [97–99]. However, questions have been raised about the efficacy of PRP in treating carpal tunnel syndrome [100].

PRP is similarly effective when added to vein grafts [67, 101–104], conduits composed of many different materials [105–111], and when combined with other cells, such as nMSCs [80] applied outside [86] or inside acellular allografts [88], when conduits are composed of platelet gel [112] or platelet-rich fibrin (PRF) [113, 114]. The PRP can induce axon regeneration that is as effective as autologous nerve grafts [112]. It is important to note that when PRP is applied to a rat sciatic nerve crush site, its influence is increased by surrounding the site with a collagen tube [70].

Clinically, bridging nerve gaps with an autograft within a PRP-filled collagen tube [115–118], or only a PRP-filled collagen

tube [118], induces meaningful recovery under conditions where allografts alone are ineffective. Thus, platelet-released factors alone can induce axon regeneration.

PRP-containing leukocytes

Leukocytes are reported to negatively affect axon regeneration by releasing catabolic cytokines and inducing inflammation [119, 120], while leukocyte-poor PRP (LP-PRP) exerts anabolic effects that promote axon regeneration [121, 122]. However, PRP efficacy is reported to increase with increasing leukocytes and white blood cells concentrations, and bioactivity of platelet-released factors. Platelet growth factor concentrations in leukocyte-rich PRP (LR-PRP) depend on the leukocyte concentrations, with the catabolic protease MMP-9 expressed at a considerably high concentration in the LR-PRP [121]. LR-PRP releases significantly more inflammatory mediators, such as TNF- α , IL-6, and IFN- γ than LP-PRP. However, it also increases the release of the anti-inflammatory mediators IL-4 and IL-10 [123, 124]. The combination and concentration of PRP platelets, leukocytes, and erythrocytes influence the extent of these factors' release [120].

A case report showed that LR-PRP induces meaningful recoveries despite long nerve gaps being repaired with a long repair delay, even in an older subject [118]. This influence is greater than that seen in other studies. The better recovery may be because the PRP was prepared using the Zimmer Biomet GPS III centrifuge system, which increases the platelet concentration 9.3-fold and leukocyte concentration 5-fold (Zimmer Biomet Data on File. Validation Report, GPS III Platelet Concentrator, Test new design for GPS III Buoy re-design, OT000183, 2007), which is at least two times higher than in PRP prepared using other devices [125–127].

The influence of PRP is also affected by its concentration of factors, which is influenced by how PRP is prepared [128]. FGF and TGF are rapidly released from platelets, with their concentration decreasing over time, while PDGF and VEGF are released at a constant rate for 7 days [128]. PRP from the Biomet GPS III has the highest concentrations of VEGF and MMP-9 but the lowest TGF concentration [128]. However, it has also been shown that the concentration of cytokines is not directly related to the cellular composition of PRP [128].

Angiogenesis

Proteomics analysis found that the local application of PRP significantly increases integrin β -8 (ITGB8) expression [95], which promotes angiogenesis [129, 130]. In addition to providing oxygenation to the region of the regenerating axons, Schwann cells use these new blood vessels as their pathway to migrate into the injury site, forming Schwann cell cords that

facilitate axon regeneration [55]. Thus, it has been proposed that PRP-released factors contribute significantly to axon regeneration by promoting vascularization, leading to the migration of cells by activating the FAK pathway mediated by integrin β 1 [131, 132].

Limitations of PRP

While many studies show that PRP promotes axon regeneration and recovery, the extent of the efficacy varies greatly. This is unsurprising because no standard techniques exist for preparing or applying PRP. The simplest and least expensive PRP preparation technique is single spin separation, which yields an increased platelet concentration of 2.67-fold [133], while the double spin technique increased it by 2.48 - 5.71-fold, with a mean of 3.47-fold [134]. A PRP 2.5-3.5-fold increased platelet concentration is considerably less effective in rats than a 4.5 - 6.5- or 7.5 - 8.5-fold increase, although both higher concentrations induce similar influences [135].

Working with New Zealand white rabbit 5 mm nerve gaps, PRP with a 2.5–3.5-fold increased platelet concentration induces limited axon regeneration, significantly greater with the higher concentration of 4.5–6.5-fold and 7.5–8.5-fold [95]. Although a 5-fold increased platelet concentration is recommended as the minimum to exert a meaningful physiological effect [136], the optimal concentration for maximal analgesia remains unknown.

pH

Various devices yield PRP with higher acidification than normal blood, reducing it from 7.35 to 6.8–6.5 [137, 138]. This decreases platelet aggregation by >25% [139–141] and reduces platelet sensitivity to thrombin, resulting in decreased platelet activation, which reduces PRP efficacy. Therefore, it is necessary to avoid PRP acidification during its preparation.

Glucose

Different PRP preparation devices yield PRP with glucose concentrations increased 3- to 6-fold over the starting blood [138]. Increasing PRP glucose concentration increases platelet activation [142]. Therefore, maximizing the efficacy of PRP required avoiding changes in its glucose level.

Diet and physiology affect PRP efficacy

A patient's physiology and diet can greatly affect PRP efficacy. Smoking increases platelet aggregation [143], while

alcohol consumption decreases platelet activation and aggregation [144] and reduces platelet responses to thrombin [145] and collagen. Diets including isoflavones [146], caffeine [147], quercetin, a flavonoid [148], and anthocyanins [149] reduce platelet aggregation. Conversely, diets of high saturated fats [150], simple carbohydrates [150], or excessive sugar [151] increase platelet aggregation. Platelets in patients with high blood pressure have lower concentrations of factors than platelets of patients with normal blood pressure [152] and have a decreased whole blood platelet count [153].

Platelet activation methods

The PRP efficacy is influenced by (1) whether its platelets are activated before or when PRP is applied, (2) the timing of platelet release, (3) the ratios of the various platelet released factors, and (4) their level of bioactivity [154]. Therefore, PRP that does not comply with the necessary physiological parameters will not exert maximal effects [155].

Potential mechanisms by which platelet-released factors increase axon regeneration

Platelets contain more than 300 identified factors [156, 157]. Many of these have been shown to play important roles in promoting axon regeneration and recovery. However, space limitations do now allow a discussion of these factors.

Conclusion

Over the past 70 years, little progress has been made clinically in increasing the percentage of patients who recover meaningful function following peripheral nerve injuries and repairs. Two

significant steps forward are the demonstration that, clinically, electrical stimulation and the application of PRP enhance axon regeneration and the extent of recovery. However, the efficacy of PRP varies greatly, within and between studies, which may result from differences in how the PRP is prepared and applied, as well as the patient's physiological status. Therefore, to optimize the influence of PRP, it is necessary to develop a standardized PRP preparation and application protocol. However, it is also necessary to determine which of a subject's physiological properties, such as diet, consumption of drugs, smoking, and alcohol, must be changed to allow PRP to exert its maximal influences.

Author contributions

All authors contributed to the article and approved the submitted version.

Funding

The author(s) declare that no financial support was received for the research and/or publication of this article.

Conflict of interest

The authors declare that the research was conducted in the absence of any commercial or financial relationships that could be construed as a potential conflict of interest.

Generative AI statement

The author(s) declare that no Generative AI was used in the creation of this manuscript.

References

- Nichols CM, Brenner MJ, Fox IK, Tung TH, Hunter DA, Rickman SR, et al. Effects of motor versus sensory nerve grafts on peripheral nerve regeneration. *Exp Neurol* (2004) **190**(2):347–55. doi:10.1016/j.expneurol.2004.08.003
- Kornfeld T, Vogt PM, Radtke C. Nerve grafting for peripheral nerve injuries with extended defect sizes. *Wien Med Wochenschr* (2019) **169**(9–10):240–51. doi:10.1007/s10354-018-0675-6
- Karabeg R, Jakirlic M, Dujso V. Sensory recovery after forearm median and ulnar nerve grafting. *Medicinski Arhiv* (2009) **63**(2):97–9.
- Ruijs AC, Jaquet JB, Kalmijn S, Giele H, Hovius SER. Median and ulnar nerve injuries: a meta-analysis of predictors of motor and sensory recovery after modern microsurgical nerve repair. *Plast Reconstr Surg* (2005) **116**(2):484–94. doi:10.1097/01.prs.0000172896.86594.07
- Shergill G, Bonney G, Munshi P, Birch R. The radial and posterior interosseous nerves. Results of 260 repairs. *The J Bone Jt Surg Br volume* (2001) **83-B**(5):646–9. doi:10.1302/0301-620x.83b5.0830646
- Lohmeyer JA, Sommer B, Siemers F, Mailänder P. Nerve injuries of the upper extremity-expected outcome and clinical examination. *Plast Surg Nurs* (2009) **29**(2):88–93. doi:10.1097/01.psn.0000356867.18220.73
- Pan D, Mackinnon SE, Wood MD. Advances in the repair of segmental nerve injuries and trends in reconstruction. *Muscle and Nerve* (2020) **61**(6):726–39. doi:10.1002/mus.26797
- Hoben GM, Ee X, Schellhardt L, Yan Y, Hunter DA, Moore AM, et al. Increasing nerve autograft length increases senescence and reduces regeneration. *Plast and Reconstr Surg* (2018) **142**(4):952–61. doi:10.1097/prs.0000000000004759
- Campodonico A, Pangrazi PP, De Francesco F, Riccio M. Reconstruction of a long defect of the median nerve with a free nerve conduit flap. *Arch Plast Surg* (2020) **47**(2):187–93. doi:10.5999/aps.2019.00654
- Lee YH, Chung MS, Gong HS, Chung JY, Park JH, Baek GH. Sural nerve autografts for high radial nerve injury with nine centimeter or greater defects. *J Hand Surg* (2008) **33**(1):83–6. doi:10.1016/j.jhnsa.2007.10.004

11. Wolfe SW, Johnsen PH, Lee SK, Feinberg JH. Long-nerve grafts and nerve transfers demonstrate comparable outcomes for axillary nerve injuries. *J Hand Surg* (2014) **39**(7):1351–7. doi:10.1016/j.jhssa.2014.02.032
12. Grinsell D, Keating CP. Peripheral nerve reconstruction after injury: a review of clinical and experimental therapies. *Biomed Res Int* (2014) **2014**:1–13. doi:10.1155/2014/698256
13. Yang M, Rawson JL, Zhang EW, Arnold P, Lineaweaver W, Zhang F. Comparisons of outcomes from repair of median nerve and ulnar nerve defect with nerve graft and tubulization: a meta-analysis. *J Reconstr Microsurg* (2011) **27**(8):451–60. doi:10.1055/s-0031-1281526
14. Fawcett JW, Verhaagen J. Intrinsic determinants of axon regeneration. *Develop Neurobiol* (2018) **78**(10):890–7. doi:10.1002/dneu.22637
15. Furey MJ, Midha R, Xu QG, Belkas J, Gordon T. Prolonged target deprivation reduces the capacity of injured motoneurons to regenerate. *Neurosurgery* (2007) **60**(4):723–33. doi:10.1227/01.neu.0000255412.63184.cc
16. Gordon T. The physiology of neural injury and regeneration: the role of neurotrophic factors. *J Commun Disord* (2010) **43**(4):265–73. doi:10.1016/j.jcomdis.2010.04.003
17. Singh B, Xu QG, Franz CK, Zhang R, Dalton C, Gordon T, et al. Accelerated axon outgrowth, guidance, and target reinnervation across nerve transection gaps following a brief electrical stimulation paradigm. *J Neurosurg* (2012) **116**(3):498–512. doi:10.3171/2011.10.jns11612
18. Fu SY, Gordon T. Contributing factors to poor functional recovery after delayed nerve repair: prolonged denervation. *J Neurosci* (1995) **15**(5 Pt 2):3886–95. doi:10.1523/jneurosci.15-05-03886.1995
19. Jessen KR, Mirsky R. The repair Schwann cell and its function in regenerating nerves. *J Physiol* (2016) **594**(13):3521–31. doi:10.1113/jp270874
20. Gordon T, Tetzlaff W. Regeneration-associated genes decline in chronically injured rat sciatic motoneurons. *Eur J Neurosci* (2015) **42**(10):2783–91. doi:10.1111/ejn.13070
21. Michalski B, Bain JR, Fahnstock M. Long-term changes in neurotrophic factor expression in distal nerve stump following denervation and reinnervation with motor or sensory nerve. *J Neurochem* (2008) **105**(4):1244–52. doi:10.1111/j.1471-4159.2008.05224.x
22. Saheb-Al-Zamani M, Yan Y, Farber SJ, Hunter DA, Newton P, Wood MD, et al. Limited regeneration in long acellular nerve allografts is associated with increased Schwann cell senescence. *Exp Neurol* (2013) **247**:165–77. doi:10.1016/j.expneurol.2013.04.011
23. Verma P, Chierzi S, Codd AM, Campbell DS, Meyer RL, Holt CE, et al. Axonal protein synthesis and degradation are necessary for efficient growth cone regeneration. *J Neurosci* (2005) **25**(2):331–42. doi:10.1523/jneurosci.3073-04.2005
24. Ji SJ, Jaffrey SR. Axonal transcription factors: novel regulators of growth cone-to-nucleus signaling. *Develop Neurobiol* (2014) **74**(3):245–58. doi:10.1002/dneu.22112
25. Pacheco A, Merianda TT, Twiss JL, Gallo G. Mechanism and role of the intra-axonal Calreticulin translation in response to axonal injury. *Exp Neurol* (2020) **323**:113072. doi:10.1016/j.expneurol.2019.113072
26. van Erp S, van Berkel AA, Feenstra EM, Sahoo PK, Wagstaff LJ, Twiss JL, et al. Age-related loss of axonal regeneration is reflected by the level of local translation. *Exp Neurol* (2021) **339**:113594. doi:10.1016/j.expneurol.2020.113594
27. Parhad IM, Scott JN, Cellars LA, Bains JS, Krekoski CA, Clark AW. Axonal atrophy in aging is associated with a decline in neurofilament gene expression. *J Neurosci Res* (1995) **41**(3):355–66. doi:10.1002/jnr.490410308
28. Fricker FR, Antunes-Martins A, Galino J, Paramsothy R, La Russa F, Perkins J, et al. Axonal neuregulin 1 is a rate limiting but not essential factor for nerve remyelination. *Brain* (2013) **136**(Pt 7):2279–97. doi:10.1093/brain/awt148
29. Lamoureux PL, O'Toole MR, Heidemann SR, Miller KE. Slowing of axonal regeneration is correlated with increased axonal viscosity during aging. *BMC Neurosci* (2010) **11**:140. doi:10.1186/1471-2202-11-140
30. Verdu E, Ceballos D, Vilches JJ, Navarro X. Influence of aging on peripheral nerve function and regeneration. *J Peripher Nervous Syst* (2000) **5**(4):191–208. doi:10.1046/j.1529-8027.2000.00026.x
31. Kerezoudi E, King RH, Muddle JR, O'Neill JA, Thomas PK. Influence of age on the late retrograde effects of sciatic nerve section in the rat. *J Anat* (1995) **187**(Pt 1):27–35.
32. Low PA, Schmelzer JD, Ward KK. The effect of age on energy metabolism and resistance to ischaemic conduction failure in rat peripheral nerve. *J Physiol* (1986) **374**:263–71. doi:10.1113/jphysiol.1986.sp016078
33. Sahoo PK, Kar AN, Samra N, Terenzio M, Patel P, Lee SJ, et al. A Ca²⁺-dependent switch activates axonal casein kinase 2 α translation and drives G3BP1 granule disassembly for axon regeneration. *Curr Biol* (2020) **30**(24):4882–95.e6. doi:10.1016/j.cub.2020.09.043
34. Joung I, Yoo M, Woo JH, Chang CY, Heo H, Kwon YK. Secretion of EGF-like domain of heregulin β promotes axonal growth and functional recovery of injured sciatic nerve. *Mol Cell* (2010) **30**(5):477–84. doi:10.1007/s10059-010-0137-5
35. Chen LE, Liu K, Seaber AV, Katragadda S, Kirk C, Urbaniak JR. Recombinant human glial growth factor 2 (rhGGF2) improves functional recovery of crushed peripheral nerve (a double-blind study). *Neurochem Int* (1998) **33**(4):341–51. doi:10.1016/s0197-0186(98)00037-0
36. Heermann S, Schwab MH. Molecular control of Schwann cell migration along peripheral axons: keep moving. *Cell Adhes and Migration* (2013) **7**(1):18–22. doi:10.4161/cam.22123
37. Gambarotta G, Fregnan F, Gnani S, Perroteau I. Neuregulin 1 role in Schwann cell regulation and potential applications to promote peripheral nerve regeneration. *Int Rev Neurobiol* (2013) **108**:223–56. doi:10.1016/b978-0-12-410499-0.00009-5
38. Ronchi G, Cillino M, Gambarotta G, Fornasari BE, Raimondo S, Pugliese P, et al. Irreversible changes occurring in long-term denervated Schwann cells affect delayed nerve repair. *J Neurosurg* (2017) **127**(4):843–56. doi:10.3171/2016.9.jns16140
39. Fricker FR, Lago N, Balarajah S, Tsantoulas C, Tanna S, Zhu N, et al. Axonally derived neuregulin-1 is required for remyelination and regeneration after nerve injury in adulthood. *J Neurosci* (2011) **31**(9):3225–33. doi:10.1523/jneurosci.2568-10.2011
40. Chang HM, Shyu MK, Tseng GF, Liu CH, Chang HS, Lan CT, et al. Neuregulin facilitates nerve regeneration by speeding Schwann cell migration via ErbB2/3-dependent FAK pathway. *PLoS One* (2013) **8**(1):e53444. doi:10.1371/journal.pone.0053444
41. Monje PV, Athauda G, Wood PM. Protein kinase A-mediated gating of neuregulin-dependent ErbB2-ErbB3 activation underlies the synergistic action of cAMP on Schwann cell proliferation. *J Biol Chem* (2008) **283**(49):34087–100. doi:10.1074/jbc.m802318200
42. Gordon T, Udina E, Verge VM, de Chaves EIP. Brief electrical stimulation accelerates axon regeneration in the peripheral nervous system and promotes sensory axon regeneration in the central nervous system. *Motor Control* (2009) **13**(4):412–41. doi:10.1123/mcj.13.4.412
43. Koppes AN, Seggio AM, Thompson DM. Neurite outgrowth is significantly increased by the simultaneous presentation of Schwann cells and moderate exogenous electric fields. *J Neural Eng* (2011) **8**(4):046023. doi:10.1088/1741-2560/8/4/046023
44. English AW, Schwartz G, Meador W, Sabatier MJ, Mulligan A. Electrical stimulation promotes peripheral axon regeneration by enhanced neuronal neurotrophin signaling. *Develop Neurobiol* (2007) **67**(2):158–72. doi:10.1002/dneu.20339
45. Zuo KJ, Shafa G, Antonyshyn K, Chan K, Gordon T, Borschel GH. A single session of brief electrical stimulation enhances axon regeneration through nerve autografts. *Exp Neurol* (2020) **323**:113074. doi:10.1016/j.expneurol.2019.113074
46. Elzinga K, Tyreman N, Ladak A, Savaryn B, Olson J, Gordon T. Brief electrical stimulation improves nerve regeneration after delayed repair in Sprague Dawley rats. *Exp Neurol* (2015) **269**:142–53. doi:10.1016/j.expneurol.2015.03.022
47. Huang J, Zhang Y, Lu L, Hu X, Luo Z. Electrical stimulation accelerates nerve regeneration and functional recovery in delayed peripheral nerve injury in rats. *Eur J Neurosci* (2013) **38**(12):3691–701. doi:10.1111/ejn.12370
48. Xu C, Kou Y, Zhang P, Han N, Yin X, Deng J, et al. Electrical stimulation promotes regeneration of defective peripheral nerves after delayed repair intervals lasting under one month. *PLoS One* (2014) **9**(9):e105045. doi:10.1371/journal.pone.0105045
49. Kroner A, Greenhalgh AD, Zarruk JG, Passos dos Santos R, Gaestel M, David S. TNF and increased intracellular iron alter macrophage polarization to a detrimental M1 phenotype in the injured spinal cord. *Neuron* (2014) **83**(5):1098–116. doi:10.1016/j.neuron.2014.07.027
50. Kigerl KA, Gensel JC, Ankeny DP, Alexander JK, Donnelly DJ, Popovich PG. Identification of two distinct macrophage subsets with divergent effects causing either neurotoxicity or regeneration in the injured mouse spinal cord. *J Neurosci* (2009) **29**(43):13435–44. doi:10.1523/jneurosci.3257-09.2009
51. Wagstaff LJ, Gomez-Sanchez JA, Fazal SV, Otto GW, Kilpatrick AM, Michael K, et al. Failures of nerve regeneration caused by aging or chronic denervation are rescued by restoring Schwann cell c-Jun. *Elife* (2021) **10**:e62232. doi:10.7554/elif.62232
52. Yi S, Yuan Y, Chen Q, Wang X, Gong L, Liu J, et al. Regulation of Schwann cell proliferation and migration by miR-1 targeting brain-derived neurotrophic factor after peripheral nerve injury. *Sci Rep* (2016) **6**:29121. doi:10.1038/srep29121

53. Pola R, Aprahamian TR, Bosch-Marce M, Curry C, Gaetani E, Flex A, et al. Age-dependent VEGF expression and intraneural neovascularization during regeneration of peripheral nerves. *Neurobiol Aging* (2004) 25(10):1361–8. doi:10.1016/j.neurobiolaging.2004.02.028
54. Van Steenwinckel J, Auvynet C, Sapienza A, Reaux-Le Goazigo A, Combadière C, Melik Parsadaniantz S. Stromal cell-derived CCL2 drives neuropathic pain states through myeloid cell infiltration in injured nerve. *Brain Behav Immun* (2015) 45:198–210. doi:10.1016/j.bbi.2014.10.016
55. Cattin AL, Burden JJ, Van Emmenis L, Mackenzie F, Hoving J, Garcia Calavia N, et al. Macrophage-induced blood vessels guide schwann cell-mediated regeneration of peripheral nerves. *Cell* (2015) 162(5):1127–39. doi:10.1016/j.cell.2015.07.021
56. Kang H, Lichtman JW. Motor axon regeneration and muscle reinnervation in young adult and aged animals. *J Neurosci* (2013) 33(50):19480–91. doi:10.1523/jneurosci.4067-13.2013
57. Painter MW, Brosius Lutz A, Cheng YC, Latremoliere A, Duong K, Miller C, et al. Diminished Schwann cell repair responses underlie age-associated impaired axonal regeneration. *Neuron* (2014) 83(2):331–43. doi:10.1016/j.neuron.2014.06.016
58. Tung TH, Mackinnon SE. Nerve transfers: indications, techniques, and outcomes. *J Hand Surg* (2010) 35(2):332–41. doi:10.1016/j.jhsa.2009.12.002
59. Zou Y, Chiu H, Zinovyeva A, Ambros V, Chuang CF, Chang C. Developmental decline in neuronal regeneration by the progressive change of two intrinsic timers. *Science* (2013) 340(6130):372–6. doi:10.1126/science.1231321
60. Arthur-Farraj PJ, Latouche M, Wilton DK, Quintes S, Chabrol E, Banerjee A, et al. c-Jun reprograms Schwann cells of injured nerves to generate a repair cell essential for regeneration. *Neuron* (2012) 75(4):633–47. doi:10.1016/j.neuron.2012.06.021
61. Yamada Y, Ohazama A, Maeda T, Seo K. The Sonic Hedgehog signaling pathway regulates inferior alveolar nerve regeneration. *Neurosci Lett* (2018) 671:114–9. doi:10.1016/j.neulet.2017.12.051
62. Huang L, Xia B, Shi X, Gao J, Yang Y, Xu F, et al. Time-restricted release of multiple neurotrophic factors promotes axonal regeneration and functional recovery after peripheral nerve injury. *FASEB J* (2019) 33(7):8600–13. doi:10.1096/fj.201802065rr
63. Bond CW, Angeloni N, Harrington D, Stupp S, Podlasek CA. Sonic Hedgehog regulates brain-derived neurotrophic factor in normal and regenerating cavernous nerves. *J Sex Med* (2013) 10(3):730–7. doi:10.1111/jsm.12030
64. Wan L, Xia R, Ding W. Short-term low-frequency electrical stimulation enhanced remyelination of injured peripheral nerves by inducing the promyelination effect of brain-derived neurotrophic factor on Schwann cell polarization. *J Neurosci Res* (2010) 88(12):2578–87. doi:10.1002/jnr.22426
65. Hu M, Hong L, Liu C, Hong S, He S, Zhou M, et al. Electrical stimulation enhances neuronal cell activity mediated by Schwann cell derived exosomes. *Sci Rep* (2019) 9(1):4206. doi:10.1038/s41598-019-41007-5
66. Koppes AN, Nordberg AL, Paolillo GM, Goodsell NM, Darwish HA, Zhang L, et al. Electrical stimulation of schwann cells promotes sustained increases in neurite outgrowth. *Tissue Eng A* (2014) 20(3–4):494–506. doi:10.1089/ten.tea.2013.0012
67. Park J, Kim J, Jeon W, Kim D, Rhyu I, Kim Y, et al. An inside-out vein graft filled with platelet-rich plasma for repair of a short sciatic nerve defect in rats. *Neural Regen Res* (2014) 9(14):1351–7. doi:10.4103/1673-5374.137587
68. Hontanilla B, Auba C, Gorria O. Nerve regeneration through nerve autografts after local administration of brain-derived neurotrophic factor with osmotic pumps. *Neurosurgery* (2007) 61(6):1268–75. doi:10.1227/01.neu.0000306106.70421.ed
69. Giannesi E, Coli A, Stornelli MR, Pirone A, Lenzi C, Burchielli S, et al. An autologously generated platelet-rich plasma sutureable membrane may enhance peripheral nerve regeneration after neurotomy in an acute injury model of sciatic nerve neurotmesis. *J Reconstr Microsurg* (2014) 30(9):617–26. doi:10.1055/s-0034-1372483
70. Vares P, Dehghan MM, Bastami F, Biazar E, Shamloo N, Heidari Keshel S, et al. Effects of platelet-rich fibrin/collagen membrane on sciatic nerve regeneration. *J Craniofac Surg* (2021) 32(2):794–8. doi:10.1097/scs.00000000000007003
71. Alsousou J, Ali A, Willett K, Harrison P. The role of platelet-rich plasma in tissue regeneration. *Platelets* (2013) 24(3):173–82. doi:10.3109/09537104.2012.684730
72. Alsousou J, Thompson M, Hulley P, Noble A, Willett K. The biology of platelet-rich plasma and its application in trauma and orthopaedic surgery: a review of the literature. *J Bone Jt Surg Br volume* (2009) 91-B(8):987–96. doi:10.1302/0301-620x.91b8.22546
73. Sanchez M, Anitua E, Delgado D, Prado R, Sánchez P, Fiz N, et al. Ultrasound-guided plasma rich in growth factors injections and scaffolds hasten motor nerve functional recovery in an ovine model of nerve crush injury. *J Tissue Eng Regen Med* (2017) 11(5):1619–29. doi:10.1002/term.2079
74. Ding XG, Li SW, Zheng XM, Hu LQ, Hu WL, Luo Y. The effect of platelet-rich plasma on cavernous nerve regeneration in a rat model. *Asian J Androl* (2009) 11(2):215–21. doi:10.1038/aja.2008.37
75. Emel E, Ergun SS, Kotan D, Gürsoy EB, Parman Y, Zengin A, et al. Effects of insulin-like growth factor-I and platelet-rich plasma on sciatic nerve crush injury in a rat model. *J Neurosurg* (2011) 114(2):522–8. doi:10.3171/2010.9.jns.091928
76. Wu YN, Wu CC, Sheu MT, Chen KC, Ho HO, Chiang HS. Optimization of platelet-rich plasma and its effects on the recovery of erectile function after bilateral cavernous nerve injury in a rat model. *J Tissue Eng Regen Med* (2016) 10(10):E294–E304. doi:10.1002/term.1806
77. Torul D, Bereket MC, Onger ME, Altun G. Comparison of the regenerative effects of platelet-rich fibrin and plasma rich in growth factors on injured peripheral nerve: an experimental study. *J Oral Maxillofac Surg* (2018) 76(8):1823 e1–1823.e12. doi:10.1016/j.joms.2018.04.012
78. Wu CC, Wu YN, Ho HO, Chen KC, Sheu MT, Chiang HS. The neuroprotective effect of platelet-rich plasma on erectile function in bilateral cavernous nerve injury rat model. *J Sex Med* (2012) 9(11):2838–48. doi:10.1111/j.1743-6109.2012.02881.x
79. Farrag TY, Lehar M, Verhaegen P, Carson KA, Byrne PJ. Effect of platelet rich plasma and fibrin sealant on facial nerve regeneration in a rat model. *The Laryngoscope* (2007) 117(1):157–65. doi:10.1097/01.mlg.0000249726.98801.77
80. Cho HH, Jang S, Lee SC, Jeong H, Park J, Han J, et al. Effect of neural-induced mesenchymal stem cells and platelet-rich plasma on facial nerve regeneration in an acute nerve injury model. *The Laryngoscope* (2010) 120(5):907–13. doi:10.1002/lary.20860
81. Kucuk L, Gunay H, Erbas O. Effects of platelet-rich plasma on nerve regeneration in a rat model. *Acta Orthop Traumatol Turc* (2014) 48(4):449–54. doi:10.3944/aott.2014.13.0029
82. Elgazzar RF, Mutabagani MA, Abdelal SE, Sadakah A. Platelet rich plasma may enhance peripheral nerve regeneration after cyanoacrylate reanastomosis: a controlled blind study on rats. *Int J Oral Maxillofac Surg* (2008) 37(8):748–55. doi:10.1016/j.ijom.2008.05.010
83. Liao CH, Chang CJ, Chen KC, Rajneesh CP, Tseng XW, Cheng JH, et al. Effects of platelet-rich plasma glue placement at the prostatectomy site on erectile function restoration and cavernous nerve preservation in a nerve-sparing prostatectomy rat model. *Biomed and Pharmacother* (2023) 161:114499. doi:10.1016/j.biopha.2023.114499
84. Anjayani S, Wirohadidjojo YW, Adam AM, Suwandi D, Seweng A, Amiruddin MD. Sensory improvement of leprosy peripheral neuropathy in patients treated with perineural injection of platelet-rich plasma. *Int J Dermatol* (2014) 53(1):109–13. doi:10.1111/ijd.12162
85. Park GY, Kwon DR. Platelet-rich plasma limits the nerve injury caused by 10% dextrose in the rabbit median nerve. *Muscle Nerve* (2014) 49(1):56–60. doi:10.1002/mus.23863
86. Teymur H, Tiftikcioglu YO, Cavusoglu T, Tiftikcioglu BI, Erbas O, Yigiturk G, et al. Effect of platelet-rich plasma on reconstruction with nerve autografts. *Kaohsiung J Med Sci* (2017) 33(2):69–77. doi:10.1016/j.kjms.2016.11.005
87. Ikumi A, Hara Y, Yoshioka T, Kanamori A, Yamazaki M. Effect of local administration of platelet-rich plasma (PRP) on peripheral nerve regeneration: an experimental study in the rabbit model. *Microsurgery* (2018) 38(3):300–9. doi:10.1002/micr.30263
88. Zheng C, Zhu Q, Liu X, Huang X, He C, Jiang L, et al. Improved peripheral nerve regeneration using acellular nerve allografts loaded with platelet-rich plasma. *Tissue Eng A* (2014) 20(23–24):3228–40. doi:10.1089/ten.tea.2013.0729
89. Garcia de Cortazar U, Padilla S, Lobato E, Delgado D, Sánchez M. Intraneural platelet-rich plasma injections for the treatment of radial nerve section: a case report. *J Clin Med* (2018) 7(2):13. doi:10.3390/jcm7020013
90. Ikumi A, Hara Y, Okano E, Kohyama S, Arai N, Taniguchi Y, et al. Intraoperative local administration of platelet-rich plasma (PRP) during neurolysis surgery for the treatment of digital nerve crush injury. *Case Rep Orthopedics* (2018) 2018:1–6. doi:10.1155/2018/1275713
91. Ricci E, Riva G, Dagna F, Cavalot AL. The use of platelet-rich plasma gel in superficial parotidectomy. *Acta Otorhinolaryngol Ital* (2019) 39(6):363–6. doi:10.14639/0392-100x-2093
92. Sariguney Y, Yavuzer R, Elmas C, Yenicesu I, Bolay H, Atabay K. Effect of platelet-rich plasma on peripheral nerve regeneration. *J Reconstr Microsurg* (2008) 24(3):159–67. doi:10.1055/s-2008-1076752
93. Sanchez M, Yoshioka T, Ortega M, Delgado D, Anitua E. Ultrasound-guided platelet-rich plasma injections for the treatment of common peroneal nerve palsy

associated with multiple ligament injuries of the knee. *Knee Surg Sports Traumatol Arthrosc* (2014) 22(5):1084–9. doi:10.1007/s00167-013-2479-y

94. Fahandezh-Saddi Diaz H, Rios Luna A, Villanueva Martínez M, Cantero Yubero ME, Prado R, Padilla S, et al. Surgical treatment of saphenous nerve injury assisted by plasma rich in growth factors (PRGF): lessons from a case report. *Clin Pract* (2023) 13(5):1090–9. doi:10.3390/clinpract13050097

95. Wang YS, Wang SL, Liu XL, Kang ZC. Platelet-rich plasma promotes peripheral nerve regeneration after sciatic nerve injury. *Neural Regen Res* (2023) 18(2):375–81. doi:10.4103/1673-5374.346461

96. Zhang Y, Yi D, Hong Q, Cao J, Geng X, Liu J, et al. Platelet-rich plasma-derived exosomes boost mesenchymal stem cells to promote peripheral nerve regeneration. *J Controlled Release* (2024) 367:265–82. doi:10.1016/j.jconrel.2024.01.043

97. Klifto KM, Klifto CS, Pidgeon TS. Platelet-rich plasma versus corticosteroid injections for the treatment of mild-to-moderate carpal tunnel syndrome: a markov cost-effectiveness decision analysis. *Hand* (2022) N Y:15589447221092056. doi:10.1002/micr.30263

98. Uzun H, Bitik O, Uzun O, Ersoy US, Aktaş E. Platelet-rich plasma versus corticosteroid injections for carpal tunnel syndrome. *J Plast Surg Hand Surg* (2017) 51(5):301–5. doi:10.1080/2000656x.2016.1260025

99. Wu YT, Ho TY, Chou YC, Ke MJ, Li TY, Huang GS, et al. Six-month efficacy of platelet-rich plasma for carpal tunnel syndrome: a prospective randomized, single-blind controlled trial. *Sci Rep* (2017) 7(1):94. doi:10.1038/s41598-017-00224-6

100. Raeissadat SA, Karimzadeh A, Hashemi M, Bagherzadeh L. Safety and efficacy of platelet-rich plasma in treatment of carpal tunnel syndrome; a randomized controlled trial. *BMC Musculoskelet Disord* (2018) 19(1):49. doi:10.1186/s12891-018-1963-4

101. Sabongi RG, De Rizzo LA, Fernandes M, Valente S, dos Santos J, Faloppa F, et al. Nerve regeneration: is there an alternative to nervous graft? *J Reconstr Microsurg* (2014) 30(9):607–16. doi:10.1055/s-0034-1372477

102. Firat C, Aytakin AH, Durak MA, Geyik Y, Erbatur S, Dogan M, et al. Comparison of the effects of PRP and hyaluronic acid in promoting peripheral nerve regeneration an experimental study with vascular conduit model in rats. *Ann Ital Chir* (2016) 87:362–74.

103. Roque JS, Pomini KT, Buchaim RL, Buchaim DV, Andreo JC, Roque DD, et al. Inside-out and standard vein grafts associated with platelet-rich plasma (PRP) in sciatic nerve repair. A histomorphometric study. *Acta Cir Bras* (2017) 32(8):617–25. doi:10.1590/s0102-865020170080000003

104. Zhu Y, Peng N, Wang J, Jin Z, Zhu L, Wang Y, et al. Peripheral nerve defects repaired with autogenous vein grafts filled with platelet-rich plasma and active nerve microtissues and evaluated by novel multimodal ultrasound techniques. *Biomater Res* (2022) 26(1):24. doi:10.1186/s40824-022-00264-8

105. Sahin MM, Cayonu M, Dinc SK. Effects of chitosan and platelet-rich plasma on facial nerve regeneration in an animal model. *Eur Arch Otorhinolaryngol* (2021). doi:10.1007/s00405-021-06859-6

106. Ye F, Li H, Qiao G, Chen F, Tao H, Ji A, et al. Platelet-rich plasma gel in combination with Schwann cells for repair of sciatic nerve injury. *Neural Regen Res* (2012) 7(29):2286–92. doi:10.3969/j.issn.1673-5374.2012.29.007

107. Chuang MH, Ho LH, Kuo TF, Sheu SY, Liu YH, Lin PC, et al. Regenerative potential of platelet-rich fibrin releasate combined with adipose tissue-derived stem cells in a rat sciatic nerve injury model. *Cell Transpl* (2020) 29:096368972091943. doi:10.1177/0963689720919438

108. Abbasipour-Dalivand S, Mohammadi R, Mohammadi V. Effects of local administration of platelet rich plasma on functional recovery after bridging sciatic nerve defect using silicone rubber chamber; an experimental study. *Bull Emerg Trauma* (2015) 3(1):1–7.

109. Hama S, Yokoi T, Orita K, Uemura T, Takamatsu K, Okada M, et al. Peripheral nerve regeneration by bioabsorbable nerve conduits filled with platelet-rich fibrin. *Clin Neurol Neurosurg* (2024) 236:108051. doi:10.1016/j.clineuro.2023.108051

110. Lu CF, Wang B, Zhang PX, Han S, Pi W, Kou Y, et al. Combining chitin biological conduits with small autogenous nerves and platelet-rich plasma for the repair of sciatic nerve defects in rats. *CNS Neurosci Ther* (2021) 27(7):805–19. doi:10.1111/cns.13640

111. Kim JW, Kim JM, Choi ME, Jeon EJ, Park JM, Kim YM, et al. Platelet-rich plasma loaded nerve guidance conduit as implantable biocompatible materials for recurrent laryngeal nerve regeneration. *NPJ Regen Med* (2022) 7(1):49. doi:10.1038/s41536-022-00239-2

112. Kaplan S, Pişkin A, Ayyıldız M, Aktaş A, Kõksal B, Ulkay MB, et al. The effect of melatonin and platelet gel on sciatic nerve repair: an electrophysiological and stereological study. *Microsurgery* (2011) 31(4):306–13. doi:10.1002/micr.20876

113. Fernandes M, Valente S, Santos J, Furukawa R, Fernandes C, Leite V, et al. Platelet-rich fibrin conduits as an alternative to nerve autografts for peripheral nerve repair. *J Reconstr Microsurg* (2017) 33(8):549–56. doi:10.1055/s-0037-1603355

114. Huang ML, Zhai Z, Chen ZX, Yang XN, Qi ZL. Platelet-rich fibrin membrane nerve guidance conduit: a potentially promising method for peripheral nerve injuries. *Chin Med J* (2020) 133(8):999–1001. doi:10.1097/cm9.0000000000000726

115. Foy CA, Micheo WF, Kuffler DP. Inducing ulnar nerve function while eliminating claw hand and reducing chronic neuropathic pain. *Plast Reconstr Surg - Glob Open* (2023) 11(4):e4927. doi:10.1097/gox.0000000000004927

116. Micheo WF, Foy CA, Kuffler DP. A novel technique restores function while eliminating intractable neuropathic pain in a 71-year-old diabetic patient under challenging injury conditions. *J Reconstr Microsurg Open* (2023) 08(1):e23–e27. doi:10.1055/s-0042-1757323

117. Foy CA, Micheo WF, Kuffler DP. Functional recovery following repair of long nerve gaps in senior patient 2.6 Years posttrauma. *Plast Reconstr Surg - Glob Open* (2021) 9(9):e3831. doi:10.1097/gox.0000000000003831

118. Kuffler DP, Reyes O, Sosa IJ, Santiago-Figueroa J. Neurological recovery across a 12-cm-long ulnar nerve gap repaired 3.25 years post trauma: case report. *Neurosurgery* (2011) 69(6):E1321–6. doi:10.1227/neu.0b013e31822a9fd2

119. Moojen DJ, Everts PA, Schure RM, Overvest EP, van Zundert A, Knappe JT, et al. Antimicrobial activity of platelet-leukocyte gel against *Staphylococcus aureus*. *J Orthopaedic Res* (2008) 26(3):404–10. doi:10.1002/jor.20519

120. Nishio H, Saita Y, Kobayashi Y, Takaku T, Fukusato S, Uchino S, et al. Platelet-rich plasma promotes recruitment of macrophages in the process of tendon healing. *Regenerative Ther* (2020) 14:262–70. doi:10.1016/j.reth.2020.03.009

121. Kobayashi Y, Saita Y, Nishio H, Ikeda H, Takazawa Y, Nagao M, et al. Leukocyte concentration and composition in platelet-rich plasma (PRP) influences the growth factor and protease concentrations. *J Orthopaedic Sci* (2016) 21(5):683–9. doi:10.1016/j.jos.2016.07.009

122. Simental-Mendia M, Vilchez-Cavazos F, Garcia-Garza R, Lara-Arias J, Montes-de-Oca-Luna R, Said-Fernández S, et al. The matrix synthesis and anti-inflammatory effect of autologous leukocyte-poor platelet rich plasma in human cartilage explants. *Histol Histopathol* (2018) 33(6):609–18. doi:10.14670/HH-11-961

123. Braun HJ, Kim HJ, Chu CR, Dragoo JL. The effect of platelet-rich plasma formulations and blood products on human synoviocytes: implications for intra-articular injury and therapy. *Am J Sports Med* (2014) 42(5):1204–10. doi:10.1177/0363546514525593

124. Sundman EA, Cole BJ, Fortier LA. Growth factor and catabolic cytokine concentrations are influenced by the cellular composition of platelet-rich plasma. *Am J Sports Med* (2011) 39(10):2135–40. doi:10.1177/0363546511417792

125. Rittner HL, Machelska H, Stein C. Leukocytes in the regulation of pain and analgesia. *J Leukoc Biol* (2005) 78(6):1215–22. doi:10.1189/jlb.0405223

126. Machelska H, Stein C. Leukocyte-derived opioid peptides and inhibition of pain. *J Neuroimmune Pharmacol* (2006) 1(1):90–7. doi:10.1007/s11481-005-9002-2

127. Celik MO, Labuz D, Henning K, Busch-Dienstfert M, Gaveriaux-Ruff C, Kieffer BL, et al. Leukocyte opioid receptors mediate analgesia via Ca(2+)-regulated release of opioid peptides. *Brain Behav Immun* (2016) 57:227–42. doi:10.1016/j.bbi.2016.04.018

128. Dragoo JL, Braun HJ, Durham JL, Ridley BA, Odegaard JL, Luong R, et al. Comparison of the acute inflammatory response of two commercial platelet-rich plasma systems in healthy rabbit tendons. *Am J Sports Med* (2012) 40(6):1274–81. doi:10.1177/0363546512442334

129. Moyle M, Napier MA, McLean JW. Cloning and expression of a divergent integrin subunit beta 8. *J Biol Chem* (1991) 266(29):19650–8. doi:10.1016/s0021-9258(18)55042-0

130. Ma L, Shen F, Jun K, Bao C, Kuo R, Young WL, et al. Integrin $\beta 8$ deletion enhances vascular dysplasia and hemorrhage in the brain of adult Alk1 heterozygous mice. *Transl Stroke Res* (2016) 7(6):488–96. doi:10.1007/s12975-016-0478-2

131. Qin J, Wang L, Sun Y, Sun X, Wen C, Shahmoradi M, et al. Concentrated growth factor increases Schwann cell proliferation and neurotrophic factor secretion and promotes functional nerve recovery in vivo. *Int J Mol Med* (2016) 37(2):493–500. doi:10.3892/ijmm.2015.2438

132. Qin J, Wang L, Zheng L, Zhou X, Zhang Y, Yang T, et al. Concentrated growth factor promotes Schwann cell migration partly through the integrin $\beta 1$ -mediated activation of the focal adhesion kinase pathway. *Int J Mol Med* (2016) 37(5):1363–70. doi:10.3892/ijmm.2016.2520

133. Anitua E, Aguirre JJ, Algorta J, Ayerdi E, Cabezas AI, Orive G, et al. Effectiveness of autologous preparation rich in growth factors for the treatment of

chronic cutaneous ulcers. *J Biomed Mater Res B: Appl Biomater* (2008) **84B**(2): 415–21. doi:10.1002/jbm.b.30886

134. Machado ES, Soares FP, Yamaguchi RS, Felipe WK, Meves R, Souza TAC, et al. A simple double-spin closed method for preparing platelet-rich plasma. *Cureus* (2022) **14**(1):e20899. doi:10.7759/cureus.20899

135. Aufiero D, Vincent H, Sampson S, Bodor M. Regenerative injection treatment in the spine: review and case series with platelet rich plasma. *J Stem Cell Res Rev and Rep* (2015) **2**:1019.

136. Marx RE. Platelet-rich plasma: evidence to support its use. *J Oral Maxillofacial Surg* (2004) **62**(4):489–96. doi:10.1016/j.joms.2003.12.003

137. Patscheke H. Shape and functional properties of human platelets washed with acid citrate. *Pathophysiology Haemost Thromb* (1981) **10**(1):14–27. doi:10.1159/000214383

138. Fitzpatrick J, Bulsara MK, McCrory PR, Richardson MD, Zheng MH. Analysis of platelet-rich plasma extraction: variations in platelet and blood components between 4 common commercial kits. *Orthopaedic J Sports Med* (2017) **5**(1):2325967116675272. doi:10.1177/2325967116675272

139. Engstrom M, Schott U, Romner B, Reinstrup P. Acidosis impairs the coagulation: a thromboelastographic study. *J Trauma Inj Infect Crit Care* (2006) **61**(3):624–8. doi:10.1097/01.ta.0000226739.30655.75

140. Flatow FA, Jr, Freireich EJ. The increased effectiveness of platelet concentrates prepared in acidified plasma. *Blood* (1966) **27**(4):449–59. doi:10.1182/blood.v27.4.449.449

141. Zavoico GB, Cragoe EJ, Jr, Feinstein MB. Regulation of intracellular pH in human platelets. Effects of thrombin, A23187, and ionomycin and evidence for activation of Na⁺/H⁺ exchange and its inhibition by amiloride analogs. *J Biol Chem* (1986) **261**(28):13160–7. doi:10.1016/s0021-9258(18)69284-1

142. Keating FK, Sobel BE, Schneider DJ. Effects of increased concentrations of glucose on platelet reactivity in healthy subjects and in patients with and without diabetes mellitus. *Am J Cardiol* (2003) **92**(11):1362–5. doi:10.1016/j.amjcard.2003.08.033

143. Belch JJ, McArdle BM, Burns P, Lowe GDO, Forbes CD. The effects of acute smoking on platelet behaviour, fibrinolysis and haemorheology in habitual smokers. *Thromb Haemost* (1984) **51**(1):006–8. doi:10.1055/s-0038-1660996

144. Mukamal KJ, Massaro JM, Ault KA, Mittleman MA, Sutherland PA, Lipinska I, et al. Alcohol consumption and platelet activation and aggregation among women and men: the Framingham Offspring Study. *Alcohol Clin and Exp Res* (2005) **29**(10):1906–12. doi:10.1097/01.alc.0000183011.86768.61

145. Olas B, Wachowicz B, Saluk-Juszczak J, Zieliński T. Effect of resveratrol, a natural polyphenolic compound, on platelet activation induced by endotoxin

or thrombin. *Thromb Res* (2002) **107**(3–4):141–5. doi:10.1016/s0049-3848(02)00273-6

146. Williams JK, Clarkson TB. Dietary soy isoflavones inhibit *in-vivo* constrictor responses of coronary arteries to collagen-induced platelet activation. *Coron Artery Dis* (1998) **9**(11):759–64. doi:10.1097/00019501-199809110-00009

147. Frary CD, Johnson RK, Wang MQ. Food sources and intakes of caffeine in the diets of persons in the United States. *J Am Diet Assoc* (2005) **105**(1):110–3. doi:10.1016/j.jada.2004.10.027

148. Hubbard GP, Wolfram S, Lovegrove JA, Gibbins J. Ingestion of quercetin inhibits platelet aggregation and essential components of the collagen-stimulated platelet activation pathway in humans. *J Thromb Haemost* (2004) **2**(12):2138–45. doi:10.1111/j.1538-7836.2004.01067.x

149. Alvarez-Suarez JM, Giampieri F, Tulipani S, Casoli T, Di Stefano G, González-Paramás AM, et al. One-month strawberry-rich anthocyanin supplementation ameliorates cardiovascular risk, oxidative stress markers and platelet activation in humans. *J Nutr Biochem* (2014) **25**(3):289–94. doi:10.1016/j.jnutbio.2013.11.002

150. de Lorgeril M, Renaud S, Mamelle N, Salen P, Martin JL, Monjaud I, et al. Mediterranean alpha-linolenic acid-rich diet in secondary prevention of coronary heart disease. *Lancet* (1994) **343**(8911):1454–9. doi:10.1016/s0140-6736(94)92580-1

151. Sudic D, Razmara M, Forslund M, Ji Q, Hjendahl P, Li N. High glucose levels enhance platelet activation: involvement of multiple mechanisms. *Br J Haematol* (2006) **133**(3):315–22. doi:10.1111/j.1365-2141.2006.06012.x

152. Yokogoshi H, Wurtman RJ. Meal composition and plasma amino acid ratios: effect of various proteins or carbohydrates, and of various protein concentrations. *Metabolism* (1986) **35**(9):837–42. doi:10.1016/0026-0495(86)90225-8

153. Ahmed Y, van Iddekinge B, Paul C, Sullivan MHF, Elder MG. Retrospective analysis of platelet numbers and volumes in normal pregnancy and in pre-eclampsia. *BJOG: An Int J Obstet and Gynaecol* (1993) **100**(3):216–20. doi:10.1111/j.1471-0528.1993.tb15233.x

154. Cavallo C, Roffi A, Grigolo B, Mariani E, Pratelli L, Merli G, et al. Platelet-rich plasma: the choice of activation method affects the release of bioactive molecules. *Biomed Res Int* (2016) **2016**:1–7. doi:10.1155/2016/6591717

155. Mazzocca AD, McCarthy MB, Chowanec DM, Cote MP, Romeo AA, Bradley JP, et al. Platelet-rich plasma differs according to preparation method and human variability. *J Bone Jt Surg* (2012) **94**(4):308–16. doi:10.2106/jbjs.k.00430

156. Golebiewska EM, Poole AW. Platelet secretion: from haemostasis to wound healing and beyond. *Blood Rev* (2015) **29**(3):153–62. doi:10.1016/j.blre.2014.10.003

157. Baidildinova G, Nagy M, Jurk K, Wild PS, ten Cate H, van der Meijden PEJ. Soluble platelet release factors as biomarkers for cardiovascular disease. *Front Cardiovasc Med* (2021) **8**:684920. doi:10.3389/fcvm.2021.684920



OPEN ACCESS

*CORRESPONDENCE

Damien P. Kuffler,
✉ dkuffler@hotmail.com

RECEIVED 05 March 2025

ACCEPTED 22 April 2025

PUBLISHED 30 June 2025

CITATION

Kuffler DP and Foy CA (2025)
Mechanisms for reducing/eliminating
chronic neuropathic pain with a focus
on platelet-rich plasma.
Exp. Biol. Med. 250:10567.
doi: 10.3389/ebm.2025.10567

COPYRIGHT

© 2025 Kuffler and Foy. This is an open-
access article distributed under the
terms of the [Creative Commons
Attribution License \(CC BY\)](#). The use,
distribution or reproduction in other
forums is permitted, provided the
original author(s) and the copyright
owner(s) are credited and that the
original publication in this journal is
cited, in accordance with accepted
academic practice. No use, distribution
or reproduction is permitted which does
not comply with these terms.

Mechanisms for reducing/ eliminating chronic neuropathic pain with a focus on platelet-rich plasma

Damien P. Kuffler^{1*} and Christian A. Foy²

¹Institute of Neurobiology, Medical School, University of Puerto Rico, San Juan, PR, United States,

²Department of Orthopedic Surgery, Medical School, University of Puerto Rico, San Juan, PR,
United States

Abstract

Peripheral nerve trauma commonly results in chronic neuropathic pain by up-regulating the synthesis and release of pro-inflammatory mediators from local and invading cells and inducing hyperexcitability of nociceptive neurons and spontaneous electrical activity. The pain decreases when these cells down-regulate genes supporting the pro-inflammatory state, up-regulate genes for expressing anti-inflammatory factors, and modulate genes that reduce nociceptive neuron spontaneous electrical activity. Pharmacological agents, the primary technique for reducing pain, do not eliminate pain, and <50% of patients achieve benefits because they do not address the underlying causes of pain. Alternative techniques providing longer lasting, but not complete or long-term pain relief include surgical interventions, electrical stimulation, and antibody treatment. Anti-inflammatory mediators can reduce pain, but the effect is not complete or long-lasting. Platelet-rich plasma (PRP) contains a readably available evolutionarily developed cocktail of factors that induce longer-lasting and more significant, but not complete, pain relief than other techniques. However, a novel study shows that unique formulations of PRP can induce long-term pain elimination. This review examines (1) the efficacy of drugs, regenerative peripheral nerve interface (RPNI), targeted muscle reinnervation (TMR), and PRP in reducing chronic neuropathic pain, (2) recent clinical data showing that a novel PRP application technique induces long-term chronic neuropathic pain reduction/elimination, and (3) discusses why the novel PRP may be more effective in reducing/eliminating chronic neuropathic pain.

KEYWORDS

axon regeneration, chronic neuropathic pain, nerve repair, pain elimination, plateletrich plasma, platelets

Impact statement

Peripheral nerve trauma and surgical interventions result in 60% of individuals suffering chronic neuropathic pain. The standard technique for reducing pain is pharmacological agents, although they may not be effective, may reduce but not eliminate pain, are not long-lasting, are strongly addictive, and their side effects may preclude their use. Physiologically, chronic pain is reduced/eliminated when injured axons reinnervate their targets. However, because, following nerve repairs, <50% of patients recover function, most patients suffer chronic pain. Novel techniques are required that induce meaningful recovery or directly reduce/eliminate chronic neuropathic pain. This review examines the efficacy of pharmacological agents and other techniques for their analgesic efficacies. It then discusses a novel technique involving platelet-rich plasma (PRP), which reliably and rapidly induces long-term chronic neuropathic pain reduction/elimination. Finally, it briefly discusses various platelet-released factors that may be responsible for this influence and their mechanisms of action.

Introduction

Up to 16% of the US population suffers chronic neuropathic pain due to trauma, amputation, and surgery [1, 2], with peripheral nerve trauma and surgical interventions leading to pain in 60% of patients [3–5]. For those who undergo peripheral nerve surgical procedures, one study found >50% have significant pain reduction [6], while another 73% continued to have or developed pain [7]. The pain was chronic and intense for about 30% [3, 8], debilitating for many [9], and challenging to treat [10, 11]. Of patients presenting to pain clinics reporting chronic neuropathic pain, 78% suffered pain after 6 months, decreasing to 56% after 12 months [12].

Surgical interventions [13–15], electrical stimulation [16–18] antibodies against pro-inflammatory mediators and their receptors [19, 20], and drugs that block nociceptive neurons' hyperexcitability and spontaneous ectopic electrical activity [21–23] provide long-term chronic neuropathic pain relief, but not elimination, to <50% of patients [24, 25].

Extensive evidence shows that injury-induced inflammation underlies neuropathic pain [3]. This suggests that administering anti-inflammatory agents should reduce chronic pain. However, clinically, administering anti-inflammatory drugs prolongs rather than shortens the time to pain elimination, while administering pro-inflammatory mediators reduces pain more rapidly [26]. While counterintuitive, this is because inflammation induces neutrophil invasion and up-regulates the synthesis and release of pro-inflammatory factors, which trigger an anti-inflammatory response [26]. Therefore, reducing/eliminating chronic neuropathic pain requires understanding which cells

are recruited by injuries, the sequences of their recruitment, and what leads to the up- or down-regulation of specifically released factors.

This paper examines the efficacy of drugs and PRP in reducing pain and the results of two novel clinical techniques involving PRP, which induce long-term chronic neuropathic pain reduction/elimination. Finally, the paper discusses the pro-algesic and analgesic roles played by some platelet-released factors that induce pain reduction/elimination.

Pharmaceutical agents

Clinically, pharmacological agents are best for reducing pain and providing adequate pain control to 30%–40% of patients [27]. Among the most effective opioid receptor agonists are strong [1, 28–34] followed by weak [35, 36] opioids [28], anticonvulsive drugs [37], such as gabapentin [38–42], tricyclic antidepressants [43], and the selective norepinephrine and anti-epileptic drug pregabalin [44]. While opioids are the most effective [45], their efficacies are increased by combining them with other drugs [46]. The clinical efficacies of other techniques, such as the local application of capsaicin [47] and lidocaine [48], are less well-established and are still being tested [49]. Recently, suzetrigine was FDA approved (first in class JAN 2025) as a non-opioid analgesic of comparable efficacy to higher-potency opioids. [50]. Its efficacy compared to PRP is not known. However, it has been shown to induce mild to moderate severe adverse events [50], while PRP induces no known adverse events.

The anesthetic ketamine is effective against chronic neuropathic pain [51]. It is considered to act by inhibiting the N-methyl-D-aspartate (NMDA) receptor and possibly other mechanisms, such as enhancing descending inhibition and central site anti-inflammatory actions [51]. However, short-term NMDA infusions induced potent analgesia only during its administration, while prolonged infusion (4–14 days) induces analgesia for up to 3 months following infusion [51]. Unfortunately, ketamine's clinical side effects include nausea/vomiting, psychedelic symptoms (hallucinations, memory defects, panic attacks), cardiovascular stimulation, and somnolence, with a minority of patients suffering hepatotoxicity [51].

No pharmacological agent provides long-term analgesia [52], and for patients with chronic pain, 54% use opioid medications daily, despite up to 97% reporting inadequate pain relief [6, 53]. However, their use is limited because of adverse effects [54, 55] and problems with abuse, dependence, overdose, and death [54, 55]. Therefore, it is essential to balance opioid pain control and the development of opioid dependence [56]. These difficulties can be reduced by multimodal analgesic plans, non-opioid medications, and regional application techniques [31, 56]. Nevertheless, novel pain relief techniques are required [57],

including developing alternative forms of nerve surgery [6], and pharmacological agents.

Targeted muscle reinnervation (TMR) and regenerative peripheral nerve interface (RPNI)

Removing painful neuromas reduces but does not eliminate pain [13], and there is a high rate of neuroma and pain redevelopment [58]. However, following neuroma removal, the pain that normally develops is reduced by securing the nerve stump to an autograft or allograft [59, 60]. For lower extremity amputations, pain is reduced by nerve capping or implanting nerve stumps in bone [24, 61]. However, there is still no long-term chronic neuropathic pain reduction [62].

The most effective techniques for preventing or reducing chronic neuropathic pain or post-amputation neuroma pain are regenerative peripheral nerve interface (RPNI) and targeted muscle reinnervation (TMR) [63–67]. RPNI involves coapting a nerve stump into a small denervated muscle grafts, while TMR involves coapting the proximal nerve stump to the proximal motor nerve innervating a small muscle graft. Thus, following neuroma excision, both RPNI and TMR reduce pain development [68] and clinically reduce post-amputation neuroma pain in 75–100% of patients [64–67, 69–71] and phantom limb pain in 45–80%. However, TMR has the significant limitation of being only effective if applied <3 months post-trauma [72], requires sacrificing a motor nerve and cannot be used if a goal is to both reduce pain and restore function.

Target reinnervation and cessation of axon regeneration

Abnormal spontaneous electrical activity of regenerating dorsal root axons is closely associated with chronic neuropathic pain [73–75]. Clinically, chronic pain reduction/elimination occurs only slightly before or in association with initial signs of functional recovery [76]. These findings led to the hypothesis that pain remains chronic when axons are regenerating [73] and only decreases or is eliminated when axons reinnervate targets, stop regenerating [63, 73, 77, 78], take up a target-derived factor/s [76, 79–81], which silence hyperexcitable nociceptive axons [63].

Supporting this hypothesis is that the extent of pain reduction decreases proportionately with the increasing extent of functional recovery [82, 83]. In rats, pain behavior is reduced or eliminated when axon regeneration is stopped/inhibited [73, 84], such as by applying semaphorin 3A [85] and injecting small-interfering RNA (siRNA) into axotomized sensory ganglia to

block growth-associated protein-43 (GAP-43) expression [73, 86]. This hypothesis is consistent with studies showing that TMR reduces/eliminates chronic neuropathic pain [69, 77, 87], including complex regional pain syndrome (CRPST) type II [88]. This idea is also consistent with rat chronic pain behavior being blocked by tetrodotoxin (TTX), GAP-43 knockdown, and semaphorin 3A, which stop axon regeneration and the electrical activity of nociceptive neurons [73]. Target reinnervation and the cessation of axon regeneration are consistent with TMR and RPNI reducing/eliminating chronic neuropathic pain, which occurs in 71%–100% of the subjects [66, 69].

PRP and the reduction/elimination of chronic neuropathic pain

One of the challenges in using PRP is consistency in the findings between different studies. Thus, some clinical studies concluded that PRP provided little or no pain relief for tendinosis or rotator cuff tears [89–91]. Meta-analyses of multiple studies support this conclusion [89, 92, 93]. However, other clinical studies found that PRP reduced pain associated with tendinosis [94, 95], tendon injury [96–98], rotator cuff tears [99, 100] osteoarthritis [101, 102], plantar fasciitis [103], and muscle injuries [104]. These findings were supported by meta-analysis [105]. Animal model studies show PRP reduces pain caused by many types of injuries [106, 107], such as skin burn-induced neuropathic pain [108], painful lesions caused by *mycobacterium leprae* (leprosy bacteria) [109], and rat spinal cord injury sites [110]. Clinically, PRP also reduces peripheral nerve pain when applied to digital [111] and sciatic [112] nerve crush sites, pudendal nerve neurolysis surgery sites [113], the median nerve at the carpal tunnel's proximal edge [114], and when injected into the perineurium of patients suffering from diabetic neuropathic pain [115]. These techniques result in >80% of patients achieving ca. three months of pain relief [116].

Clinically, a single epidural PRP injection provides lower back pain relief for up to 6 months [117, 118] while reducing complex chronic degenerative spinal pain [119]. Multiple PRP epidural injections provide temporary lumbar radicular pain relief [120], which is significantly increased by adding corticosteroids, although this is effective for only about 50% of patients [121, 122]. In comparative studies, the analgesic efficacy of PRP is similar to [120, 123] or better than [94, 124] that is provided by injecting a corticosteroid. An effective alternative technique for rats involves wrapping nerves in a PRP-coated NeuraWrap Nerve Protector [125]. Nevertheless, two meta-analyses found that in animal models and clinically, although PRP induces pain relief and nerve regeneration, the effect is not long-lasting [114, 126].

Variability in PRP efficacy in reducing neuropathic pain

The efficacy of PRP in reducing pain and the duration of the suppression varies significantly between individuals [127] and studies [128]. This variability is best explained by significant differences in the composition of the PRP due to how it is prepared [129]. These techniques include single vs. double-spin PRP separation and >30 different types of commercially available PRP separation systems [130–132]. These different techniques yield PRP with platelet concentrations ranging from 0.52- to 9.3-fold relative to whole blood [133]. PRP differences are also caused by how and when the platelets are activated before or when the PRP is applied, and the centrifugation parameters [132, 134, 135], which affect the ratios of unactivated vs. activated platelets, numbers of other different cell types, levels of bioactive factors, and leukocyte concentration [128, 130, 135–138], when platelets release their factors, (3) the ratios of the factors released, and (4) the level of factor bioactivity [139].

When comparing the analgesic efficacy of PRP, parameters that are never considered are how it is prepared and applied and the uncontrolled differences in the physiology, health, and products consumed by patients [128, 140, 141]. Thus, platelet aggregation, and therefore its efficacy, is increased by smoking [142], while platelet activation and aggregation are decreased by alcohol consumption [143], which also reduces the response of platelets to thrombin [144] and collagen. Platelet aggregation is also reduced by diets containing isoflavones [145], caffeine [146], quercetin (a flavonoid) [147], and anthocyanins [148]. However, platelet aggregation is increased by diets high in saturated fats [149], sugar [150], and simple carbohydrates [149]. Finally, platelets of patients with high blood pressure have a decreased whole blood platelet count [151], and their platelets have lower bioactive factor concentrations than those with normal blood pressure [152]. Therefore, without standardizing how PRP is prepared and applied, it is not possible to eliminate the variability in the efficacy of PRP and to ensure that PRP exerts its maximum potential effects [138].

Novel clinical PRP application techniques induce long-term chronic neuropathic pain reduction/elimination

Recent case studies show that PRP induces long-lasting and complete pain elimination. These applications involved bridging nerve gaps with an autograft within a PRP-filled collagen tube [153–158] or only a PRP-filled collagen tube [159, 160]. The first technique reduced the pain in 8% and eliminated it in 92% of subjects, while the second eliminated pain in all the subjects. The pain reduction/elimination lasted throughout the 1.1–15 years follow-up. Thus, platelet-released

factors have the capacity to induce long-term pain elimination.

Novel PRP techniques are superior to TMR and RPNI

The novel PRP techniques are superior to TMR and RPNI. (1) They reduce/eliminate pain while promoting meaningful recovery. (2) While TMR is effective when applied up to 3 months post-trauma, its efficacy decreases with longer delays [72]. (3) RPNI requires survival or a small muscle graft, which PRP does not. (4) RPNI requires sacrificing a motor nerve, while using PRP does not.

What underlies the high level of efficacy of the novel PRP application techniques?

While PRP provides short-term pain reduction/elimination [161, 162], the pain returns to 86% of patients [163]. This raises the question of why the novel PRP application techniques induce long-term pain reduction/elimination in 92%–100% of patients. The best explanation is in how the PRP was prepared and applied. First, applying PRP in a liquid form (without fibrin polymerization) causes the platelets to release all their factors within a few hours, while applying PRP in a polymerized fibrin form allows the platelets to release their factors over days [164], thus allowing the factors significantly more time to act. The novel PRP technique involved applying PRP in a polymerized fibrin form.

Second, although the optimal platelet concentration to provide maximal pain relief has not been determined, the degree of pain relief provided by PRP is reported to be linearly related to the number of platelets, the number and concentration of the growth and inflammatory factors they contain, and the number of neutrophils and monocytes [165]. Double centrifugation is the most commonly used PRP separation technique, yielding a ca. 4-fold increase in platelet concentration. This concentration is consistent with the finding that the degree of pain reduction associated with tennis elbow increases as the PRP platelet concentration is increased to 4–6-fold [166], while for knee osteoarthritis [167] and tendinopathies [168], a 3–4 fold concentration increase is recommended. However, it has also been reported that while a 2-fold increased platelet concentration yields good results for tissue healing, a 5-fold increase reduces healing [169, 170], and *in vitro* kills human tenocytes [171]. However, PRP used in the novel techniques prepared using GPS III concentrator tubes (Zimmer Biomet, Warsaw, IN) had a 9.3-fold increased platelet concentration.

Third, PRP from the GPS III concentrator tubes increased leukocytes by four-fold. Fourth, while most studies involve

applying a small amount of PRP (≤ 1 mL), long-term pain relief is associated with the application of a significantly larger volume (4–6 mL). Fifth, long-term pain relief was associated with applying PRP to long (4–16 cm) vs. short (<0.5 cm) lengths of nerve [172]. Sixth, most studies showing a temporary analgesic influence of PRP involve applying it to the surface of nerves. However, PRP provides longer-lasting analgesia when the nerve and applied PRP are surrounded by a collagen tube. The tube reduces the diffusion of platelet-released factors away from the site, resulting in a higher effective concentration of the factors, which allows them to act on the axons for a longer time. This hypothesis is supported by the finding that the efficacy of PRP applied to a rat nerve crush site is increased by surrounding the application site with a collagen tube [112].

Platelet-released factors

Platelets contain and release >300 identified factors [173]. While some are pre-packaged, with different types of platelet granules containing different factors, others are synthesized by platelets. The platelet's environment determines the factor synthesis and release pattern [174–176]. Thus, physiologically, platelets release their factors in a specific order, with some released fast and others more slowly [173, 177, 178]. For example, nerve growth factor (NGF) is released within minutes, while brain-derived neurotrophic factor (BDNF) is released more slowly [176]. This sequence is critical to allow the factors to perform specifically timed functions, such as releasing pro-inflammatory factors first, followed by releasing anti-inflammatory factors, which suppress pain [179].

Platelet-released factors reduce/eliminate pain by additional mechanisms, but journal length limitations do not allow a complete discussion of the platelet-released factors that may be involved in reducing/eliminating pain. However, nerve injury induces voltage gated sodium channel (Na(v)) 1.3 channel expression in nociceptive and higher-order spinal sensory neurons, leading to their hyperexcitability, spontaneous ectopic electrical activity, and the development of neuropathic pain [180–182]. Therefore, one mechanism for reducing/eliminating chronic neuropathic pain is to down-regulate the expression of these channels, thus eliminating the spontaneous electrical activity that underlies pain.

Drugs, such as local anesthetics and other Na(v) channel-blocking techniques, reduce neuropathic pain by inhibiting nociceptive axon spontaneous ectopic nerve activity and hyperactivity [183–185]. The pharmacological blockade of sodium channel activity reduces ectopic electrical activity [185, 186] and reverses nerve injury-induced hyperalgesia [187]. This has been attributed to the blocking of Na(v) 1.8 and Na(v) 1.7 channels, leading to reduced or eliminated nociceptive neuron hyperexcitability. However, the role of Na(v)

1.7 in neuropathic pain must be further investigated, and new analysis of a mouse Na(v)1.8 knockout suggests it is not involved in changing the neurons' post-injury pain threshold following peripheral nerve injury [188]. However, it has also been shown that administering antisense oligonucleotides against Na(v) 1.8 administered intrathecally completely reverses neuropathic pain behavior [189].

This is in contrast to the finding of Lai et al who reported that antisense oligonucleotides directed against Na(v) 1.8 administered intrathecally completely reverse neuropathic pain behavior [18]. It is possible that this discrepancy could be due to the up-regulation of the Na(v)1.7 channel seen in the Na(v)1.8 knockout mouse [12], which might mask an otherwise important role for Na(v)1.8 in neuropathic pain.

However, the pain suppression is not long-lasting. However, in rats, nerve injury-induced chronic pain is reduced by Na(v) 1.3 knockdown [190]. Further, intrathecal IL-10 infusion reduces neuropathic pain [191, 192] in part by down-regulating sodium channel expression in dorsal root ganglion (DRG) neurons [179], resulting in blocking nociceptive neurons' hyperexcitability and spontaneous ectopic electrical activity [21–23, 185, 189, 193]. Although platelets do not contain IL-10, they release large amounts of prostaglandin E2 (PGE2), which induces interleukin-10 (IL-10) release [194, 195], which reduces pain [196–198]. Thus, multiple platelet-released factors can induce long-term chronic neuropathic pain reduction/elimination.

Conclusion

Tissue injury-induced inflammation is the primary trigger of neuropathic pain, with chronic inflammation resulting in chronic pain. Injury induces the release of pro-inflammatory factors from local cells and other cells recruited to the injury site. While inflammation and pain are adverse events, they are required to trigger the normal physiological responses that induce the transition of a pro-inflammatory environment into an anti-inflammatory one, which is necessary for healing and pain elimination. Although some factors initially play pro-inflammatory roles, over time, they begin to play anti-inflammatory roles. Their roles depend on when they act after injury, what other factors are present, the cells on which they act, and the receptors on those cells. Thus, controlling pain requires controlling which factors are released and when. Platelets are an evolutionarily developed toolbox containing a physiological cocktail of factors for controlling cellular environments to promote healing and pain relief. While most studies find PRP only induces short-lived pain relief, two novel clinical techniques show that PRP can induce long-term chronic neuropathic pain elimination in all subjects. Further studies must determine which platelet-released factors, ratios, and concentrations induce these effects.

Author contributions

All authors contributed to the article and approved the submitted version.

Funding

The author(s) declare that no financial support was received for the research and/or publication of this article.

References

- DiBonaventura MD, Sadosky A, Concialdi K, Hopps M, Kudel I, Parsons B, et al. The prevalence of probable neuropathic pain in the US: results from a multimodal general-population health survey. *J Pain Res* (2017) **10**:2525–38. doi:10.2147/jpr.s127014
- Toth C, Lander J, Wiebe S. The prevalence and impact of chronic pain with neuropathic pain symptoms in the general population. *Pain Med* (2009) **10**(5): 918–29. doi:10.1111/j.1526-4637.2009.00655.x
- Teixeira MJ, da Paz MG, Bina MT, Santos SN, Raicher I, Galhardoni R, et al. Neuropathic pain after brachial plexus avulsion—central and peripheral mechanisms. *BMC Neurol* (2015) **15**:73. doi:10.1186/s12883-015-0329-x
- Campbell J, Neuroma Pain In, Gebhart GF, Schmidt RF, editors. *Encyclopedia of pain* 2. Berlin: Springer-Verlag (2013). p. 2056–8.
- Poppler LH, Mackinnon SE. The role of the peripheral nerve surgeon in the treatment of pain. *Neurotherapeutics* (2019) **16**(1):9–25. doi:10.1007/s13311-018-00695-z
- Felder JM, Ducic I. Impact of nerve surgery on opioid and medication use in patients with chronic nerve injuries. *Plast Reconstr Surg Glob open* (2021) **9**(9): e3789. doi:10.1097/gox.0000000000003789
- Miclescu A, Straatmann A, Gkatziani P, Butler S, Karlsten R, Gordh T. Chronic neuropathic pain after traumatic peripheral nerve injuries in the upper extremity: prevalence, demographic and surgical determinants, impact on health and on pain medication. *Scand J Pain* (2019) **20**(1):95–108. doi:10.1515/sjpain-2019-0111
- Samii M, Bear-Henney S, Ludemann W, Tatagiba M, Blömer U. Treatment of refractory pain after brachial plexus avulsion with dorsal root entry zone lesions. *Neurosurgery* (2001) **48**(6):1269–77. doi:10.1227/00006123-200106000-00016
- Colloca L, Ludman T, Bouhassira D, Baron R, Dickenson AH, Yarnitsky D, et al. Neuropathic pain. *Nat Rev Dis Primers* (2017) **3**:17002. doi:10.1038/nrdp.2017.2
- Attal N, Cruccu G, Haanpaa M, Hansson P, Jensen TS, Nurmikko T, et al. EFNS guidelines on pharmacological treatment of neuropathic pain. *Eur J Neurol* (2006) **13**(11):1153–69. doi:10.1111/j.1468-1331.2006.01511.x
- Finnerup NB, Otto M, Jensen TS, Sindrup SH. An evidence-based algorithm for the treatment of neuropathic pain. *MedGenMed* (2007) **9**(2):36.
- Hayes C, Browne S, Lantry G, Burstal R. Neuropathic pain in the acute pain service: a prospective survey. *Acute Pain* (2002) **4**(2):45–8. doi:10.1016/s1366-0071(02)00026-8
- Nikolajsen L, Black JA, Kroner K, Jensen TS, Waxman SG. Neuroma removal for neuropathic pain: efficacy and predictive value of lidocaine infusion. *The Clin J Pain* (2010) **26**(9):788–93. doi:10.1097/ajp.0b013e3181ed0823
- Souza JM, Cheesborough JE, Ko JH, Cho MS, Kuiken TA, Dumanian GA. Targeted muscle reinnervation: a novel approach to postamputation neuroma pain. *Clin Orthopaedics and Relat Res* (2014) **472**(10):2984–90. doi:10.1007/s11999-014-3528-7
- Calcagni M, Zimmermann S, Scaglioni MF, Giesen T, Giovanoli P, Fakin RM. The novel treatment of SVF-enriched fat grafting for painful end-neuromas of superficial radial nerve. *Microsurgery* (2018) **38**(3):264–9. doi:10.1002/micr.30122
- Lopez-Alvarez VM, Cobiañchi S, Navarro X. Chronic electrical stimulation reduces hyperalgesia and associated spinal changes induced by peripheral nerve injury. *Neuromodulation: Technology Neural Interf* (2019) **22**(5):509–18. doi:10.1111/ner.12927

Conflict of interest

The author(s) declared no potential conflicts of interest with respect to the research, authorship, and/or publication of this article.

Generative AI statement

The author(s) declare that no Generative AI was used in the creation of this manuscript.

- Billet B, Hanssens K, De Coster O, Santos A, Rotte A, Minne V. High-frequency (10 kHz) spinal cord stimulation for the treatment of focal, chronic postsurgical neuropathic pain: results from a prospective study in Belgium. *Pain Manag* (2021) **12**:75–85. doi:10.2217/pmt-2021-0045
- Lee KY, Bae C, Lee D, Kagan Z, Bradley K, Chung JM, et al. Low-intensity, kilohertz frequency spinal cord stimulation differently affects excitatory and inhibitory neurons in the rodent superficial dorsal horn. *Neuroscience* (2020) **428**:132–9. doi:10.1016/j.neuroscience.2019.12.031
- Kato K, Kikuchi S, Shubayev VI, Myers R. Distribution and tumor necrosis factor- α isoform binding specificity of locally administered etanercept into injured and uninjured rat sciatic nerve. *Neuroscience* (2009) **160**(2):492–500. doi:10.1016/j.neuroscience.2009.02.038
- Kremer M, Yalcin I, Goumon Y, Wurtz X, Nexon L, Daniel D, et al. A dual noradrenergic mechanism for the relief of neuropathic allodynia by the antidepressant drugs duloxetine and amitriptyline. *J Neurosci* (2018) **38**(46): 9934–54. doi:10.1523/jneurosci.1004-18.2018
- Suter MR, Papaloizos M, Berde CB, Woolf C, Gilliard N, Spahn D, et al. Development of neuropathic pain in the rat spared nerve injury model is not prevented by a peripheral nerve block. *Anesthesiology* (2003) **99**(6):1402–8. doi:10.1097/0000542-200312000-00025
- Capano A, Weaver R, Burkman E. Evaluation of the effects of CBD hemp extract on opioid use and quality of life indicators in chronic pain patients: a prospective cohort study. *Postgrad Med* (2020) **132**(1):56–61. doi:10.1080/00325481.2019.1685298
- Chaplan SR, Guo HQ, Lee DH, Luo L, Liu C, Kuei C, et al. Neuronal hyperpolarization-activated pacemaker channels drive neuropathic pain. *J Neurosci* (2003) **23**(4):1169–78. doi:10.1523/jneurosci.23-04-01169.2003
- Wu J, Chiu DT. Painful neuromas: a review of treatment modalities. *Ann Plast Surg* (1999) **43**(6):661–7. doi:10.1097/0000637-199912000-00016
- Allen CB, Williamson TK, Norwood SM, Gupta A. Do electrical stimulation devices reduce pain and improve function? A comparative review. *Pain Ther* (2023) **12**(6):1339–54. doi:10.1007/s40122-023-00554-6
- Parisien M, Lima LV, Dagostino C, El-Hachem N, Drury GL, Grant AV, et al. Acute inflammatory response via neutrophil activation protects against the development of chronic pain. *Sci Transl Med* (2022) **14**(644):eabj9954. doi:10.1126/scitranslmed.abj9954
- Decrouy-Duruz V, Christen T, Raffoul W. Evaluation of surgical treatment for neuropathic pain from neuroma in patients with injured peripheral nerves. *J Neurosurg* (2018) **128**(4):1235–40. doi:10.3171/2017.1.jns.161778
- Freeman R. New and developing drugs for the treatment of neuropathic pain in diabetes. *Curr Diab Rep* (2013) **13**(4):500–8. doi:10.1007/s11892-013-0396-6
- Finnerup NB, Sindrup SH, Jensen TS. The evidence for pharmacological treatment of neuropathic pain. *Pain* (2010) **150**(3):573–81. doi:10.1016/j.pain.2010.06.019
- Caruso R, Ostuzzi G, Turrini G, Ballette F, Recla E, Dall'Olio R, et al. Beyond pain: can antidepressants improve depressive symptoms and quality of life in patients with neuropathic pain? A systematic review and meta-analysis. *Pain* (2019) **160**:2186–98. doi:10.1097/j.pain.0000000000001622
- Gisev N, Nielsen S, Campbell G, Santo T, Jr, Mant A, Bruno R, et al. Antidepressant use among people prescribed opioids for chronic noncancer pain. *Pain Med* (2019) **20**:2450–8. doi:10.1093/pm/pnz009

32. Lovaglio AC, Socolovsky M, Di Masi G, Bonilla G. Treatment of neuropathic pain after peripheral nerve and brachial plexus traumatic injury. *Neurol India* (2019) **67**(Suppl. ment):S32–S37. doi:10.4103/0028-3886.250699
33. Watson PCN, Moulin D, Watt-Watson J, Gordon A, Eisenhoffer J. Controlled-release oxycodone relieves neuropathic pain: a randomized controlled trial in painful diabetic neuropathy. *Pain* (2003) **105**(1–2):71–8. doi:10.1016/s0304-3959(03)00160-x
34. Sindrup SH, Andersen G, Madsen C, Smith T, Brøsen K, Jensen TS. Tramadol relieves pain and allodynia in polyneuropathy: a randomised, double-blind, controlled trial. *Pain* (1999) **83**(1):85–90. doi:10.1016/s0304-3959(99)00079-2
35. Harati Y, Gooch C, Swenson M, Edelman S, Greene D, Raskin P, et al. Double-blind randomized trial of tramadol for the treatment of the pain of diabetic neuropathy. *Neurology* (1998) **50**(6):1842–6. doi:10.1212/wnl.50.6.1842
36. Sato R, Sekiguchi M, Konno SI. Acetaminophen combined with tramadol is more effective than acetaminophen or tramadol to reduce neuropathic root pain: an experimental study with application of nucleus pulposus in a rat model. *Eur Spine J* (2020) **29**(1):169–78. doi:10.1007/s00586-019-06190-z
37. Vinik A. Clinical review: use of antiepileptic drugs in the treatment of chronic painful diabetic neuropathy. *The J Clin Endocrinol and Metab* (2005) **90**(8):4936–45. doi:10.1210/jc.2004-2376
38. Backonja MM. Gabapentin monotherapy for the symptomatic treatment of painful neuropathy: a multicenter, double-blind, placebo-controlled trial in patients with diabetes mellitus. *Epilepsia* (1999) **40**:S57–S74. doi:10.1111/j.1528-1157.1999.tb00934.x
39. Vannier JL, Belkheyar Z, Oberlin C, Montravers P. Management of neuropathic pain after brachial plexus injury in adult patients: a report of 60 cases. *Ann Françaises d'Anesthésie de Réanimation* (2008) **27**(11):890–5. doi:10.1016/j.annfar.2008.08.013
40. Sindou MP, Blondet E, Emery E, Mertens P. Microsurgical lesioning in the dorsal root entry zone for pain due to brachial plexus avulsion: a prospective series of 55 patients. *J Neurosurg* (2005) **102**(6):1018–28. doi:10.3171/jns.2005.102.6.1018
41. van Dongen R, Cohen SP, van Kleef M, Mekhail N, Huygen F. 22. Traumatic plexus lesion. *Pain Pract* (2011) **11**(4):414–20. doi:10.1111/j.1533-2500.2011.00451.x
42. Allegri N, Mennuni S, Rulli E, Vanacore N, Corli O, Floriani I, et al. Systematic review and meta-analysis on neuropsychological effects of long-term use of opioids in patients with chronic noncancer pain. *Pain Pract* (2019) **19**(3):328–43. doi:10.1111/papr.12741
43. Guan J, Tanaka S, Kawakami K. Anticonvulsants or antidepressants in combination pharmacotherapy for treatment of neuropathic pain in cancer patients: a systematic review and meta-analysis. *The Clin J Pain* (2016) **32**(8):719–25. doi:10.1097/ajp.0000000000000310
44. Rosenstock J, Tuchman M, LaMoreaux L, Sharma U. Pregabalin for the treatment of painful diabetic peripheral neuropathy: a double-blind, placebo-controlled trial. *Pain* (2004) **110**(3):628–38. doi:10.1016/j.pain.2004.05.001
45. Torrance N, Smith BH, Watson MC, Bennett MI. Medication and treatment use in primary care patients with chronic pain of predominantly neuropathic origin. *Fam Pract* (2007) **24**(5):481–5. doi:10.1093/fampra/cmm042
46. Stein C. New concepts in opioid analgesia. *Expert Opin Investig Drugs* (2018) **27**(10):765–75. doi:10.1080/13543784.2018.1516204
47. Papagianni A, Siedler G, Sommer C, Üçeyler N. Capsaicin 8% patch reversibly reduces A-delta fiber evoked potential amplitudes. *PAIN Rep* (2018) **3**(2):e644. doi:10.1097/pr9.0000000000000644
48. Wolff RF, Bala MM, Westwood M, Kessels A, Kleijnen J. 5% lidocaine medicated plaster in painful diabetic peripheral neuropathy (DPN): a systematic review. *Swiss Med Wkly* (2010) **140**(21–22):297–306. doi:10.4414/smw.2010.12995
49. Schreiber AK, Nones CF, Reis RC, Chichorro JG, Cunha JM. Diabetic neuropathic pain: physiopathology and treatment. *World J Diabetes* (2015) **6**(3):432–44. doi:10.4239/wjd.v6.i3.432
50. Bertoch T, D'Aunno D, McCoun J. Suzetrigine, a non-opioid NaV1.8 inhibitor for treatment of moderate-to-severe acute pain: two phase 3 randomized clinical trials. *Anesthesiology* (2025). doi:10.1097/ALN.0000000000005460
51. Niesters M, Martini C, Dahan A. Ketamine for chronic pain: risks and benefits. *Br J Clin Pharmacol* (2014) **77**(2):357–67. doi:10.1111/bcp.12094
52. Piotrowska A, Starnowska-Sokół J, Makuch W, Mika J, Witkowska E, Tymecka D, et al. Novel bifunctional hybrid compounds designed to enhance the effects of opioids and antagonize the pronociceptive effects of non-opioid peptides as potent analgesics in a rat model of neuropathic pain. *Pain* (2020) **162**:432–45. doi:10.1097/j.pain.0000000000002045
53. American Pain Foundation. Overview of American pain surveys: 2005–2006. *J Pain Palliat Care Pharmacother* (2008) **22**(1):33–8. doi:10.1080/15360280801989344
54. Benyamin R, Trescot AM, Datta S, Buenaventura R, Adlaka R, Sehgal N, et al. Opioid complications and side effects. *Pain Physician* (2008) **11**(2 Suppl. 1):S105–20.
55. Katz WA, Barkin RL. Dilemmas in chronic/persistent pain management. *Disease-a-Month* (2010) **56**(4):233–50. doi:10.1016/j.disamonth.2009.12.006
56. Gross JL, Perate AR, Elkassabany NM. Pain management in trauma in the age of the opioid crisis. *Anesthesiology Clin* (2019) **37**(1):79–91. doi:10.1016/j.anclin.2018.09.010
57. Lin CS, Lin YC, Lao HC, Chen CC. Interventional treatments for postherpetic neuralgia: a systematic review. *Pain Physician* (2019) **22**(3):209–28.
58. Pet MA, Ko JH, Friedly JL, Smith DG. Traction neurectomy for treatment of painful residual limb neuroma in lower extremity amputees. *J Orthopaedic Trauma* (2015) **29**(9):e321–5. doi:10.1097/bot.0000000000000337
59. Zuniga JR, Yates DM. Factors determining outcome after trigeminal nerve surgery for neuropathic pain. *J Oral Maxillofacial Surg* (2016) **74**(7):1323–9. doi:10.1016/j.joms.2016.02.005
60. Ducic I, Yoon J, Eberlin KR. Treatment of neuroma-induced chronic pain and management of nerve defects with processed nerve allografts. *Plast Reconstr Surg - Glob Open* (2019) **7**(12):e2467. doi:10.1097/gox.0000000000002467
61. Mass DP, Ciano MC, Tortosa R, Newmeyer WL, Kilgore ES. Treatment of painful hand neuromas by their transfer into bone. *Plast Reconstr Surg* (1984) **74**(2):182–5. doi:10.1097/00006534-198408000-00002
62. Ives GC, Kung TA, Nghiem BT, Ursu DC, Brown DL, Cederna PS, et al. Current state of the surgical treatment of terminal neuromas. *Neurosurgery* (2018) **83**(3):354–64. doi:10.1093/neuros/nyx500
63. Chappell AG, Jordan SW, Dumanian GA. Targeted muscle reinnervation for treatment of neuropathic pain. *Clin Plast Surg* (2020) **47**(2):285–93. doi:10.1016/j.cps.2020.01.002
64. Dumanian GA, Potter BK, Mioton LM, Ko JH, Cheesborough JE, Souza JM, et al. Targeted muscle reinnervation treats neuroma and phantom pain in major limb amputees: a randomized clinical trial. *Ann Surg* (2019) **270**(2):238–46. doi:10.1097/sla.0000000000003088
65. Janes LE, Fracol ME, Dumanian GA, Ko JH. Targeted muscle reinnervation for the treatment of neuroma. *Hand Clin* (2021) **37**(3):345–59. doi:10.1016/j.hcl.2021.05.002
66. Mauch JT, Kao DS, Friedly JL, Liu Y. Targeted muscle reinnervation and regenerative peripheral nerve interfaces for pain prophylaxis and treatment: a systematic review. *PM&R* (2023) **15**:1457–65. doi:10.1002/pmrj.12972
67. Al-Ajam Y, Woollard A, Kang N. Advances in upper limb loss rehabilitation: the role of targeted muscle reinnervation and regenerative peripheral nerve interfaces. *Plast Aesthet Res* (2022) **9**(63):63. doi:10.20517/2347-9264.2022.24
68. Senger JLB, Hardy P, Thorkelsson A, Duia S, Hsiao R, Kemp SWP, et al. A direct comparison of targeted muscle reinnervation and regenerative peripheral nerve interfaces to prevent neuroma pain. *Neurosurgery* (2023) **93**(5):1180–91. doi:10.1227/neu.0000000000002541
69. Shamoun F, Shamoun V, Akhavan A, Tuffaha SH. Target receptors of regenerating nerves: neuroma formation and current treatment options. *Front Mol Neurosci* (2022) **15**:859221. doi:10.3389/fnmol.2022.859221
70. Valerio IL, Dumanian GA, Jordan SW, Mioton LM, Bowen BJ, West JM, et al. Preemptive treatment of phantom and residual limb pain with targeted muscle reinnervation at the time of major limb amputation. *J Am Coll Surgeons* (2019) **228**(3):217–26. doi:10.1016/j.jamcollsurg.2018.12.015
71. Dellon AL, Mackinnon SE. Treatment of the painful neuroma by neuroma resection and muscle implantation. *Plast Reconstr Surg* (1986) **77**(3):427–36. doi:10.1097/00006534-198603000-00016
72. Roth E, Linehan A, Weihrauch D, Stucky C, Hogan Q, Hoben G. Targeted muscle reinnervation prevents and reverses rat pain behaviors after nerve transection. *Pain* (2023) **164**(2):316–24. doi:10.1097/j.pain.0000000000002702
73. Xie W, Strong JA, Zhang JM. Active nerve regeneration with failed target reinnervation drives persistent neuropathic pain. *eNeuro* (2017) **4**(1):ENEURO.0008–17.2017. doi:10.1523/eneuro.0008-17.2017
74. Serra J, Bostock H, Sola R, Aleu J, García E, Cokic B, et al. Microneurographic identification of spontaneous activity in C-nociceptors in neuropathic pain states in humans and rats. *Pain* (2012) **153**(1):42–55. doi:10.1016/j.pain.2011.08.015
75. Xie W, Strong JA, Meij JTA, Zhang JM, Yu L. Neuropathic pain: early spontaneous afferent activity is the trigger. *Pain* (2005) **116**(3):243–56. doi:10.1016/j.pain.2005.04.017
76. Woolf CJ, Salter MW. Neuronal plasticity: increasing the gain in pain. *Science* (2000) **288**(5472):1765–8. doi:10.1126/science.288.5472.1765

77. Lanier ST, Jordan SW, Ko JH, Dumanian GA. Targeted muscle reinnervation as a solution for nerve pain. *Plast and Reconstr Surg* (2020) **146**(5):651e–63e. doi:10.1097/prs.00000000000007235
78. Peters BR, Russo SA, West JM, Moore AM, Schulz SA. Targeted muscle reinnervation for the management of pain in the setting of major limb amputation. *SAGE Open Med* (2020) **8**:2050312120959180. doi:10.1177/2050312120959180
79. Jankowski MP, Lawson JJ, McIlwraith SL, Rau KK, Anderson CE, Albers KM, et al. Sensitization of cutaneous nociceptors after nerve transection and regeneration: possible role of target-derived neurotrophic factor signaling. *J Neurosci* (2009) **29**(6):1636–47. doi:10.1523/jneurosci.3474-08.2009
80. Pet MA, Ko JH, Friedly JL, Mourad PD, Smith DG. Does targeted nerve implantation reduce neuroma pain in amputees? *Clin Orthopaedics and Relat Res* (2014) **472**(10):2991–3001. doi:10.1007/s11999-014-3602-1
81. Valerio I, Schulz SA, West J, Westenberg RF, Eberlin KR. Targeted muscle reinnervation combined with a vascularized pedicled regenerative peripheral nerve interface. *Plast Reconstr Surg - Glob Open* (2020) **8**(3):e2689. doi:10.1097/gox.0000000000002689
82. Kato N, Htut M, Taggart M, Carlstedt T, Birch R. The effects of operative delay on the relief of neuropathic pain after injury to the brachial plexus: a review of 148 cases. *The J Bone Joint Surg Br volume* (2006) **88-B**(6):756–9. doi:10.1302/0301-620x.88b6.16995
83. Berman JS, Birch R, Anand P. Pain following human brachial plexus injury with spinal cord root avulsion and the effect of surgery. *Pain* (1998) **75**(2-3):199–207. doi:10.1016/s0304-3959(97)00220-0
84. Decosterd I, Woolf CJ. Spared nerve injury: an animal model of persistent peripheral neuropathic pain. *Pain* (2000) **87**(2):149–58. doi:10.1016/s0304-3959(00)00276-1
85. Zhang J, Liu W, Zhang X, Lin S, Yan J, Ye J. Sema3A inhibits axonal regeneration of retinal ganglion cells via ROCK2. *Brain Res* (2020) **1727**:146555. doi:10.1016/j.brainres.2019.146555
86. Wu F, Miao X, Chen J, Sun Y, Liu Z, Tao Y, et al. Down-regulation of GAP-43 by inhibition of caspases-3 in a rat model of neuropathic pain. *Int J Clin Exp Pathol* (2012) **5**(9):948–55.
87. Lister RC, Tsui JM, Naram A. A technical guide for sciatic nerve targeted muscle reinnervation in a transfemoral amputee. *Plast Reconstr Surg - Glob Open* (2022) **10**(9):e4525. doi:10.1097/gox.00000000000004525
88. Shin SE, Haffner ZK, Chang BL, Kleiber GM. A pilot investigation into targeted muscle reinnervation for complex regional pain syndrome, type II. *Plast Reconstr Surg - Glob Open* (2022) **10**(12):e4718. doi:10.1097/gox.00000000000004718
89. Fu CJ, Sun JB, Bi ZG, Wang XM, Yang CL. Evaluation of platelet-rich plasma and fibrin matrix to assist in healing and repair of rotator cuff injuries: a systematic review and meta-analysis. *Clin Rehabil* (2017) **31**(2):158–72. doi:10.1177/0269215516634815
90. Ribeiro Ad G, Ricioli Junior W, Silva AR, Polesello GC, Guimarães RP. Prp in the treatment of trochanteric syndrome: a pilot study. *Acta Ortop Bras* (2016) **24**(4):208–12. doi:10.1590/1413-785220162404159837
91. Verhaegen F, Brys P, Debeer P. Rotator cuff healing after needling of a calcific deposit using platelet-rich plasma augmentation: a randomized, prospective clinical trial. *J Shoulder Elbow Surg* (2016) **25**(2):169–73. doi:10.1016/j.jse.2015.10.009
92. Grassi A, Napoli F, Romandini I, Samuelsson K, Zaffagnini S, Candrian C, et al. Is platelet-rich plasma (PRP) effective in the treatment of acute muscle injuries? A systematic review and meta-analysis. *Sports Med* (2018) **48**(4):971–89. doi:10.1007/s40279-018-0860-1
93. Khan M, Bedi A. Cochrane in CORR ®: platelet-rich therapies for musculoskeletal soft tissue injuries (review). *Clin Orthopaedics and Relat Res* (2015) **473**(7):2207–13. (Review). doi:10.1007/s11999-015-4207-z
94. Fitzpatrick J, Bulsara MK, O'Donnell J, McCrory PR, Zheng MH. The effectiveness of platelet-rich plasma injections in gluteal tendinopathy: a randomized, double-blind controlled trial comparing a single platelet-rich plasma injection with a single corticosteroid injection. *Am J Sports Med* (2018) **46**:933–9. doi:10.1177/0363546517745525
95. Yoshida M, Funasaki H, Marumo K. Efficacy of autologous leukocyte-reduced platelet-rich plasma therapy for patellar tendinopathy in a rat treadmill model. *Muscle Ligaments Tendons J* (2019) **06**(2):205–15. doi:10.32098/mltj.02.2016.07
96. Cook JL, Smith PA, Bozynski CC, Kuroki K, Cook CR, Stoker AM, et al. Multiple injections of leukoreduced platelet rich plasma reduce pain and functional impairment in a canine model of ACL and meniscal deficiency. *J Orthopaedic Res* (2016) **34**(4):607–15. doi:10.1002/jor.23054
97. Dyson-Hudson TA, Hogaboom NS, Nakamura R, Terry A, Malanga GA. Ultrasound-guided platelet-rich plasma injection for the treatment of recalcitrant rotator cuff disease in wheelchair users with spinal cord injury: a pilot study. *The J Spinal Cord Med* (2020) **45**:42–8. doi:10.1080/10790268.2020.1754676
98. Moezi M, Tahririan M, Motifard M, Nemati M, Nemati A. Ultrasound guided platelet-rich plasma injection for the treatment of rotator cuff tendinopathy. *Adv Biomed Res* (2016) **5**:200. doi:10.4103/2277-9175.190939
99. Kim SJ, Kim EK, Kim SJ, Song DH. Effects of bone marrow aspirate concentrate and platelet-rich plasma on patients with partial tear of the rotator cuff tendon. *J Orthop Surg Res* (2018) **13**(1):1. doi:10.1186/s13018-017-0693-x
100. Sengodan VC, Kurian S, Ramasamy R. Treatment of partial rotator cuff tear with ultrasound-guided platelet-rich plasma. *J Clin Imaging Sci* (2017) **7**(32):32. doi:10.4103/jcis.jcis_26_17
101. Sanchez M, Guadilla J, Fiz N, Andia I. Ultrasound-guided platelet-rich plasma injections for the treatment of osteoarthritis of the hip. *Rheumatology* (2012) **51**(1):144–50. doi:10.1093/rheumatology/ker303
102. Patel S, Dhillon MS, Aggarwal S, Marwaha N, Jain A. Treatment with platelet-rich plasma is more effective than placebo for knee osteoarthritis: a prospective, double-blind, randomized trial. *Am J Sports Med* (2013) **41**(2):356–64. doi:10.1177/0363546512471299
103. Wilson JJ, Lee KS, Miller AT, Wang S. Platelet-rich plasma for the treatment of chronic plantar fasciopathy in adults: a case series. *Foot and Ankle Specialist* (2014) **7**(1):61–7. doi:10.1177/1938640013509671
104. Rossi LA, Molina Romoli AR, Bertona Altieri BA, Burgos Flor JA, Scordo WE, Elizondo CM. Does platelet-rich plasma decrease time to return to sports in acute muscle tear? A randomized controlled trial. *Knee Surg Sports Traumatol Arthrosc* (2017) **25**(10):3319–25. doi:10.1007/s00167-016-4129-7
105. Hurley ET, Lim Fat D, Moran CJ, Mullett H. The efficacy of platelet-rich plasma and platelet-rich fibrin in arthroscopic rotator cuff repair: a meta-analysis of randomized controlled trials. *Am J Sports Med* (2018) **47**:753–61. doi:10.1177/0363546517751397
106. Fitzpatrick J, Bulsara M, Zheng MH. The effectiveness of platelet-rich plasma in the treatment of tendinopathy: a meta-analysis of randomized controlled clinical trials. *Am J Sports Med* (2017) **45**(1):226–33. doi:10.1177/0363546516643716
107. Kuffler DP. Platelet-rich plasma and the elimination of neuropathic pain. *Mol Neurobiol* (2013) **48**(2):315–32. doi:10.1007/s12035-013-8494-7
108. Huang SH, Wu SH, Lee SS, Lin YN, Chai CY, Lai CS, et al. Platelet-rich plasma injection in burn scar areas alleviates neuropathic scar pain. *Int J Med Sci* (2018) **15**(3):238–47. doi:10.7150/ijms.22563
109. Anjayani S, Wirohadidjojo YW, Adam AM, Suwandi D, Seweng A, Amiruddin MD. Sensory improvement of leprosy peripheral neuropathy in patients treated with perineural injection of platelet-rich plasma. *Int J Dermatol* (2014) **53**(1):109–13. doi:10.1111/ijd.12162
110. Behrooz Z, Ramezani F, Janzadeh A, Rahimi B, Nasirinezhad F. Platelet-rich plasma in umbilical cord blood reduces neuropathic pain in spinal cord injury by altering the expression of ATP receptors. *Physiol and Behav* (2021) **228**:113186. doi:10.1016/j.physbeh.2020.113186
111. Ikumi A, Hara Y, Okano E, Kohyama S, Arai N, Taniguchi Y, et al. Intraoperative local administration of platelet-rich plasma (PRP) during neurolysis surgery for the treatment of digital nerve crush injury. *Case Rep Orthopedics* (2018) **2018**:1–6. doi:10.1155/2018/1275713
112. Vares P, Dehghan MM, Bastami F, Biazar E, Shamloo N, Heidari Keshel S, et al. Effects of platelet-rich fibrin/collagen membrane on sciatic nerve regeneration. *J Craniofac Surg* (2021) **32**(2):794–8. doi:10.1097/scs.00000000000007003
113. Hibner M, Castellanos ME, Drachman D, Balducci J. Repeat operation for treatment of persistent pudendal nerve entrapment after pudendal neurolysis. *J Minimally Invasive Gynecol* (2012) **19**(3):325–30. doi:10.1016/j.jmig.2011.12.022
114. Dong C, Sun Y, Qi Y, Zhu Y, Wei H, Wu D, et al. Effect of platelet-rich plasma injection on mild or moderate carpal tunnel syndrome: an updated systematic review and meta-analysis of randomized controlled trials. *Biomed Res Int* (2020) **2020**:5089378. doi:10.1155/2020/5089378
115. Hassanien M, Elawamy A, Kamel EZ, Khalifa WA, Abolfadl GM, Roushdy ASI, et al. Perineural platelet-rich plasma for diabetic neuropathic pain, could it make a difference? *Pain Med* (2020) **21**(4):757–65. doi:10.1093/pm/pnz140
116. Hernández G, Ospina-Tascón GA, Damiani LP, Estenssoro E, Dubin A, Hurtado J, et al. Effect of a resuscitation strategy targeting peripheral perfusion status vs serum lactate levels on 28-day mortality among patients with septic shock: the ANDROMEDA-SHOCK randomized clinical trial. *JAMA* (2019) **321**(7):654–64. doi:10.1001/jama.2019.0071
117. Bhatia R, Chopra G. Efficacy of platelet rich plasma via lumbar epidural route in chronic prolapsed intervertebral disc patients-A pilot study. *J Clin Diagn Res : JCDR* (2016) **10**(9):UC05–UC07. doi:10.7860/JCDR/2016/21863.8482

118. Anitua E, Kirchner F. Intradiscal and intra-articular facet infiltrations with plasma rich in growth factors reduce pain in patients with chronic low back pain. *J Craniovertebral Junction Spine* (2016) 7(4):250–6. doi:10.4103/0974-8237.193260
119. Ruiz-Lopez R, Tsai YC. A randomized double-blind controlled pilot study comparing leucocyte-rich platelet-rich plasma and corticosteroid in caudal epidural injection for complex chronic degenerative spinal pain. *Pain Pract* (2020) 20(6):639–46. doi:10.1111/papr.12893
120. Bise S, Dallaudiere B, Pesquer L, Pedram M, Meyer P, Antoun MB, et al. Comparison of interlaminar CT-guided epidural platelet-rich plasma versus steroid injection in patients with lumbar radicular pain. *Eur Radiol* (2020) 30(6):3152–60. doi:10.1007/s00330-020-06733-9
121. Centeno C, Markle J, Dodson E, Stemper I, Hyzy M, Williams C, et al. The use of lumbar epidural injection of platelet lysate for treatment of radicular pain. *J Exp Orthopaedics* (2017) 4(1):38. doi:10.1186/s40634-017-0113-5
122. Auffero D, Vincent H, Sampson S. Regenerative injection treatment in the spine: review and case series with platelet rich plasma. *J Stem Cells Res Rev and Rep* (2015) 2:1019.
123. Becker C, Heidersdorf S, Drewlo S, de Rodriguez SZ, Krämer J, Willburger RE. Efficacy of epidural perineural injections with autologous conditioned serum for lumbar radicular compression: an investigator-initiated, prospective, double-blind, reference-controlled study. *Spine (Phila Pa 1976)* (2007) 32(17):1803–8. doi:10.1097/brs.0b013e3181076514
124. Uzun H, Bitik O, Uzun O, Ersoy US, Aktaş E. Platelet-rich plasma versus corticosteroid injections for carpal tunnel syndrome. *J Plast Surg Hand Surg* (2017) 51(5):301–5. doi:10.1080/2000656x.2016.1260025
125. Hibner M, Castellanos ME, Drachman D, Balducci J. Repeat operation for treatment of persistent pudendal nerve entrapment after pudendal neurolysis. *J Minimally Invasive Gynecol* (2012) 19:325–30. doi:10.1016/j.jmig.2011.12.022
126. Lin CP, Chang KV, Huang YK, Wu WT, Özçakar L. Regenerative injections including 5% dextrose and platelet-rich plasma for the treatment of carpal tunnel syndrome: a systematic review and network meta-analysis. *Pharmaceuticals (Basel)* (2020) 13(3):49. doi:10.3390/ph13030049
127. Kuffler DP. Differing efficacies of autologous platelet-rich plasma in reducing pain following rotator-cuff injury in a single patient. *J Pain Res* (2018) 11:2239–45. doi:10.2147/jpr.s169647
128. Kuffler DP. Variables affecting the potential efficacy of PRP in providing chronic pain relief. *J Pain Res* (2018) 12:109–16. doi:10.2147/jpr.s190065
129. Shao S, Pan R, Chen Y. Autologous platelet-rich plasma for diabetic foot ulcer. *Trends Endocrinol and Metab* (2020) 31(12):885–90. doi:10.1016/j.tem.2020.10.003
130. Castillo TN, Pouliot MA, Kim HJ, Drago J. Comparison of growth factor and platelet concentration from commercial platelet-rich plasma separation systems. *Am J Sports Med* (2011) 39(2):266–71. doi:10.1177/0363546510387517
131. Hsu WK, Mishra A, Rodeo SR, Fu F, Terry MA, Randelli P, et al. Platelet-rich plasma in orthopaedic applications: evidence-based recommendations for treatment. *J Am Acad Orthopaedic Surgeons* (2013) 21(12):739–48. doi:10.5435/jaas-22-08-469
132. Oudelaar BW, Peerbooms JC, Huis in 't Veld R, Vochoeteloo AJ. Concentrations of blood components in commercial platelet-rich plasma separation systems: a review of the literature. *Am J Sports Med* (2019) 47(2):479–87. doi:10.1177/0363546517746112
133. Marx RE. Platelet-rich plasma (PRP): what is PRP and what is not PRP? *Implant Dentistry* (2001) 10(4):225–8. doi:10.1097/00008505-200110000-00002
134. Arora S, Agnihotri N. Platelet derived biomaterials for therapeutic use: review of technical aspects. *Indian J Hematol Blood Transfus* (2017) 33(2):159–67. doi:10.1007/s12288-016-0669-8
135. Dohan Ehrenfest DM, Pinto NR, Pereda A, Jiménez P, Corso MD, Kang BS, et al. The impact of the centrifuge characteristics and centrifugation protocols on the cells, growth factors, and fibrin architecture of a leukocyte- and platelet-rich fibrin (L-PRF) clot and membrane. *Platelets* (2018) 29(2):171–84. doi:10.1080/09537104.2017.1293812
136. Weibrich G, Kleis WK, Hitzler WE, Hafner G. Comparison of the platelet concentrate collection system with the plasma-rich-in-growth-factors kit to produce platelet-rich plasma: a technical report. *The Int J Oral and Maxill Implants* (2005) 20(1):118–23.
137. Schar MO, Diaz-Romero J, Kohl S, Zumstein MA, Nesic D. Platelet-rich concentrates differentially release growth factors and induce cell migration *in vitro*. *Clin Orthopaedics and Relat Res* (2015) 473(5):1635–43. doi:10.1007/s11999-015-4192-2
138. Mazzocca AD, McCarthy MB, Chowaniec DM, Cote MP, Romeo AA, Bradley JP, et al. Platelet-rich plasma differs according to preparation method and human variability. *J Bone Joint Surg* (2012) 94(4):308–16. doi:10.2106/jbjs.k.00430
139. Cavallo C, Roffi A, Grigolo B, Mariani E, Pratelli L, Merli G, et al. Platelet-rich plasma: the choice of activation method affects the release of bioactive molecules. *Biomed Res Int* (2016) 2016:1–7. doi:10.1155/2016/6591717
140. Eppley BL, Woodell JE, Higgins J. Platelet quantification and growth factor analysis from platelet-rich plasma: implications for wound healing. *Plast Reconstr Surg* (2004) 114(6):1502–8. doi:10.1097/01.prs.0000138251.07040.51
141. Kuffler DP. Platelet-rich plasma promotes axon regeneration, wound healing, and pain reduction: fact or fiction. *Mol Neurobiol* (2015) 52(2):990–1014. doi:10.1007/s12035-015-9251-x
142. Belch JJ, McArdle BM, Burns P, Lowe GDO, Forbes CD. The effects of acute smoking on platelet behaviour, fibrinolysis and haemorheology in habitual smokers. *Thromb Haemost* (1984) 51(1):006–8. doi:10.1055/s-0038-1660996
143. Mukamal KJ, Massaro JM, Ault KA, Mittleman MA, Sutherland PA, Lipinska I, et al. Alcohol consumption and platelet activation and aggregation among women and men: the Framingham Offspring Study. *Alcohol Clin and Exp Res* (2005) 29(10):1906–12. doi:10.1097/01.alc.0000183011.86768.61
144. Olas B, Wachowicz B, Saluk-Juszczak J, Zieliński T. Effect of resveratrol, a natural polyphenolic compound, on platelet activation induced by endotoxin or thrombin. *Thromb Res* (2002) 107(3–4):141–5. doi:10.1016/s0049-3848(02)00273-6
145. Williams JK, Clarkson TB. Dietary soy isoflavones inhibit *in-vivo* constrictor responses of coronary arteries to collagen-induced platelet activation. *Coron Artery Dis* (1998) 9(11):759–64. doi:10.1097/00019501-199809110-00009
146. Frary CD, Johnson RK, Wang MQ. Food sources and intakes of caffeine in the diets of persons in the United States. *J Am Diet Assoc* (2005) 105(1):110–3. doi:10.1016/j.jada.2004.10.027
147. Hubbard GP, Wolfram S, Lovegrove JA, Gibbins J. Ingestion of quercetin inhibits platelet aggregation and essential components of the collagen-stimulated platelet activation pathway in humans. *J Thromb Haemost* (2004) 2(12):2138–45. doi:10.1111/j.1538-7836.2004.01067.x
148. Alvarez-Suarez JM, Giampieri F, Tulipani S, Casoli T, Di Stefano G, González-Paramás AM, et al. One-month strawberry-rich anthocyanin supplementation ameliorates cardiovascular risk, oxidative stress markers and platelet activation in humans. *The J Nutr Biochem* (2014) 25(3):289–94. doi:10.1016/j.jnutbio.2013.11.002
149. de Lorgeril M, Renaud S, Mamelle N, Salen P, Martin JL, Monjaud I, et al. Mediterranean alpha-linolenic acid-rich diet in secondary prevention of coronary heart disease. *Lancet* (1994) 343(8911):1454–9. doi:10.1016/s0140-6736(94)92580-1
150. Sudic D, Razmara M, Forslund M, Ji Q, Hjendahl P, Li N. High glucose levels enhance platelet activation: involvement of multiple mechanisms. *Br J Haematol* (2006) 133(3):315–22. doi:10.1111/j.1365-2141.2006.06012.x
151. Ahmed Y, van Iddekinge B, Paul C, Sullivan MHF, Elder MG. Retrospective analysis of platelet numbers and volumes in normal pregnancy and in pre-eclampsia. *BJOG: An Int J Obstet and Gynaecol* (1993) 100(3):216–20. doi:10.1111/j.1471-0528.1993.tb15233.x
152. Yokogoshi H, Wurtman RJ. Meal composition and plasma amino acid ratios: effect of various proteins or carbohydrates, and of various protein concentrations. *Metabolism* (1986) 35(9):837–42. doi:10.1016/0026-0495(86)90225-8
153. Micheo WF, Foy CA, Kuffler DP. A novel technique restores function while eliminating intractable neuropathic pain in a 71-year-old diabetic patient under challenging injury conditions. *J Reconstr Microsurg Open* (2023) 08(1):e23–e27. doi:10.1055/s-0042-1757323
154. Foy CA, Micheo WF, Kuffler DP. Inducing ulnar nerve function while eliminating claw hand and reducing chronic neuropathic pain. *Plast Reconstr Surg - Glob Open* (2023) 11(4):e4927. doi:10.1097/gox.0000000000004927
155. Micheo WF, Foy CA, Kuffler DP. Novel technique for restoring function and eliminating chronic neuropathic pain to a 71-year-old diabetic patient with a 12 cm peripheral nerve gap repaired 1.3 years post-trauma. *J Reconstr Microsurg Open* (2022). (in press). doi:10.1055/s-0042-1757323
156. Foy CA, Micheo WF, Kuffler DP. Functional recovery following repair of long nerve gaps in senior patient 2.6 Years posttrauma. *Plast Reconstr Surg - Glob Open* (2021) 9(9):e3831. doi:10.1097/gox.0000000000003831
157. Foy C, Micheo W, Kuffler DP. Sensory and motor recovery following the repair of three long nerve gap in a senior patient 2.6 Years post-trauma. *Plast and Reconstr Surg* (2021). (in press). doi:10.1097/GOX.0000000000003831
158. Santiago Figureoa JP. KD. Novel technique for the long-term elimination of chronic excruciating neuropathic pain. *J Pain Management* (2021). (in press). doi:10.1055/s-0042-1757323
159. Kuffler DP, Reyes O, Sosa JJ, Santiago-Figureoa J. Neurological recovery across a 12-cm-long ulnar nerve gap repaired 3.25 years post trauma: case report. *Neurosurgery* (2011) 69(6):E1321–E1326. doi:10.1227/neu.0b013e31822a9fd2

160. Reyes O, Sosa JJ, Santiago J, Kuffler DP. A novel technique leading to complete sensory and motor recovery across a long peripheral nerve gap. *PR Health Sci J* (2007) **26**(3):225–8.
161. Sucuoğlu H, Üstünsoy S. The short-term effect of PRP on chronic pain in knee osteoarthritis. *Agri* (2019) **31**(2):63–9. doi:10.14744/agri.2019.81489
162. Urits I, Viswanath O, Galasso AC, Sottosani ER, Mahan KM, Aiudi CM, et al. Platelet-rich plasma for the treatment of low back pain: a comprehensive review. *Curr Pain Headache Rep* (2019) **23**(7):52. doi:10.1007/s11916-019-0797-6
163. Salomon D, Miloro M, Kolokythas A. Outcomes of immediate allograft reconstruction of long-span defects of the inferior alveolar nerve. *J Oral Maxillofac Surg* (2016) **74**(12):2507–14. doi:10.1016/j.joms.2016.05.029
164. Barber FA. PRP as an adjunct to rotator cuff tendon repair. *Sports Med Arthrosc Rev* (2018) **26**(2):42–7. doi:10.1097/jsa.0000000000000193
165. Sundman EA, Cole BJ, Fortier LA. Growth factor and catabolic cytokine concentrations are influenced by the cellular composition of platelet-rich plasma. *Am J Sports Med* (2011) **39**(10):2135–40. doi:10.1177/0363546511417792
166. Raeissadat SA, Sedighpour L, Rayegani SM, Bahrami MH, Bayat M, Rahimi R. Effect of platelet-rich plasma (PRP) versus autologous whole blood on pain and function improvement in tennis elbow: a randomized clinical trial. *Pain Res Treat* (2014) **2014**:1–8. doi:10.1155/2014/191525
167. Milants C, Bruyere O, Kaux JF. Response to: comment on responders to platelet-rich plasma in osteoarthritis: a technical analysis. *Biomed Res Int* (2018) **2018**:1–2. doi:10.1155/2018/2718156
168. Kaux JF, Bouvard M, Lecut C, Oury C, Gothot A, Sanchez M, et al. Reflections about the optimisation of the treatment of tendinopathies with PRP. *Muscle Ligaments Tendons J* (2019) **05**(1):1–4. doi:10.32098/mltj.01.2015.01
169. Yamaguchi R, Terashima H, Yoneyama S, Tadano S, Ohkohchi N. Effects of platelet-rich plasma on intestinal anastomotic healing in rats: PRP concentration is a key factor. *J Surg Res* (2012) **173**(2):258–66. doi:10.1016/j.jss.2010.10.001
170. Laver L, Marom N, Dnyanesh L, Mei-Dan O, Espregueira-Mendes J, Gobbi A. PRP for degenerative cartilage disease: a systematic review of clinical studies. *Cartilage* (2017) **8**(4):341–64. doi:10.1177/1947603516670709
171. Giusti I, D'Ascenzo S, Mancò A, Di Stefano G, Di Francesco M, Rugghetti A, et al. Platelet concentration in platelet-rich plasma affects tenocyte behavior *in vitro*. *Biomed Res Int* (2014) **2014**:630870. doi:10.1155/2014/630870
172. Santiago-Figueroa J, Sosa JJ, Reyes O. Reducing and eliminating human neuropathic pain following peripheral nerve trauma. *J Pain Management. J Pain Management* (2011) **4**(4):387–94.
173. Golebiewska EM, Poole AW. Platelet secretion: from haemostasis to wound healing and beyond. *Blood Rev* (2015) **29**(3):153–62. doi:10.1016/j.blre.2014.10.003
174. Lindemann S, Tolley ND, Dixon DA, McIntyre TM, Prescott SM, Zimmerman GA, et al. Activated platelets mediate inflammatory signaling by regulated interleukin 1 β synthesis. *The J Cell Biol* (2001) **154**(3):485–90. doi:10.1083/jcb.200105058
175. Weyrich AS, Schwartz H, Kraiss LW, Zimmerman G. Protein synthesis by platelets: historical and new perspectives. *J Thromb Haemost* (2009) **7**(2):241–6. doi:10.1111/j.1538-7836.2008.03211.x
176. Kniewallner KM, Grimm N, Humpel C. Platelet-derived nerve growth factor supports the survival of cholinergic neurons in organotypic rat brain slices. *Neurosci Lett* (2014) **574**:64–9. doi:10.1016/j.neulet.2014.05.033
177. Jonnalagadda D, Izu LT, Whiteheart SW. Platelet secretion is kinetically heterogeneous in an agonist-responsive manner. *Blood* (2012) **120**(26):5209–16. doi:10.1182/blood-2012-07-445080
178. Mariani E, Roffi A, Cattini L, Pulsatelli L, Assirelli E, Krishnakumar GS, et al. Release kinetic of pro- and anti-inflammatory biomolecules from platelet-rich plasma and functional study on osteoarthritis synovial fibroblasts. *Cytotherapy* (2020) **22**(7):344–53. doi:10.1016/j.jcyt.2020.02.006
179. Shen KF, Zhu HQ, Wei XH, Wang J, Li YY, Pang RP, et al. Interleukin-10 down-regulates voltage gated sodium channels in rat dorsal root ganglion neurons. *Exp Neurol* (2013) **247**:466–75. doi:10.1016/j.expneurol.2013.01.018
180. Estacion M, Waxman SG. The response of Na(V)1.3 sodium channels to ramp stimuli: multiple components and mechanisms. *J Neurophysiol* (2013) **109**(2):306–14. doi:10.1152/jn.00438.2012
181. Hains BC, Klein JP, Saab CY, Craner MJ, Black JA, Waxman SG. Upregulation of sodium channel Nav1.3 and functional involvement in neuronal hyperexcitability associated with central neuropathic pain after spinal cord injury. *J Neurosci* (2003) **23**(26):8881–92. doi:10.1523/jneurosci.23-26-08881.2003
182. Cummins TR, Sheets PL, Waxman SG. The roles of sodium channels in nociception: implications for mechanisms of pain. *Pain* (2007) **131**(3):243–57. doi:10.1016/j.pain.2007.07.026
183. Burchiel KJ. Carbamazepine inhibits spontaneous activity in experimental neuromas. *Exp Neurol* (1988) **102**(2):249–53. doi:10.1016/0014-4886(88)90101-x
184. Matzner O, Devor M. Hyperexcitability at sites of nerve injury depends on voltage-sensitive Na⁺ channels. *J Neurophysiol* (1994) **72**(1):349–59. doi:10.1152/jn.1994.72.1.349
185. Devor M, Wall PD, Catalan N. Systemic lidocaine silences ectopic neuroma and DRG discharge without blocking nerve conduction. *Pain* (1992) **48**(2):261–8. doi:10.1016/0304-3959(92)90067-1
186. Omana-Zapata I, Khabbaz MA, Hunter JC, Clarke DE, Bley KR. Tetrodotoxin inhibits neuropathic ectopic activity in neuromas, dorsal root ganglia and dorsal horn neurons. *Pain* (1997) **72**(1-2):41–9. doi:10.1016/s0304-3959(97)00012-2
187. Chabal C, Jacobson L, Little J. Intrathecal fentanyl depresses nociceptive flexion reflexes in patients with chronic pain. *Anesthesiology* (1989) **70**(2):226–9. doi:10.1097/0000542-198902000-00008
188. Kerr BJ, Souslova V, McMahon SB, Wood JN. A role for the TTX-resistant sodium channel Nav 1.8 in NGF-induced hyperalgesia, but not neuropathic pain. *Neuroreport* (2001) **12**(14):3077–80. doi:10.1097/00001756-2001110080-00019
189. Lai J, Gold MS, Kim CS, Bian D, Ossipov MH, Hunter JC, et al. Inhibition of neuropathic pain by decreased expression of the tetrodotoxin-resistant sodium channel, Nav1.8. *Pain* (2002) **95**(1-2):143–52. doi:10.1016/s0304-3959(01)00391-8
190. Samad OA, Tan AM, Cheng X, Foster E, Dib-Hajj SD, Waxman SG. Virus-mediated shRNA knockdown of Na(v)1.3 in rat dorsal root ganglion attenuates nerve injury-induced neuropathic pain. *Mol Ther* (2013) **21**(1):49–56. doi:10.1038/mt.2012.169
191. Ledeboer A, Jekich BM, Sloane EM, Mahoney JH, Langer SJ, Milligan ED, et al. Intrathecal interleukin-10 gene therapy attenuates paclitaxel-induced mechanical allodynia and proinflammatory cytokine expression in dorsal root ganglia in rats. *Brain Behav Immun* (2007) **21**(5):686–98. doi:10.1016/j.bbi.2006.10.012
192. Yao MZ, Gu JF, Wang JH, Sun LY, Lang MF, Liu J, et al. Interleukin-2 gene therapy of chronic neuropathic pain. *Neuroscience* (2002) **112**(2):409–16. doi:10.1016/s0306-4522(02)00078-7
193. Gonzalez-Darder JM, Barbera J, Abellan MJ. Effects of prior anaesthesia on autotomy following sciatic transection in rats. *Pain* (1986) **24**(1):87–91. doi:10.1016/0304-3959(86)90029-1
194. Dokka S, Shi X, Leonard S, Wang L, Castranova V, Rojanasakul Y. Interleukin-10-mediated inhibition of free radical generation in macrophages. *Am J Physiology-Lung Cell Mol Physiol* (2001) **280**(6):L1196–202. doi:10.1152/ajplung.2001.280.6.L1196
195. Linke B, Schreiber Y, Picard-Willems B, Slattery P, Nüsing RM, Harder S, et al. Activated platelets induce an anti-inflammatory response of monocytes/macrophages through cross-regulation of PGE2 and cytokines. *Mediators Inflamm* (2017) **2017**:1–14. doi:10.1155/2017/1463216
196. Zheng W, Huang W, Liu S, Levitt RC, Candiotti KA, Lubarsky DA, et al. IL-10 mediated by herpes simplex virus vector reduces neuropathic pain induced by HIV gp120 combined with ddC in rats. *Mol Pain* (2014) **10**:49. doi:10.1186/1744-8069-10-49
197. Plunkett JA, Yu CG, Easton JM, Bethea JR, Yezierski RP. Effects of interleukin-10 (IL-10) on pain behavior and gene expression following excitotoxic spinal cord injury in the rat. *Exp Neurol* (2001) **168**(1):144–54. doi:10.1006/exnr.2000.7604
198. Yu ML, Wei RD, Zhang T, Wang J, Cheng Y, Qin F, et al. Electroacupuncture relieves pain and attenuates inflammation progression through inducing IL-10 production in CFA-induced mice. *Inflammation* (2020) **43**(4):1233–45. doi:10.1007/s10753-020-01203-2

**EBM is the official journal of the Society
for Experimental Biology and Medicine**

Experimental Biology and Medicine (EBM)
is a global, peer-reviewed journal dedicated
to the publication of multidisciplinary and
interdisciplinary research in the biomedical
sciences.

Discover more of our Special Issues

See more →

Contact

development@ebm-journal.org

See more

ebm-journal.org

publishingpartnerships.frontiersin.org/our-partners

